CROSS-TALK BETWEEN CELLULAR AND MOLECULAR COMPARTMENTS DURING LIVER INJURY

EDITED BY: Chao Yan, Jianpeng Sheng, Xiaojun Chen and Liang Wen

PUBLISHED IN: Frontiers in Medicine

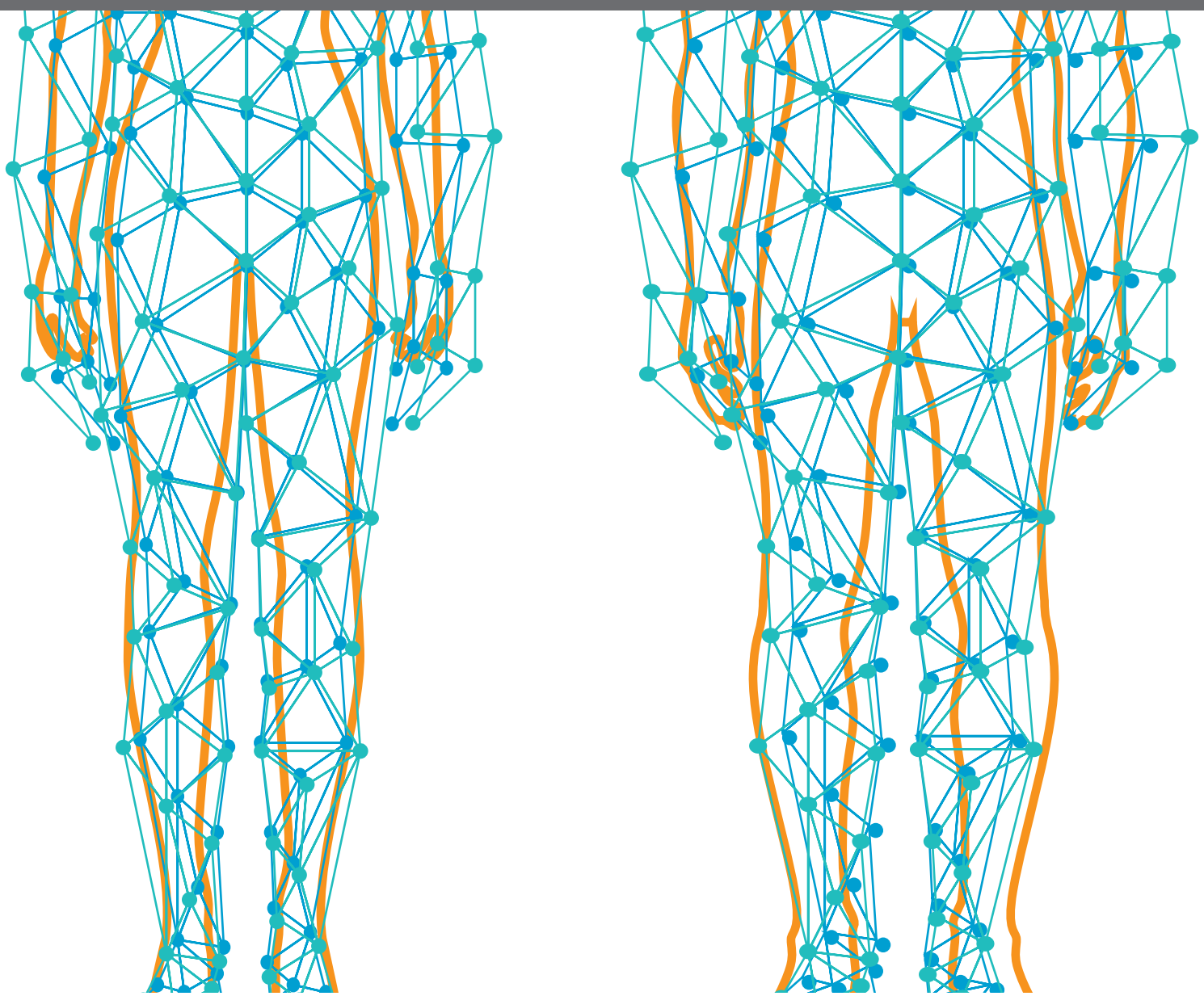

frontiers Research Topics

ISSN 1664-8714
ISBN 978-2-88974-997-3
DOI 10.3389/978-2-88974-997-3

About Frontiers

Frontiers is more than just an open-access publisher of scholarly articles: it is a pioneering approach to the world of academia, radically improving the way scholarly research is managed. The grand vision of Frontiers is a world where all people have an equal opportunity to seek, share and generate knowledge. Frontiers provides immediate and permanent online open access to all its publications, but this alone is not enough to realize our grand goals.

Frontiers Journal Series

The Frontiers Journal Series is a multi-tier and interdisciplinary set of open-access, online journals, promising a paradigm shift from the current review, selection and dissemination processes in academic publishing. All Frontiers journals are driven by researchers for researchers; therefore, they constitute a service to the scholarly community. At the same time, the Frontiers Journal Series operates on a revolutionary invention, the tiered publishing system, initially addressing specific communities of scholars, and gradually climbing up to broader public understanding, thus serving the interests of the lay society, too.

Dedication to Quality

Each Frontiers article is a landmark of the highest quality, thanks to genuinely collaborative interactions between authors and review editors, who include some of the world's best academicians. Research must be certified by peers before entering a stream of knowledge that may eventually reach the public - and shape society; therefore, Frontiers only applies the most rigorous and unbiased reviews.
Frontiers revolutionizes research publishing by freely delivering the most outstanding research, evaluated with no bias from both the academic and social point of view. By applying the most advanced information technologies, Frontiers is catapulting scholarly publishing into a new generation.

What are Frontiers Research Topics?

Frontiers Research Topics are very popular trademarks of the Frontiers Journals Series: they are collections of at least ten articles, all centered on a particular subject. With their unique mix of varied contributions from Original Research to Review Articles, Frontiers Research Topics unify the most influential researchers, the latest key findings and historical advances in a hot research area! Find out more on how to host your own Frontiers Research Topic or contribute to one as an author by contacting the Frontiers Editorial Office: frontiersin.org/about/contact

CROSS-TALK BETWEEN CELLULAR AND MOLECULAR COMPARTMENTS DURING LIVER INJURY

Topic Editors:
Chao Yan, Xuzhou Medical University, China
Jianpeng Sheng, Nanyang Technological University, Singapore
Xiaojun Chen, Nanjing Medical University, China
Liang Wen, Zhejiang University, China

Citation: Yan, C., Sheng, J., Chen, X., Wen, L., eds. (2022). Cross-Talk Between Cellular and Molecular Compartments During Liver Injury. Lausanne: Frontiers Media SA. doi: 10.3389/978-2-88974-997-3

Table of Contents

frontiers in Medicine

REVIEW
published: 24 September 2020
doi: 10.3389/fmed.2020.583691

Roles of Macrophages and Exosomes in Liver Diseases

Mengyi Shen[1†], Yi Shen[1†], Xiaoli Fan[1], Ruoting Men[1], Tinghong Ye[2] and Li Yang[1*]*

[1] Department of Gastroenterology and Hepatology, Sichuan University-University of Oxford Huaxi Joint Centre for Gastrointestinal Cancer, Frontiers Science Center for Disease-Related Molecular Network, West China Hospital, Sichuan University, Chengdu, China, [2] Laboratory of Liver Surgery, State Key Laboratory of Biotherapy/Collaborative Innovation Center for Biotherapy, West China Hospital, Sichuan University, Chengdu, China

Exosomes are small discoid extracellular vesicles (EVs) originating from endosomes that are 30–150 nm in diameter and have a double lipid layer. They participate in the immune response, cell migration, cell differentiation, and tumor invasion and mediate intercellular communication, regulating the biological activity of receptor cells through the proteins, nucleic acids, and lipids that they carry. Exosomes also play vital roles in the diagnosis and treatment of liver diseases. Macrophages, which show unique phenotypes and functions in complex microenvironments, can be divided into M1 and M2 subtypes. M1 macrophages function in immune surveillance, and M2 macrophages downregulate the immune response. Recent studies have shown that macrophages are involved in non-alcoholic fatty liver disease, liver fibrosis, and hepatocellular carcinoma. Moreover, several studies have demonstrated that liver diseases are associated with exosomes derived from or transferred to macrophages. This review focuses on the participation of macrophages and exosomes in liver diseases.

Keywords: macrophages, exosomes, hepatitis virus, alcoholic liver disease, non-alcoholic fatty liver disease, acute liver failure, hepatocellular carcinoma

OPEN ACCESS

Edited by:
Jianpeng Sheng, Nanyang Technological University, Singapore

Reviewed by:
Jafar Rezaie, Urmia University of Medical Sciences, Iran
Reza Rahbarghazi, Tabriz University of Medical Sciences, Iran

***Correspondence:**
Tinghong Ye
yeth1309@scu.edu.cn
Li Yang
yangli_hx@scu.edu.cn

[†]These authors have contributed equally to this work

Specialty section:
This article was submitted to Gastroenterology, a section of the journal Frontiers in Medicine

Received: *15 July 2020*
Accepted: *13 August 2020*
Published: *24 September 2020*

Citation:
Shen M, Shen Y, Fan X, Men R, Ye T and Yang L (2020) Roles of Macrophages and Exosomes in Liver Diseases. Front. Med. 7:583691. doi: 10.3389/fmed.2020.583691

INTRODUCTION

Exosomes are small discoid extracellular vesicles (EVs) originating from endosomes that are 30–150 nm in diameter and have a double lipid layer (1). The exosome formation process involves invagination of the cell membrane to form an endosome, which then develops into a multivesicular body (MVB) that subsequently fuses with the cell membrane, releases the particles outside of the cell, and forms the exosome (2). A variety of cells can secrete exosomes under normal and pathological conditions (3). In addition, exosomes are also widely found in bodily fluids, including blood, saliva, urine, ascites, and cerebrospinal fluid (4, 5). The function of an exosome depends on the type of cell from which it originates. In general, exosomes can participate in processes such as immune response, cell migration, cell differentiation, and tumor invasion (6). Exosomes mediate intercellular communication, regulating the biological activity of receptor cells through the proteins, nucleic acids, and lipids they carry (7, 8). Exosomes also play a vital role in the diagnosis and treatment of liver diseases (9).

Macrophages are a heterogeneous population of cells that exhibit a unique phenotype and function in the complex microenvironment *in vivo*. According to differences in their activation state and function, macrophages can be divided into classically activated macrophages (CAMs or M1) and alternatively activated macrophages (AAMs or M2). M1 macrophages participate

in the immune response and in immune surveillance by presenting antigens and secreting pro-inflammatory cytokines such as IL-6 and tumor necrosis factor-α (TNF-α). M2 macrophages have a weak antigen presentation ability and play an important role in immune regulation by downregulating the immune response *via* the secretion of the inhibitory cytokines IL-10, transforming growth factor-β (TGF-β) and mannose receptor (Mrc) (10–12). It has been suggested that macrophages have a series of continuous functional states, and M1 and M2 macrophages are the two extremes of this continuous state (13). Moreover, recent studies have found that macrophages are involved in non-alcoholic fatty liver disease (NAFLD) (14, 15), liver fibrosis (16), and hepatocellular carcinoma (HCC) (17).

Exosomes secreted by hepatocytes exposed to alcohol can be ingested by macrophages, thereby promoting the secretion of cytokines (18). In cholestatic liver disease, exosomal long non-coding RNA (lncRNA) H19 from bile duct cells promotes the M1 polarization of Kupffer cells and the production of chemokine ligand 2 and interleukin 6 (19). In melatonin-treated HCC cells, exosomes change the immunosuppression status of macrophages (20). In this review, we summarize the effects and interaction of macrophages and exosomes in liver diseases (**Table 1**).

CHARACTERISTICS OF EXOSOMES

Cells release bilayer membranous vesicles called EVs, which can be divided into exosomes, microvesicles (MVs), ectosomes, migrasomes, apoptotic bodies, and oncosomes according to their size and origin (37). Exosomes are the smallest EVs, with a diameter of 30–150 nm. Further, exosomes can be divided into small exosomes (60–80 nm) and large exosomes (90–120 nm). Proteomic analyses have shown that small exosomes carry proteins that are associated with endosomes, MVBs, and phagocytic vesicles, indicating that small exosomes are classical exosomes from the endosomal compartment. In contrast, large exosomes include plasma membrane proteins, cellular connexins, and late endosomal proteins and may be atypical exosomes from plasma membrane germination (38). Medium-sized EVs, 100–1,000 nm in diameter, include MVs, ectosomes, and microparticles (39). Ectosomes depend on the plasma membrane, while exosomes depend on endocytic membranes. These two distinct types of EVs differ in size, composition, and release regulation mechanisms. For ectosomes and exosomes, the goods on the surface and in the lumen differ when EVs are released by different cell types or individual cells in different functional conditions. After release, the two types of EVs move through the extracellular fluid at different times and for different distances (40). Migrasomes, apoptotic bodies, and oncosomes are large EVs (a few thousand nanometers) that have been found to be associated with migration, phagocytosis, and cancer, respectively. Migrasomes are newly identified organelles that depend on migration, leaving long retractable fibers upon cell migration, and vesicles grow atop the tips and intersections of fibers. Eventually, the fibers that connect the vesicles to the main cell body break apart, and the vesicles are released into the extracellular space or absorbed directly by the surrounding cells (41). Apoptotic bodies, small bodies released by programmed cell death, can be formed in two ways: the sprouting and shedding mechanism and the autophagosome mechanism (42). The term "oncosomes" was originally used to describe abnormally large EVs, although it is often used to refer to EVs released by cancer cells (43). Oncosomes derived from prostate cancer cells strongly promote the establishment of a tumor-supporting environment by inducing new interstitial reprogramming (44). In fact, EVs should not be classified into subtypes according to their sizes because their diameters overlap; for example, some MVs, whose size range is very large (100–1,000 nm), can be easily confused with large exosomes (45). At present, the origin is the only basis for distinguishing exosomes from other EVs. Other EVs are formed by the protrusion and shedding of cell membranes, whereas exosomes are derived from intracellular endosomes, which can form MVBs that are then degraded by lysosomes or fused with the cytoplasmic membrane, released and enter the receiving cell through fusion, endocytosis or receptors (46). According to the MISEV2018 guidelines, exploring the biogenesis of EVs remains a challenge without the use of live imaging techniques. Therefore, operational terms are still recommended for the description of EV subtypes according to their size, density, biochemical composition, and cell or organ origin (47).

The exosome formation process involves invagination of the cell membrane to form an endosome, which then develops into MVBs. Some of these MVBs directly fuse with lysosomes and degrade, some are transported to the Golgi for recovery, and some fuse with the cell membrane to release small vesicles outside of the cell and form exosomes. Regarding the mechanisms associated with exosome biogenesis and abscission, many molecules play an important role. First, the endosomal sorting complex required for transport (ESCRT) and other proteins, such as tumor susceptibility gene 101 protein (TSG101) and ALG-2 interacting protein X (ALIX), are involved in cargo sorting into exosomes (3). Apart from ESCRT, other ESCRT-independent mechanisms, including lipid rafts and tetraspanins CD63 and CD81, are conducive to exosome biogenesis (48). Finally, the Rab-GTPase family contributes to the intracellular trafficking and fusion of MVBs with the cell membrane to release exosomes. Some studies clarified that sphingomyelinase, protein kinase D family, and argonaute-2 are involved in the formation of exosomes (49) (**Figure 1**).

Exosomes are composed of nucleic acids (including DNA and RNA), proteins, and lipids. Exosomal RNAs mainly play key roles in the target cell and mainly include mRNAs, microRNAs, lncRNAs, circRNAs, etc. (50). MicroRNAs are now the most widely and deeply studied type of RNA in exosomes, often due to their relationship with the occurrence and development of diseases (51). Exosomal proteins can be divided into membrane proteins and intramembrane proteins. Membrane proteins, including tetraspanins (CD63, CD81, and CD9) and some cell-specific proteins, such as A33 (colon epithelial cell source), MHC-II, and CD86 (antigen-presenting cell sources), participate in exosome transport. Intracellular exosomal proteins include the heat shock protein family (HSP60, HSP70, HSP90, HSPA5, and CCT2), a variety of metabolic enzymes (GAPDH, PKM2,

TABLE 1 | Summary of exosome and macrophage participation in liver diseases.

Disease	Exosome component	Pathway/mediator	Effect	References
HBV	HBV-miR-3	SOCS5/STAT1	M1 polarization and IL-6 secretion	(21)
	HBV-infected hepatocyte exosomes	MyD88, TICAM-1, and MAVS	Resistance to the host's inherent immune response	(22)
HCV	Anti-HCV miRNA-29	TLR3-activated macrophages	Inhibition of the HCV replication	(23)
	Exosome-packaged HCV	TLR7/8	Monocytes tend to differentiate into macrophages	(24)
ALD	miR-155	Hsp90	Increase in inflammatory macrophages	(25)
	miR-27A	CD206 on monocytes	M2 polarization	(26)
	CD40L (TNFSF5)	Caspase-3	M1 polarization	(27)
	miR-122	HO-1	Reprogramming ability to make monocytes sensitive to LPS	(18)
	Mitochondrial double-stranded RNA	TLR3 in Kupffer cells	Increase in IL-1β and IL−17A levels	(28)
NAFLD	mi R-192-5p	Rictor/Akt/FoxO1	M1 polarization	(29)
	Hepatocyte-derived EV	DR5/Caspase/ROCK1	Macrophage pro-inflammatory response	(30)
	Lipotoxic EVs	ITGβ1	Promotion of monocyte adhesion and liver inflammation	(31)
	miR122-5p	lysosome	M1 polarization	(32)
ALF	miR-17	TXNIP	Inhibition of inflammatory factor activation in hepatic macrophages	(33)
HCC	lncRNA TUC339	Toll-like receptor signaling and FcγR-mediated phagocytosis	Reduction in pro-inflammatory cytokine production and amelioration of phagocytosis	(34)
	Exo-con	STAT3	Upregulation of PD-L1 expression and cytokine secretion in macrophages	(20)
	miR-23a-3p	PTEN/AKT	Upregulation of PD-L1 expression in macrophages and inhibition of T-cell function	(35)
	miR-142-3p	RAC1	Propofol stimulates the transfer of miR-142-3p from macrophages to HCC cells. MiR-142-3p downregulates RAC1 expression and inhibits HCC cell migration and invasion	(36)

HBV, Hepatitis B virus; HCV, Hepatitis C virus; ALD, Alcoholic liver disease; NAFLD, Nonalcoholic fatty liver disease; ALF, Acute liver failure; HCC, Hepatocellular carcinoma; Exo-con, Hepatocellular carcinoma-derived exosomes; M1, M1 macrophages; M2, M2 macrophages.

PGK1, PDIA3, antioxidant proteins), ribosomal proteins (RPS3), signal transduction factors (melanoma differentiation-related factors, ARF1, CDC42), adhesion factors (MFGE8, integrin), cytoskeletal proteins, and ubiquitin (52, 53). Lipids are important components of the exosomal membrane, and exosomes contain more specific lipids than parent cells. Several studies have found that the percentages of different lipid categories in cells and exosomes vary among several cell types, such as human B cells and dendritic cells. Specifically, in human B cells, cholesterol, and sphingomyelins have been found to be enriched from cells to exosomes (54) (**Figure 2**).

Exosomes have several functions. First, they function as a shuttle bus between cells, mediate cell-cell communication and play a role in immunity. Exosomes have been identified as important mediators of intercellular communication through the transfer of encapsulated cargo, such as bioactive lipids, non-coding RNAs, mRNAs, and proteins (55). These bioactive molecules are stable because they are covered with a biofilm capable of avoiding degradation. In addition, due to the characteristics of their surface proteins, exosomes also show relatively high target specificity to receptor cells. All these characteristics make exosomes important mediators of communication between cells, especially between organs. Second, the occurrence and progression of diseases [e.g., tumor metastasis (56–58), cardiovascular disease risk (59, 60), neurological diseases (61, 62)] can be predicted by studying the relationship among the exosome type, number, size, and content. Finally, several recent studies have reported on targeted drugs for exosomes. Exosomes can be used as carriers to deliver drugs to target areas, providing hope for the treatment of many diseases (63, 64).

HEPATITIS VIRUS

Hepatitis B virus (HBV) infection is characterized by long-term chronic infection accompanied by hepatocyte injury due to the complicated interaction between HBV and the immune system. In addition, according to the World Health Organization, more than 185 million people are infected with hepatitis C virus (HCV) (65). In the process of HCV infection, the interaction between macrophages and hepatocytes is an important part of liver innate immunity.

HBV encodes a microRNA (HBV-miR-3) that inhibits HBV replication by impeding transcription. Type I interferons (IFNs) constitute important immune responses to viral infection and can thus be used to treat some infectious viruses, including HBV and HCV. IFN-I interacts with its receptor to activate the Janus kinase (JAK)/STAT pathway, and STAT1/2 is then phosphorylated and transferred to the nucleus to bind to the IFN-stimulating response element, initiating the transcription of

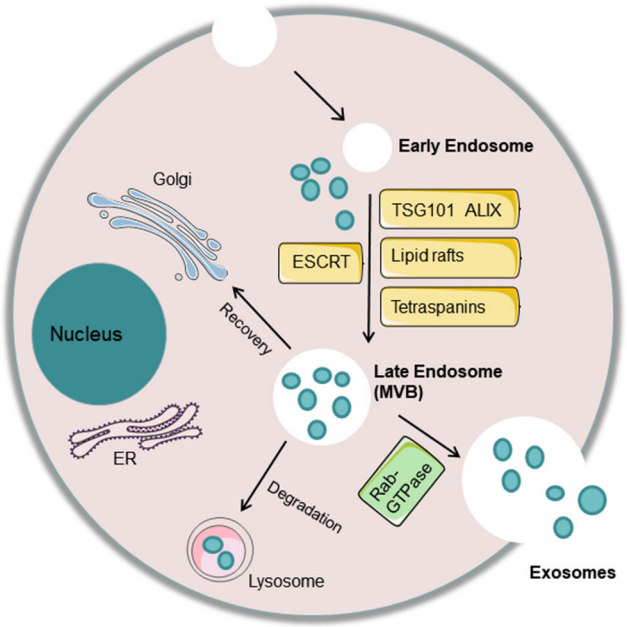

FIGURE 1 | Exosome biogenesis and abscission. The cell membrane invaginates to form an endosome, which then develops into a late endosome or multivesicular body (MVB) with processing of the rough endoplasmic reticulum and Golgi. Some of these MVBs directly fuse with lysosomes and degrade, some are transported to the Golgi for recovery, and some fuse with the cell membrane to release small vesicles outside of the cell and form exosomes. Many molecules play an important role in exosome biogenesis and abscission. First, the endosomal sorting complex required for transport (ESCRT) and other proteins, such as tumor susceptibility gene 101 protein (TSG101) and ALG-2 interacting protein X (ALIX), are involved in cargo sorting into exosomes. In addition, other ESCRT-independent mechanisms, including lipid rafts and tetraspanins CD63 and CD81, are conducive to exosome biogenesis. Finally, the Rab-GTPase family contributes to the intracellular trafficking and fusion of MVBs with the cell membrane to release exosomes.

IFN-stimulated genes. SOCS5, an E3 ubiquitin ligase, negatively regulates the mechanism described above; specifically, it inhibits JAK kinase activity by interacting with JAKs through its JAK interaction region. Exosomal HBV-miR-3 promotes macrophage differentiation into the M1 phenotype and IL-6 secretion through the SOCS5/STAT1 pathway (21). Macrophage exosomes rely on T cell immunoglobulin and the hepatitis A virus receptor mucin receptor 1 to enter liver cells and then promote anti-HBV activity induced by IFN-α. In addition, the two main endocytic pathways for viral infection, namely, reticular protein-mediated endocytosis and macrophage phagocytosis, cooperate to allow exosome entry into liver cells and transfer of this activity (66). HBV-infected hepatocyte exosomes carry viral nucleic acids and prompt the expression of NKG2D ligands in macrophages. Compared to normal hepatocytes, HBV-infected hepatocyte exosomes show higher expression levels of immunoregulatory microRNAs, which are transported to macrophages and then restrict IL-12p35 mRNA expression in macrophages, leading to resistance to the host's inherent immune response (22).

Exosomes derived from macrophages play a key role in inhibiting the replication of HCV. TLR3-activated macrophages release exosomes containing anti-HCV microRNA (miRNA)-29 family members (23). Further studies show that interferon-stimulated macrophage-derived EVs inhibit HCV replication and participate in antiviral immune responses, while polyunsaturated fatty acids weaken this process (67). On the other hand, exosomes can also affect macrophages. Concretely, monocytes tend to differentiate into macrophages that show high expression of M2 surface markers and produce pro- and anti-inflammatory cytokines when cocultured with exosome-packaged HCV, which is mediated by TLR7/8 (24).

ALCOHOLIC LIVER DISEASE

Alcoholic liver disease (ALD) or alcoholic hepatitis (AH) is a liver disease caused by long-term heavy drinking. The effects of alcohol, alcohol metabolites, and gut-derived endotoxins cause liver damage in patients with ALD (68, 69). The initial manifestation is usually fatty liver, which can develop into AH, liver fibrosis, and liver cirrhosis (70). Approximately 3.3 million people die each year from excessive drinking, accounting for almost 5.9% of all global deaths. According to the World Health Organization, Europe has the highest amount of alcohol consumption per adult. In EU countries, 41% of all liver deaths are attributed to alcohol. Since ALD patients have not shown any clinical symptoms or abnormal laboratory indicators in the past, screening should be carried out in high-risk groups (71).

A recent study focused on the potential correlation between autophagy and exosomes since autophagosome and exosome biogenesis involve the same components. The researchers found autophagy damage in ALD and AH mouse models and in the livers of patients with ALD. Moreover, this autophagy occurs at the lysosome level by reducing the expression of lysosome-associated membrane protein 1 (LAMP1) and lysosome-associated membrane protein 2 (LAMP2). The expression of microRNA 155 (miR-155) is increased by alcohol, and its action targets are LAMP1, LAMP2, mechanistic target of rapamycin, and Ras homolog enriched in the brain. In line with this, miR-155 gene-deficient mice exhibited less alcohol-induced autophagic damage and less exosome production than control mice. Downregulation of LAMP1 or LAMP2 increases the number of exosomes released by hepatocytes and macrophages. These results reveal that the increased exosome content induced by alcohol is related to the destruction of autophagy and the impaired function of autophagosomes and lysosomes (25). Another study clarified that atypical exosomes can eliminate lysosomal waste to combat lysosomal dysfunction, thus maintaining dynamic equilibrium (72). In addition, researchers have found that EVs in patients with ALD carry a unique protein cargo and induce macrophage activation by heat shock protein 90 (73). Another study found that alcohol increases the EV (mainly exosomes) production of primary human monocytes and THP-1 monocytes, and monocytes exposed to alcohol communicate with primitive monocytes through EVs. Furthermore, miR-27A in exosomes polarizes primitive monocytes into M2 macrophages (26). Similarly, patients with AH and alcohol-fed mice produced more EVs than normal

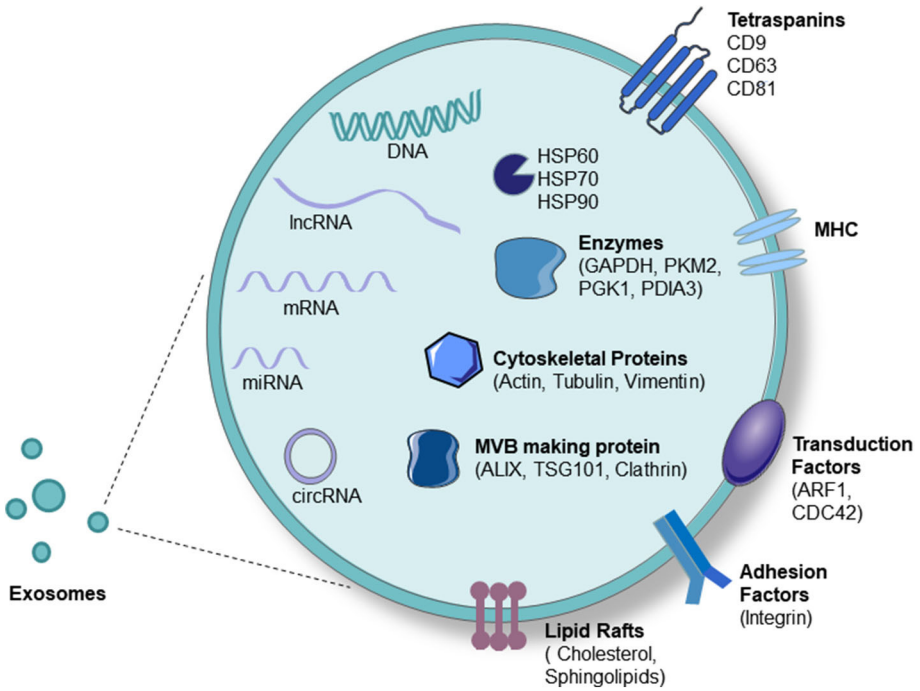

FIGURE 2 | Exosome components. Exosomes carry proteins, nucleic acids, and lipids. Proteins include tetraspanins (CD63, CD81, and CD9), some cell-specific proteins such as MHC-II (antigen-presenting cell source), heat-shock protein family (HSP60, HSP70, HSP90), a variety of metabolic enzymes (GAPDH, PKM2, PGK1, PDIA3, antioxidant proteins), signal transduction factors (ARF1, CDC42), adhesion factors (MFGE8, integrin), cytoskeletal proteins (Actin, Tubulin, Vimentin), and MVB-producing proteins (Alixs, Tsg101, Clathrin). Nucleic acids include DNA, mRNA, microRNA, lncRNA, and circRNA.

controls. Exosomal miRNA-192, miRNA-122, and miRNA-30a secreted into the blood could be used as diagnostic biomarkers of ALD (74). In addition, a previous study in mice demonstrated that ethanol promotes the secretion of EVs *via* CYP2E1 and revealed for the first time that the caspase-3 pathway is involved in this process. EVs contain CD40L (TNFSF5) and can activate pro-inflammatory macrophages (27). Liver cells exposed to alcohol secrete exosomes containing increased concentrations of miR-122, which is absorbed by macrophages and makes them sensitive to lipopolysaccharide (LPS), thereby enhancing cytokine secretion (18). In addition, mitochondria have also attracted much attention. Ethanol exposure can activate toll-like receptor 3 in Kupffer cells by hepatic mitochondrial double-stranded RNA (MtdsRNA) through exosomal delivery, resulting in increased IL-1β levels, which promotes the production of IL-17A. MtdsRNA and TLR3 can be used as therapeutic targets for ALD (28, 75). Hence, blocking these pathways may protect against alcohol-induced liver injury.

NON-ALCOHOLIC FATTY LIVER DISEASE

NAFLD is characterized by the excessive accumulation of liver fat and insulin resistance, which is defined by histological analysis as >5% hepatocyte steatosis or by proton density as a fat content of >5.6%. NAFLD includes two kinds of pathological diagnoses with different prognoses: non-alcoholic fatty liver (NAFL) and non-alcoholic steatohepatitis (NASH). The latter is more severe than the former and includes fibrosis, liver cirrhosis, and HCC (76). High-calorie diets, excessive intake of saturated fats, refined carbohydrates, sugary drinks, and fructose and Western diets are all associated with increased body mass, obesity, and especially NAFLD (77). High-fructose intake increases the risk of NASH and advanced liver fibrosis (78, 79). In addition, it is generally recognized that monocyte-derived macrophages recruited in the liver are involved in the inflammatory response of NASH.

The pathological features of NASH are lipid-induced hepatocyte apoptosis (apoptosis induced by toxic lipid mediators) and infiltration by inflammatory cells, some of which are activated macrophages (80). The latest research indicates that the number and miR-192-5p level of serum exosomes in NASH patients, and NASH model rats are significantly higher than those in their respective control groups. Furthermore, the exosomes released by lipotoxic hepatocytes can be ingested by macrophages, resulting in activation of M1 macrophages and hepatic inflammation by regulating the Rictor/Akt/FoxO1 signaling pathway (29). Another study showed that in a mouse model of NASH, EVs derived from lipotoxic hepatocytes are rich in active integrin β1 (ITGβ1), mediating the adhesion of monocytes to hepatic sinusoidal endothelial cells, which is a necessary step in hepatic inflammation. ITGβ1 inhibition reduces liver injury (31). In addition, it has been reported that exosomes isolated from melatonin-treated adipocytes significantly attenuate liver steatosis induced by a high-fat diet and resistin-mediated ER stress. Further research has shown

that melatonin reduces the level of exosomal resistin derived from adipocytes through Bmal1 transcription inhibition and M6A RNA demethylation in adipocytes (81). Several studies have observed that macrophage-derived exosomes contribute to insulin resistance through paracrine or endocrine mechanisms (55, 82, 83). Another study found elevated levels of exosomes derived from natural killer T cells and macrophages among patients with NAFLD or NASH (84). Moreover, lipids have been shown to stimulate death receptor 5, promoting the release of EVs from hepatocytes; subsequently, these EVs activate the inflammatory phenotype in macrophages, which ultimately causes NASH (30). Cholesterol damages the lysosomal function of hepatocytes, leading to the secretion of hepatocyte-derived exosomal miR122-5p, which enters macrophages to promote M1 polarization and the occurrence of inflammation (32). Hepatocytes treated with ezetimibe can inhibit inflammasome formation in macrophages and IL-1 secretion as well as alleviate NASH liver inflammation through exosomes (85).

ACUTE LIVER FAILURE

Acute liver failure (ALF), a clinical syndrome characterized by jaundice, ascites, hepatic encephalopathy, and coagulation dysfunction, refers to the extensive necrosis of hepatocytes or severe liver function damage caused by various factors, such as viruses, drugs, and toxins. The treatments for ALF are liver transplantation and artificial liver therapy. However, there are limitations associated with liver transplantation due to a lack of appropriate donor livers and a variety of complications. Additionally, the efficacy of artificial liver therapy is relatively limited (86).

The transplantation of mesenchymal stem cells (MSCs) might become a potential approach for treating liver disease (87). Researchers administered human umbilical cord MSC-derived exosomes (hucMSC-Ex) to mice *via* their tail vein or oral gavage. The hucMSC-Exs exhibited antioxidant functions and antiapoptotic effects and rescued the mice from liver failure induced by CCl4 (88). Another study further explored the role of macrophages in this process. The researchers treated mice with LPS and D-galactosamine (LPS/GalN) and immediately injected adipose MSC (AMSC)-derived exosomes (AMSC-Exos) intravenously. AMSC-Exos colocalized with hepatic macrophages and reduced the secretion of inflammatory factors by inhibiting the activation of inflammatory factors in macrophages. Exosome-encapsulated miR-17 plays an important role in the treatment of ALF by targeting TXNIP and inhibiting the activation of inflammatory factors in hepatic macrophages (33). Exosomes secreted by MSCs may improve the therapeutic efficacy of MSCs by mediating intercellular communication and transporting paracrine factors (89).

HCC

The incidence of liver cancer is on the rise worldwide, with the number of newly diagnosed cases increasing by 75% between 1990 and 2015 (90). It is predicted that liver cancer will be the sixth most common cancer in the world and the fourth-largest cause of cancer-related death. According to statistics by the International Agency for Research on Cancer, there were approximately 842,080 new cases of liver cancer and 781,631 deaths in 2018. Liver cancer includes HCC (75–85% of cases), intrahepatic cholangiocarcinoma (10–15% of cases) and other rare types (91). Because patients with early HCC exhibit no obvious clinical symptoms, early diagnosis is quite difficult. Currently, screening methods for HCC rely on mainly serum tumor markers and imaging tests. Clinical serological tests include α-fetoprotein (AFP), des-γ-carboxy prothrombin, and the AFP-L3 fraction. Imaging-based diagnostic methods include computed tomography and magnetic resonance imaging. If necessary, pathological examination may be used, but this method is not ideal in early HCC monitoring (92–94). Surgical resection is suggested as the first choice for the treatment of HCC patients with non-cirrhosis. However, those who undergo surgery have a recurrence rate of 70% (95). Therefore, a need exists for improved diagnostic and treatment methods for liver cancer.

Recent studies have shown that tumor-derived exosomes can be absorbed by fibroblasts and macrophages in the tumor microenvironment, change their phenotype, and ultimately promote tumor progression and metastasis (96). Several studies have noted that HCC-derived exosomes can be ingested by macrophages and thereby promote tumor progression. A recent study showed that exosomes derived from HCC contain a large amount of the lncRNA TUC339, which is taken up along with exosomes by macrophages in the tumor microenvironment, reducing the secretion of pro-inflammatory cytokines from these macrophages, increasing the secretion of anti-inflammatory cytokines, and causing the phenotypic conversion of macrophages. These phenotypically transformed macrophages can inhibit immune-mediated tumor cell death and promote tumor immune escape, thus facilitating rapid tumor growth progression (34). The exosomes secreted by hepatoma cells and released by melatonin-induced hepatoma cells can be phagocytosed and ingested by macrophages. The immune response is affected by regulating the expression of PD-L1 and the inflammatory factors IL-6, IL-10, and TNF-α. The melatonin-induced release of exosomes from HCC cells downregulates the expression of PD-L1 in macrophages by downregulating the protein expression of STAT3 (20). Another HCC study showed that endoplasmic reticulum (ER)-stressed HCC cells release exosomes, upregulate PD-L1 expression in macrophages, and then inhibit T cell function through the exosomal miR-23a-PTEN-AKT pathway. These results provide new insights into how tumor cells escape antitumor immunity (35). Hepatoma cells transmit miRNA-21 to hepatic stellate cells and activate the tumor suppressor gene PTEN through exosomes to activate the transition of hepatic stellate cells into cancer-associated fibroblasts (CAFs) via the PDK1/AKT signaling pathway. Activated CAFs further secrete angiogenic cytokines, including vascular endothelial growth factor (VEGF), MMP2, and MMP9, increasing the number of blood vessels and promoting the development of HCC (97). In contrast, the expression of miR-122 in serum or circulating exosomes is lower in HCC patients

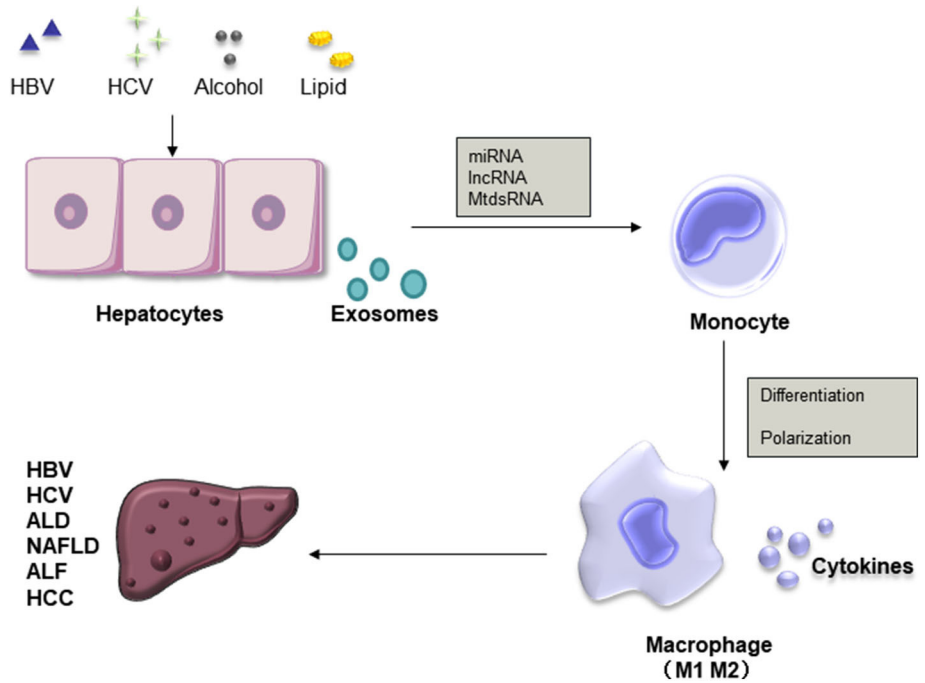

FIGURE 3 | Roles of exosomes and macrophages in liver diseases. Exosomal miRNAs, lncRNAs, and MtdsRNAs released from injured hepatocytes promote the differentiation of macrophages into the M1 or M2 phenotype and the secretion of cytokines, thereby promoting inflammation.

than in healthy subjects (98, 99). In tumor-bearing mice, propofol inhibits the invasion of HCC cells by stimulating the transfer of microvesicular miR-142-3p from tumor-associated macrophages to HCC cells (36). ER stress induces the release of exosomes from HCC cells, and by regulating the expression of programmed death ligand 1 in macrophages, the mir-23a-PTEN-AKT pathway inhibits T cell function and weakens antitumor immunity (35). Macrophages and exosomes also play an important role in tumor metastasis. Some scholars have found that in pancreatic ductal adenocarcinoma cells, tumor-derived exosomes can recruit bone marrow-derived macrophages to form a preliver metastatic environment and promote tumor metastasis (100).

EXOSOME ROLES IN PROGNOSIS AND TREATMENT

In the process of HCV infection, the interaction between retained macrophages and hepatocytes is an important part of liver innate immunity. Exosomes derived from macrophages play a key role in inhibiting the replication of HCV. Further study shows that TLR3-activated macrophages release exosomes containing anti-HCV miRNA-29 family members (23). Virus entry mechanisms and pathways have also been applied to study the exosome-mediated transfer of antiviral activity between cells. In HBV infection, macrophage-derived exosomes can use hepatitis A virus receptors to enter liver cells. Subsequently, exosomes utilize clathrin-mediated endocytosis and macrophage phagocytosis and then fuse with endosomes to effectively transmit the anti-HBV activity induced by IFN-α (66). Together, these studies suggest that exosomes have great potential as delivery vehicles for disease treatment. Exosomes can also be used for prognostic analyses. Circulating EV concentrations and sphingolipid carrier characteristics can be used not only for the diagnosis and differentiation of AH, decompensated alcoholic cirrhosis, and other end-stage liver diseases but also for the prediction of the 90-day survival time (101).

CONCLUSIONS AND PERSPECTIVES

Macrophage activation is an important force driving liver injury. Exosomes are important vesicles that are released by almost all cell types and play an important role in intercellular communication. Increasing evidence indicates that exosomes have outstanding functions, suggesting their potential use for future applications. In all liver diseases, studies on the effects and connections between macrophages and exosomes have concentrated on ALD, NAFLD, and HCC areas and have provided ideas for the non-invasive diagnosis and treatment of these diseases (**Table 1**). Generally, exosomes from damaged hepatocytes or tumors can promote the activation and differentiation of macrophages, thereby promoting inflammation. On the other hand, macrophage-derived exosomes also play a role in target hepatocytes (**Figure 3**). Nevertheless, the identification of novel specific biomarkers is required. In addition, it is

worth investigating macrophages and exosomes in other liver diseases.

AUTHOR CONTRIBUTIONS

MS and YS drafted the manuscript. LY and TY conceived the idea. XF and RM provided critical feedback. All authors read and approved the final version. All authors contributed to the article and approved the submitted version.

FUNDING

This manuscript was funded by the National Natural Science Foundation of China (No. 81770568 to LY), the 1.3.5 project for disciplines of excellence, West China Hospital, Sichuan University (No. ZYGD20012 to LY), and the 1.3.5 project for disciplines of excellence, West China Hospital, Sichuan University (No. ZYJC18008 to LY).

REFERENCES

1. Colombo M, Raposo G, Thery C. Biogenesis, secretion, and intercellular interactions of exosomes and other extracellular vesicles. *Annu Rev Cell Dev Biol.* (2014) 30:255–89. doi: 10.1146/annurev-cellbio-101512-122326
2. Thery C, Zitvogel L, Amigorena S. Exosomes: composition, biogenesis and function. *Nat Rev Immunol.* (2002) 2:569–79. doi: 10.1038/nri855
3. Andaloussi SEL, Mager I, Breakefield XO, Wood MJ. Extracellular vesicles: biology and emerging therapeutic opportunities. *Nat Rev Drug Discov.* (2013) 12:347–57. doi: 10.1038/nrd3978
4. Bang C, Thum T. Exosomes: new players in cell-cell communication. *Int J Biochem Cell Biol.* (2012) 44:2060–4. doi: 10.1016/j.biocel.2012.08.007
5. Vlassov AV, Magdaleno S, Setterquist R, Conrad R. Exosomes: current knowledge of their composition, biological functions, and diagnostic and therapeutic potentials. *Biochim Biophys Acta.* (2012) 1820:940–8. doi: 10.1016/j.bbagen.2012.03.017
6. Raposo G, Stoorvogel W. Extracellular vesicles: exosomes, microvesicles, and friends. *J Cell Biol.* (2013) 200:373–83. doi: 10.1083/jcb.201211138
7. Tkach M, Thery C. Communication by extracellular vesicles: where we are and where we need to go. *Cell.* (2016) 164:1226–32. doi: 10.1016/j.cell.2016.01.043
8. Jabbari N, Akbariazar E, Feqhhi M, Rahbarghazi R, Rezaie J. Breast cancer-derived exosomes: tumor progression and therapeutic agents. *J Cell Physiol.* (2020) 235:6345–56. doi: 10.1002/jcp.29668
9. Sato K, Meng F, Glaser S, Alpini G. Exosomes in liver pathology. *J Hepatol.* (2016) 65:213–21. doi: 10.1016/j.jhep.2016.03.004
10. Tacke F, Zimmermann HW. Macrophage heterogeneity in liver injury and fibrosis. *J Hepatol.* (2014) 60:1090–6. doi: 10.1016/j.jhep.2013.12.025
11. Wynn TA, Vannella KM. Macrophages in tissue repair, regeneration, and fibrosis. *Immunity.* (2016) 44:450–62. doi: 10.1016/j.immuni.2016.02.015
12. Lawrence T, Natoli G. Transcriptional regulation of macrophage polarization: enabling diversity with identity. *Nat Rev Immunol.* (2011) 11:750–61. doi: 10.1038/nri3088
13. Mantovani A, Sica A, Sozzani S, Allavena P, Vecchi A, Locati M. The chemokine system in diverse forms of macrophage activation and polarization. *Trends Immunol.* (2004) 25:677–86. doi: 10.1016/j.it.2004.09.015
14. Bala S, Csak T, Saha B, Zatsiorsky J, Kodys K, Catalano D, et al. The pro-inflammatory effects of miR-155 promote liver fibrosis and alcohol-induced steatohepatitis. *J Hepatol.* (2016) 64:1378–87. doi: 10.1016/j.jhep.2016.01.035
15. Kazankov K, Jorgensen SMD, Thomsen KL, Moller HJ, Vilstrup H, George J, et al. The role of macrophages in nonalcoholic fatty liver disease and nonalcoholic steatohepatitis. *Nat Rev Gastroenterol Hepatol.* (2019) 16:145–59. doi: 10.1038/s41575-018-0082-x
16. Weiskirchen R, Tacke F. Liver fibrosis: from pathogenesis to novel therapies. *Dig Dis.* (2016) 34:410–22. doi: 10.1159/000444556
17. Yin Z, Huang J, Ma T, Li D, Wu Z, Hou B, et al. Macrophages activating chemokine (C-X-C motif) ligand 8/miR-17 cluster modulate hepatocellular carcinoma cell growth and metastasis. *Am J Transl Res.* (2017) 9:2403–11.
18. Momen-Heravi F, Bala S, Kodys K, Szabo G. Exosomes derived from alcohol-treated hepatocytes horizontally transfer liver specific miRNA-122 and sensitize monocytes to LPS. *Sci Rep.* (2015) 5:9991. doi: 10.1038/srep09991
19. Li X, Liu R, Wang Y, Zhu W, Zhao D, Wang X, et al. Cholangiocyte-derived exosomal lncRNA H19 promotes macrophage activation and hepatic inflammation under cholestatic conditions. *Cells.* (2020) 9:190. doi: 10.3390/cells9010190
20. Cheng L, Liu J, Liu Q, Liu Y, Fan L, Wang F, et al. Exosomes from melatonin treated hepatocellularcarcinoma cells alter the immunosupression status through STAT3 pathway in macrophages. *Int J Biol Sci.* (2017) 13:723–34. doi: 10.7150/ijbs.19642
21. Zhao X, Sun L, Mu T, Yi J, Ma C, Xie H, et al. An HBV-encoded miRNA activates innate immunity to restrict HBV replication. *J Mol Cell Biol.* (2020) 12:263–76. doi: 10.1093/jmcb/mjz104
22. Kouwaki T, Fukushima Y, Daito T, Sanada T, Yamamoto N, Mifsud EJ, et al. Extracellular vesicles including exosomes regulate innate immune responses to hepatitis B virus infection. *Front Immunol.* (2016) 7:335. doi: 10.3389/fimmu.2016.00335
23. Zhou Y, Wang X, Sun L, Zhou L, Ma TC, Song L, et al. Toll-like receptor 3-activated macrophages confer anti-HCV activity to hepatocytes through exosomes. *FASEB J.* (2016) 30:4132–40. doi: 10.1096/fj.201600696R
24. Saha B, Kodys K, Adejumo A, Szabo G. Circulating and exosome-packaged hepatitis c single-stranded RNA induce monocyte differentiation via TLR7/8 to polarized macrophages and fibrocytes. *J Immunol.* (2017) 198:1974–84. doi: 10.4049/jimmunol.1600797
25. Babuta M, Furi I, Bala S, Bukong TN, Lowe P, Catalano D, et al. Dysregulated autophagy and lysosome function are linked to exosome production by micro-RNA 155 in alcoholic liver disease. *Hepatology.* (2019) 70:2123–41. doi: 10.1002/hep.30766
26. Saha B, Momen-Heravi F, Kodys K, Szabo G. MicroRNA cargo of extracellular vesicles from alcohol-exposed monocytes signals naive monocytes to differentiate into M2 macrophages. *J Biol Chem.* (2016) 291:149–59. doi: 10.1074/jbc.M115.694133
27. Verma VK, Li H, Wang R, Hirsova P, Mushref M, Liu Y, et al. Alcohol stimulates macrophage activation through caspase-dependent hepatocyte derived release of CD40L containing extracellular vesicles. *J Hepatol.* (2016) 64:651–60. doi: 10.1016/j.jhep.2015.11.020
28. Lee JH, Shim YR, Seo W, Kim MH, Choi WM, Kim HH, et al. Mitochondrial double-stranded RNA in exosome promotes interleukin-17 production through toll-like receptor 3 in alcoholic liver injury. *Hepatology.* (2019) 72:609–25. doi: 10.1002/hep.31041
29. Liu XL, Pan Q, Cao HX, Xin FZ, Zhao ZH, Yang RX, et al. Lipotoxic hepatocyte-derived exosomal miR-192-5p activates macrophages via Rictor/Akt/FoxO1 signaling in NAFLD. *Hepatology.* (2019) 72:454–69. doi: 10.1002/hep.31050
30. Hirsova P, Ibrahim SH, Krishnan A, Verma VK, Bronk SF, Werneburg NW, et al. Lipid-Induced signaling causes release of inflammatory extracellular vesicles from hepatocytes. *Gastroenterology.* (2016) 150:956–67. doi: 10.1053/j.gastro.2015.12.037
31. Guo Q, Furuta K, Lucien F, Gutierrez Sanchez LH, Hirsova P, Krishnan A, et al. Integrin beta1-enriched extracellular vesicles mediate monocyte adhesion and promote liver inflammation in murine NASH. *J Hepatol.* (2019) 71:1193–205. doi: 10.1016/j.jhep.2019.07.019
32. Zhao Z, Zhong L, Li P, He K, Qiu C, Zhao L, et al. Cholesterol impairs hepatocyte lysosomal function causing M1 polarization of macrophages via exosomal miR-122-5p. *Exp Cell Res.* (2020) 387:111738. doi: 10.1016/j.yexcr.2019.111738
33. Liu Y, Lou G, Li A, Zhang T, Qi J, Ye D, et al. AMSC-derived exosomes alleviate lipopolysaccharide/d-galactosamine-induced acute liver failure by miR-17-mediated reduction of TXNIP/NLRP3

inflammasome activation in macrophages. *EBioMedicine.* (2018) 36:140–50. doi: 10.1016/j.ebiom.2018.08.054
34. Li X, Lei Y, Wu M, Li N. Regulation of macrophage activation and polarization by HCC-derived exosomal lncRNA TUC339. *Int J Mol Sci.* (2018) 19:2958. doi: 10.3390/ijms19102958
35. Liu J, Fan L, Yu H, Zhang J, He Y, Feng D, et al. Endoplasmic reticulum stress causes liver cancer cells to release exosomal miR-23a-3p and up-regulate programmed death ligand 1 expression in macrophages. *Hepatology.* (2019) 70:241–58. doi: 10.1002/hep.30607
36. Zhang J, Shan WF, Jin TT, Wu GQ, Xiong XX, Jin HY, et al. Propofol exerts anti-hepatocellular carcinoma by microvesicle-mediated transfer of miR-142-3p from macrophage to cancer cells. *J Transl Med.* (2014) 12:279. doi: 10.1186/s12967-014-0279-x
37. Maas SLN, Breakefield XO, Weaver AM. Extracellular vesicles: unique intercellular delivery vehicles. *Trends Cell Biol.* (2017) 27:172–88. doi: 10.1016/j.tcb.2016.11.003
38. Zhang H, Freitas D, Kim HS, Fabijanic K, Li Z, Chen H, et al. Identification of distinct nanoparticles and subsets of extracellular vesicles by asymmetric flow field-flow fractionation. *Nat Cell Biol.* (2018) 20:332–43. doi: 10.1038/s41556-018-0040-4
39. Wu AY, Ueda K, Lai CP. Proteomic analysis of extracellular vesicles for cancer diagnostics. *Proteomics.* (2019) 19:e1800162. doi: 10.1002/pmic.201800162
40. Meldolesi J. Exosomes and ectosomes in intercellular communication. *Curr Biol.* (2018) 28:R435–44. doi: 10.1016/j.cub.2018.01.059
41. Ma L, Li Y, Peng J, Wu D, Zhao X, Cui Y, et al. Discovery of the migrasome, an organelle mediating release of cytoplasmic contents during cell migration. *Cell Res.* (2015) 25:24–38. doi: 10.1038/cr.2014.135
42. Crescitelli R, Lasser C, Szabo TG, Kittel A, Eldh M, Dianzani I, et al. Distinct RNA profiles in subpopulations of extracellular vesicles: apoptotic bodies, microvesicles and exosomes. *J Extracell Vesicles.* (2013) 2:20677. doi: 10.3402/jev.v2i0.20677
43. Meehan B, Rak J, Di Vizio D. Oncosomes - large and small: what are they, where they came from? *J Extracell Vesicles.* (2016) 5:33109. doi: 10.3402/jev.v5.33109
44. Minciacchi VR, Spinelli C, Reis-Sobreiro M, Cavallini L, You S, Zandian M, et al. MYC mediates large oncosome-induced fibroblast reprogramming in prostate cancer. *Cancer Res.* (2017) 77:2306–17. doi: 10.1158/0008-5472.CAN-16-2942
45. Zaborowski MP, Balaj L, Breakefield XO, Lai CP. Extracellular vesicles: composition, biological relevance, and methods of study. *Bioscience.* (2015) 65:783–97. doi: 10.1093/biosci/biv084
46. Genschmer KR, Russell DW, Lal C, Szul T, Bratcher PE, Noerager BD, et al. Activated PMN exosomes: pathogenic entities causing matrix destruction and disease in the lung. *Cell.* (2019) 176:113–26.e15. doi: 10.1016/j.cell.2018.12.002
47. Thery C, Witwer KW, Aikawa E, Alcaraz MJ, Anderson JD, Andriantsitohaina R, et al. Minimal information for studies of extracellular vesicles 2018. (MISEV2018): a position statement of the International Society for Extracellular Vesicles and update of the MISEV2014 guidelines. *J Extracell Vesicles.* (2018) 7:1535750. doi: 10.1080/20013078.2018.1461450
48. Rezaie J, Nejati V, Khaksar M, Oryan A, Aghamohamadzadeh N, Shariatzadeh MA, et al. Diabetic sera disrupted the normal exosome signaling pathway in human mesenchymal stem cells *in vitro*. *Cell Tissue Res.* (2018) 374:555–65. doi: 10.1007/s00441-018-2895-x
49. Rezaie J, Rahbarghazi R, Pezeshki M, Mazhar M, Yekani F, Khaksar M, et al. Cardioprotective role of extracellular vesicles: a highlight on exosome beneficial effects in cardiovascular diseases. *J Cell Physiol.* (2019) 234:21732–45. doi: 10.1002/jcp.28894
50. Lloret-Llinares M, Karadoulama E, Chen Y, Wojenski LA, Villafano GJ, Bornholdt J, et al. The RNA exosome contributes to gene expression regulation during stem cell differentiation. *Nucleic Acids Res.* (2018) 46:11502–13. doi: 10.1093/nar/gky817
51. Neviani P, Fabbri M. Exosomic microRNAs in the tumor microenvironment. *Front Med.* (2015) 2:47. doi: 10.3389/fmed.2015.00047
52. Dorayappan KDP, Gardner ML, Hisey CL, Zingarelli RA, Smith BQ, Lightfoot MDS, et al. A microfluidic chip enables isolation of exosomes and establishment of their protein profiles and associated signaling pathways in ovarian cancer. *Cancer Res.* (2019) 79:3503–13. doi: 10.1158/0008-5472.CAN-18-3538
53. Jabbari N, Karimipour M, Khaksar M, Akbariazar E, Heidarzadeh M, Mojarad B, et al. Tumor-derived extracellular vesicles: insights into bystander effects of exosomes after irradiation. *Lasers Med Sci.* (2020) 35:531–45. doi: 10.1007/s10103-019-02880-8
54. Skotland T, Sandvig K, Llorente A. Lipids in exosomes: current knowledge and the way forward. *Prog Lipid Res.* (2017) 66:30–41. doi: 10.1016/j.plipres.2017.03.001
55. Ying W, Riopel M, Bandyopadhyay G, Dong Y, Birmingham A, Seo JB, et al. Adipose tissue macrophage-derived exosomal miRNAs can modulate *in vivo* and *in vitro* insulin sensitivity. *Cell.* (2017) 171:372–84.e12. doi: 10.1016/j.cell.2017.08.035
56. Hoshino A, Costa-Silva B, Shen TL, Rodrigues G, Hashimoto A, Tesic Mark M, et al. Tumour exosome integrins determine organotropic metastasis. *Nature.* (2015) 527:329–35. doi: 10.1038/nature15756
57. Lan J, Sun L, Xu F, Liu L, Hu F, Song D, et al. M2 macrophage-derived exosomes promote cell migration and invasion in colon cancer. *Cancer Res.* (2019) 1:146–58. doi: 10.1158/0008-5472.CAN-18-0014
58. Jabbari N, Nawaz M, Rezaie J. Ionizing radiation increases the activity of exosomal secretory pathway in MCF-7 human breast cancer cells: a possible way to communicate resistance against radiotherapy. *Int J Mol Sci.* (2019) 20:3649. doi: 10.3390/ijms20153649
59. Eleftheriou D, Moraitis E, Hong Y, Turmaine M, Venturini C, Ganesan V, et al. Microparticle-mediated VZV propagation and endothelial activation: Mechanism of VZV vasculopathy. *Neurology.* (2020) 94:e474–80. doi: 10.1212/WNL.0000000000008885
60. Tian C, Gao L, Zimmerman MC, Zucker IH. Myocardial infarction-induced microRNA-enriched exosomes contribute to cardiac Nrf2 dysregulation in chronic heart failure. *Am J Physiol Heart Circ Physiol.* (2018) 314:H928–39. doi: 10.1152/ajpheart.00602.2017
61. Xu B, Zhang Y, Du XF, Li J, Zi HX, Bu JW, et al. Neurons secrete miR-132-containing exosomes to regulate brain vascular integrity. *Cell Res.* (2017) 27:882–97. doi: 10.1038/cr.2017.62
62. Yu Z, Shi M, Stewart T, Fernagut PO, Huang Y, Tian C, et al. Reduced oligodendrocyte exosome secretion in multiple system atrophy involves SNARE dysfunction. *Brain.* (2020) 143:1780–97. doi: 10.1093/brain/awaa110
63. Li S, Wu Y, Ding F, Yang J, Li J, Gao X, et al. Engineering macrophage-derived exosomes for targeted chemotherapy of triple-negative breast cancer. *Nanoscale.* (2020) 12:10854–62. doi: 10.1039/D0NR00523A
64. Elsharkasy OM, Nordin JZ, Hagey DW, de Jong OG, Schiffelers RM, Andaloussi SE, et al. Extracellular vesicles as drug delivery systems: why and how? *Adv Drug Deliv Rev.* (2020). doi: 10.1016/j.addr.2020.04.004. [Epub ahead of print].
65. Messina JP, Humphreys I, Flaxman A, Brown A, Cooke GS, Pybus OG, et al. Global distribution and prevalence of hepatitis C virus genotypes. *Hepatology.* (2015) 2:77–87. doi: 10.1002/hep.27259
66. Yao Z, Qiao Y, Li X, Chen J, Ding J, Bai L, et al. Exosomes exploit the virus entry machinery and pathway to transmit alpha interferon-induced antiviral activity. *J Virol.* (2018) 92:e01578-18. doi: 10.1128/JVI.01578-18
67. Cai C, Koch B, Morikawa K, Suda G, Sakamoto N, Rueschenbaum S, et al. Macrophage-derived extracellular vesicles induce long-lasting immunity against hepatitis c virus which is blunted by polyunsaturated fatty acids. *Front Immunol.* (2018) 9:723. doi: 10.3389/fimmu.2018.00723
68. Szabo G, Bala S. Alcoholic liver disease and the gut-liver axis. *World J Gastroenterol.* (2010) 16:1321–9. doi: 10.3748/wjg.v16.i11.1321
69. Nagy LE. The role of innate immunity in alcoholic liver disease. *Alcohol Res.* (2015) 37:237–50.
70. O'Shea RS, Dasarathy S, McCullough AJ, Practice Guideline Committee of the American Association for the Study of Liver D, Practice Parameters Committee of the American College of G. Alcoholic liver disease. *Hepatology.* (2010) 1:307–28. doi: 10.1002/hep.23258
71. European Association for the Study of the Liver. Electronic address EEE, European Association for the Study of the L. EASL clinical practice guidelines: management of alcohol-related liver disease. *J Hepatol.* (2018) 57:154–81. doi: 10.1016/j.jhep.2018.03.018
72. Miranda AM, Lasiecka ZM, Xu Y, Neufeld J, Shahriar S, Simoes S, et al. Neuronal lysosomal dysfunction releases exosomes harboring APP

C-terminal fragments and unique lipid signatures. *Nat Commun.* (2018) 9:291. doi: 10.1038/s41467-017-02533-w
73. Saha B, Momen-Heravi F, Furi I, Kodys K, Catalano D, Gangopadhyay A, et al. Extracellular vesicles from mice with alcoholic liver disease carry a distinct protein cargo and induce macrophage activation through heat shock protein 90. *Hepatology.* (2018) 67:1986–2000. doi: 10.1002/hep.29732
74. Momen-Heravi F, Saha B, Kodys K, Catalano D, Satishchandran A, Szabo G. Increased number of circulating exosomes and their microRNA cargos are potential novel biomarkers in alcoholic hepatitis. *J Transl Med.* (2015) 13:261. doi: 10.1186/s12967-015-0623-9
75. Cai Y, Xu MJ, Koritzinsky EH, Zhou Z, Wang W, Cao H, et al. Mitochondrial DNA-enriched microparticles promote acute-on-chronic alcoholic neutrophilia and hepatotoxicity. *JCI Insight.* (2017) 2:e92634. doi: 10.1172/jci.insight.92634
76. European Association for the Study of the L, European Association for the Study of D, European Association for the Study of O. EASL-EASD-EASO Clinical Practice Guidelines for the management of non-alcoholic fatty liver disease. *J Hepatol.* (2016) 60:1388–402. doi: 10.1007/s00125-016-3902-y
77. Barrera F, George J. The role of diet and nutritional intervention for the management of patients with NAFLD. *Clin Liver Dis.* (2014) 18:91–112. doi: 10.1016/j.cld.2013.09.009
78. Chiu S, Sievenpiper JL, de Souza RJ, Cozma AI, Mirrahimi A, Carleton AJ, et al. Effect of fructose on markers of non-alcoholic fatty liver disease (NAFLD): a systematic review and meta-analysis of controlled feeding trials. *Eur J Clin Nutr.* (2014) 68:416–23. doi: 10.1038/ejcn.2014.8
79. Gerber L, Otgonsuren M, Mishra A, Escheik C, Birerdinc A, Stepanova M, et al. Non-alcoholic fatty liver disease (NAFLD) is associated with low level of physical activity: a population-based study. *Aliment Pharmacol Ther.* (2012) 36:772–81. doi: 10.1111/apt.12038
80. Hirsova P, Gores GJ. Death receptor-mediated cell death and proinflammatory signaling in nonalcoholic steatohepatitis. *Cell Mol Gastroenterol Hepatol.* (2015) 1:17–27. doi: 10.1016/j.jcmgh.2014.11.005
81. Rong B, Feng R, Liu C, Wu Q, Sun C. Reduced delivery of epididymal adipocyte-derived exosomal resistin is essential for melatonin ameliorating hepatic steatosis in mice. *J Pineal Res.* (2019) 66:e12561. doi: 10.1111/jpi.12561
82. Antonyak MA, Lukey MJ, Cerione RA. Lipid-filled vesicles modulate macrophages. *Science.* (2019) 363:931–2. doi: 10.1126/science.aaw6765
83. Flaherty SE III, Grijalva A, Xu X, Ables E, Nomani A, Ferrante AW Jr. A lipase-independent pathway of lipid release and immune modulation by adipocytes. *Science.* (2019) 363:989–93. doi: 10.1126/science.aaw2586
84. Kornek M, Lynch M, Mehta SH, Lai M, Exley M, Afdhal NH, et al. Circulating microparticles as disease-specific biomarkers of severity of inflammation in patients with hepatitis C or nonalcoholic steatohepatitis. *Gastroenterology.* (2012) 143:448–58. doi: 10.1053/j.gastro.2012.04.031
85. Kim SH, Kim G, Han DH, Lee M, Kim I, Kim B, et al. Ezetimibe ameliorates steatohepatitis via AMP activated protein kinase-TFEB-mediated activation of autophagy and NLRP3 inflammasome inhibition. *Autophagy.* (2017) 13:1767–81. doi: 10.1080/15548627.2017.1356977
86. Patel P, Okoronkwo N, Pyrsopoulos NT. Future approaches and therapeutic modalities for acute liver failure. *Clin Liver Dis.* (2018) 22:419–27. doi: 10.1016/j.cld.2018.01.011
87. Volarevic V, Nurkovic J, Arsenijevic N, Stojkovic M. Concise review: therapeutic potential of mesenchymal stem cells for the treatment of acute liver failure and cirrhosis. *Stem Cells.* (2014) 32:2818–23. doi: 10.1002/stem.1818
88. Yan Y, Jiang W, Tan Y, Zou S, Zhang H, Mao F, et al. hucMSC exosome-derived GPX1 is required for the recovery of hepatic oxidant injury. *Mol Ther.* (2017) 25:465–79. doi: 10.1016/j.ymthe.2016.11.019
89. Lou G, Chen Z, Zheng M, Liu Y. Mesenchymal stem cell-derived exosomes as a new therapeutic strategy for liver diseases. *Exp Mol Med.* (2017) 6:e346. doi: 10.1038/emm.2017.63
90. Global Burden of Disease Liver Cancer C, Akinyemiju T, Abera S, Ahmed M, Alam N, Alemayohu MA, et al. The burden of primary liver cancer and underlying etiologies from 1990 to 2015 at the global, regional, and national level: results from the global burden of disease study 2015. *JAMA Oncol.* (2017) 12:1683–91. doi: 10.1001/jamaoncol.2017.3055
91. Bray F, Ferlay J, Soerjomataram I, Siegel RL, Torre LA, Jemal A. Global cancer statistics 2018: GLOBOCAN estimates of incidence and mortality worldwide for 36 cancers in 185 countries. *CA Cancer J Clin.* (2018) 68:394–424. doi: 10.3322/caac.21492
92. European Association for the Study of the Liver. Electronic address EEE, European Association for the Study of the L. EASL clinical practice guidelines: management of hepatocellular carcinoma. *J Hepatol.* (2018) 69:182–236. doi: 10.1016/j.jhep.2018.03.019
93. Lok AS, Sterling RK, Everhart JE, Wright EC, Hoefs JC, Di Bisceglie AM, et al. Des-gamma-carboxy prothrombin and alpha-fetoprotein as biomarkers for the early detection of hepatocellular carcinoma. *Gastroenterology.* (2010) 138:493–502. doi: 10.1053/j.gastro.2009.10.031
94. Marrero JA, Feng Z, Wang Y, Nguyen MH, Befeler AS, Roberts LR, et al. Alpha-fetoprotein, des-gamma carboxyprothrombin, and lectin-bound alpha-fetoprotein in early hepatocellular carcinoma. *Gastroenterology.* (2009) 137:110–8. doi: 10.1053/j.gastro.2009.04.005
95. Lee WC, Lee CF, Cheng CH, Wu TJ, Chou HS, Wu TH, et al. Outcomes of liver resection for hepatocellular carcinoma in liver transplantation era. *Eur J Surg Oncol.* (2015) 14:1144–52. doi: 10.1016/j.ejso.2015.05.024
96. Hui L, Chen Y. Tumor microenvironment: sanctuary of the devil. *Cancer Lett.* (2015) 368:7–13. doi: 10.1016/j.canlet.2015.07.039
97. Zhou Y, Ren H, Dai B, Li J, Shang L, Huang J, et al. Hepatocellular carcinoma-derived exosomal miRNA-21 contributes to tumor progression by converting hepatocyte stellate cells to cancer-associated fibroblasts. *J Exp Clin Cancer Res.* (2018) 37:324. doi: 10.1186/s13046-018-0965-2
98. Sohn W, Kim J, Kang SH, Yang SR, Cho JY, Cho HC, et al. Serum exosomal microRNAs as novel biomarkers for hepatocellular carcinoma. *Exp Mol Med.* (2015) 47:e184. doi: 10.1038/emm.2015.68
99. Wu X, Wu S, Tong L, Luan T, Lin L, Lu S, et al. miR-122 affects the viability and apoptosis of hepatocellular carcinoma cells. *Scand J Gastroenterol.* (2009) 44:1332–9. doi: 10.3109/00365520903215305
100. Costa-Silva B, Aiello NM, Ocean AJ, Singh S, Zhang H, Thakur BK, et al. Pancreatic cancer exosomes initiate pre-metastatic niche formation in the liver. *Nat Cell Biol.* (2015) 17:816–26. doi: 10.1038/ncb3169
101. Sehrawat TS, Arab JP, Liu M, Amrollahi P, Wan M, Fan J, et al. Circulating extracellular vesicles carrying sphingolipid cargo for the diagnosis and dynamic risk profiling of alcoholic hepatitis. *Hepatology.* (2020) doi: 10.1002/hep.31256. [Epub ahead of print].

Conflict of Interest: The authors declare that the research was conducted in the absence of any commercial or financial relationships that could be construed as a potential conflict of interest.

frontiers in Medicine

ORIGINAL RESEARCH
published: 20 October 2020
doi: 10.3389/fmed.2020.584342

Multicenter Analysis of Liver Injury Patterns and Mortality in COVID-19

Huikuan Chu[1†], Tao Bai[1†], Liuying Chen[1], Lilin Hu[1], Li Xiao[1], Lin Yao[1], Rui Zhu[2], Xiaohui Niu[3], Zhonglin Li[1], Lei Zhang[1], Chaoqun Han[1], Shuangning Song[1], Qi He[1], Ying Zhao[4], Qingjing Zhu[4], Hua Chen[5], Bernd Schnabl[6], Ling Yang[1] and Xiaohua Hou[1]**

[1] Division of Gastroenterology, Union Hospital, Tongji Medical College, Huazhong University of Science and Technology, Wuhan, China, [2] Department of Integrated Chinese and Western Medicine, Union Hospital, Tongji Medical College, Huazhong University of Science and Technology, Wuhan, China, [3] College of Informatics, Huazhong Agricultural University, Wuhan, China, [4] Liver and Infectious Diseases Department, Wuhan Jinyintan Hospital, Wuhan, China, [5] Tuberculosis and Respiratory Department, Wuhan Jinyintan Hospital, Wuhan, China, [6] Department of Medicine, University of California, San Diego, La Jolla, CA, United States

Background and Aim: Liver test abnormalities are common in COVID-19 patients. The aim of our study was to determine risk factors for different liver injury patterns and to evaluate the relationship between liver injury patterns and prognosis in patients with COVID-19.

Methods: We retrospectively analyzed patients admitted between January 1st to March 10th, with laboratory-confirmed COVID-19 and followed them up to April 20th, 2020. Information of clinical features of patients was collected for analysis.

Results: As a result, a total of 838 hospitalized patients with confirmed COVID-19, including 48.8% (409/838) patients with normal liver function and 51.2% (429/838) patients with liver injury were analyzed. Abnormal liver function tests are associated with organ injuries, hypoxia, inflammation, and the use of antiviral drugs. Hepatocellular injury pattern was associated with hypoxia. The mortality of the hepatocellular injury pattern, cholestatic pattern and mixed pattern were 25, 28.2, and 22.3%, respectively, while the death rate was only 6.1% in the patients without liver injury. Multivariate analyses showed that liver injury with cholestatic pattern and mixed pattern were associated with increased mortality risk.

Conclusions: Our study confirmed that hepatocellular injury pattern that may be induced by hypoxia was not risk factor for mortality in SARS-COV-2 infection, while liver injury with mixed pattern and cholestatic pattern that might be induced by SARS-CoV-2 directly might be potential risk factors for increased mortality in COVID-19 patients.

Keywords: liver impairment, hepatocellular pattern, cholestatic pattern, mixed pattern, prognosis

OPEN ACCESS

Edited by:
Liang Wen,
Zhejiang University, China

Reviewed by:
Ming-Hua Zheng,
First Affiliated Hospital of Wenzhou Medical University, China
Hiroshi Nakase,
Sapporo Medical University, Japan

***Correspondence:**
Ling Yang
hepayang@163.com
Xiaohua Hou
houxh@hust.edu.cn

[†]These authors have contributed equally to this work

Specialty section:
This article was submitted to Gastroenterology, a section of the journal Frontiers in Medicine

Received: *17 July 2020*
Accepted: *11 September 2020*
Published: *20 October 2020*

Citation:
Chu H, Bai T, Chen L, Hu L, Xiao L, Yao L, Zhu R, Niu X, Li Z, Zhang L, Han C, Song S, He Q, Zhao Y, Zhu Q, Chen H, Schnabl B, Yang L and Hou X (2020) Multicenter Analysis of Liver Injury Patterns and Mortality in COVID-19. Front. Med. 7:584342. doi: 10.3389/fmed.2020.584342

INTRODUCTION

The severe acute respiratory syndrome coronavirus 2 (SARS-Cov-2) disease, which is also called Corona Virus Disease 2019 (COVID-19), has been considered as a public health emergency of international concern by World Health Organization (WHO). Currently, SARS-CoV-2 has spread to over 200 countries and areas with 11, 327, 790 confirmed cases, including 532, 340 deaths globally until July 6 (1). Although COVID-19 mainly affects the lower

respiratory tract and manifests as pneumonia in humans, a subset of COVID-19 patients present with different degrees of liver injury (2–4).

On the basis of previous reports from China, 15–26% of COVID-19 patients develop severe pneumonia with increased mortality (5). Organ dysfunction including acute kidney injury and liver injury is common in patients with severe pneumonia (5–8). 16–53% of COVID-19 patients had liver injury with abnormal levels of alanine aminotransferase (ALT) and/or aspartate aminotransferase (AST) accompanied by slightly elevated bilirubin levels during disease progression (2–4). The incidence of liver injury in COVID-19 patients with severe disease (62%) was significantly higher than that in patients with mild disease (25%) (4, 9). In addition, hepatic steatosis and liver injury were also confirmed by liver biopsy from a deceased patient infected with COVID-19 (10), and 78% of deceased COVID-19 patients had liver injury (11). However, whether liver injury is related with the progression of COVID-19 remains controversial (12–14). Besides, liver injury with hepatocyte pattern or mixed pattern had significantly higher risks of developing severe pneumonia in a single-center study of 148 patients (13), while the risk factors for different liver injury patterns remain unclear and a large-scale, multicenter study on the detailed relationships between different liver injury patterns and progression of COVID-19 was absent. In this study, we analyzed data from 838 hospitalized COVID-19 patients in multiple centers, explored the risk factors of liver injury among COVID-19 patients and evaluated the relationship between different patterns of liver injury and the progression of COVID-19. We found that liver injury was closely related with organ injuries, hypoxia, inflammation and the utilization of antiviral drugs, hepatocellular injury pattern that was associated with hypoxia was not risk factor for increased mortality, while liver injury with cholestatic pattern and mixed pattern that may be induced by SARS-CoV-2 directly increased mortality risk for COVID-19 patients.

METHODS

Study Design and Participants

This study was conducted in accordance with the principles of the Declaration of Helsinki and approved by the Institutional Ethics Board of Union Hospital, Tongji Medical College, Huazhong University of Science and Technology, and Jinyintan Hospital in China. We obtained the clinical and laboratory data at admission of confirmed COVID-19 patients from two centers including Union Hospital, Tongji Medical College, Huazhong University of Science and Technology, and Jinyintan Hospital that were designated hospitals in Wuhan to manage patients with COVID-19. We retrospectively analyzed patients admitted between January 1st to March 10th, 2020, and followed them up to April 20th, 2020, with laboratory-confirmed COVID-19 based on real-time reverse-transcriptase polymerase-chain-reaction (RT-PCR) assay for nasal and pharyngeal swab specimens (9). The inclusion criteria were: 1. Patients confirmed with COVID-19; 2. Adult patients aged >18 years; 3. Patients had definite clinical outcome (cured or died) before April 20th. Exclusion criteria were: 1. Patients had pre-existing liver disease; 2. Patients aged <18 years. All patients with COVID-19 enrolled in this study were diagnosed according to The World Health Organization Interim Guidance.

Data Collection

The medical records of patients were collected and analyzed by the search team from Union Hospital, Tongji Medical College, Huazhong University of Science and Technology, and Jinyintan Hospital. The clinical symptoms on admission, vital signs, and the pre-existing comorbidities of the patients were obtained from the electronic medical records. The results of the laboratory and imaging examinations on admission were obtained from the electronic system of laboratory and imaging examination. Diagnoses of acute kidney injuries and cardiac injuries were defined according to the Berlin Definition, improving global outcome definition and elevated cardiac biomarker, respectively (10, 15, 16). The degree of severity of COVID-19 (severe vs. non-severe) was defined using the American Thoracic Society guidelines for community-acquired pneumonia (17). For the diagnosis of three patterns of liver injury, initially ALT activity [patients ALT/upper limit of normal (ULN) of ALT] and alkaline phosphatase (ALP) activity (patients ALP/ULN of ALP) is calculated. Then ALT/ALP ratio (R) is determined. Hepatocellular pattern: If ALT alone is elevated ≥5-fold above ULN or R ≥5. Cholestatic pattern: ALP alone is elevated ≥2-fold above ULN or R ≤2. Mixed pattern: R >2 to <5 (18, 19).

Statistical Analysis

Categorical variables were presented as numbers and percentages. Chi-square tests with Bonferoni corrections for intragroup comparisons and Fisher's exact tests were used for categorical variables. Continuous values were expressed as means (standard deviations), and were calculated using the Student's *t*-test or one-way ANOVA for parametric data. Continuous values were expressed as median [interquartile range (IQR)], and were calculated using the Mann–Whitney U or Kruskal-Wallis H test with Bonferoni corrections for intragroup comparisons for non-parametric data. The correlation of hypoxia/inflammation and abnormal liver function test was examined using Spearman Rho's (ρ) correlation. To identify the risk factors for poor outcomes, univariate and multivariate Cox regression analyses were performed and reported as hazard ratios (HRs) and 95% confidence intervals (95% CIs). All statistical analyses were performed using SPSS (Statistical Package for the Social Sciences) (version 13.0, IBM Corp,

Abbreviations: ACE2, angiotensin converting enzyme II; ALP, alkaline phosphatase; ALT, alanine aminotransferase; AST, aspartate aminotransferase; Cis, confidence intervals; COVID-19, Corona Virus Disease 2019; CRP, C-reactive protein; GGT, gamma glutamyltransferase; HRs, hazard ratios; IL-6, Interleukin 6; IQR, interquartile range; ORs, odds ratios; PCT, procalcitonin; R, ratio; RT-PCR, real-time reverse-transcriptase polymerase-chain-reaction; SARS-Cov-2, severe acute respiratory syndrome coronavirus 2; SIRS, systemic inflammatory response syndrome; TNF-α, tumor necrosis factor-α; WHO, World Health Organization; ULN, upper limit of normal.

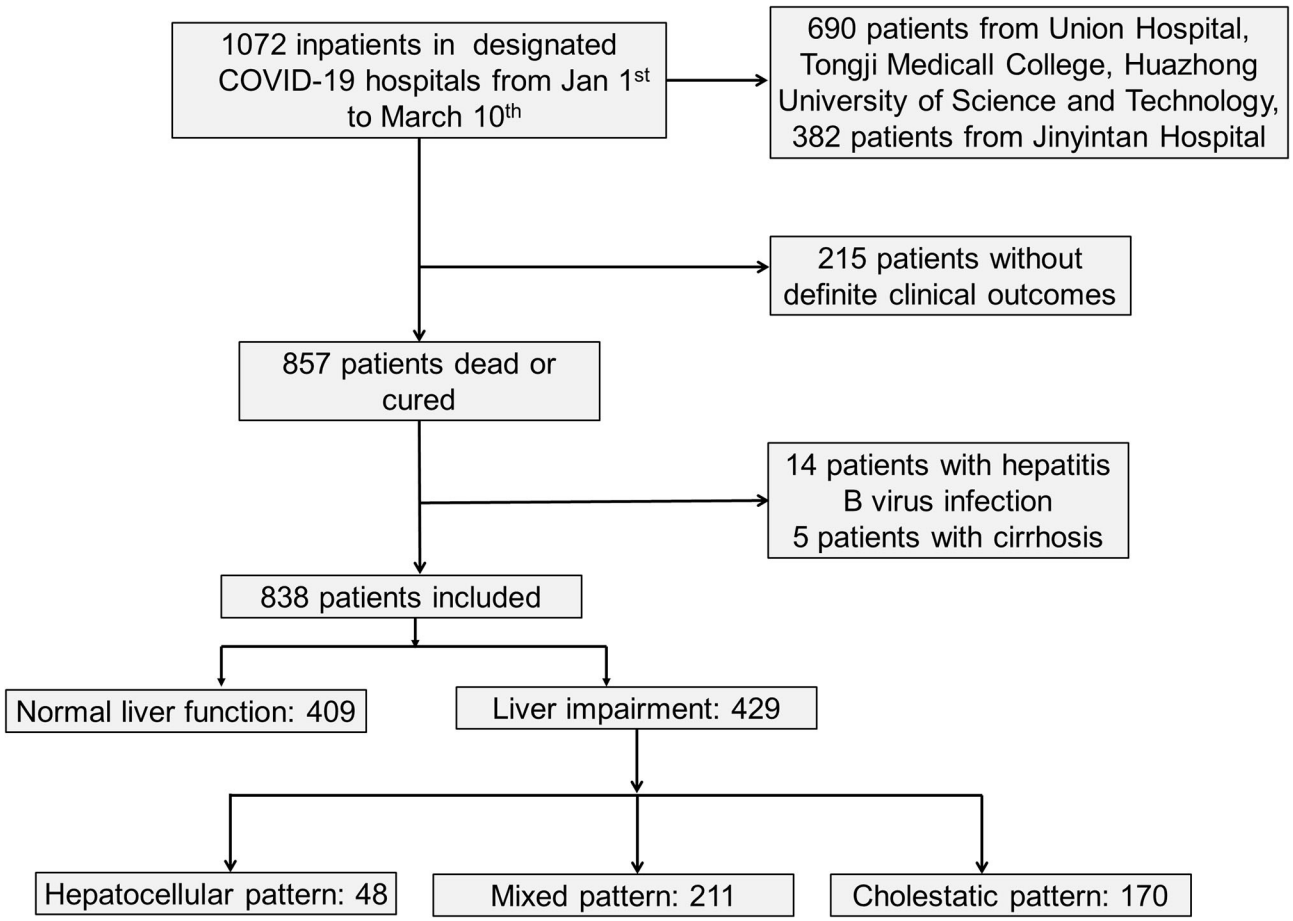

FIGURE 1 | Selection diagram of included patients.

Armonk, NY, USA). A significance level of $P \leq 0.05$ was used for all models (two-sided).

RESULTS

Clinical Characteristics of Patients

As shown in **Figure 1** and **Table 1**, a total of 838 hospitalized patients with confirmed COVID-19, including 48.8% (409/838) patients with normal liver function and 51.2% (429/838) patients with liver injury were analyzed. A total of 65.3% (280/429) male patients had liver injury, while in female patients, this proportion was significantly lower. The average age for patients with liver injury was 61, which is older than that in patients with normal liver function. In addition, more patients with liver injury had severe COVID-19. These results indicated that male and older patients and patients with more severe disease were more susceptible to liver injury.

Among them, 31.8% (267/838) had hypertension, 15.3% (128/838) had diabetes, and 7.8% (65/838) had coronary heart diseases (**Table 1**). A higher proportion of COVID-19 patients with liver injury had pre-existing hypertension, coronary heart diseases and malignant tumor, while there was no difference in pre-existing diabetes or chronic renal diseases between the subgroups with normal liver function and liver injury (**Table 1**).

Liver Biochemical Abnormalities Were Related With Organ Injuries

We evaluated the relationship between liver biochemical abnormalities and other laboratory results in COVID-19 patients. Patients with liver biochemical abnormalities showed more severe lymphocytopenia with lower counts of lymphocytes, more inflammation as indicated by elevated level of serum white blood cells, C-reactive protein (CRP) and procalcitonin (PCT), higher level of D-dimers, kidney injury as indicated by elevated level of serum creatinine, and higher level of serum ferritin. Importantly, patients with liver biochemical abnormalities had a higher incidence of cardiac injury, kidney injury, and systemic inflammatory response syndrome (SIRS) (**Table 1**). These results indicated that liver biochemical abnormalities were closely associated with cardiac injury, kidney injury and systemic inflammatory response that play important roles in COVID-19 patients.

TABLE 1 | Clinical and laboratory characteristics of patients with COVID-19.

Variables	Normal liver function	Liver injury	*P*-values
	n (%) or median (IQR)	n (%) or median (IQR)	
Sex			***
Male	184 (45.0)	280 (65.3)	
Female	225 (55.0)	149 (34.7)	
Age (years)	56 (43–66)	61 (49–69)	***
Severe	45 (11.0)	141 (32.9)	***
Hypertension	105 (25.7)	162 (37.8)	***
Diabetes	57 (13.9)	71 (16.6)	0.293
Coronary heart disease	24 (5.9)	41 (9.6)	*
Chronic kidney disease	7 (1.7)	12 (2.8)	0.291
Malignant tumor	8 (2.0)	20 (4.7)	*
Blood oxygen saturation (%)	97 (95–98)	95 (91–98)	***
White blood cell (10^9/L)	5.4 (4.1–6.8)	6.5 (4.8–9.0)	***
Lymphocyte (10^9/L)	1.2 (0.8–1.6)	0.9 (0.6–1.4)	***
Neutrophils (10^9/L)	3.6 (2.6–4.9)	5.1 (3.4–7.6)	***
Hemoglobin	125 (114–136)	130 (119–140)	***
Platelets (10^9/L)	204 (160–268)	205 (148–280)	0.806
Liver function test			
Total bilirubin (μmol/L)	9.6 (7.0–11.9)	13.2 (9.6–20.0)	***
Alanine aminotransferase (U/L)	19 (14–26)	49 (32–71)	***
Aspartate aminotransferase (U/L)	23 (18–29)	44 (31–59)	***
Alkaline phosphatase (U/L)	58 (47–70)	69 (52–95)	***
Gamma glutamyltransferase (U/L)	22 (15–31)	49 (26–93)	***
Albumin (g/L)	34.4 (30.0–38.5)	30.8 (27.1–35.2)	***
Creatinine (μmol/L)	65.0 (54.0–77.0)	72.7 (60.7–88.5)	***
Prothrombin time (s)	12.9 (11.8–13.7)	13.1 (12.0–14.3)	**
Activated partial thromboplastin time (s)	36.6 (34.0–38.8)	36.5 (32.6–40.2)	0.780
D-dimer (mg/L)	0.43 (0.23–0.98)	0.80 (0.41–3.06)	***
International normalized ratio	0.98 (0.93–1.06)	1.00 (0.94–1.09)	**
C-reactive protein (mg/L)	10.6 (2.9–41.8)	41.7 (9.1–90.5)	***
Procalcitonin (ug/L)	0.05 (0.04–0.09)	0.09 (0.05–0.23)	***
Ferritin (ug/L)	281.3 (129.0–567.4)	651.2 (329.0–1390.4)	***
Troponin I (μg/L)	3.2 (1.4–7.5)	5.4 (2.3–20.1)	***
Creatine Kinase (U/L)	67 (46–115)	99 (53–228)	***
Cardiac injury	18 (4.4)	77 (17.9)	***
Kidney injury	8 (2.0)	20 (4.7)	*
Systemic inflammatory response syndrome	79 (19.3)	114 (26.6)	*

*$P < 0.05$, **$P < 0.01$, ***$P < 0.001$.ULN, upper limit of normal; IQR, interquartile range.

Liver Biochemical Abnormalities Were Closely Associated With Hypoxia/Inflammation

Hypoxia and inflammatory cytokine storm are considered as risk factor for liver biochemical abnormalities in patients with COVID-19 (20). Therefore, we analyzed the relationship between liver biochemical abnormalities and hypoxia or inflammatory cytokines. As shown in **Table 1**, patients with liver injury had much lower blood oxygen saturation. Correlation analysis showed that blood oxygen saturation was negatively related with ALT, AST, TBIL, ALP, and GGT indicating that hypoxia might contribute to liver injury (**Table 2**).

To determine which inflammatory cytokine is associated with liver injury, we measured serum level of Interleukin (IL)-2, IL-4, IL-6, IL-8, IL-10, and tumor necrosis factor-α (TNF-α) in patients with normal liver function and with liver injury. As shown in **Supplementary Table 1**, serum IL-6 and TNF-α were significantly increased in the liver injury group. IL-6 was positively correlated with the increased AST, TBIL, and ALP. IL-8 was positively correlated with increased AST, and TNF-α was positively correlated with increased ALT, AST, and GGT

TABLE 2 | Correlation between hypoxia/inflammation and liver biochemical abnormalities in COVID-19.

		ALT	AST	TBIL	ALP	GGT
Blood oxygen saturation (%)	rho	−0.229	−0.375	−0.173	−0.136	−0.226
	P-value	***	***	***	***	***
IL-2	rho	−0.299	−0.237	0.134	−0.328	−0.109
	P-value	0.177	0.288	0.551	0.136	0.628
IL-4	rho	−0.278	−0.200	0.194	−0.071	−0.026
	P-value	0.211	0.373	0.387	0.755	0.906
IL-6	rho	0.115	0.223	0.289	0.182	0.094
	P-value	0.052	***	***	**	0.114
IL-8	rho	0.136	0.363	0.103	0.129	0.104
	P-value	0.277	**	0.412	0.304	0.405
IL-10	rho	−0.017	0.146	−0.131	−0.053	0.055
	P-value	0.876	0.176	0.222	0.622	0.609
TNF-alpha	rho	0.216	0.307	−0.006	0.160	0.246
	P-value	0.043	**	0.958	0.136	*

*Data are given as Spearman's rho correlation coefficients and P-value. *P < 0.05, **P < 0.01, ***P < 0.001.*
ALP, alkaline phosphatase; ALT, alanine aminotransferase; AST, aspartate aminotransferase; GGT, gamma glutamyltransferase; IL-2, Interleukin 2; TBIL, Total bilirubin.

(**Table 2**). These results indicate that inflammatory cytokines might contribute to liver injury in patients with COVID-19.

Lopinavir/Litonavir and Ribavirin Increased the Risk of Liver Biochemical Abnormalities

Antiviral drugs recommended to treat COVID-19 include umifenovir (arbidol hydrochloride), lopinavir/litonavir, ribavirin and interferon, which are metabolized in liver and can induce hepatotoxicity. We tested an association of antiviral drug use and liver injury in COVID-19 patients. As shown in **Table 3**, the level of ALT, AST, ALP, GGT, and TBil showed no significant difference between patients with and without umifenovir treatment. Patients treated with lopinavir/litonavir had higher levels of AST and GGT (**Table 3**). In addition, use of ribavirin slightly increased the level of ALP (**Table 3**). These results indicate that there is an association between the use of lopinavir /litonavir and ribavirin as the antiviral drugs and increased liver injury in COVID-19 patients.

Hepatocellular Injury Pattern Was Closely Related With Hypoxia

To further understand the characteristic of liver injury in patients with COVID-19, we classified the liver biochemical abnormalities as hepatocellular pattern, cholestatic pattern and mixed pattern according to the ALT/ALP ratio. Most patients (49.2%) manifested with a mixed liver injury pattern (211/429), and 39.6% of patients presented with cholestatic pattern (170/429). Hepatocellular pattern only accounted for 11.2% of patients (48/429). There was no difference between these three liver injury patterns in terms of gender, age, severity of COVID-19 and pre-existing diseases (**Supplementary Table 2**).

We further evaluated the relationship between different liver injury patterns and laboratory parameters (**Supplementary Table 2**). Patients with a hepatocellular injury pattern had lower blood oxygen saturation, higher ferritin level and increased kidney injury (**Supplementary Table 2**). These results indicated that hypoxia might play a critical role in hepatocytes death in COVID-19 patients.

The Association Between Liver Injury and COVID-19 Severity

We finally evaluated the relationship between different patterns of liver injury and COVID-19 outcome (**Table 4**). It was worth noting that 47.9, 29.4, and 32.2% of COVID-19 patients with hepatocellular pattern, cholestatic pattern and mixed pattern, respectively, were severe cases compared with 11% of patients with normal liver function (**Table 4**). The death rates of the COVID-19 patients with hepatocellular pattern, cholestatic pattern, and mixed pattern were 25, 28.2, and 22.3%, respectively, compared with 6.1% of patients with normal liver function (**Table 4**).

Multivariate analyses showed that the liver injury was associated with increased mortality risk in patients with COVID-19, with an adjusted hazard ratio of 2.65 (1.22–5.76) compared with normal liver function (**Table 5**). In addition, other factors such as platelet count and coagulation factors that represent the state of liver's ability to function were also associated with increased mortality risk in patients with COVID-19 (**Supplementary Tables 3**, **4**). The levels of platelet count decreased in deceased patients with COVID-19, while prothrombin time, D-dimer and international normalized ratio increased in deceased patients with COVID-19 (**Supplementary Table 3**). Further analysis showed that liver injury with cholestatic pattern and mixed pattern were associated with increased mortality risks in patients with COVID-19 (**Table 5**). These results indicate that liver injury with cholestatic pattern and mixed pattern are associated with worse prognosis in patients with COVID-19.

TABLE 3 | The association of anti-viral treatment and abnormal liver function test in COVID-19.

		ALT (U/L)	AST (U/L)	TBIL (μmol/L)	ALP (U/L)	GGT (U/L)	
Umifenovir	No	34 (20–59)	26 (18–75)	10.6 (8.6–13.6)	54 (47–89)	34 (19–103)	
	Yes	34 (20–54)	31 (23–46)	10.7 (8.0–14.3)	53 (43–71)	29 (19–54)	
	P-value	0.670	0.826	0.857	0.174	0.417	
Lopinavir /litonavir	No	33 (20–52)	29 (22–45)	10.7 (8.1–14.0)	53 (43–69)	28 (19–52)	
	Yes	41 (23–68)	39 (29–69)	9.8 (7.6–15.2)	52 (42–73)	45 (24–79)	
	P-value	0.060	**	0.744	0.893	**	
Ribavirin	No	34 (21–56)	32 (23–47)	10.6 (8.0–14.0)	52 (42–69)	29 (19–54)	
	Yes	34 (20–64)	26 (20–46)	11.6 (8.0–15.3)	56 (49–87)	41 (22–78)	
	P-value	0.994	0.288	0.526	*	0.186	
Interferon	No	34 (21–57)	32 (23–47)	10.8 (8.1–14.6)	54 (43–71)	30 (20–56)	
	Yes	32 (19–46)	30 (23–44)	10.1 (7.7–12.8)	49 (41–61)	27 (19–53)	
	P-value	0.120	0.577	0.251	*	0.283	

*Data for the level of ALT, AST, TBIL, ALP, and GGT were expressed as median (interquartile range). *P < 0.05, **P < 0.01. ALP, alkaline phosphatase; ALT, alanine aminotransferase; AST, aspartate aminotransferase; GGT, gamma glutamyltransferase; TBIL, Total bilirubin.*

TABLE 4 | Relationship between liver injury pattern and disease progress.

Variables	No liver injury (*n* = 409)	Hepatocellular pattern (*n* = 48)	Cholestatic pattern (*n* = 170)	Mixed pattern (n = 211)	P_1	P_2	P_3
	n (%) or median (IQR)	n (%) or median (IQR)	n (%) or median (IQR)	n (%) or median (IQR)			
D-dimer (mg/L)	0.43 (0.23–0.98)	0.83 (0.42–2.62)	0.85 (0.43–4.94)	0.72 (0.41–2.33)	***	***	***
International normalized ratio	0.98 (0.93–1.06)	0.99 (0.94–1.06)	1.01 (0.94–1.13)	1.00 (0.93–1.09)	0.495	**	0.088
C-reactive protein (mg/L)	10.6 (2.9–41.8)	40.8 (14.2–102.1)	46.4 (8.9–104.9)	39.2 (8.0–79.6)	***	***	***
Procalcitonin (ug/L)	0.05 (0.04–0.09)	0.12 (0.05–0.41)	0.09 (0.05–0.23)	0.09 (0.05–0.23)	***	***	***
Ferritin (ug/L)	281.3 (129.0–567.4)	1171.8 (601.8–2000.0)	636.5 (351.9–1543.7)	579.8 (284.1–1257.8)	***	***	***
Cardiac injury	18 (4.4)	12 (25.0)	32 (18.8)	33 (15.6)	***	***	***
Kidney injury	8 (2.0)	5 (10.4)	10 (5.9)	5 (2.4)	**	*	0.771
Systemic inflammatory response syndrome	79 (19.3)	19 (39.6)	47 (27.6)	48 (22.7)	***	*	0.316
Severe	45 (11.0)	23 (47.9)	50 (29.4)	68 (32.2)	***	***	***
Deceased	25 (6.1)	12 (25.0)	48 (28.2)	47 (22.3)	***	***	***

*P_1, Hepatocellular pattern vs. no liver injury; P_2, Cholestatic pattern vs. no liver injury; P_3, Mixed pattern vs. no liver injury. *P < 0.05, **P < 0.01, ***P < 0.001. IQR, interquartile range.*

DISCUSSION

Severe respiratory failure is more likely to be the main cause of mortality in COVID-19 patients (21). Other potential factors such as older age, high Sequential Organ Failure Assessment (SOFA) score, and d-dimer > 1 μg/mL were also associated with poor prognosis (22). On the basis of previous reports from China, some COVID-19 patients present with liver injury (7, 8, 23). Since subtypes of liver injury include hepatocellular pattern, cholestatic pattern, and mixed pattern, we mainly evaluated the incidence of three subtypes in COVID-19 patients and assessed their relationship with prognosis of COVID-19. In this study, we found that liver injury with cholestatic and mixed pattern were associated with worse prognosis of patients with COVID-19.

Our data indicate that SARS-CoV-2 associated liver injury correlates with hypoxia/ inflammation. The mechanism by which COVID-19 patients present with liver injury is still unclear. It was reported that SARS-CoV-2 uses angiotensin converting enzyme II (ACE2) for cell entry (24). Apart from the lung alveolar epithelial cells, liver cholangiocytes also express of ACE2 (24, 25). Besides, coronavirus particles were also identified in the liver of two deceased SARS-CoV-2 patients (26). These suggest that SARS-CoV-2 may damage cholangiocytes directly and lead to cholestatic and mixed pattern liver injury in COVID-19 patients. Interestingly, viral inclusions were not observed in the liver biopsy specimens of some COVID-19 patient with liver injury (10), indicating that SARS-CoV-2 may induce liver injury through other mechanisms. Inflammation may also contribute

TABLE 5 | Multivariate Cox regression analyses of liver injury association with mortality.

Variables	HR	95%CI	*P*-value
liver injury	2.65	1.22–5.76	*
Hepatocellular pattern	1.74	0.61–4.97	0.301
Cholestatic pattern	3.05	1.29–7.22	*
Mixed pattern	2.70	1.19–6.15	*

*P-values were adjusted by age, sex, on admission blood oxygen saturation, kidney injury or cardiac injury. *P < 0.05. CI, confidence interval; HR, Hazard ratio.*

to liver injury as patients with liver injury had higher level of inflammatory markers, such as CRP and PCT (9, 27). Wang et al. (28) confirmed that the inflammatory storm is closely related to multiple organ damage or death in COVID-19 patients. Our data also confirmed that liver injury correlates with inflammatory cytokines. In addition, hypoxia presenting as one of the common symptoms in COVID-19 patients, may be also related with liver injury (29). Our data show that liver injury is negatively correlated with blood oxygen saturation. Adverse effect of some drugs may be another factor to cause liver injury (30, 31). The use of lopinavir/ritonavir before admission was significantly higher in patients with emerging liver injury than that in patients with normal liver functions, suggesting that application of antiviral drugs may lead to liver injury during the process of COVID-19 treatment (27). Our data confirmed that liver injury for COVID-19 patients was associated with the use of certain antiviral drugs, such as lopinavir /litonavir and ribavirin.

Our data show that patients with liver injury had higher level of serum ferritin and more severe hypoxia especially for patients with hepatocellular injury pattern. It was reported that SARS-CoV-2 destroys hemoglobin in red blood cells, dissociating iron and deoxyhemoglobin, causing less hemoglobin that can carry oxygen, and producing symptoms of respiratory distress and hypoxia (32). Besides, iron dissociated from heme will be stored in ferritin, thus the level of ferritin in serum will be increased (32). In addition, hypoxia may also induce liver injury (29), and damage hepatocytes. Therefore, we propose that the elevated level of serum ferritin and hypoxia are related with hepatocyte injury.

Similar to other reports (6, 33), our study showed that liver injury in COVID-19 patients was frequent but mild in nature. The patterns of liver injury were mostly cholestatic and mixed pattern, which maybe induced by SARS-CoV-2 directly. Besides, liver injury with cholestatic and mixed patterns were associated with the worse prognosis of COVID-19. Thus, clinical physicians should pay more attention to COVID-19 patients with cholestatic and mixed pattern liver injury and give effective treatment method.

Our study has some limitations. Liver injury in COVID-19 is associated with hepatotoxic drug intake and tissue hypoxia. Therefore, increased liver injury induced by hypoxia, or hepatotoxic drug intake may not be reflective of risk factors for mortality in SARS-COV-2 infection. Although large enough to conduct valid comparisons among groups, the sample size remains limited. Larger studies should be performed to further evaluate the predictive value of liver injury for prognosis of COVID-19. In addition, this was a retrospective study, and an unknown bias may exist.

In summary, our study demonstrates that liver injury is closely related with organ injuries, hypoxia, inflammation, and the use of antiviral drugs. Hepatocellular injury pattern is associated with hypoxia, and increased hepatocellular injury may not be risk factor for mortality in SARS-COV-2 infection, while liver injury with cholestatic, and mixed patterns that may be induced by SARS-CoV-2 directly may be potential risk factors for increased mortality in patients with COVID-19. COVID-19 patients with liver injury especially for cholestatic and mixed patterns should be monitored and evaluated frequently and performed effective treatment.

DATA AVAILABILITY STATEMENT

All datasets generated for this study are included in the article/**Supplementary Material**.

ETHICS STATEMENT

The studies involving human participants were reviewed and approved by Union Hospital, Tongji Medical College, Huazhong University of Science and Technology, and Jinyintan Hospital. Written informed consent for participation was not required for this study in accordance with the national legislation and the institutional requirements.

AUTHOR CONTRIBUTIONS

HChu was responsible for study concept and design, analysis and interpretation of data, and drafting of the manuscript. TB was responsible for acquisition, analysis of data, and critical revision of the manuscript. LH, LX, LYao, RZ, ZL, LZ, CH, SS, QH, and YZ provided assistance in data acquisition and revision of the manuscript. LC and XN provided assistance in data analysis and revision of the manuscript. QZ, HChe, and BS provided critical revision of the manuscript. LYan and XH was responsible for the study concept and design, critical revision of the manuscript, and study supervision. All authors contributed to the article and approved the submitted version.

FUNDING

This study was supported by Hubei Province Novel Pneumonia Emergency Research (No. 2020FCA014 to XH) and the NIH funded San Diego Digestive Diseases Research Center (P30 DK120515 to BS).

SUPPLEMENTARY MATERIAL

The Supplementary Material for this article can be found online at: https://www.frontiersin.org/articles/10.3389/fmed.2020.584342/full#supplementary-material

REFERENCES

1. World Health Organization. *Coronavirus Disease 2019 (COVID-19) Situation Report-209*. Available online at: https:// https://www.who.int/docs/default-source/coronaviruse/situation-reports/20200816-covid-19-sitrep-209.pdf (accessed August 16, 2020).
2. Xu XW, Wu XX, Jiang XG, Xu KJ, Ying LJ, Ma CL, et al. Clinical findings in a group of patients infected with the 2019 novel coronavirus (SARS-Cov-2) outside of Wuhan, China: retrospective case series. *BMJ*. (2020) 368:m606. doi: 10.1136/bmj.m606
3. Shi H, Han X, Jiang N, Cao Y, Alwalid O, Gu J, et al. Radiological findings from 81 patients with COVID-19 pneumonia in Wuhan, China: a descriptive study. *Lancet Infect Dis.* (2020) 20:425–34. doi: 10.1016/S1473-3099(20)30086-4
4. Guan WJ, Ni ZY, Hu Y, Liang WH, Ou CQ, He JX, et al. China medical treatment expert group for, clinical characteristics of coronavirus disease 2019 in China. *N Engl J Med.* (2020) 382:1708–20. doi: 10.1056/NEJMoa2002032
5. Special Expert Group for Control of the Epidemic of Novel Coronavirus Pneumonia of the Chinese Preventive Medicine Association. An update on the epidemiological characteristics of novel coronavirus pneumoniaCOVID-19. *Zhonghua Liu Xing Bing Xue Za Zhi*. (2020) 41:139–44. doi: 10.3760/cma.j.issn.0254-6450.2020.02.002
6. Wang D, Hu B, Hu C, Zhu F, Liu X, Zhang J, et al. Clinical characteristics of 138 hospitalized patients with 2019 novel coronavirus-infected pneumonia in Wuhan, China. *JAMA*. (2020) 323:1061–69. doi: 10.1001/jama.2020.1585
7. Cui Y, Tian M, Huang D, Wang X, Huang Y, Fan L, et al. A 55-day-old female infant infected with 2019 novel coronavirus disease: presenting with pneumonia, liver injury, heart damage. *J Infect Dis.* (2020) 221:1775–81. doi: 10.1093/infdis/jiaa113
8. Yang X, Yu Y, Xu J, Shu H, Xia J, Liu H, et al. Clinical course and outcomes of critically ill patients with SARS-CoV-2 pneumonia in Wuhan, China: a single-centered, retrospective, observational study. *Lancet Respir Med.* (2020) 8:475–81. doi: 10.1016/S2213-2600(20)30079-5
9. Huang C, Wang Y, Li X, Ren L, Zhao J, Hu Y, et al. Clinical features of patients infected with 2019 novel coronavirus in Wuhan, China. *Lancet*. (2020) 395:497–506. doi: 10.1016/S0140-6736(20)30183-5
10. Xu Z, Shi L, Wang Y, Zhang J, Huang L, Zhang C, et al. Pathological findings of COVID-19 associated with acute respiratory distress syndrome. *Lancet Respir Med.* (2020) 8:420–22. doi: 10.1016/S2213-2600(20)30076-X
11. Zhang B, Zhou X, Qiu Y, Song Y, Feng F, Feng J, et al. Clinical characteristics of 82 cases of death from COVID-19. *PLoS ONE*. (2020) 15:e0235458. doi: 10.1371/journal.pone.0235458
12. Zhang Y, Zheng L, Liu L, Zhao M, Xiao J, Zhao Q. Liver impairment in COVID-19 patients: a retrospective analysis of 115 cases from a single center in Wuhan city, China. *Liver Int.* (2020) 40:2095–103. doi: 10.1111/liv.14455
13. Cai Q, Huang D, Yu H, Zhu Z, Xia Z, Su Y, et al. COVID-19: abnormal liver function tests. *J Hepatol.* (2020) 73:566–74. doi: 10.1016/j.jhep.2020.04.006
14. Lei F, Liu YM, Zhou F, Qin JJ, Zhang P, Zhu L, et al. Longitudinal association between markers of liver injury and mortality in COVID-19 in China. *Hepatology.* (2020) 72:389–98. doi: 10.1002/hep.31301
15. Force ADT, Ranieri VM, Rubenfeld GD, Thompson BT, Ferguson ND, Caldwell E, et al. Acute respiratory distress syndrome: the berlin definition. *JAMA*. (2012) 307:2526–33. doi: 10.1001/jama.2012.5669
16. Kellum JA, Lameire N, K.Group AGW. Diagnosis, evaluation, and management of acute kidney injury: a KDIGO summary (Part 1). *Critical Care*. (2013) 17:204. doi: 10.1186/cc11454
17. Metlay JP, Waterer GW, Long AC, Anzueto A, Brozek J, Crothers K, et al. Diagnosis and treatment of adults with community-acquired pneumonia. An official clinical practice guideline of the American thoracic society and infectious diseases society of America. *Am J Respir Crit Care Med.* (2019) 200:e45–67. doi: 10.1164/rccm.201908-1581ST
18. Danan G, Benichou C. Causality assessment of adverse reactions to drugs–I. A novel method based on the conclusions of international consensus meetings: application to drug-induced liver injuries. *J Clin Epidemiol.* (1993) 46:1323–30. doi: 10.1016/0895-4356(93)90101-6
19. Kang Y, Kim SH, Park SY, Park BY, Lee JH, An J, et al. Evaluation of drug-induced liver injury developed during hospitalization using electronic health record (EHR)-based algorithm. *Allergy Asthma Immunol Res.* (2020) 12:430–42. doi: 10.4168/aair.2020.12.3.430
20. Feng G, Zheng KI, Yan QQ, Rios RS, Targher G, Byrne CD, et al. COVID-19 and liver dysfunction: current insights and emergent therapeutic strategies. *J Clin Transl Hepatol.* (2020) 8:18–24. doi: 10.14218/JCTH.2020.00018
21. Li X, Ma X. Acute respiratory failure in COVID-19: is it "typical" ARDS? *Crit Care.* (2020) 24:198. doi: 10.1186/s13054-020-02911-9
22. Zhou F, Yu T, Du R, Fan G, Liu Y, Liu Z, et al. Clinical course and risk factors for mortality of adult inpatients with COVID-19 in Wuhan, China: a retrospective cohort study. *Lancet*. (2020) 395:1054–62. doi: 10.1016/S0140-6736(20)30566-3
23. Zhang C, Shi L, Wang FS. Liver injury in COVID-19: management and challenges. *Lancet Gastroenterol Hepatol.* (2020) 5:428–30. doi: 10.1016/S2468-1253(20)30057-1
24. Zhou P, Yang XL, Wang XG, Hu B, Zhang L, Zhang W, et al. A pneumonia outbreak associated with a new coronavirus of probable bat origin. *Nature*. (2020) 579:270–3. doi: 10.1038/s41586-020-2012-7
25. Qi F, Qian S, Zhang S, Zhang Z. Single cell RNA sequencing of 13 human tissues identify cell types and receptors of human coronaviruses. *Biochem Biophys Res Commun.* (2020) 526:135–40. doi: 10.1016/j.bbrc.2020.03.044
26. Wang Y, Liu S, Liu H, Li W, Lin F, Jiang L, et al. SARS-CoV-2 infection of the liver directly contributes to hepatic impairment in patients with COVID-19. *J Hepatol.* (2020) 73:807–16. doi: 10.1016/j.jhep.2020.05.002
27. Fan Z, Chen L, Li J, Cheng X, Yang J, Tian C, et al. Clinical features of COVID-19-related liver functional abnormality. *Clin Gastroenterol Hepatol.* (2020) 18:1561–6. doi: 10.1016/j.cgh.2020.04.002
28. Wang C, Xie J, Zhao L, Fei X, Zhang H, Tan Y, et al. Alveolar macrophage dysfunction and cytokine storm in the pathogenesis of two severe COVID-19 patients. *EBioMedicine*. (2020) 57:102833. doi: 10.1016/j.ebiom.2020.102833
29. Yang L, Wang W, Wang X, Zhao J, Xiao L, Gui W, et al. Creg in hepatocytes ameliorates liver ischemia/reperfusion injury in a TAK1-dependent manner in mice. *Hepatology*. (2019) 69:294–313. doi: 10.1002/hep.30203
30. Yancheva N, Tzonev R. A case of late presentation of darunavir-related cholestatic hepatitis. *Int J STD AIDS*. (2019) 30:620–2. doi: 10.1177/0956462419826723
31. Marty FM, Vidal-Puigserver J, Clark C, Gupta SK, Merino E, Garot D, et al. Intravenous zanamivir or oral oseltamivir for hospitalised patients with influenza: an international, randomised, double-blind, double-dummy, phase 3 trial. *Lancet Respir Med*. (2017) 5:135–46. doi: 10.1016/S2213-2600(16)30435-0
32. LiuW, Li H. *COVID-19: Attacks the 1-Beta Chain of Hemoglobin and Captures the Porphyrin to Inhibit Human Heme Metabolism*. Available online at: https://chemrxiv.org/articles/COVID-19_Disease_ORF8_and_SurfaceGlycoprotein_Inhibit_Heme_Metabolism_by_Binding_to_Porphyrin/11938173 (accessed April 25, 2020).
33. Ji D, Qin E, Xu J, Zhang D, Cheng G, Wang Y, et al. Non-alcoholic fatty liver diseases in patients with COVID-19: a retrospective study. *J Hepatol.* (2020) 73:451–3. doi: 10.1016/j.jhep.2020.03.044

Conflict of Interest: The authors declare that the research was conducted in the absence of any commercial or financial relationships that could be construed as a potential conflict of interest.

frontiers in Medicine

REVIEW
published: 27 October 2020
doi: 10.3389/fmed.2020.584250

Evaluation of Intra-Tumoral Vascularization in Hepatocellular Carcinomas

Qi Zhang[1,2,3,4†], *Jiajun Wu*[1†], *Xueli Bai*[1,2,3,4*] *and Tingbo Liang*[1,2,3,4*]

[1] Department of Hepatobiliary and Pancreatic Surgery, The First Affiliated Hospital, Zhejiang University School of Medicine, Hangzhou, China, [2] Zhejiang Provincial Key Laboratory of Pancreatic Disease, The First Affiliated Hospital, Zhejiang University School of Medicine, Hangzhou, China, [3] The Innovation Center for the Study of Pancreatic Diseases of Zhejiang Province, Hangzhou, China, [4] Zhejiang Clinical Research Center of Hepatobiliary and Pancreatic Diseases, Hangzhou, China

Intratumoral neovascularization has intricate effects on tumor growth, metastasis, and treatment. Over the last 30 years, Microvessel density (MVD) has been the standard method for laboratory and clinical evaluation of angiogenesis. Hepatocellular carcinoma (HCC) is a typical hypervascularized tumor, and the predictive value of MVD for prognosis is still controversial. According to previous viewpoints, this has been attributed to the determination of hotspot, counting methods, vascular endothelial markers, and different definitions of high and low vascular density; however, the heterogeneity of tumor angiogenesis patterns should be factored. The breakthroughs in artificial intelligence and algorithm can improve the objectivity and repeatability of MVD measurement, thus saving a lot of manpower. Presently, anti-angiogenesis therapy is the only effective systematic treatment for liver cancer, and the use of imaging technology-assisted MVD measurement is expected to be a reliable index for evaluating the curative effect. MVD in multinodular hepatocellular carcinoma represents a subject area with huge understudied potential, and exploring it might advance our understanding of tumor heterogeneity.

Keywords: tumor vascularization, liver cancer, microvascular density, vascular pattern, cell marker

OPEN ACCESS

Edited by:
Chao Yan,
Xuzhou Medical University, China

Reviewed by:
Giuseppe Losurdo,
University of Bari Medical School, Italy
Wen-Ming Cong,
Eastern Hepatobiliary Surgery Hospital, China

***Correspondence:**
Tingbo Liang
liangtingbo@zju.edu.cn
Xueli Bai
shirleybai@zju.edu.cn

[†]These authors have contributed equally to this work

Specialty section:
This article was submitted to Gastroenterology, a section of the journal Frontiers in Medicine

Received: *16 July 2020*
Accepted: *07 September 2020*
Published: *27 October 2020*

Citation:
Zhang Q, Wu J, Bai X and Liang T (2020) Evaluation of Intra-Tumoral Vascularization in Hepatocellular Carcinomas. Front. Med. 7:584250. doi: 10.3389/fmed.2020.584250

INTRODUCTION

Liver cancer is the fourth leading cause of cancer-related death with a 5-year overall survival rate of 18% globally (1). Hepatocellular carcinoma (HCC) is the most prevalent primary liver cancer, and its incidence is increasing in different populations in recent decades, specifically in Asian countries due to hepatitis B virus infection. Whilst acknowledging the continuous progress in the treatment of HCC, its prognosis remains poor (2). This is attributed to the fact that only a small part of HCC patients are diagnosed in early stages and receive curative treatments like hepatectomy and liver transplantation. However, the recurrence rate after surgical resection is high, and the application of liver transplantation is limited by the shortage of grafts.

Angiogenesis, a process that facilitates oxygen and nutrient delivery to the tumor cells, is the hallmark of cancer (3). Generally, it is believed that the absence of neovascularization causes the size of the solid tumor to remain in a dormant state of only 2–3 mm^3 (4). Neovascularization supports tumor cell proliferation and provides a pathway for metastasis (5). Therefore, a tumor with rich blood supply is considered to have a growth advantage and early metastasis compared to poorly vascularized tumors. Liver cancer is a hypervascularized tumor, and angiogenesis regulates disease recurrence, progression, and metastasis. Thus, anti-angiogenesis

strategies are developed for liver cancer and are particularly attractive. Currently, sorafenib and lenvatinib, two multi-kinase inhibitors with potent anti-angiogenic capacity, are first-line therapy for hepatocellular carcinoma (HCC) that accounts for 80% of primary liver cancer (6, 7). In addition, evaluation of vascularization might be valuable for predicting prognosis and decision-making for clinical practice (8). For instance, postoperative transcatheter arterial chemoembolization is recommended for patients with microvascular invasion of tumor cells (9). The abundance of micro-vessels is associated with poor outcomes; however, the quantification of micro-vessel abundance is challenging and several methods have been developed (10). As a classical and most widely used measurement of angiogenic activity, microvascular density (MVD) has an effective predictive value in the clinical behavior of many kinds of tumors since it was first proposed by Weidner in 1991 (11). Therefore, it is considered that the measurement of angiogenesis in liver cancer tissue might be of great significance for the prognosis and treatment of liver cancer (12). Herein, we review the progress, agreements, and controversies of microvascular quantification in liver cancer, and its roles in the prognosis and treatment of HCC.

BIOLOGICAL CHARACTERISTICS OF MICROVASCULAR DENSITY

Although highly vascularized tumor is supposed to obtain better blood perfusion and more oxygen supply, in practice, the relationship between tumor MVD and local hypoxia is complicated. Vascular endothelial growth factor (VEGF) is a hexose-modified multifunctional protein, which has a specific binding site of hypoxia-inducible factor-1α (HIF-1α), and can act on vascular endothelial cells and induce micro-angiogenesis. In the development of HCC, hypoxia enhances the transcriptional activity of VEGF, and increases the stability of VEGF mRNA in a HIF-1α-dependent manner (13–15). However, high MVD is prone to but does not always represent a satisfactory blood supply of tumors. Because of the compression by overproliferated tumor cells and the immature vascular structure, tumor neovascularization is structurally abnormal with compromised functions, which will still cause acidosis and hypoxia within the tumor (16). Hypoxia enhances the malignant characteristics of tumor cells by inducing epithelial-to-mesenchymal transition and consequently causing drug resistance and metastasis (17, 18). Certainly, reversing microenvironmental hypoxia in tumor by direct delivery of oxygen or improvement of angiogenesis stimulate the effectiveness of chemotherapy and radiotherapy (19–22). Nevertheless, abundant neovascularization in tumor does promote distant metastasis of tumor cells (23). Therefore, precise evaluation of tumor vascularization and methods for regulation of vascularization in HCC are vital for clinical practice.

However, quantification of both vascular abundance and maturity is formidable. Currently, reliable *in vivo* methods to evaluate vascularization of tumors are unavailable, and *ex vivo* methods are based on two-dimensional analysis, which is not the case in real tumors. So far, MVD is still the most applied and accepted index for the measurement of tumor vascularization. Neovascularization in tumors with high MVD has been confirmed to be positively related to distant metastasis and increased number of circulating tumor cells (24–26). However, debate exists about the association between MVD and the differentiation degree of HCC. Studies by Wada et al. and Hisai et al. found that angiopoietin-2 expression was positively correlated with MVD and that MVD of well-differentiated HCCs is significantly lower than that of moderately and poorly differentiated HCCs (14, 27), whereas other reports showed that there was no correlation between the two groups (28). Regarding drug perfusion and distribution, it is not intuitive that tumors with high MVD can exhibit better drug perfusion. Immature vessels and interstitial fluid pressure can severely hinder the penetration and distribution of drugs, although this feature can be also utilized by nanomaterials to boost drug delivery through the enhanced permeability and retention effect (29). In contrast, the elaborate use of anti-angiogenesis strategy might promote tumor vascular normalization and enhance blood perfusion and drug delivery (16, 30, 31).

ADVANCES IN THE METHODOLOGY OF MVD MEASUREMENT

The quantitation method of MVD in the tumor was first proposed by Weidner in 1991 (32). This technique means counting the outline of the blood vessel wall stained by routine immunohistochemistry in tissue slide, and eventually obtaining the number of micro-vessels per square millimeter. Briefly, this method begins from scanning the whole section under a low-power microscope field to identify several "hot spots" with the highest blood vessel density, followed by counting single new micro-vessels under a high-power microscope field (33). The obscurity of whether it was a neovascularization was resolved by an agreement between two researchers using a double-ended microscope, and each procedure took 7–10 min. In our experience, the selection of hot spots should be spaced at an appropriate distance and reflects the overall situation of the whole slice. Neovascularization is distinguished if single new micro-vessels, which are defined as any stained epithelial cells (EC) or clusters separated from adjacent blood vessels, with or without lumen or red blood cells, are observed. Blood vessels containing muscle walls and vessels in the tumor sclerosis area are not counted. In this earliest work, Weidner found that the MVD in breast tumors with poor prognosis and metastasis was twice as high as that in breast tumors with good prognosis and no metastasis. Despite being revolutionary, this method has inherent shortcomings. First, the subjective definition of hotspot causes poor repeatability, thus the inter-observer and intra-observer heterogeneity are significant. For example, de Jong and colleagues reported that the average inter-observer coefficient of variation was about 24% (34). Second, the judgment of neovascularization is subjective with no objective parameters for quality control. Last, manual calculation is time-consuming, particularly for tumors with hypervascularization and size larger than 10 cm. In addition, the cut-off values between high and low MVD in

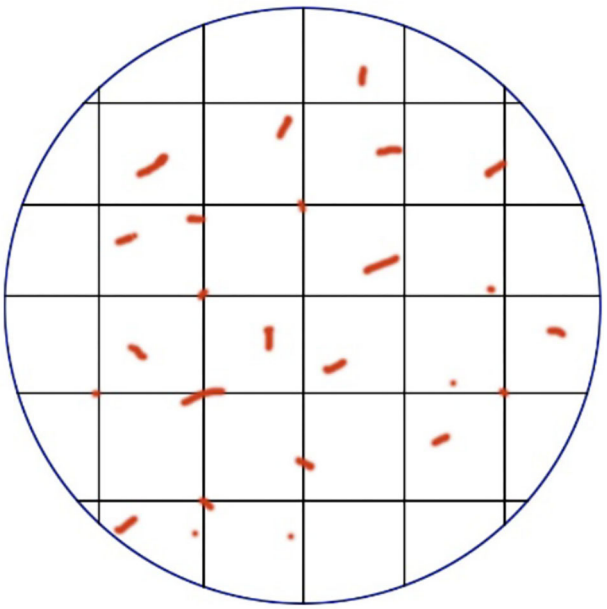

FIGURE 1 | A demonstration diagram of the Chalkley method. The vertical lines that are intersected in the circular eyepiece form a grid, and the vessels were counted when collided with the grid point.

different trials ranged from 4 to 106.3. This may be due to the wide range of antibodies, patient groups, treatments, and data interpretations. Therefore, cross-sectional comparisons of cut-off values are meaningless.

The Chalkley method, also called point-overlap morphometry, is based on the systematic random sampling theory to approximate the relative area of neovascularization in a limited area (35). Like the Weidner method, it requires the subjective selection of several hotspots with the highest neovascularization density, but does not need to calculate all micro-vessels. A special attachment called "Chalkley point array graticule" installed on the eyepiece of the microscope was used (**Figure 1**), there are 25 randomly distributed fixed points on the Chalkley graticule, and the direction of the grid points can be changed by moving clockwise or counterclockwise (36). The observer can find a unique location where there is the highest grid point overlap with the micro-vessels, and record the total number of intersections as a Chalkley count, where Chalkley count is a unitless parameter. Since there is no need for observers to frequently determine whether the stained microvessels conform to the principles of neovascularization, the Chalkley method is relatively more objective and time-saving than the Weidner method.

To improve the reproducibility of measurement and reduce inter-observer and intra-observer variations, computer-aided technology has been applied to microvessel counting. Unfortunately, no computer software that can automatically analyze and measure MVD is up to date, primarily because manual intervention is necessary to select vascular hotspots. Some investigators have attempted automated image analysis algorithms to generate geographical microvessel maps by calculating entire tumor slices, which can be more objective in counting microvessels (37). Although they conquer the subjectivity of previous methods, the excessive time consumption limits its application, and hence it is worth investigating whether MVD in the whole section represents the real angiogenic activity of the tumor. In recent years, Marien et al. developed a semi-automatic system based on systematic uniform random sampling, i.e., AutoTag and AutoSnap as a substitute for the classical method of identifying hotspots manually by pathologists to confirm areas of interest (ROI). Then, a self-written Photoshop automatically integrates the digital grid with the ROI captured by the system to produce a new image for computer microvascular counting (38). Due to the automatic nature of AutoSnap, workforce hours can be saved, and each image has a tag corresponding to it, making the result traceable. In addition, the random sampling method can reflect the overall vascular growth in the tumor and minimize the variation caused by the experience of the observer at the time of sampling. This technique was further validated by Marien and colleagues in colorectal cancer, glioblastoma multiforme, ovarian carcinoma, and renal cell carcinoma (39), despite being not verified by other investigators. The measurement method of MVD is currently immature and will keep evolving toward being more standard, objective, repeatable, and efficient. With the emergence of computer algorithm and artificial intelligence technology, it is believed that real automatic vascular technology analysis will emerge in the near future. But it must be noted that due to the heterogeneity of tumor vascular growth patterns, certain methods of sampling or measurement might not be suitable for all tumors. Also, the identification of vascular growth patterns and their clinical significance are critical in different types of tumors as well as in different patients with the same types of tumor.

ENDOTHELIAL CELL MARKERS USED TO MEASURE MVD

Many pan-endothelial and special endothelial cell markers are used for vascular labeling in HCC. Among all these markers, the widely used ones include vWF (factor VIII-related antigen), CD31, CD34, and CD105. vWF is a glycoprotein primarily found in endothelial cell Weibel-Palade bodies, and it mediates platelet adhesion to endothelial cells at the sites of vascular injury (40). vWF is probably the most specific endothelial marker, which can well distinguish endothelial cells from other surrounding tissues, due to its exclusive expression on vascular endothelial cells despite a small part of it being stored in megakaryocytes (41). In normal liver, only scattered positive reactions are observed in vascular endothelial cells in the portal area, and vWF is not expressed in normal hepatic sinusoidal endothelial cells. However, positive staining may be found in the background of chronic hepatitis and cirrhosis, whereas strong positive staining is often detected in HCCs (42). These characteristics make vWF one of the most reliable endothelial markers in measuring the MVD of HCC.

TABLE 1 | Measurement and prognosis of MVD in different trials.

References	*N*	Marker	Proportion of sinusoid-like vessels	Counting method	Preoperative treatment	No. of hotspots	Correlation between high-MVD and poor prognosis
Tanigawa et al. (53)	43	CD34 and vWF	5 out of 43	Weidner	TAE (12 cases)	5	Positive
El-assal et al. (54)	71	vWF	NM	Weidner	None	3	Positive
Sun et al. (28)	78	CD34	19 out of 78	Weidner	None	5	Irrelevant
Poon et al. (55)	100	CD34 and vWF	NM	CIAS	None	5	Positive (only for CD34 in tumor ≤5 cm)
Ho et al. (56)	86	CD34 and CD105	NM	Weidner	None	5	Irrelevant
Zhang et al. (57)*	82	CD34	NM	CIAS	NM	5	Positive
Yang et al. (58)	113	CD34 and CD105	NM	Weidner	None	3	Positive (only for CD105-MVD)
Sakaguchi et al. (59)	51	CD34 and CL-5	NA	Weidner	NM	5	Positive (only for CL-5-MVD)
Huang et al. (60)	100	CD34 and Endocan	NM	Weidner	None	3	Positive (only for Endocan -MVD)
Zhang et al. (61)	75	CD34	NA	Weidner	None	5	Positive
Zeng et al. (62)	69	CD34	NM	Chalkley	None	3	Negative
Kitamura et al. (63)	63	CD34	NM	CIAS	None	10	Negative
Wang et al. (64)	305	CD34	NM	CIAS	None	5	Positive
Qiu et al. (65)	103	CD34	NM	CIAS	None	NM	Positive
Murakami et al. (66)	136	CD34	20 out of 136	Weidner	None	5	Negative
Luo et al. (67)	90	CD34	NA	Weidner	None	5	Positive

*N, numbers of patients; NM, not mentioned; NA, sinusoid-like vessels were measured, but the data is not available; CIAS, computerized image analysis system; *patients received liver transplantation.*

CD31, which belongs to the immunoglobulin superfamily, is a component of endothelial cell junction and also appears on the surface of platelets, monocytes, macrophages, plasma cells, neutrophils, as well as other inflammatory cells (43, 44). The expression of CD31 is homogeneous and strongly expressed relative to the vascular type-specific expression of VWF and CD34, and it often cross-reacts with plasma cells (41). However, CD31 is rarely used for MVD study in HCC.

CD34, a transmembrane glycoprotein of 110 kDa, is another endothelial marker broadly used in HCC. Like the vWF and CD31, CD34 is a pan-endothelial marker and is usually located in vascular endothelial cells and hematopoietic progenitor cells (45). In normal liver, CD34 is only expressed in the area around the portal vein, and most of the sinusoids in the central lobule are negative for CD34 (43). A study by Ohmori et al. discovered that there were CD34-positive but vWF-negative sinusoidal endothelial cells in the liver of patients with hepatitis C virus-related chronic liver disease, and the high expression of these CD34-positive sinusoidal endothelial cells was a risk factor for HCC carcinogenesis in these patients (46). This implies that CD34 might be a preferable endothelial marker rather than vWF for the study of HCC.

None of the pan-vascular endothelial markers mentioned above can distinguish between resting and proliferating blood vessels, while CD105 is a transmembrane glycoprotein highly and precisely expressed on activated endothelial cells (47). CD105, also known as endoglin, is a co-receptor of transforming growth factor β (TGF-β). It is involved in the development and remodeling of blood vessels, and its expression is up-regulated when resting endothelial cells become proliferative, thus representing the proliferation of hepatic sinusoidal endothelial cells in the liver (48). However, in practical application, it did not meet the expectations. Elsewhere, Qian et al. compared CD31 and CD105 in the determination of a more stable endothelial marker. The results showed that in 90 HCCs, all tumor vessels showed CD31 expression, 39 cases (43.3%) showed weak or no CD105 expression in tumors and their vessels, of which 29 cases (74.4%) were poorly differentiated HCCs, indicating that CD105 might not be expressed in poorly differentiated HCC cells (49). Evidence from Yu et al. found that CD105 was expressed in neovessels of HCC and sinusoidal endothelial cells in cirrhotic liver (50). Furthermore, given that CD105 can be expressed in tumor cells (49, 51, 52), contamination with CD105-positive tumor cells is inevitable. Therefore, the application of CD105 in the measurement of MVD in HCC is limited. CD34 is still the most widely applied endothelial marker in calculating MVD in HCC (**Table 1**).

VASCULAR PATTERNS THAT INFLUENCE MVD

Pathological angiogenesis of HCC is often referred to as capillarization, in which normal sinusoids turn into thicker and continuous endothelial cells with fewer fenestrations (68). Two classic morphologies can ordinarily be observed in the

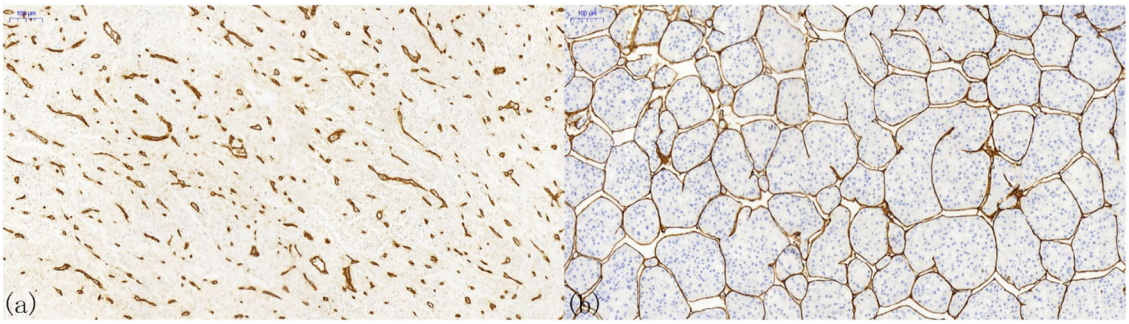

FIGURE 2 | Patterns of microvessels in hepatocellular carcinoma. **(a)** Capillary-like microvessels have discrete, disconnected blood vessels with small or no lumen; **(b)** Sinusoid-like microvessels, in which the endothelial cells are interconnected, can entirely encapsulate the cancer nest to form a cobweb-like structure.

immunohistochemical staining of HCC tissues (**Figure 2**). One is capillary-like microvessels, and the other is sinusoid-like microvessels (also known as vessels that encapsulate tumor clusters, VETC) (66). Generally, the former has small, scattered capillaries with no or a narrow lumen, whereas the latter has continuous branches and an apparent lumen. However, the clinicopathological differences between these two distinct vascular patterns have scarcely been observed.

The latter vascular pattern presents a hurdle to the counting of MVD in HCC. It becomes impossible to count vascular endothelial cells connected using the conventional counting principle. Therefore, Tanigawa proposed a modified counting method by defining every 40-μm lumen length as one point (53). Nonetheless, the efficacy and clinical significance of this method have not been thoroughly verified, and no one proposed a better solution after that. In addition to the measurement method being different from the conventional microvascular evaluation, sinusoidal-like vessels have a great impact on the clinical outcomes of HCC patients. An investigation by Sugino et al. checked immunohistochemical slices on 80 autopsy HCC cases and speculated that this special vascular pattern could encircle multiple tumor cells to spread in the form of multicellular tumor emboli, rather than cancer cells invading the blood vessel wall alone (69). This observation suggested an invasion-independent metastasis phenomenon in HCC. The clinical significance of this conjecture was validated by later studies. Dingand and colleagues revealed that the sinusoidal-like vascular patterns were associated with a low overall survival rate and high early recurrence rate (70). Additionally, Fang et al. unprecedentedly used three-dimensional reconstruction to confirm that sinus vessels formed an interconnected network around a single HCC nodule, while capillaries showed discrete and disorganized patterns (71, 72). They suggested that this vascular pattern was an effective mode of HCC metastasis independent of epithelial-to-mesenchymal transition. In 2019, Renne et al. demonstrated that it was an independent risk factor for early recurrence and decreased overall survival in a large multi-institutional cohort containing 541 resected HCCs from Italy, South Korea, and Japan (73). Seemingly, it reminds us that the MVD influence the clinical outcomes of HCC, and the heterogeneity of vascular patterns might regulate HCC progression.

PROGNOSTIC VALUE OF MVD IN HCC

Tanigawa, one of the pioneers exploring the association between MVD and prognosis of HCC patients, demonstrated that patients with MVD<290 showed a better overall survival and were more likely to remain tumor-free (53). The negative correlation between MVD and prognosis of patients was confirmed in several subsequent studies and summarized in a meta-analysis (54, 55, 57–61, 64, 65, 67, 74). However, an ambiguous connection and even a positive correlation between MVD and survival in HCC patients were also observed by other investigators (28, 56, 62, 63, 66). For instance, in a retrospective study of 136 HCC patients reported by Murakami et al., low MVD was identified as an independent predictor of poor 2-year DFS and OS, which contrasted with previous findings (66). Further, other researchers tried to combine MVD with other factors in predicting the prognosis of HCC patients. Qiu and colleagues used Beclin-1 and MVD to predict survival (65), and Murakami suggested that the 10-year OS rate and 2-year DFS rate in the low vasohibin1/MVD group (vasohibin1/CD34-MVD $\leq$ 0.459) were significantly higher than those in the high vasohibin1/CD34-MVD group (75). These conflicting results were partly due to the influence of methodological factors including endothelial markers, hotspot selection, counting methods, microvascular patterns, and patients. For example, in the study by Murakami, sinusoidal-like microvessels were identified in about 15% of cases. This special microvascular pattern, which ranges from 18.9 to 45.2% in HCC (70, 71, 73), ordinarily has a lower blood vessel density than ordinary capillary-like pattern and tends to form a large vessel lumen (76). Importantly, it has independent negative effects on OS and DFS (69–73). Neglecting the possible impacts of microvascular pattern on prognosis will cause unpredictable interference for the judgment of the actual role of MVD. Unfortunately, the importance of microvascular patterns has been underestimated in the studies reported so far, and its subgroup analysis is largely understudied. This kind of sinus vessel occurs frequently only in HCC, thyroid carcinoma, and clear cell renal carcinoma, but it is rare in malignant tumors originating from stomach, colon, breast, pancreas, lung, uterus, and esophagus (77). Also, this might partially explain why MVD is less controversial as a prognostic factor in tumors that

significantly induce angiogenesis, such as breast, prostate, and hematologic malignancies. Therefore, in analyzing the effect of MVD on tumor prognosis, the heterogeneity of microvascular patterns should be factored. In addition, differences of inclusion criteria in these trials might also have a significant impact; in particular, some subjects received preoperative radiofrequency ablation and transhepatic artery catheterization chemotherapy, while others did not. Since necrosis has a great impact on tumor angiogenesis, under the influence of such confounding factors, whether such a research could reflect the impact of MVD on tumor prognosis was highly susceptible. Therefore, it is essential to conduct a rigorously designed study where the samples are relatively uniform or with suitable layers.

Microvascular invasion (MVI) is defined as the presence of tumor cells in the endothelium-lined vascular lumen that is visible only under a microscope. Its diagnosis depends on the histological evaluation of the tumor and its surrounding liver tissue (78). In HCC, both MVI and MVD are considered to be positively correlated with earlier recurrence and shorter overall survival (79). High tumor neovascularization often represents high invasiveness. However, whether there is a correlation between MVI and high-MVD remains to be further studied. A few researchers have elaborated on this. For example, Franco et al. believed that there was a significant correlation between peri-tumor vessel invasion and MVD (80). However, the cause of invasiveness does not necessarily depend on blood vessel density. As mentioned earlier, the sinusoidal-like vascular in HCC is highly invasive. Fang et al. showed that endothelium-wrapped tumor emboli were always seen in adjacent non-tumor blood vessels (71); however, this vascular pattern is not necessarily associated with high-MVD.

THE PREDICTIVE ROLE OF MVD IN ANTI-ANGIOGENESIS THERAPIES

HCC tends to show vascular invasion because of its vascularization feature, and anti-angiogenic therapy is supposed to be a promising approach. Most advanced HCC treatments are currently approved in first- and second-line settings target angiogenic pathways (12). Although numerous anti-angiogenic agents have been tested or are under development, sorafenib, regorafenib, and lenvatinib are currently the only anti-angiogenic agents approved globally to enhance survival in patients with advanced HCC (81).

As the most direct indicator of angiogenesis in tumor tissue, MVD might play a vital role in regulating the efficacy of anti-angiogenic agents, but its performance was unsatisfactory. The traditional histological immunohistochemical method for measuring MVD failed in the acquisition of tumor samples greatly, which hinders its application in the evaluation of anti-angiogenic therapy. The development of a repeatable, accurate, and preferably non-invasive tumor angiogenesis evaluation technique has great clinical value in the follow-up of these targeted treatments. To overcome this, few investigators have tried to identify imaging indicators equivalent to traditional MVD for evaluating the efficacy of anti-angiogenic therapy. For example, Zhou et al. utilized contrast-enhanced ultrasound perfusion imaging to measure blood perfusion in a mouse HCC model and proved high consistency with MVD, which can be used to monitor perfusion alteration after anti-angiogenic therapy (82). Again, Song et al. used dynamic contrast-enhanced MRI to affirm if their evaluation function equals the traditional MVD (83). Recently, Lee et al. used intra-voxel incoherent motion imaging to confirm that the perfusion fraction was significantly correlated with MVD in HCC, which thus could be used to evaluate the anti-angiogenic effect of sorafenib (84). Yang and colleagues jointly introduced ultra-small superparamagnetic iron oxide enhanced susceptibility-weighted imaging (USPIO-enhanced SWI) and mean vessel density imaging into the evaluation of tumor vessels at the macro- and micro-vasculature levels, and revealed positive correlation between mean vessel density and traditional histological MVD (85). Specifically, the intra-tumoral susceptibility signal scoring in the sorafenib treatment group was significantly lower than that of control group at each time point (7 days, $P = 0.006$; 14 days, $P = 0.013$; 21 days, $P = 0.012$) (85). Previous studies could not directly demonstrate tumor microvessels, but evaluated the functional characteristics of tumor angiogenesis, while Yang's method directly reflected the changes of tumor neovascularization after treatment. This method may be useful for other anti-angiogenic chemicals in identifying those patients who might benefit from such a strategy. Despite these studies being young, clinical applications are promising. And perhaps with its advancement, MVD will guide clinical practice in a new perspective.

DRAWBACKS

In addition to the special microvascular pattern in HCC, there are several points worth mentioning. First, all existing studies on microvessel density in HCC focused on inter-tumoral heterogeneity (86), but little is known about the intra-tumoral heterogeneity of angiogenesis in HCC. Recently, intra-tumoral heterogeneity of HCC has been carried out with significant differences in genomics, transcriptomics, proteomics, metabolomics, and local immunity (87, 88), but the intra-tumoral heterogeneity of neovascularization in HCC has rarely been explored, specifically, in the case of multiple lesions in the liver, which could be intrahepatic metastases of a single tumor or multi-centric carcinogenesis of several independent tumors (89). In previous investigations, the investigators normally chose only one nodular as a representative MVD measurement (62) despite three to five regions with the highest MVD being selected. Understanding the intratumoral heterogeneity of angiogenesis in HCC might help us better classify HCC and improve prognosis and antiangiogenic therapy.

Second, current indicators for identification of MVD are endothelial cell markers, however, other components of blood vessels including vascular smooth muscle cells and pericytes are not well reflected and influence the integrity of microvessels (90). It is alleged that HCC with high MVD but poor vascular quality might have worse blood perfusion, drug penetration, and more likely to metastasize than patients with low MVD but

better vascular quality. Reports suggest that α-SMA was used in reflecting the maturity of microvessels in HCC, and was proved to have a certain prognostic value (64). The understanding of microvascular quality needs to be further elucidated, and this can be resolved with the discovery of novel and effective pericyte markers and the progress of imaging technology.

CONCLUSIONS AND PROSPECT

We reviewed the previous literature on the measurement of MVD and its roles in predicting the prognosis and reflecting the underlying evaluation of HCC. Then, we introduced a particular but not rare microvasculature pattern. With the rapid development of computer-aided technology, the measurement of MVD could facilitate automation and standardization in future applications. CD34 is still the predominant marker, however, it has been applied for 20 years. Also, the sinusoidal-like vessels in HCC might suggest clinical significance such as survival and treatment response, and its underlying biological characteristics are impressive. The intra-tumoral heterogeneity and the maturity of microvessels should be reiterated in future clinical studies, which might be helpful for the advancement of anti-angiogenesis therapy. Finally, the combination of MVD with new imaging techniques is a potential strategy for the evaluation of the treatment efficacy.

AUTHOR CONTRIBUTIONS

QZ and JW conceived the idea and wrote the manuscript. TL and XB supervised the study, interpreted the clinical significance, and made critical revisions to the draft. All authors contributed to the article and approved the submitted version.

FUNDING

This work was financially supported by the National Natural Science Foundation of China (81871320 and 81830089), Zhejiang Provincial Foundation for Distinguished Youth (No. LR20H160002), and the Fundamental Research Funds for the Central Universities (2020FZZX003-02-10, 2019XZZX005-4-05).

REFERENCES

1. Villanueva A. Hepatocellular carcinoma. *N Engl J Med.* (2019) 380:1450–62. doi: 10.1056/NEJMra1713263
2. Lurje I, Czigany Z, Bednarsch J, Roderburg C, Isfort P, Neumann UP, et al. Treatment strategies for hepatocellular carcinoma (-) a multidisciplinary approach. *Int J Mol Sci.* (2019) 20:6. doi: 10.3390/ijms20061465
3. Hanahan D, Weinberg RA. Hallmarks of cancer: the next generation. *Cell.* (2011) 144:646–74. doi: 10.1016/j.cell.2011.02.013
4. Folkman J. Tumor angiogenesis: therapeutic implications. *N Engl J Med.* (1971) 285:1182–6. doi: 10.1056/NEJM197111182852108
5. Sharma S, Sharma MC, Sarkar C. Morphology of angiogenesis in human cancer: a conceptual overview, histoprognostic perspective and significance of neoangiogenesis. *Histopathology.* (2005) 46:481–9. doi: 10.1111/j.1365-2559.2005.02142.x
6. Kudo M, Finn RS, Qin S, Han KH, Ikeda K, Piscaglia F, et al. Lenvatinib versus sorafenib in first-line treatment of patients with unresectable hepatocellular carcinoma: a randomised phase 3 non-inferiority trial. *Lancet.* (2018) 391:1163–73. doi: 10.1016/S0140-6736(18)30207-1
7. Llovet JM, Ricci S, Mazzaferro V, Hilgard P, Gane E, Blanc JF, et al. Sorafenib in advanced hepatocellular carcinoma. *N Engl J Med.* (2008) 359:378–90. doi: 10.1056/NEJMoa0708857
8. Roma-Rodrigues C, Mendes R, Baptista PV, Fernandes AR. Targeting tumor microenvironment for cancer therapy. *Int J Mol Sci.* (2019) 20:4. doi: 10.3390/ijms20040840
9. Qi YP, Zhong JH, Liang ZY, Zhang J, Chen B, Chen CZ, et al. Adjuvant transarterial chemoembolization for patients with hepatocellular carcinoma involving microvascular invasion. *Am J Surg.* (2019) 217:739–44. doi: 10.1016/j.amjsurg.2018.07.054
10. Ntellas P, Perivoliotis K, Dadouli K, Koukoulis GK, Ioannou M. Microvessel density as a surrogate prognostic marker in patients with multiple myeloma: a Meta-Analysis. *Acta Haematol.* (2017) 138:77–84. doi: 10.1159/000478085
11. Hasan J, Byers R, Jayson GC. Intra-tumoural microvessel density in human solid tumours. *Br J Cancer.* (2002) 86:1566–77. doi: 10.1038/sj.bjc.6600315
12. Berretta M, Cobellis G, Franco R, Panarese I, Rinaldi B, Nasti G, et al. Features of microvessel density (MVD) and angiogenesis inhibitors in therapeutic approach of hepatocellular carcinoma (HCC). *Eur Rev Med Pharmacol Sci.* (2019) 23:10139–50. doi: 10.26355/eurrev_201911_19584
13. Wang W, Xu GL, Jia WD, Wang ZH, Li JS, Ma JL, et al. Expression and correlation of hypoxia-inducible factor-1alpha, vascular endothelial growth factor and microvessel density in experimental rat hepatocarcinogenesis. *J Int Med Res.* (2009) 37:417–25. doi: 10.1177/147323000903700217
14. Wada H, Nagano H, Yamamoto H, Yang Y, Kondo M, Ota H, et al. Expression pattern of angiogenic factors and prognosis after hepatic resection in hepatocellular carcinoma: importance of angiopoietin-2 and hypoxia-induced factor-1 alpha. *Liver Int.* (2006) 26:414–23. doi: 10.1111/j.1478-3231.2006.01243.x
15. Huang GW, Yang LY, Lu WQ. Expression of hypoxia-inducible factor 1alpha and vascular endothelial growth factor in hepatocellular carcinoma: impact on neovascularization and survival. *World J Gastroenterol.* (2005) 11:1705–8. doi: 10.3748/wjg.v11.i11.1705
16. Al-Abd AM, Aljehani ZK, Gazzaz RW, Fakhri SH, Jabbad AH, Alahdal AM, et al. Pharmacokinetic strategies to improve drug penetration and entrapment within solid tumors. *J Control Release.* (2015) 219:269–77. doi: 10.1016/j.jconrel.2015.08.055
17. Zhang Q, Bai X, Chen W, Ma T, Hu Q, Liang C, et al. Wnt/β-catenin signaling enhances hypoxia-induced epithelial-mesenchymal transition in hepatocellular carcinoma via crosstalk with hif-1α signaling. *Carcinogenesis.* (2013) 34:962–73. doi: 10.1093/carcin/bgt027
18. Du B, Shim JS. Targeting epithelial-Mesenchymal transition (EMT) to overcome drug resistance in cancer. *Molecules.* (2016) 21:7. doi: 10.3390/molecules21070965
19. Qiao Y, Yang F, Xie T, Du Z, Zhong D, Qi Y, et al. Engineered algae: a novel oxygen-generating system for effective treatment of hypoxic cancer. *Sci Adv.* (2020) 6:eaba5996. doi: 10.1126/sciadv.aba5996
20. Gao M, Liang C, Song X, Chen Q, Jin Q, Wang C, et al. Erythrocyte-Membrane-Enveloped perfluorocarbon as nanoscale artificial red blood cells to relieve tumor hypoxia and enhance cancer radiotherapy. *Adv Mater.* (2017) 29:35.doi: 10.1002/adma.201701429
21. Bai XL, Zhang Q, Ye LY, Hu QD, Fu QH, Zhi X, et al. Inhibition of protein phosphatase 2A enhances cytotoxicity and accessibility of chemotherapeutic drugs to hepatocellular carcinomas. *Mol Cancer Ther.* (2014) 13:2062–72. doi: 10.1158/1535-7163.MCT-13-0800
22. Bai X, Zhi X, Zhang Q, Liang F, Chen W, Liang C, et al. Inhibition of protein phosphatase 2A sensitizes pancreatic cancer to chemotherapy by increasing drug perfusion via hIF-1α-VEGF mediated angiogenesis. *Cancer Lett.* (2014) 355:281–7. doi: 10.1016/j.canlet.2014.09.048
23. Folkman J. Role of angiogenesis in tumor growth and metastasis. *Semin Oncol.* (2002) 29(6 Suppl 16):15–8. doi: 10.1016/S0093-7754(02)70065-1

24. Tien YW, Chang KJ, Jeng YM, Lee PH, Wu MS, Lin JT, et al. Tumor angiogenesis and its possible role in intravasation of colorectal epithelial cells. *Clin Cancer Res.* (2001) 7:1627–32.
25. Maeda R, Ishii G, Ito M, Hishida T, Yoshida J, Nishimura M, et al. Number of circulating endothelial progenitor cells and intratumoral microvessel density in non-small cell lung cancer patients: differences in angiogenic status between adenocarcinoma histologic subtypes. *J Thorac Oncol.* (2012) 7:503–11. doi: 10.1097/JTO.0b013e318241780e
26. Sun C, Li J, Wang B, Shangguan J, Figini M, Shang N, et al. Tumor angiogenesis and bone metastasis - correlation in invasive breast carcinoma. *J Immunol Methods.* (2018) 452:46–52. doi: 10.1016/j.jim.2017.10.006
27. Hisai H, Kato J, Kobune M, Murakami T, Miyanishi K, Takahashi M, et al. Increased expression of angiogenin in hepatocellular carcinoma in correlation with tumor vascularity. *Clin Cancer Res.* (2003) 9:4852–9.
28. Sun HC, Tang ZY, Li XM, Zhou YN, Sun BR, Ma ZC. Microvessel density of hepatocellular carcinoma: its relationship with prognosis. *J Cancer Res Clin Oncol.* (1999) 125:419–26. doi: 10.1007/s004320050296
29. Golombek SK, May JN, Theek B, Appold L, Drude N, Kiessling F, et al. Tumor targeting via ePR: strategies to enhance patient responses. *Adv Drug Deliv Rev.* (2018) 130:17–38. doi: 10.1016/j.addr.2018.07.007
30. Minchinton AI, Tannock IF. Drug penetration in solid tumours. *Nat Rev Cancer.* (2006) 6:583–92. doi: 10.1038/nrc1893
31. Kerbel RS. Antiangiogenic therapy: a universal chemosensitization strategy for cancer? *Science.* (2006) 312:1171–5. doi: 10.1126/science.1125950
32. Weidner N, Semple JP, Welch WR, Folkman J. Tumor angiogenesis and metastasis–correlation in invasive breast carcinoma. *N Engl J Med.* (1991) 324:1–8. doi: 10.1056/NEJM199101033240101
33. Weidner N, Folkman J, Pozza F, Bevilacqua P, Allred EN, Moore DH, et al. Tumor angiogenesis: a new significant and independent prognostic indicator in early-stage breast carcinoma. *J Natl Cancer Inst.* (1992) 84:1875–87. doi: 10.1093/jnci/84.24.1875
34. Vermeulen PB, Gasparini G, Fox SB, Toi M, Martin L, McCulloch P, et al. Quantification of angiogenesis in solid human tumours: an international consensus on the methodology and criteria of evaluation. *Eur J Cancer.* (1996) 32:2474–84. doi: 10.1016/S0959-8049(96)00379-6
35. Vermeulen PB, Gasparini G, Fox SB, Colpaert C, Marson LP, Gion M, et al. Second international consensus on the methodology and criteria of evaluation of angiogenesis quantification in solid human tumours. *Eur J Cancer.* (2002) 38:1564–79. doi: 10.1016/S0959-8049(02)00094-1
36. Karslioglu Y, Yigit N, Onguru O. Chalkley method in the angiogenesis research and its automation via computer simulation. *Pathol Res Pract.* (2014) 210:161–8. doi: 10.1016/j.prp.2013.11.010
37. Belien JA, Somi S, de Jong JS, van Diest PJ, Baak JP. Fully automated microvessel counting and hot spot selection by image processing of whole tumour sections in invasive breast cancer. *J Clin Pathol.* (1999) 52:184–92. doi: 10.1136/jcp.52.3.184
38. Marien KM, Andries L, De Schepper S, Kockx MM, De Meyer GR. AutoTag and autoSnap: standardized, semi-automatic capture of regions of interest from whole slide images. *MethodsX.* (2015) 2:272–7. doi: 10.1016/j.mex.2015.05.002
39. Marien KM, Croons V, Waumans Y, Sluydts E, De Schepper S, Andries L, et al. Development and validation of a histological method to measure microvessel density in whole-Slide images of cancer tissue. *PLoS ONE.* (2016) 11:e0161496. doi: 10.1371/journal.pone.0161496
40. Warhol MJ, Sweet JM. The ultrastructural localization of von willebrand factor in endothelial cells. *Am J Pathol.* (1984) 117:310–5.
41. Nico B, Benagiano V, Mangieri D, Maruotti N, Vacca A, Ribatti D. Evaluation of microvascular density in tumors: pro and contra. *Histol Histopathol.* (2008) 23:601–7. doi: 10.14670/HH-23.601
42. Hattori M, Fukuda Y, Imoto M, Koyama Y, Nakano I, Urano F. Histochemical properties of vascular and sinusoidal endothelial cells in liver diseases. *Gastroenterol Jpn.* (1991) 26:336–43. doi: 10.1007/BF02781922
43. Pusztaszeri MP, Seelentag W, Bosman FT. Immunohistochemical expression of endothelial markers cD31, cD34, von willebrand factor, and fli-1 in normal human tissues. *J Histochem Cytochem.* (2006) 54:385–95. doi: 10.1369/jhc.4A6514.2005
44. Muller AM, Hermanns MI, Skrzynski C, Nesslinger M, Muller KM, Kirkpatrick CJ. Expression of the endothelial markers pECAM-1, vWf, and cD34 *in vivo* and *in vitro*. *Exp Mol Pathol.* (2002) 72:221–9. doi: 10.1006/exmp.2002.2424
45. Jennings RN, Miller MA, Ramos-Vara JA. Comparison of cD34, cD31, and factor vIII-related antigen immunohistochemical expression in feline vascular neoplasms and cD34 expression in feline nonvascular neoplasms. *Vet Pathol.* (2012) 49:532–7. doi: 10.1177/0300985811429312
46. Ohmori S, Shiraki K, Sugimoto K, Sakai T, Fujikawa K, Wagayama H, et al. High expression of cD34-positive sinusoidal endothelial cells is a risk factor for hepatocellular carcinoma in patients with hCV-associated chronic liver diseases. *Hum Pathol.* (2001) 32:1363–70. doi: 10.1053/hupa.2001.29678
47. Li C, Hampson IN, Hampson L, Kumar P, Bernabeu C, Kumar S. CD105 antagonizes the inhibitory signaling of transforming growth factor beta1 on human vascular endothelial cells. *Faseb j.* (2000) 14:55–64. doi: 10.1096/fasebj.14.1.55
48. Kasprzak A, Adamek A. Role of endoglin (CD105) in the progression of hepatocellular carcinoma and anti-Angiogenic therapy. *Int J Mol Sci.* (2018) 19:12. doi: 10.3390/ijms19123887
49. Qian H, Yang L, Zhao W, Chen H, He S. A comparison of cD105 and cD31 expression in tumor vessels of hepatocellular carcinoma by tissue microarray and flow cytometry. *Exp Ther Med.* (2018) 16:2881–8. doi: 10.3892/etm.2018.6553
50. Yu D, Zhuang L, Sun X, Chen J, Yao Y, Meng K, et al. Particular distribution and expression pattern of endoglin (CD105) in the liver of patients with hepatocellular carcinoma. *BMC Cancer.* (2007) 7:122. doi: 10.1186/1471-2407-7-122
51. Saroufim A, Messai Y, Hasmim M, Rioux N, Iacovelli R, Verhoest G, et al. Tumoral cD105 is a novel independent prognostic marker for prognosis in clear-cell renal cell carcinoma. *Br J Cancer.* (2014) 110:1778–84. doi: 10.1038/bjc.2014.71
52. Bai S, Zhu W, Coffman L, Vlad A, Schwartz LE, Elishaev E, et al. CD105 is expressed in ovarian cancer precursor lesions and is required for metastasis to the ovary. *Cancers (Basel).* (2019) 11:11. doi: 10.3390/cancers11111710
53. Tanigawa N, Lu C, Mitsui T, Miura S. Quantitation of sinusoid-like vessels in hepatocellular carcinoma: its clinical and prognostic significance. *Hepatology.* (1997) 26:1216–23. doi: 10.1002/hep.510260520
54. El-Assal ON, Yamanoi A, Soda Y, Yamaguchi M, Igarashi M, Yamamoto A, et al. Clinical significance of microvessel density and vascular endothelial growth factor expression in hepatocellular carcinoma and surrounding liver: possible involvement of vascular endothelial growth factor in the angiogenesis of cirrhotic liver. *Hepatology.* (1998) 27:1554–62. doi: 10.1002/hep.510270613
55. Poon RTP, Ng IOL, Lau C, Yu WC, Yang ZF, Fan ST, et al. Tumor microvessel density as a predictor of recurrence after resection of hepatocellular carcinoma: a prospective study. *J Clin Oncol.* (2002) 20:1775–85. doi: 10.1200/JCO.2002.07.089
56. Ho JW, Poon RT, Sun CK, Xue WC, Fan ST. Clinicopathological and prognostic implications of endoglin (CD105) expression in hepatocellular carcinoma and its adjacent non-tumorous liver. *World J Gastroenterol.* (2005) 11:176–81. doi: 10.3748/wjg.v11.i2.176
57. Zhang Q, Chen X, Zhou J, Zhang L, Zhao Q, Chen G, et al. CD147, mMP-2, mMP-9 and mVD-CD34 are significant predictors of recurrence after liver transplantation in hepatocellular carcinoma patients. *Cancer Biol Ther.* (2006) 5:808–14. doi: 10.4161/cbt.5.7.2754
58. Yang LY, Lu WQ, Huang GW, Wang W. Correlation between cD105 expression and postoperative recurrence and metastasis of hepatocellular carcinoma. *BMC Cancer.* (2006) 6:110. doi: 10.1186/1471-2407-6-110
59. Sakaguchi T, Suzuki S, Higashi H, Inaba K, Nakamura S, Baba S, et al. Expression of tight junction protein claudin-5 in tumor vessels and sinusoidal endothelium in patients with hepatocellular carcinoma. *J Surg Res.* (2008) 147:123–31. doi: 10.1016/j.jss.2007.07.013
60. Huang GW, Tao YM, Ding X. Endocan expression correlated with poor survival in human hepatocellular carcinoma. *Dig Dis Sci.* (2009) 54:389–94. doi: 10.1007/s10620-008-0346-3
61. Zhang ZB, Cai L, Zheng SG, Xiong Y, Dong JH. Overexpression of caveolin-1 in hepatocellular carcinoma with metastasis and worse prognosis: correlation with vascular endothelial growth factor, microvessel density and unpaired artery. *Pathol Oncol Res.* (2009) 15:495–502. doi: 10.1007/s12253-008-9144-7
62. Zeng W, Gouw AS, van den Heuvel MC, Molema G, Poppema S, van der Jagt EJ, et al. Hepatocellular carcinomas in cirrhotic and noncirrhotic human

livers share angiogenic characteristics. *Ann Surg Oncol.* (2010) 17:1564–71. doi: 10.1245/s10434-009-0900-z
63. Kitamura K, Hatano E, Higashi T, Narita M, Seo S, Nakamoto Y, et al. Proliferative activity in hepatocellular carcinoma is closely correlated with glucose metabolism but not angiogenesis. *J Hepatol.* (2011) 55:846–57. doi: 10.1016/j.jhep.2011.01.038
64. Wang WQ, Liu L, Xu HX, Luo GP, Chen T, Wu CT, et al. Intratumoral alpha-SMA enhances the prognostic potency of cD34 associated with maintenance of microvessel integrity in hepatocellular carcinoma and pancreatic cancer. *PLoS ONE.* (2013) 8:e71189. doi: 10.1371/journal.pone.0071189
65. Qiu DM, Wang GL, Chen L, Xu YY, He S, Cao XL, et al. The expression of beclin-1, an autophagic gene, in hepatocellular carcinoma associated with clinical pathological and prognostic significance. *BMC Cancer.* (2014) 14:327. doi: 10.1186/1471-2407-14-327
66. Murakami K, Kasajima A, Kawagishi N, Ohuchi N, Sasano H. Microvessel density in hepatocellular carcinoma: prognostic significance and review of the previous published work. *Hepatol Res.* (2015) 45:1185–94. doi: 10.1111/hepr.12487
67. Luo LM, Xia H, Shi R, Zeng J, Liu XR, Wei M. The association between aquaporin-1 expression, microvessel density and the clinicopathological features of hepatocellular carcinoma. *Oncol Lett.* (2017) 14:7077–84. doi: 10.3892/ol.2017.7106
68. Haratake J, Scheuer PJ. An immunohistochemical and ultrastructural study of the sinusoids of hepatocellular carcinoma. *Cancer.* (1990) 65:1985–93. doi: 10.1002/1097-0142(19900501)65:9<1985::AID-CNCR2820650918>3.0.CO;2-C
69. Sugino T, Yamaguchi T, Hoshi N, Kusakabe T, Ogura G, Goodison S, et al. Sinusoidal tumor angiogenesis is a key component in hepatocellular carcinoma metastasis. *Clin Exp Metastasis.* (2008) 25:835–41. doi: 10.1007/s10585-008-9199-6
70. Ding T, Xu J, Zhang Y, Guo RP, Wu WC, Zhang SD, et al. Endothelium-coated tumor clusters are associated with poor prognosis and micrometastasis of hepatocellular carcinoma after resection. *Cancer.* (2011) 117:4878–89. doi: 10.1002/cncr.26137
71. Fang JH, Zhou HC, Zhang C, Shang LR, Zhang L, Xu J, et al. A novel vascular pattern promotes metastasis of hepatocellular carcinoma in an epithelial-mesenchymal transition-independent manner. *Hepatology.* (2015) 62:452–65. doi: 10.1002/hep.27760
72. Fang JH, Xu L, Shang LR, Pan CZ, Ding J, Tang YQ, et al. Vessels that encapsulate tumor clusters (VETC) pattern is a predictor of sorafenib benefit in patients with hepatocellular carcinoma. *Hepatology.* (2019) 70:824–39. doi: 10.1002/hep.30366
73. Renne SL, Woo HY, Allegra S, Rudini N, Yano H, Donadon M, et al. Vessels encapsulating tumor clusters (VETC) is a powerful predictor of aggressive hepatocellular carcinoma. *Hepatology.* (2020) 71:183–95. doi: 10.1002/hep.30814
74. Li Y, Ma X, Zhang J, Liu X, Liu L. Prognostic value of microvessel density in hepatocellular carcinoma patients: a meta-analysis. *Int J Biol Markers.* (2014) 29:e279–87. doi: 10.5301/jbm.5000087
75. Murakami K, Kasajima A, Kawagishi N, Sekiguchi S, Fujishima F, Watanabe M, et al. The prognostic significance of vasohibin 1-associated angiogenesis in patients with hepatocellular carcinoma. *Hum Pathol.* (2014) 45:589–97. doi: 10.1016/j.humpath.2013.10.028
76. Chen ZY, Wei W, Guo ZX, Lin JR, Shi M, Guo RP. Morphologic classification of microvessels in hepatocellular carcinoma is associated with the prognosis after resection. *J Gastroenterol Hepatol.* (2011) 26:866–74. doi: 10.1111/j.1440-1746.2010.06511.x
77. Sugino T, Yamaguchi T, Ogura G, Saito A, Hashimoto T, Hoshi N, et al. Morphological evidence for an invasion-independent metastasis pathway exists in multiple human cancers. *BMC Med.* (2004) 2:9. doi: 10.1186/1741-7015-2-9
78. Erstad DJ, Tanabe KK. Prognostic and therapeutic implications of microvascular invasion in hepatocellular carcinoma. *Ann Surg Oncol.* (2019) 26:1474–93. doi: 10.1245/s10434-019-07227-9
79. Dekel Y, Koren R, Kugel V, Livne PM, Gal R. Significance of angiogenesis and microvascular invasion in renal cell carcinoma. *Pathol Oncol Res.* (2002) 8:129–32. doi: 10.1007/BF03033722
80. Franco R, Pirozzi G, Scala S, Cantile M, Scognamiglio G, Camerlingo R, et al. CXCL12-binding receptors expression in non-small cell lung cancer relates to tumoral microvascular density and cXCR4 positive circulating tumoral cells in lung draining venous blood. *Eur J Cardiothorac Surg.* (2012) 41:368–75. doi: 10.1016/j.ejcts.2011.05.009
81. Heo YA, Syed YY. Regorafenib: a Review in hepatocellular carcinoma. *Drugs.* (2018) 78:951–8. doi: 10.1007/s40265-018-0932-4
82. Zhou JH, Zheng W, Cao LH, Liu M, Luo RZ, Han F, et al. Contrast-enhanced ultrasonic parametric perfusion imaging in the evaluation of antiangiogenic tumor treatment. *Eur J Radiol.* (2012) 81:1360–5. doi: 10.1016/j.ejrad.2011.01.099
83. Song KD, Choi D, Lee JH, Im GH, Yang J, Kim JH, et al. Evaluation of tumor microvascular response to brivanib by dynamic contrast-enhanced 7-T mRI in an orthotopic xenograft model of hepatocellular carcinoma. *AJR Am J Roentgenol.* (2014) 202:W559–66. doi: 10.2214/AJR.13.11042
84. Lee Y, Lee SS, Cheong H, Lee CK, Kim N, Son WC, et al. Intravoxel incoherent motion mRI for monitoring the therapeutic response of hepatocellular carcinoma to sorafenib treatment in mouse xenograft tumor models. *Acta Radiol.* (2017) 58:1045–53. doi: 10.1177/0284185116683576
85. Yang S, Lin J, Lu F, Han Z, Fu C, Gu H. Use of ultrasmall superparamagnetic iron oxide enhanced susceptibility weighted imaging and mean vessel density imaging to monitor antiangiogenic effects of sorafenib on experimental hepatocellular carcinoma. *Contrast Media Mol Imaging.* (2017) 2017:9265098. doi: 10.1155/2017/9265098
86. Liu J, Dang H, Wang XW. The significance of intertumor and intratumor heterogeneity in liver cancer. *Exp Mol Med.* (2018) 50:e416. doi: 10.1038/emm.2017.165
87. Xu LX, He MH, Dai ZH, Yu J, Wang JG, Li XC, et al. Genomic and transcriptional heterogeneity of multifocal hepatocellular carcinoma. *Ann Oncol.* (2019) 30:990–7. doi: 10.1093/annonc/mdz103
88. Zhang Q, Lou Y, Yang J, Wang J, Feng J, Zhao Y, et al. Integrated multiomic analysis reveals comprehensive tumour heterogeneity and novel immunophenotypic classification in hepatocellular carcinomas. *Gut.* (2019) 68:2019–31. doi: 10.1136/gutjnl-2019-318912
89. Chianchiano P, Pezhouh MK, Kim A, Luchini C, Cameron A, Weiss MJ, et al. Distinction of intrahepatic metastasis from multicentric carcinogenesis in multifocal hepatocellular carcinoma using molecular alterations. *Hum Pathol.* (2018) 72:127–34. doi: 10.1016/j.humpath.2017.11.011
90. Raza A, Franklin MJ, Dudek AZ. Pericytes and vessel maturation during tumor angiogenesis and metastasis. *Am J Hematol.* (2010) 85:593–8. doi: 10.1002/ajh.21745

Conflict of Interest: The authors declare that the research was conducted in the absence of any commercial or financial relationships that could be construed as a potential conflict of interest.

frontiers in Medicine

ORIGINAL RESEARCH
published: 06 November 2020
doi: 10.3389/fmed.2020.583943

CML/RAGE Signal Bridges a Common Pathogenesis Between Atherosclerosis and Non-alcoholic Fatty Liver

*Qiwen Pang[1], Zhen Sun[1], Chen Shao[1], Honghua Cai[2], Zhengyang Bao[3], Lin Wang[1], Lihua Li[4], Lele Jing[1], Lili Zhang[1] and Zhongqun Wang[1]**

[1] Department of Cardiology, Affiliated Hospital of Jiangsu University, Zhenjiang, China, [2] Department of Burn Surgery, Affiliated Hospital of Jiangsu University, Zhenjiang, China, [3] Department of Internal Medicine, Affiliated Hospital of Wuxi Maternity and Child Health of Nanjing Medical University, Wuxi, China, [4] Department of Pathology, Affiliated Hospital of Jiangsu University, Zhenjiang, China

Non-alcoholic fatty liver disease (NAFLD) has become a common chronic disease in the world. NAFLD is not only a simple intrahepatic lesion, but also affects the occurrence of a variety of extrahepatic complications. In particular, cardiovascular complications are particularly serious, which is the main cause of death in patients with NAFLD. To study the relationship between NAFLD and AS may be a new way to improve the quality of life in patients with NAFLD. As we all known, inflammatory response plays an important role in the occurrence and development of NAFLD and AS. In this study, we found that the accumulation of Nε-carboxymethyllysine (CML) in the liver leads to hepatic steatosis. CML can induce the expression of interleukin (IL-1β), interleukin (IL-6), tumor necrosis factor (TNF-α), C-reactionprotein (CRP) by binding with advanced glycosylation end-product receptor (RAGE) and accelerate the development of AS. After silencing RAGE expression, the expression of pro-inflammatory cytokines was inhibited and liver and aorta pathological changes were relieved. In conclusion, CML/RAGE signal promotes the progression of non-alcoholic fatty liver disease and atherosclerosis. We hope to provide new ideas for the study of liver vascular dialogue in multi organ communication.

Keywords: atherosclerosis (AS), non-alcoholic fatty liver disease (NAFLD), Nε-carboxymethyllysine (CML), advanced glycosylation end-product receptor (RAGE), pro-inflammatory

OPEN ACCESS

Edited by:
Chao Yan,
Xuzhou Medical University, China

Reviewed by:
Giuseppe Losurdo,
University of Bari Medical School, Italy
Yuncheng Lv,
Guilin Medical University, China

***Correspondence:**
Zhongqun Wang
wangtsmc@126.com

Specialty section:
This article was submitted to Gastroenterology, a section of the journal Frontiers in Medicine

Received: *16 July 2020*
Accepted: *07 October 2020*
Published: *06 November 2020*

Citation:
Pang Q, Sun Z, Shao C, Cai H, Bao Z, Wang L, Li L, Jing L, Zhang L and Wang Z (2020) CML/RAGE Signal Bridges a Common Pathogenesis Between Atherosclerosis and Non-alcoholic Fatty Liver. Front. Med. 7:583943. doi: 10.3389/fmed.2020.583943

INTRODUCTION

With economic development, improvement in living standards, the prevalence of a high-fat, high-calorie diet, the acceleration of life and the prevalence of a lifestyle of less movement and more sitting, the prevalence of non-alcoholic fatty liver disease (NAFLD) is increasing (1, 2). NAFLD refers to excessive fat deposition in the liver in the absence of ethanol and other clear causes. The main characteristics of this disease are accumulation and diffuse fatty degeneration of hepatocytes (3, 4). NAFLD is the most common chronic liver disease (4, 5), and NAFLD has become a worldwide public health problem that endangers human health. According to statistics, the global prevalence of NAFLD has reached 25.2% (6). NAFLD has no obvious symptoms in the early stage, and liver fat infiltration of 30% or more can be diagnosed by liver ultrasound (7–9). As NAFLD is difficult to diagnose and its prevalence is likely to be underestimated.

As early as 1950, researchers found that NAFLD is associated with Atherosclerosis (AS) (10). NAFLD and AS often share common pathogenic factors. Exploring its common pathogenic factors not only inhibits the occurrence of NAFLD, it may even protect NAFLD patients from AS (11, 12).

At present, the "second strike" hypothesis is widely accepted regarding the pathogenesis of NAFLD, which is mainly caused by excessive lipid accumulation in the liver and oxidative stress caused by lipid peroxidation (13). Lipid peroxidation induces inflammation in the liver and promotes the formation of advanced glycation end products (AGEs) (14–17). Once AGEs are formed, they are difficult to degrade and accumulate in the body with age. Nε-carboxymethyllysine (CML) is the most important active center of AGEs (18). By binding with its receptor for AGEs (RAGE), it destroys cell antioxidant defense and the production of ROS (19). CML activate the receptor RAGE to cause cell activation and increase the production of pro-inflammatory cytokines (such as IL-1β, IL-6, TNF-α, CRP), leading to the occurrence of various diseases (20–22). Our previous research found that CML/RAGE signaling plays an important role in the development of AS (23). CML-RAGE interaction can change the role of the endothelial barrier, increase the permeability of endothelial cells, and destroy the normal function of vascular endothelial cells (24). CML-RAGE also promotes smooth muscle cells to take up excessive cholesterol and induces the formation of vascular smooth muscle cell-derived foam cells (25). Eventually promote the formation and progression of AS.

Liver is an important metabolic center of AGEs in the body (26). Existing research shows that AGEs research has found that AGEs have a significant effect on liver cells, such as promoting the release of pro-inflammatory cytokines and participating in the formation of liver fibrosis. We hypothesized that CML/RAGE signaling may be a common risk factor for the development of NAFLD and AS.

In this study, we collected liver biopsies from atherosclerotic patients, and used an *in vivo* model to explored the role of CML/RAGE in the development of NAFLD and AS.

METHODS

Patients

Liver biopsy specimens of 80 individuals undergoing liver biopsy were collected from the affiliated hospital of Jiangsu University (The clinical baseline data in **Supplementary Table 1**). Liver biopsies were fixed in formalin and embedded in paraffin. We divided the patients into 4 groups according to the degree of steatosis:control group (no steatosis or steatotic liver cells <5%) the low steatosis group (steatotic liver cells 5–33%); the moderate steatosis group (steatotic liver cells 33–66%); and the severe steatosis group (steatotic liver cells> 66%).

Inclusion Criteria

1. Age: 40–75 years;
2. Voluntarily undergo liver biopsy and sign the consent form.

Exclusion Criteria

1. Drinking history (daily alcohol intake: female <20 g/d, male <30 g/d);
2. Viral hepatitis, drug-induced liver disease, total parenteral nutrition, hepatolenticular degeneration, autoimmune liver disease and other specific diseases that can cause fatty liver;
3. Excluded drugs (amiodarone, tamoxifen, sodium valproate, glucocorticoid, methotrexate, etc.), total parenteral nutrition, inflammatory bowel disease, hypothyroidism, etc. Special conditions of fatty liver;
4. History of infection or tissue damage in the last 1 month;
5. A history of malignant tumors or autoimmune diseases; and a history of liver transplant surgery.

ANIMALS

Six-week-old ApoE$^{-/-}$ mice on a C57BL/6J background were purchased fromurchased from Cavens (Changzhou, China), Animals are kept in the barrier system of Jiangsu University Laboratory Animal Research Center. All animal experiments were approved by Institutional Animal Care and Use Committee of Jiangsu University. 10^{12} DNAse-resistant particles of adeno-associated viral (AAV) vectors consisting of AAV-shscramble (as a control group), AAV-shRAGE (Han HengBiological Technology Co., Ltd. Shanghai China) solution was injected into mice via the tail vein. 3 weeks after AAV injection, the high-fat diet (HFD) was introduced. Inject CML (10 mg/kg/day) into the tail vein of mice. The mice were randomly divided into 5 groups: control group (normal diet); model group (high-fat diet); CML group (high-fat diet+CML 10 mg/kg/d), AAV-shscramble group (high-fat diet +CML 10 mg/kg/d+AAV-shscramble); AAV-shRAGE group (high-fat diet +CML 10 mg/kg/d+AAV-shRAGE). Observe the pathological changes of the liver and aorta at 4, 8, 16 weeks after CML injection. Blood samples were collected through the tail vein at 16 weeks. After the mice were euthanized, the abdominal cavity and chest cavity were opened, liver tissues were removed, and the liver wet weight was accurately weighed to calculate the liver index. The liver index was calculated as follows: liver index = wet liver weight (g)/body weight (g).

Biochemical Analysis

The levels of total cholesterol (TC), triglyceride (TG), low-density lipoprotein (LDL-C), high-density lipoprotein (HDL-C), alanine aminotransferase (ALT), aspartate aminotransferase (AST) were measured by automatic biochemical instrument.

Immunohistochemical Staining

Paraffin sections were dewaxed, rehydrated and boiled in citric acid buffer for 10 min for antigen repair. The sections were blocked with 5% goat serum at room temperature for 1 h. Human liver samples were incubated with CML antibody (Abcam, 1:200) and RAGE antibody (Abcam, 1:200). ApoE$^{-/-}$ mice liver and aorta samples were incubated with RAGE antibody (Abcam, 1:200) overnight at 4°C. Then, we used a rabbit and mouse HRP kit (Conway, China Century Biotechnology Co., Ltd.) sample was photographed under a microscope.

H&E Staining

The aorta and liver tissue were fixed in 4% formaldehyde buffer and then embedded in paraffin. Paraffin embedded tissue was cut into 5 μm thick sections and stained with hematoxylin and eosin. The stained samples were photographed under a microscope.

Oil Red O Staining

Frozen sections of mice liver were fixed with 4% paraformaldehyde for 1 h and washed with isopropanol 3 times (15 s each time). Then, the slices were dyed in oil red O working solution (3 oil red O stock solution: 2 distilled solution) for 30 min and washed in isopropanol 3 times. The stained samples were photographed under a microscope.

Detection of Gene Expression by Real-time Quantitative PCR

Total RNA was extracted from the mice liver and aorta using TRIzol reagent (Invitrogen, Carlsbad, CA, USA). The RNA concentration was determined by measuring the optical density at 260 and 280 nm. Then, the RNA was reverse transcribed into cDNA. Real-time PCR was performed using primers for mice IL-1β, IL-6, TNF-α, CRP, and β-actin (synthesized by Sangon). The primer sequences are detailed in **Supplementary Table 1**. The RT-PCR reaction conditions were as follows: 94°C for 1 min, followed by 33 cycles at 94°C for 30 s, 63°C for 30 s, and 72°C for 1 min, and a final extension at 72°C for 7 min.

Statistical Analysis

All data are expressed as mean ± SD.SPSS 25.0 was used for analysis. The multiple groups were compared using a one-way analysis of variance and between two groups by Student's *t*-test analysis. $p < 0.05$ was considered statistically significant.

RESULTS

CML Accumulation in Liver Tissue of Patients With Non-alcoholic Fatty Liver

We performed liver biopsies on 80 individuals in the affiliated hospital of Jiangsu University. The degree of fatty degeneration of the liver was divided into four groups according to H&E staining (**Figure 1A**). To investigate whether CML accumulates in the liver, we performed immunohistochemical staining. We observed no obvious CML staining in the liver tissue of the control group (**Figures 1A,B**). With steatosis of the liver, CML staining gradually increased. We detected the expression of the CML receptor RAGE by immunohistochemistry and found that RAGE was significantly expressed on the steatotic liver cell membrane (**Figures 1A,C**). We hypothesize that liver steatosis may be related to CML accumulation and CML may play a role in inducing liver inflammation by binding with RAGE.

CML Promotes High Fat-Induced Liver Steatosis and Intravascular Plaque Formation in ApoE$^{-/-}$ Mice

The pathological changes of liver and aorta of ApoE$^{-/-}$ mice were detected by H&E staining in 4 and 8 weeks (**Figure 2**). At the time of 4 weeks, the hepatocytes were arranged in a radial pattern, hepatocytes were uniform in size, the nucleus was centrally distributed, thickness of the vascular intima was uniform, and the endoplasm was neatly arranged in the control group. In the model group, hepatocytes showed balloon-like degeneration, hepatocytes were uneven in size, the nucleus shifted to one side, and the vascular endoplasmic arrangement was disordered, the thickness of intima and media was uneven. In the CML group, hepatocytes were larger in size, with obvious balloon-like degeneration of hepatocytes and the thickness of intima and media increased, and a large number of monocytes gathered (**Figure 2A**). At the time of 8 weeks (**Figures 2B,C**), the fatty degeneration of liver cells in mice was further aggravated, and foam cells and fibrous plaques can be seen under the vascular intima, which protrude into the lumen, and the basement membrane is destroyed. After CML intervention, the mice liver steatosis and severe changes in aortic plaque compared with the model group.

All ApoE$^{-/-}$ mice were euthanized after 16 weeks. By observing the general picture of mice liver (**Figure 3A**), we found that compared with the control group, the liver volume of the model group was significantly increased ($P < 0.05$), and the liver surface was greasy. Under CML stimulation, there was no significant change in liver volume ($P > 0.05$), but the liver color was pale, which we speculated may be related to lipid deposition. To prove this idea, we calculate the liver index (**Figure 3B**). We found that the liver indices of the mice under CML interventions significantly increased compared with the control group ($P < 0.05$), but there was no significant difference in body weights ($P > 0.05$) (**Figure 3C**). The formation of NAFLD is accompanied by disorders of lipid metabolism and liver damage. Therefore, we measured the levels of TC, TG, LDL-C, HDL-C, AST, and ALT in the serum (**Figure 4**). After CML intervention, the level of TC, TG, LDL-C, AST, and ALT were significantly higher ($P < 0.05$), But the level of HDL-C is obviously reduced compare with the control group ($P < 0.05$).

H&E and Oil Red O staining were used to observe the liver pathological changes in the mice (**Figures 5A,B**). The control group showed normal structures in the liver, without obvious lipid droplet infiltration. After CML intervention, the liver tissue structure was unclear, and typical vacuole-like steatotic cells and red spherical lipid droplets formed. CML effectively induces the formation of NAFLD. Then observe the pathological changes of the aorta by H&E staining and Masson staining (**Figures 5A,C**). There was no obvious plaque formation in the control group. In the model group showed plaque protruding into the lumen. However, CML group had a significantly larger plaque area in the vascular lumen, a large amount of cholesterol crystals, a weak fiber cap, and poor plaque stability.

CML Promotes the Expression of Pro-inflammatory Cytokines in the Liver and Blood Vessels of ApoE$^{-/-}$ Mice

To investigate whether the pathogenic role of CML in the liver and aorta is related to inflammation, we examined the expression of IL-1β, IL-6, TNF-α, CRP mRNA in the liver and aorta. We found that IL-1β, IL-6, TNF-α, CRP mRNA expression increased

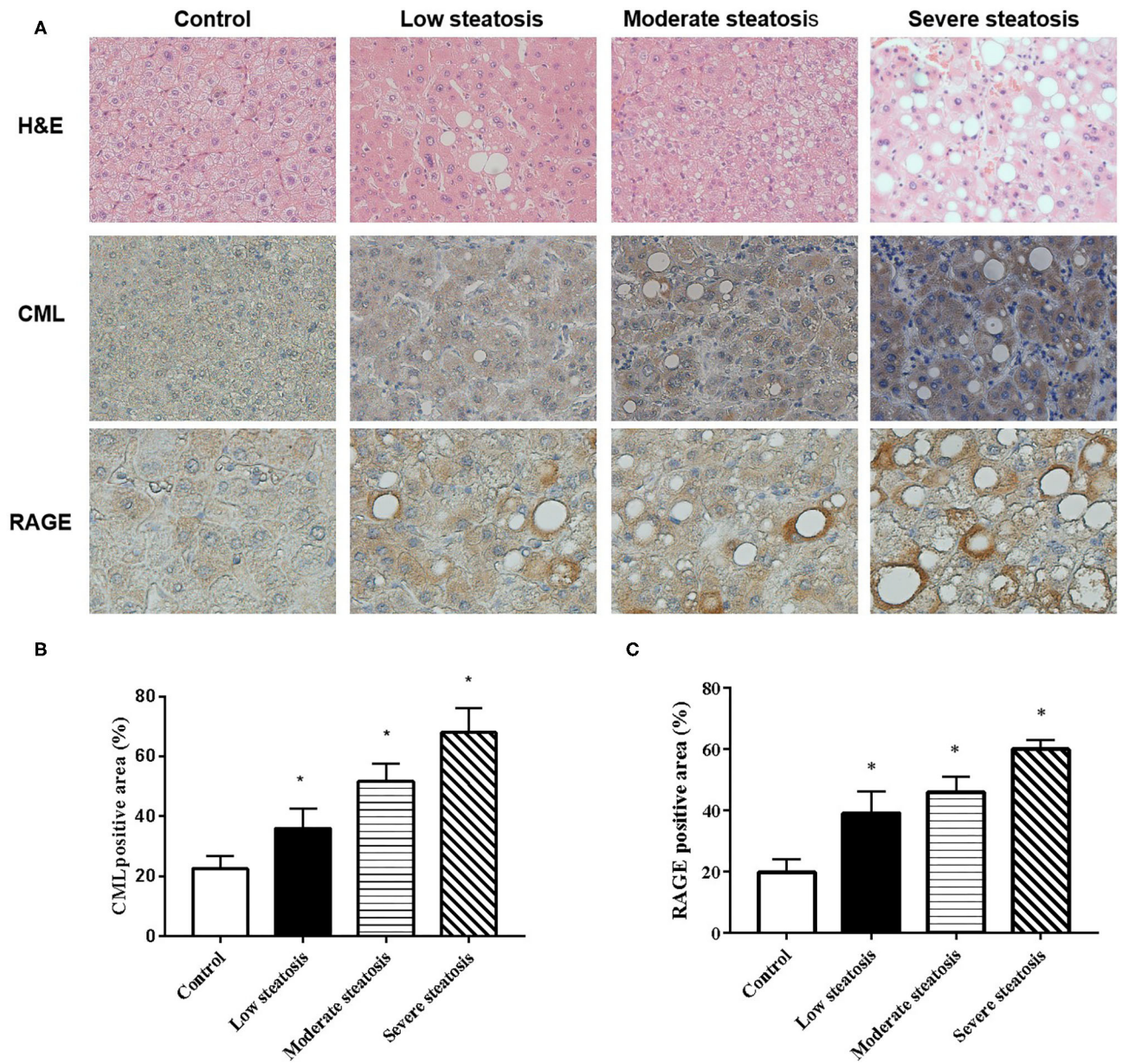

FIGURE 1 | CML accumulation in liver tissue of patients with non-alcoholic fatty liver **(A)**. First row: Liver biopsy H&E (×200). Second and third row: immunohistochemistry shows the expression of CML (×200) and RAGE (×400) **(B)**. Percentage of CML-positive immunohistochemical staining area **(C)**. Percentage of RAGE-positive immunohistochemical staining area. The proportion of the positive area to the total liver area was calculated by ImageJ. All data are expressed as the means ± SEM. *$P < 0.05$, compared to control group.

by 1.68, 2.0, 1.85, 2.51 times in liver tissues respectively compared with the control group (**Figure 6**), while IL-1β, IL-6,TNF-α CRP mRNA expression increased by 1.32, 1.87, 1.19,1.61 times in aorta (**Figure 6**).

CML Promotes the Expression of Pro-inflammatory Cytokines by RAGE

Inflammatory cell infiltration in liver and aorta were observed by H&E staining (**Figure 7**). There was no significant inflammatory cell infiltration in the control group. In the model group, infiltration of inflammatory cells in liver tissue and aortic plaques can be observed. However, after CML intervention, the inflammatory cell infiltration in the liver tissue and aortic plaques were significantly aggravated, focal necrosis of hepatocytes was observed. After silencing the expression of RAGE, the inflammatory cell infiltration in the liver tissue and aortic plaques were significantly reduced. To detect whether CML promotes the expression of pro-inflammatory cytokines by

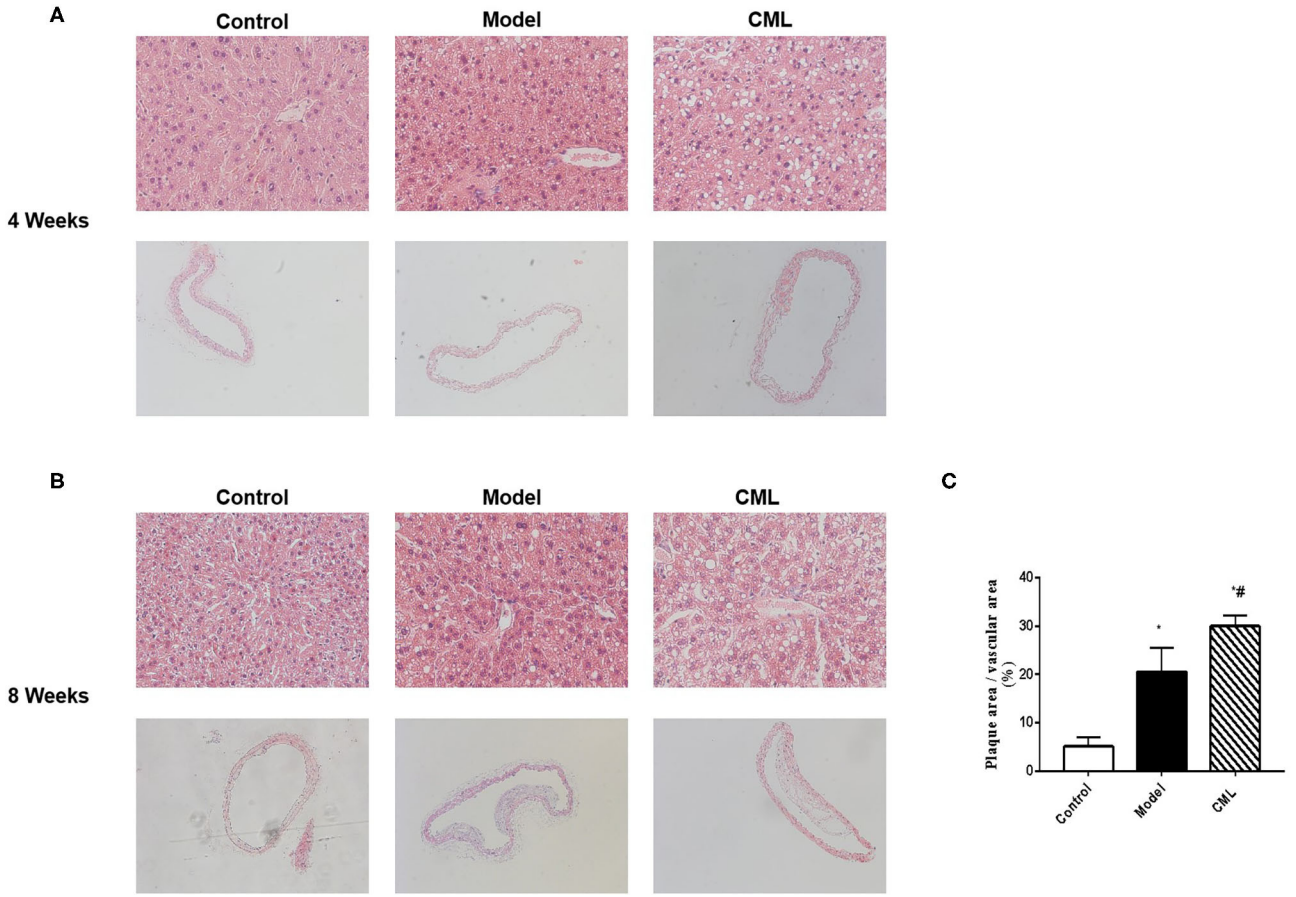

FIGURE 2 | CML promotes high fat-induced liver steatosis and intravascular plaque formation in ApoE$^{-/-}$ mice **(A,B)**. At the time of 4, 8 weeks, ApoE$^{-/-}$ mice liver (×200) and aorta H&E staining (×100) **(C)**. Image J analyzes plaque area.*$P < 0.05$, compared to control group; $^{\#}P < 0.05$, compared to model group.

upregulating the expression of RAGE, we used CML combined with AAV treatment (AAV-shRAGE and AAV-shscramble). Immunohistochemistry and quantification showed that RAGE expression did not change significantly after the injection of AAV-shscramble. AAV-shRAGE significantly downregulated the expression of RAGE (**Figures 8A,B,G,H**). We measured the expression of IL-1β, IL-6, TNF-α, and CRP mRNA in the liver and aorta (**Figures 8C–F**). The results showed that the levels of IL-1β, IL-6, TNF-α, and CRP mRNA in liver and aorta were significantly lower in the AAV-shRAGE group compared with the CML group ($P < 0.05$). This may be related to silencing the expression of RAGE down-regulating the expression of pro-inflammatory cytokines.

DISCUSSION

At present, there is a high prevalence of NAFLD in the world, which has attracted increasing attention. NAFLD includes a series of diseases, from simple fatty liver to non-alcoholic steatohepatitis (NASH), which may develop into liver cirrhosis or even liver cancer (27). Studies have shown that in the past 10 years, NAFLD has been associated with liver related incidence rate or mortality (28, 29). But most of NAFLD deaths are due to AS (30–33). In recent years, researchers have found that NAFLD may be the cause of AS, indicating that the relationship between NAFLD and AS is bidirectional or both diseases are caused by a common pathogenic link (34–37). Therefore, it is very important to find the common pathogenic factors between them.

Abnormal lipid metabolism is the basis for the occurrence of AS. Hyperlipidemia can directly cause endothelial cell dysfunction, increase the permeability of endothelial cells, and provide a basis for lipid deposition on the vascular inner membrane and platelet adhesion (38). Therefore, lipids Metabolic abnormalities are believed to be related to the acceleration of the progression of AS. As early as 1998, Professor ROSS proved that AS is a chronic persistent inflammatory disease (39). The development process of AS can be divided into lipid streak stage, fibrous plaque stage, atheroma stage, unstable plaque stage, plaque rupture and thrombosis stage. In the different development stages of AS, AS is always accompanied by inflammatory reactions (40). IL-1β, CRP, TNF-α, and IL-6 are commonly used indicators to assess the risk of cardiovascular events (41, 42). These pro-inflammatory cytokines are also closely related to the occurrence and prognosis of NAFLD disease (43,

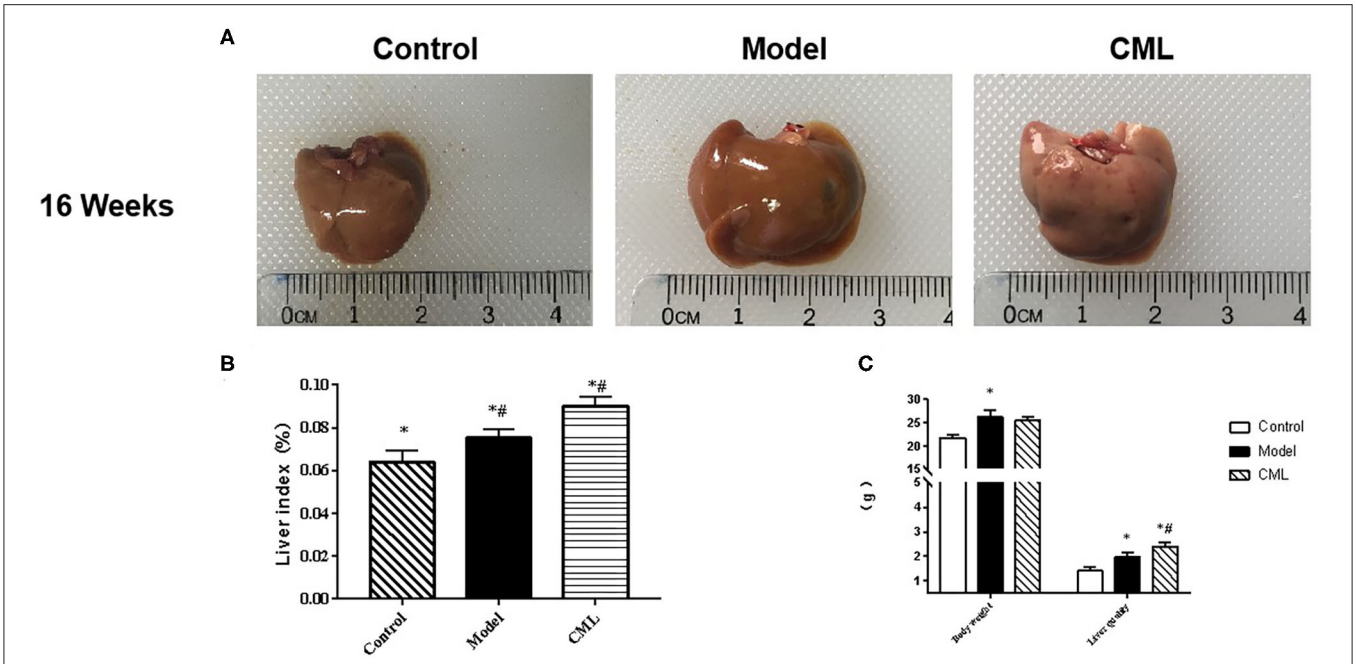

FIGURE 3 | Effect of CML on liver lipid accumulation **(A)**. Observation of overall liver morphology **(B)**. Liver body mass indexin ApoE$^{-/-}$ mice **(C)**. ApoE$^{-/-}$ mice body weight and wet liver weight. *$P < 0.05$ compared with control group; $^{\#}P < 0.05$ compared with model group.

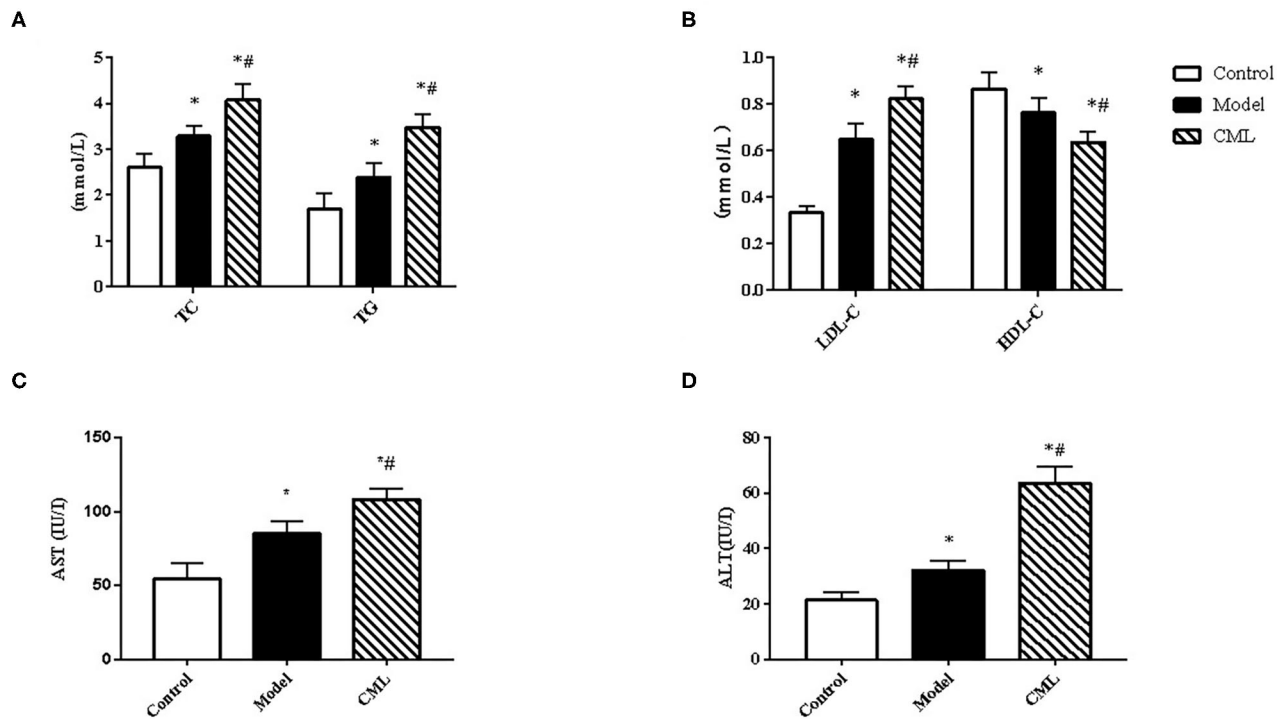

FIGURE 4 | Observe the effect of 16 weeks CML on related biochemical indexes of ApoE$^{-/-}$ mice **(A)**. Total cholesterol (TC), Triglyceride (TG) **(B)**. Low-density lipoprotein (LDL-C) and high-density lipoprotein (HDL-C) **(C)**. Aspartate aminotransferase (AST) **(D)**. Alanine aminotransferase (ALT) levels were measured using an automatic biochemical analyzer. All data are expressed as the means ± SEM. *$P < 0.05$, compared with control group; $^{\#}P < 0.05$, compared with model group.

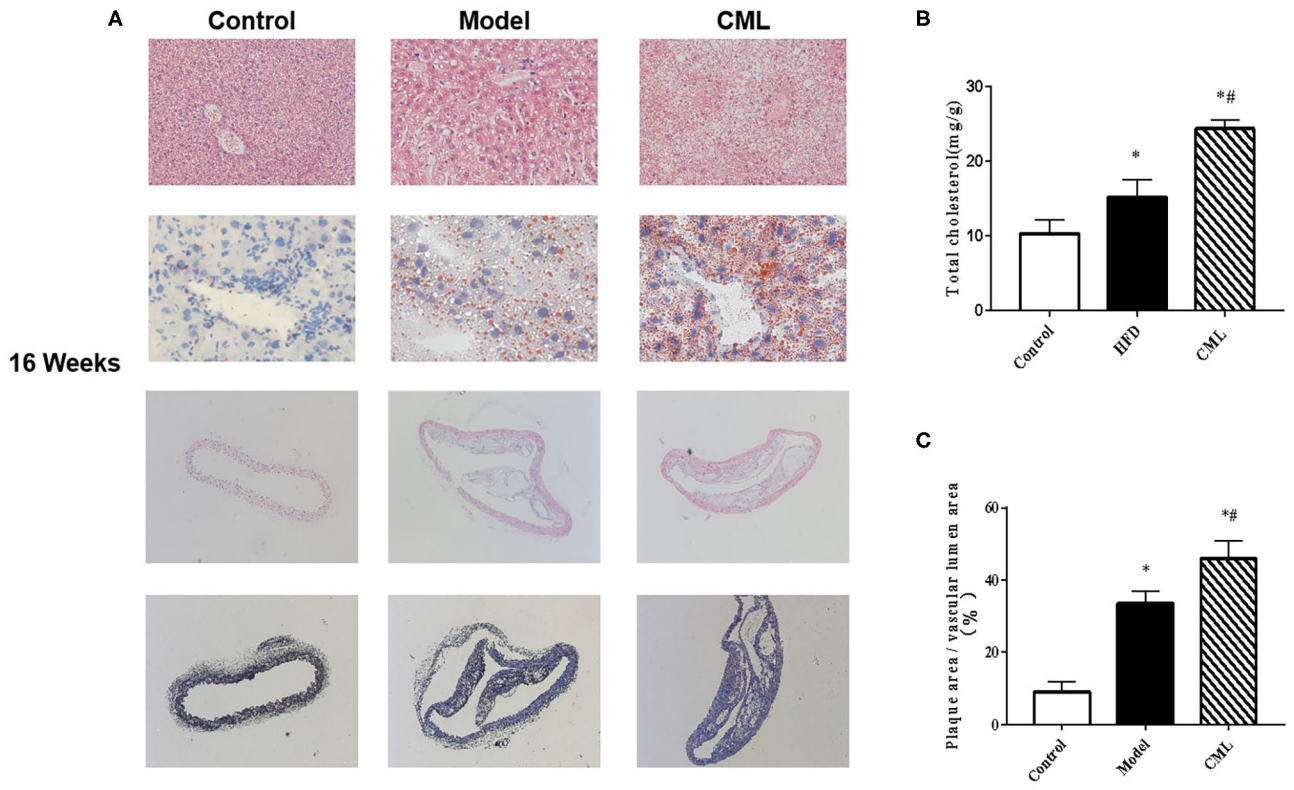

FIGURE 5 | Pathological changes of liver and aorta after ApoE$^{-/-}$ mice at the time of 16 weeks **(A)**. First row: H&E staining of ApoE$^{-/-}$ mice liver (×200). Second row: Oil Red O staining of ApoE$^{-/-}$ mice liver (×400). Third row: H&E staining of ApoE$^{-/-}$ mice aorta (×100). Fourth row: Masson staining of liver aorta in ApoE$^{-/-}$ mice (×100). **(B)**. Total cholesterol content in ApoE$^{-/-}$ mice liver **(C)**. Quantification of vascular plaque area by Image J. $^{*}P < 0.05$, compared with control group; $^{\#}P < 0.05$, compared with model group.

44). Therefore, regulating lipids and inhibiting inflammation have become an important way to combat AS in recent years. Increased fatty liver inflammation is a sign of the progression of NAFLD, therefore, inhibiting inflammation damage is also an important way to prevent and treat NAFLD (45).

Studies have found that NAFLD is formed during the occurrence and development of AS and can promote the development of AS (46). The main mechanism may be that the formation of NAFLD causes the body to be in a chronic inflammatory state for a long time, promotes the release of pro-inflammatory cytokines, leads to damage to the endothelial cells of the vascular intima, and accelerates the formation of atherosclerosis (47–49). The blood lipid metabolism disorder of NAFLD patients is manifested by plasma hypertriglyceridemia, increased low-density lipoprotein and decreased high-density lipoprotein levels, which also contribute to the development of AS (50).

In our clinical study, we found that CML aggregation in liver tissue of NAFLD patients, with the progress of liver steatosis, the expression of CML significantly increased. Therefore, we hypothesized that CML participated in the development of NAFLD, to explore the relationship between CML and non-alcoholic fatty liver and atherosclerosis. We established an *in vivo* model of ApoE$^{-/-}$ mice and monitored the liver and vascular lesions at 4, 8, and 16 weeks respectively. It was found that the fatty degeneration of the liver and the change of the plaque in the aorta gradually increased with the change of time. Moreover, fatty degeneration of liver occurs earlier than atherosclerosis.

NAFLD is a disease characterized by dyslipidemia and impaired liver function (51). Hyperlipidemia is an important risk factor for fatty liver formation. 20–92% of patients with hyperlipidemia have fatty liver (52). NAFLD is not only the excessive deposition of liver fat, but also the damage of liver cell function. AST and ALT in serum were commonly used as indexes to measure the function of hepatocytes (53). After 16 weeks of experimental intervention, serum related biochemical indexes and morphological changes of liver were detected. We found that the serum TG, TC, LDL-C, ALT, AST levels increased and HDL-C levels decreased in the model group after 16 weeks of continuous high fat feeding. The model of mice NAFLD was established successfully, and obvious plaque formation was found in the vascular lumen. After CML stimulation, the lesions of mice non-alcoholic fatty liver were aggravated and the plaque was more unstable. This confirms our hypothesis that CML is the link of NAFLD and AS.

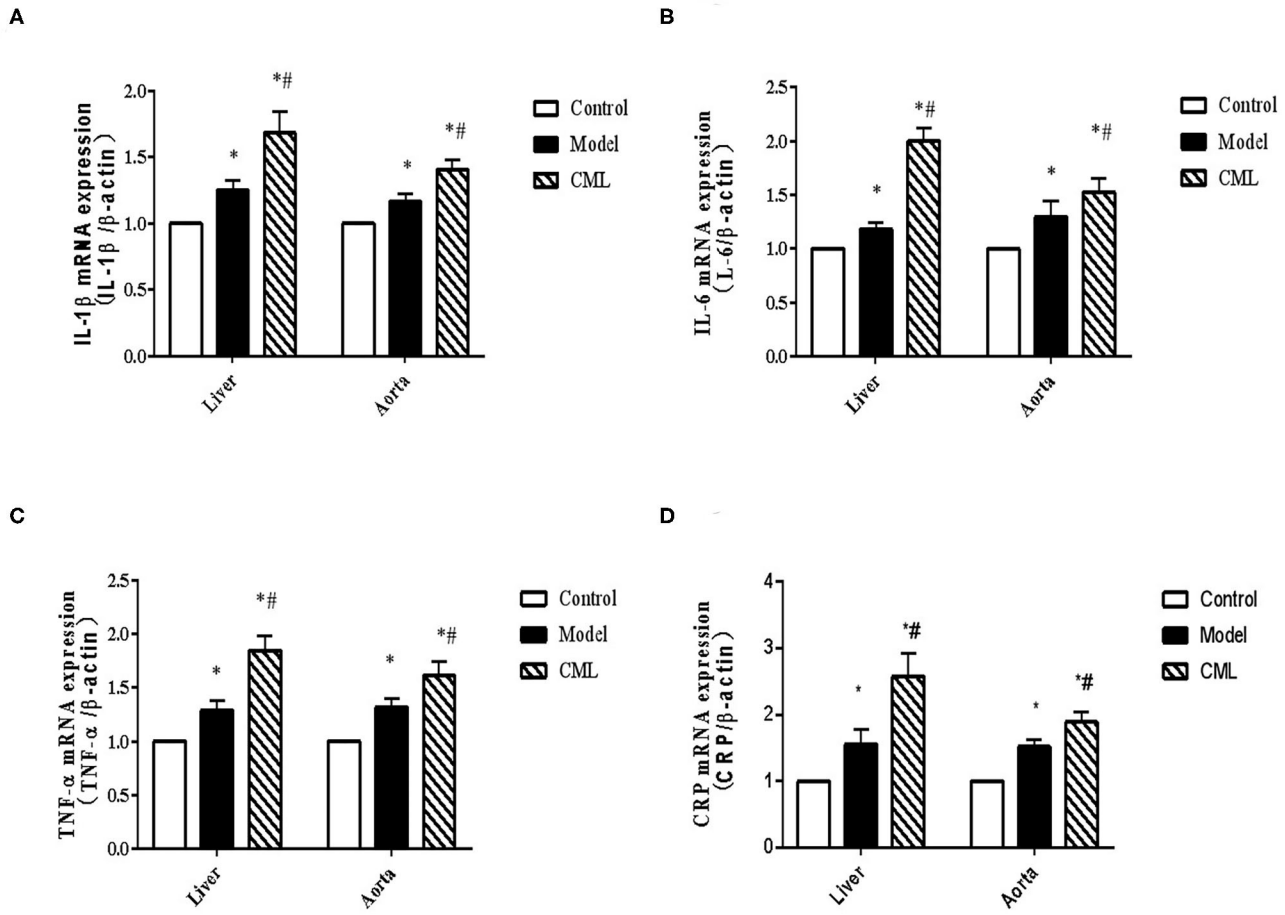

FIGURE 6 | CML promotes the expression of pro-inflammatory cytokines in liver and blood vessels of ApoE$^{-/-}$ mice **(A–D)** Detection of IL-1β, IL-6, TNF-α, CRP mRNA expression levels in liver and aorta by PCR. *$P < 0.05$, compared with control group; #$P < 0.05$, compared with model group.

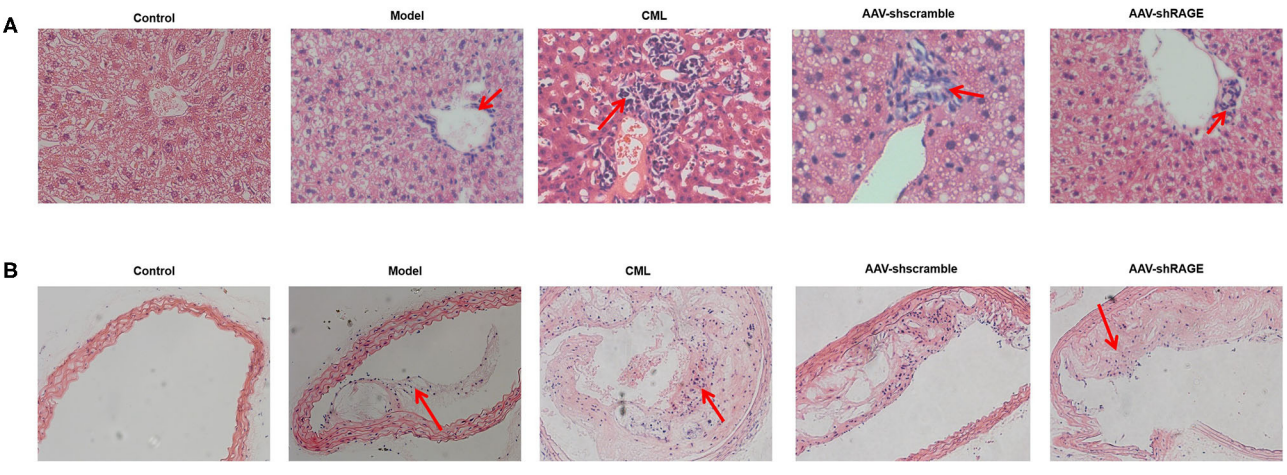

FIGURE 7 | CML increases the density of inflammatory cells infiltrating the plaque and liver **(A)** H&E staining of ApoE$^{-/-}$ mice liver (×200) **(B)** H&E staining of ApoE$^{-/-}$ mice aotra plaque (×200).The red arrow points to the location of inflammatory cell infiltration.

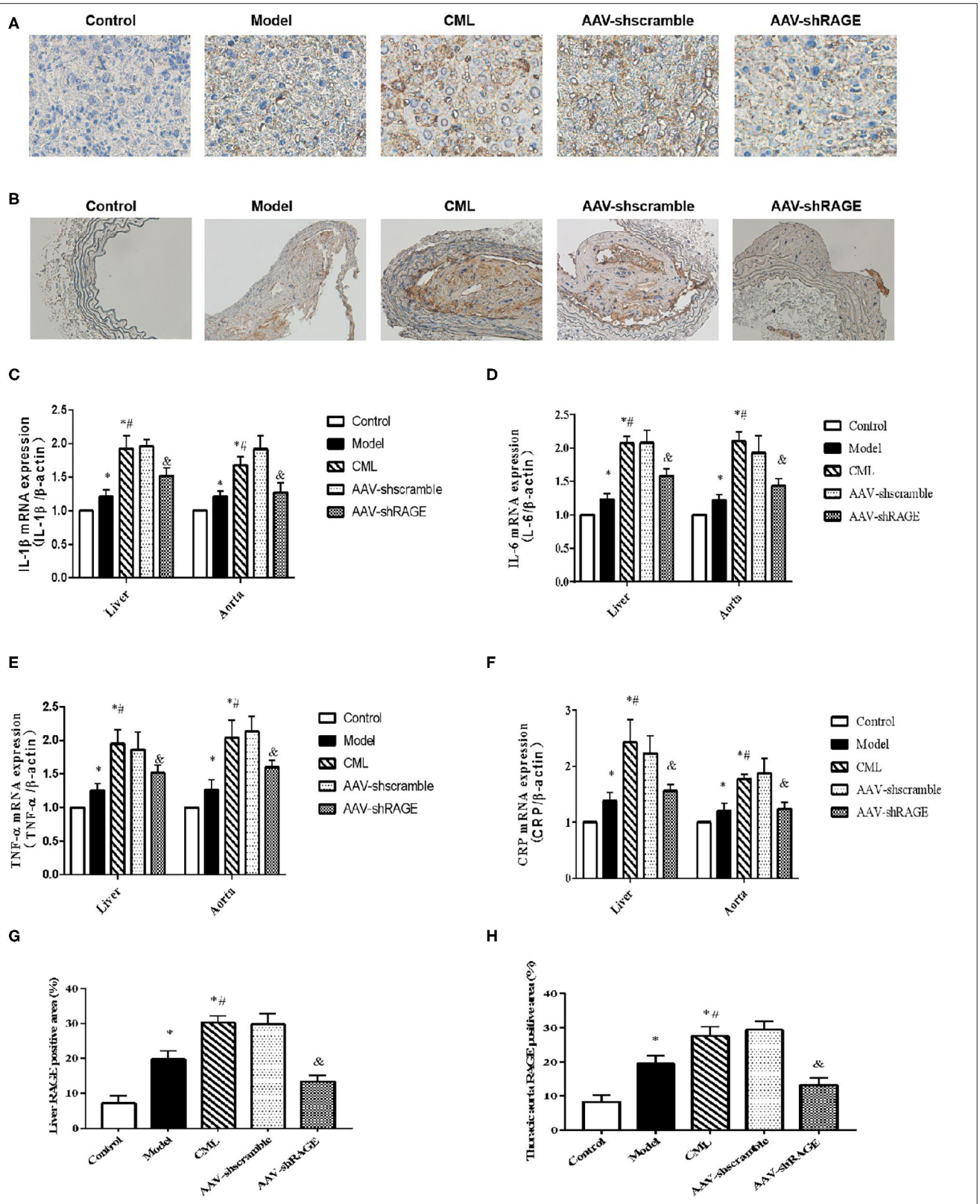

FIGURE 8 | After AAV injection, the expression of RAGE in liver and aorta changed **(A)** and **(B)** Immunohistochemistry shows the expression of RAGE (×400). **(C–F)** Detection of IL-1β, IL-6, TNF-α, CRP mRNA expression levels in liver and aorta by PCR **(G,H)** Percentage of RAGE positive immunohistochemical staining area. The proportion of the positive area to the total Liver area was calculated by ImageJ. $^{*}P < 0.05$, compared with normal control group; $^{\#}P < 0.05$, compared with model group;$^{\&}P < 0.05$, compared with CML group.

How CML mediates the pathogenesis of NAFLD and AS has attracted our attention. In clinical trials, we found that in the liver samples of NAFLD, RAGE staining was stronger and positively correlated with fatty liver degeneration. Studies have shown that RAGE is an important receptor for CML, which is difficult to clear after binding to its receptor and can activate multiple signal cascades, target genes that regulate the inflammatory response (54). Excessive inflammation is not only a sign of the progression of NAFLD to Non-alcoholic steatohepatitis (NASH) but also an important influencing factor of as progress (55–57). *In vivo* study, we found that after CML stimulation, significant infiltration of inflammatory cells and focal necrosis were observed in liver tissue. This may indicate that CML can promote the progression of NAFLD to NASH.

The expression levels of RAGE and pro-inflammatory cytokines IL-1β, IL-6, TNF-α, CRP in liver and aorta were significantly increased after CML stimulation. In this study, when RAGE was silenced, the expression level of pro-inflammatory cytokines was down regulated, which significantly alleviated the pathological changes of NAFLD and AS. This finding indicates that CML is responsible for the up-regulation of pro-inflammatory cytokines by up-regulating RAGE expression.

In this study, we confirmed that the activation of CML/RAGE signal leads to an imbalance in pro-inflammatory cytokine expression mediates the development of NAFLD and AS. Inhibition of CML/RAGE signal in liver can inhibit the occurrence of NAFLD and delay the progression of AS. It is hoped that our findings could provide a worthwhile intervention target for the treatment and prevention of AS in NAFLD.

DATA AVAILABILITY STATEMENT

The datasets presented in this study can be found in online repositories. The names of the repository/repositories and accession number(s) can be found in the article/**Supplementary Material**.

ETHICS STATEMENT

The animal study was reviewed and approved by Institutional Animal Care and Use Committee at Jiangsu University. Human studies conform to the principles outlined in the Declaration of Helsinki (1964) and was approved by the Ethical Committee of the Affiliated Hospital of Jiangsu University. All patients agreed and signed informed consent before enrollment.

AUTHOR CONTRIBUTIONS

QP designed experimental ideas, completed experiments, and analyzed data. ZW provided suggestions for experimental design. ZB and ZS assisted the analysis of experimental data. LZ and LJ assisted in collecting clinical data. LL assisted in preparing sections and assessing the degree of liver tissue lesion. CS, HC, and LW supervised the experiment and read and approved the final draft. QP completed the manuscript with the help of everyone. All authors are involved in experimental research.

FUNDING

This work was supported as follows: the National Natural Science Foundation of China (81770450, 81370408); the related Foundation of Jiangsu Province (WSN-044, LGY2018092, QNRC2016836); Postgraduate Research & Practice Innovation Program of Jiangsu Province (SJKY19_2585, KYCX20_2881); Zhenjiang Cardiovascular Clinical Research Center Project (SS2018008).

SUPPLEMENTARY MATERIAL

The Supplementary Material for this article can be found online at: https://www.frontiersin.org/articles/10.3389/fmed.2020.583943/full#supplementary-material

REFERENCES

1. Zelber-Sagi S, Ratziu V, Oren R. Nutrition and physical activity in NAFLD: an overview of the epidemiological evidence. *World J Gastroenterol.* (2011) 17:3377–89. doi: 10.3748/wjg.v17.i29.3377
2. Dongiovanni P, Romeo S, Valenti L. Genetic factors in the pathogenesis of nonalcoholic fatty liver and steatohepatitis. *Biomed Res Int.* (2015) 2015:1–10. doi: 10.1155/2015/460190
3. Romero FA, Jones CT, Xu Y, Fenaux M, Halcomb RL. The race to bash NASH: emerging targets and drug development in a complex liver disease. *J Med Chem.* (2020) 63:5031–73. doi: 10.1021/acs.jmedchem.9b01701
4. Sherif ZA, Saeed A, Ghavimi S, Nouraie SM, Laiyemo AO, Brim H, et al. Global epidemiology of non-alcoholic fatty liver disease and perspectives on US minority populations. *Dig Dis Sci.* (2016) 61:1214–25. doi: 10.1007/s10620-016-4143-0
5. Ismail MH. Nonalcoholic fatty liver disease and type 2 diabetes mellitus: the hidden epidemic. *Am J Med Sci Jun.* (2011) 341:485–92. doi: 10.1097/MAJ.0b013e3182018598
6. Younossi ZM, Golabi P, de Avila L, Paik JM, Srishord M, Fukui N, et al. The global epidemiology of NAFLD NASH in patients with type 2 diabetes: a systematic review meta-analysis. *J Hepatol.* (2019) 71:793–801. doi: 10.1016/j.jhep.2019.06.021
7. Fracanzani AL, Valenti L, Bugianesi E, Andreoletti M, Colli A, Vanni E, et al. Risk of severe liver disease in nonalcoholic fatty liver disease with normal aminotransferase levels: a role for insulin resistance and diabetes. *Hepatology.* (2008) 48:792–8. doi: 10.1002/hep.22429
8. Kotronen A, Juurinen L, Hakkarainen A, Westerbacka J, Cornér A, Bergholm R, et al. Liver fat is increased in type 2 diabetic patients and underestimated by serum alanine aminotransferase compared with equally obese nondiabetic subjects. *Diabetes Care.* (2008) 31:165–9. doi: 10.2337/dc07-1463
9. Gastaldelli A, Cusi K, Pettiti M, Hardies J, Miyazaki Y, Berria R, et al. Relationship between hepatic/visceral fat and hepatic insulin resistance in nondiabetic and type 2 diabetic subjects. *Gastroenterology.* (2007) 133:496–506. doi: 10.1053/j.gastro.2007.04.068
10. Mantovani A. Nonalcoholic Fatty Liver Disease (NAFLD) and risk of cardiac arrhythmias: a new aspect of the liver-heart axis. *J Clin Transl Hepatol.* (2017) 5:134–41. doi: 10.14218/JCTH.2017.00005
11. Tana C, Ballestri S, Ricci F, Di Vincenzo A, Ticinesi A, Gallina S, et al. Cardiovascular risk in non-alcoholic fatty liver disease: mechanisms and therapeutic implications. *Int J Environ Res Public Health.* (2019) 16:3104–23. doi: 10.3390/ijerph16173104

12. Sookoian S, Pirola CJ. Non-alcoholic fatty liver disease is strongly associated with carotid atherosclerosis: a systematic review. *J Hepatol.* (2008) 49:600–7. doi: 10.1016/j.jhep.2008.06.012
13. Day CP, James OF. Steatohepatitis: a tale of two "hits"? *Gastroenterology.* (1998) 114:842–5. doi: 10.1016/S0016-5085(98)70599-2
14. Dos Santos JM, Tewari S, Mendes RH. The role of oxidative stress in the development of diabetes mellitus and its complications. *J Diabetes Res.* (2019) 2019:189813. doi: 10.1155/2019/4189813
15. Baynes JW, Thorpe SR. Role of oxidative stress in diabetic complications: a new perspective on an old paradigm. *Diabetes.* (1999) 48:1–9. doi: 10.2337/diabetes.48.1.1
16. Gaens KH, Stehouwer CD, Schalkwijk CG. The N^{ε}-(carboxymethyl)lysine -RAGE axis: putative implications for the pathogenesis of obesity-related complications. *Endocrinol Metab.* (2010) 5:839–54. doi: 10.1586/eem.10.68
17. Fu MX, Requena JR, Jenkins AJ, Lyons TJ, Baynes JW, Thorpe SR. The advanced glycation end product, Nepsilon-(carboxymethyl)lysine, is a product of both lipid peroxidation and glycoxidation reactions. *J Biol Chem.* (1996) 271:9982–6. doi: 10.1074/jbc.271.17.9982
18. Wang Z, Jiang Y, Liu N, Ren L, Zhu Y, An Y, et al. Advanced glycation end-product N^{ε}-carboxymethyl-Lysine accelerates progression of atherosclerotic calcification in diabetes. *Atherosclerosis.* (2012) 221:387–96. doi: 10.1016/j.atherosclerosis.2012.01.019
19. Stojsavljević S, Gomerčić Palčić M, Virović Jukić L, Smirčić Duvnjak L, Duvnjak M. Adipokines proinflammatory cytokines, the key mediators in the pathogenesis of nonalcoholic fatty liver disease. *World J Gastroenterol.* (2014) 20:18070–91. doi: 10.3748/wjg.v20.i48.18070
20. Nonaka K, Kajiura Y, Bando M, Sakamoto E, Inagaki Y, Lew JH, et al. Advanced glycation end-products increase IL-6 and ICAM-1 expression via RAGE, MAPK and NF-κB pathways in human gingival fibroblasts. *J Periodontal Res.* (2018) 53:334–44. doi: 10.1111/jre.12518
21. Liu SH, Sheu WH, Lee MR, Lee WJ, Yi YC, Yang TJ, et al. Advanced glycation end product N^{ε} - carboxymethyllysine induces endothelial cell injury: the involvement of SHP-1-regulated VEGFR-2 dephosphorylation. *Pathology.* (2013) 230:215–27. doi: 10.1002/path.4045
22. Wood TT, Winden DR, Marlor DR, Wright AJ, Jones CM, Chavarria M, et al. Acute secondhand smoke-induced pulmonary inflammation is diminished in RAGE knockout mice. *Am J Physiol Lung Cell Mol Physiol.* (2014) 307:758–64. doi: 10.1152/ajplung.00185.2014
23. Wang Z, Yan J, Li L, Liu N, Liang Y, Yuan W, et al. Effects of N^{ε} - carboxymethyl-lysine on ERS-mediated apoptosis in diabetic atherosclerosis. *Int J Cardiol.* (2014) 172:478–83. doi: 10.1016/j.ijcard.2014.01.031
24. Araki E, Nishikawa T. Oxidative stress: a cause and therapeutic target of diabetic complications. *J Diabetes Investig.* (2010) 1:90–6. doi: 10.1111/j.2040-1124.2010.00013.x
25. Allahverdian S, Chehroudi AC, McManus BM, Abraham T, Francis GA. Contribution of intimal smooth muscle cells to cholesterol accumulation and macrophage-like cells in human atherosclerosis. *Circulation.* (2014) 129:1551–9. doi: 10.1161/CIRCULATIONAHA.113.005015
26. Butscheid M, Hauptvogel P, Fritz P, Klotz U, Alscher DM. Hepaticexpressionofgalectin-3 and receptor for advanced glycationend products inpatients with liver disease. *J Clin Pathol.* (2007) 60:415–8. doi: 10.1136/jcp.2005.032391
27. Oates JR, McKell MC, Moreno-Fernandez ME, Damen MSMA, Deepe GS, Qualls JE, et al. Macrophage function in the pathogenesis of non-alcoholic fatty liver disease: the mac attack. *Front Immunol.* (2019) 10:2893–920. doi: 10.3389/fimmu.2019.02893
28. Angulo P, Hui JM, Marchesini G, Bugianesi E, George J, Farrell GC, et al. The NAFLD fibrosis score: a noninvasive system that identifies liver fibrosis in patients with NAFLD. *Hepatology.* (2007) 45:846–54. doi: 10.1002/hep.21496
29. Chalasani N, Younossi Z, Lavine JE, Diehl AM, Brunt EM, Cusi K, et al. The diagnosis and management of non-alcoholic fatty liver disease: practice guideline by the American gastroenterological association, American Association for the study of liver diseases, and American College of Gastroenterology. *Gastroenterology.* (2012) 142:1592–609. doi: 10.1053/j.gastro.2012.04.001
30. Ong JP, Pitts A, Younossi ZM. Increased overall mortality and liver-related mortality in non-alcoholic fatty liver disease. *J Hepatol.* (2008) 49:608–12. doi: 10.1016/j.jhep.2008.06.018
31. Söderberg C, Stål P, Askling J, Glaumann H, Lindberg G, Marmur J, et al. Decreased survival of subjects with elevated liver function tests during a 28-year follow-up. *Hepatology.* (2010) 51:595–602. doi: 10.1002/hep.23314
32. Lonardo A, Targher G. Cardiovascular risk in NAFLD: an intimate relationship? *Dig Dis Sci.* (2019) 5:595–602. doi: 10.1007/s10620-019-05996-7
33. Stepanova M, Younossi ZM. Independent association between nonalcoholic fatty liver disease and cardiovascular disease in the US population. *Clin Gastroenterol Hepatol.* (2012) 10:646–50. doi: 10.1016/j.cgh.2011.12.039
34. Targher G, Byrne CD, Lonardo A, Zoppini G, Barbui C. Nonalcoholic fatty liver disease and risk of incident cardiovascular disease: a meta-analysis of observational studies. *J Hepatol.* (2016) 65:589–600. doi: 10.1016/j.jhep.2016.05.013
35. Baratta F, Pastori D, Angelico F, Balla A, Paganini AM, Cocomello N, et al. Nonalcoholic fatty liver disease and fibrosis associated with increased risk of cardiovascular events in a prospective study. *Clin Gastroenterol Hepatol.* (2020) 18:2324–31.e4. doi: 10.1016/j.cgh.2019.12.026
36. Lonardo A, Lombardini S, Scaglioni F, Ballestri S, Verrone AM, Bertolotti M, et al. Fatty liver, carotid disease and gallstones: a study of age related associations. *World J Gastroenterol.* (2006) 12:5826–33. doi: 10.3748/wjg.v12.i36.5826
37. Santos RD, Valenti L, Romeo S. Does nonalcoholic fatty liver disease cause cardiovascular disease? Current knowledge and gaps. *Atherosclerosis.* (2019) 282:110–20. doi: 10.1016/j.atherosclerosis.2019.01.029
38. Novák J, Bienertová-Vašku J, Kára T, Novák M. MicroRNAs involved in the lipid metabolism and their possible implications for atherosclerosis development and treatment. *Mediat Inflamm.* (2014) 2014:1–14. doi: 10.1155/2014/275867
39. Ross R. Atherosclerosis an inflamrnatory disease. *N Engl J Med.* (1999) 340:15–26. doi: 10.1056/NEJM199901143400207
40. Kim MJ, Jung SK. Nutraceuticals for prevention of atherosclerosis: targeting monocyte infiltration to the vascular endotheliu. *J Food Biochem.* (2020) 446:1–12. doi: 10.1111/jfbc.13200
41. Wang J, Du A, Wang H, Li Y. MiR-599 regulates LPS-mediated apoptosis and inflammatory responses through the JAK2/STAT3 signaling pathway via targeting ROCK1 in human umbilical vein endothelial cells. *Clin Exp Pharmacol Physiol.* (2020) 478:1420–8. doi: 10.1111/1440-1681.13316
42. Tuttolomondo A, Di Raimondo D, Pecoraro R, Arnao V, Pinto A, Licata G. Atherosclerosis as an inflammatory disease. *Curr Pharm Des.* (2012) 18:4266–88. doi: 10.2174/138161212802481237
43. Lizardi-Cervera J, Chavez-Tapia NC, Pérez-Bautista O, Ramos MH, Uribe M. Association among C-reactive protein, fatty liver disease, and cardiovascular risk. *Curr Pharm Des.* (2007) 52:2375–9. doi: 10.1007/s10620-006-9262-6
44. Zhou Y, Dong B, Kim KH, Choi S, Sun Z, Wu N, et al. Vitamin D receptor activation in liver macrophages protects against hepatic endoplasmic reticulum stress in mice. *Hepatology.* (2020) 71:1453–66. doi: 10.1002/hep.30887
45. Fabbrini E, Sullivan S, Klein S. Obesity and nonalcoholic fatty liver disease: biochemical, metabolic, and clinical implications. *Hepatology.* (2010) 51:679–89. doi: 10.1002/hep.23280
46. Zhang L, She ZG, Li H, Zhang XJ. Non-alcoholic fatty liver disease: a metabolic burden promoting atherosclerosis. *Clin Sci.* (2020) 134:1775–99. doi: 10.1042/CS20200446
47. Srivastava RAK. Life-style-induced metabolic derangement and epigenetic changes promote diabetes and oxidative stress leading to NASH and atherosclerosis severity. *J Diabetes Metab Disord.* (2018) 17:381–91. doi: 10.1007/s40200-018-0378-y
48. Haukeland JW, Damås JK, Konopski Z, Løberg EM, Haaland T, Goverud I, et al. Systemic inflammation in nonalcoholic fatty liver disease is characterized by elevated levels of CCL2. *Hepatology.* (2006) 44:1167–74. doi: 10.1016/j.jhep.2006.02.011
49. Lombardi R, Fargion S, Fracanzani AL. Brain involvement in non-alcoholic fatty liver disease (NAFLD): a systematic review. *Dig Liver Dis.* (2019) 51:1214–22. doi: 10.1016/j.dld.2019.05.015
50. Deprince A, Haas JT, Staels B. Dysregulated lipid metabolism links NAFLD to cardiovascular disease. *Mol Metab.* (2020) 30:1–45. doi: 10.1016/j.molmet.2020.101092

51. Bellentani S, Scaglioni F, Marino M, Bedogni G. Epidemiology of non-alcoholic fatty liver disease. *Digest Dis.* (2010) 28:55–61. doi: 10.1159/000282080
52. Cullis PR, Chonn A, Semple SC. Interactions of liposomes and lipid-based carrier systems with blood proteins: relation to clearance behaviour *in vivo*. *Adv Drug Deliver Rev.* (1998) 32:3–17. doi: 10.1016/S0169-409X(97)00128-2
53. Verma S, Jensen D, Hart J, Mohanty SR. Predictive value of ALT levels for non-alcoholic steatohepatitis (NASH) and advanced fibrosis in non-alcoholic fatty liver disease (NAFLD). *Liver Int.* (2013) 33:398–405. doi: 10.1111/liv.12226
54. Kislinger T, Fu C, Huber B, Qu W, Taguchi A, Du Yan S, et al. N(epsilon)-(carboxymethyl)lysine adducts of proteins are ligands for receptor for advanced glycation end products that activate cell signaling pathways and modulate gene expression. *J Biol Chem.* (1999) 274:31740–9. doi: 10.1074/jbc.274.44.31740
55. Katsiki N, Imprialos K, Vlachopoulos C. Editorial: arterial stiffness, central haemodynamics and nonalcoholic fatty liver disease: links with cardiovascular risk and effects of drug treatment. *Curr Vasc Pharmacol.* (2018) 16:401–4. doi: 10.2174/1570161116666171205105402
56. Lonardo A, Lugari S, Ballestri S, Nascimbeni F, Baldelli E, Maurantonio M. A round trip from nonalcoholic fatty liver disease to diabetes: molecular targets to the rescue? *Acta Diabetol.* (2019) 56:385–96. doi: 10.1007/s00592-018-1266-0
57. Schulz E, Anter E, Keaney JF. Oxidative stress, antioxidants, and endothelial function. *Curr Med Chem.* (2004) 11:1093–104. doi: 10.2174/0929867043365369

Conflict of Interest: The authors declare that the research was conducted in the absence of any commercial or financial relationships that could be construed as a potential conflict of interest.

frontiers in Medicine

ORIGINAL RESEARCH
published: 10 November 2020
doi: 10.3389/fmed.2020.584871

Preoperative Albumin–Bilirubin Grade With Prognostic Nutritional Index Predicts the Outcome of Patients With Early-Stage Hepatocellular Carcinoma After Percutaneous Radiofrequency Ablation

*Jingying Pan, Shuochun Chen, Guo Tian and Tianan Jiang**

Department of Ultrasound, The First Affiliated Hospital of Zhejiang University, Hangzhou, China

OPEN ACCESS

Edited by:
Xiaojun Chen,
Nanjing Medical University, China

Reviewed by:
Mousumi Chaudhury,
Arkansas Children's Nutrition Center, United States
Xiaofei Sun,
University of California, San Francisco, United States

***Correspondence:**
Tianan Jiang
tiananjiang@zju.edu.cn

Specialty section:
This article was submitted to Gastroenterology, a section of the journal Frontiers in Medicine

Received: *18 July 2020*
Accepted: *12 October 2020*
Published: *10 November 2020*

Citation:
Pan J, Chen S, Tian G and Jiang T (2020) Preoperative Albumin–Bilirubin Grade With Prognostic Nutritional Index Predicts the Outcome of Patients With Early-Stage Hepatocellular Carcinoma After Percutaneous Radiofrequency Ablation. Front. Med. 7:584871. doi: 10.3389/fmed.2020.584871

Background: Prognostic nutritional index (PNI) that was designed to assess the nutritional and immunological status of patients and albumin–bilirubin (ALBI) grades can be used as an assessment tool for hepatic function. Both nutritional and immunological statuses have been reported to be independent prognostic factors of patients with hepatocellular carcinoma (HCC). This study aimed to investigate whether PNI together with ALBI could be a better predictor in patients with early-stage HCC undergoing radiofrequency ablation (RFA).

Method: The information of 110 patients with newly diagnosed HCC within the Milan criteria receiving RFA as the initial therapy between 2014 and 2015 was retrospectively collected. Pretreatment PNI, ALBI, and PNI-ALBI grades were calculated. Overall survival (OS) and recurrence-free survival (RFS) were estimated by the Kaplan–Meier method, and multivariate analysis was used to identify prognostic factors.

Result: The 1-, 3-, and 5-years OS rates of patients were 80.0, 30.9, and 23.9%, respectively. Multivariate analysis showed that the tumor size [hazard ratio (HR) = 1.966, 95% confidence interval (CI) = 1.091–3.545, $P = 0.025$], PNI grade (H = 2.558, 95% CI = 1.289–5.078, $P = 0.007$), and PNI-ALBI grade (HR = 3.876, 95% CI = 1.729–8.690, $P = 0.001$) were independent risk factors for OS, whereas only the elevated α-fetoprotein (HR = 1.732, 95% CI = 1.003–2.991, $P = 0.049$) and the size of the tumor (HR = 1.640, 95% CI = 1.015–2.647, $P = 0.43$) were independent predictors for better RFS.

Conclusion: This study demonstrates that preoperative PNI-ALBI grade is a simple and useful predictor for OS in patients with early-stage HCC after RFA.

Keywords: hepatocellular carcinoma, radiofrequency ablation, prognostic nutritional index, albumin-bilirubin, overall survival

INTRODUCTION

Liver cancer is the sixth most frequent malignancy, ranked as the fifth most common in men, and ninth in women, respectively. It is the fourth leading cause of cancer-related deaths worldwide, next to lung, colorectal, and stomach cancers (1). Hepatocellular carcinoma (HCC) accounts for ∼75% of all liver cancers and is the most common primary liver tumor (2).

The main risk factors for HCC include chronic infection with hepatitis B virus (HBV) or hepatitis C virus (HCV), aflatoxin exposure, etc. However, in most cases, particularly in high-risk areas, HCC develops as a sequela to protracted chronic infection with the HBV or HCV, with or without the development of liver cirrhosis (3).

Although there is a significant improvement in the clinical diagnosis and treatment of HCC, however, with the deterioration in the liver function, high recurrence rates, and distant metastasis, the rates of morbidity and mortality of HCC continue to increase (4).

Percutaneous radiofrequency ablation (RFA) is recognized as an important alternative treatment for small HCCs and cases where resection cannot be performed, due to location, tumor size, multimodality, or inadequate function. RFA can cause necrosis of the tissues of hepatic carcinoma by thermal coagulation (5). It was confirmed to be an effective therapy in patients with hepatic cirrhosis and in single HCC $\leq$5 cm in diameter or up to three HCCs each 3 cm or smaller, and there was no significant difference between the survival rate of RFA and surgical resection (6, 7). Thus, the good candidates for RFA are patients with early-stage HCC (single tumor $\leq$5 cm in diameter, or tumor number $\leq$3 with the maximum diameter of each $\leq$3 cm) (8). But if the HCC diameter is larger than 4 cm, it is not considered to be much effective (9). In RFA, a solitary inserted electrode can cause necrosis of an area with a diameter of $\leq$3 cm and ablate 2-cm tumor completely (10). Also, RFA has effects that are similar to the microwave ablation and cryoablation, but it has become more common because of the prevalence and convenience of the device. However, the methods for assessing the survival outcomes of the postoperative patients were limited.

The assessment of liver function and failure is vital in predicting overall survival (OS) of the patients with HCC. The Child–Pugh (C-P) grade has been widely used in the assessment of preoperative liver function in clinical practice, and it is based on a score derived from five parameters, including conventional liver function tests, extent of ascites, and degree of hepatic encephalopathy. However, the grading of ascites and encephalopathy can be highly subjective, which could introduce confounding evaluation (11, 12). A new model named the albumin–bilirubin (ALBI) grade was first defined by Johnson et al. (13), and it is one of the best indicators of liver function and showed better discriminative performance than C-P grade. A recent study found that the ALBI grade predicted recurrence-free survival (RFS) and OS more accurately than the CP grade in patients with HCC undergoing liver resection with curative intent (14, 15). ALBI was calculated by two objective variables (albumin and bilirubin), and it was used to stratify patients with HCC into three categories of liver function risk. The higher the ALBI grade, the poorer was the patient's outcome. For the ALBI grade, the following formula was used: ALBI = ($\log_{10}$ bilirubin (μmol/L) $\times$ 0.66) + (albumin (g/L) $\times$ −0.085) (13). ALBI values had three grades. The cutoff points were as follows: grade 0 (<-2.60), grade 1 (>-2.60 to ≤ -1.39), and grade 2 (>-1.39).

The prognostic nutritional index (PNI) was originally proposed to assess the nutritional status and predict the surgical risk in gastrointestinal surgery patients by Buzby et al. (16), and Onodera et al. corroborated this in 1984 (17). Since then, further function of PNI was investigated, and a large amount of recent studies found this index to be associated with the prognosis of patients with different types of solid tumors, such as lung cancer, gastric cancer, colorectal cancer, and esophageal carcinoma (18–21). In patients with early-stage HCC, increasing evidence shows that PNI is an effective independent factor of the OS after RFA (15). The following formula was used for PNI: serum albumin (g/L) + 0.005 $\times$ absolute lymphocyte count (per mm^3) (17). However, the combination of ALBI and PNI, which can evaluate both the nutritional immunological status and hepatic function, has never been applied in the prognosis of the HCC patients. In this study, a new index, the PNI-ALBI grade, was put up, and its prognostic significance in HCC patients was assessed.

PATIENTS AND METHODS

The study was conducted in patients with HCC receiving RFA as initial therapy in the First Affiliated Hospital of Zhejiang University between January 2014 and December 2015.

All early-stage HCC patients during the same period who met the following criteria were included in this retrospective study: (1) early-stage HCC (single tumor $\leq$5 cm in diameter, or tumor number $\leq$3, a maximum diameter of each $\leq$3 cm), (2) no extrahepatic metastasis or major vascular invasion, (3) platelet count >50,000/mm^3, (4) patients who refused surgical treatment, (5) the patients with a pathological diagnosis of

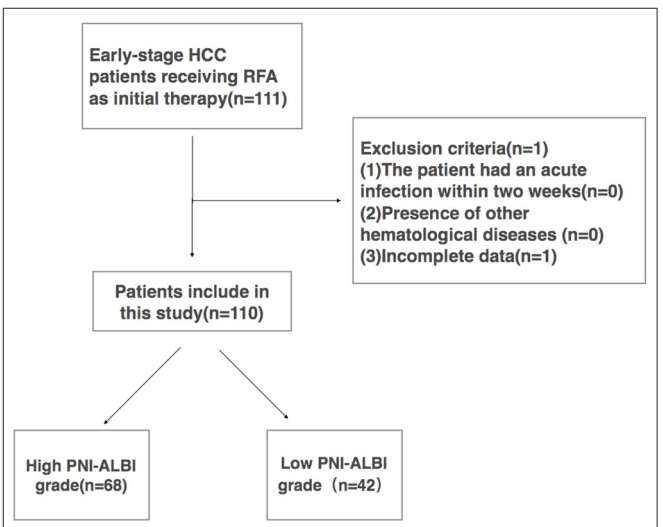

FIGURE 1 | Flowchart of this study. RFA, radiofrequency ablation.

TABLE 1 | Baseline characteristics of the patients.

Clinicopathological feature	Number (%) of patients or Mean ± *SD*
Age	
<55 years	43 (39.1%)
≥55 years	67 (60.9%)
Gender	
Female	18 (16.4%)
Male	92 (83.6%)
Family cases	
Yes	16 (14.5%)
No	96 (85.5%)
Tumor size	
>2.5 cm	30 (27.3%)
≤2.5 cm	80 (72.7%)
TNM stage	
I	112 (93.3%)
II	8 (6.7%)
Hypertension	
Yes	21 (19.1%)
No	89 (80.9%)
Diabetes mellitus	
Yes	19 (17.3%)
No	91 (82.7%)
Ascites	
Yes	14 (12.7%)
No	96 (87.3%)
Splenomegaly	
Yes	79 (71.8%)
No	31 (27.3%)
Cirrhosis	
Yes	80 (72.7%)
No	30 (27.3%)
HBsAg	
Present	101 (91.8%)
Absent	9 (8.2%)
AFP (μg/L)	
Normal	90 (81.8%)
Abnormal	20 (18.2%)
ALBI grade	
1	54 (49.1%)
2	54 (49.1%)
3	2 (1.8%)
PNI	
>47.2	47 (42.7%)
≤ 47.2	63 (57.3%)
PNI-ALBI grade	
0	42 (38.2%)
1	68 (61.8%)
WBC ($\times 10^3/\mu L$)	4.39 ± 1.72
Platelet count ($\times 10^9$/L)	106.31 ± 57.46
Prothrombin time (s)	16.02 ± 34.78
Albumin (g/L)	39.06 ± 5.16
Total bilirubin (μmol/L)	19.01 ± 9.48

SD, standard deviation; TNM, tumor–node–metastasis; HBsAg, positive hepatitis B surface antigen; AFP, α-fetoprotein; ALBI, albumin–bilirubin; PNI, prognostic nutritional index; WBC, white blood cell count.

HCC, and (6) patients who had not undergone chemotherapy or other preoperative antitumor treatment before. The patients were excluded if (1) the patient had an acute infection within 2 weeks, (2) presence of other hematological diseases, or (3) incomplete data. A total of 111 patients met the inclusion criteria, and 1 patient was excluded because of incomplete data. Finally, 110 patients were enrolled in this study (**Figure 1**).

The subsequent clinical parameters recorded were gender; age at diagnosis; size of the tumor; conditions such as diabetes, hypertension, ascites, schistosomiasis, and cirrhosis; and HBV-DNA levels. Besides, the laboratory blood investigations were carried out before RFA, including white blood cell (WBC) count, platelet count, prothrombin time, absolute lymphocyte count, serum albumin, total bilirubin, and serum α-fetoprotein (AFP).

Authors have access to information that could identify individual participants during or after data collection. This study was provided by the Research Ethics Committee of the First Affiliated Hospital of Zhejiang University. Written informed consent was obtained from patients before treatment. The study was conducted in accordance with the ethical principles stated in the Declaration of Helsinki. All methods were performed in accordance with the relevant guidelines and regulations.

Statistical Analysis

All statistical analyses were performed using SPSS 21.0 (SPSS Company, Chicago, IL, USA) for Windows. Categorical variables were examined using Fisher exact test. All continuous variables were expressed as the mean ± standard deviation, and the comparison between them was analyzed using the *t*-test.

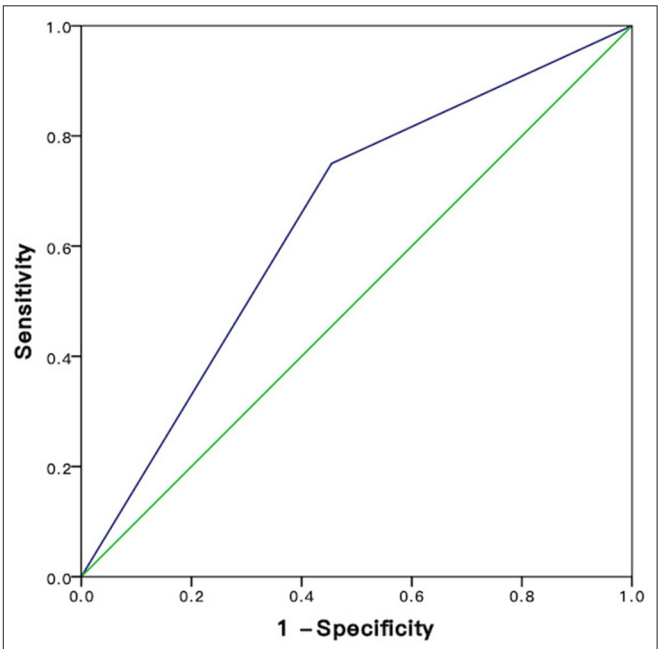

FIGURE 2 | ROC analysis for sensitivity and specificity of PNI. HCC, hepatocellular carcinoma; RFA, radiofrequency ablation; PNI, prognostic nutritional index; ALBI, albumin-bilirubin.

Spearman correlation was determined to analyze the correlation between PNI and PNI-ALBI grade. A time-dependent receiver operating characteristic (ROC) curve analysis was used to determine the cutoff values of PNI. In order to assess the ability of different models in predicting postoperative prognosis, our analysis was performed using the c-statistic equivalent to the area under the ROC curve (AUC). The RFS and OS were determined using the Kaplan–Meier method, and comparisons were determined using the log-rank test. The independent risk factors for the RFS and OS were identified using Cox regression analysis. The variables found to be significant ($P < 0.05$) in the univariate analysis were included in the multivariate analysis. A $P < 0.05$ was considered statistically significant.

RESULTS

A total of 110 patients were included in this study. Among them, there were 18 (16.4%) females and 92 (83.6%) males. The average age was 57.38 ±10.10 years. Sixteen (14.5%) patients had similar cases in their families. According to tumor–node–metastasis (TNM) staging system, 112 of the cases were stage I, 8 were stage II, and none of them were stage III or IV. There were 21 patients (19.1%) who had hypertension, and 19 (17.3%) had diabetes mellitus. There were 14 (12.7%) patients with ascites and 29 with schistosomiasis. A total of 80 (72.7%) patients had cirrhosis, and 101 patients had a positive HBV-DNA load. The average tumor size was 2.25 ± 0.67 cm. The size of the tumor was between 0.8 and 4.1 cm. Only one patient had HCC ≤1 cm

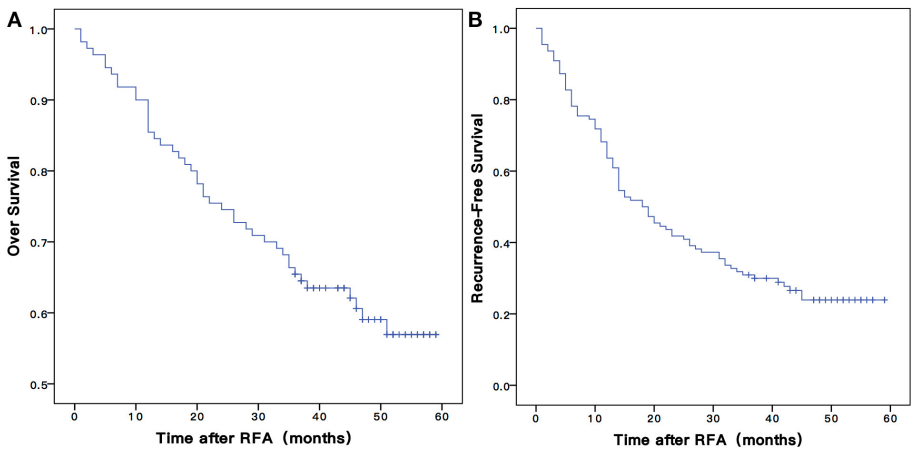

FIGURE 3 | The Kaplan-Meier overall **(A)** and recurrence-free **(B)** survival curves for early stage HCC patients undergoing RFA of this study. RFA, radiofrequency ablation.

TABLE 2 | Univariate and multivariate analyses of baseline prognosticators for overall survival in patients with early-stage hepatocellular carcinoma after radiofrequency ablation.

Variables	Univariate analysis		Multivariate analysis	
	HR (95% CI)	*P*-value	HR (95% CI)	*P*-value
Age, years (<55/≥55)	1.097 (0.594–2.029)	0.766		
Gender (female/male)	0.588 (0.290–1.191)	0.140		
Family cases (yes/no)	0.679 (0.316–1.462)	0.323		
Tumor size (>2.5/≤2.5 cm)	2.524 (1.387–4.593)	0.003	1.966 (1.091–3.545)	0.025
TNM stage (I/II)	0.796 (0.285–2.225)	0.663		
Hypertension (yes/no)	0.995 (0.503–1.970)	0.989		
Diabetes mellitus (yes/no)	1.959 (0.773–4.968)	0.157		
Ascites	0.598 (0.214–1.672)	0.327		
Schistosomiasis	1.937 (0.902–4.161)	0.040		
Cirrhosis	1.456(0.650–3.261)	0.361		
HBsAg (+/–)	1.041 (0.373–2.910)	0.938		
AFP (μg/L) (≥200/<200)	1.924 (0.993–3.729)	0.050		
ALBI grade (1/2,3)	2.447 (1.301–4.604)	0.006		
PNI (≥ 47.2/<47.2)	2.778 (1.406–5.488)	0.003	2.558 (1.289–5.078)	0.007
PNI-ALBI grade (0/1)	3.876 (1.792–8.690)	0.001	3.876 (1.729–8.690)	0.001

HR, hazard ratio; CI, confidence interval; TNM, tumor-node-metastasis; HBsAg, hepatitis B surface antigen; AFP, α-fetoprotein; PNI, prognostic nutritional index; ALBI, albumin-bilirubin.

in diameter, and the nodule was 0.8 cm in diameter. There was one patient with HCC ≥4 cm, and the nodule was 4.1 cm. WBC, platelet count, prothrombin time, total bilirubin, and AFP of patients before RFA are shown in **Table 1**.

Based on ROC curves, the cutoff value of PNI was 47.2 (**Figure 2**). A PNI ≥47.2 was considered as a high PNI, and a PNI < 47.2 was considered as a low PNI.

Patients with a high PNI were allocated a score of 0; otherwise, the patients were allocated a score of 1. Patients with ALBI grade 0 were allocated a score of 0, grade 1 a score of 1, and grade 2 were allocated a score of 2.

The combination of the ALBI and PNI (PNI-ALBI) scores was the summation of the two scores. They ranged from 0 to 3. There were 47 patients with high PNI. The number of patients in ALBI grades 1 and 2 was 54 each. There was only one patient in ALBI grade 3. The PNI-ALBI scores ranged from 0 to 3. The patients with a score of 0 were considered to have a low PNI-ALBI grade (PNI-ALBI grade 0), and the patients with scores of more than 0 were defined as high PNI-ALBI grade (PNI-ALBI grade 1). Among all the patients in this study, 68 (61.8%) patients were reclassified into PNI-ALBI grade 1, and 42 (38.2%) were into PNI-ALBI grade 0. Spearman correlation was performed

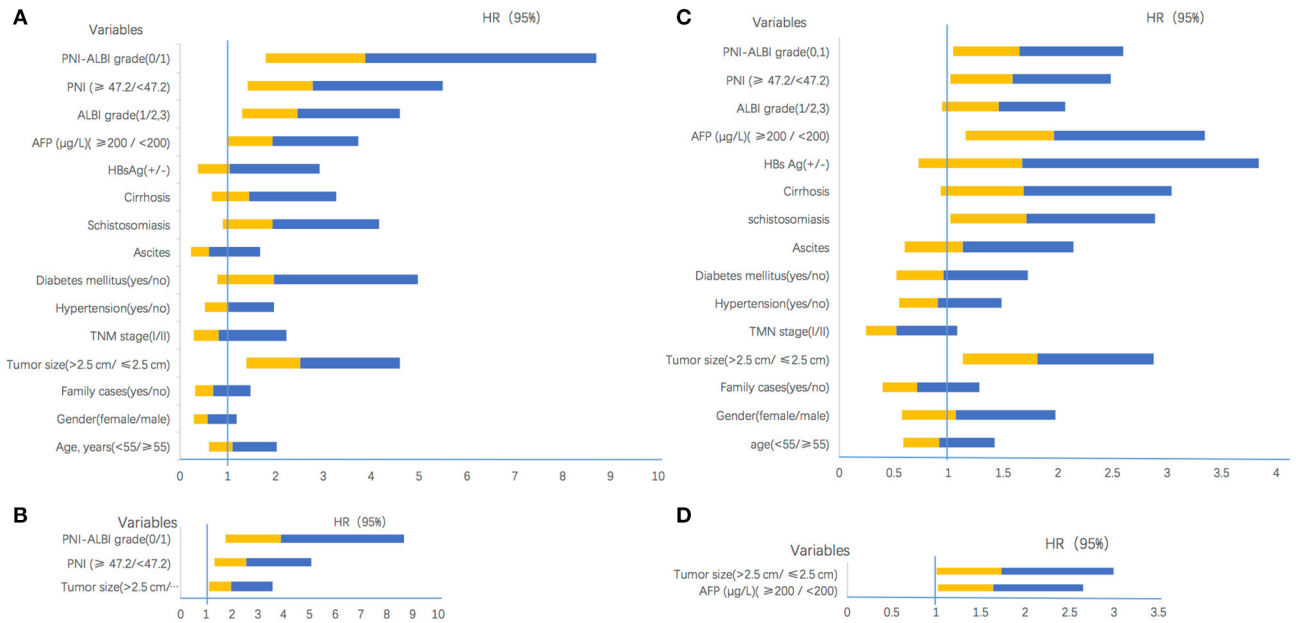

FIGURE 4 | Confidence interval charts of univariate and multivariate analyses. **(A)** The univariate analyses results for overall survival. **(B)** The multivariate analyses results for overall survival. **(C)** The univariate analyses results for recurrence-free survival. **(D)** The multivariate analyses results for recurrence-free survival. HR, hazard ratio; CI, confidence interval; TMN, tumor-node-metastasis; HBs Ag, hepatitis B surface antigen; AFP, α-fetoprotein; PNI, prognostic nutritional index; ALBI, albumin-bilirubin.

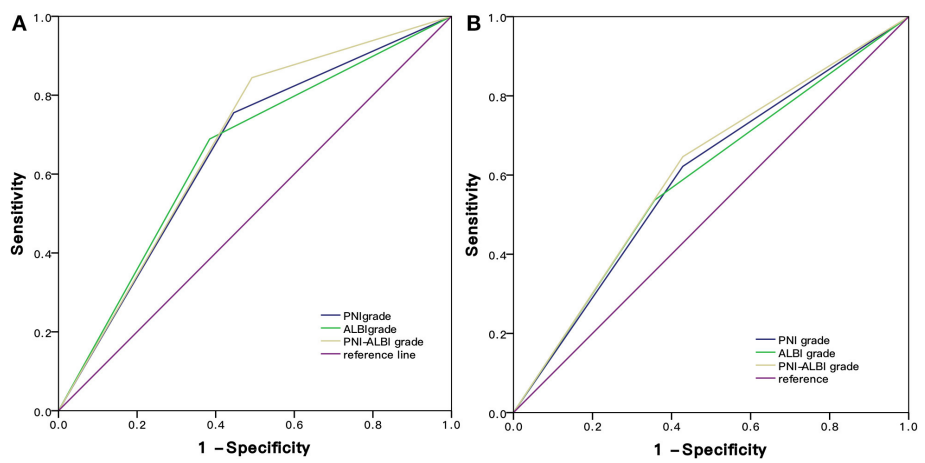

FIGURE 5 | Comparison of the AUC of PNI-ALBI grade, PNI, and ALBI in predicting survival **(A)** and postoperative recurrence **(B)**. RFA, radiofrequency ablation; AUC, area under the receiver operating characteristic curve; PNI, prognostic nutritional index; ALBI, albumin-bilirubin.

to find that PNI was highly correlated with PNI-ALBI grade ($r = 0.814$, $P < 0.01$).

Analyses for OS

The mean follow-up time was 47.5 ±14.8 months, and in between, 45 (40.9%) patients died. The 1-, 3-, and 5-years OS rates of patients were 80.0, 30.9, and 23.9%, respectively (**Figure 3A**).

As shown in **Table 2**, the univariate analysis showed potential association of OS with the following parameters: tumor size [HR = 2.524, 95% confidence interval (CI) = 1.387–4.593, $P = 0.003$], schistosomiasis (HR = 1.937, 95% CI = 0.902–4.161, $P = 0.040$), high AFP level (HR = 1.924, 95% CI = 0.993–3.729, $P = 0.050$), ALBI grade (HR = 2.447, 95% CI = 1.301–4.604, $P = 0.006$), PNI grade (HR = 2.778, 95% CI = 1.406–5.488, $P = 0.003$), and PNI-ALBI grade (HR = 3.876, 95% CI = 1.792–8.690, $P = 0.001$). The result is shown in the CI chart (**Figure 4A**).

However, in the multivariate analysis, only tumor size (HR = 1.966, 95% CI = 1.091–3.545, $P = 0.025$), PNI (HR = 2.558, 95% CI = 1.289–5.078, $P = 0.007$), and PNI-ALBI grade (HR = 3.876, 95% CI = 1.729–8.690, $P = 0.001$) were independent risk factors for OS (**Figure 4B**). It confirmed that the PNI-ALBI grade was a strong predictor of OS. The predictive abilities for OS of PNI-ALBI, ALBI, and PNI were compared.

Based on the ROC curves, the AUC of PNI-ALBI grade was 0.676, PNI grade was 0.655, and ALBI grade was 0.652. The PNI-ALBI had the highest AUC, which indicated that the PNI-ALBI might be a better factor to predict the OS of the patients with HCC after RFA (**Figure 5A**).

Analyses for RFS

There were 82 (74.5%) patients who suffered from recurrence during the follow-up periods. The 1-, 3-, and 5-years RFS rates were 63.6, 53.2, and 35.0%, respectively (**Figure 3B**). The univariate Cox proportional hazards model showed that tumor size (HR = 1.808, 95% CI = 1.135–2.882, $P = 0.013$), schistosomiasis (HR = 1. 713, 95% CI = 1.014–2.895, $P = 0.044$), AFP (HR = 1.962, 95% CI = 1.152–3.342, $P = 0.013$), and PNI-ALBI grade (HR = 1.647, 95% CI = 1.043–2.600, $P = 0.032$) were independent risk factors for RFS, as shown in **Table 3**. But in multivariate Cox proportional hazards model, only the AFP (HR = 1.732, 95% CI = 1.003–2.991, $P = 0.049$) and the size of tumor (HR = 1.640, 95% CI = 1.015–2.647, $P = 0.43$) turned out to be independent predictors for better RFS (**Figures 4C,D**).

Based on the ROC curves, the AUC of PNI-ALBI grade was 0.609, PNI was 0.590, and ALBI grade was 0.597 (**Figure 5B**). For predicting postoperative RFS, the PNI-ALBI grade had the highest AUC, followed by ALBI grade and PNI.

The Difference Between the Patients With Low and High PNI-ALBI Grade

As shown in **Figure 6A**, the 1-, 3-, and 5-years OS rates were 93.3, 82.8, and 79.9%, respectively, for patients with low PNI-ALBI grade. For patients with high PNI-ALBI grade, they were 71.1, 39.6, and 33.5%, respectively, and the difference was statistically significant ($P < 0.001$). As shown in **Figure 6B**, the 1-, 3-, and 5-years RFS rates for patients with low PNI-ALBI grade were 80.0, 52.2, and 41.4%, respectively; and 58.8, 23.1, and 17.3%, respectively, for patients with high PNI-ALBI grade ($P < 0.001$).

We compared the clinicopathological characteristics of patients with different PNI-ALBI grades (**Table 4**). Patients with high PNI-ALBI grade had a higher incidence of larger tumor size (≥2.5 cm), ascites, splenomegaly, cirrhosis, AFP, lower albumin, and higher total bilirubin compared with low PNI-ALBI grade.

DISCUSSION

HCC ranks third in the cancer-related causes of the deaths worldwide (22). Ablation is the recommended treatment for early HCC, and RFA is the most mature and widely used treatment among them (23). It is recommended as the first-line therapy for HCC <3 cm in diameter, as it has a similar survival outcome compared with surgical resection (24). Because of the metabolic function of the liver, the PNI, which was initially designed to evaluate the immunological and nutritional status of patients after surgery of the gastrointestinal tract, was applied in patients with HCC and turned out to be an independent predictor of OS (15, 25–27). Patients with a lower PNI tend to have a worse OS. Low PNI may be caused by hypoalbuminemia and/or lymphocytopenia. The question arises: How do hypoalbuminemia and lymphocytopenia contribute to tumor development and progression? Lymphocytes are important in the adaptive immune system that acts against cancer. They are the cellular foundation for cancer immunosurveillance and immunoediting, and a previous study had proven that a higher lymphocyte count could guarantee an effective antitumor cellular immune response. Likewise, a lower lymphocyte count might weaken the antitumor immune defense, indicating a poor prognosis (28). Hypoalbuminemia in patients with HCC is caused by an impaired liver function due to the underlying chronic liver disease and is also associated with a sustained systemic inflammatory response, either as a host reaction or from the tumor itself.

Rather than advanced-stage diseases, PNI was a better prognostic predictor in patients with an early stage (29), and all the patients in our study were in the early stage. A previous study found that ALBI grade, known as a new assessment method for the hepatic function, was proposed, which was reported to be better than CP and Model for End-stage Liver Disease (MELD) scale in the assessment ability for hepatic function (30). The MELD score was calculated by three objective variables, which were total bilirubin, creatinine, and international normalized ratio (INR). But INR was reported not to sufficiently reflect coagulopathy and consequently liver function in liver cirrhosis (31). The CP score was inferior in terms of stability, because two parameters in the score, namely, ascites and encephalopathy, were variable and were mostly subjective to the observer. In comparison, ALBI grade is a simple and more objective way to assess liver function and therefore could be a better tool in the evaluation of patients with HCC (32). HCC patients with relatively well-preserved hepatic function are more likely to receive appropriate

TABLE 3 | Univariate and multivariate analyses of baseline prognosticators for recurrence-free survival in patients with early-stage HCC after RFA.

Variables	Univariate analysis		Multivariate analysis	
	HR (95% CI)	*P*-value	HR (95% CI)	*P*-value
Age (<55/≥55)	0.908 (0.581–1.418)	0.671		
Gender (female/male)	1.068 (0.578–1.974)	0.833		
Family cases (yes/no)	0.708 (0.390–1.283)	0.254		
Tumor size (>2.5/≤2.5 cm)	1.808 (1.135–2.882)	0.013	1.640 (1.015–2.647)	0.43
TNM stage (I/II)	0.517 (0.249–1.075)	0.077		
Hypertension (yes/no)	0.900 (0.543–1.490)	0.681		
Diabetes mellitus (yes/no)	0.951 (0.526–1.721)	0.868		
Ascites	1.135 (0.601–2.145)	0.696		
Schistosomiasis	1. 713 (1.014–2.895)	0.044		
Cirrhosis	1.682 (0.929–3.046)	0.086		
HBsAg (+/–)	1.668 (0.726–3.833)	0.228		
AFP (μg/L) (≥200/<200)	1.962 (1.152–3.342)	0.013	1.732 (1.003–2.991)	0.049
ALBI grade (1/2,3)	1.457 (0.942–2.066)	0.091		
PNI (≥47.2/<47.2)	1.587 (1. 012–2.488)	0.044		
PNI-ALBI grade (0, 1)	1.647 (1.043–2.600)	0.032		

HCC, hepatocellular carcinoma; RFA, radiofrequency ablation; HR, hazard ratio; CI, confidence interval; TNM, tumor–node–metastasis; HBsAg, hepatitis B surface antigen; AFP, a-fetoprotein; PNI, prognostic nutritional index; ALBI, albumin–bilirubin.

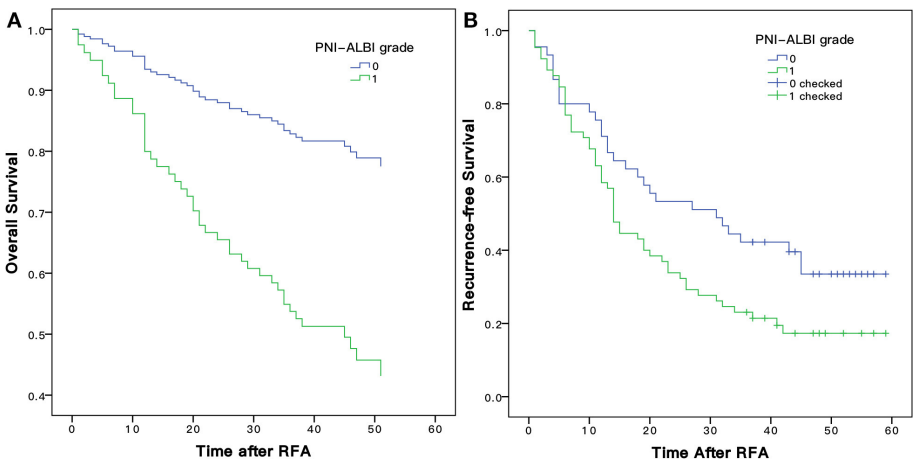

FIGURE 6 | Comparison of Kaplan-Meier overall **(A)** and recurrence-free **(B)** survival curves for early stage HCC patients with different PNI-ALBI grade. PNI, prognostic nutritional index; ALBI, albumin-bilirubin; HCC, hepatocellular carcinoma.

therapy, and poor liver function is associated with increased treatment-related toxicity and inferior survival. Also, patients with better liver function can recover faster with fewer complications (33). More and more studies confirmed that ALBI grade is an independent predictor of OS in patients with HCC (34, 35).

It is hypothesized that the combination of PNI and ALBI would increase the accuracy of prognostic evaluation after RFA for HCC, as the combination could evaluate both the nutritional status and the hepatic function of patients with HCC. In this retrospective study, 110 patients with newly diagnosed HCC were included, and all the patients received the RFA. The multivariate analysis and univariate analysis results showed that the PNI-ALBI grade was an independent influencing factor for the OS of the patients with HCC after RFA. More importantly, the performance of PNI-ALBI grade in predicting OS of the HCC patients was better than PNI or ALBI alone. Patients with high PNI-ALBI grades were more likely to have a worse OS. But for RFS, the univariate analysis found that the AFP and PNI-ALBI grade seems to be a predictor; however, in multivariate analysis, the prognostic values of the ALBI and PNI for RFS are uncertain in patients with early-stage HCC receiving RFA as initial therapy. Okamura et al. found the PNI predicts only OS and not RFS in HCC patients after hepatectomy (36). Chu et al. also demonstrated that an elevated AFP level of ≥200 ng/mL was a significant factor associated with RFS by univariate and

TABLE 4 | Comparison of clinicopathologic characteristics between patients with low PNI-ALBI grade and high PNI-ALBI grade.

Clinicopathological feature	Low PNI-ALBI grade	High PNI-ALBI grade	*P*-value
Age			
<55 years	18 (42.9%)	25 (36.8%)	0.525
≥55 years	24 (57.1%)	43 (63.2%)	
Gender			
Female	5 (11.9%)	13 (19.1%)	0.320
Male	37 (88.1%)	55 (80.9%)	
Family cases			
Yes	7 (16.7%)	9 (13.2%)	0.828
No	35 (83.3%)	59 (86.8%)	
Tumor size			
>2.5 cm	6 (14.3%)	24 (35.3%)	0.016
≤2.5 cm	36 (85.7%)	44 (64.7%)	
TNM stage			
I	39 (92.9%)	63 (92.6%)	0.97
II	3 (7.1%)	5 (7.4%)	
Hypertension			
Yes	10 (23.8%)	17 (25.0%)	0.538
No	32 (76.2%)	51 (75.0%)	
Diabetes mellitus			
Yes	9 (21.4%)	10 (14.7%)	0.439
No	33 (78.6%)	58 (85.3%)	
Ascites			
Yes	2 (4.8%)	12 (17.6%)	0.042
No	40 (95.2%)	56 (82.4%)	
Splenomegaly			
Yes	19 (45.2%)	60 (88.2%)	<0.001
No	23 (54.8%)	8 (11.8%)	
Cirrhosis			
Yes	25 (59.5%)	62 (91.2%)	<0.001
No	27 (64.3%)	6 (8.8%)	
HBsAg			
Present	37 (88.1%)	63 (92.6%)	0.332
Absent	6 (14.3%)	5 (7.4%)	
AFP (μg/L)			
Normal	39 (92.9%)	51 (75.0%)	0.022
Abnormal	3 (7.1%)	17 (25.0%)	
WBC ($\times 10^3$/μL)	5.09 ± 1.49	3.96 ± 1.73	0.382
Platelet count ($\times 10^9$/L)	136.90 ± 61.03	87.41 ± 46.29	0.157
Prothrombin time (s)	12.10 ± 1.74	18.44 ± 44.16	0.146
Albumin (g/L)	43.74 ± 2.65	36.18 ± 4.11	0.002
Total bilirubin (μmol/L)	15.57 ± 7.62	21.12 ± 9.93	0.028

HR, hazard ratio; CI, confidence interval; TNM, tumor–node–metastasis; HBsAg, hepatitis B surface antigen; AFP, α-fetoprotein; PNI, prognostic nutritional index; ALBI, albumin–bilirubin.

multivariate analyses, whereas PNI had limited prognostic value for RFS in early-stage HCC patients undergoing RFA (15). However, a study conducted by Chan et al. showed that the PNI could be an important prognostic parameter for HCC patients who underwent hepatectomy (37). Regarding ALBI, several studies have evidenced that it could have a predictive value in OS. But fewer studies were performed to evaluate the predictive role of ALBI in estimating HCC recurrence (38). No clear explanation for this difference is available at present. Further research with larger sample size and longer follow-up time on this issue may show the PNI and ALBI to be a significant predictor of both OS and RFS. A significant difference in the PNI-ALBI grade was identified in the current univariate analysis for RFS.

Our results indicated that the PNI-ALBI grade could better reflect the long-term survival for patients with HCC after RFA, compared with either score alone. The results of our study can help us to identify patients who had a potentially poor prognosis and take interventions before the RFA.

Although, to our best knowledge, this is the first study to combine PNI and ALBI to evaluate the prognostic value in patients with early-stage HCC after RFA, this study had several potential limitations. First, this was a retrospective study. Second, this was a single-center study, and patients involved were confined to the east of China. Third, the sample size of the study was limited, and a further larger sample size cohort is needed. Fourth, some other well-known indicators, including the platelet-to-lymphocyte ratio, C-reactive protein level, and Glasgow prognostic score, were not evaluated in our cohort, although they have been proposed earlier as prognostic factors for patients with HCC.

In conclusion, this study demonstrated that the PNI-ALBI grade was a more accurate marker for predicting the OS of patients with early-stage HCC treated with RFA in comparison to PNI or ALBI alone. Patients with high PNI-ALBI grade are more likely to have a worse outcome, which suggests that we should check out the patients' liver function and nutritional status before performing the RFA.

DATA AVAILABILITY STATEMENT

All datasets generated for this study are included in the article/**Supplementary Material**.

ETHICS STATEMENT

The studies involving human participants were reviewed and approved by the Research Ethics Committee of The First Affiliated Hospital of Zhejiang University. The ethics committee waived the requirement of written informed consent for participation.

AUTHOR CONTRIBUTIONS

JP conceived the study and wrote the manuscript. SC collected the data. JP and GT performed statistical analyses. TJ provided support and helped with manuscript revision. All authors were involved in analyzing the results.

FUNDING

This study was supported by grants from National Key R&D Program of China (No. 2018YFC0114900), the National Natural

Science Foundation of China (No. 81971623), the Major Research plan of the National Natural Science Foundation of China (No. 91630311), the Natural Science Foundation of Zhejiang Province (No. LZ20H180001), and National S&T Major Project of China (No. 2018ZX10301201).

SUPPLEMENTARY MATERIAL

The Supplementary Material for this article can be found online at: https://www.frontiersin.org/articles/10.3389/fmed.2020.584871/full#supplementary-material

REFERENCES

1. Bray F, Ferlay J, Soerjomataram I, Siegel RL, Torre LA, Jemal A. Global cancer statistics 2018: GLOBOCAN estimates of incidence and mortality worldwide for 36 cancers in 185 countries. *CA A Cancer J Clin*. (2018) 68:394–424. doi: 10.3322/caac.21492
2. Mittal S, El-Serag HB. Epidemiology of hepatocellular carcinoma: consider the population. *J Clin Gastroenterol.* (2013) 47:S2–6. doi: 10.1097/MCG.0b013e3182872f29
3. Yang, JD, Hainaut, P, Gores, GJ, et al. A global view of hepatocellular carcinoma: trends, risk, prevention and management. *Nat Rev Gastroenterol Hepatol.* (2019) 16:589–604. doi: 10.1038/s41575-019-0186-y
4. Altekruse SF, McGlynn KA, Reichman ME. Hepatocellular carcinoma incidence, mortality, and survival trends in the United States from 1975 to 2005. *J Clin Oncol*. (2009) 27:1485–91. doi: 10.1200/JCO.2008.20.7753
5. Luo W, Zhang Y, He G, Yu M, Zheng M, Liu L, et al. Effects of radiofrequency ablation versus other ablating techniques on hepatocellular carcinomas: a systematic review and meta-analysis. *World J Surg Oncol.* (2017) 15:126. doi: 10.1186/s12957-017-1196-2
6. Lencioni RA, Allgaier HP, Cioni D, Olschewski M, Deibert P, Crocetti L, et al. Small hepatocellular carcinoma in cirrhosis: randomized comparison of radiofrequency thermal ablation versus percutaneous ethanol injection. *Radiology*. (2003) 228:235–40. doi: 10.1148/radiol.2281020718
7. Feng K, Yan J, Li X, Xia F, Ma K, Wang S, et al. A randomized controlled trial of radiofrequency ablation and surgical resection in the treatment of small hepatocellular carcinoma. *J Hepatol.* (2012) 57:794–802. doi: 10.1016/j.jhep.2012.05.007
8. Zhu ZX, Huang JW, Liao MH, Zeng Y. Treatment strategy for hepatocellular carcinoma in China: radiofrequency ablation versus liver resection. *Jpn J Clin Oncol.* (2016) 46:1075–80. doi: 10.1093/jjco/hyw134
9. Dhir M, Melin AA, Douaiher J, Lin C, Zhen WK, Hussain SM, et al. A review and update of treatment options and controversies in the management of hepatocellular carcinoma. *Ann Surg.* (2016) 263:1112–25. doi: 10.1097/SLA.0000000000001556
10. Livraghi T, Meloni F, Di Stasi M, Rolle E, Solbiati L, Tinelli C, et al. Sustained complete response and complications rates after radiofrequency ablation of very early hepatocellular carcinoma in cirrhosis: is resection still the treatment of choice? *Hepatology.* (2008) 47:82–9. doi: 10.1002/hep.21933
11. Durand F, Valla D. Assessment of prognosis of cirrhosis. *Semin Liver Dis.* (2008) 28:110–22. doi: 10.1055/s-2008-1040325
12. Shetty K, Rybicki L, Carey WD. The child-Pugh classification as a prognostic indicator for survival in primary sclerosing cholangitis. *Hepatology.* (1997) 25:1049–53. doi: 10.1002/hep.510250501
13. Johnson PJ, Berhane S, Kagebayashi C, Satomura S, Teng M, Reeves HL, et al. Assessment of liver function in patients with hepatocellular carcinoma: a new evidence-based approach-the ALBI grade. *J Clin Oncol.* (2015) 33:550–8. doi: 10.1200/JCO.2014.57.9151
14. Johnson PJ, Berhane S, Kagebayashi C, Satomura S, Teng M, Reeves HL, et al. Prognostic significance of combined albumin–bilirubin and tumor–node–metastasis staging system in patients who underwent hepatic resection for hepatocellular carcinoma. *Hepatol Res.* (2015) 47:1289–98. doi: 10.1111/hepr.12868
15. Chu MO, Shen CH, Chang TS, Xu HW, Yen CW, Lu SN, et al. Pretreatment inflammation-based markers predict survival outcomes in patients with early stage hepatocellular carcinoma after radiofrequency ablation. *Sci Rep.* (2018) 8:16611. doi: 10.1038/s41598-018-34543-z
16. Buzby GP, Mullen JL, Matthews DC, Hobbs CL, Rosato EF. Prognostic nutritional index in gastrointestinal surgery. *Am J Surg.* (1980) 139:160–7. doi: 10.1016/0002-9610(80)90246-9
17. Onodera T, Goseki N, Kosaki G. Prognostic nutritional index in gastrointestinal surgery of malnourished cancer patients. *Nihon Geka Gakkai Zasshi.* (1984) 85:1001–5.
18. Shimizu K, Okita R, Saisho S, Yukawa T, Maeda A, Nojima Y, et al. Prognostic nutritional index before adjuvant chemotherapy predicts chemotherapy compliance and survival among patients with non-small-cell lung cancer. *Ther Clin Risk Manag.* (2015) 11:1555–61. doi: 10.2147/TCRM.S92961
19. Nozoe T, Kimura Y, Ishida M, Saeki H, Korenaga D, Sugimachi K. Correlation of pre-operative nutritional condition with post-operative complications in surgical treatment for oesophageal carcinoma. *Eur J Surg Oncol.* (2002) 28:396–400. doi: 10.1053/ejso.2002.1257
20. Nozoe T, Kohno M, Iguchi T, Mori E, Maeda T, Matsukuma A, et al. The prognostic nutritional index can be a prognostic indicator in colorectal carcinoma. *Surg Today.* (2012) 42:532–5. doi: 10.1007/s00595-011-0061-0
21. Abe A, Kurita K, Hayashi H, Ishihama T, Ueda A. Correlation between prognostic nutritional index and occlusal status in gastric cancer. *Oral Dis.* (2020) 26:465–72. doi: 10.1111/odi.13242
22. Ferlay J, Soerjomataram I, Dikshit R, Eser S, Mathers C, Rebelo M, et al. Cancer incidence and mortality worldwide: sources, methods and major patterns in GLOBOCAN (2012). *Int J Cancer.* (2015) 136:E359–86. doi: 10.1002/ijc.29210
23. Aubé C, Bouvier A, Lebigot J, Vervueren L, Cartier V, Oberti F. Radiological treatment of HCC: interventional radiology at the heart of management. *Diagn Interv Imaging.* (2015) 96:625–36. doi: 10.1016/j.diii.2015.04.008
24. Mazzaferro V, Lencioni R, Majno P. Early hepatocellular carcinoma on the procrustean bed of ablation, resection, and transplantation. *Semin Liver Dis.* (2014) 34:415–26. doi: 10.1055/s-0034-1394365
25. Ke M, Xu T, Li N, Ren Y, Shi A, Lv Y, et al. Prognostic nutritional index predicts short-term outcomes after liver resection for hepatocellular carcinoma within the Milan criteria. *Oncotarget.* (2016) 7:81611–20. doi: 10.18632/oncotarget.13151
26. Ji F, Liang Y, Fu S, Chen D, Cai X, Li S, et al. Prognostic value of combined preoperative prognostic nutritional index and body mass index in HCC after hepatectomy. *HPB.* (2017) 9:695–705. doi: 10.1016/j.hpb.2017.04.008
27. Pinato DJ, North BV, Sharma R. A novel, externally validated inflammation-based prognostic algorithm in hepatocellular carcinoma: the prognostic nutritional index (PNI). *Br J Cancer.* (2012) 106:1439–45. doi: 10.1038/bjc.2012.92
28. Hoffmann TK, Dworacki G, Tsukihiro T, Meidenbauer N, Gooding W, Johnson JT, et al. Spontaneous apoptosis of circulating t lymphocytes in patients with head and neck cancer and its clinical importance. *Clin Cancer Res.* (2002) 8:2553–62.
29. Okamura Y, Sugiura T, Ito T, Yamamoto Y, Ashida R, Uesaka K. The optimal cutoff value of the preoperative prognostic nutritional index for the survival differs according to the TNM stage in hepatocellular carcinoma. *Surg Today.* (2017) 47:986–93. doi: 10.1007/s00595-017-1491-0
30. Hiraoka A, Kumada T, Kudo M, Hirooka M, Tsuji K, Itobayashi E, et al. Albumin-Bilirubin (ALBI) grade as part of the evidence-based clinical practice guideline for HCC of the Japan society of hepatology: a comparison with the liver damage and child-pugh classifications. *Liver Cancer.* (2017) 6:204–15. doi: 10.1159/000452846
31. Bedreli S, Sowa JP, Gerken G, Saner FH, Canbay A. Management of acute-on-chronic liver failure: rotational thromboelastometry may reduce

substitution of coagulation factors in liver cirrhosis. *Gut.* (2016) 65:357–8. doi: 10.1136/gutjnl-2015-309922

32. Peng Y, Qi X, Guo X. Child-pugh versus meld score for the assessment of prognosis in liver cirrhosis: a systematic review and meta-analysis of observational studies. *Medicine.* (2016) 95:e2877. doi: 10.1097/MD.0000000000002877
33. Zou H, Yang X, Li QL, Zhou QX, Xiong L, Wen Y. A comparative study of albumin-bilirubin score with child-pugh score, model for end-stage liver disease score and indocyanine green R15 in predicting posthepatectomy liver failure for hepatocellular carcinoma patients. *Digest Dis.* (2018) 36:236–43. doi: 10.1159/000486590
34. Ho SY, Liu PH, Hsu CY, Hsia CY, Su CW, Huang YH. An Albumin-Bilirubin (ALBI) grade-based prognostic model for patients with hepatocellular carcinoma within milan criteria. *Am J Clin Oncol.* (2019) 42:698–704. doi: 10.1097/COC.0000000000000581
35. Nguyen TTH, Nguyen VH, Nguyen VH, Nguyen TL, Le VQ. Role of baseline albumin-bilirubin grade on predict overall survival among sorafenib-treated patients with hepatocellular carcinoma in Vietnam. *Cancer Control.* (2019) 26:1073274819865269. doi: 10.1177/1073274819865269
36. Okamura Y, Ashida R, Ito T, Sugiura T, Mori K, Uesaka K. Preoperative neutrophil to lymphocyte ratio and prognostic nutritional index predict overall survival after hepatectomy for hepatocellular carcinoma. *World J Surg.* (2015) 39:1501–9. doi: 10.1007/s00268-015-2982-z
37. Chan AW, Chan SL, Wong GL, Wong VW, Chong CC, Lai PB, et al. Prognostic Nutritional Index (PNI) predicts tumor recurrence of very early/early stage hepatocellular carcinoma after surgical resection. *Ann Surg Oncol.* (2015) 22:4138–48. doi: 10.1245/s10434-015-4516-1
38. Peng Y, Wei Q, He Y, Xie Q, Liang Y, Zhang L, et al. ALBI versus child-pugh in predicting outcome of patients with HCC: a systematic review. *Expert Rev Gastroenterol Hepatol.* (2020) 14:383–400. doi: 10.1080/17474124.2020.1748010

Conflict of Interest: The authors declare that the research was conducted in the absence of any commercial or financial relationships that could be construed as a potential conflict of interest.

frontiers in Medicine

ORIGINAL RESEARCH
published: 16 November 2020
doi: 10.3389/fmed.2020.588928

Gut Microbiota Modulates Intestinal Pathological Injury in *Schistosoma japonicum*-Infected Mice

Beibei Zhang[1,2,3,4,5†], *Xiaoying Wu*[6†], *Qiuyue Song*[1,2,3†], *An Ning*[7], *Jinyi Liang*[1,2,3], *Langui Song*[1,2,3], *Jiahua Liu*[1,2,3], *Yishu Zhang*[8], *Dongjuan Yuan*[9*], *Xi Sun*[1,2,3*] and *Zhongdao Wu*[1,2,3*]

[1] Department of Parasitology of Zhongshan School of Medicine, Sun Yat-sen University, Guangzhou, China, [2] Key Laboratory of Tropical Disease Control, Ministry of Education, Sun Yat-sen University, Guangzhou, China, [3] Provincial Engineering Technology Research Center for Biological Vector Control, Sun Yat-sen University, Guangzhou, China, [4] Jiangsu Key Laboratory of Immunity and Metabolism, Department of Pathogenic Biology and Immunology, Xuzhou Medical University, Xuzhou, China, [5] Laboratory of Infection and Immunity, Xuzhou Medical University, Xuzhou, China, [6] Department of Gastroenterology, Third Affiliated Hospital of Sun Yat-sen University, Guangzhou, China, [7] Jiangxi Provincial Institute of Parasitic Diseases, Nanchang, China, [8] College of Basic Medical Sciences, Guilin Medical University, Guilin, China, [9] College of Veterinary Medicine, South China Agricultural University, Guangzhou, China

OPEN ACCESS

Edited by:
Xiaojun Chen,
Nanjing Medical University, China

Reviewed by:
Zhipeng Xu,
Nanjing Medical University, China
Jijia Shen,
Anhui Medical University, China

***Correspondence:**
Zhongdao Wu
wuzhd@mail.sysu.edu.cn
Xi Sun
sunxi2@mail.sysu.edu.cn
Dongjuan Yuan
yuandj@scau.edu.cn

†These authors have contributed equally to this work and share first authorship

Specialty section:
This article was submitted to Gastroenterology, a section of the journal Frontiers in Medicine

Received: *29 July 2020*
Accepted: *12 October 2020*
Published: *16 November 2020*

Citation:
Zhang B, Wu X, Song Q, Ning A, Liang J, Song L, Liu J, Zhang Y, Yuan D, Sun X and Wu Z (2020) Gut Microbiota Modulates Intestinal Pathological Injury in Schistosoma japonicum-Infected Mice. Front. Med. 7:588928. doi: 10.3389/fmed.2020.588928

Trapping of *Schistosoma japonicum* (*S. japonicum*) eggs in host tissue, mainly in the intestine and liver, causes severe gastrointestinal and hepatic granulomatous immune responses and irreversible fibrosis. Although the gut microbiota plays a central role in regulating pathological responses in several diseases, the effect of the gut microbiota on the pathologenesis progression of schistosomiasis remains largely unknown. In this study, we aimed to investigate the regulatory function of the gut microbiota in schistosomiasis japonica. We found that the depletion of the gut microbiota significantly ameliorated egg granulomas formation and fibrosis in the intestine of infected mice. This role of the gut microbiota in intestinal granuloma formation and fibrosis was reinforced when normal and infected mice were housed together in one cage. Notably, changes in the gut microbiota induced by *S. japonicum* infection were partly reversible with microbiota transfer in the cohousing experiment. Transfer of the gut microbiota from normal to infected mice attenuated the intestinal pathological responses. Depletion of the gut microbiota by antibiotics, or transfer of the gut microbiota from normal to infected mice decreased the levels of IL-4, IL-5, and IL-13 and promoted the production of cytokines and mRNA levels of IL-10 and TGF-β in infected mice. Our findings indicated a regulatory effect of the gut microbiota on intestinal pathological injury associated with schistosomiasis japonica in mice, and thus suggested a potential strategy for schistosomiasis treatment.

Keywords: schistosomiasis japonica, gut microbiota, intestinal pathological injury, immune response, regulatory effect

INTRODUCTION

Schistosomiasis japonica is a severe zoonotic disease that can lead to irreversible fibrosis and portal hypertension and eventually give rise to splenomegaly, ascites and, gastrointestinal varices (1). *Schistosoma japonicum* (*S. japonicum*) infection remains one of the most important public health problems in tropical and subtropical areas; by 2018, there are still 29,214 advanced schistosomiasis cases were documented in China (2). The infections are initiated by cercariae, the invasive

larvae of *Schistosoma* spp., which enter the bodies of humans and other definitive hosts through the skin. Immature male and female schistosomula, then migrate downstream to the hepatic portal-mesenteric system via the circulatory system, in which females lay inside the groves of males, and release thousands of eggs. Some of the eggs are permanently intravenously trapped in the intestinal wall, or are deposited in the liver via the portal system (3). Mounting evidence has indicated that deposited eggs, which are the major pathogenic factors of these parasites, induce granuloma formation by stimulating dominant $CD4^+$ Th2 immune responses accompanied by eosinophil, macrophage, hepatic stellate cell and lymphocyte recruitment (4). However, the exact immunopathological mechanisms that are involved in schistosomiasis japonica remain to be fully defined.

The mammalian gut harbors a vast number of microbes. These microbes play essential roles in regulating host immunity through their surface antigens or their small metabolic molecules (5). The composition of the gut microbiota is dynamic and can be influenced by drug treatment, infection, host nutritional status and genetic factors (6, 7). Microbial dysbiosis can induce a series of autoimmune intestinal diseases, including Crohn's disease and ulcerative colitis (8), and even extra-intestinal diseases such as obesity, asthma, alcoholic liver disease, and rheumatoid arthritis (9–11). Intestinal schistosomiasis is caused by trapping of schistosome eggs in the intestinal mucosa, which may lead to a granulomatous response (12). The disease presents as abdominal pain and loss of appetite commonly accompanied by diarrhea (13). Intestinal schistosomiasis may result in extensive fibrosis and even hepatosplenic disease if it cannot be controlled in a timely manner. Many researchers have attempted to clarify the pathogenesis and regulatory mechanism of intestinal schistosomiasis. For example, Zhao et al. reported that intestinal egg granulomas induce alterations in the gut microbiome (14). However, until now, it has remained unclear whether the gut microbiota participates in modulating the progression of intestinal pathological responses induced by *S. japonicum* infection.

To explore the regulatory function of the gut microbiota in intestinal schistosomiasis, we used antibiotics treatment and cohousing experiment to investigate the relationship between the alteration of gut microbiota and the pathological progression of *S. japonicum* infection. We found that *S. japonicum* infection influenced the gut microbial community in mice. Depletion of the gut microbiota by antibiotics or transfer of the gut microbiota from normal mice to infected mice through cohousing attenuated granuloma formation and fibrotic responses in the intestines of infected mice. The regulatory function of the gut microbiota was mediated by the modulation of the immune response in the intestine of mice.

MATERIALS AND METHODS

Mice, Infection, Antibiotic Treatment, and Cohousing Experiments

Six-week-old male Balb/c mice around 21 ± 1 g were purchased from the Experimental Animal Center of Southern Medical University and kept at the Biosafety Level-2 (BSL-2) laboratory of Sun Yat-sen University with a 12-h light and 12-h dark cycle. The temperature of the housing room was kept at 21–26°C and the humidity was 40–70%. The mice were fed sterile food and given water as needed. All the procedures of animal experiments and reporting follow to the ARRIVE guidelines.

All mice were acclimatized for 1 week before further processing. Mice were randomly divided into two groups (n = 5 per group). Each mouse was infected with 15 *S. japonicum* specimens in the infective form (cercariae) as described previously (15). In brief, *S. japonicum* cercariae were released from *Oncomelania hupehensis*, and each mouse was infected percutaneously with the cercariae. A broad-spectrum antibiotic cocktail was used to disturb the diversity and composition of the gut microbiota. In brief, mice were divided randomly into four groups (n = 4–5 per group): a normal group, an infected group; a group of normal mice receiving antibiotics, and a group of infected mice receiving antibiotics. The infected mice were percutaneously infected with 15 cercariae each. The antibiotic-treated mice received 0.2 g/l ampicillin (Dalian Meilun Biotech, Dalian, China), 0.2 g/l metronidazole (Dalian Meilun Biotech, Dalian, China), 0.1 g/l vancomycin (MDBio Inc., Qingdao, China), and 0.2 g/l neomycin (Dalian Meilun Biotech, China) in their water beginning on the first day of infection, and treatment continued for 7 weeks. For the cohousing experiment, normal mice and mice infected with 15 cercariae each were housed in one cage or housed separately beginning on the first day of infection (n = 4–5 per group). Before collecting samples, all mice were euthanized under deep anesthesia and unconsciousness via intraperitoneal injection with pentobarbital sodium at a dose of 150 mg/kg.

DNA Isolation and 16S rDNA Illumina Sequencing Analysis

After dissecting each mouse and exposing the sterile abdominal cavity, the contents of the colon were collected individually and stored in sterile tubes. All fecal samples were frozen at −80°C for genomic DNA isolation. For each sample, 100–200 mg of colonic fecal material was used for the extraction of genomic DNA. DNA isolation was conducted with a HiPure Stool DNA Kit (Magen, Guangzhou, China) according to the manufacturer's instructions. The V3-V4 region of 16S rDNA (approximately 500 bp) was amplified by PCR using specific bacterial primers (338F: 5′-ACTCCTACGGGAGGCAGCA-3′; 806R: 5′-GGACTACHVGGGTWTCTAAT-3′). Water was used as a template for negative control. An amplicon library was generated from the individual specimens and high-throughput sequencing was performed on an Illumina HiSeq platform. After demultiplexing, the raw paired-end reads from the original DNA fragments were merged in FLASH (version 1.2.11, minimum overlap of 10 bp, maximum mismatch rate of 0.2), and the high-quality sequences were filtered with Trimmomatic (version 0.33, minimum average quality score of 20, window size of 50 bp). The effective tags were obtained after chimera filtering with UCHIME (version 8.1) software. USEARCH (version 10.0) software was used for operational taxonomic unit (OTU) clustering with a

97% similarity cut-off. The OTUs were annotated based on the Silva database (http://www.arb-silva.de/) with UCLUST with a minimum similarity 80% OTUs accounting for more than 0.0005% of all the effective tags were retained for further analyses. The remaining OTUs were used for calculation of alpha diversity indexes with Mothur (version 1.30) software. Beta diversity analysis among the different groups was based on the thetaYC distance variance.

Sampling and Histopathological Analysis

Serum was collected for Alanine transaminase (ALT) and alanine transaminase (AST) measurements in KingMed Diagnostics. Left liver lobes and colons were harvested and immediately fixed in 4% paraformaldehyde. Paraffin sections were de-waxed for hamatoxylin and eosin (H&E) staining and Masson's trichrome staining. All images were captured under an inverted microscope (Olympus, Tokyo, Japan). For quantitative analysis of the percentage of the fibrotic area, each section stained with Masson's trichrome staining was examined under a ZEISS Axio Scan.Z1 automated slide scanner microscope (Carl Zeiss AG, Oberkochen, Germany), and an image of the whole tissue was obtained. Then, the area of the whole tissue and the blue positive region were analyzed with Image-Pro Plus 6.0 software (Media Cybernetics, Inc, Maryland, USA) as previously described (16). The percentage was calculated by dividing the area of the blue-labeled region by that of the whole tissue. For immunohistochemistry, de-waxed sections were washed three times in PBS and heated in boiling citrate solution for 30 min. After cooling for 2 h at room temperature and being washed three times in PBS, the slides were incubated in 3% hydrogen peroxide for 10 min at room temperature and washed. One percentage BSA was used to block the sections for 1 h at room temperature. The sections were then incubated overnight at 4°C with primary antibodies against IL-4 (GB11111, Wuhan Servicebio Technology CO., Ltd., Wuhan, China, used at a 1:200 dilution), IL-5 (AB41062, A Brand of Bioscience, Baltimore, USA, used at a 1:500 dilution), IL-13 (BA1208-1, BOSTER, Wuhan, China, used at a 1:1,000 dilution), IL-10 (BA1201-1, Boster, Wuhan, China, used at a 1:500 dilution), and TGF-β (21898-1-AP, Proteintech, Wuhan, China, used at a 1:500 dilution). After washing the sections three times with PBS, each section was incubated with one drop of ready-to-use HRP labeled anti-mouse or anti-rabbit general secondary antibodies (Dako, Copenhagen, Denmark) was used to incubate each section for 45 min at room temperature, respectively. Then, each section was monitored carefully after 50 μl of substrates were added. Finally, to study the nuclear structures, the sections were counterstained with hematoxylin, dehydrated and covered with neutral gum. Images were acquired using an inverted microscope (Olympus, Tokyo, Japan). For quantitative analysis of the positive area, the entire tissue was again imaged with a Zeiss Axio Scan.Z1 microscope, and the total area of the entire tissue and the area of the positive region were analyzed with Image-Pro Plus 6.0 software. The positivity is presented as the positive area vs. the total area.

Determination of Worm Length, Worm Burden, and Egg Burden

Male and female worms were obtained from the portal vein by cardiac perfusion 7 weeks post-infection. Then the numbers of male and female worms were recorded. The length of each worm was measured under a stereoscopic microscope (Leica, Wetzlar, Germany).

Egg burden was determined as previously described (17). Briefly, liver tissues and colons were removed, weighed and cut into pieces. Tissues were digested in 1 ml of 4% potassium hydroxide at 37°C in an orbital shaker for 6 h. Then, the eggs in 10 μl of the resulting suspension were counted under a microscope; counting was repeated six times for each sample. Finally, the total number of eggs per gram was calculated by multiplying the average number of eggs in 10 μl of suspension by 100 and dividing the resulting number by the weight of the tissue.

Acetic Red Staining

Worms were fixed in 4% paraformaldehyde, washed in 70% ethanol, and stained with 10 mg/ml acetic red (Sigma, St. Louis, USA) for 10 min. Subsequently, the worms were destained in 70% ethanol with 2% HCl, and dehydrated with graded ethanol. Fast Green (Sigma, St. Louis, USA) was used to stain the worm cuticles. The worms were isolated and mounted on glass slides. Photographs were taken using an inverted microscope (Olympus, Japan).

Real-Time qPCR Detection

The collected liver and intestine tissues were lysed with Trizol reagent (Qigen) for RNA extraction. We employed 3 μg total RNA to synthesize complementary DNA (cDNA). Specific primers for IL-4 (forward 5′-TTGTCATCCTGCTCTTCTTTCTCG-3′ and reverse 5′-CTCACTCTCTGTGGTGTTCTTCGTT-3′), IL-5 (forward 5′-AAAGAGAAGTGTGGCGAGGA-3′ and reverse 5′-ACCAAGGAACTCTTGCAGGT-3′), IL-13 (forward 5′-GCAGCATGGTATGGAGTGTG-3′ and reverse 5′-GGAATCCAGGGCTACACAGA-3′), IL-10 (forward 5′-GGAAGACAATAACTGCACCCACT-3′ and reverse 5′-GGAAGACAATAACTGCACCCACT-3′), TGF-β (forward 5′-CCACCTGCAAGACCATCGAC-3′ and reverse 5′-CTGGCGAGCCTTAGTTTGGAC-3′), and GAPDH (forward 5′-ACTCCACTCACGGCAAATTC-3′ and reverse 5′-TCTCCATGGTGGTGAAGACA-3′) were designed for Real-time qPCR analysis. The amplification was performed with 0.5 μl template according to the manufacturer's instruction (TaKaRa, Japan). Then, the reactions were started with LightCycler® 480 Real-time qPCR instrument (Roche, USA).

Statistical Analysis

All data are presented as the mean ± SEM. SPSS 19.0 software (SPSS, Inc., Chicago, USA) was used for statistical analysis. Comparisons between two groups were conducted with independent-sample *t*-tests, and significant differences among multiple groups were detected by one-way ANOVA followed by least significant difference (LSD) or Kruskal-Wallis H tests. $P < 0.05$ was considered to indicate statistical significance.

RESULTS

Changes in the Gut Microbiota in *S. japonicum* Infected Mice

To investigate whether gut microbiota homeostasis could be disturbed in mice with *S. japonicum* infection, mice were infected with 15 cercariae for 7 weeks. H&E staining revealed granuloma formation around the eggs in the livers of the infected mice (**Supplementary Figure 1A**). Granuloma formation contributed to the Pseudotuberculosis, microulceration, villus structural disorder, and intestinal wall perforation, which were the main pathological changes in the intestine (**Supplementary Figure 1D**). Fibrotic responses were detected by Masson's trichrome staining. The fibrotic area became extensive in both the liver and the intestine in infected mice (**Supplementary Figures 1B,C,E,F**).

16S rDNA high-throughput sequencing was performed to analyze the composition and diversity of the gut microbiota. The average OTU numbers were 372 and 302 in nromal group and infected group, respectively. For alpha diversity analysis, Shannon index (3.67) and ACE index (344.11) in the infected group were higher than those in normal group (**Figures 1A–C**). All the data indicated that the diversity of the gut microbiota was reduced in mice with *S. japonicum* infection compared to normal mice. Taxonomic analyses showed that the abundance of the phylum *Firmicutes* decreased, while that of the phylum *Bacteroidetes* increased with infection. *Proteobacteria* accounted for as little as 2.3% of all bacteria in normal mice but up to 9.2% in infected mice (**Figure 1D**). The abundances of the top 20 bacterial genera were analyzed (**Figure 1E**), and the relative abundances of *Bacteroides*, *Helicobacter* and *Parabacteroides* in the normal group were found to be 3.04, 0.65, and 0.47%, respectively. In contrast, the abundances of these bacteria in the infected group had increased to 23.8, 2.6, and 4%, respectively. The relative abundance of *Alistipes* was higher in the infected group (6.13%) than that in the normal group (2.13%). In contrast, the abundances of *Lachnospiraceae_NK4A136_group* and *Ruminiclostridium* decreased in infected mice. All these data suggested that the gut microbiota composition was disturbed in mice infected with *S. japonicum*.

Depletion of the Gut Microbiota by Antibiotics Attenuated the Intestinal Pathological Injuries in *S. japonicum*-Infected Mice

Antibiotics were administered to explore the impact of the gut microbiota on pathological injuries associated with schistosomiasis. The numbers of OTUs in both normal and infected mice decreased dramatically with antibiotic treatment ($p < 0.001$) (**Figure 2A**). The Shannon index and the ACE index in the antibiotic treatment group were much lower than in the non-treatment group among infected mice (**Figure 2B**), indicating that antibiotic treatment depleted the gut microbiota and reduced species diversity successfully. In detail, the relative abundances of *Bacteroidetes* and *Firmicutes* among all bacteria decreased from >90% in untreated normal mice to <1% in antibiotic-treated normal mice. Only the phylum of *Proteobacteria* (up to 99.9%) could be detected after antibiotic treatment. In infected mice, *Proteobacteria* was also the dominant phylum after antibiotics treatment, with a relative abundance of 60%, much higher than that in infected mice not treated with antibiotics. The abundance of *Bacteroidetes* and *Firmicutes* decreased significantly with the antibiotic treatment (**Figure 2C**). Thus, antibiotic treatment effectively depleted gut microbiota.

To elucidate the effects of antibiotics on the development and reproduction of *S. japonicum*, male worms from mice without and with the antibiotic treatment were stained with acetic red. Six to eight testicular lobes were in the testes, and no difference in the reproductive systems was observed between the two groups (**Figure 3A**). In addition, the lengths and numbers of adult worms from the mice did not differ significantly between the groups (**Figure 3B**). The burden of deposited eggs in the liver and intestine was also not influenced by antibiotic treatment. These results demonstrated that antibiotic treatment depleted the gut microbiota and reduced the species diversity in mice with *S. japonicum* infection but has no significant impact on the development or reproduction of adult worms.

We also examined the effects of gut microbiota depletion on pathological injury in infected mice. Significant alleviation of granulomas was identified in the intestine upon depletion of the gut microbiota with antibiotic treatment (**Figure 3C**). Detection of fibrous collagen by Masson's trichrome staining revealed severe fibrosis in the intestines ($p < 0.01$) of infected mice; however, the fibrotic area decreased obviously with antibiotic treatment ($p < 0.01$) (**Figures 3D,E**). We also observed the pathological changes in the liver in infected mice, and found that these changes were slightly ameliorated with antibiotic treatment (**Supplementary Figure 2A**). Besides, there were no differences of ALT and AST between infected infected mice with the antibiotic treatment or not (**Supplementary Figure 2C**). Thus, we propose that the depletion of the gut microbiota ameliorated the intestinal pathological progress in *S. japonicum*-infected mice.

Gut Microbiota Depletion Modulated the Intestinal Immune Response in Infected Mice

In individuals with schistosomiasis, specific cytokines secreted by immune cells regulated the granulomas and fibrosis development (18). In this study, we examed the expression of IL-4, IL-5, IL-13, IL-10, and TGF-β by immunohistochemistry. All cytokines were expressed at basal levels in normal mice with and without the antibiotic treatment, and no visible differences were observed between treated and untreated mice (data was not shown.). Compared with non-antibiotic-treated infected mice, only IL-10 ($p < 0.05$) was increased in the livers of mice in the antibiotic treatment group; the levels of IL-4, IL-5, IL-13, and TGF-β remained unchanged (**Supplementary Figure 3**). However, antibiotic-treated infected mice exhibited significantly decreased production of cytokines IL-4 ($p < 0.05$), IL-5 ($p < 0.05$), and IL-13 ($p < 0.05$) in the intestine (**Figures 4A,B**). Production of IL-10 ($p < 0.01$) and TGF-β ($p < 0.05$) was increased in the intestines

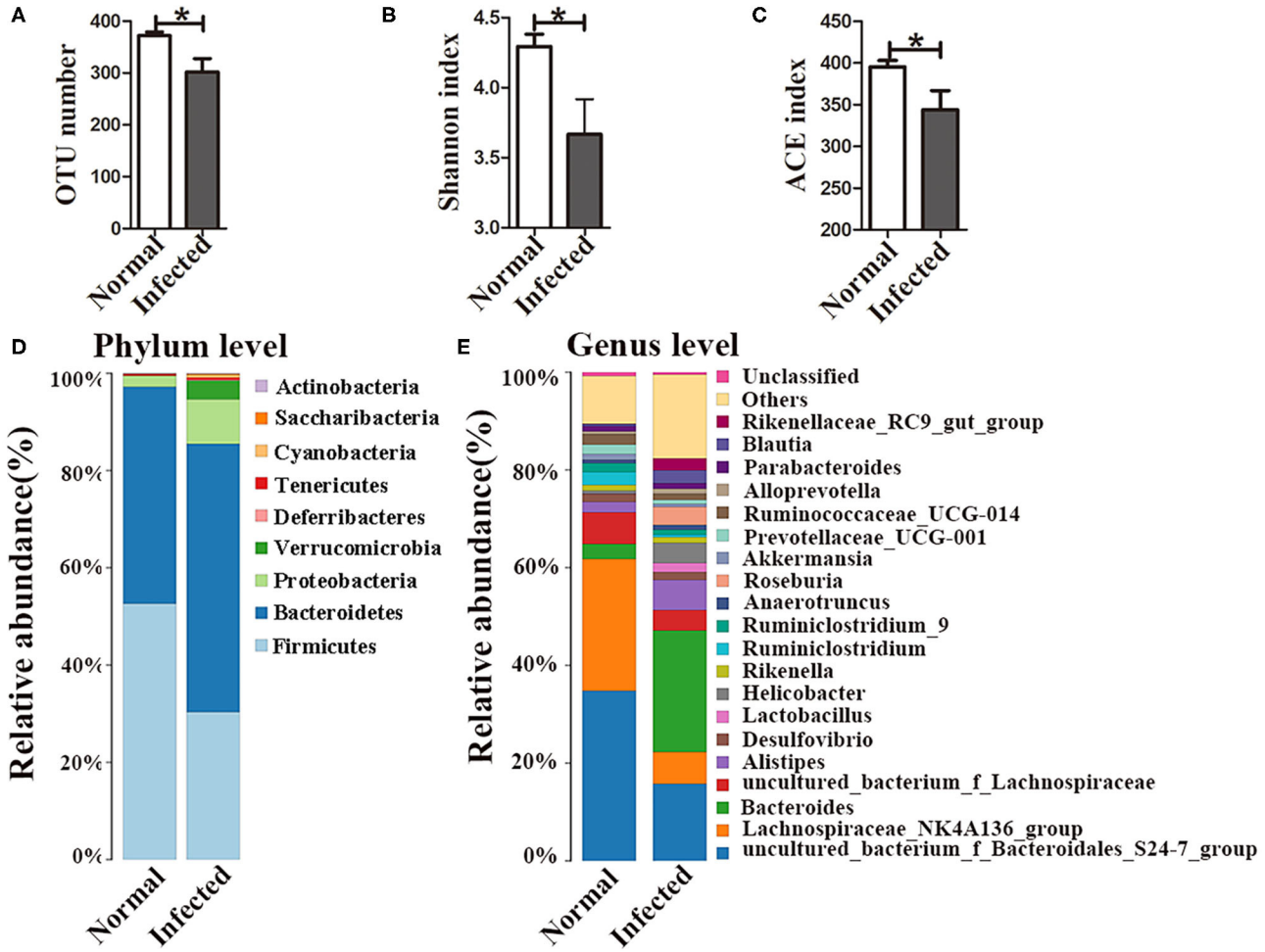

FIGURE 1 | Changes in the gut microbiota in *S. japonicum* infected mice. **(A)** OTU numbers. **(B)** Shannon index values. **(C)** ACE index values. The stacked bar chart indicates the species distributions at the phylum level **(D)** and the genus level **(E)**. * = $p < 0.05$.

of antibiotic-treated infected mice compared to those of non-antibiotic-treated infected mice (**Figures 4A,B**). The mRNA expression profiles of these cytokines in intestine were also tested by Real-time qPCR and showed similar trends (**Figure 4C**) Thus, depletion of the gut microbiota might participate in the regulation of the intestinal inflammatory cytokines expression.

Transfer of the Gut Microbiota From Normal to Infected Mice Attenuated the Intestinal Pathological Injury in Infected Mice

Given that the depletion of the gut microbiota significantly impacts the microbial community on pathogenesis in infected mice, the regulatory role of the gut microbiota in mice was further explored by cohousing infected mice with normal mice for 7 weeks. To profile the microbiota, 16S rDNA high-throughput sequencing was performed on the colons of infected and normal littermate mice. Both the number of OTUs ($p < 0.05$) and the Shannon index ($p < 0.05$) were significantly lower in infected mice than in separately housed groups ($p < 0.05$), but no differences were observed cohoused infected mice and normal mice (**Figures 5A,B**). Taxonomic analyses showed that in the separately housed groups, the infected mice had a higher abundance of the phylum *Proteobacteria* (9.71%) than the normal mice (2.31%) (**Figure 5C**), however, the abundance in infected mice was only 8.03% in the cohousing groups. *Bacteroidetes* and *Firmicutes* were the most dominant bacterial phyla in normal mice. The ratio of *Bacteroidetes* to *Firmicutes* was 0.8 in normal mice and 1.87 in infected mice under separate housing conditions, while the ratio was 2.8 in normal mice and 2.18 in infected mice under cohousing conditions. This fluctuation indicated that the gut microbiota could be transferred between normal and infected littermate mice. The abundances of *Bacteroides* and *Parabacteroides* were significantly higher in infected mice than in normal mice under separate housing conditions, but they were nearly at normal levels in infected mice cohoused with normal mice (**Figure 5D** and **Supplementary Figures 4A,D**). Among separately housed mice, the abundances of *Lachnospiraceae_NK4A136_group* (p

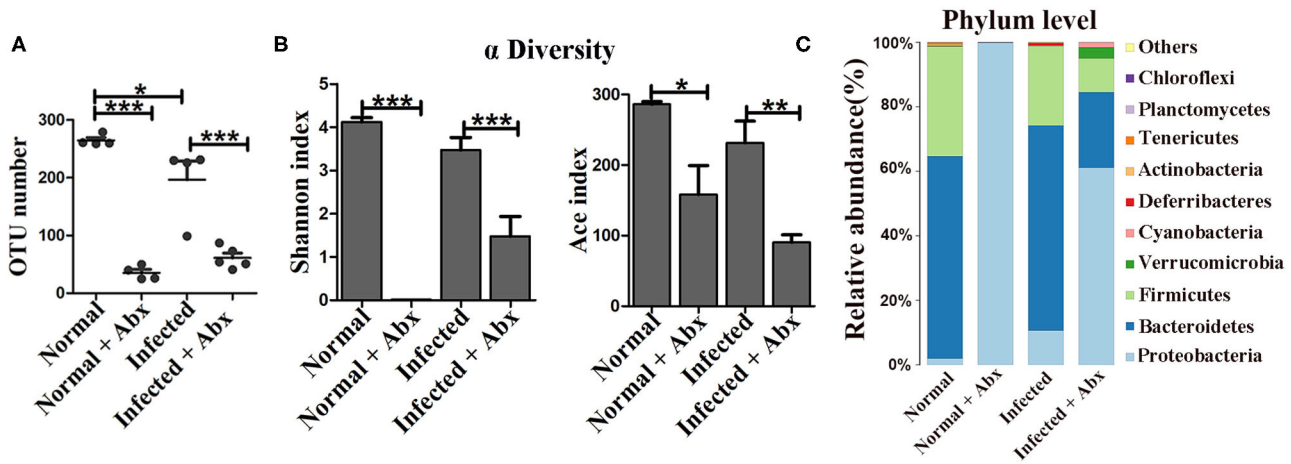

FIGURE 2 | The antibiotic treatment depleted the gut microbiota in mice. In the antibiotic-treated groups, normal and infected mice were given water with an antibiotic cocktail for 7 weeks. **(A)** OTU numbers in the four different groups. **(B)** Alpha diversity (Shannon and ACE index) analysis for the four groups. **(C)** Stacked bar chart showing the species distributions at the phylum level. * = $p < 0.05$, ** = $p < 0.01$, *** = $p < 0.001$.

< 0.05) and *Ruminiclostridium* ($p < 0.01$) were significantly lower in infected mice than in normal mice. However, under cohousing conditions, the abundances of these two genera were slightly decreased in normal mice and increased in infected mice (**Figure 5D** and **Supplementary Figures 4C,F**). Interestingly, the abundances of *Alistipes* and *Helicobacter* were increased in infected mice under separate housing conditions, but remained unchanged in infected mice cohoused with normal mice (**Figure 5D** and **Supplementary Figures 4B,E**). These results suggested that the alteration in the microbiota induced by *S. japonicum* infection could be reversed through microbiota transfer by cohousing of normal and infected mice in the same cage.

Next, we also found that the infected mice which co-housed with normal mice demonstrated attenuation of intestinal granuloma formation and fibrotic responses compared with infected mice housed separately from normal mice (**Figures 6A–C**). Such remission was not obvious in the liver (**Supplementary Figure 2B**). The hepatic function was showed no improvement in infected mice which co-housed with normal mice (**Supplementary Figure 2D**). In contrast, there were no significant differences in worm counts and the number of eggs deposited in the liver and the intestine between infected mice housed separately and cohoused (**Figure 6D**). Therefore, the transfer of gut microbiota from normal mice to infected mice attenuated the histopathology in infected mice but did not influence eggs release in tissues.

Transfer of the Gut Microbiota From Normal to Infected Mice Modulated the Intestinal Immune Responses in Infected Mice

The severity of schistosomiasis related cytokines was also detected by immunohistochemistry. Compared with infected mice housed separately, the liver level of IL-10 was increased ($p < 0.01$) in infected mice which cohoused with normal mice. However, IL-4, IL-5, IL-13, and TGF-β were unchanged (**Supplementary Figure 5**). But, in intestine, IL-4, IL-5, and IL-13 decreased significantly in cohoused infected mice ($p < 0.01$) (**Figures 7A,B**). With regard to anti-inflammatory factors, the intestinal levels of IL-10 ($p < 0.01$) and TGF-β ($p < 0.05$) were higher in the cohoused infected group than in the separately housed infected group. The mRNA levels of these cytokines in intestine exihibited the same trend (**Figure 7C**). Together, these data suggested that the transfer of the gut microbiota from normal to infected mice could modulate immune responses by regulating inflammatory cytokine production in infected mice.

DISCUSSION

Although increasing numbers of studies have tried to elucidate the mechanisms of *S. japonicum*-induced schistosomiasis (12, 18), the role of the gut microbiota has not previously been addressed. Our findings demonstrated that the depletion of the gut microbiota through antibiotics treatment alleviated granuloma formation and fibrotic responses in the intestine, but did not influence the development or fecundity of worms. Changes in the gut microbiota in infected mice upon cohousing with normal mice further suggested that the gut microbiota modulated histopathological injuries, and the intestinal immune response was probably get involved into this process.

In our study, mice infected with *S. japonicum* had a lower diversity of the gut microbiota than normal mice. The abundance of the phylum *Firmicutes* decreased, while that of the phylum *Bacteroidetes* and *Proteobacteria* increased with infection. These data are consistent with the findings of Zhao et al. (14). Schistosomiasis is characterized by inflammation, fibrosis, and chronic pathological injuries. The intestine tissue is the first defensive line to the microbiota (19, 20). In the context of

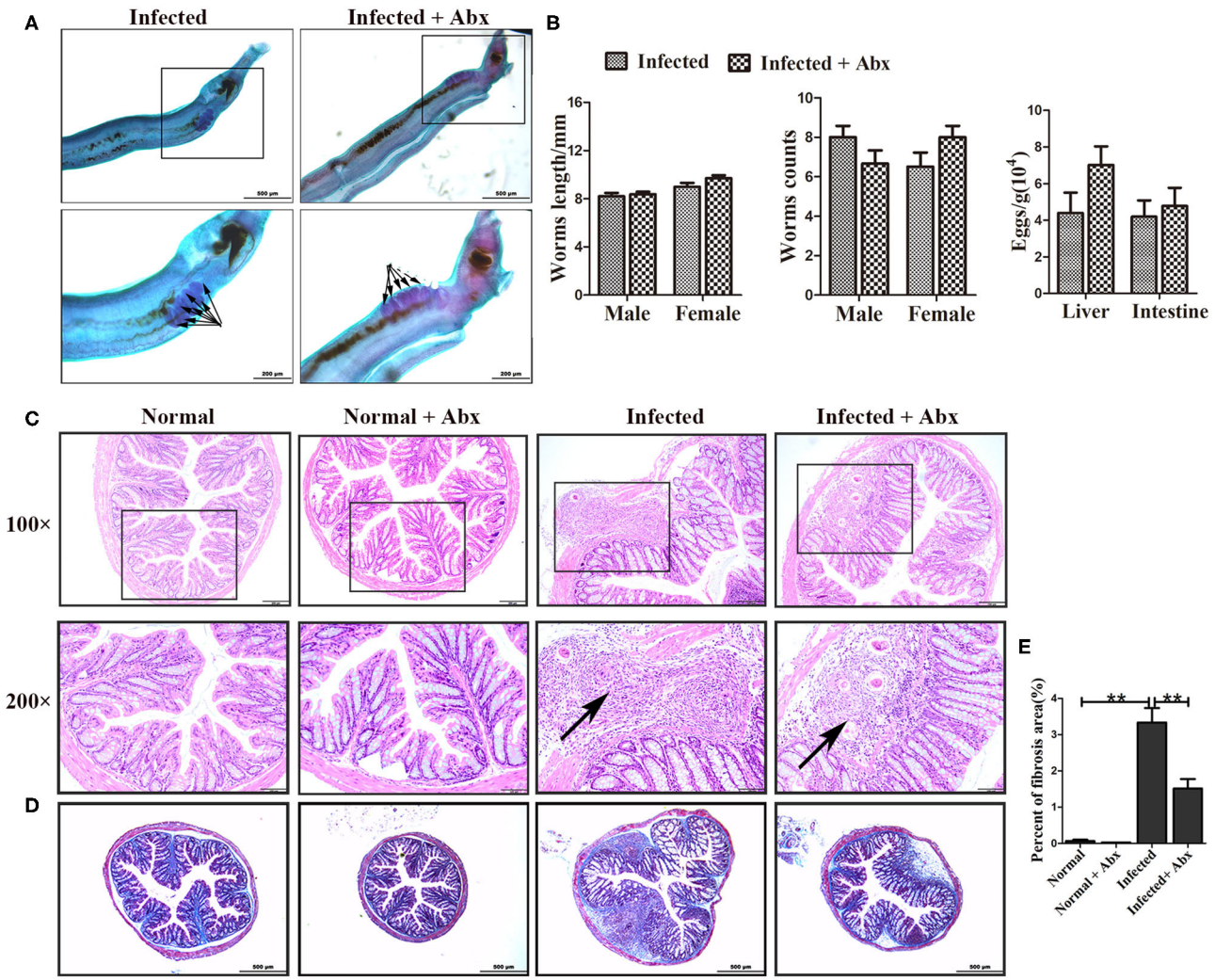

FIGURE 3 | Depletion of the gut microbiota attenuated pathological injuries of the intestine in *S. japonicum* infected mice. **(A)** Morphology of adult males. The arrows indicate the testes of the worms. **(B)** Worm lengths, worm counts, and egg counts per gram in the livers and intestines of infected mice. **(C)** Histopathological changes in the intestine were observed by H&E staining and arrows indicate the eggs granuloma. **(D)** Fibrosis was examined by Masson's trichrome staining. **(E)** The value of fibrotic area in the intestine was analyzed with Image-Pro Plus 6.0 software. ** = $p < 0.01$.

some diseases, reduction or shifts in the composition of the gut microbiota induce pathological injuries in mammals, through the breakdown of the well-established interaction between the microbiota and the host (21–23). Gram-negative *Bacteroidetes* and gram-positive *Firmicutes* are the most dominant taxa in the mammal gut microbiota (24). Mixed broad-spectrum antibiotics depleted the majority of *Firmicutes* and *Bacteroidetes*, leaving only *Parabacteroides* at detectable levels. The depletion of the majority of gut microbes significantly attenuated the intestinal histopathology changes in infected mice. We found that the histopathological remission in the liver was less evident than that in the intestine, showing the depletion of the microbiota affected the liver to a lesser extent compared to the intestine, probably due to the filtering function of the liver (25).

Gut microbes can be transferred among mice that are cohoused. Changes in the microbiota induced by *S. japonicum* infection were partially reversed upon cohousing of normal and infected mice in one cage. Infected mice harbor more bacteria with associations with pro-inflammatory and pro-fibrotic effects. When the homeostatic microbiota in normal mice is transferred to infected mice, granulomas formation and fibrosis in intestinal tissue were both attenuated. This was contributed by the overall regulatory effect of the alterative microbiota. The differences in some phyla between separately housed and cohoused are worth noting. For example, the abundances of the genera *Bacteroides* and *Parabacteroides* in the phylum *Bacteroidetes* were significantly higher in infected mice than in normal mice under separate housing conditions. However, compared with infected mice housed separately, the

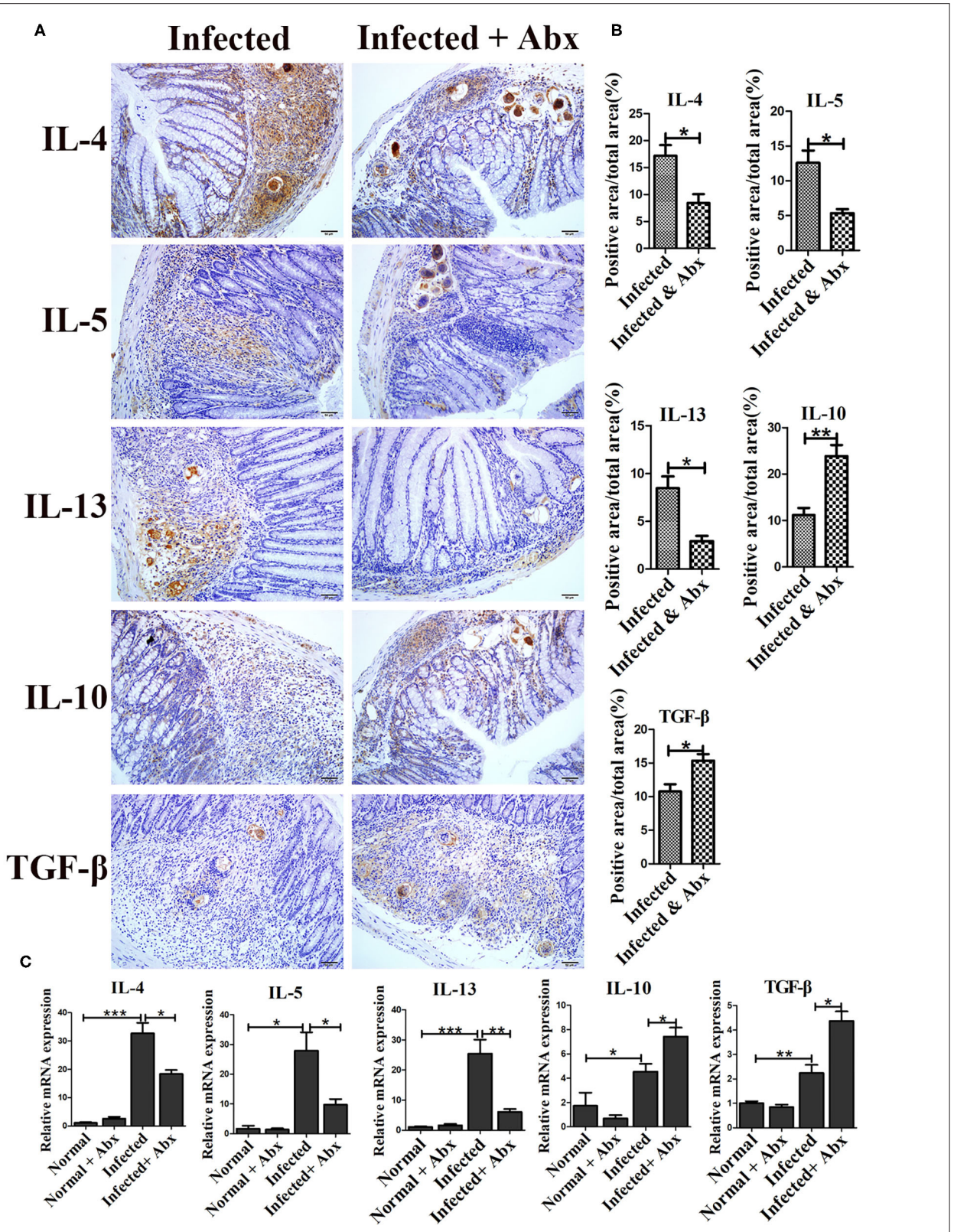

FIGURE 4 | Depletion of the gut microbiota regulated intestinal inflammatory cytokine production in infected mice. **(A)** The levels of IL-4, IL-5, IL-13, IL-10, and TGF-β in the intestine were detected by immunohistochemistry. Cell nuclei were counterstained with haematoxylin. **(B)** The area of the entire tissue and the positive area were analyzed with Image-Pro Plus 6.0 software. **(C)** The mRNA of IL-4, IL-5, IL-13, IL-10, and TGF-β in the intestine were detected by Real-time qPCR. * = $p < 0.05$, ** = $p < 0.01$, *** = $p < 0.001$.

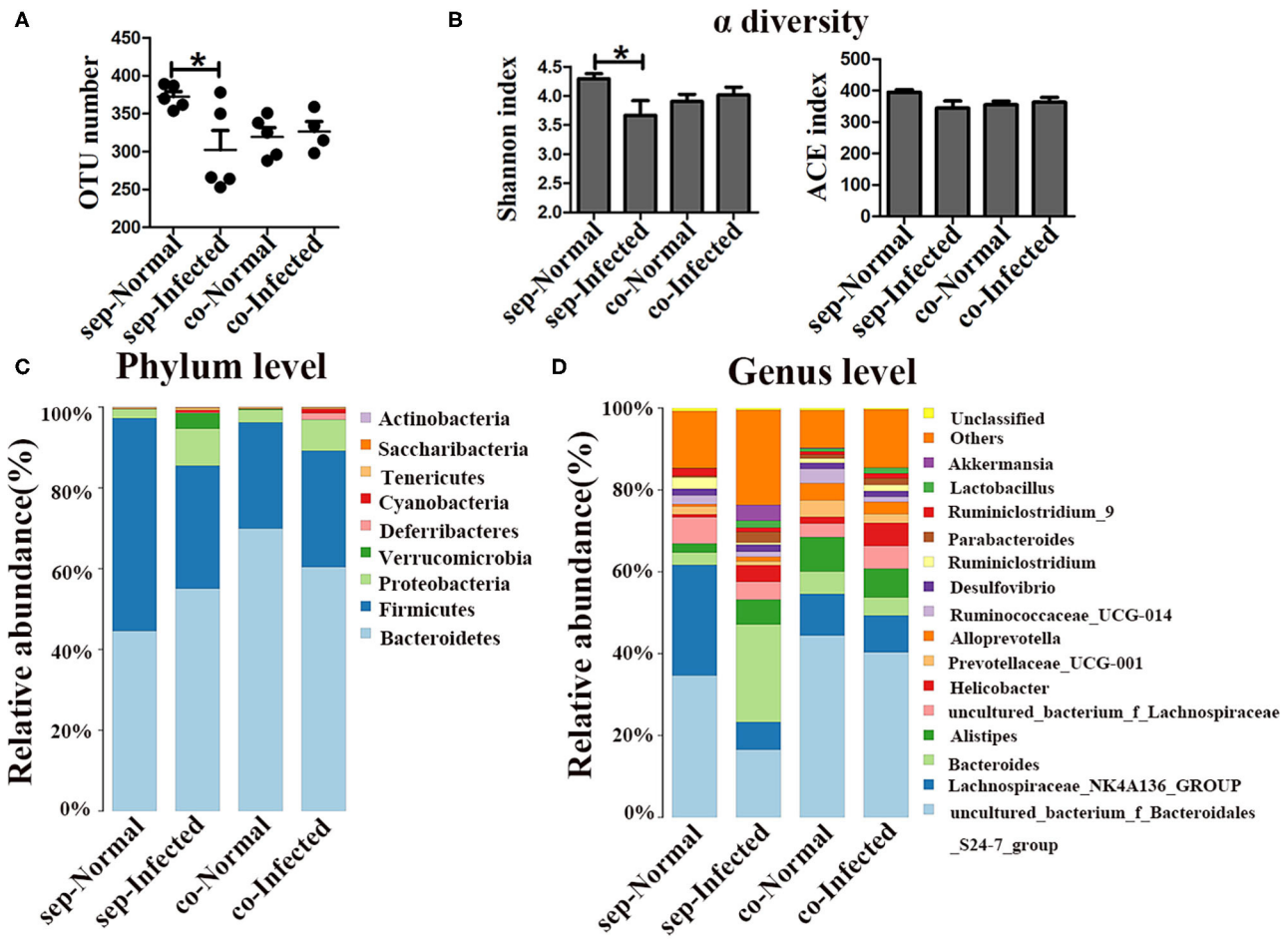

FIGURE 5 | Transfer of the gut microbiota from normal mice to infected mice. Normal mice and infected mice were cohoused or housed separately for 7 weeks. **(A)** OTU numbers in the four different groups. **(B)** Alpha diversity (Shannon and ACE index) analysis for each group. **(C)** Stacked bar chart showing the species-distribution at the phylum level. **(D)** Histogram showing the species distributions at the genus level. * = $p < 0.05$.

levels of bacteria in these taxa were reduced in infected mice under cohousing conditions. Species in the genera of *Bacteroides* and *Parabacteroides* are frequently involved in infectious diseases such as bacteremia and in intra-abdominal processes (26, 27). Over-growth of genus *Bacteroides* has been reported to contribute to the inflammatory changes in patients with Crohn's disease (28). In addition, specific species of *Bacteroides* have been reported to be associated with inflammation and colorectal cancer (29, 30). However, another bacterium, *Bacteroides acidifaciens,* regulates energy metabolism and insulin resistance and thus might be a potential therapeutic agent for diabetes and obesity (31). The abundances of *Lachnospiraceae_NK4A136* and *Ruminiclostridium* declined in *S. japonicum*-infected mice but slightly increased when the infected mice were cohoused with normal mice. The relative abundances of *Lachnospiraceae* species have been reported to be reduced in patients with cirrhosis, inflammatory bowel disease and *Clostridium difficile*-associated colitis compared to healthy individuals (29, 32). Loss of *Lachnospiraceae* might result in decreased production of short-chain fatty acids, which promotes inflammation in mice (32). Further understanding the exact functions of these taxa in schisosomiasis is important and will be beneficial for elucidating the detailed mechanisms of the progression of pathological injuries.

Several drugs, such as nitrofuran, niridazole, amoscanate, and traditional Chinese medicines have been used for the schistosomiasis treatment (33). Most of these drugs damage the ultrastructures of the worms or even kill them directly. However, the antibiotic cocktail used in this study had no effects on worm load, growth, reproductive systems or reproductive capacity. In addition, there were no significant differences in worm burden or deposited egg burden deposition in the liver or the intestine between separately housed and cohoused infected mice. These data indicated that the remission of intestinal histopathological injuries was majorly caused by changes in the gut microbiota

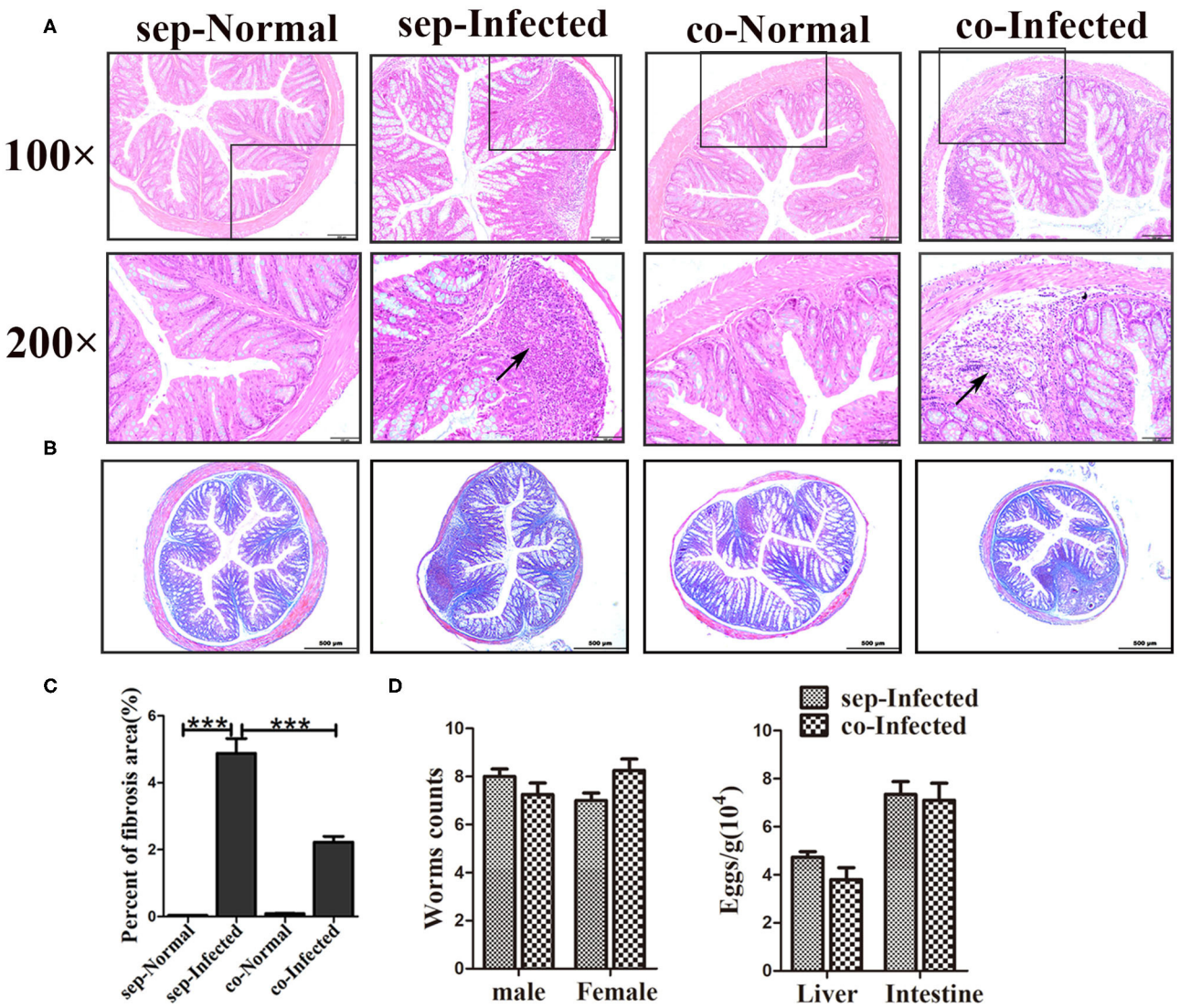

FIGURE 6 | Transfer of the gut microbiota from normal mice to infected mice attenuated pathological injuries of the intestine in *S. japonicum* infected mice. Normal mice and infected mice were cohoused or housed separately for 7 weeks. **(A)** Histopathological changes in the liver were observed by H&E staining and arrows indicate the eggs granuloma. **(B)** Fibrosis formation was examined by Masson's trichrome staining. **(C)** The value of the fibrotic area in the liver was analyzed with Image-Pro Plus6 software. **(D)** Worm counts and egg counts in the livers and intestines of infected mice. *** = $p < 0.001$.

rather than by direct killing of the worms or reductions in egg excretion.

Th2-associated cytokines including IL-4, IL-5, and IL-13, have been identified as important contributors to granulomatous immune responses and fibrosis (18). The immunoregulatory properties of Tregs are driven by IL-10 and TGF-β, to limit excessive Th1 and Th2 immune responses induced by *Schistosoma* infection (34–36). In our study, depletion of the gut microbiota in infected mice by antibiotics, or transfer of the microbiota from normal mice to infected mice, reduced the levels of the IL-4, IL-5, and IL-13 and increased the production of cytokines IL-10 and TGF-β. These effects suggested that the regulatory function of the gut microbiota in intestinal schisosomiasis was mediated by the modulation of the local immune response.

In conclusion, we identified the potential associations among the gut microbiota, immune responses, and pathological injuries in the context of intestinal schistosomiasis. *S. japonicum* infection altered the gut microbiota composition in mice, while changes in microbial composition in infected mice mediated by the antibiotic treatment or microbiota transfer from normal mice alleviated the intestinal pathological injuries. Our work supports a regulatory function of the gut microbiota in the pathogenesis of schistosomiasis and provides insights into the development of new strategies against schistosomiasis japonica.

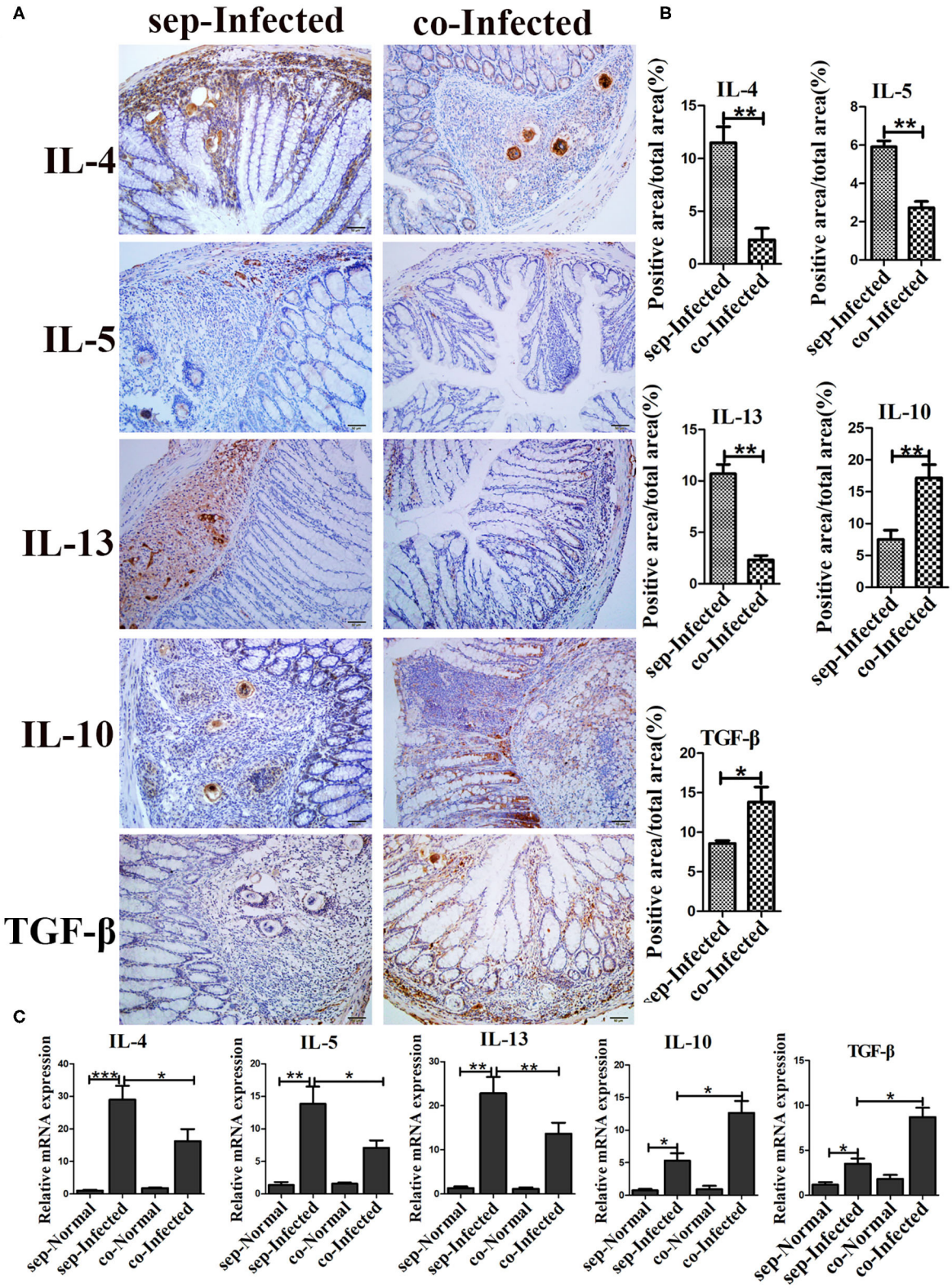

FIGURE 7 | Transfer of the gut microbiota from normal mice to infected mice regulated intestinal inflammatory cytokine production in infected mice. **(A)** The levels of IL-4, IL-5, IL-13, IL-10, and TGF-β in the intestine were detected by immunohistochemistry. Cell nuclei were counterstained with haematoxylin. **(B)** The area of the entire tissue and the positive area were analyzed with Image-Pro Plus 6.0 software. **(C)** The mRNA of IL-4, IL-5, IL-13, IL-10, and TGF-β in the intestine were detected by Real-time qPCR. * = $p < 0.05$, ** = $p < 0.01$, *** = $p < 0.001$.

DATA AVAILABILITY STATEMENT

The datasets presented in this study can be found in online repositories. The names of the repository/repositories and accession number(s) can be found in the article/**Supplementary Material**.

ETHICS STATEMENT

All experiments were conducted in strict accordance with the Guide for the Care and Use of Laboratory Animals of the National Institutes of Health. The experimental procedure was supported by the Committee for Animal Research following the guidelines of Sun Yat-sen University (Permit No: 2016-104).

AUTHOR CONTRIBUTIONS

ZW, XS, DY, and BZ designed the experiments. BZ, QS, AN, JLia, and JLiu performed the experiments. BZ, XW, QS, LS, and YZ contributed to the data analysis. BZ and DY wrote the paper. ZW and XS reviewed the final version of the manuscript and supervised the project. All authors contributed to the article and approved the submitted version.

FUNDING

This work was supported by the National Natural Science Foundation of China (Grant Numbers: 81871682, 81572014, and 81601781), the China Postdoctoral Science Foundation (Grant Number: 2016M591605), and the Science and Technology Program of Guangzhou, China (Grant Number: 201804010006).

ACKNOWLEDGMENTS

We thank the Chinese Center for Disease Control and Prevention for providing us with *Oncomelania hupehensis* (*O. hupehensis*) infected with *S. japonicum* cercariae and Professor Tao Ding for editing our manuscript.

SUPPLEMENTARY MATERIAL

The Supplementary Material for this article can be found online at: https://www.frontiersin.org/articles/10.3389/fmed.2020.588928/full#supplementary-material

REFERENCES

1. McManus DP, Dunne DW, Sacko M, Utzinger J, Vennervald BJ, Zhou XN. Schistosomiasis. *Nat Rev Dis Primers.* (2018) 4:13. doi: 10.1038/s41572-018-0013-8
2. Zhang LJ, Xu ZM, Guo JY, Dai SM, Dang H, Lv S, et al. [Endemic status of schistosomiasis in People's Republic of China in 2018]. *Zhongguo xue xi chong bing fang zhi za zhi.* (2019) 6:576–82.
3. McManus DP, Gray DJ, Li Y, Feng Z, Williams GM, Stewart D, et al. Schistosomiasis in the People's Republic of China: the era of the Three Gorges Dam. *Clin Microbiol Rev.* (2010) 23:442–66. doi: 10.1128/CMR.00044-09
4. Burke ML, Jones MK, Gobert GN, Li YS, Ellis MK, McManus DP. Immunopathogenesis of human schistosomiasis. *Parasite Immunol.* (2009) 31:163–76. doi: 10.1111/j.1365-3024.2009.01098.x
5. Sender R, Fuchs S. Revised estimates for the number of human and bacteria cells in the body. *PLoS Biol.* (2016) 14:e1002533. doi: 10.1371/journal.pbio.1002533
6. Goodrich JK, Waters JL, Poole AC, Sutter JL, Koren O, Blekhman R, et al. Human genetics shape the gut microbiome. *Cell.* (2014) 159:789–99. doi: 10.1016/j.cell.2014.09.053
7. Rangan KJ, Hang HC. Biochemical mechanisms of pathogen restriction by intestinal bacteria. *Trends Biochem Sci.* (2017) 42:887–98. doi: 10.1016/j.tibs.2017.08.005
8. Knights D, Silverberg MS, Weersma RK, Gevers D, Dijkstra G, Huang H, et al. Complex host genetics influence the microbiome in inflammatory bowel disease. *Genome Med.* (2014) 6:107. doi: 10.1186/s13073-014-0107-1
9. Turnbaugh PJ, Hamady M, Yatsunenko T, Cantarel BL, Duncan A, Ley RE, et al. A core gut microbiome in obese and lean twins. *Nature.* (2009) 457:480–4. doi: 10.1038/nature07540
10. Henao-Mejia J, Elinav E, Jin C, Hao L, Mehal WZ, Strowig T, et al. Inflammasome-mediated dysbiosis regulates progression of NAFLD and obesity. *Nature.* (2012) 482:179–85. doi: 10.1038/nature10809
11. Bodkhe R, Balakrishnan B, Taneja V. The role of microbiome in rheumatoid arthritis treatment. *Ther Adv Musculoskelet Dis.* (2019) 11:1759720x19844632. doi: 10.1177/1759720X19844632
12. Carson JP, Ramm GA, Robinson MW, McManus DP, Gobert GN. *Schistosome*-induced fibrotic disease: the role of hepatic stellate cells. *Trends Parasitol.* (2018) 34:524–40. doi: 10.1016/j.pt.2018.02.005
13. Colley DG, Bustinduy AL, Secor WE, King CH. Human schistosomiasis. *Lancet.* (2014) 383:2253–64. doi: 10.1016/S0140-6736(13)61949-2
14. Zhao Y, Yang S, Li B, Li W, Wang J, Chen Z, et al. Alterations of the mice gut microbiome via *Schistosoma japonicum* ova-induced granuloma. *Front Microbiol.* (2019) 10:352. doi: 10.3389/fmicb.2019.00352
15. Peng H, Zhang Q, Li X, Liu Z, Shen J, Sun R, et al. IL-33 Contributes to *Schistosoma japonicum*-induced hepatic pathology through induction of M2 macrophages. *Sci Rep.* (2016) 6:29844. doi: 10.1038/srep29844
16. Yan C, Wang L, Li B, Zhang BB, Zhang B, Wang YH, et al. The expression dynamics of transforming growth factor-beta/Smad signaling in the liver fibrosis experimentally caused by Clonorchis sinensis. *Parasites Vectors.* (2015) 8:70. doi: 10.1186/s13071-015-0675-y
17. Shen J, Lai DH. Nitric oxide blocks the development of the human parasite *Schistosoma japonicum*. *Proc Natl Acad Sci USA*. (2017) 114:10214–9. doi: 10.1073/pnas.1708578114
18. Chuah C, Jones MK, Burke ML, McManus DP, Gobert GN. Cellular and chemokine-mediated regulation in *schistosome*-induced hepatic pathology. *Trends Parasitol.* (2014) 30:141–50. doi: 10.1016/j.pt.2013.12.009
19. Johansson ME, Sjovall H, Hansson GC. The gastrointestinal mucus system in health and disease. *Nat Rev Gastroenterol Hepatol.* (2013) 10:352–61. doi: 10.1038/nrgastro.2013.35
20. Tropini C, Earle KA, Huang KC, Sonnenburg JL. The gut microbiome: connecting spatial organization to function. *Cell Host Microbe.* (2017) 21:433–42. doi: 10.1016/j.chom.2017.03.010
21. Turnbaugh PJ, Ley RE, Mahowald MA, Magrini V, Mardis ER, Gordon JI. An obesity-associated gut microbiome with increased capacity for energy harvest. *Nature.* (2006) 444:1027–31. doi: 10.1038/nature05414
22. Belkaid Y, Hand TW. Role of the microbiota in immunity and inflammation. *Cell.* (2014) 157:121–41. doi: 10.1016/j.cell.2014.03.011
23. Tilg H, Cani PD, Mayer EA. *Gut* microbiome and liver diseases. *Gut.* (2016) 65:2035–44. doi: 10.1136/gutjnl-2016-312729
24. Eckburg PB, Bik EM, Bernstein CN, Purdom E, Dethlefsen L, Sargent M, et al. Diversity of the human intestinal microbial flora. *Science.* (2005) 308:1635–8. doi: 10.1126/science.1110591
25. Haque TR, Barritt AS. Intestinal microbiota in liver disease. *Best Pract Res Clin Gastroenterol.* (2016) 30:133–42. doi: 10.1016/j.bpg.2016.02.004
26. Aldridge KE. The occurrence, virulence, and antimicrobial resistance of anaerobes in polymicrobial infections. *Am J Surg.* (1995) 169 (5A Suppl.):2s—7s.

27. Boente RF, Ferreira LQ, Falcao LS, Miranda KR, Guimaraes PL, Santos-Filho J, et al. Detection of resistance genes and susceptibility patterns in Bacteroides and Parabacteroides strains. *Anaerobe*. (2010) 16:190–4. doi: 10.1016/j.anaerobe.2010.02.003
28. Ramanan D, Tang MS, Bowcutt R, Loke P, Cadwell K. Bacterial sensor Nod2 prevents inflammation of the small intestine by restricting the expansion of the commensal Bacteroides vulgatus. *Immunity*. (2014) 41:311–24. doi: 10.1016/j.immuni.2014.06.015
29. Zackular JP, Baxter NT, Iverson KD, Sadler WD, Petrosino JF, Chen GY, et al. The gut microbiome modulates colon tumorigenesis. *MBio*. (2013) 4:e00692–13. doi: 10.1128/mBio.00692-13
30. Yang JY, Lee YS, Kim Y, Lee SH, Ryu S, Fukuda S, et al. Gut commensal *Bacteroides* acidifaciens prevents obesity and improves insulin sensitivity in mice. *Mucosal Immunol.* (2017) 10:104–16. doi: 10.1038/mi.2016.42
31. Bajaj JS, Heuman DM, Hylemon PB, Sanyal AJ, White MB, Monteith P, et al. Altered profile of human gut microbiome is associated with cirrhosis and its complications. *J Hepatol.* (2014) 60:940–7. doi: 10.1016/j.jhep.2013.12.019
32. Bajaj JS, Kakiyama G, Savidge T, Takei H, Kassam ZA, Fagan A, et al. Antibiotic-associated disruption of microbiota composition and function in cirrhosis is restored by fecal transplant. *Hepatology*. (2018) 68:1549–58. doi: 10.1002/hep.30037
33. Xiao SH, Sun J, Chen MG. Pharmacological and immunological effects of praziquantel against *Schistosoma japonicum*: a scoping review of experimental studies. *Infect Dis Poverty*. (2018) 7:9. doi: 10.1186/s40249-018-0391-x
34. Wilson MS, Mentink-Kane MM, Pesce JT, Ramalingam TR, Thompson R, Wynn TA. Immunopathology of schistosomiasis. *Immunol Cell Biol.* (2007) 85:148–54. doi: 10.1038/sj.icb.7100014
35. Wang X, Zhou S, Chi Y, Wen X, Hoellwarth J, He L, et al. CD4+CD25+ Treg induction by an HSP60-derived peptide SJMHE1 from Schistosoma. *Eur J Immunol.* (2009) 39:3052–65. doi: 10.1002/eji.200939335
36. Romano A, Hou X, Sertorio M, Dessein H, Cabantous S, Oliveira P, et al. FOXP3^{+} regulatory T cells in hepatic fibrosis and splenomegaly caused by *Schistosoma japonicum*: the spleen may be a major source of Tregs in subjects with splenomegaly. *PLoS Negl Trop Dis.* (2016) 10:e0004306. doi: 10.1371/journal.pntd.0004306

Conflict of Interest: The authors declare that the research was conducted in the absence of any commercial or financial relationships that could be construed as a potential conflict of interest.

frontiers in Medicine

SYSTEMATIC REVIEW
published: 03 December 2020
doi: 10.3389/fmed.2020.592472

Efficacy and Safety of Glecaprevir/Pibrentasvir in HCV Patients With Previous Direct-Acting Antiviral Therapy Failures: A Meta-Analysis

Chao Shen[1†], Haozhi Fan[2†], Zhijun Ge[3], Weihua Cai[4], Jianguo Shao[5], Chen Dong[6], Hong Xue[7], Zuqiang Fu[1], Jun Li[8], Yun Zhang[1,9] and Ming Yue[8]*

[1] Key Laboratory of Infectious Diseases, Department of Epidemiology and Biostatistics, School of Public Health, Nanjing Medical University, Nanjing, China, [2] Department of Information, First Affiliated Hospital of Nanjing Medical University, Nanjing, China, [3] Department of Critical Care Medicine, The Affiliated Yixing Hospital of Jiangsu University, Yixing, China, [4] Department of General Surgery, Third Affiliated Hospital of Nantong University, Nantong, China, [5] Department of Digestive Medicine, Third Affiliated Hospital of Nantong University, Nantong, China, [6] Department of Epidemiology and Statistics, School of Public Health, Medical College of Soochow University, Suzhou, China, [7] Department of Severe Infectious Diseases, Third Affiliated Hospital of Nantong University, Nantong, China, [8] Department of Infectious Diseases, First Affiliated Hospital of Nanjing Medical University, Nanjing, China, [9] Institute of Epidemiology and Microbiology, Eastern Theater Command Centers for Disease Prevention and Control, Nanjing, China

OPEN ACCESS

Edited by:
Chao Yan,
Xuzhou Medical University, China

Reviewed by:
Hui Jin,
Southeast University, China
Mousumi Chaudhury,
Arkansas Children's Nutrition Center, United States
Wenshi Wang,
Heidelberg University Hospital, Germany

***Correspondence:**
Ming Yue
yueming@njmu.edu.cn

[†]These authors have contributed equally to this work

Specialty section:
This article was submitted to Gastroenterology, a section of the journal Frontiers in Medicine

Received: 07 August 2020
Accepted: 13 November 2020
Published: 03 December 2020

Citation:
Shen C, Fan H, Ge Z, Cai W, Shao J, Dong C, Xue H, Fu Z, Li J, Zhang Y and Yue M (2020) Efficacy and Safety of Glecaprevir/Pibrentasvir in HCV Patients With Previous Direct-Acting Antiviral Therapy Failures: A Meta-Analysis. Front. Med. 7:592472. doi: 10.3389/fmed.2020.592472

Background: Since a greater number of hepatitis C virus (HCV) patients have access to direct-acting antiviral (DAA) based therapies, the number of patients not properly responding to prior DAA regimens is increasing. The objective of this comprehensive analysis was to assess the efficacy and safety of glecaprevir/pibrentasvir (GLE/PIB) in HCV patients who experienced previous DAA therapy failures.

Methods: Bibliographic databases were systematically searched for relevant articles published by November 2020. The main endpoints were sustained viral response after 12 weeks (SVR12), adverse events (AEs; any grade) and severe adverse events (SAEs). Publication bias assessment was performed using funnel plots and the Egger's test.

Results: Fourteen studies consisting of a total of 1,294 subjects were included in this study and the pooled estimate of SVR12, AEs and SAEs rates were 96.8% (95%CI: 95.1–98.2), 47.1% (95%CI: 26.0–69.3), and 1.8% (95%CI: 0.7–3.4), respectively. Subgroup analysis showed that pooled SVR12 rates were 97.9% (95%CI: 96.7–98.9) for Japan and 91.1% (95%CI: 87.3–94.3) for the United States; 95.8% (95%CI: 93.9–97.4) for genotype (GT)1 and 100.0% (95%CI: 99.6–100.0) for GT2; 95.3% (95%CI: 92.4–97.2) for cirrhosis and 96.3% (95%CI: 94.2–97.7) for non-cirrhosis cases. There was no publication bias included this study.

Conclusion: This comprehensive analysis revealed that GLE/PIB is an effective and secure retreatment option for patients who did not optimally respond to DAA treatment, especially the Asian population with GT1-2.

Keywords: pibrentasvir, retreatment, DAAs therapy failures, meta-analysis, glecaprevir

INTRODUCTION

Hepatitis C virus infection is a common disease affecting ∼180 million individuals worldwide (1, 2). According to the World Health Organization (WHO), ∼71 million people develop chronic HCV infections that may lead to cirrhosis, hepatocellular carcinoma (HCC) and liver-related deaths (3, 4). In addition to prevention, effective regimens are critical to achieve the WHO goal of eliminating HCV as a major global public health threat by 2030 (5).

Treatment of HCV has evolved over the past decade. Before direct-acting antiviral, interferon (IFN)-based regimens were the main method of HCV, but the cure rate using this regimen was only 40–65% (6). In addition, the incidence of SAEs and discontinuation of these treatments were both frequent (7). Compared with IFN-based regimens, the efficacy and safety of DAA-based therapies for HCV resulted in dramatical improvements, including high sustained virologic response (SVR) rates, shorter treatment duration, better tolerability, and less SAEs. Despite excellent efficacy of DAA-based regimens, about 5% of patients still failed to achieve SVR and have just drawn public attention in recent years (8). Given the size of the HCV infected population, the absolute number of patients with DAA treatment failure is substantial and increasing as more patients have access to DAA-based therapies. Thus, effective and alternative treatment strategies for these individuals are particularly important.

In 2017, the combination of glecaprevir (GLE; a second-generation NS3/4 protease inhibitor) and pibrentasvir (PIB; a second-generation NS5A inhibitor) was approved and this combination shows high anti-HCV activity across genotypes 1–6 with a high *in vitro* barrier to resistance (9, 10). In clinical trials, GLE/PIB regimens showed high efficacy and favorable safety for all six major HCV genotypes (11, 12). In addition, GLE/PIB treatments were also effective and well-tolerated in patients with compensated cirrhosis or those with severe renal impairment (13, 14). Furthermore, recent studies uncovered that GLE/PIB regimens are highly effective in patients who failed to achieve SVR after prior DAA therapies (15, 16). However, the relevant researches were just conducted recently and there haven't been a lot of researches in this population. The European Association for the Study of the Liver (EASL) recommended the GLE/PIB regimen to treat treatment-experienced (pegylated IFN-a and ribavirin, pegylated IFN-a, ribavirin, and sofosbuvir, or sofosbuvir and ribavirin) HCV patients, but did not explicitly recommended this regimen to retreat patients with DAA treatment failure on account of insufficient supporting evidences.

Even though the latest guidelines from China recommended using GLE/PIB to retreat patients with prior DAA failure (17), further research is needed to increase the confidence of this recommendation. The aim of this systematic review was to assess the efficacy and safety of GLE/PIB regimens for patients who experienced DAA treatment failure.

METHOD

Search Strategy

Preferred reporting items for systematic review and meta-analyses (PRISMA) were followed to conduct this study (18). Two investigators independently performed a systematic and comprehensive literature search using multiple databases including PubMed, Embase, Web of Science, Cochrane Library, CNKI, and WanFang Data. Key search terms included (Hepacivirus OR Hepaciviruses OR Hepatitis C-Like Viruses OR Hepatitis C Like Viruses OR Hepatitis C virus OR Hepatitis C viruses OR HCV) AND (glecaprevir OR ABT-493) AND (pibrentasvir OR ABT-530). A manual search was also performed by checking related references and reviewing citations included in the selected publications. There were no language restrictions. The literature search was last updated in November 2020.

Selection Criteria

Studies were be included if they met all the following criteria: (1) HCV patients with previous DAA therapy failures (defined as failure to achieve SVR12 after DAA treatment); (2) retreatment with GLE/PIB; (3) the primary endpoint was SVR12.

Studies were excluded if they met any of the following criteria: (1) patients without a DAA treatment history; (2) patients with a DAA treatment history, but unclear information as to whether they experienced DAA therapy failure; (3) patients who were liver transplant recipients with recurrent hepatitis C; (4) a sample size <10; (5) reports that did not provide the primary endpoint (SVR12); (6) case reports, letters, meta-analysis, editorials or reviews; (7) pharmacokinetics or pharmacodynamics studies.

Outcome Measures

The primary outcome was the percentage of SVR12, which was defined as plasma HCV RNA below the lower limit of quantification (LLOQ) 12 weeks after end of treatment (EOT). Additional secondary primary outcomes included the percentage of patients with on-treatment breakthrough and post-treatment relapse. Breakthrough was defined as HCV RNA becoming detectable after HCV RNA below LLOQ during the treatment period. Relapse was defined as undetectable HCV RNA at EOT but became detectable within 12 weeks after. We assessed safety in terms of the incidence and intensity of AEs (any grade), common AEs (CAEs), SAEs, and discontinuation due to AEs. Analyses of secondary primary and safety outcomes included only studies reporting these data.

Study Selection and Data Extraction

Study selection and data extraction performed by two independent researchers (CS and HZF). Study selection followed the predetermined selection criteria. Records found through primary search were initially reviewed by title and abstract. The full texts of potentially eligible studies were reviewed and eligible studies were included.

Required data were extracted from eligible studies and respected the original description. The extracted data included study characteristics (the first author's name, year of publication,

region, study design, setting, publication type, sample size, subgroup number of patients, regimen, and treatment duration); patient characteristics (age, sex, HCV genotype, treatment history, resistance-associated substitutions, and presence of cirrhosis) and study outcomes (SVR12, on-treatment breakthrough, post-treatment relapse, AEs, CAEs, SAEs, and discontinuation due to AEs).

During this process, any conflicts arising between the two reviewers were resolved by consensus with the help of a third researcher (ZQF).

Quality Assessment

The quality of studies included was assessed using the Newcastle-Ottawa quality assessment scale (NOS) for observational studies, including eight items with a total score of nine. Low quality was scored as 0–5 points, moderate quality as 6–7 points, and high quality as 8–9 points (19). The quality of randomized studies was assessed using the Cochrane Collaboration's tool. The Cochrane Collaboration's tool addresses seven specific domains including randomization, allocation concealment, blinding of subjects, blinding of outcome assessors, reporting of incomplete outcome data, selective outcome reporting, and other potential sources of bias. In each domain, every study took one of three categories: "low risk," "high risk," or "unclear risk" for bias (20). The quality of each included study was independently assessed by two investigators.

Statistical Analysis

Effect sizes were collected as pooled event incidences with corresponding 95% confidence intervals (95% CI) using the inverse variance method. Zero events were estimated using Freeman-Tukey double arcsine transformation. Heterogeneity between studies was assessed using Cochran Q-statistics and I^2 statistics. An $I^2 < 50\%$ indicated little or no heterogeneity and then the fixed-effects model was used; When the $I^2 \geq 50\%$, this indicated moderate or substantial heterogeneity and the random-effects model was used. To effectively evaluate the efficacy and safety of GLE/PIB, we conducted subgroup analyses of SVR12 by region, setting, duration of treatment, HCV genotype, treatment history, and presence of cirrhosis. Publication bias was explored using funnel plots and the Egger's test. All statistical tests were two-sided, with a $p < 0.05$ considered as statistically significant. All statistical analyses were conducted using R version 3.6.3.

RESULTS

Study Selection and Basic Information

Our initial search retrieved 1,500 records. After removing 770 overlapping studies, the titles and abstracts of 730 articles were screened. After assessing the full text of 63 articles, 49 articles were excluded for various reasons, and 14 articles (21–34) were eventually added to this study (**Figure 1**).

The 14 studies were all published since 2018, including 12 full-articles and two conference abstracts. All studies came from two regions: 12 from Japan and two from the United States. Overall 1,294 subjects showed chronic HCV infection with GT1-3, DAA treatment experience and some were presented with cirrhosis. The treatment regimens were fixed-dose combinations of GLE (300 mg/d) and PIB (120 mg/d) with or without ribavirin (RBV). Treatment courses included 12 and 16 weeks, respectively. Details of study and patient characteristics are shown in **Tables 1**, **2**.

Quality of the Included Studies

Twelve observational studies were assessed by NOS. Among these studies, three were of high quality, six were of moderate quality and the others were of low quality. The quality assessment scores are shown in **Supplementary Table 1**.

Two clinical trials (26, 32) were assessed using the Cochrane Collaboration's tool. Among these assessed items, randomization, allocation concealment, reporting of incomplete outcome data, selective outcome reporting, and other potential sources of bias were reported in these two different studies. These results are represented in **Supplementary Figure 1**.

Efficacy of Outcomes

SVR12

Data on SVR12 rates of GLE/PIB retreatment for HCV infection were available in all studies (1,294 cases). The pooled estimation of the SVR12 rate from the random-effect model was 96.8% (95%CI: 95.1–98.2, $I^2 = 37.1\%$, $P = 0.08$) (**Figure 2A**).

Breakthroughs and Relapses

In nine studies (21–27, 29, 32), only 11 of the 503 HCV patients retreated with GLE/PIB showed an on-treatment breakthrough with a pooled rate being 0.92% (95%CI: 0.08–2.32, $I^2 = 13.1\%$, $P = 0.33$) (**Figure 2B**). Furthermore, 19 of the 617 patients from 10 studies (21–27, 29, 31, 32) showed a post-treatment relapse with a pooled rate being 1.96% (95%CI: 0.78–3.50, $I^2 = 0.0\%$, $P = 0.55$) (**Figure 2C**).

Subgroup Analysis of the SVR12 Rate

Based on settings, regions, genotypes, treatment history, treatment durations and the presence or absence of cirrhosis, we conducted subgroup analyses as detailed in **Table 3**. The rate of SVR12 was 96.0% (95%CI: 93.4–97.5) in multi-center and 96.1% (95%CI: 92.3–98.0) in single-center studies. Approximately 97.9% of patients (95%CI: 96.7–98.9) in Japan presented achieved SVR12 rate, while the SVR12 rate of the United States subgroup was 91.1% (95%CI: 87.3–94.3). As for genotypes, the pooled SVR12 rates in GT1, GT2, and GT3 were 95.8% (95%CI: 93.9–97.4), 100.0% (95%CI: 99.6–100.0), and 100.0% (95%CI:66.74–100.0). In subgenotype subgroups, GT1a, GT1b, GT2a, and GT2b were 90.3% (95%CI: 84.4–94.2), 94.8% (95%CI: 90.3–97.3), 100.0% (95%CI: 99.7–100.0), and 100.0% (95%CI: 98.3–100.0), respectively. Among the patients who had treatment history available for analysis, the SVR12 rates of sofosbuvir/ribavirin (SOF/RBV), daclatasvir/asunaprevir (DCV/ASV), ledipasvir/sofosbuvir (LDV/SOF), ombitasvir/paritaprevir/ritonavir (OBV/PTV/r), elbasvir/grazoprevir (EBV/GZR), and other DAAs were 100.0% (95%CI: 99.2–100.0), 97.6% (95%CI: 92.9–100.0), 99.3% (95%CI: 86.0–100.0), 100.0% (95%CI: 73.9–100.0), 97.4% (95%CI: 62.0–100.0), and 96.5% (95%CI: 95.1–97.7), respectively. Nine studies

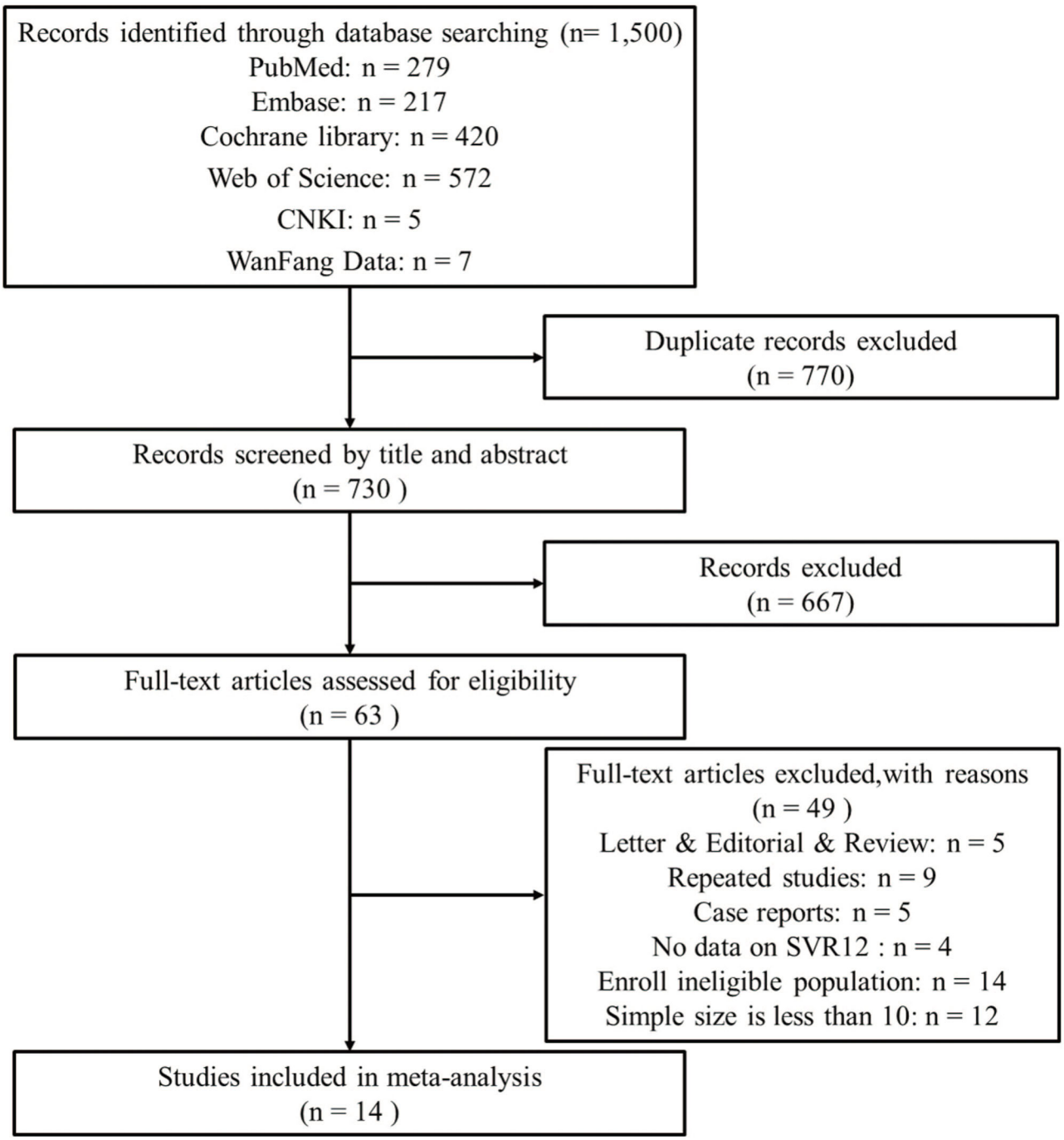

FIGURE 1 | The flow diagram of literature screening and following the preferred reporting items of systematic reviews and meta-analyses (PRISMA).

including 784 patients provided data for subgroup analysis with the presence or absence of cirrhosis. The SVR12 rates for patients with or without cirrhosis were 95.3% (95% CI: 92.4–97.2) and 96.3% (95% CI: 94.2–97.7), respectively.

Additionally, the SVR12 rate of the Japan subgroup was higher than the United States subgroup ($P = 0.0003$) and the GT1 was lower than the GT2-3 ($P = 0.0064$). However, there were no significant differences between the other subgroups analyzed.

Safety

Six studies reported numbers for AEs, CAEs, SAEs, and discontinuation due to AEs were 288, 273, 12, and 4, respectively.

TABLE 1 | Characteristics of the studies included in this comprehensive analysis.

Study	Year	Study design	Publication type	Region	Setting	Regimen	Sample size	Duration (weeks)
Shunji Watanabe	2019	Observational study	Full	Japan	Multi-center	GLE/PIB	13	12
Hayato Uemura	2019	Cohort study	Full	Japan	Single-center	GLE/PIB	42	12
Atsushi Suetsugu	2019	Observational study	Conference abstract	Japan	NA	GLE/PIB	13	12
Hitomi Sezak	2019	Prospective cohort study	Full	Japan	Single-center	GLE/PIB	88	12
Mitsutaka Osawa	2019	Observational study	Full	Japan	Single-center	GLE/PIB	30	12
Anna S. Lok	2019	Clinical trial	Full	United States	Multi-center	GLE/PIB ± RBV	177	12/16
Atsunori Kusakabe	2019	Observational study	Full	Japan	Multi-center	GLE/PIB	28	12
Masayuki Kurosaki	2019	Observational study	Conference abstract	Japan	Multi-center	GLE/PIB	237	12
Norio Akuta	2018	Observational study	Full	Japan	Single-center	GLE/PIB	20	12
Fred Poordad	2018	Clinical trial	Full	United States	Multi-center	GLE/PIB	91	12/16
Hidenori Toyoda	2019	Prospective cohort study	Full	Japan	Multi-center	GLE/PIB	199	12
Akihiro Tamori	2019	Observational study	Full	Japan	Multi-center	GLE/PIB	115	12
Ayumi Sugiura	2020	Cohort study	Full	Japan	Single-center	GLE/PIB	23	12
Akito Nozaki	2020	Observational study	Full	Japan	Multi-center	GLE/PIB	218	12/16

GLE, glecaprevir; PIB, pibrentasvir; RBV, ribavirin; NA, not applicable.

The pooled rates of AEs, CAEs, SAEs, and discontinuation due to AEs were 47.1% (95%CI: 26.0–69.3), 45.2% (95%CI: 25.3–66.7), 1.8% (95%CI: 0.7–3.4), and 0.1% (95%CI: 0.0–0.9), respectively (**Table 4**). The main CAEs were fatigue (6.8%), headache (8.1%), nausea (4.1%), pruritus (11.8%), and appetite loss (1.3%). Furthermore, three studies observed treatment-related laboratory abnormalities in seven patients, including elevation of total bilirubin (5/254) and serum ALT levels (2/254).

Publication Bias and Sensitivity Analysis

Funnel plots for the SVR12 rate are shown in **Supplementary Figures 2, 3**. The Egger's test for evaluating publication bias showed that no publication bias was identified in these studies ($t = 1.72$, $P = 0.11$). Furthermore, the results from the sensitivity analysis manifested that the pooled estimate of SVR12 did not depend on a single study (**Supplementary Figure 4**).

DISCUSSION

This study provided estimates regarding the efficacy and safety following GLE/PIB retreatment for patients who experienced prior DAA treatment failure. These results indicated that GLE/PIB for patients experiencing DAA therapy failure can achieve high SVR12 rates at 12 and 16 weeks, regardless of sex, age, genotype, the presence or absence of cirrhosis or other demographic factors. The rates of SAEs and discontinuation due to adverse events were minimal in GLE/PIB. Thus, GLE/PIB is an effective and secure retreatment option for patients who experience DAA treatment failure and this is critical information for global HCV treatment guidelines.

In this meta-analysis, the pooled SVR12, breakthrough, and relapse rates were 96.8% (95%CI: 95.1–98.2), 0.92% (95%CI: 0.08–2.32), and 1.96% (95%CI: 0.78–3.50), respectively. Compared with sofosbuvir/velpatasvir/voxilaprevir (35), and sofosbuvir/elbasvir/grazoprevirs ± ribavirin (36) retreatments, their SVR12 rates were similar. The incidence of failure of GLE/PIB was lower than other regimens, such as sofosbuvir/daclatasvir (5.7%) and sofosbuvir/velpatasvir (3.4%) (37). Although sofosbuvir/velpatasvir/ voxilaprevir was considered as a highly effective option for the re-treatment of HCV patients, the AEs (100%), SAEs (6.5%), and discontinuation due to AEs rates (5.2%) rates were higher than what was observed for GLE/PIB (AEs = 47.1%, SAEs = 1.8%, and discontinuation due to AEs = 0.1%) (35, 38), which explained an advantage for the GLE/PIB regimen.

Our findings revealed that the SVR12 rate among individuals in Japan was significantly higher than individuals in the United States. Only two studies ($n = 268$) were derived from the United States, so this analysis may be restricted by a finite sample size. Alternatively, a possible explanation was that therapy efficacy was related to race. Kanwal et al. reported differences among gender and race subgroups in the DAA treatment group (39). Most patients in Japan were Asians while most patients in the United States were White, Hispanic or Black. In addition, retreatment data from Asians were limited and available research showed that the SVR24 rate was 91.2% in patients with previous therapy failures (40). Therefore, our study suggested that GLE/PIB was of great significance for the retreatment of Asians with HCV therapy failures and more studies are needed for further evaluation in the United States.

In terms of genotype, there were significant differences among GTs 1-3 while no significant differences were in subgenotype subgroups (GT1a vs. GT1b; GT2a vs. GT2b). In previous studies, patients with GT3 infection showed lower SVR rates compared with other GTs. However, our data were inconsistent with previous studies since the SVR12 rates of GTs2-3 were 100% higher than GT1 (95.4%). On one hand, the sample size of GT3 was small ($n = 6$) which caused poor accuracy and reliability so more GT3 cases should be included to obtain enough evidence. We inferred that GLE/PIB still had a high efficacy for GT3 in patients with previous DAA therapy failures,

TABLE 2 | Patient characteristics of the studies enrolled in this comprehensive analysis.

Study	Year	Age (year)	Sex (M/F)	Cirrhosis (Yes/NO)	HCV-RNA (log^{10} IU/mL)	AST (IU/L)	ALT (IU/L)	HCV genotype	RASs in NS3 or NS5A	Treatment history
Shunji Watanabe	2019	65 (52–81)	8/5	6/7	NA	NA	NA	GT 2, 3	NA	SOF/RBV
Hayato Uemura	2019	68 (36–86)	17/25	11/31	6.2 (4.0–7.2)	34 (14–156)	30 (11–132)	GT 1-3	38	DCV/ ASV, LDV/SOF, SOF/RBV, VEL/SOF+ RBV, OBV/ PTV/ r ± RBV
Atsushi Suetsugu	2019	NA	NA	NA	NA	NA	NA	GT 1, 2	NA	DCV/ASV, LDV/SOF, EBV/ GZR, SOF/RBV
Hitomi Sezak	2019	69 (58–76)	42/46	57/31	6.6 (6.0–7.0)	34 (25–55)	29 (21–56)	GT 1-3	NA	Others
Mitsutaka Osawa	2019	75 (48–86)	16/14	19/11	6.3 (5.4–7.4)	39 (18–115)	31 (9–130)	GT 1-3	26	DCV/ ASV, LDV/SOF, Other
Anna S. Lok	2019	NA	NA	50/127	NA	NA	NA	GT 1	70	SOF/LDV, SOF/VEL, SOF/DCV
Atsunori Kusakabe	2019	68.1 ± 12.5	20/8	20/8	6.06 ± 1.04	NA	59.1 ± 60.0	GT 2	NA	SOF/RBV
Masayuki Kurosaki	2019	NA	NA	NA	NA	NA	NA	GT 1	NA	Others
Norio Akuta	2018	74 (49–84)	8/12	NA	6.8 (3.1–7.5)	48 (20–123)	46 (10–128)	GT 1, 2	16	DCV/ASV, EBR/GZR, SOF/RBV, LDV/SOF, DCV/ASV
Fred Poordad	2018	NA	NA	NA	NA	NA	NA	GT 1, 4	NA	SOF/LDV, SOF/SIM, OBV/PTV/r, Others
Hidenori Toyoda	2019	69 (64–77)	90/109	93/106	6.3 (5.9–6.8)	35 (26–50)	30 (21–49)	GT 1, 2, 3	NA	Others
Akihiro Tamori	2019	NA	NA	37/78	NA	NA	NA	GT 1, 2	111	ASV/DCV, SOF/RBV, SOF/LDV, PTV/ r/OBV GZR/EBR
Ayumi Sugiura	2020	68	9/14	20/3	NA	33 (19–90)	27 (15–141)	GT 1, 2	NA	DCV/ASV, LDV/SOF, EBR/GZR, OMV/PTV/r
Akito Nozaki	2020	NA	NA	NA	NA	NA	NA	GT 1, 2, 3	NA	Others

AST, aspartate aminotransferase; ALT, alanine aminotransferase; GT, genotype; RASs, resistance-associated substitutions; SOF, sofosbuvir; RBV, ribavirin; DCV, daclatasvir; ASV, asunaprevir; LDV, ledipasvir; VEL, velpatasvir; OBV, ombitasvir; PTV, paritaprevir; r, ritonavir; EBV, elbasvir; GZR, grazoprevir; SIM, simeprevir; EBR, elbasvir; Others, any other combination of DAA regimens; NA, not applicable.

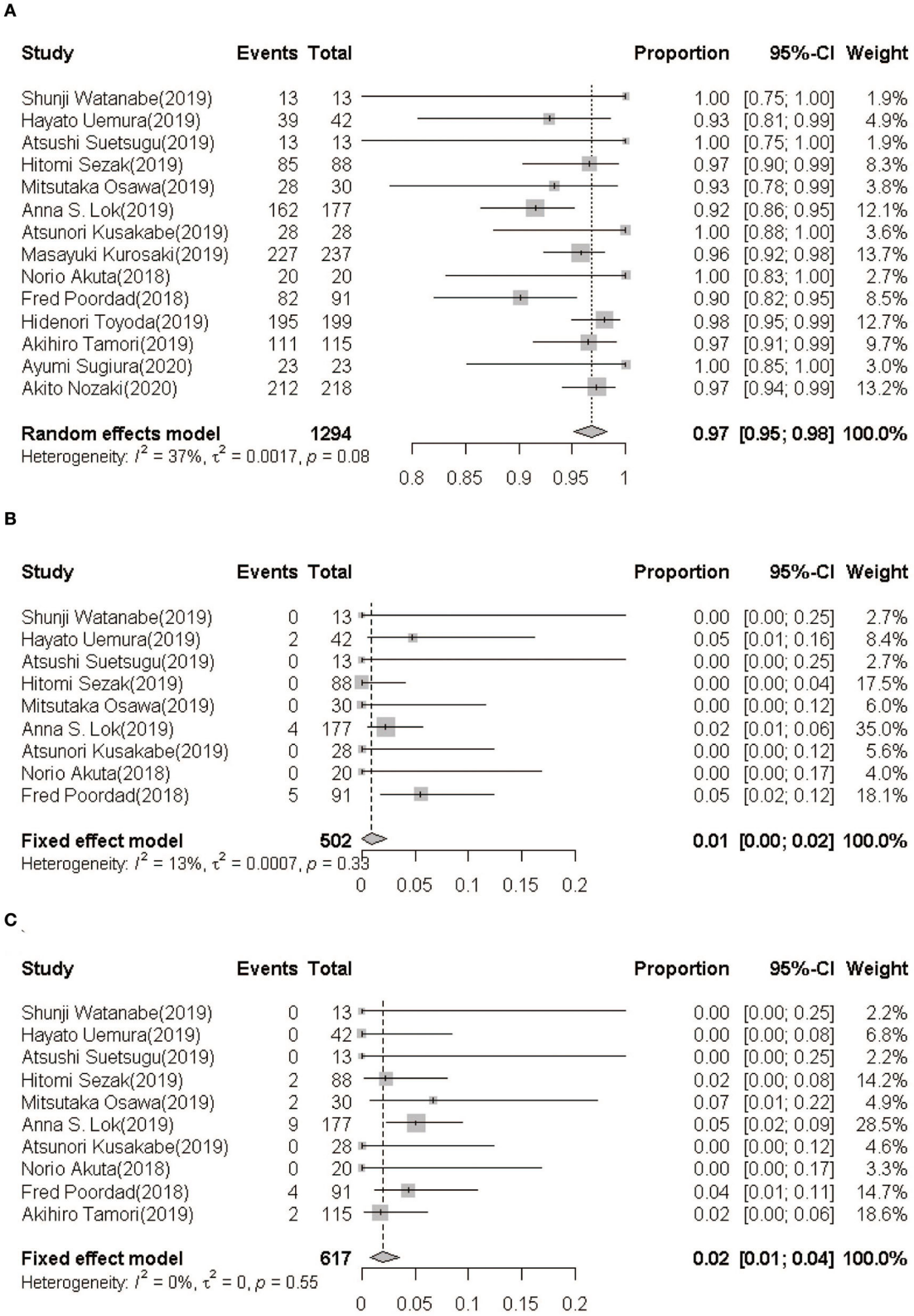

FIGURE 2 | (A) SVR12 rate following GLE/PIB treatment. **(B)** On-treatment breakthrough rate following GLE/PIB treatment. **(C)** Post-treatment relapse rate following GLE/PIB treatment. GLE/PIB, glecaprevir/pibrentasvir; CI, confidence interval.

TABLE 3 | SVR12 by settings, regions, genotypes, treatment history, treatment durations, and the presence or absence of cirrhosis.

Response	SVR12 (N = 1,294)		Heterogeneity		P**-value	Studies
	Total, n/N	Rate (95%CI)	I^2 (%)	P*		N
Overall	1238/1294	96.8 (95.1–98.2)	37.1	0.08		14
By settings					0.9483	
Single-center	195/203	96.1 (92.3–98.0)	0.0	0.91		5
Multi-center	1030/1078	96.0 (93.4–97.5)	56.9	0.03		8
By regions						
Japan	994/1026	97.9 (96.7–98.9)	0.0	0.77	0.0003	12
United States	244/268	91.1 (87.3–94.3)	0.0	0.67		2
By genotypes					0.0064[a]	
1	637/674	95.8 (93.9–97.4)	0.0	0.46	0.1325[b]	9
1a	131/145	90.3 (84.4–94.2)	0.0	1.00		3
1b	164/173	94.8 (90.3–97.3)	0.0	0.80		5
2	165/165	100.0 (99.6–100.0)	0.0	1.00	0.7802[c]	9
2a	72/72	100.0 (99.7–100.0)	0.0	0.98		7
2b	53/53	100.0 (98.3–100.0)	0.0	0.99		7
3	6/6	100.0 (66.7–100.0)	0.0	0.99		4
By treatment history					0.2787	
SOF/RBV	81/81	100.0 (99.2–100.0)	0.0	0.99		7
DCV/ASV	120/126	97.6 (92.9–100.0)	0.0	0.81		5
LDV/ SOF	27/29	99.3 (86.0–100.0)	0.0	0.95		5
OBV/PTV/r	7/7	100.0 (73.9–100.0)	0.0	0.94		3
EBV/GZR	8/9	97.4 (62.0–100.0)	0.0	0.70		4
Others	829/863	96.5 (95.1–97.7)	47.6	0.09		6
By treatment durations					0.2349	
12	1121/1169	95.9 (94.6–96.9)	43.6	0.15		14
16	117/125	93.6 (87.7–96.8)	0.0	0.46		2
By the presence or absence of cirrhosis					0.4681	
Cirrhosis	304/319	95.3 (92.4–97.2)	0.0	0.63		9
Non-cirrhosis	448/465	96.3 (94.2–97.7)	39.0	0.28		9

SOF, sofosbuvir; RBV, ribavirin; DCV, daclatasvir; ASV, asunaprevir; LDV, ledipasvir; OBV, ombitasvir; PTV, paritaprevir; r, ritonavir; EBV, Elbasvir; GZR, grazoprevir r; Others, any other combination of DAA regimen; CI, confidence interval.

**Test of heterogeneity.*

***Test for subgroup differences.*

[a] *Test for subgroup (genotype1-3) difference.*

[b] *Test for subgroup (genotype1a and 1b) difference.*

[c] *Test for subgroup (genotype2a and 2b) difference.*

considering that a systematic review demonstrated that GLE/PIB had distinct performance (SVR12 rate = 96.1%) when it came to the treatment of GT3 (41). On the other hand, five studies have found baseline resistance-associated substitutions (RASs) in NS3 or NS5A region and these RASs were mostly in subjects with GT1 (261/384). Moreover, at least 25 of 37 patients with GT1 who failed to achieve SVR12 had detected RASs in the NS3 or NS5A region. RASs were produced by the error-prone replication of HCV that could decrease efficacy of the DAA regimens (42). We suspected that the existence of RASs caused the decrease of the SVR12 rate in GT1. Even so, the SVR12 rate was still $\geq$ 95% in GT1, which suggested an ideal curative effect. Thus, GLE/PIB, one of the NS3/4/NS5A combination regimens, is extremely effective and a strong choice for the HCV population with RASs.

Currently, there are three major classes of antiviral HCV drugs including: inhibitors of the NS3/NS4A protease (PIs), inhibitors of the NS5A complex and inhibitors of the NS5B polymerase (43). In our study, main DAA treatment histories included SOF/RBV and DCV/ASV, belonging to the three classes of DAAs mentioned. As the first pan-genotypic DAA agent that was approved, SOF was widely used in many countries, but about 10% of people treated with SOF-containing regimens did not achieve SVR (44). DCV is a DAA agent that was approved by the European Medicines Agency for combination with other medicinal products for treating chronic HCV genotype 1, 3, or 4 infections (45). Administered with an NS3 protease inhibitor (ASV), DCV achieves greater than a 90% HCV eradication rate, while around 5–10% will not be cured (46). Furthermore, except for four studies without a clear DAA treatment history,

TABLE 4 | Rate of safety outcomes GLE/PIB for patients with HCV.

Outcomes	Safety		Heterogeneity studies		
	Total, n/N	Rate%(95%CI)	I^2 (%)	*P*	
AEs	288/550	47.1 (26.0–69.3)	95.1	<0.01	6
CAEs	273/550	45.2 (25.3–66.7)	94.8	<0.01	6
SAEs	12/550	1.8 (0.7–3.4)	0.0	0.47	6
Discontinuation due to AEs	4/550	0.1 (0.0–0.9)	0.0	0.70	6

GLE/PIB, glecaprevir/pibrentasvir; CI, confidence interval; AEs, any adverse events; CAEs, common adverse events; SAEs, serious adverse events.

these prior DAA treatments mostly were PIs and NS5A or NS5B inhibitor-containing regimens. Although DAA treatment histories were varied, GLE/PIB obtained favorable SVR rates (>95%), especially sofosbuvir-containing regimens (100%), which implied its wide application and fantastic efficacy.

Interestingly, treatment duration did not increase the response rate of GLE/PIB in our subgroup analysis. However, only two studies contained a 16-weeks GLE/PIB therapy period and showed that the SVR rates of the 16-weeks treatment subgroup were higher than the 12-weeks treatment subgroup. These two studies came from the United States with relatively low SVR12 rates. This may explain why the 16-weeks treatment SVR rate did not increase. In addition, there was no significant observed difference between patients with or without cirrhosis. It can be inferred that re-treatment with 12 weeks of GLE/PIB is highly effective in HCV patients with or without cirrhosis and future guidelines should consider recommending a 12-weeks therapy.

Our comprehensive analysis exhibited several strengths. First, our study was the first to evaluate the efficacy and safety of GLE/PIB for HCV patients with previous DAA therapy failures. We screened 14 studies including 1,294 individuals, which allowed us to accurately assess the pooled SVR12 rate, breakthrough, relapse, AE and SAE rates of populations who had previous DAA treatment failure. In addition, the heterogeneity among the included studies for most analyses was small, which indicated that this study is reliable and may help clinicians effectively retreat HCV subjects.

However, despite these strengths, this study still contained several limitations. First, only the efficacy and safety rates were analyzed along with the 95% CI. The relative risk (RR) for the various subgroups was not analyzed due to the absence of a control group. Second, most included studies were from Japan and focused on patients with GT1-3. Our data may not be relatable to other nations and genotypes. Third, some studies offered the frequency of prior DAA treatment but we did not perform subgroup analysis on this subject due to insufficient data.

CONCLUSION

This comprehensive analysis supports that the GLE/PIB regimen has strong efficacy and increased safety for HCV patients with previous DAAs therapy failures, especially the Asian population with GT1-2 regardless of treatment duration, and the presence or absence of cirrhosis. Furthermore, GLE/PIB is appropriate for subjects with various DAA treatment failures, such as sofosbuvir-containing regimens.

DATA AVAILABILITY STATEMENT

The original contributions presented in the study are included in the article/**Supplementary Materials**, further inquiries can be directed to the corresponding author/s.

AUTHOR CONTRIBUTIONS

CS, MY, and HF participated in the design of the study. CS, HF, ZG, WC, and ZF took charge of literature retrieval, data collection, and quality control. CS, JS, and JL performed the statistical analysis. HX, HF, CD, and MY contributed to analysis. CS, HF, and WC wrote the paper. All authors read and approved the final manuscript.

FUNDING

This study was supported by the National Natural Science Foundation of China (81773499), Open Research Fund Program of the State Key Laboratory of Virology of China (2019KF005), Key Project of Natural Science Foundation of Yunnan Province (2019FA005), Science Foundation for Distinguished Young Scholars of Jiangsu Province (BK20190106), Jiangsu Program for Young Medical Talents (QNRC2016616), and Novel Coronavirus Pneumonia Project of Nantong (HS2020002).

SUPPLEMENTARY MATERIAL

The Supplementary Material for this article can be found online at: https://www.frontiersin.org/articles/10.3389/fmed.2020.592472/full#supplementary-material

REFERENCES

1. Manns MP, Buti M, Gane E, Pawlotsky JM, Razavi H, Terrault N, et al. Hepatitis C virus infection. *Nat Rev Dis Primers.* (2017) 3:17006. doi: 10.1038/nrdp.2017.6
2. Messina JP, Humphreys I, Flaxman A, Brown A, Cooke GS, Pybus OG, et al. Global distribution and prevalence of hepatitis C virus genotypes. *Hepatology.* (2015) 61:77–87. doi: 10.1002/hep.27259
3. Collaborators TPOH. Global prevalence and genotype distribution of hepatitis C virus infection in 2015: a modelling study. *Lancet Gastroenterol Hepatol.* (2017) 2:161–76. doi: 10.1016/S2468-1253(16)30181-9
4. WHO. *Hepatitis C.* (2019). Available online at: https://www.who.int/news-room/fact-sheets/detail/hepatitis-c (accessed 9 July, 2020).
5. Organization WH. *Global Heath Strategy on Viral Hepatitis 2016–2021 Towards Ending Viral Hepatitis.* (2016). Geneva: World Health Organization.

6. Chao DT, Abe K, Nguyen MH. Systematic review: epidemiology of hepatitis C genotype 6 and its management. *Aliment Pharmacol Ther.* (2011) 34:286–96. doi: 10.1111/j.1365-2036.2011.04714.x
7. Sulkowski MS, Cooper C, Hunyady B, Jia J, Ogurtsov P, Peck-Radosavljevic M, et al. Management of adverse effects of Peg-IFN and ribavirin therapy for hepatitis C. *Nat Rev Gastroenterol Hepatol.* (2011) 8:212–23. doi: 10.1038/nrgastro.2011.21
8. Naggie S, Muir AJ. Oral combination therapies for hepatitis C virus infection: successes, challenges, and unmet needs. *Annu Rev Med.* (2017) 68:345–58. doi: 10.1146/annurev-med-052915-015720
9. Ng TI, Tripathi R, Reisch T, Lu L, Middleton T, Hopkins TA, et al. *In vitro* antiviral activity and resistance profile of the next-generation hepatitis C virus NS3/4A protease inhibitor glecaprevir. *Antimicrob Agents Chemother.* (2018) 62:17. doi: 10.1128/AAC.01620-17
10. Ng TI, Krishnan P, Pilot-Matias T, Kati W, Schnell G, Beyer J, et al. *In vitro* antiviral activity and resistance profile of the next-generation hepatitis C virus NS5A inhibitor pibrentasvir. *Antimicrob Agents Chemother.* (2017) 61:16. doi: 10.1128/AAC.02558-16
11. Kwo PY, Poordad F, Asatryan A, Wang S, Wyles DL, Hassanein T, et al. Glecaprevir and pibrentasvir yield high response rates in patients with HCV genotype 1-6 without cirrhosis. *J Hepatol.* (2017) 67:263–71. doi: 10.1016/j.jhep.2017.03.039
12. Asselah T, Kowdley KV, Zadeikis N, Wang S, Hassanein T, Horsmans Y, et al. Efficacy of glecaprevir/pibrentasvir for 8 or 12 weeks in patients with hepatitis C virus genotype 2, 4, 5, or 6 infection without cirrhosis. *Clin Gastroenterol Hepatol.* (2018) 16:417–26. doi: 10.1016/j.cgh.2017.09.027
13. Forns X, Lee SS, Valdes J, Lens S, Ghalib R, Aguilar H, et al. Glecaprevir plus pibrentasvir for chronic hepatitis C virus genotype 1, 2, 4, 5, or 6 infection in adults with compensated cirrhosis (EXPEDITION-1): a single-arm, open-label, multicentre phase 3 trial. *Lancet Infect Dis.* (2017) 17:1062–8. doi: 10.1016/S1473-3099(17)30496-6
14. Gane E, Lawitz E, Pugatch D, Papatheodoridis G, Bräu N, Brown A, et al. Glecaprevir and pibrentasvir in patients with HCV and severe renal impairment. *N Engl J Med.* (2017) 377:1448–55. doi: 10.1056/NEJMoa1704053
15. Puoti M, Foster GR, Wang S, Mutimer D, Gane E, Moreno C, et al. High SVR12 with 8-weeks and 12-weeks glecaprevir/pibrentasvir therapy: an integrated analysis of HCV genotype 1–6 patients without cirrhosis. *J Hepatol.* (2018) 69:293–300. doi: 10.1016/j.jhep.2018.03.007
16. Wyles D, Poordad F, Wang S, Alric L, Felizarta F, Kwo PY, et al. Glecaprevir/pibrentasvir for hepatitis C virus genotype 3 patients with cirrhosis and/or prior treatment experience: a partially randomized phase 3 clinical trial. *Hepatology.* (2018) 67:514–23. doi: 10.1002/hep.29541
17. Chinese Society of Hepatology, Chinese Society of Infectious Diseases, Chinese Medical Association. Guidelines for the prevention and treatment of hepatitis C (2019 version). *Zhonghua Gan Zang Bing Za Zhi.* (2019) 27:962–79. doi: 10.3760/cma.j.issn.1007-3418.2019.12.008
18. Liberati A, Altman DG, Tetzlaff J, Mulrow C, Gøtzsche PC, Ioannidis JP, et al. The PRISMA statement for reporting systematic reviews and meta-analyses of studies that evaluate health care interventions: explanation and elaboration. *J Clin Epidemiol.* (2009) 62:e1–34. doi: 10.1016/j.jclinepi.2009.06.006
19. Margulis AV, Pladevall M, Riera-Guardia N, Varas-Lorenzo C, Hazell L, Berkman ND, et al. Quality assessment of observational studies in a drug-safety systematic review, comparison of two tools: the Newcastle-Ottawa Scale and the RTI item bank. *Clin Epidemiol.* (2014) 6:359–68. doi: 10.2147/CLEP.S66677
20. Cumpston M, Li T, Page MJ, Chandler J, Welch VA, Higgins JP, et al. Updated guidance for trusted systematic reviews: a new edition of the Cochrane Handbook for Systematic Reviews of Interventions. *Cochrane Database Syst Rev.* (2019) 10:Ed000142. doi: 10.1002/14651858.ED000142
21. Watanabe S, Miura K, Morimoto N, Murohisa T, Tano S, Tahara T, et al. Efficacy and safety of glecaprevir/pibrentasvir combination therapy for patients with genotype 2 chronic hepatitis C infection who failed HCV eradication by SOF+RBV treatment. *Acta Hepatol Japonica.* (2019) 60:77–9. doi: 10.2957/kanzo.60.77
22. Uemura H, Uchida Y, Kouyama J-i, Naiki K, Tsuji S, Sugawara K, et al. NS5A-P32 deletion as a factor involved in virologic failure in patients receiving glecaprevir and pibrentasvir. *J Gastroenterol.* (2019) 54:459–70. doi: 10.1007/s00535-018-01543-9
23. Suetsugu A, Naiki T, Shimizu S, Sugihara J, Tomita E, Shimizu M. Efficacy of Glecaprevir/Pibrentasvir in patients with hepatitis C virus genotype 1 or 2 and past direct-acting antiviral treatment failure. *Hepatol Int.* (2019) 13:S92–3. doi: 10.1007/s12072-019-09936-5
24. Sezaki H, Suzuki F, Hosaka T, Fujiyama S, Kawamura Y, Akuta N, et al. Initial- and re-treatment effectiveness of glecaprevir and pibrentasvir for Japanese patients with chronic hepatitis C virus-genotype 1/2/3 infections. *J Gastroenterol.* (2019) 54:916–27. doi: 10.1007/s00535-019-01575-9
25. Osawa M, Imamura M, Teraoka Y, Uchida T, Morio K, Fujino H, et al. Real-world efficacy of glecaprevir plus pibrentasvir for chronic hepatitis C patient with previous direct-acting antiviral therapy failures. *J Gastroenterol.* (2019) 54:291–6. doi: 10.1007/s00535-018-1520-9
26. Lok AS, Sulkowski MS, Kort JJ, Willner I, Reddy KR, Shiffman ML, et al. Efficacy of glecaprevir and pibrentasvir in patients with genotype 1 hepatitis C virus infection with treatment failure after NS5A Inhibitor plus sofosbuvir therapy. *Gastroenterology.* (2019) 157:1506. doi: 10.1053/j.gastro.2019.08.008
27. Kusakabe A, Kurosaki M, Itakura J, Joko K, Akahane T, Tsuji K, et al. Efficacy and safety of glecaprevir/pibrentasvir as retreatment therapy for patients with genotype 2 chronic hepatitis C who failed prior sofosbuvir plus ribavirin regimen. *Hepatol Res.* (2019) 49:1121–6. doi: 10.1111/hepr.13387
28. Kurosaki M, Itakura J, Izumi N. ns5a resistance profile of genotype 1b virological failures that impacts outcome of re-treatment by glecaprevir/pibrentasvir: nation-wide real world study. *J Hepatol.* (2019) 70:E111. doi: 10.1016/S0618-8278(19)30198-7
29. Akuta N, Sezaki H, Suzuki F, Fujiyama S, Kawamura Y, Hosaka T, et al. Favorable efficacy of glecaprevir plus pibrentasvir as salvage therapy for HCV failures to prior direct-acting antivirals regimens. *J Med Virol.* (2019) 91:102–6. doi: 10.1002/jmv.25278
30. Toyoda H, Atsukawa M, Watanabe T, Nakamuta M, Uojima H, Nozaki A, et al. Real-world experience of 12-weeks direct-acting antiviral regimen of glecaprevir and pibrentasvir in patients with chronic hepatitis C virus infection. *J Gastroenterol Hepatol.* (2020) 35:855–61. doi: 10.1111/jgh.14874
31. Tamori A, Inoue K, Kagawa T, Takaguchi K, Nouso K, Iwasaki Y, et al. Intention-to-treat assessment of glecaprevir + pibrentasvir combination therapy for patients with chronic hepatitis C in the real world. *Hepatol Res.* (2019) 49:1365–73. doi: 10.1111/hepr.13410
32. Poordad F, Pol S, Asatryan A, Buti M, Shaw D, Hézode C, et al. Glecaprevir/Pibrentasvir in patients with hepatitis C virus genotype 1 or 4 and past direct-acting antiviral treatment failure. *Hepatology.* (2018) 67:1253–60. doi: 10.1002/hep.29671
33. Nozaki A, Atsukawa M, Kondo C, Toyoda H, Chuma M, Nakamuta M, et al. The effectiveness and safety of glecaprevir/pibrentasvir in chronic hepatitis C patients with refractory factors in the real world: a comprehensive analysis of a prospective multicenter study. *Hepatol Int.* (2020) 14:225–38. doi: 10.1007/s12072-020-10019-z
34. Sugiura A, Joshita S, Yamashita Y, Yamazaki T, Fujimori N, Kimura T, et al. Effectiveness of glecaprevir/pibrentasvir for hepatitis C: real-world experience and clinical features of retreatment cases. *Biomedicines.* (2020) 8:74. doi: 10.3390/biomedicines8040074
35. Wilson E, Covert E, Hoffmann J, Comstock E, Emmanuel B, Tang L, et al. A pilot study of safety and efficacy of HCV retreatment with sofosbuvir/velpatasvir/voxilaprevir in patients with or without HIV (RESOLVE STUDY). *J Hepatol.* (2019) 71:498–504. doi: 10.1016/j.jhep.2019.05.021
36. Papaluca T, Sinclair M, Gow P, Pianko S, Sievert W, Arachchi N, et al. Retreatment with elbasvir, grazoprevir, sofosbuvir ± ribavirin is effective for GT3 and GT1/4/6 HCV infection after relapse. *Liver Int.* (2019) 39:2285–90. doi: 10.1111/liv.14201
37. Pawlotsky JM. Retreatment of hepatitis C virus-infected patients with direct-acting antiviral failures. *Semin Liver Dis.* (2019) 39:354–68. doi: 10.1055/s-0039-1687823
38. Mathur P, Kottilil S, Wilson E. Sofosbuvir/velpatasvir/voxilaprevir: a highly effective option for retreatment of hepatitis C in difficult-to-treat patients. *Antivir Ther.* (2019) 24:1–10. doi: 10.3851/IMP3264

39. Kanwal F, Kramer JR, El-Serag HB, Frayne S, Clark J, Cao Y, et al. Race and gender differences in the use of direct acting antiviral agents for hepatitis C virus. *Clin Infect Dis.* (2016) 63:291–9. doi: 10.1093/cid/ciw249
40. Wei L, Zhang M, Xu M, Chuang WL, Lu W, Xie W, et al. A phase 3, open-label study of daclatasvir plus asunaprevir in Asian patients with chronic hepatitis C virus genotype 1b infection who are ineligible for or intolerant to interferon alfa therapies with or without ribavirin. *J Gastroenterol Hepatol.* (2016) 31:1860–7. doi: 10.1111/jgh.13379
41. Wang X, Fan X, Deng H, Zhang X, Zhang K, Li N, et al. Efficacy and safety of glecaprevir/pibrentasvir for chronic hepatitis C virus genotypes 1-6 infection: a systematic review and meta-analysis. *Int J Antimicrob Agents.* (2019) 54:780–9. doi: 10.1016/j.ijantimicag.2019.07.005
42. Sarrazin C, Dvory-Sobol H, Svarovskaia ES, Doehle BP, Pang PS, Chuang SM, et al. Prevalence of resistance-associated substitutions in HCV NS5A, NS5B, or NS3 and outcomes of treatment with ledipasvir and sofosbuvir. *Gastroenterology.* (2016) 151:501–12.e1. doi: 10.1053/j.gastro.2016.06.002
43. Spengler U. Direct antiviral agents (DAAs)—a new age in the treatment of hepatitis C virus infection. *Pharmacol Ther.* (2018) 183:118–26. doi: 10.1016/j.pharmthera.2017.10.009
44. Tang L, Ward H, Kattakuzhy S, Wilson E, Kottilil S. Dual sofosbuvir and ribavirin therapy for chronic hepatitis C infection. *Expert Rev Gastroenterol Hepatol.* (2016) 10:21–36. doi: 10.1586/17474124.2016.1119042
45. Agency EM. *Daklinza (Daclatasvir): EU Summmary of Product Characteristics.* (2016). Available online at: http://www.ema.europa.eu/ (accessed November 20, 2020).
46. Keating GM. Daclatasvir: a review in chronic hepatitis C. *Drugs.* (2016) 76:1381–91. doi: 10.1007/s40265-016-0632-x

Conflict of Interest: The authors declare that the research was conducted in the absence of any commercial or financial relationships that could be construed as a potential conflict of interest.

frontiers in Medicine

ORIGINAL RESEARCH
published: 17 December 2020
doi: 10.3389/fmed.2020.589011

The Protective Effect of Aspirin Eugenol Ester on Paraquat-Induced Acute Liver Injury Rats

*Zhen-Dong Zhang, Ya-Jun Yang, Xi-Wang Liu, Zhe Qin, Shi-Hong Li and Jian-Yong Li**

Key Lab of New Animal Drug Project of Gansu Province, Key Lab of Veterinary Pharmaceutical Development of Ministry of Agriculture and Rural Affairs, Lanzhou Institute of Husbandry and Pharmaceutical Sciences of CAAS, Lanzhou, China

Aspirin eugenol ester (AEE) possesses anti-inflammatory and anti-oxidative effects. The study was conducted to evaluate the protective effect of AEE on paraquat-induced acute liver injury (ALI) in rats. AEE was against ALI by decreasing alanine transaminase and aspartate transaminase levels in blood, increasing superoxide dismutase, catalase, and glutathione peroxidase levels, and decreasing malondialdehyde levels in blood and liver. A total of 32 metabolites were identified as biomarkers by using metabolite analysis of liver homogenate based on ultra-performance liquid chromatography-tandem mass spectrometry, which belonged to purine metabolism, phenylalanine, tyrosine and tryptophan biosynthesis, glycerophospholipid metabolism, primary bile acid biosynthesis, aminoacyl-tRNA biosynthesis, phenylalanine metabolism, histidine metabolism, pantothenate, and CoA biosynthesis, ether lipid metabolism, beta-Alanine metabolism, lysine degradation, cysteine, and methionine metabolism. Western blotting analyses showed that Bax, cytochrome C, caspase-3, caspase-9, and apoptosis-inducing factor expression levels were obviously decreased, whereas Bcl-2 expression levels obviously increased after AEE treatment. AEE exhibited protective effects on PQ-induced ALI, and the underlying mechanism is correlated with antioxidants that regulate amino acid, phospholipid and energy metabolism metabolic pathway disorders and alleviate liver mitochondria apoptosis.

Keywords: aspirin eugnol ester, paraquat, metabolites, hepatotoxicity, antioxidation

OPEN ACCESS

Edited by:
Jianpeng Sheng, Nanyang Technological University, Singapore

Reviewed by:
Haijun Li, Jilin University, China
Wei Li, Jilin University, China

****Correspondence:***
Jian-Yong Li
lijy1971@163.com

Specialty section:
This article was submitted to Gastroenterology, a section of the journal Frontiers in Medicine

Received: *30 July 2020*
Accepted: *30 November 2020*
Published: *17 December 2020*

Citation:
Zhang Z-D, Yang Y-J, Liu X-W, Qin Z, Li S-H and Li J-Y (2020) The Protective Effect of Aspirin Eugenol Ester on Paraquat-Induced Acute Liver Injury Rats. Front. Med. 7:589011. doi: 10.3389/fmed.2020.589011

INTRODUCTION

PQ is a non-selective herbicide with excellent effect, which has been widely used in the world for many years (1–3). PQ is extremely toxic to humans (4, 5). Studies have shown that when taking about 10 ml PQ, patients can die of multiple organ failure a few hours later (6). The accumulation of PQ can damage the main organs such as lung, kidney, liver and heart (7). It is reported that the liver is one of the main target organs of PQ poisoning, which is often accompanied by the formation of free radicals (8, 9). The liver is the main metabolic and detoxifying organ of the human body (10, 11). A multiple potentially harmful stimuli challenge the liver, including free radicals. It is well known that drugs and other substances are further transformed and metabolized after being absorbed by the body, resulting in the production of free radicals in the liver. Excessive free radicals produce oxidative stress on the liver, which in turn leads to oxidative damage to the liver (12).

Currently, the molecular mechanism of hepatotoxicity induced by PQ is not completely understood. It is known that the redox response is one of the main factors involved in the toxic effects of PQ (13). It has been reported that PQ molecules can interfere with the electron transport chain and then inhibit the synthesis of NADPH (14). Excessive production of ROS was observed during PQ poisoning, indicating that oxidative stress was involved in the pathological changes induced by PQ. Excessive ROS and excessive free radicals lead to oxidative stress by destroying DNA, proteins and lipids (15). Therefore, the premise of the toxic effect of PQ is its induced oxidative stress. At present, the main methods for the treatment of PQ poisoning are immunosuppressant and hemodialysis (16). Existing clinical treatments for severe PQ poisoning only relieve symptoms (17). In recent decades, new drugs to treat the toxicity of PQ have been developed. In the early stages of poisoning, the use of antioxidants has been shown to effectively reduce the damage of PQ to organs. Therefore, it is imperative to develop potential effective drugs for the treatment of PQ poisoning.

AEE is a new potential pharmaceutical compound possessing anti-inflammatory and anti-oxidative stress pharmacological activity (18–22). The effect of AEE against H_2O_2-induced oxidative stress of human umbilical vein endothelial cells is consistent with the AEE-enhanced expression of Bcl-2 and Nrf2 (18, 23). It has been well documented that AEE could alleviate H_2O_2-induced dysfunction of mitochondria, the generation of ROS productions and the increase of apoptosis via enhancing the expression of Bcl-2 and Nrf2 (18, 23). It is well known that the dysfunction of mitochondria could release cytochrome C, apoptosis inducing factor (AIF), and other factor into cytoplasm to mediate downstream apoptotic signals causing cell apoptosis (24, 25), while the exacerbation of reactive oxygen species (ROS) induced by the dysfunction of mitochondria is also vital incentive of cell apoptosis (26, 27).

MATERIALS AND METHODS

Chemicals

AEE (99.5%) was prepared in Lanzhou Institute of Husbandry and Pharmaceutical Sciences of CAAS (Lanzhou, China). MS-gradeacetonitrile was purchased from Thermo Fisher Scientific (Waltham, MA, USA). Formic Acid (98.0%, for LC-MS) was purchased from Tokyo Chemical Industry (Shanghai, China). Catalase assay kit was purchased from Solarbio (Beijing, China). Glutathione peroxidase (GPx), GSH and GSSG assay kit, superoxide dismutase (SOD), and malondialdehyde (MDA) assay kit were purchased from Beyotime (Shanghai, China). Caspase-3 assay kit was purchased from Jianglai Chemical Biotechnology (Shanghai, China). The antibodies of Caspase-9, Caspase-3, Bax, Bcl-2, Cyt C, AIF, and IgG were purchased from abcam (Shanghai, China). Alanine aminotransferase kit and aspartate aminotransferase kit were purchased from Mlbio (Shanghai, China).

Animal Experiment

Eighteen male specific pathogen-free SD rats (6 weeks old) weighing 120–130 g were purchased from the Laboratory Animal Center of Lanzhou Veterinary Research Institute (Lanzhou, China). All animals were placed in groups in SPF-class housing of laboratory at a controlled relative humidity (55–65%), 12 h light/dark cycle and temperature (24 ± 2°C). The rats were randomly divided into three groups ($n = 6$): (1) control group, in which rats were administrated equivalent saline by intraperitoneal injection (ip); (2) PQ group, in which rats were administrated PQ (20 mg/kg body weight, ip) (28–30); (3) AEE groups, in which rats were pre-administrated AEE (54 mg/kg/day body weight) by gavage once a day for 1 week before being administrated PQ. The rats in the different groups were sacrificed after a single intraperitoneal injection of 20 mg/kg PQ for 24 h. All experimental protocols and procedures were approved by the Institutional Animal Care and Use Committee of Lanzhou Institute of Husbandry and Pharmaceutical Science of Chinese Academy of Agricultural Sciences (Approval No. NKMYD201907018; Approval Date: 18 July 2019). Animal welfare and experimental procedures were performed strictly in accordance with the Guidelines for the Care and Use of Laboratory Animals issued by the US National Institutes of Health.

Metabonomic Analysis

Hepatic Tissue Sample Preparation

The hepatic tissue samples were homogenized with ice-cold physiological saline (10%, wt%, 1 g tissue in 10 mL of physiological saline) in an Ultra Turrax tissue homogenizer. After vortex mixing for 3 min, the samples were centrifuged at 12,000 rpm for 10 min at 4°C. The supernatant was subsequently analyzed by UPLC-QTOF-MS/MS.

UPLC-QTOF-MS/MS Conditions

Liquid chromatography was executed on DAD 1290 UPLC system (Agilent Technologies Inc., California, USA). Separation was performed on an Agilent SB C18 RRHD Column (2.1 × 150 mm, 1.8 μm). The temperature of the column was set to 35°C. Injection volume was 3 μL and autosampler temperature was set at 4°C. Mobile phase A consisted of water containing 0.1% formic acid and mobile phase B was acetonitrile containing 0.1% formic acid at a flow rate of 0.3 mL/min. The gradient elution of A was as follows: 98%A from 0 to 2 min, 98–55% A from 2 to 9 min, 55–30% A from 9 to 15 min, 30–2% A from 15 to 22 min, 2% A from 22 to 23 min, 2–98% A from 23 to 24 min and held at 98% A from 24 to 27 min. The mass spectrometer was operated in both positive and negative ionization modes. The fragment voltage was set to 135V and the skimmer voltage was set to 65 V. In positive ion mode, capillary voltage was 4.0 KV, while in negative ion mode, it was 3.5 KV. The temperature and the flow of the drying gas were 350°C and 10 L/min, respectively. The nebulizer pressure was set to 45 psig. Ions were scanned over a region of 50–1000 m/z.

Metabolomics Data Analysis

The raw MS data were initially processed with the Mass Profiler Professional (MPP) software (Agilent Technologies, USA) to filter noise, correct the baseline, align peaks, and identity and quantify peaks. The match tolerance of mass span is 10 ppm,

and the match tolerance of retention time's span is 0.10 min. The obtained data were imported into SIMCA-P (version 13.0, Umetrics AB, Umea, Sweden), where a principal component analysis (PCA) and partial least squares discriminant analysis (OPLS-DA) were performed on the dataset. The quality of OPLS-DA models was described by R^2X, R^2Y, and Q^2, and its validity was evaluated by performing permutation testing (with 200 permutations). The variable importance in the projection (VIP > 1) value of the validated OPLS-DA model and the p values from one-way ANOVA ($p < 0.05$) were used as the measurement indices to select potential metabolites. Metabolites were identified through a mass-based search followed by manual verification. Accurate mass values of the molecular ions of interest in TOF-MS data were searched against METLIN and Human Metabolome Database (HMDB). Then, an MS/MS analysis was conducted to confirm the structure of potential biomarkers by matching the masses of the fragments. The parent ion mass tolerance is ± 10 ppm and mass/charge (m/z) of products tolerance is ± 10 ppm. The clustering analysis of the potential biomarkers and pathway analysis were performed using MetaboAnalyst 4.0 and the metabolic pathways were identified using the KEGG database.

Histopathology

Liver specimens were fixed with 10% formaldehyde. After fixation, the liver tissue was embedded in paraffin wax, sectioned to a thickness of 5 μm and stained with hematoxylin-eosin staining.

Analysis of MDA, SOD, Caspase-3, GSH/GSSH, and GPx

The levels of MDA, SOD and the activity of caspase-3, the ratio of GSH/GSSH and GPx in the rat serum were assessed using the corresponding commercial kits according to the manufacturer's protocols.

Protein Expression Analysis

The expression of AIF, Bax, Bcl-2, Caspase-3, Caspase-9, and Cyt c among different treatment was assessed by Western blot analysis. In brief, total protein of the liver was extracted using RIPA, quantified by bicinchoninic acid (BCA) method, and separated by precast SDS-PAGE Gel (15%, 4–20%). The separated proteins were transferred onto polyvinylidene fluoride (PVDF) membrane using standard procedures. Blots were incubated with the primary antibody followed by horseradish peroxidase-conjugated secondary antibody. Results were detected using the G: Box Chemi XRQ Imaging System (Cambridge, UK).

RESULTS

AEE Reduces PQ-Induced Liver Injury in Rat

To verify whether AEE has a protective effect on PQ-induced hepatotoxicity *in vivo*, we explored the effect of AEE pretreatment on PQ-induced liver injury in rats. The results showed that PQ (20 mg/kg) could significantly cause liver tissue necrosis, cell atrophy and portal hyperemia in rats. Pretreatment with 54 mg/kg AEE for seven consecutive days by gavage markedly attenuated the pathological injury of liver tissue induced by PQ (**Figure 1**). The results showed that AEE could effectively reduce the liver injury induced by PQ in rats.

AEE Attenuates PQ-Induced Oxidative Stress in the Liver of Rats

The results for CAT, MDA, SOD, GPx, and GSH/GSSH ratio in serum were shown in **Figure 2**. AEE significantly attenuated the increase in MDA and prevented the decrease in CAT, SOD, GPx activity, GSH/GSSH ratio caused by PQ in rats (**Figure 2**). These results suggested that AEE could effectively inhibit oxidative stress induced by PQ in rat liver.

Metabolomics Analysis of AEE Effect on PQ-Induced ALI in Rats

Analysis of Liver Metabolites

In this study, an unsupervised PCA was performed with the data from three experimental groups. In both positive and negative modes, the first two principal components explained 61.4 and 58.9% of the total variance, respectively. As shown in the PCA plots (**Figures 3A,B,G,H**), the three groups showed obvious separation in both positive and negative ion modes. In order to further maximize the separation and identification of metabolites, supervised orthogonal partial least squares discriminant analysis (OPLS-DA) was used. Then an OPLS-DA model was established between the PQ group and other groups to enhance the variation. The OPLS-DA score plots presented an obvious separation between the PQ group and other groups without any overlap in either the positive or negative modes (**Figures 3C,E,I,K**). The R^2X, R^2Y, and Q^2 values of the OPLS-DA model showed that the models were robust and had predictive abilities (**Figures 3D,F,J,L**).

Differential metabolites contributing to the separation were identified using variable importance in the projection (VIP) value and p value. The potential metabolites were screened with a VIP value > 1 and $p < 0.05$. As shown in **Table 1**, 32 metabolites were identified as potential metabolites, including dephospho-CoA, taurochenodesoxycholic acid, lysoPC(14:1), chenodeoxyglycocholic acid, PA(22:2), PA(22:2), cholic acid, 5,9,11-trihydroxyprosta-6E,14Z-dien-1-oate, lysoPE(18:2), lysoPE(20:4), lysoPE(16:0), lysoPC(16:0), L-Histidine, pipecolic acid, glycerophosphocholine, acetylglycine, N-(2-Methylpropyl)acetamide, D-Asparagine, hypoxanthine, inosine, xanthosine, L-Phenylalanine, melatonin radical, ophthalmic acid, nonyl isovalerate, glutamylarginine, glutamylleucine, pipecolic acid, S-(PGJ2)-glutathione, L-Octanoylcarnitine, lysoPC(16:0), argininic acid, deoxycholic acid glycine conjugate, N-Undecanoylglycine. After AEE treatment, the levels of these metabolites normalized either due to upregulation or downregulation.

Metabolic Pathway Analysis

The related metabolic pathway analysis was performed on MetaboAnalyst 4.0. The metabolic pathway analysis data are shown as a bar chart and a bubble chart in **Figure 4**. There are 12 main metabolic pathways: purine metabolism, phenylalanine, tyrosine and tryptophan biosynthesis, glycerophospholipid

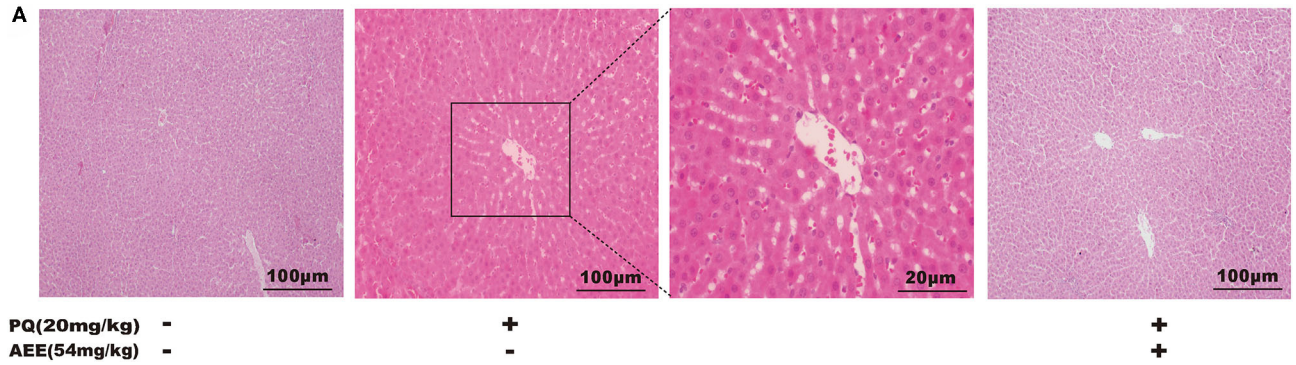

FIGURE 1 | AEE reduces PQ-induced liver injury in rat. **(A)** Histopathological H&E staining of rat liver tissue (scale bar = 100 μm). Values are presented as the means ± SD where applicable ($n = 6$).

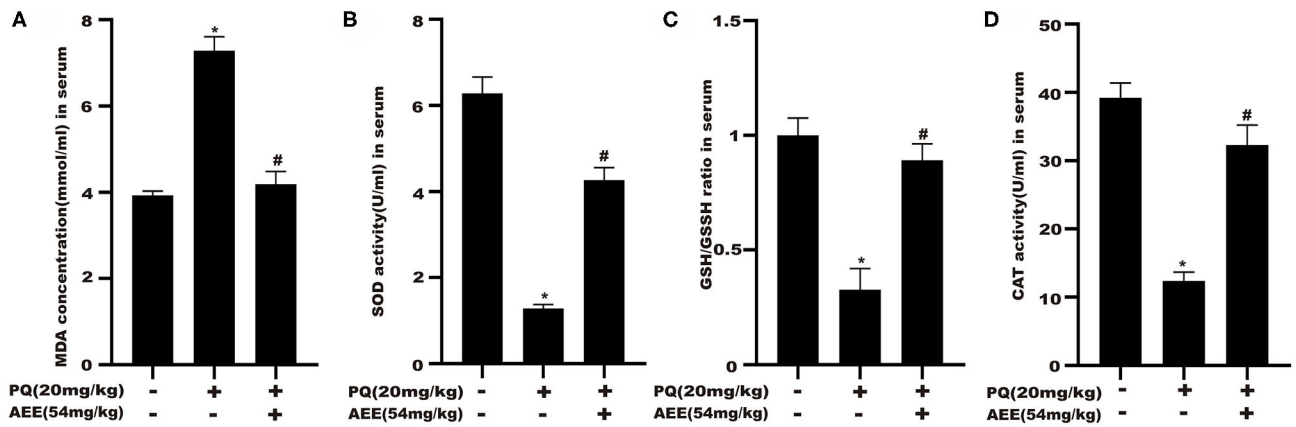

FIGURE 2 | AEE attenuates PQ-induced oxidative stress in the liver of rat. **(A)** The activity of malondialdehyde (MDA) in serum of different treatment groups was detected. **(B)** The activity of superoxide dismutase (SOD) in serum of different treatment groups was detected. **(C)** The ratio of reduced glutathione/oxidized glutathione disulfide (GSH/GSSH) in serum different treatment groups was detected. **(D)** The activity of catalase (CAT) in serum of different treatment groups was detected. Values are presented as the means ± SD where applicable ($n = 6$). $^{*}p < 0.05$ compared with the control group; $^{\#}p < 0.05$ compared with the PQ group.

metabolism, primary bile acid biosynthesis, aminoacyl-tRNA biosynthesis, phenylalanine metabolism, histidine metabolism, pantothenate and CoA biosynthesis, ether lipid metabolism, beta-Alanine metabolism, lysine degradation, cysteine and methionine metabolism. As shown in **Figure 4**, there are significant differences in metabolic pathways, including Methylhistidine Metabolism, Bile Acid Biosynthesis, Purine Metabolism, Pantothenate and CoA Biosynthesis, Mitochondrial Beta-Oxidation of Short ($p < 0.05$). The influence of the path is mainly concentrated in Phenylalanine, tyrosine and tryptophan biosynthesis, Purine metabolism, Glycerophospholipid metabolism, and Primary bile acid biosynthesis. PQ-induced ALI in rats is mainly reflected in redox reaction and energy metabolism. The results showed that ALI induced by PQ caused metabolic disorder in rats, and AEE could effectively regulate this imbalance.

As shown in **Table 1**, AEE could increase the levels of L-Histidine, D-Asparagine, and L-Phenylalanine compared with PQ group. Some studies have shown that L-Histidine and D-Asparagine have the effect of anti-apoptosis (31–33). The deficiency of L-Histidine can cause apoptosis through mitochondrial dysfunction, and as a substrate of asparagine biosynthesis, the deficiency of D-asparagine can also promote apoptosis (31, 32). Interestingly, higher concentrations of L-Phenylalanine also inhibited mitochondrial function and cause apoptosis (33). It is necessary to detect the expression of mitochondrial apoptosis-related proteins.

AEE Decreased the Level of Apoptosis-Related Proteins in Rat Liver Tissue Induced by PQ

To delineate the effector pathways of PQ-induced apoptosis, we examined the expression of mitochondrial apoptosis-related proteins and the expression of caspases, the central executioners of cell apoptosis. Compared with the control group, the expression of Caspase-3, Caspase-9, Bax, Cyt C, and AIF in the model group increased, while the expression

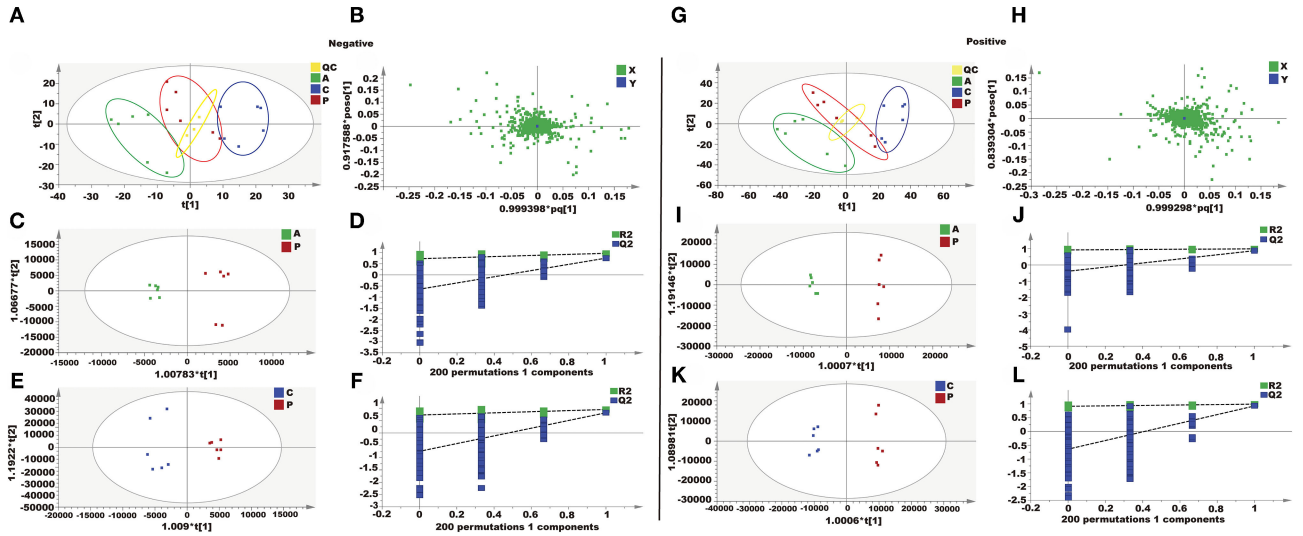

FIGURE 3 | Metabolomics analysis of the effect of AEE on PQ-induced ALI in rats. **(A,G)** PCA score plots based on supernatant of rat liver tissue of the control, PQ and AEE groups in positive and negative modes, ESI+: $R^2 = 0.614$, ESI–: $R^2 = 0.589$. **(B,H)** The loading plot of AEE and PQ groups in positive and negative modes. **(C,I)** OPLS-DA score plots of the AEE and PQ groups in positive and negative modes, ESI+: $R^2X = 0.566$, $R^2Y = 0.994$, $Q^2 = 0.878$; ESI–: $R^2X = 0.502$, $R^2Y = 0.969$, $Q^2 = 0.752$. **(D,J)** Permutation test of the OPLS-DA model, ESI+: the intercepts of $R^2 = 0.926$ and $Q^2 = -0.387$, ESI–: the intercepts of $R^2 = 0.726$ and $Q^2 = -0.640$. **(E,K)** OPLS-DA score plots of the control and PQ groups in positive and negative modes, ESI+: $R^2X = 0.592$, $R^2Y = 0.993$, $Q^2 = 0.927$; ESI–: $R^2X = 0.405$, $R^2Y = 0.952$, $Q^2 = 0.820$. **(F,L)** Permutation test of the OPLS-DA model, ESI+: the intercepts of $R^2 = 0.915$ and $Q^2 = -0.641$, ESI–: the intercepts of $R^2 = 0.727$ and $Q^2 = -0.744$. Values are presented as the means ± SD where applicable ($n = 6$).

of Bcl-2 decreased (**Figure 5**). In AEE pretreatment group, AEE could inhibit the increase of Caspase-3, Caspase-9, Bax, Cyt C, and AIF induced by PQ, and enhance the expression of Bcl-2. Western blotting analysis showed that AEE reduced the apoptosis of liver cells via inhibiting the expression of apoptosis-related proteins in rat liver tissue induced by PQ.

DISCUSSION

AEE is synthesized by combining aspirin with eugenol based on the prodrug principal (21). As a new potential compound with anti-inflammatory and antioxidant stress pharmacological activities, AEE plays an active role in many aspects (18–21, 23, 34–38). AEE can prevent tail thrombosis induced by c kappa-carrageenan in rats (19). At the same time, AEE can attenuate thrombus induced with high-fat diet in rats by regulating platelet aggregation, hemorheology, TXB2/6-keto-PGF1α, and blood biochemistry (38). With further study, a rat model of blood stasis was established and it was observed that AEE could alleviate the symptoms of blood stasis in rats (39). It was also found that AEE can inhibit agonist-induced platelet aggregation in rats by regulating PI3K/Akt, MAPK, and Sirt1/CD40L signal pathways (35). AEE has not only the effects of anti-inflammation, anti-thrombosis and anti-blood stasis, but also the effect of anti-atherosclerosis and other cardiovascular diseases. AEE can reduce the oxidative stress of human umbilical vein endothelial cells induced by H_2O_2 through mitochondrial-lysosomal axis and Nrf2 signaling pathway, and then reduce the oxidative damage of vascular endothelial cells (18, 23).

PQ poisoning is caused by the selective accumulation of PQ molecules that can cause multiple organ failure and can cause severe damage to the liver (15). Although progress has been made in the comprehensive treatment of PQ poisoning, the mortality rate remains high due to the lack of effective treatment (40, 41). The underlying mechanism of PQ poisoning has not been fully elucidated, but it may be multifactorial. Studies have shown that an important cause of PQ poisoning is the excessive production of ROS (42). The overproduction of reactive oxygen species could cause excessive oxidative stress and oxidant injury in cells (43, 44). ALT and AST are enzymes found in hepatocytes. When the liver cell membrane lipid peroxidation occurs, two enzymes are easily released into the blood. The elevated levels of AST and ALT in liver and serum may indicate PQ-induced ALI. MDA is the end product of lipid peroxidation and its level can be used to assess the extent of damage from peroxidative damage (45–47). Downregulation of AST, ALT, and MDA levels meant that AEE could reduce lipid peroxidation damage. Antioxidant enzymes such as SOD, CAT and GSH-Px play an important role in ROS removal. SOD is the most important antioxidant enzyme for removing H_2O_2 from $O_2\cdot^-$ (48–50). CAT and GSH-Px are the major enzymes that convert H_2O_2 to O_2 and H_2O (51–54). In the model group, ROS produced by PQ increased MDA levels and decreased SOD, GSH-Px, and CAT levels. After

TABLE 1 | Statistics of differential metabolites in the rat liver.

No	RT	VIP	Formula	Metabolites	SM	m/z	Fold Change	
							PQ/C	AEE/PQ
1	1.036	1.08	$C_6H_9N_3O_2$	L-Histidine	ESI+	155.1546	0.86	1.03
2	1.146	2.51	$C_6H_{11}NO_2$	Pipecolic acid	ESI+	129.157	0.78	1.16*
3	1.154	1.06	$C_8H_{20}NO_6P$	Glycerophosphocholine	ESI+	257.223	1.34	0.74*
4	1.213	3.14	$C_4H_7NO_3$	Acetylglycine	ESI+	117.1033	0.77	1.63*
5	1.314	1.05	$C_6H_{13}NO$	N-(2-Methylpropyl)acetamide	ESI+	115.1735	1.04	1.47*
6	1.817	2.46	$C_4H_8N_2O_3$	D-Asparagine	ESI+	132.1179	0.92	1.55*
7	3.638	1.17	$C_5H_4N_4O$	Hypoxanthine	ESI+	136.1115	1.37	0.92*
8	3.646	1.09	$C_{10}H_{12}N_4O_5$	Inosine	ESI+	268.2261	0.85	1.15*
9	4.517	2.84	$C_{10}H_{12}N_4O_6$	Xanthosine	ESI+	284.2255	0.98	1.85*
10	4.627	4.61	C9H11NO2	L-Phenylalanine	ESI+	165.1891	0.46	1.48*
11	4.779	2.43	$C_{13}H_{17}N_2O_3$	Melatonin radical	ESI+	249.2857	0.39	0.75*
12	4.959	1.73	$C_{11}H_{19}N_3O_6$	Ophthalmic acid	ESI+	289.2851	0.40	0.85*
13	5.379	1.24	$C_{14}H_{28}O_2$	Nonyl isovalerate	ESI+	228.3709	0.91	0.80
14	5.717	1.42	$C_{11}H_{21}N_5O_5$	Glutamylarginine	ESI+	303.319	0.49	0.98*
15	5.802	1.26	$C_{11}H_{20}N_2O_5$	Glutamylleucine	ESI+	260.29	0.91	0.64
16	6.368	1.57	$C_6H_{11}NO_2$	Pipecolic acid	ESI+	129.157	1.47	1.04*
17	6.682	1.07	$C_{30}H_{47}N_3O_{10}S$	S-(PGJ2)-glutathione	ESI+	641.773	0.65	1.19*
18	9.368	1.04	$C_{15}H_{29}NO_4$	L-Octanoylcarnitine	ESI+	287.3951	0.60	2.18*
19	9.419	1.46	$C_{24}H_{50}NO_6P$	LysoPC(P-16:0)	ESI+	479.6307	1.80	3.18*
20	10.117	1.06	$C_6H_{13}N_3O_3$	Argininic acid	ESI+	175.1857	0.79	1.78*
21	13.354	2.48	$C_{26}H_{43}NO_5$	Deoxycholic acid glycine conjugate	ESI+	449.6233	0.85	0.82
22	13.969	2.42	$C_{13}H_{25}NO_3$	N-Undecanoylglycine	ESI+	243.3425	0.89	1.07
23	4.995	3.96	$C_{21}H_{35}N_7O_{13}P_2S$	Dephospho-CoA	ESI-	687.15	1.95	1.04*
24	9.331	5.39	$C_{26}H_{45}NO_6S$	Taurochenodesoxycholic acid	ESI-	499.3	1.44	0.89*
25	10.677	1.07	$C_{22}H_{44}NO_7P$	LysoPC(14:1)	ESI-	465.561	2.15	1.04*
26	10.776	3.14	$C_{26}H_{43}NO_5$	Chenodeoxyglycocholic acid	ESI-	449.6233	1.97	2.33
27	11.221	2.03	$C_{47}H_{89}O_8P$	PA(22:2)	ESI-	813.195	1.29	1.11
28	12.143	2.50	$C_{24}H_{40}O_5$	Cholic acid	ESI-	408.5714	2.05	0.82*
29	14.502	1.11	$C_{30}H_{37}NO_8$	5,9,11-trihydroxyprosta-6E,14Z-dien-1-oate	ESI-	539.625	1.29	0.77*
30	14.897	1.61	$C_{23}H_{44}NO_7P$	LysoPE(18:2)	ESI-	477.5717	1.33	0.92*
31	14.973	1.15	$C_{25}H_{44}NO_7P$	LysoPE(20:4)	ESI-	501.5931	2.06	0.75*
32	15.650	1.69	$C_{21}H_{44}NO_7P$	LysoPE(16:0)	ESI-	453.5503	1.65	1.01*

*RT, retention time; VIP, variable importance in the projection; SM, scan mode; +, metabolites identified in positive mode; –, metabolites identified in negative mode. Metabolites identified in both positive and negative modes; *$p < 0.05$ compared with the PQ group; C/PQ, control group compared with the PQ group; AEE/PQ, AEE group compared with the PQ group.*

AEE administration, SOD, GSH-Px, and CAT increased. This indicates that AEE could restore ALI in PQ-induced rats via ROS scavenging.

Arginine synthesis and the metabolism of arginine and proline involved in L-arginine may be one of the most important metabolic pathways in which AEE plays a protective role in PQ-induced lung injury. L-arginine is a semi-essential amino acid needed for cell proliferation, and is the substrate of arginase 1 (Arg-1) and inducible nitric oxide synthase (iNOS), which is involved in the oxidative stress of the body to external stimuli. Metabonomic results showed that the biosynthesis pathway of L-arginine was inhibited in PQ group. L-arginine is a scavenger of free radicals in the body (55). L-arginine increases the activity of antioxidant enzymes and reduces the content of MDA by promoting the production of nitric oxide (NO), thus reducing the tissue damage caused by oxidative stress (56). After pretreatment with AEE, the production of L-arginine increased, which in turn promoted the increase of SOD, GSH-Px and CAT. It is suggested that AEE may alleviate PQ-induced lung injury in rats by scavenging excessive ROS.

Glycerophospholipid metabolites, including PC and LysoPE are key components of the lipid bilayer of cells, as well as being involved in metabolism and signaling (57–59). A previous study suggested that various PCs and LysoPEs were significantly increased in rat acute blood stasis model and AEE could significantly inhibit the increase of PC and LysoPE (39). AEE increased high-density lipoprotein cholesterol serum level and decreased low-density lipoprotein cholesterol serum level in hyperlipidemia model induced by high-fat diet. Notably, the

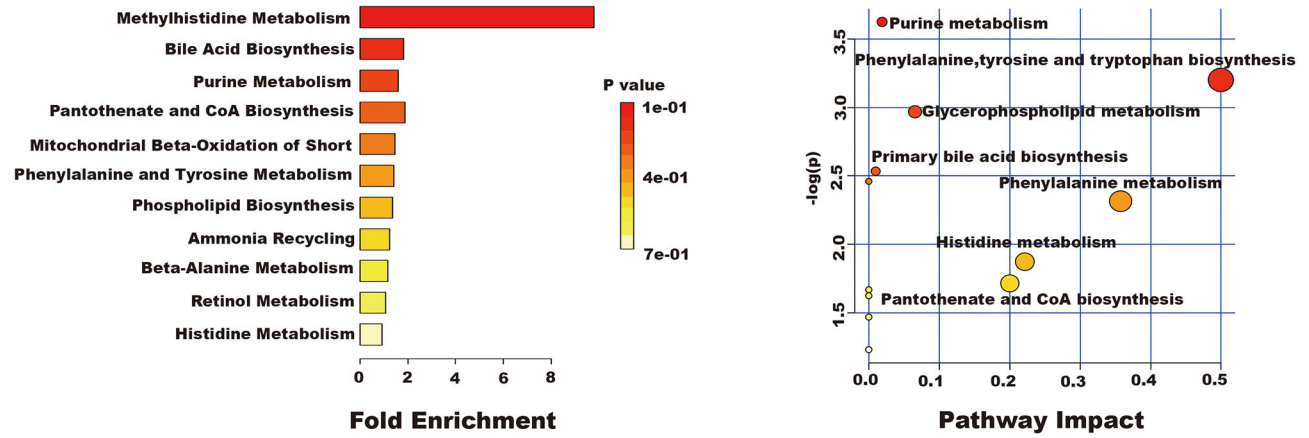

FIGURE 4 | The results of fold enrichment and path analysis of potential metabolites in the supernatant of liver tissue.

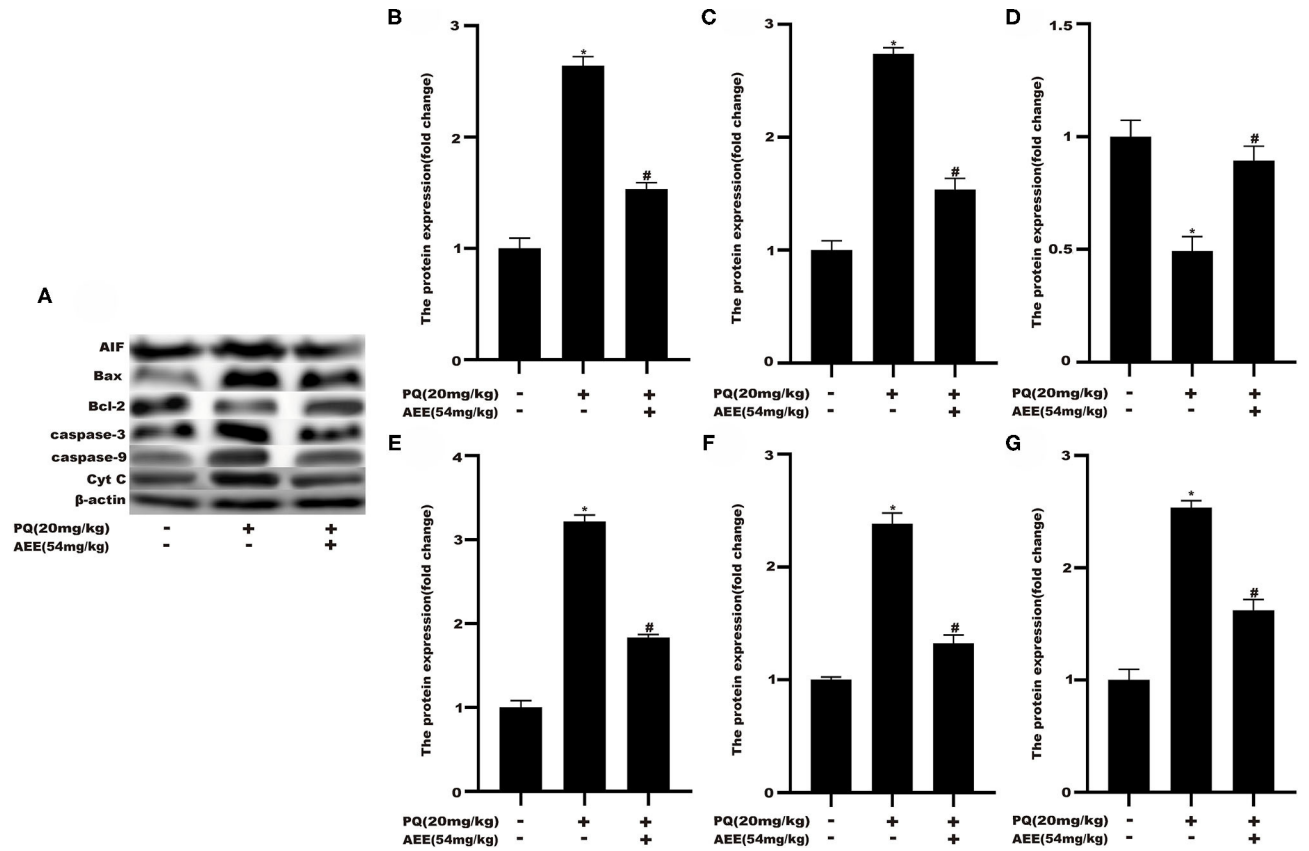

FIGURE 5 | AEE decreased the level of apoptosis-related proteins in rat liver tissue induced by PQ. **(A,B)** The expression of AIF protein in liver tissue of different treatment groups was detected. **(A,C)** The expression of Bax protein in liver tissue of different treatment groups was detected. **(A,D)** The expression of Bcl-2 protein in liver tissue of different treatment groups was detected. **(A,E)** The expression of Caspase-3 protein in liver tissue of different treatment groups was detected. **(A,F)** The expression of Caspase-9 protein in liver tissue of different treatment groups was detected. **(A,G)** The expression of Cyt C protein in liver tissue of different treatment groups was detected. Values are presented as the means ± SD where applicable ($n = 6$). $^{*}p < 0.05$ compared with the control group; $^{\#}p < 0.05$ compared with the PQ group.

elevated TG and TC serum levels were also reversed by AEE. All of the above implied that lipid metabolism was partly restored by AEE.

Mitochondrial damage was present due to impaired energy, amino acid, and fatty acid metabolism. The production of ROS can also cause mitochondrial apoptosis (60–62). Therefore,

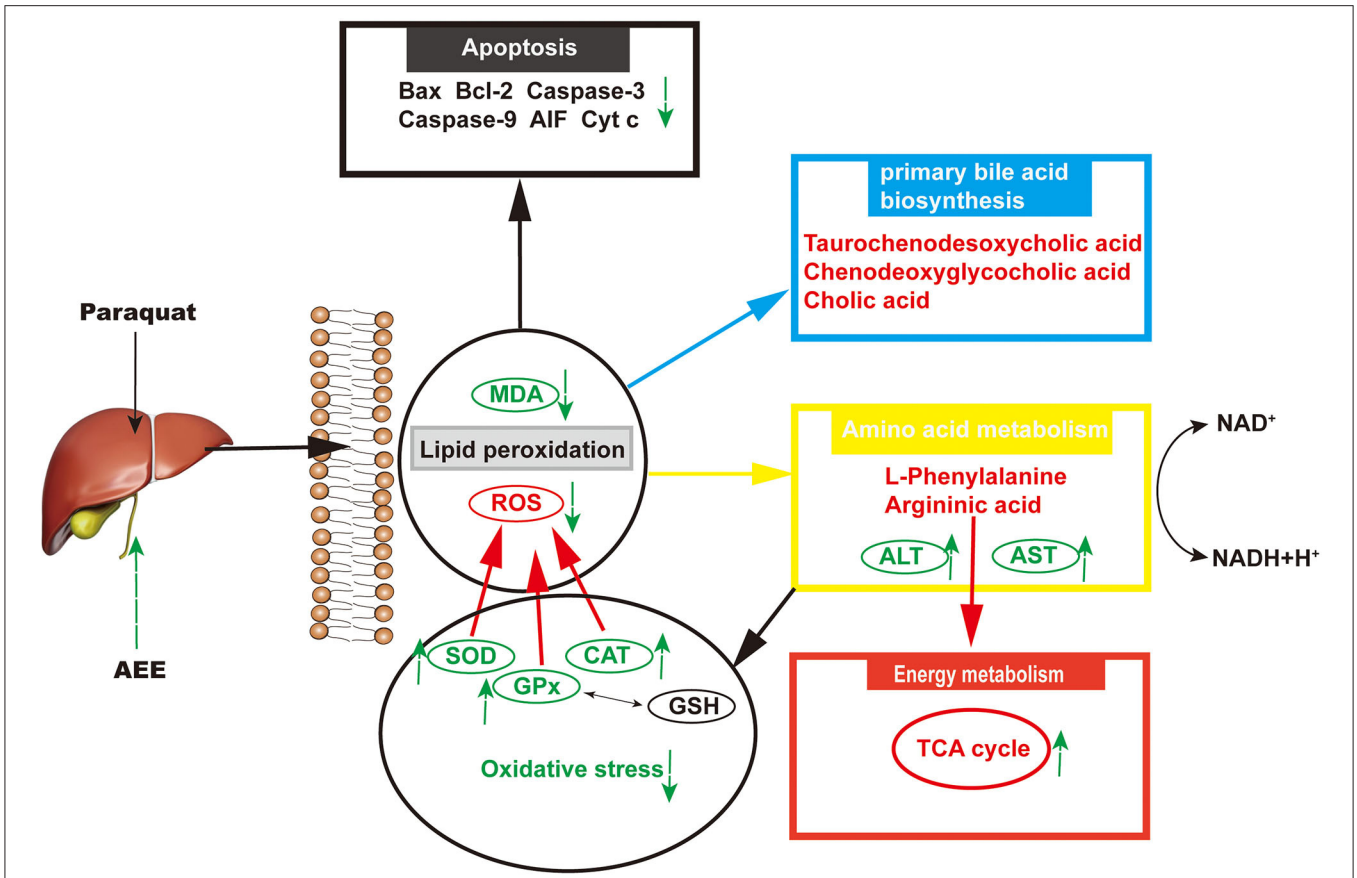

FIGURE 6 | The results of hepatoprotective effect of AEE on ALI rats.

apoptosis may play an important role in the pathogenesis of liver injury. In this study, the hepatic apoptotic cell rate was increased in the model group. The low percentage of hepatic apoptotic cells in the AEE group suggests that AEE enhanced antioxidant activity and attenuated apoptosis. On the other hand, the results of Western blotting analysis suggest that the expression levels of Caspase-9, Bax, Cyt C, Caspase-3, and AIF were decreased, whereas that of Bcl-2 was increased in the AEE group. **Figure 6** summarizes the protective effects of AEE on ALI rats. As shown in **Figure 6**, PQ could induce excessive production of ROS in liver tissue. Excessive ROS could further increase the excessive production of MDA and decrease the activities of antioxidant enzymes such as SOD, CAT, and GSH-Px. The decrease of antioxidant enzyme activity would lead to the release of apoptotic proteins, including Caspase-9, Bax, Cyt C, Caspase-3, and AIF. There is no doubt that when apoptosis occurs, the energy supply of mitochondria in the cell will be insufficient, and the synthesis and metabolism of some amino acids will be hindered. In this study, the metabolism and synthesis of chenodeoxycholic acid, chenodeoxycholic acid, and cholic acid were affected to some extent. Undoubtedly, during the amino acid metabolism process, the levels of L-Phenylalanine and Argininic acid decreased significantly after PQ treatment. The metabolism of amino acids would further affect the energy metabolism of cells, especially in the TCA cycle.

CONCLUSION

AEE exhibited protective effects on PQ-induced ALI. The underlying mechanism was correlated with antioxidants that regulate amino acid, phospholipid and energy metabolism metabolic pathway disorders and alleviate liver mitochondria apoptosis.

DATA AVAILABILITY STATEMENT

The original contributions presented in the study are included in the article/supplementary materials, further inquiries can be directed to the corresponding author/s.

ETHICS STATEMENT

The animal study was reviewed and approved by the Institutional Animal Care and Use Committee of Lanzhou Institute of Husbandry and Pharmaceutical Science of Chinese Academy

of Agricultural Sciences (Approval No. NKMYD201907018; Approval Date: 18 July 2019).

AUTHOR CONTRIBUTIONS

Z-DZ designed and performed the experiments. Y-JY synthesized and purified AEE. X-WL, S-HL, and ZQ assisted with the animal experiments. J-YL supervised the study and revised the manuscript.

FUNDING

This study was supported by grants from the National Natural Science Foundation of China (No. 31872518).

REFERENCES

1. Shao Y, Zhao Y, Zhu T, Zhang F, Chang X, Zhang Y, et al. Paraquat preferentially induces apoptosis of late stage effector lymphocyte and impairs memory immune response in mice. *Int J Environ Res Public Health.* (2019) 16:60. doi: 10.3390/ijerph16112060
2. Chen HG, Yang RJ, Tang Y, Fu XY. Effects of curcumin on artery blood gas index of rats with pulmonary fibrosis caused by paraquat poisoning and the expression of Smad 4, Smurf 2, interleukin-4 and interferon-. *Exp Ther Med.* (2019) 17:3664–70. doi: 10.3892/etm.2019.7341
3. Sun L, Li GQ, Yan PB, Liu Y, Li GF, Wei LQ. Prediction of outcome following paraquat poisoning by arterial lactate concentration-time data. *Exp Ther Med.* (2014) 8:652–6. doi: 10.3892/etm.2014.1773
4. Chen F, Liu ZL, Li W, Li D, Yan BL. The significance of serum HMGB1 level in humans with acute paraquat poisoning. *Sci Rep*. (2019) 9:1. doi: 10.1038/s41598-019-43877-1
5. Xu CW, Luo JJ, He L, Montell C, Perrimon N. Oxidative stress induces stem cell proliferation via TRPA1/RyR-mediated Ca2+ signaling in the Drosophila midgut. *Elife*. (2017) 6:40. doi: 10.7554/eLife.22441.040
6. Feng MX, Li YN, Ruan WS, Lu YQ. Predictive value of the maximum serum creatinine value and growth rate in acute paraquat poisoning patients. *Sci Rep*. (2018) 8:298. doi: 10.1038/s41598-018-29800-0
7. Yan B, Chen F, Xu L, Xing J, Wang X. HMGB1-TLR4-IL23-IL17A axis promotes paraquat-induced acute lung injury by mediating neutrophil infiltration in mice. *Sci Rep*. (2017) 7:597. doi: 10.1038/s41598-017-00721-8
8. Han JY, Zhang ZJ, Yang SB, Wang J, Yang XL, Tan DH. Betanin attenuates paraquat-induced liver toxicity through a mitochondrial pathway. *Food Chem Toxicol.* (2014) 70:100–6. doi: 10.1016/j.fct.2014.04.038
9. El-Boghdady NA, Abdeltawab NF, Nooh MM. Resveratrol and montelukast alleviate paraquat-induced hepatic injury in mice: modulation of oxidative stress, inflammation, and apoptosis. *Oxid Med Cell Long.* (2017) 2017:425. doi: 10.1155/2017/9396425
10. Jung E, Kim J. Aloin inhibits muller cells swelling in a rat model of thioacetamide-induced hepatic retinopathy. *Molecules*. (2018) 23:6. doi: 10.3390/molecules23112806
11. Zhang L, Wang X, Chen S, Wang S, Tu Z, Zhang G, et al. Medium-chain triglycerides attenuate liver injury in lipopolysaccharide-challenged pigs by inhibiting necroptotic and inflammatory signaling pathways. *Int J Mol Sci.* (2018) 19:97. doi: 10.3390/ijms19113697
12. Parvez MK, Arbab AH, Al-Dosari MS, Al-Rehaily AJ, Alam P, Ibrahim KE, et al. Protective effect of *Atriplex suberecta* extract against oxidative and apoptotic hepatotoxicity. *Exp Ther Med.* (2018) 15:3883–91. doi: 10.3892/etm.2018.5919
13. Ren Y, Yang ZZ, Sun ZR, Zhang W, Chen X, Nie SN. Curcumin relieves paraquat-induced lung injury through inhibiting the thioredoxin interacting protein/NLR pyrin domain containing 3-mediated inflammatory pathway. *Mol Med Rep.* (2019) 20:5032–40. doi: 10.3892/mmr.2019.10612
14. Gao C, Huang Q, Lan Q, Feng Y, Tang F, Hoi MPM, et al. A user-friendly herbicide derived from photo-responsive supramolecular vesicles. *Nat Commun.* (2018) 9:2967. doi: 10.1038/s41467-018-05437-5
15. Qian JY, Deng P, Liang YD, Pang L, Wu LC, Yang LL, et al. 8-formylophiopogonanone b antagonizes paraquat-induced hepatotoxicity by suppressing oxidative stress. *Front Pharmacol.* (2019) 10:1283. doi: 10.3389/fphar.2019.01283
16. Chen D, Ma T, Liu XW, Yang C, Liu Z. Rapamycin reverses paraquat-induced acute lung injury in a rat model through inhibition of NF kappa B activation. *Int J Clin Exp Pathol.* (2015) 8:4627–38.
17. Gawarammana IB, Buckley NA. Medical management of paraquat ingestion. *Br J Clin Pharmacol.* (2011) 72:745–57. doi: 10.1111/j.1365-2125.2011.04026.x
18. Huang MZ, Yang YJ, Liu XW, Qin Z, Li JY. Aspirin eugenol ester attenuates oxidative injury of vascular endothelial cells by regulating NOS and Nrf2 signalling pathways. *Br J Pharmacol.* (2019) 176:906–18. doi: 10.1111/bph.14592
19. Ma N, Liu XW, Yang YJ, Li JY, Mohamed I, Liu GR, et al. Preventive effect of aspirin eugenol ester on thrombosis in kappa-carrageenan-induced rat tail thrombosis model. *PLoS ONE.* (2015) 10:e0133125. doi: 10.1371/journal.pone.0133125
20. Ma N, Yang GZ, Liu XW, Yang YJ, Mohamed I, Liu GR, et al. Impact of aspirin eugenol ester on cyclooxygenase-1, cyclooxygenase-2, C-reactive protein, prothrombin and arachidonate 5-lipoxygenase in healthy rats. *Iran J Pharm Res.* (2017) 16:1443–51. doi: 10.22037/ijpr.2017.2119
21. Li JY, Yu YG, Wang QW, Zhang JY, Yang YJ, Li B, et al. Synthesis of aspirin eugenol ester and its biological activity. *Med Chem Res.* (2012) 21:995–9. doi: 10.1007/s00044-011-9609-1
22. Li JY, Wang QW, Yu YG, Yang YJ, Niu JR, Zhou XZ, et al. Anti-inflammatory effects of aspirin eugenol ester and the potential mechanism. *Chin J Pharm Toxicol.* (2011) 25:57–61. doi: 10.3867/j.issn.1000-3002.2011.01.011
23. Huang MZ, Yang YJ, Liu XW, Qin Z, Li JY. Aspirin eugenol ester reduces H2O2-induced oxidative stress of HUVECs via mitochondria-lysosome axis. *Oxid Med Cell Longev.* (2019) 2019:8098135. doi: 10.1155/2019/8098135
24. Abate M, Festa A, Falco M, Lombardi A, Luce A, Grimaldi A, et al. Mitochondria as playmakers of apoptosis, autophagy and senescence. *Semin Cell Dev Biol.* (2020) 98:139–53. doi: 10.1016/j.semcdb.2019.05.022
25. Hasnat M, Yuan Z, Ullah A, Naveed M, Raza F, Ashraf Baig MMF, et al. Mitochondria-dependent apoptosis in triptolide-induced hepatotoxicity is associated with the Drp1 activation. *Toxicol Mech Methods.* (2019) 2019:1–10. doi: 10.1080/15376516.2019.1669247
26. Meng LQ, Wang Y, Luo YH, Piao XJ, Liu C, Wang Y, et al. Quinalizarin induces apoptosis through reactive oxygen species (ROS)-mediated mitogen-activated protein kinase (MAPK) and signal transducer and activator of transcription 3 (STAT3) signaling pathways in colorectal cancer cells. *Med Sci Monit.* (2018) 24:3710–9. doi: 10.12659/MSM.907163
27. Moradzadeh M, Hosseini A, Rakhshandeh H, Aghaei A, Sadeghnia HR. Cuscuta campestris induces apoptosis by increasing reactive oxygen species generation in human leukemic cells. *Avicenna J Phytomed.* (2018) 8:237–45.
28. Tan D, Wang Y, Bai B, Yang X, Han J. Betanin attenuates oxidative stress and inflammatory reaction in kidney of paraquat-treated rat. *Food Chem Toxicol.* (2015) 78:141–6. doi: 10.1016/j.fct.2015.01.018
29. Li GP, Yang H, Zong SB, Liu Q, Li L, Xu ZL, et al. Diterpene ginkgolides meglumine injection protects against paraquat-induced lung injury and pulmonary fibrosis in rats. *Biomed Pharmacother.* (2018) 99:746–54. doi: 10.1016/j.biopha.2018.01.135
30. Javad-Mousavi SA, Hemmati AA, Mehrzadi S, Hosseinzadeh A, Houshmand G, Rashidi Nooshabadi MR, et al. Protective effect of *Berberis vulgaris* fruit extract against Paraquat-induced pulmonary fibrosis in rats. *Biomed Pharmacother.* (2016) 81:329–36. doi: 10.1016/j.biopha.2016.04.027
31. Gwinn DM, Lee AG, Briones-Martin-Del-Campo M, Conn CS, Simpson DR, Scott AI, et al. Oncogenic KRAS regulates amino acid homeostasis and asparagine biosynthesis via ATF4 and alters sensitivity to L-asparaginase. *Cancer Cell.* (2018) 33:91–107.e106. doi: 10.1016/j.ccell.2017.12.003

32. Zhang J, Fan J, Venneti S, Cross JR, Takagi T, Bhinder B, et al. Asparagine plays a critical role in regulating cellular adaptation to glutamine depletion. *Mol Cell.* (2014) 56:205–18. doi: 10.1016/j.molcel.2014.08.018
33. Chen S, Sun M, Zhao X, Yang Z, Liu W, Cao J, et al. Neuroprotection of hydroxysafflor yellow A in experimental cerebral ischemia/reperfusion injury via metabolic inhibition of phenylalanine and mitochondrial biogenesis. *Mol Med Rep.* (2019) 19:3009–20. doi: 10.3892/mmr.2019.9959
34. Li J, Yu Y, Yang Y, Liu X, Zhang J, Li B, et al. A 15-day oral dose toxicity study of aspirin eugenol ester in Wistar rats. *Food Chem Toxicol.* (2012) 50:1980–5. doi: 10.1016/j.fct.2012.03.080
35. Shen DS, Yang YJ, Kong XJ, Ma N, Liu XW, Li SH, et al. Aspirin eugenol ester inhibits agonist-induced platelet aggregation in vitro by regulating PI3K/Akt, MAPK and Sirt 1/CD40L pathways. *Eur J Pharmacol.* (2019) 852:1–13. doi: 10.1016/j.ejphar.2019.02.032
36. Ma N, Liu XW, Kong XJ, Li SH, Jiao ZH, Qin Z, et al. Aspirin eugenol ester regulates cecal contents metabolomic profile and microbiota in an animal model of hyperlipidemia. *BMC Vet Res.* (2018) 14:405. doi: 10.1186/s12917-018-1711-x
37. Huang MZ, Lu XR, Yang YJ, Liu XW, Qin Z, Li JY. Cellular metabolomics reveal the mechanism underlying the anti-atherosclerotic effects of aspirin eugenol ester on vascular endothelial dysfunction. *Int J Mol Sci.* (2019) 20:165. doi: 10.3390/ijms20133165
38. Ma N, Liu XW, Yang YJ, Shen DS, Zhao XL, Mohamed I, et al. Evaluation on antithrombotic effect of aspirin eugenol ester from the view of platelet aggregation, hemorheology, TXB2/6-keto-PGF1alpha and blood biochemistry in rat model. *BMC Vet Res.* (2016) 12:108. doi: 10.1186/s12917-016-0738-0
39. Shen D, Ma N, Yang Y, Liu X, Qin Z, Li S, et al. UPLC-Q-TOF/MS-based plasma metabolomics to evaluate the effects of aspirin eugenol ester on blood stasis in rats. *Molecules.* (2019) 24:80. doi: 10.3390/molecules24132380
40. Hu S, Qiao C, Yuan Z, Li M, Ye J, Ma H, et al. Therapy with high-dose long-term antioxidant free radicals for severe paraquat poisoning: A pilot study. *Exp Ther Med.* (2018) 16:5149–55. doi: 10.3892/etm.2018.6823
41. Gu SY, Yeh TY, Lin SY, Peng FC. Unfractionated bone marrow cells attenuate paraquat-induced glomerular injury and acute renal failure by modulating the inflammatory response. *Sci Rep.* (2016) 6:23287. doi: 10.1038/srep23287
42. Sun S, Wang H, Zhao G, An Y, Guo Y, Du L, et al. Complement inhibition alleviates paraquat-induced acute lung injury. *Am J Respir Cell Mol Biol.* (2011) 45:834–42. doi: 10.1165/rcmb.2010-0444OC
43. Wang Y, Wu Y, Quadri F, Prox JD, Guo L. Cytotoxicity of ZnO nanowire arrays on excitable cells. *Nanomaterials*. (2017). 7:80. doi: 10.3390/nano7040080
44. Kumar M, Padula MP, Davey P, Pernice M, Jiang Z, Sablok G, et al. Proteome analysis reveals extensive light stress-response reprogramming in the seagrass Zostera muelleri (Alismatales, Zosteraceae) metabolism. *Front Plant Sci.* (2016) 7:2023. doi: 10.3389/fpls.2016.02023
45. Yue QM, Peng Y, Zhao Y, Lu RX, Fu QY, Chen Y, et al. Dual-targeting for brain-specific drug delivery: synthesis and biological evaluation. *Drug Del.* (2018) 25:426–434. doi: 10.1080/10717544.2018.1431978
46. Yang BY, Zhang XY, Guan SW, Hua ZC. Protective effect of procyanidin B2 against CCl4-induced acute liver injury in mice. *Molecules.* (2015) 20:12250–65. doi: 10.3390/molecules200712250
47. Ali A, Guo D, Mahar A, Ma F, Li RH, Shen F, et al. Streptomyces pactum assisted phytoremediation in Zn/Pb smelter contaminated soil of Feng County and its impact on enzymatic activities. *Sci Rep*. (2017) 7:87. doi: 10.1038/srep46087
48. Wang YP, Yang L, Chen X, Ye TT, Zhong B, Liu RJ, et al. Major latex protein-like protein 43 (MLP43) functions as a positive regulator during abscisic acid responses and confers drought tolerance in *Arabidopsis thaliana*. *J Exp Botany*. (2016) 67:421–34. doi: 10.1093/jxb/erv477
49. Liu ZH, Shi XY, Li S, Zhang LL, Song XY. Oxidative stress and aberrant programmed cell death are associated with pollen abortion in isonuclear alloplasmic male-sterile wheat. *Front Plant Sci*. (2018) 9:595. doi: 10.3389/fpls.2018.00595
50. Huang CP, Qin NN, Sun L, Yu MY, Hu WZ, Qi ZY. Selenium improves physiological parameters and alleviates oxidative stress in strawberry seedlings under low-temperature stress. *Int J Mol Sci*. (2018) 19:1913. doi: 10.3390/ijms19071913
51. Belhadj S, Hentati O, Hamdaoui G, Fakhreddine K, Maillard E, Dal S, et al. Beneficial effect of jojoba seed extracts on hyperglycemia-induced oxidative stress in rinm5f beta cells. *Nutrients*. (2018) 10:384. doi: 10.3390/nu10030384
52. Yang GY, Zhang CL, Liu XC, Qian G, Deng DQ. Effects of cigarette smoke extracts on the growth and senescence of skin fibroblasts *in vitro*. *Int J Biol Sci.* (2013) 9:613–23. doi: 10.7150/ijbs.6162
53. Volpato GT, Damasceno DC, Sinzato YK, Ribeiro VM, Rudge MVC, Calderon IMP. Oxidative stress status and placental implications in diabetic rats undergoing swimming exercise after embryonic implantation. *Reprod Sci.* (2015) 22:602–8. doi: 10.1177/1933719114556485
54. Etani R, Kataoka T, Kanzaki N, Sakoda A, Tanaka H, Ishimori Y, et al. Protective effects of hot spring water drinking and radon inhalation on ethanol-induced gastric mucosal injury in mice. *J Rad Res.* (2017) 58:614–25. doi: 10.1093/jrr/rrx021
55. Roder P, Hille C. Local tissue manipulation via a force- and pressure-controlled AFM micropipette for analysis of cellular processes. *Sci Rep*. (2018) 8:9. doi: 10.1038/s41598-018-24255-9
56. Liu YN, Paterson M, Baumgardt SL, Irwin MG, Xia ZY, Bosnjak ZJ, et al. Vascular endothelial growth factor regulation of endothelial nitric oxide synthase phosphorylation is involved in isoflurane cardiac preconditioning. *Cardiovasc Res.* (2019) 115:168–78. doi: 10.1093/cvr/cvy157
57. Jiang P, Zhang X, Huang Y, Cheng N, Ma Y. Hepatotoxicity induced by *Sophora flavescens* and hepatic accumulation of kurarinone, a major hepatotoxic constituent of *Sophora flavescens* in rats. *Molecules*. (2017) 22:809. doi: 10.3390/molecules22111809
58. Xu J, Casas-Ferreira AM, Ma Y, Sen A, Kim M, Proitsi P, et al. Lipidomics comparing DCD and DBD liver allografts uncovers lysophospholipids elevated in recipients undergoing early allograft dysfunction. *Sci Rep.* (2015) 5:17737. doi: 10.1038/srep17737
59. Srivastava NK, Sharma S, Sharma R, Sinha N, Mandal SK, Sharma D. Metabolic fingerprinting of joint tissue of collagen-induced arthritis (CIA) rat: *In vitro*, high resolution NMR (nuclear magnetic resonance) spectroscopy based analysis. *EXCLI J.* (2018) 17:257–72. doi: 10.17179/excli2017-938
60. Jiang XS, Chen XM, Wan JM, Gui HB, Ruan XZ, Du XG. Autophagy protects against palmitic acid-induced apoptosis in podocytes *in vitro*. *Sci Rep*. (2017) 7:64. doi: 10.1038/srep42764
61. Qin JL, Shen WY, Chen ZF, Zhao LF, Qin QP, Yu YC, et al. Oxoaporphine metal complexes (Co-II, Ni-II, Zn-II) with high antitumor activity by inducing mitochondria-mediated apoptosis and S-phase arrest in HepG2. *Sci Rep.* (2017) 7:56. doi: 10.1038/srep46056
62. Winckelmans E, Nawrot TS, Tsamou M, Den Hond E, Baeyens W, Kleinjans J, et al. Transcriptome-wide analyses indicate mitochondrial responses to particulate air pollution exposure. *Environ Health.* (2017) 16:7. doi: 10.1186/s12940-017-0292-7

Conflict of Interest: The authors declare that the research was conducted in the absence of any commercial or financial relationships that could be construed as a potential conflict of interest.

frontiers in Medicine

ORIGINAL RESEARCH
published: 15 January 2021
doi: 10.3389/fmed.2020.584888

Comparison of Liver Biomarkers in 288 COVID-19 Patients: A Mono-Centric Study in the Early Phase of Pandemic

*Haozhi Fan[1†], Jinyuan Cai[2†], Anran Tian[2†], Yuwen Li[3], Hui Yuan[2], Zhengyi Jiang[4], Yunxi Yu[5], Lili Ruan[6], Pingping Hu[2], Ming Yue[2], Nian Chen[2], Jun Li[2] and Chuanlong Zhu[2,7]**

[1] Department of Information, The First Affiliated Hospital of Nanjing Medical University, Nanjing, China, [2] Department of Infectious Disease, The First Affiliated Hospital of Nanjing Medical University, Nanjing, China, [3] Department of Pediatrics, The First Affiliated Hospital of Nanjing Medical University, Nanjing, China, [4] State Key Laboratory for Diagnosis and Treatment of Infectious Diseases, Collaborative Innovation Center for Diagnosis and Treatment of Infectious Diseases, College of Medicine, The First Affiliated Hospital, Zhejiang University, Hangzhou, China, [5] Emergency Department, Huangshi Hospital of Traditional Chinese Medicine, Huangshi, China, [6] Department of Anesthesiology, The Fifth Hospital of Huangshi, Huangshi, China, [7] Department of Tropical Diseases, The Second Affiliated Hospital of Hainan Medical University, Haikou, China

OPEN ACCESS

Edited by:
Chao Yan,
Xuzhou Medical University, China

Reviewed by:
Roberto Gramignoli,
Karolinska Institutet (KI), Sweden
Huikuan Chu,
Huazhong University of Science and Technology, China

***Correspondence:**
Chuanlong Zhu
chuanlong@yahoo.com

†These authors have contributed equally to this work

Specialty section:
This article was submitted to Gastroenterology, a section of the journal Frontiers in Medicine

Received: *18 July 2020*
Accepted: *14 December 2020*
Published: *15 January 2021*

Citation:
Fan H, Cai J, Tian A, Li Y, Yuan H, Jiang Z, Yu Y, Ruan L, Hu P, Yue M, Chen N, Li J and Zhu C (2021) Comparison of Liver Biomarkers in 288 COVID-19 Patients: A Mono-Centric Study in the Early Phase of Pandemic. Front. Med. 7:584888. doi: 10.3389/fmed.2020.584888

Background and Aims: Recent reports have indicated that hepatic dysfunction occurred in a proportion of patients with coronavirus disease 2019 (COVID-19). We aimed to compare and describe the liver biomarkers in different subtypes of COVID-19 patients.

Methods: This study enrolled 288 COVID-19 patients in Huangshi Hospital of Traditional Chinese Medicine. All patients were divided into ordinary, severe, and critical groups according to the *Diagnosis and Treatment Protocol for Novel Coronavirus Pneumonia (Trial Version 7)*. Demographic, clinical characteristics and liver biomarkers were compared among the three groups.

Results: During hospitalization, AST, TBiL, and ALP levels in ordinary and severe patients fluctuated within the normal range with a rising trend in critical patients except AST. ALT and GGT levels fluctuated within the normal range showing an upward trend, while LDH levels in the critical group exceeded the normal range. Prealbumin showed an upward trend, especially in the severe group. At discharge, AST and LDH levels in ordinary and severe groups were lower than their baselines but increased in the critical group. In contrast to albumin, TBiL levels were increased in ordinary and critical groups while decreased in the severe group. The stratified analysis revealed factors affecting liver function in critical cases included highest temperature $\geq$38.0°C, age $\geq$60 and symptom of hypoxemia.

Conclusions: COVID-19 can cause severe hepatic dysfunction in critical patients, requiring early monitoring and intervention. LDH, ALP, GGT, TBiL, prealbumin, and albumin may be helpful for evaluating and predicting disease prognosis due to their correlation with disease severity in COVID-19.

Keywords: COVID-19, SARS-CoV-2, liver biomarkers, liver injury, hepatic dysfunction

INTRODUCTION

Since December 2019, a pneumonia of unknown cause broke out in Wuhan. Epidemiological evidence shows that this pneumonia can spread among people through close contact and respiratory droplets, and people are generally susceptible (1–3). Different from severe acute respiratory syndrome (SARS) and middle east respiratory syndrome coronavirus (MERS) (4), a novel coronavirus named severe acute respiratory syndrome coronavirus 2 (SARS-CoV-2) was identified as the pathogen. Subsequently, this unique pneumonia was named coronavirus disease 2019 (COVID-19) by World Health Organization (WHO). Common clinical manifestations of SARS-CoV-2 infection include fever, fatigue and dry cough (5–9). In the early stage of infection, chest computed tomography (CT) only exhibits multiple small spot shadows and interstitial changes, and this then develops into multiple ground-glass opacities and infiltration in both lungs. In some severe cases, acute respiratory distress syndrome (ARDS), sepsis and even multiple organ failure may occur (5). Although the fatality rate of SARS-CoV-2 is not as high as that of SARS, its transmission and pathogenicity are even stronger. COVID-19 has already become a worldwide pandemic, so it is urgent to control the epidemic.

At present, there is still no specific drug or vaccine for COVID-19. Patients mainly receive symptomatic and supportive treatment during hospitalization to prevent serious complications. Clinical reports show that ALT, AST, TBiL, and other liver-related biochemical indexes of some patients with COVID-19 have increased to varying degrees (5–9). It suggests that in addition to cardiopulmonary injury, substantial hepatic impairment also exists, especially in severe and critical cases. Unfortunately, there is little research involving the mechanism of liver injury caused by COVID-19, nor does any pathological report prove that SARS-CoV-2 can directly attack the liver. Thus, the cause of liver dysfunction in COVID-19 remains unclear.

In clinical operations, serum biochemical examinations are more accessible than complicated operations such as liver biopsy and ultrasonography. Thus, indicators related to liver function in blood biochemical examination were selected as observation indicators. In serum biochemical examination, AST, ALT, and LDH are indicators of liver function that reflect the damage and severity of liver cells. ALP, GGT, and TBiL are indicators of liver function that reflect bilirubin metabolism and cholestasis. As for prealbumin and albumin, they are indicators that reflect liver synthesis and reserve function. In this study, we compared the clinical manifestations and liver biomarkers among different subtypes of COVID-19 patients, focusing on the baseline characteristics and dynamic change trend of the above liver biomarkers at admission and during hospitalization. Besides, we discussed the potential mechanism of hepatic impairment in critical cases to provide novel insights for clinical decision-making and drug development.

METHODS

Study Participants

This retrospective study enrolled a total of 288 COVID-19 patients in Huangshi Hospital of Traditional Chinese Medicine in Hubei Province from January to April 2020. Among them, male and female patients numbered 147 and 141, respectively. According to the *Diagnosis and Treatment Protocol for Novel Coronavirus Pneumonia (Trial Version 7)* (10), COVID-19 patients were confirmed by positive real-time reverse transcriptase-polymerase chain reaction (RT-PCR) and chest CT test. Clinical and laboratory information of these patients should be completed.

Patients infected with other common respiratory viruses, including influenza A and B viruses, respiratory syncytial virus, parainfluenza virus, adenovirus, SARS coronavirus, or MERS coronavirus or a combination with chronic liver diseases, such as viral hepatitis, autoimmune liver disease, alcoholic fatty liver disease, or liver cancer, were excluded from this study.

Data Collection

Clinical information, including age, gender, epidemic history, basic diseases, clinical symptoms, imaging findings, laboratory tests, and treatment measures were obtained from medical records.

Grouping Methods

The degrees of COVID-19 infection were categorized into ordinary, severe, and critical based on *Diagnosis and Treatment Protocol for Novel Coronavirus Pneumonia (Trial Version 7)* (10). In brief, ordinary or mild patients exhibited mild clinical symptoms with or without imaging changes. Adult patients with severe type were characterized by at least one of the following symptoms: respiratory frequency $\geq$30/min, blood oxygen saturation at rest $\leq$93%, PaO_2/FiO_2 ratio $<$300 mmHg and lung infiltrates $>$50% within 24–48 h. Critical cases were those exhibiting respiratory failure with mechanical ventilation, septic shock and/or multiple organ dysfunction/failure, and they needed ICU monitoring. With the purpose of optimizing this study design, ordinary, and mild types were combined into the ordinary type in this study.

At the end of the study, each group was divided into smaller subgroups according to age, hypertension, highest temperature, chest tightness, glucocorticoid therapy, and hypoxemia to further analyze potential confounding factors.

Statistical Analysis

SPSS (version 22.0) was used to perform statistical analyses. Continuous data with normal distribution were expressed as means $\pm$ standard deviation (SD) and were analyzed by analysis of variance (ANOVA). Continuous data with non-normal distribution medians were expressed as the interquartile range (P25-P75) and were analyzed by non-parametric test. Categorical data were expressed as numbers (%) and were compared by Chi-squared test. The Mann-Kendal test was used to test the trend of each liver function index with hospitalization time. When the sample size was insufficient, the Fisher exact test was adopted. A $p < 0.05$ was considered to indicate statistical significance.

Study Approval

This study was approved by the Ethics Committee of the Huangshi Hospital of Traditional Chinese Medicine in Hubei Province (HSZYPJ-2020-021-01) in compliance with the

principles of the Declaration of Helsinki and according to Good Clinical Practice guidelines. Written informed consent was waived due to the rapid emergence of this infectious disease.

RESULTS

Demographic and Clinical Characteristics of COVID-19 Patients in Different Groups

As shown in **Table 1**, the average age in the critical group (71.9 ± 11.6) was significantly older than that in the ordinary (49.3 ± 14.1) and severe groups(61.4 ± 13.9). The frequency of patients with hypertension (19.4%) and cardiovascular complications (12.9%) in the critical group was higher than that in the ordinary (6.2%, 0.9%) and severe groups (17.4%, 4.3%).

As shown in **Table 2**, the proportion of severe (47.8%) and critical (54.8%) patients with chest tightness at admission were significantly higher than that of ordinary patients (17.5%). High fever (more than 39°C) was more common in the severe group. During hospitalization, 21.2% of patients developed hypoxemia, of which that of severe patients (65.2%) and critical patients (51.6%) was significantly higher than that of ordinary patients (7.1%), and more severe patients (82.2%) and critical patients (80.8%) received glucocorticoid therapy compared with ordinary patients (16.5%). After standardized treatment, the averaged days of nucleic acid turning negative and CT symptoms disappear had significant differences among the three groups. In the critical group, only one patient achieved negative nucleic acid and CT symptoms disappeared before the study deadline. A total of 23 patients died, and the mortality of the critical group was significantly higher than that of the other two groups.

Dynamic Changes in Liver Function Indexes in Different Groups of COVID-19 Patients During Hospitalization

To observe the dynamic impact of SARS-CoV-2 infection and clinical treatment on the liver function of patients, a violin plot was used to show the results of AST, ALT, GGT, LDH, ALP, TBiL, prealbumin, and albumin at different times after admission, as shown in **Figure 1**. The trend of each liver biomarker index with hospitalization time according to the Mann-Kendal test showed in **Supplementary Table 1**.

The median levels of AST, TBiL, and ALP in ordinary and severe patients fluctuated within the normal range (**Figures 1A,D,F**). Moreover, the median levels of ALP in severe patients ($Z = 2.021$, $P = 0.043$) and the median levels of TBiL in critical patients ($Z = 2.205$, $P = 0.027$) had a significant upward trend. As shown in **Figures 1B,E**, ALT and GGT levels among the three groups were fluctuated around the normal range and showed an upward trend ($Z > 0$, $P > 0.05$), except for ALT median levels in critical patients. Differently, LDH level in critical patients fluctuated above the normal value (**Figure 1C**), higher than that of the ordinary and severe groups ($P < 0.05$) and showed a significantly downward trend in ordinary and severe patients ($Z = -2.205$, $P = 0.028$). We also observed that prealbumin levels among the three groups fluctuated below the normal value, showing an upward trend especially in the severe group ($Z = 2.205$, $P = 0.027$), and the critical group was lower than that in the other two groups (**Figure 1G**, $P < 0.05$). Albumin levels in the ordinary group fluctuated within the normal range, higher than the severe and critical groups (**Figure 1H**, $P < 0.05$), and their albumin level fluctuated around the normal.

Changes From Baseline in Liver Biomarkers Among Different Groups of COVID-19 Patients at Discharge

As shown in **Table 3**, the baseline levels of AST and LDH in the critical group [(46.0, P25–P75:32.0–59.3), (390, P25–P75:290–516), respectively] were significantly higher than that in ordinary group [(28.0, P25–P75:23.0–38.0), (326, P25–P75:195–293), respectively], whereas prealbumin and albumin levels showed opposite trends. Also, ALP levels were increased than their baseline among three groups (8.0, 12.0, 25.0, respectively), and the change of the critical group was significantly higher than that of the ordinary group ($P < 0.05$). Furthermore, there were differences in the baseline levels of TBiL among three groups ($P = 0.016$), but no difference was found between the two groups after Bonferroni correction.

At discharge, AST and LDH levels were decreased than their baseline in ordinary (−4.5, −46, respectively) and severe groups (−9.0, −129, respectively), while increased in critical group (6.0, 166, respectively), and the change of the critical group was significantly higher than that of the severe group ($P < 0.05$). In contrast to albumin, TBiL levels were increased in ordinary and critical groups (0.2, 15.4, respectively), while decreased in the severe group (−1.3). Prealbumin levels were increased among the ordinary, severe and critical groups (126, 146, 7, respectively).

For exploring the affecting factors of liver function in critical cases, we carried out a stratified analysis. We summarized that the factors affecting liver function (AST, ALP, and LDH) in critical patients included highest temperature ≥38.0°C, age ≥60 and symptom of hypoxemia (**Supplementary Figures 1, 2, 4, 9, 11, 12**). No significant associations between the variables (age, hypertension, highest temperature, chest tightness, glucocorticoid therapy, and hypoxemia) and the changed TBiL and prealbumin were observed (**Supplementary Figures 5–8**).

DISCUSSION

As of April 17, 2020, a total of 2,074,529 COVID-19 cases have been confirmed, with 139,378 deaths (11), and the epidemic is still expanding. In this retrospective study, the critical group had an average age of 71.9, 87.1% (27/31) were over 60.0, and it showed the highest fatality rate 67.7% (21/31). In view of the elderly patients often combined with chronic basic diseases and weakened immunity, their condition was more likely to deteriorate. Recent studies found that patients with a longer time from onset to admission are more likely to develop hepatic impairment (12), and pathological evidence also showed moderate microvascular steatosis and mild lobular inflammation in the liver tissue of patients with COVID-19 (13), indicating that COVID-19 infection can lead to liver injury in some patients.

TABLE 1 | Demographics and baseline characteristics of patients infected with SARS-CoV-2.

Characteristics	All patients ($n = 288$)	Disease severity			*P*-value
		Ordinary ($n = 211$)	Severe ($n = 46$)	Critical ($n = 31$)	
Age (mean ± *SD*), yr	53.7 ± 15.8	49.3 ± 14.1	61.4 ± 13.9	71.9 ± 11.6	<0.001
Age groups, No. (%)					<0.001
<50 yr	112 (38.9)	103 (48.7)	8 (17.5)	1 (3.2)	
50–59 yr	72 (25.0)	59 (28.0)	10 (21.7)	3 (9.7)	
60–69 yr	59 (20.5)	36 (17.1)	14 (30.4)	9 (29.0)	
>70 yr	45 (15.6)	13 (6.2)	14 (30.4)	18 (58.1)	
Sex, No. (%)					0.679
Female	141 (49.0)	106 (50.2)	22 (47.8)	13 (41.9)	
Male	147 (51.0)	105 (49.8)	24 (52.2)	18 (58.1)	
Exposure history[†], No. (%)	107 (37.2)	83 (39.3)	13 (28.3)	11 (35.5)	0.148
Coexisting disorders, No. (%)					
Hypertension	27 (9.4)	13 (6.2)	8 (17.4)	6 (19.4)	0.006*
Diabetes	24 (8.3)	14 (6.6)	6 (13.0)	4 (12.9)	0.187*
Cardiovascular disease	8 (2.8)	2 (0.9)	2 (4.3)	4 (12.9)	0.002*
Malignancy	3 (1.0)	1 (0.5)	1 (2.2)	1 (3.2)	0.175*
Chronic kidney disease	3 (1.0)	1 (0.5)	2 (4.3)	0	0.099*
Incubation (mean ± *SD*)[‡], day	5.8 ± 4.1	5.5 ± 4.2	7.0 ± 3.2	6.4 ± 4.6	0.580

**P-value of Fisher's exact test between two groups, T < 1 or 2 cells (25.0%) have T < 5.*

[†] Represents a clear history of contact with infected patients.

[‡] Represents days from possible contact with an infected person to illness onset.

Moreover, Xie et al. found the increase of ALT or AST was also observed in nearly one-third of patients in non-ICU group (14). To further explore the effects of COVID-19 on liver function, we conducted a mono-centric study in the early phase of the pandemic to analyze the changes of serological hepatic biomarkers in COVID-19 patients during hospitalization and at discharge.

During hospitalization, we found LDH was increased in all three groups, especially exceeding the normal range in the critical group. After treatment, AST and LDH levels in ordinary and severe cases gradually tended to be normal, but it should be noted that the levels of LDH in critical cases were increased until discharge. There are various factors contributing to the elevation of LDH. Chen et al. (6) found that COVID-19 patients with cardiovascular events are more likely to have heart injury and heart failure, illuminating that the increase of LDH may also be related to heart function damage. A case-control study found that a high level of LDH was an independent factor associated with 1-month mortality in older COVID-19 inpatients (15). Moreover, a meta-analysis indicated that the abnormal changes of serological examination results, such as LDH, are related to multiple organ dysfunction and its severity (16). Increased liver function indicator levels, such as ALT, AST, ALP, and TBiL, were involved in the increased mortality risk of COVID-19 (17). However, in our study, the levels of raised ALT and AST were limited, which was consistent with the previous study (18). These findings showed the correlation between liver injury and the prognosis of the disease and the monitoring of LDH in COVID-19 patients, especially in critical patients should be paid enough attention.

At present, few researchers have reported a significant increase in serum ALP levels in COVID-19. The current study found that the median levels of ALP and GGT among the three groups shown an upward trend, especially the increasing trend of ALP median levels in severe patients was significant. Apart from the effects of age, elevated ALP may imply the injury of the bile duct. It has been fully confirmed that the co-expression of angiotensin-converting enzyme 2 (ACE2) (19, 20) and transmembrane protease serine 2 (TMPRSS2) (21, 22) is necessary for SARS-CoV-2 to enter the cells. Trophoblast cell surface antigen 2 (TROP2) protein is expressed in putative bipotent liver epithelial progenitors as well as biliary cells (23). Moreover, a recent scRNA-seq analysis reported that adult human liver TROP2+ progenitors co-express ACE2 and TMPRSS2 (24), indicating that the liver could be a potential target of SARS-CoV-2. However, previous results of sequencing showed that the expression of ACE2 in hepatocytes was very low, while the expression of ACE2 in bile duct epithelial cells was 20 times higher than that in hepatocytes (15, 25). Given that ACE2 is the crucial factor (26), SARS-hepatic inflammation may be more likely to induce bile duct epithelial cell damage than direct liver damage. Combined with our detection of markedly increased TBiL in the critical group, it is speculated that SARS-CoV-2 could induce the injury of bile duct cells and then bring certain damage to liver function.

TABLE 2 | Clinical characteristics and outcomes of patients infected with SARS-CoV-2.

Characteristics	All patients ($n = 288$)	Disease severity			*P*-value
		Ordinary ($n = 211$)	Severe ($n = 46$)	Critical ($n = 31$)	
Signs and symptoms at admission, No. (%)					
Fever	215 (74.7)	159 (75.4)	37 (80.4)	19 (61.3)	0.150
Dry cough	134 (46.5)	97 (46.0)	27 (58.7)	10 (32.3)	0.070
Fatigue	44 (15.3)	29 (13.7)	12 (26.1)	3 (9.7)	0.071
Chest tightness	76 (26.4)	37 (17.5)	22 (47.8)	17 (54.8)	<0.001
Expectoration	14 (4.9)	7 (3.3)	7 (15.2)	0	0.005*
Diarrhea	22 (7.6)	15 (7.1)	4 (8.7)	3 (9.7)	0.814*
Pharyngalgia	5 (1.7)	3 (1.4)	2 (4.3)	0	0.226*
Anorexia	27 (9.4)	16 (7.6)	9 (19.6)	2 (6.5)	0.050*
Dizzy	13 (4.5)	11 (5.2)	2 (4.3)	0 (0)	0.570*
Treatments and outcomes					
Glucocorticoid therapy, No. (%)	90 (34.0)	32 (16.5)	37 (82.2)	21 (80.8)	<0.001
Highest temperature, °C					0.005
<37.3	72 (25.0)	51 (24.2)	10 (21.7)	11 (35.5)	
37.3–37.9	70 (24.3)	64 (30.3)	4 (8.7)	2 (6.5)	
38.0–38.9	80 (27.8)	52 (24.6)	18 (39.2)	10 (32.3)	
≥39.0	66 (22.9)	44 (20.9)	14 (30.4)	8 (25.7)	
Hypoxemia, No. (%)	61 (21.2)	15 (7.1)	30 (65.2)	16 (51.6)	<0.001
Fever days §	9.0 (7.0, 11.0)	8.0 (6.0, 11.0)	10.0 (7.0, 11.0)	11.0 (7.0, 14.8)	0.194
Nucleic acid turning negative days§	17.0 (13.0, 21.0)	16.0 (13.0, 20.0)	21.0 (17.0, 27.0)	14.0†	<0.001
CT symptoms disappear days§	14.0 (10.0, 19.0)	13.0 (10.0, 18.0)	20.0 (15.0, 26.0)	20.0†	<0.001
Inpatient days‡, §	18.0 (15.0, 23.0)	18.0 (15.0, 22.0)	23.0 (20.0,29.0)	18.0 (11.0, 26.0)	<0.001
Death, No. (%)	23 (8.0)	1 (0.5)	1 (2.2)	21 (67.7)	<0.001

**P-value of Fisher's exact test between two groups, T < 1 or 2 cells (25.0%) have T < 5.*

† Only one critical patient reported nucleic acid turning positive days and CT symptoms disappear days.

‡ Some patients have not been discharged, especially critical patients.

§ Non-normal distribution data expressed as median (Q1, Q3).

Albumin and prealbumin are valuable indicators that are capable of predicting poor body status and clinical prognosis of numerous diseases (27–29). In our study, prealbumin and albumin levels were increased among ordinary and severe groups at discharge, but the median of prealbumin was still below the limit of the normal range. Liver dysfunction can lead to hypoalbuminemia. Hypoalbuminemia and elevated AST levels were often observed in critical patients, and the correlation of albumin and AST levels with disease severity was also found (30). Therefore, it can be considered that there existed substantial hepatic dysfunction. Albumin levels in both severe and critical groups were <40.0 g /L. Also, the level of the ordinary group was higher than that of the other two groups. And in all three groups, the levels decreased first and then increased during hospitalization, which indicated an improving trend of status as well as suggested that prealbumin and albumin might be related to the condition of patients.

Clinically, COVID-19 patients with fever usually received antipyretic treatment during hospitalization. Most antipyretic drugs contain paracetamol, which has been recognized to cause serious liver injury or even induce liver failure. In addition, although there is no targeted antiviral treatment for COVID-19, many patients still take non-specific antiviral drugs such as lopinavir and ritonavir, which may have certain hepatotoxicity and induce liver injury.

We noted that critical cases had severe symptoms of chest tightness at admission, and the proportion of oxygen saturation deficiency in severe and critical cases was as high as 65.2 and 51.6%, respectively. Researchers have found oxygen deprivation, lipid accumulation, glycogen consumption and

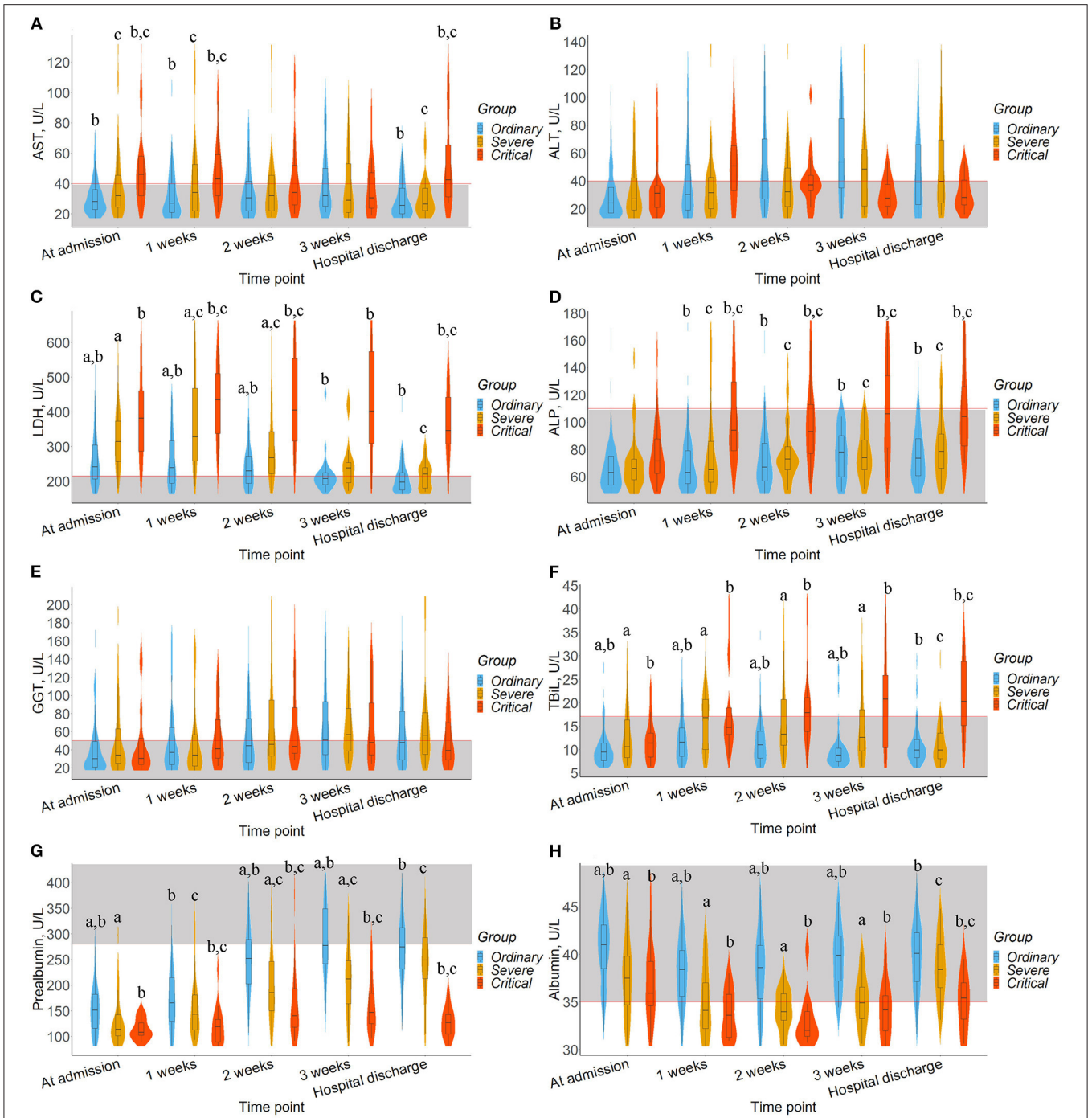

FIGURE 1 | Timeline charts illustrate dynamic changes of liver biomarkers. The box in the violin plot represents the median and quartile, the extension from the thin black line represents the 95% confidence interval, and the width of the violin plot represents the sample size at this level. In addition, the normal range was defined and drawn as gray area. [a] represents the significant difference between the ordinary and severe groups after *Bonferroni* correction. [b] represents the significant difference between ordinary and critical group after *Bonferroni* correction. [c] represents the significant difference between severe and critical group after *Bonferroni* correction. **(A)** AST. **(B)** ALT. **(C)** LDH. **(D)** ALP. **(E)** GGT. **(F)** TBiL. **(G)** Prealbumin. **(H)** Albumin.

ATP depletion in hepatocytes can rapidly lead to hepatocyte death (31). With the increase of reactive oxygen species (ROS), ROS and its peroxides act as the second messengers, activate redox-sensitive transcription factors, further activate the release of a variety of pro-inflammatory factors and then lead to liver damage (32). This indicates that the hypoxic internal

TABLE 3 | Summary of changes from baseline in liver biomarkers at discharge.

Characteristics	All patients ($n = 288$)	Disease severity			*P*-value*
		Ordinary ($n = 211$)	Severe ($n = 46$)	Critical ($n = 31$)	
AST (U/L), *n*	221	160	41	20	
Baseline	31.0 (24.0, 43.0)	28.0 (23.0, 38.0)‡	32.0 (24.0, 54.5)	46.0 (32.0, 59.3)‡	<0.001
Change from baseline	−4.0 (−14.0, 4.0)	−4.5 (−12.8, 2.0)	−9.0 (−24.0, 1.5)§	6.0 (−11.3, 72.0)§	0.013
ALT (U/L), *n*	221	160	41	20	
Baseline	22.0 (15.0, 36.0)	21.5 (14.3, 35.8)	25.0 (15.0, 45.0)	26.5 (16.0, 35.8)	0.625
Change from baseline	9.0 (−0.5, 33.5)	9.5 (1.0, 35.5)	4.0 (−6.0, 37.5)	5.5 (−4.0, 19.8)	0.335
LDH (U/L), *n*	158	122	20	16	
Baseline	260 (203, 320)	326 (195, 293)†,‡	350 (269, 396)†	390 (290, 516)‡	<0.001
Change from baseline	−47 (−10, −6.8)	−46 (−95, −11.5)†,‡	−129(−177, −49)†,§	166 (−33, 397)‡, §	<0.001
ALP (U/L), *n*	200	147	36	17	
Baseline	60.0 (51.0, 73.0)	59.0 (51.0, 72.0)	61.0 (48.3, 72.0)	69.0 (57.5, 94.0)	0.100
Change from baseline	9.0 (−1.0, 23.8)	8.0 (−3.0, 20.0)‡	12.0 (1.3, 26.5)	25.0 (9.5, 83.0)‡	0.007
GGT (U/L), *n*	200	147	36	17	
Baseline	27.0 (19.3, 52.8)	26.0 (18.0, 49.0)	34.0 (23.3, 63.5)	25.0 (21.5, 83.5)	0.172
Change from baseline	5.0 (−1.8, 26.8)	4.0 (−2.0, 23.0)	15.5 (0, 30.0)	4.0 (−34.0, 38.5)	0.148
TBiL (μmol/L), *n*	200	147	36	17	
Baseline	9.3 (7.3, 11.8)	9.0 (7.1, 11.3)	10.1 (8.0, 15.4)	11.6 (8.2, 14.0)	0.016
Change from baseline	0.4 (−1.9, 3.5)	0.2 (−1.7, 2.8)‡	−1.3 (−2.9, 1.5)§	15.4 (4.8, 26.3)‡, §	<0.001
Prealbumin (mg/L), *n*	187	140	31	16	
Baseline	134 (99, 172)	145 (109, 180)†,‡	99 (73, 132)†	103 (61, 122)‡	<0.001
Change from baseline	124 (64, 179)	126 (74, 189)‡	146 (94, 177)§	7 (−41, 48)‡, §	<0.001
Albumin (g/L), *n*	200	147	36	17	
Baseline	39.9 (36.1, 42.6)	40.8 (37.2, 43.3)†,‡	37.5 (33.7, 39.7)†	35.6 (31.9, 39.3)‡	<0.001
Change from baseline	−0.6 (−3.9, 2.6)	−0.6 (−3.7, 1.8)	0.6 (−1.9, 4.2)§	−5.7 (−10.6, 4.0)§	0.022

**Represents the P-values comparing different groups from the Kruskal-Wallis test.*

†Represents the significant difference between the ordinary and severe group after Bonferroni correction.

‡Represents the significant difference between the ordinary and critical group after Bonferroni correction.

§Represents the significant difference between the severe and critical group after Bonferroni correction.

AST, aspartate aminotransferase; ALT, alanine aminotransferase; GGT, gamma-glutamyl transpeptidase; ALP, alkaline phosphatase; TBiL, total bilirubin; LDH, lactate dehydrogenase.

environment could be one of the secondary injury factors in COVID-19 patients.

This study still has some limitations. Firstly, most dead critical cases are lack autopsy reports, and the pathological changes in the liver cannot therefore be observed in detail. Secondly, it cannot be ruled out that some changes in liver function in critical cases could also be secondary to the dysfunction of other organs or sepsis, etc. Finally, for most of the variables, data were available only for some patients and not all, and the changes in most of the variables, though different across groups, were not very remarkable.

In summary, we observed that COVID-19 has caused changes in several liver biomarkers, which may be closely related to the severity of the disease. In this study, critical cases had a worse prognosis, with higher fatality and worse liver function, for which the changes of liver biomarkers should be closely monitored, especially LDH, ALP, GGT, TBiL, prealbumin, and albumin. This will help evaluate and predict disease prognosis and disease severity in COVID-19. In addition, hepatotoxic drugs should be used with great caution during clinical treatment, and liver protection drugs could be applied appropriately when necessary.

DATA AVAILABILITY STATEMENT

The original contributions generated for the study are included in the article/**Supplementary Material**, further inquiries can be directed to the corresponding author/s.

ETHICS STATEMENT

The studies involving human participants were reviewed and approved by Ethics Committee of the Huangshi Hospital of Traditional Chinese Medicine in Hubei Province (HSZYPJ-2020-021-01). Written informed consent for participation was not required for this study in accordance with the national legislation and the institutional requirements.

AUTHOR CONTRIBUTIONS

CZ conceived the study and assumed responsibility for the paper as a whole. HF and CZ provided statistical advice and analyzed the data. JC, AT, YL, and HY drafted the manuscript. ZJ, YY, LR, PH, MY, NC, and JL collected the data. All of the authors contributed substantially to its revision, read, and approved the final manuscript.

FUNDING

This work was supported by the National Natural Science Foundation of China (Grant Nos. 81770591 and 81800778) and the Key Medical Talents Fund of Jiangsu Province (Grant No. ZDRCA2016007).

SUPPLEMENTARY MATERIAL

The Supplementary Material for this article can be found online at: https://www.frontiersin.org/articles/10.3389/fmed.2020.584888/full#supplementary-material

REFERENCES

1. Huang C, Wang Y, Li X, Ren L, Zhao J, Hu Y, et al. Clinical features of patients infected with 2019 novel coronavirus in Wuhan, China. *Lancet*. (2020) 395:497–506. doi: 10.1016/S0140-6736(20)30183-5
2. Li Q, Guan X, Wu P, Wang X, Zhou L, Tong Y, et al. Early transmission dynamics in Wuhan, China, of novel coronavirus-infected pneumonia. *N Engl J Med*. (2020) 382:1199–207. doi: 10.1056/NEJMoa2001316
3. Chan JF, Yuan S, Kok KH, To KK, Chu H, Yang J, et al. A familial cluster of pneumonia associated with the 2019 novel coronavirus indicating person-to-person transmission: a study of a family cluster. *Lancet*. (2020) 395:514–23. doi: 10.1016/S0140-6736(20)30154-9
4. Zhu N, Zhang D, Wang W, Li X, Yang B, Song J, et al. A novel coronavirus from patients with pneumonia in China, 2019. *N Engl J Med*. (2020) 382:727–33. doi: 10.1056/NEJMoa2001017
5. Wang D, Hu B, Hu C, Zhu F, Liu X, Zhang J, et al. Clinical characteristics of 138 hospitalized patients with 2019 novel coronavirus-infected pneumonia in Wuhan, China. *JAMA*. (2020) 323:1061–9. doi: 10.1001/jama.2020.1585
6. Chen T, Wu D, Chen H, Yan W, Yang D, Chen G, et al. Clinical characteristics of 113 deceased patients with coronavirus disease 2019: retrospective study. *BMJ*. (2020) 368:m1091. doi: 10.1136/bmj.m1091
7. Chen N, Zhou M, Dong X, Qu J, Gong F, Han Y, et al. Epidemiological and clinical characteristics of 99 cases of 2019 novel coronavirus pneumonia in Wuhan, China: a descriptive study. *Lancet*. (2020) 395:507–13. doi: 10.1016/S0140-6736(20)30211-7
8. Zhao X, Zhang B, Li P, Ma C, Gu J, Hou P, et al. Incidence, clinical characteristics and prognostic factor of patients with COVID-19: a systematic review and meta-analysis. *medRxiv*. (2020). doi: 10.1101/2020.03.17.20037572v1
9. Zhao D, Yao F, Wang L, Zheng L, Gao Y, Ye J, et al. A comparative study on the clinical features of COVID-19 pneumonia to other pneumonias. *Clin Infect Dis*. (2020) 71:ciaa247. doi: 10.1093/cid/ciaa247
10. National Health Commission and State Administration of Traditional Chinese Medicine. *Diagnosis and Treatment Protocol for Novel Coronavirus Pneumonia (Trial Version 7)*. (2020). Available online at: https://www.who.int/docs/default-source/wpro---documents/countries/china/covid-19-briefing-nhc/1-clinical-protocols-for-the-diagnosis-and-treatment-of-covid-19-v7.pdf?sfvrsn=c6cbfba4_2 (accessed 3 March, 2020).
11. World Health Organization. *Coronavirus disease 2019 (COVID-19): Situation Report—88*. (2020). Available online at: https://www.who.int/docs/default-source/coronaviruse/situation-reports/20200417-sitrep-88-covid-191b6cccd94f8b4f219377bff55719a6ed.pdf?sfvrsn=ebe78315_6 (accessed 17 April 2020).
12. Qi X, Liu C, Jiang Z, Gu Y, Zhang G, Shao C, et al. Multicenter analysis of clinical characteristics and outcome of COVID-19 patients with liver injury. *J Hepatol*. (2020) 73:455–8. doi: 10.1016/j.jhep.2020.04.010
13. Xu Z, Shi L, Wang Y, Zhang J, Huang L, Zhang C, et al.Pathological findings of COVID-19 associated with acute respiratory distress syndrome. *Lancet Respir Med*. (2020) 8:420–2. doi: 10.1016/S2213-2600(20)30076-X
14. Xie H, Zhao J, Lian N, Lin S, Xie Q, Zhuo H. Clinical characteristics of non-ICU hospitalized patients with coronavirus disease 2019 and liver injury: a retrospective study. *Liver Int*. (2020) 40:1321–6. doi: 10.1111/liv.14449
15. Bousquet G, Falgarone G, Deutsch D, Derolez S, Lopez-Sublet M, Goudot FX, et al. ADL-dependency, D-Dimers, LDH and absence of anticoagulation are independently associated with one-month mortality in older inpatients with Covid-19. *Aging*. (2020) 12:11306–13. doi: 10.18632/aging.103583
16. Deng X, Liu B, Li J, Zhang J, Zhao Y, Xu K. Blood biochemical characteristics of patients with coronavirus disease 2019 (COVID-19): a systemic review and meta-analysis. *Clin Chem Lab Med*. (2020) 58:1172–81. doi: 10.1515/cclm-2020-0338
17. Lei F, Liu YM, Zhou F, Qin JJ, Zhang P, Zhu L, et al. Longitudinal association between markers of liver injury and mortality in COVID-19 in China. *Hepatology*. (2020) 72:389–98. doi: 10.1002/hep.31301
18. Fan Z, Chen L, Li J, Cheng X, Yang J, Tian C, et al. Clinical features of COVID-19-related liver functional abnormality. *Clin Gastroenterol Hepatol*. (2020) 18:1561–6. doi: 10.1016/j.cgh.2020.04.002
19. Hoffmann M, Kleine-Weber H, Krüger N, Müller M, Drosten C, Pöhlmann S. The novel coronavirus 2019 (2019-nCoV) uses the SARS-coronavirus receptor ACE2 and the cellular protease TMPRSS2 for entry into target cells. *bioRxiv*. (2020). doi: 10.1101/2020.01.31.929042
20. Zhou P, Yang XL, Wang XG, Hu B, Zhang L, Zhang W, et al. A pneumonia outbreak associated with a new coronavirus of probable bat origin. *Nature*. (2020) 579:270–3. doi: 10.1038/s41586-020-2012-7
21. Hoffmann M, Kleine-Weber H, Schroeder S, Krüger N, Herrler T, Erichsen S, et al. SARS-CoV-2 cell entry depends on ACE2 and TMPRSS2 and is blocked by a clinically proven protease inhibitor. *Cell*. (2020) 181:271–80.e8. doi: 10.1016/j.cell.2020.02.052
22. Heurich A, Hofmann-Winkler H, Gierer S, Liepold T, Jahn O, Pöhlmann S. TMPRSS2 and ADAM17 cleave ACE2 differentially and only proteolysis by TMPRSS2 augments entry driven by the severe acute respiratory syndrome coronavirus spike protein. *J Virol*. (2014) 88:1293–307. doi: 10.1128/JVI.02202-13
23. Aizarani N, Saviano A, Sagar, Mailly L, Durand S, Herman JS, et al. A human liver cell atlas reveals heterogeneity and epithelial progenitors. *Nature*. (2019) 572:199–204. doi: 10.1038/s41586-019-1373-2
24. Wen Seow JJ, Pai R, Mishra A, Shepherdson E, Hon Lim TK, Goh BKP, et al. scRNA-seq reveals ACE2 and TMPRSS2 expression in TROP^{2+} liver progenitor cells: implications in COVID-19 associated liver dysfunction. *bioRxiv*. (2020). doi: 10.1101/2020.03.23.002832
25. Chai X, Hu L, Zhang Y, Han W, Lu Z, Ke W, et al. Specific ACE2 expression in cholangiocytes may cause liver damage after 2019-nCoV infection. *bioRxiv*. (2020). doi: 10.1101/2020.02.03.931766

26. Sungnak W, Huang N, Bécavin C, Berg M, Queen R, Litvinukova M, et al. SARS-CoV-2 entry factors are highly expressed in nasal epithelial cells together with innate immune genes. *Nat Med*. (2020) 26:681–7. doi: 10.1038/s41591-020-0868-6
27. Uthamalingam S, Kandala J, Daley M, Patvardhan E, Capodilupo R, Moore SA, et al. Serum albumin and mortality in acutely decompensated heart failure. *Am Heart J*. (2010) 160:1149–55. doi: 10.1016/j.ahj.2010.09.004
28. Babu MS, Kaul S, Dadheech S, Rajeshwar K, Jyothy A, Munshi A. Serum albumin levels in ischemic stroke and its subtypes: correlation with clinical outcome. *Nutrition*. (2013) 29:872–5. doi: 10.1016/j.nut.2012.12.015
29. Gao C, Zhang B, Zhang W, Pu S, Yin J, Gao Q. Serum prealbumin (transthyretin) predict good outcome in young patients with cerebral infarction. *Clin Exp Med*. (2011) 11:49–54. doi: 10.1007/s10238-010-0103-8
30. Lei P, Zhang L, Han P, Zheng C, Tong Q, Shang H, et al. Liver injury in patients with COVID-19: clinical profiles, CT findings, the correlation of the severity with liver injury. *Hepatol Int*. (2020) 14:733–42. doi: 10.1007/s12072-020-10087-1
31. Yang L, Wang W, Wang X, Zhao J, Xiao L, Gui W, et al. Creg in hepatocytes ameliorates liver ischemia/reperfusion injury in a TAK1-dependent manner in mice. *Hepatology*. (2019) 69:294–313. doi: 10.1002/hep.30203
32. Zhang XJ, Cheng X, Yan ZZ, Fang J, Wang X, Wang W, et al. An ALOX12-12-HETE-GPR31 signaling axis is a key mediator of hepatic ischemia-reperfusion injury. *Nat Med*. (2018) 24:73–83. doi: 10.1038/nm.4451

Conflict of Interest: The authors declare that the research was conducted in the absence of any commercial or financial relationships that could be construed as a potential conflict of interest.

frontiers in Medicine

ORIGINAL RESEARCH
published: 04 February 2021
doi: 10.3389/fmed.2020.589040

Hepatocyte Endoplasmic Reticulum Stress Inhibits Hepatitis B Virus Secretion and Delays Intracellular Hepatitis B Virus Clearance After Entecavir Treatment

*Huan Chen†, Maoyuan Mu†, Qichuan Liu, Han Hu, Caiyun Tian, Guoyuan Zhang, Ying Li, Fangwan Yang and Shide Lin**

Department of Infectious Diseases, Affiliated Hospital of Zunyi Medical University, Zunyi, China

Background: The aim of this study was to explore the effects of endoplasmic reticulum (ER) stress on hepatitis B virus (HBV) replication and the antiviral effect of entecavir (ETV).

Methods: Thapsigargin (TG) and stearic acid (SA) were used to induce ER stress in HepG2.2.15 cells and HepAD38 cells that contained an integrated HBV genome, while ETV was used to inhibit HBV replication. The expression levels of glucose-regulated protein 78 (GRP78) and phosphorylated eukaryotic translation initiation factor 2 subunit alpha (p-eIF2α) were measured by western blotting. Intracellular HBV DNA was determined by qPCR; HBsAg by western blotting; HBV RNA by real-time RT-qPCR; HBsAg and HBeAg in supernatants by enzyme-linked immunosorbent assay (ELISA); and HBV DNA in supernatants by qPCR.

Results: TG and SA induced ER stress in HepG2.2.15 cells and HepAD38 cells from 12 to 48 h post treatment. However, 4-phenylbutyric acid (PBA) partly alleviated the TG-induced ER stress. Moreover, TG inhibited HBsAg, HBeAg, and HBV DNA secretion from 12 to 48 h, while different concentrations of SA inhibited HBsAg and HBV DNA secretion at 48 h. TG promoted intracellular HBV DNA and HBsAg accumulation and the transcription of the HBV 3.5-kb mRNA and S mRNA. PBA treatment restored the secretion of HBsAg and HBV DNA. Finally, ER stress accelerated extracellular HBV DNA clearance but delayed intracellular HBV DNA clearance after ETV treatment.

Conclusions: Hepatocyte ER stress promoted intracellular HBV DNA and HBsAg accumulation by inhibiting their secretion. Our study also suggested that hepatocyte ER stress delayed intracellular HBV DNA clearance after ETV treatment.

Keywords: endoplasmic reticulum stress, HepG2215, thapsigargin, stearic acid, HBsAg, HBV DNA

OPEN ACCESS

Edited by:
Chao Yan,
Xuzhou Medical University, China

Reviewed by:
Jianguo Wu,
Wuhan University, China
Jiang Zheng,
Xi'an Branch of Chinese Academy of Sciences, China

***Correspondence:**
Shide Lin
linshide6@hotmail.com

†These authors have contributed equally to this work

Specialty section:
This article was submitted to Gastroenterology, a section of the journal Frontiers in Medicine

Received: *30 July 2020*
Accepted: *21 December 2020*
Published: *04 February 2021*

Citation:
Chen H, Mu M, Liu Q, Hu H, Tian C, Zhang G, Li Y, Yang F and Lin S (2021) Hepatocyte Endoplasmic Reticulum Stress Inhibits Hepatitis B Virus Secretion and Delays Intracellular Hepatitis B Virus Clearance After Entecavir Treatment. Front. Med. 7:589040. doi: 10.3389/fmed.2020.589040

INTRODUCTION

Chronic hepatitis B virus (HBV) infection constitutes a global health concern. More than 240 million people are chronically infected with HBV, which puts them at great risk of developing end-stage liver diseases such as liver failure, cirrhosis, and liver cancer (1). The progression of patients with chronic HBV infection depends on a complex interaction between the host and the virus (2).

The HBV genome contains four partially overlapping open reading frames, named C, S, P, and X, from which 3.5-, 2.4-, 2.1-, and 0.7 kb-long RNAs, respectively, are transcribed. Translation of the 2.4- and 0.7-kb fragments produces the large envelope protein and the HBx protein, respectively. The 2.1-kb mRNA yields both the middle and small envelope proteins. The 3.5-kb long RNA, also called pregenomic RNA, is the only HBV transcript required for genome replication (1, 3).

The endoplasmic reticulum (ER) is an important cellular organelle and plays a major role in protein synthesis, folding, modification, and transport, as well as in lipid synthesis and the maintenance of calcium homeostasis. When ER homeostasis is disturbed under physical or pathological stimuli, such as the disruption of calcium homeostasis, the accumulation of unfolded or misfolded proteins, glucose starvation, and hypoxia, the unfolded protein response (UPR) is activated (4). ER stress can initiate the UPR *via* the binding of glucose-regulated protein 78 (GRP78) to unfolded or misfolded proteins and by activating three different sensors: protein kinase R-like endoplasmic reticulum kinase (PERK), inositol-requiring enzyme 1 (IRE1), and activating transcription factor 6 (ATF6).

ER stress is a common pathological phenomenon in patients with liver disease, including viral hepatitis, fatty liver disease, alcoholic liver disease, drug-induced hepatitis, and ischemic liver damage, among others (5, 6). Viruses, fatty acids, alcohol, and drugs can all induce ER stress in hepatocytes, which can damage these cells and lead to metabolic disorders.

HBV and hepatocytes have a complex and close interaction. The activation of HBV enhancers largely depends on cellular factors expressed in hepatocytes (7, 8). Transcription factors in hepatocytes such as CCAAT/enhancer-binding protein (C/EBP), cyclic-adenosine monophosphate-responsive element-binding protein (CREB), and several other nuclear factors have been found to play an important role in HBV enhancer activation (8, 9). In the HBV life cycle, secretory proteins, such as HBsAg and HBeAg, are folded and assembled in the ER of hepatocytes (10). However, how hepatocyte ER stress affects HBV replication, and the antiviral effect of nucleos(t)ide analogs, remains unknown. In this study, we employed thapsigargin (TG) and stearic acid (SA) as ER stress inducers in HBV-transfected HepG2.2.15 cells and HepAD38 cells to investigate the impact of ER stress on HBV replication and the antiviral efficacy of entecavir (ETV).

MATERIALS AND METHODS

Reagents

RPMI 1640 was obtained from Thermo-Fisher Biochemical Products Co., Ltd (Beijing, China). TG, SA, and 4-phenylbutyric acid (PBA) were purchased from Sigma (St. Louis, MO, USA). Antibodies against GRP78, HBsAg, and beta-actin were purchased from Santa Cruz Biotechnology (Santa Cruz, CA, USA). The anti-phosphorylated eukaryotic translation initiation factor 2 alpha (p-eIF2α) antibody was purchased from Cell Signaling Technology (BioConcept, Allschwil, Switzerland). ETV was purchased from Solarbio Science & Technology Co., Ltd (Beijing, China). All other chemicals and reagents were obtained from Sigma (St. Louis, MO, USA).

Cell Culture

HepG2.2.15 cells and HepAD38 cells with a stably integrated HBV genome were obtained from the cell bank of the Type Culture Collection of the Chinese Academy of Sciences (Shanghai, China). HepG2.2.15 cells and HepAD38 cells were cultured to 80–100% confluence. To investigate the effects of TG and SA on ER stress, HepG2.2.15 and HepAD38 cells were treated with TG (1 μM) for 12, 24, 36, and 48 h or SA (50, 100, or 200 μM) for 48 h. Similarly, PBA was used to alleviate ER stress and ETV to inhibit HBV replication. Briefly, HepG2.2.15 cells were pretreated with PBA (1 mM) for 2 h and then incubated with TG for 96 h, whereas ETV (10 μM) and TG (1 μM) were simultaneously administered for the same length of time. SA (0.017 g) was dissolved in 3 ml of 0.1 mM NaOH in a water bath at 100°C. Stock solutions were prepared by adding 3 ml of 40% fatty acid-free bovine serum albumin to each tube and incubating for 30 min at 55°C. The final SA concentration was 10 mM. All control conditions included the corresponding vehicles at the appropriate concentrations.

Flow Cytometry

Apoptosis was determined using an Annexin V–fluorescein isothiocyanate (FITC)/propidium iodide (PI) apoptosis detection kit following the manufacturer's instructions. Briefly, 2×10^6 cells were harvested and washed twice with precooled PBS and resuspended in 500 μl of binding buffer. Then, 5 μl of Annexin V–FITC and 5 μl of PI was added to each sample followed by incubation at room temperature in the dark for 10 min. Analysis was performed by flow cytometry (Beckman Coulter Gallios, USA) according to the manufacturer's specifications.

Western Blotting

Cell lysates containing 40 μg of protein were resolved by sodium dodecyl sulfate–polyacrylamide gel electrophoresis (SDS–PAGE) using a 7–12.5% polyacrylamide gradient gel, and the fractioned proteins were subsequently transferred to polyvinylidene fluoride membranes (Millipore, Billerica, MA, USA). After being blocked with Tris-buffered saline containing 5% dry milk and 0.1% Tween 20 for 1 h, the membranes were blotted with the corresponding antibodies. The following primary antibodies were used: rabbit anti-human GRP78 (sc-376768, 1:10,000), anti-p-eIF-2α (3398, 1:10,000), mouse anti-human β-actin (sc-58673, 1:10,000), and anti-HBsAg (sc-53300, 1:1,000). The secondary antibodies were horseradish peroxidase-conjugated goat anti-rabbit IgG and horseradish peroxidase-conjugated goat anti-mouse IgG. The membranes were developed using a chemiluminescence detection system and then exposed to Kodak BioMax Light Film (Rochester, NY, USA). The band intensity for each protein was measured densitometrically and normalized to the level of β-actin.

Quantification of HBsAg and HBeAg

HepG2.2.15 and HepAD38 cells were cultured at a density of 1×10^4 cells per well in RPMI 1640 medium. After drug treatment, the levels of HBsAg and HBeAg in the supernatants were measured using an enzyme-linked immunosorbent assay (ELISA) (Kehua Bio-engineering Corp.) according to the manufacturer's recommendations.

DNA and RNA Isolation, Reverse Transcription, and Real-Time Polymerase Chain Reaction

Total DNA was extracted using a QIAamp DNA Mini Kit (Qiagen). Total RNA was extracted from HepG2.2.15 cells using a TaKaRa MiniBEST Universal RNA Extraction Kit (9767, Takara). The HBV DNA content was quantified by real-time qPCR using SYBR Green I. The primers used to amplify the HBV DNA were as follows: 5′-GTTGCCCGTTTGTCCTCTAATTC-3′ and 5′-GGAGGGATACATAGAGGTTCCTT-3′. Quantitative PCR was performed at 95°C for 30 s, 40 cycles of 95°C for 5 s, and 60°C for 34 s, followed by melting curve analysis, according to the instrument documentation. The RNA samples were first reverse transcribed into cDNA using the PrimeScript RT Reagent Kit (DRR037A, Takara). The products were then subjected to qPCR using the following primers: HBV-S mRNA, 5′-CTAGGACCCCTGCTCGTG-3′ and 5′-GATGAGGCATAGCAGCAG-3′; HBV 3.5-kb mRNA, 5′-CTCAATCTCGGGAATCTCAATGT-3′ and 5′-TGGATAAAACCTAGCAGGCATAAT-3′; and GADPH mRNA, 5′-CGACCACTTTGTCAAGCTCA-3′ and 5′-ACAGCCTGGATAGCAACG-3′. The relative HBV DNA and mRNA levels were determined using the comparative ($2^{-\Delta\Delta CT}$) method, as previously described (11).

Statistical Analysis

The results were expressed as means ± standard deviation for "n" independent observations. One-way ANOVA was used to determine the statistical differences between the mean values for the groups. The level of significance was set at $P < 0.05$.

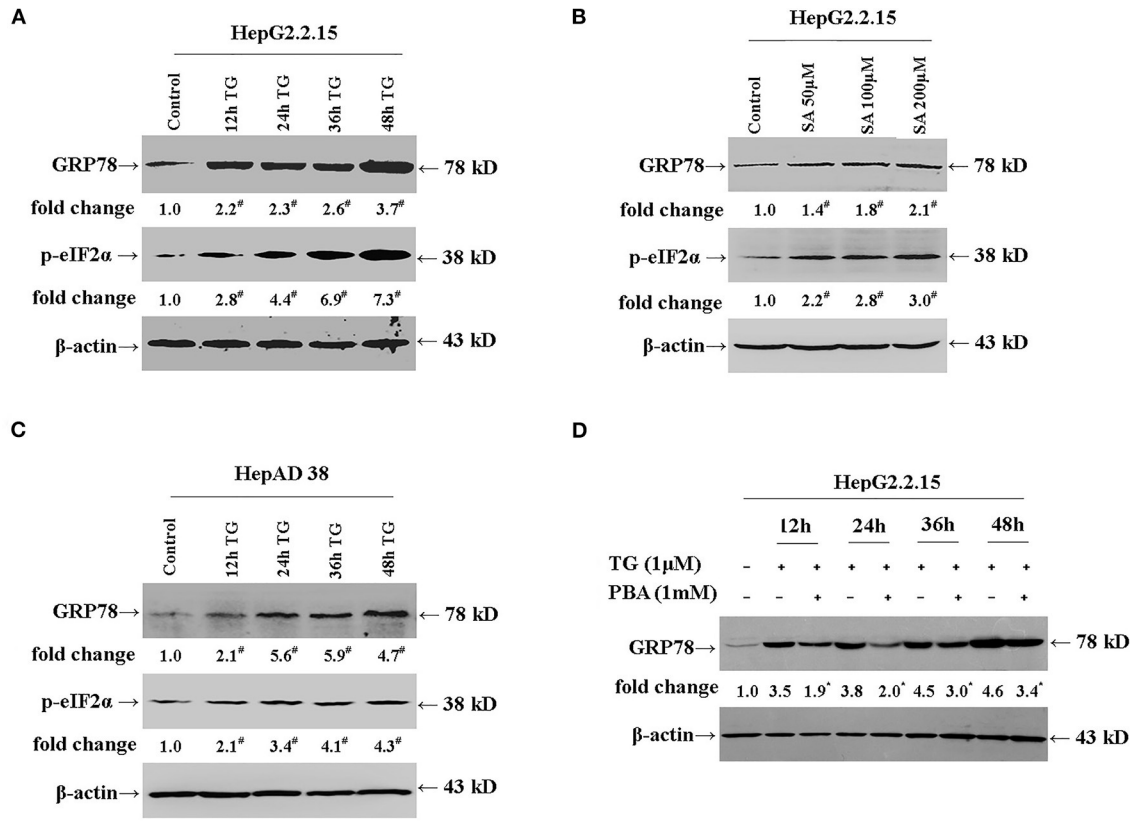

FIGURE 1 | TG and SA induced ER stress in HepG2.2.15 and HepAD38 cells, which was alleviated by PBA treatment. HepG2.2.15 and HepAD38 cells were treated with 1 μM of TG for 12, 24, 36, and 48 h or 50, 100, and 200 μM of SA for 48 h. The expression of GRP78 and p-eIF2α was assessed by western blotting. Representative blots from three independent experiments are shown. The results of the densitometric analysis are presented as fold-changes compared with control or TG. **(A)** GRP78 and p-eIF2α expression in HepG2.2.15 cells after TG treatment. #$P < 0.05$ vs. control. **(B)** GRP78 and p-eIF2α expression in HepG2.2.15 cells following SA treatment. #$P < 0.05$ vs. control. **(C)** GRP78 and p-eIF2α expression in HepAD38 cells after TG treatment. #$P < 0.05$ vs. control. **(D)** GRP78 expression in HepG2.2.15 cells after TG or PBA (1 mM) + TG treatment. *$P < 0.05$ vs. the TG group. ER, endoplasmic reticulum; GRP78, glucose-regulated protein 78; PBA, 4-phenylbutyric acid; p-eIF2α, phospho-eukaryotic translation initiation factor 2 alpha; SA, stearic acid; TG, thapsigargin.

RESULTS

Thapsigargin and Stearic Acid Treatment Induced Endoplasmic Reticulum Stress in HepG2.2.15 and HepAD38 Cells, Which Was Alleviated by Exposure to 4-Phenylbutyric Acid

We first investigated whether TG and SA induced ER stress in HepG2.2.15 and HepAD38 cells. As shown in **Figures 1A,B**, TG significantly induced GRP78 and p-eIF2α expression from 12 to 48 h post treatment at the 1-μM concentration in HepG2.2.15 cells. Similarly, SA markedly induced GRP78 and p-eIF2α expression at 48 h at the concentrations of 50, 100, and 200 μM in HepG2.2.15 cells. At 100 μM, SA significantly induced GRP78 expression from 24 to 72 h, as did TG at 24 h at the concentrations of 0.5, 1, and 2 μM in HepG2.2.15 cells (**Supplementary Figures 1, 2**). Furthermore, 1 μM of TG significantly induced GRP78 and p-eIF2α expression from 12 to 48 h post treatment in HepAD38 cells (**Figure 1C**). Our results demonstrated that both TG and SA could induce ER stress and activate the UPR in HepG2.2.15 cells and HepAD38 cells.

Next, we investigated whether PBA could alleviate the ER stress induced by TG (**Figure 1D**). We found that at the 1-mM concentration, PBA could significantly inhibit the TG-mediated induction of GRP78 expression, demonstrating that PBA could alleviate TG-induced ER stress.

We next evaluated the effect of TG and SA on the apoptosis and viability of HepG2.2.15 cells. At the concentration of 1 μM, TG treatment did not lead to a marked increase in the rate of apoptosis from 12 to 48 h post treatment, and a similar effect was observed for SA treatment (50 and 100 μM) at 48 h (**Supplementary Figure 3**).

Thapsigargin and Stearic Acid Inhibited the Secretion of HBsAg, HBeAg, and Hepatitis B Virus DNA

We subsequently explored the effect of TG (1 μM) and SA (50, 100, and 200 μM) on the secretion of HBsAg, HBeAg, and HBV DNA in HepG2.2.15 supernatants. As shown in **Figures 2**, **3**, exposure to TG significantly inhibited the secretion of HBsAg, HBeAg, and HBV DNA from 12 to 48 h post treatment. Similarly, treatment with 50, 100, and 200 μM of SA also greatly suppressed the secretion of HBsAg and HBV DNA at 48 h. We further found that TG significantly inhibited the secretion of HBsAg from 12 to 48 h post treatment in HepAD38 cells (**Figure 2C**). Western blotting results confirmed that TG significantly inhibited the secretion of HBsAg from 12 to 48 h. However, SA treatment did not significantly affect the secretion of HBeAg, at the concentration of either 50 or 100 μM (**Figure 3**). At 100 μM, SA also significantly inhibited the

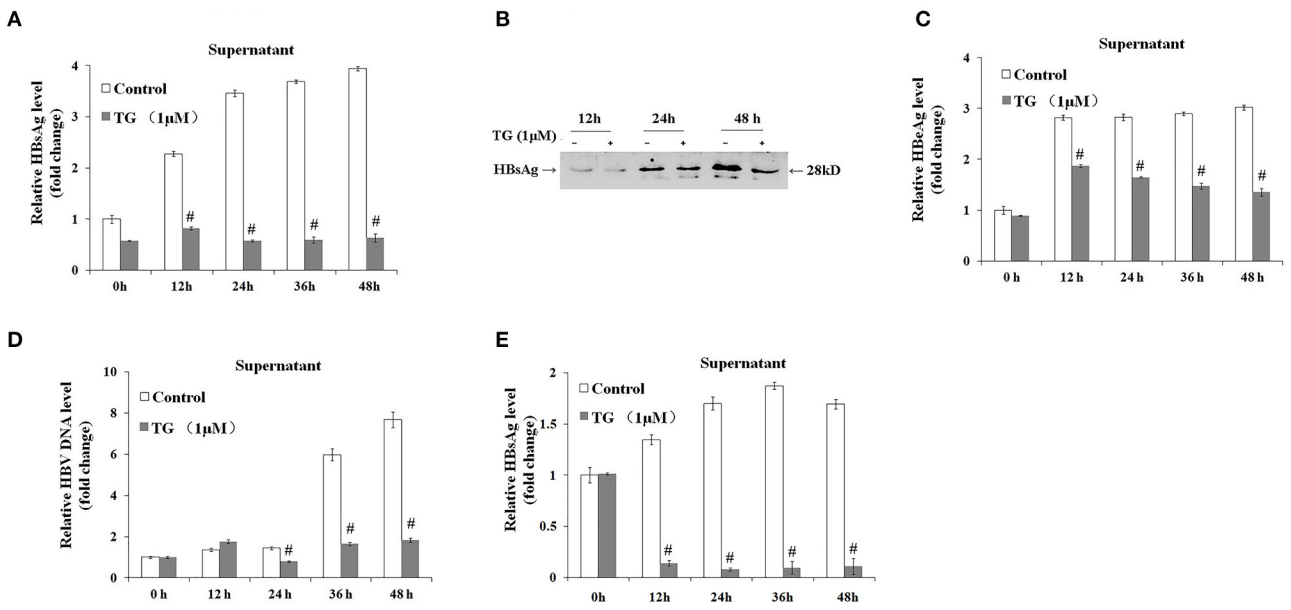

FIGURE 2 | Thapsigargin (TG) inhibited HBsAg, HBeAg, and hepatitis B virus (HBV) DNA secretion in HepG2.2.15 cells and HepAD38 cells. HepG2.2.15 cells and HepAD38 cells were treated with 1 μM of TG for 12, 24, 36, and 48 h. The supernatant levels of HBsAg and HBeAg were determined by ELISA or western blotting, while those of HBV DNA were determined by qPCR. **(A)** HBsAg levels as determined by ELISA in HepG2.2.15 cells. **(B)** HBsAg levels as determined by western blotting in HepG2.2.15 cells. **(C)** HBeAg levels as determined by ELISA in HepG2.2.15 cells. **(D)** HBV DNA levels as determined by qPCR in HepG2.2.15 cells. **(E)** HBsAg levels as determined by western blotting in HepAD38 cells. The results are presented as fold-changes compared with the control. Histograms represent the means ± *SD* of three independent experiments. $^{\#}P < 0.05$ vs. the control.

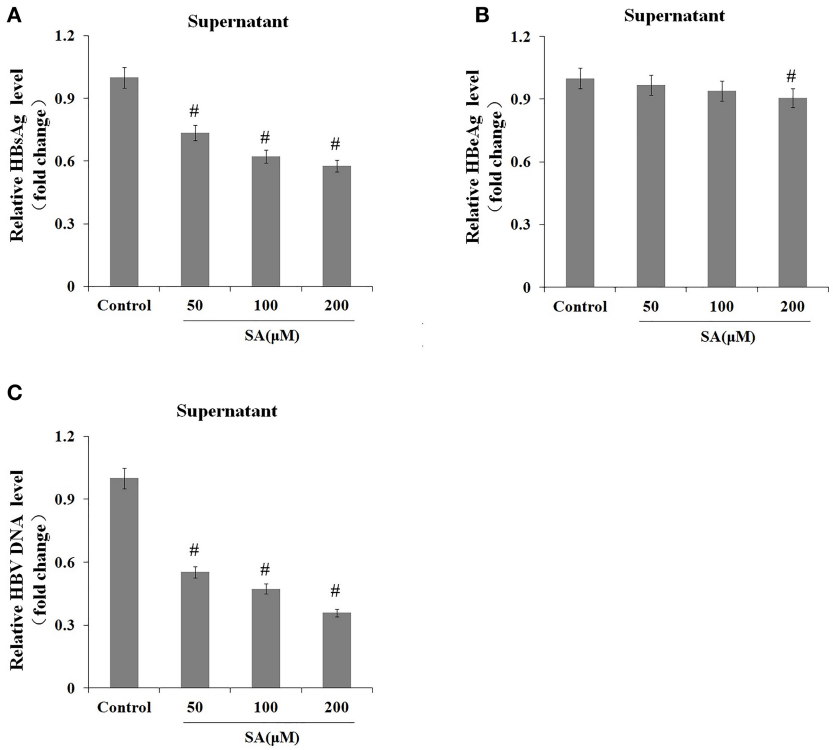

FIGURE 3 | Stearic acid (SA) inhibited the secretion of HBsAg and hepatitis B virus (HBV) DNA in HepG2.2.15 cells. HepG2.2.15 cells were treated with 50, 100, and 200 μM of SA for 48 h. The supernatant levels of HBsAg and HBeAg were determined by ELISA, while those of HBV DNA were determined by qPCR. **(A)** HBsAg levels as determined by ELISA. **(B)** HBeAg levels as determined by ELISA. **(C)** HBV DNA levels as determined by qPCR. The results are presented as fold-changes compared with the control. Histograms represent the means ± *SD* of three independent experiments. $^{\#}P < 0.05$ vs. the control.

secretion of HBsAg and HBV DNA from 24 to 72 h, as did TG at 24 h at the concentrations of 0.5, 1, and 2 μM in HepG2.2.15 cells (**Supplementary Figures 4**–7).

The Effects of Thapsigargin on the Transcription of Hepatitis B Virus DNA and Intracellular HBsAg and Hepatitis B Virus DNA Levels

We further explored the effects of TG on the expression levels of the 3.5-kb mRNA and S mRNA as well as on the intracellular levels of HBsAg and HBV DNA. As shown in **Figure 4**, TG significantly upregulated the expression of the HBV 3.5-kb mRNA fragment and S mRNA and increased the intracellular levels of HBsAg and HBV DNA. Western blotting confirmed that the intracellular level of HBsAg was significantly increased by TG from 12 to 48 h post treatment.

Thapsigargin Inhibited the Secretion of HBsAg and Hepatitis B Virus DNA *via* the Induction of Endoplasmic Reticulum Stress

We then investigated whether the inhibitory effects of TG on HBsAg and HBV DNA secretion were exerted through the induction of ER stress. As shown in **Figure 5**, the secretion of HBsAg and HBV DNA was significantly restored by PBA at 36 h post treatment. Similarly, HBeAg levels in the supernatant were also partially restored. These results strongly suggested that TG inhibited HBsAg, HBeAg, and HBV DNA secretion through the induction of ER stress.

Thapsigargin Delayed Intracellular Hepatitis B Virus Clearance After Entecavir Treatment

Finally, we assessed whether the TG-induced ER stress impaired the antiviral effect of ETV. After 96 h of ETV treatment, HBV replication was significantly inhibited (**Figure 6**). TG treatment significantly delayed the intracellular clearance of HBV DNA, HBsAg, and HBV RNA; in contrast, TG treatment significantly accelerated the extracellular clearance of HBV DNA, HBsAg, and HBeAg.

DISCUSSION

HBV assembly and HBsAg synthesis and secretion are highly dependent on ER function (10, 12). Each of the HBV envelope proteins is cotranslationally inserted into the ER membrane. The middle and small proteins have single transmembrane domains,

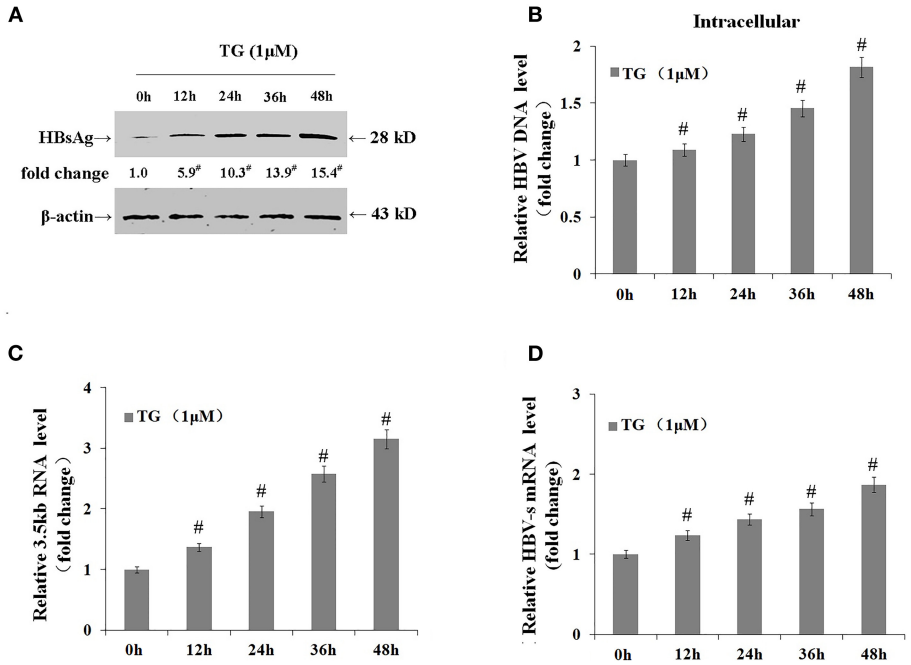

FIGURE 4 | Thapsigargin (TG) promoted hepatitis B virus (HBV) DNA transcription and the accumulation of HBV DNA and HBsAg in HepG2.2.15 cells. HepG2.2.15 cells were treated with 1 μM of TG for 12, 24, 36, and 48 h. Intracellular HBsAg, HBV DNA, and HBV RNA levels were determined by western blotting, qPCR, and real-time RT-qPCR, respectively. The results are presented as fold-changes compared with the control. Histograms represent the means ± *SD* of three independent experiments. $^{\#}P < 0.05$ vs. control. **(A)** HBsAg levels as determined by western blotting. Representative blots from three independent experiments are shown. **(B)** HBV DNA levels as determined by qPCR. **(C)** HBV 3.5-kb mRNA levels as determined by RT-qPCR. **(D)** HBV S mRNA levels as determined by RT-qPCR.

whereas the large protein has a unique dual transmembrane conformation topology in the ER. The large protein is modified by myristoylation, but this is dispensable for virion formation (13–15). Host chaperones, such as heat shock protein 70 (HSP70) and GRP78/Bip, play an important role in the correct folding of envelope proteins and the maintenance of the dual topology of the large protein in the ER (16, 17). The synthesis of HBeAg is also closely associated with the ER (18, 19). As HBV replication and antigen secretion *in vivo* are both dependent on a complex interaction between the host and the virus, such as the activation of immune cells and the regulation of cytokine levels, it is difficult to identify the direct effect of ER stress on HBV replication *in vivo*. In this study, we used TG and SA to induce ER stress in HepG2.2.15 cells containing an integrated HBV genome and HepAD38 cells, and the results obtained mostly reflect the direct effect of ER stress on HBV replication.

In this study, we found for the first time that hepatocyte ER stress greatly suppressed HBsAg and HBV DNA secretion and increased the intracellular levels of HBsAg and HBV DNA. How ER stress affects HBV replication remains unknown. Several studies have reported that the accumulation of mutated HBsAg in hepatocytes results in ER stress and the activation of the UPR both *in vitro* and *in vivo* (20–22). However, the results regarding the effect of hepatocyte ER stress on HBV replication have been contradictory, and several different mechanisms have been suggested to be involved. Xu et al. reported that hepatocyte ER stress induced by the retention of the large protein of the HBV can activate the S promoter; increase the synthesis of the middle and small proteins to restore the proportions of the large, middle, and small proteins in cells; and maintain the assembly of HBV particles (23). Additionally, the authors also found that the transcriptional activation of the S promoter was cell type-restricted and was mediated through the IRE1α/X-box binding protein 1 (XBP1) pathway. A different study demonstrated that, in HBV-infected hepatoma cells, the ER stress-associated degradation pathway was activated, leading to the degradation of the HBV envelope protein and the consequent inhibition of HBV replication (24). Cisplatin-induced ER stress in hepatocytes has also been found to evoke HBV reactivation *via* the peroxisome proliferator-activated receptor gamma coactivator 1 alpha (PPARGC1A) signaling pathway (25). GRP78 is a master ER stress regulator, the expression of which is significantly upregulated during ER stress. Several studies have demonstrated that GRP78 expression can inhibit HBV DNA replication (26–28). We do not know the reasons for these differing results. In this study, we used TG and SA to induce ER stress, and we found that both inhibited HBV DNA and HBsAg secretion, while TG also promoted intracellular HBV DNA and HBsAg accumulation. PBA is a low-molecular-weight chemical chaperone that effectively prevents misfolded protein aggregation and alleviates ER stress. After PBA administration, HBV DNA and HBsAg secretion were partly

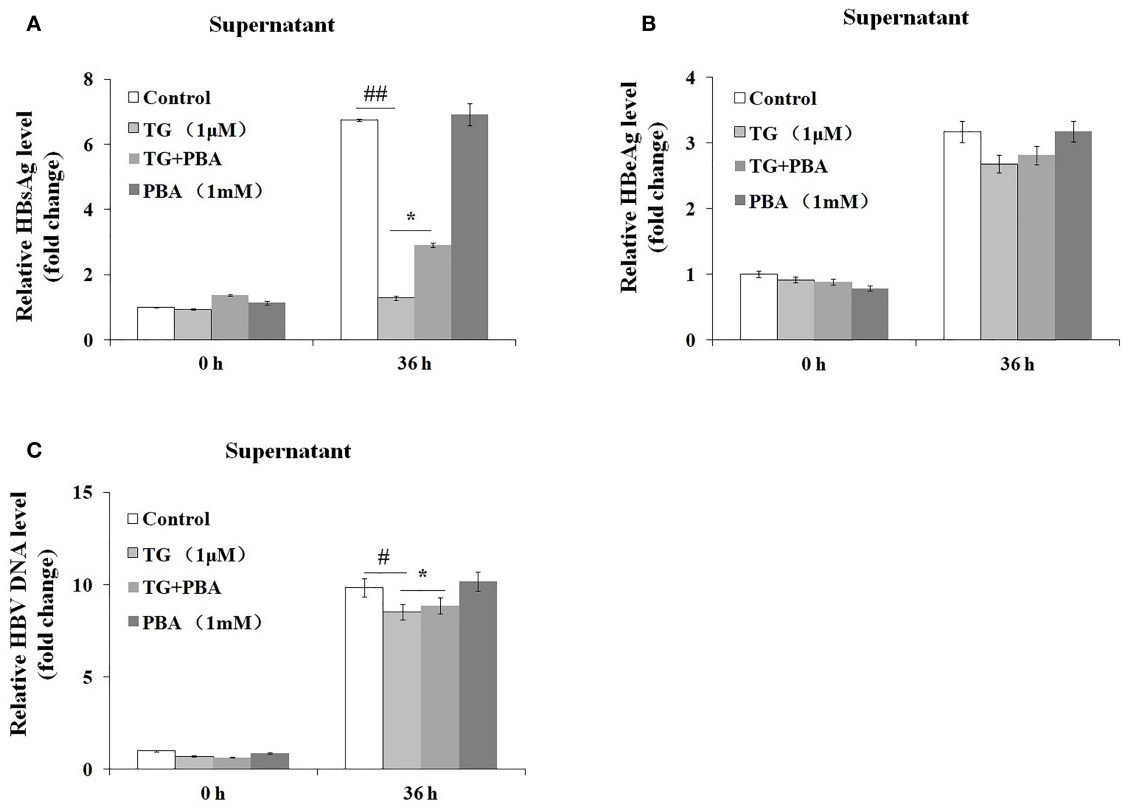

FIGURE 5 | 4-Phenylbutyric acid (PBA) pretreatment restored the secretion of hepatitis B virus (HBV) DNA, HBsAg, and HBeAg in HepG2.2.15 cells. HepG2.2.15 cells were treated with 1 μM of thapsigargin (TG) with or without 1 mM of PBA for 12, 24, 36, and 48 h. The supernatant levels of HBsAg and HBeAg were determined by ELISA, while those of HBV DNA were determined by qPCR. The results are presented as fold-changes compared with the control. Histograms represent the means ± *SD* of three independent experiments. $^{\#}P < 0.05$ vs. the control $^{\#\#}P < 0.01$, $^{\#}P < 0.05$ vs. the control; $^{*}P < 0.05$. **(A)** HBsAg and **(B)** HBeAg levels as determined by ELISA. **(C)** HBV DNA levels as determined by qPCR.

restored. These results demonstrated that the inhibitory effects of TG and SA on HBV DNA and HBsAg secretion were at least partly dependent on the induction of ER stress.

The ER is the largest Ca^{2+} store in hepatocytes. Ca^{2+} release from the ER is a common mechanism underlying the occurrence and progression of ER stress following both physical and pathological cues. TG induces ER stress by irreversibly inhibiting sarcoplasmic/ER Ca^{2+}-ATPase, which blocks the reabsorption of calcium from the cytosol to the ER and leads to an increase in the cytosolic Ca^{2+} concentration (29). Cytosolic Ca^{2+} can stimulate the Pyk2/Src kinase signal transduction pathway, thereby activating HBV reverse transcription and DNA replication (30). However, one study reported that HBV DNA replication was inhibited following the blocking of the ER Ca^{2+}-ATPase (12). How SA, a saturated fatty acid, induces ER stress remains unclear. High saturated fatty acid concentrations have been found to impair ER structure and function (31). In our study, both TG and SA inhibited the secretion of HBV DNA and HBsAg. However, these effects were partially attenuated following PBA-mediated alleviation of ER stress. These results further supported that the inhibition of HBV DNA and HBsAg secretion by TG and SA was partly mediated *via* the induction of ER stress. However, whether TG promoted the transcription of both the HBV 3.5-kb mRNA fragment and S mRNA *via* an increase in the cytosolic Ca^{2+} concentration warrants further study.

Another major finding of this study was that, although ETV displayed high antiviral efficacy in the presence of TG, treatment with TG accelerated extracellular HBV DNA, HBsAg, and HBeAg clearance but delayed the clearance of intracellular HBV DNA, HBsAg, and HBV mRNA. These results suggested that hepatocyte ER stress delayed intracellular HBV clearance. The intracellular HBV DNA and HBsAg accumulation induced by TG exposure may partly explain this result. However, the mechanism underlying the impaired HBsAg and HBV DNA secretion and the enhanced transcription of the HBV 3.5-kb mRNA and S mRNA under ER stress needs further clarification. Additionally, given that ER stress is a common pathological phenomenon in patients with liver disease, the clinical significance of the delayed intracellular HBV clearance under ER stress after ETV treatment should also be explored.

In conclusion, this study is the first to report that hepatocyte ER stress promotes intracellular HBV DNA and HBsAg accumulation by inhibiting HBV DNA and HBsAg secretion. Our

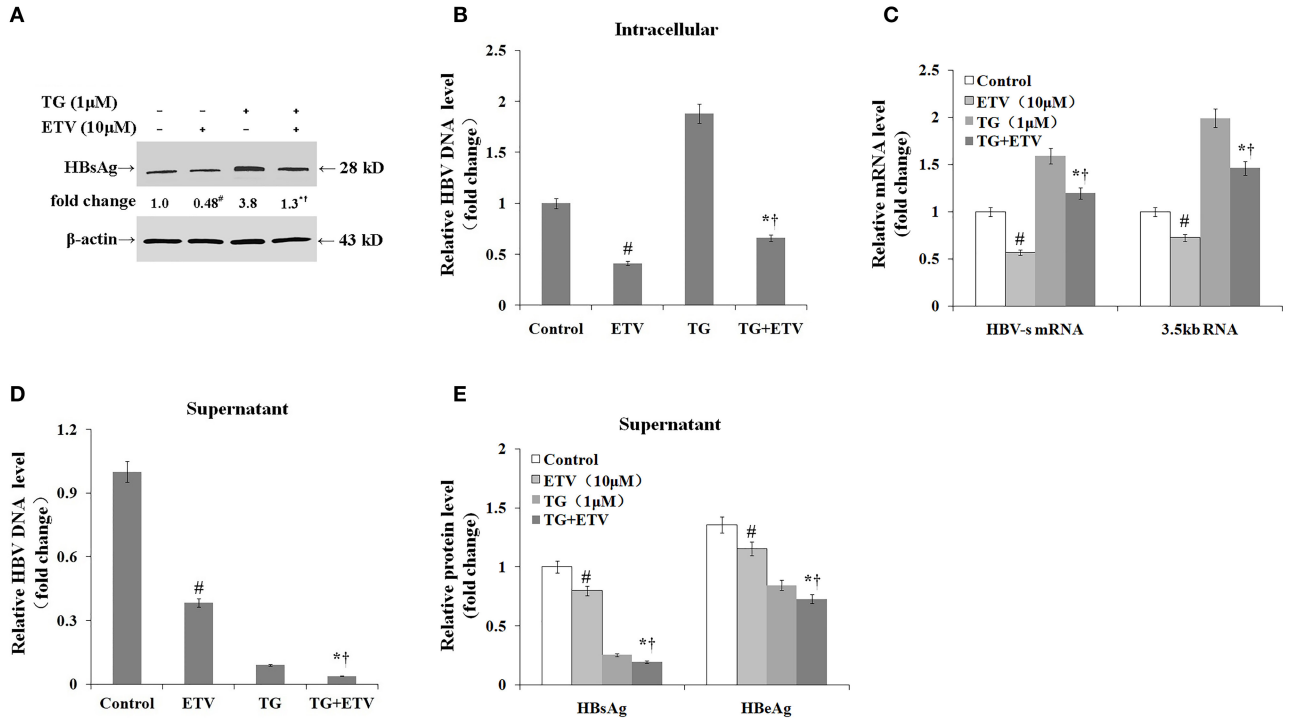

FIGURE 6 | Thapsigargin (TG) delayed intracellular hepatitis B virus (HBV) clearance after entecavir (ETV) treatment. HepG2.2.15 cells were treated with 1 μM of TG with or without 10 μM of ETV for 96 h. The supernatant levels of HBsAg and HBeAg were determined by ELISA, while those of HBV DNA were determined by qPCR. Intracellular HBsAg, HBV DNA, and HBV RNA levels were determined by western blotting, qPCR, and RT-qPCR, respectively. The results are presented as fold-changes compared with the control or TG group. Histograms represent the means ± *SD* of three independent experiments. $^{\#}P < 0.05$ vs. the control; $^{*}P < 0.05$ vs. the TG group; $^{\dagger}P < 0.05$ vs. the ETV group. **(A)** Intracellular HBsAg levels as determined by western blotting. Representative blots from three independent experiments are shown. **(B)** Intracellular HBV DNA levels as determined by qPCR. **(C)** Intracellular HBV RNA levels as determined by RT-qPCR. **(D)** HBV DNA levels in supernatants as determined by qPCR. **(E)** HBsAg and HBeAg levels in supernatants as determined by ELISA.

study also suggested that hepatocyte ER stress delays intracellular HBV DNA clearance after ETV treatment.

DATA AVAILABILITY STATEMENT

The original contributions presented in the study are included in the article/**Supplementary Materials**, further inquiries can be directed to the corresponding author/s.

AUTHOR CONTRIBUTIONS

SL designed the experiments and wrote the manuscript. HC, MM, QL, HH, and GZ performed the experiments. YL and FY revised the manuscript and analyzed the data. All authors read and approved the final manuscript.

FUNDING

This work was supported by funding from the Chinese National Natural Science Foundation Project (81460124 and 81860114). The funders had no role in the study design and analysis, decision to publish, or preparation of the manuscript. No additional external funding was received for this study.

SUPPLEMENTARY MATERIAL

The Supplementary Material for this article can be found online at: https://www.frontiersin.org/articles/10.3389/fmed.2020.589040/full#supplementary-material

REFERENCES

1. Tong S, Revill P. Overview of hepatitis B viral replication and genetic variability. *J Hepatol.* (2016) 64(1Suppl.):S4–16. doi: 10.1016/j.jhep.2016.01.027
2. European Association for the Study of the Liver. Clinical Practice Guidelines on the management of hepatitis B virus infection. *J Hepatol.* (2017) 67:370–98. doi: 10.1016/j.jhep.2017.03.021
3. Seeger C, Mason WS. Molecular biology of hepatitis B virus infection. *Virology.* (2015) 479–80:672–86. doi: 10.1016/j.virol.2015.02.031

4. Oakes SA, Papa FR. The role of endoplasmic reticulum stress in human pathology. *Annu Rev Pathol.* (2015) 10:173–94. doi: 10.1146/annurev-pathol-012513-104649
5. Wu FL, Liu WY, Van Poucke S, Braddock M, Jin WM, Xiao J, et al. Targeting endoplasmic reticulum stress in liver disease. *Expert Rev Gastroenterol Hepatol.* (2016) 10:1041–52. doi: 10.1080/17474124.2016.1179575
6. Kim SY, Kyaw YY, Cheong J. Functional interaction of endoplasmic reticulum stress and hepatitis B virus in the pathogenesis of liver diseases. *World J Gastroenterol.* (2017) 23:7657–65. doi: 10.3748/wjg.v23.i43.7657
7. Ezzikouri S, Ozawa M, Kohara M, Elmdaghri N, Benjelloun S, Tsukiyama-Kohara K. Recent insights into hepatitis B virus–host interactions. *J Med Virol.* (2014) 86:925–32. doi: 10.1002/jmv.23916
8. Kong F, You H, Kong D, Zheng K, Tang R. The interaction of hepatitis B virus with the ubiquitin proteasome system in viral replication and associated pathogenesis. *Virol J.* (2019) 16:73. doi: 10.1186/s12985-019-1183-z
9. Tang H, McLachlan A. Transcriptional regulation of hepatitis B virus by nuclear hormone receptors is a critical determinant of viral tropism. *Proc Natl Acad Sci U S A.* (2001) 98:1841–6. doi: 10.1073/pnas.98.4.1841
10. Patzer EJ, Nakamura GR, Simonsen CC, Levinson AD, Brands R. Intracellular assembly and packaging of hepatitis B surface antigen particles occur in the endoplasmic reticulum. *J Virol.* (1986) 58:884–92. doi: 10.1128/JVI.58.3.884-892.1986
11. Wu L, Wang W, Zhang X, Zhao X, Yu G. Anti-HBV activity and mechanism of marine-derived polyguluronate sulfate (PGS) *in vitro*. *Carbohydr Polym.* (2016) 143:139–48. doi: 10.1016/j.carbpol.2016.01.065
12. Xia W, Shen Y, Xie H, Zheng S. Involvement of endoplasmic reticulum in hepatitis B virus replication. *Virus Res.* (2006) 121:116–21. doi: 10.1016/j.virusres.2006.01.020
13. Bruss V, Ganem D. The role of envelope proteins in hepatitis B virus assembly. *Proc Natl Acad Sci U S A.* (1991) 88:1059–63. doi: 10.1073/pnas.88.3.1059
14. Dorobantu C, Macovei A, Lazar C, Dwek RA, Zitzmann N, Branza-Nichita N. Cholesterol depletion of hepatoma cells impairs hepatitis B Virus envelopment by altering the topology of the large envelope protein. *J Virol.* (2011) 85:13373–83. doi: 10.1128/JVI.05423-11
15. Lambert C, Prange R. Posttranslational N-glycosylation of the hepatitis B virus large envelope protein. *Virol J.* (2007) 4:45. doi: 10.1186/1743-422X-4-45
16. Cho D-Y, Yang G-H, Ryu CJ, Hong HJ. Molecular chaperone GRP78/BiP interacts with the large surface protein of hepatitis B virus *in vitro* and *in vivo*. *J Virol.* (2003) 77:2784–8. doi: 10.1128/JVI.77.4.2784-2788.2003
17. Lambert C, Prange R. Chaperone action in the posttranslational topological reorientation of the hepatitis B virus large envelope protein: implications for translocational regulation. *Proc Natl Acad Sci U S A.* (2003) 100:5199–204. doi: 10.1073/pnas.0930813100
18. Garcia PD, Ou JH, Rutter WJ, Walter P. Targeting of the hepatitis B virus precore protein to the endoplasmic reticulum membrane: after signal peptide cleavage translocation can be aborted and the product released into the cytoplasm. *J Cell Biol.* (1988) 106:1093–104. doi: 10.1083/jcb.106.4.1093
19. Wang J, Lee AS, Ou JH. Proteolytic conversion of hepatitis B virus e antigen precursor to end product occurs in a postendoplasmic reticulum compartment. *J Virol.* (1991) 65:5080–3. doi: 10.1128/JVI.65.9.5080-5083.1991
20. Xu Z, Jensen G, Yen TS. Activation of hepatitis B virus S promoter by the viral large surface protein *via* induction of stress in the endoplasmic reticulum. *J Virol.* (1997) 71:7387–92. doi: 10.1128/JVI.71.10.7387-7392.1997
21. Hsieh YH, Su IJ, Wang HC, Chang WW, Lei HY, Lai MD, et al. Pre-S mutant surface antigens in chronic hepatitis B virus infection induce oxidative stress and DNA damage. *Carcinogenesis.* (2004) 25:2023–32. doi: 10.1093/carcin/bgh207
22. Montalbano R, Honrath B, Wissniowski TT, Elxnat M, Roth S, Ocker M, et al. Exogenous hepatitis B virus envelope proteins induce endoplasmic reticulum stress: involvement of cannabinoid axis in liver cancer cells. *Oncotarget.* (2016) 7:20312–23. doi: 10.18632/oncotarget.7950
23. Huang Z-M, Tan T, Yoshida H, Mori K, Ma Y, Yen TSB. Activation of hepatitis B virus S promoter by a cell type-restricted IRE1-dependent pathway induced by endoplasmic reticulum stress. *Mol Cell Biol.* (2005) 25:7522–33. doi: 10.1128/MCB.25.17.7522-7533.2005
24. Lazar C, Macovei A, Petrescu S, Branza-Nichita N. Activation of ERAD pathway by human hepatitis B virus modulates viral and subviral particle production. *PLoS ONE.* (2012) 7:e34169. doi: 10.1371/journal.pone.0034169
25. Li X, Pan E, Zhu J, Xu L, Chen X, Li J, et al. Cisplatin enhances hepatitis B virus replication and PGC-1α expression through endoplasmic reticulum stress. *Sci Rep.* (2018) 8:3496. doi: 10.1038/s41598-018-21847-3
26. Ma Y, Yu J, Chan HL, Chen YC, Wang H, Chen Y, et al. Glucose-regulated protein 78 is an intracellular antiviral factor against hepatitis B virus. *Mol Cell Proteom.* (2009) 8:2582–94. doi: 10.1074/mcp.M900180-MCP200
27. Huang KL, Lai YK, Lin CC, Chang JM. Involvement of GRP78 in inhibition of HBV secretion by *Boehmeria nivea* extract in human HepG2 2.2.15 cells. *J Viral Hepat.* (2009) 16:367–75. doi: 10.1111/j.1365-2893.2009.01072.x
28. Shu W, Guo Z, Li L, Xiong Z, Wang Z, Yang Y, et al. Regulation of molecular chaperone GRP78 by HBV: control of viral replication and cell survival. *Mol Cell Biol.* (2019) 40:e00475–19. doi: 10.1128/MCB.00475-19
29. Wu L, Huang X, Kuang Y, Xing Z, Deng X, Luo Z. Thapsigargin induces apoptosis in adrenocortical carcinoma by activating endoplasmic reticulum stress and the JNK signaling pathway: an *in vitro* and *in vivo* study. *Drug Des Devel Ther.* (2019) 13:2787–98. doi: 10.2147/DDDT.S209947
30. Bouchard MJ, Wang LH, Schneider RJ. Calcium signaling by HBx protein in hepatitis B virus DNA replication. *Science.* (2001) 294:2376–8. doi: 10.1126/science.294.5550.2376
31. Zhu L, Jiang J, Zhai X, Baecker A, Peng H, Qian J, et al. Hepatitis B virus infection and risk of non-alcoholic fatty liver disease: a population-based cohort study. *Liver Int.* (2019) 39:70–80. doi: 10.1111/liv.13933

Conflict of Interest: The authors declare that the research was conducted in the absence of any commercial or financial relationships that could be construed as a potential conflict of interest.

frontiers in Medicine

ORIGINAL RESEARCH
published: 11 February 2021
doi: 10.3389/fmed.2020.607206

Prevalence and Characteristics of Hypoxic Hepatitis in COVID-19 Patients in the Intensive Care Unit: A First Retrospective Study

Haijun Huang[1†], Hong Li[1,2†], Shanshan Chen[1,3†], Xianlong Zhou[4,5†], Xuan Dai[1,6], Jia Wu[7], Jun Zhang[8], Lina Shao[9], Rong Yan[1], Mingshan Wang[1], Jiafeng Wang[10], Yuexing Tu[11] and Minghua Ge[10]**

[1] Department of Infectious Disease, Zhejiang Provincial People's Hospital, People's Hospital Affiliated of Hangzhou Medical College, Hangzhou, China, [2] Medical College of Qingdao University, Qingdao, China, [3] Graduate School of Clinical Medicine, Bengbu Medical College, Bengbu, China, [4] Emergency Center, Zhongnan Hospital of Wuhan University, Wuhan, China, [5] Hubei Clinical Research Center for Emergency and Resuscitation, Zhongnan Hospital of Wuhan University, Wuhan, China, [6] Hangzhou Medical College, Hangzhou, China, [7] Department of Hepatobiliary and Pancreatic Surgery and Minimally Invasive Surgery, Zhejiang Provincial People's Hospital, People's Hospital affiliated of Hangzhou Medical College, Hangzhou, China, [8] Department of Orthopaedic Surgery, Zhejiang Provincial People's Hospital, People's Hospital affiliated of Hangzhou Medical College, Hangzhou, China, [9] Department of Nephrology, Zhejiang Provincial People's Hospital, People's Hospital affiliated of Hangzhou Medical College, Hangzhou, China, [10] Department of Head, Neck and Thyroid Surgery, Zhejiang Provincial People's Hospital, People's Hospital affiliated of Hangzhou Medical College, Hangzhou, China, [11] Department of Intensive Care Unit, Zhejiang Provincial People's Hospital, People's Hospital affiliated of Hangzhou Medical College, Hangzhou, China

OPEN ACCESS

Edited by:
Jianpeng Sheng,
Nanyang Technological University, Singapore

Reviewed by:
Yiwen Yao,
Saarland University, Germany
Yimin Zhang,
Zhejiang University, China

***Correspondence:**
Minghua Ge
geminghua@hmc.edu.cn
Yuexing Tu
tuyuexing1988@163.com

[†]These authors have contributed equally to this work and share first authorship

Specialty section:
This article was submitted to Gastroenterology, a section of the journal Frontiers in Medicine

Received: 16 September 2020
Accepted: 21 December 2020
Published: 11 February 2021

Citation:
Huang H, Li H, Chen S, Zhou X, Dai X, Wu J, Zhang J, Shao L, Yan R, Wang M, Wang J, Tu Y and Ge M (2021) Prevalence and Characteristics of Hypoxic Hepatitis in COVID-19 Patients in the Intensive Care Unit: A First Retrospective Study. Front. Med. 7:607206. doi: 10.3389/fmed.2020.607206

Purpose: Coronavirus disease 2019 (COVID-19) has been associated with acute liver injury in reports worldwide. But no studies to date have described hypoxic hepatitis (HH) in patients with COVID-19. We aim to identify the prevalence of and possible mechanisms of HH in COVID-19 patients in the Intensive Care Unit (ICU).

Methods: This retrospective study was conducted on 51 patients with confirmed SARS-CoV-2 infection in the ICU at Zhongnan Hospital of Wuhan University from December 21, 2019, to March 11, 2020. Information on clinical features of enrolled patients was collected for analysis.

Results: HH was observed in 5.88% of the ICU patients with SARS-CoV-2 infection. All HH patients were progressing to respiratory failure and peak alanine aminotransferase (ALT) values were 1665, 1414, and 1140 U/L during hospitalization, respectively. All patients with HH died as a result of the deterioration of multiple organ failure (MOF). The dynamic changes of ALT, aspartate transaminase (AST), and total bilirubin (TBIL) levels were more dramatic in HH groups. Levels of TBIL, C-reactive protein (CRP), procalcitonin (PCT), and interleukin-6(IL-6) showed statistically significant elevation in HH cases compared with that in non-HH cases ($P < 0.001$). Besides, the median survival time of the HH group was significantly shorter than the non-HH group ($P < 0.05$).

Conclusions: In ICU, HH was not a rare condition in patients with severe COVID-19 and has a high mortality. The main causes of HH are respiratory and cardiac failure and

may be associated with the immune-mediated inflammatory response. Clinicians should search for any underlying hemodynamic or respiratory instability even in patients with normal ALT levels on admission.

Keywords: 2019-nCoV, SARS-CoV-2, hypoxic hepatitis, ischemia, liver injury, multiple organ failure (MOF), COVID-19

INTRODUCTION

In December 2019, a range of viral pneumonia cases started to spread in the city of Wuhan, China. On 11 February 2020, this unknown etiology was officially named severe acute respiratory syndrome coronavirus 2(SARS-CoV-2) (1), and the disease was named coronavirus disease 2019(COVID-19) by the World Health Organization. Some patients had different degrees of liver injury. Moreover, four relatively large-scale studies have reported the clinical characteristics of COVID-19 patients, including liver impairment (2–5). Although transaminase elevation is usually mild, severe liver injury has been reported (3–6). However, the reason for severe liver injury is still not clear.

Acute liver impairment can present as a life-threatening disorder and can be caused by a series of reasons, including drug-induced liver injury (DILI), acute viral hepatitis, HH, acute alcohol-induced liver injury, liver trauma, etc. Whether SARS-CoV-2 is hepatotropic like viral hepatitis A, B, C, and what roles does the virus plays in the course of liver injury is worth studying. What's more, other causes of acute liver injury, if not SARS-CoV-2, need to be identified.

HH is the most common cause of a significant but transient elevation in serum aminotransferase activities (S-AT) in most studies. In ICU, the prevalence of HH accounts for at least 1% of admission (7). Currently, the pathogenesis of HH is not very clear, but most scholars agree with the three mechanisms proposed by Dunn et al. (8) that lead to HH: hepatic ischemia caused by reduced blood flow to the liver, venous congestion caused by right heart failure, and arterial hypoxemia caused by decreased blood oxygen content. Thus, remarkedly hypoxemic conditions could result in HH. Severe COVID-19 cases have led to respiratory failure, which can decrease oxygen supply to the liver. For this reason, HH may be a possible cause of severe liver injury in COVID-19 patients. Up to date, there has been no study of HH in patients infected with SARS-CoV-2. In the largest cohort study of critically ill patients with HH, the 28-day mortality in ICU was 45.0%(9). Because of this high mortality, the prompt identification and treatment of HH are crucial to the prognosis. We aim to describe the prevalence of HH in COVID-19 patients in ICU, as well as possible mechanisms.

Abbreviations: HH, hypoxic hepatitis; SARA-CoV-2, severe acute respiratory syndrome coronavirus 2; COVID-19, coronavirus disease 19; ICU, intensive care unit; CHD, coronary heart disease; COPD, chronic obstructive pulmonary disease; DM, diabetes mellitus; ECMO, extracorporeal membrane oxygenation; SD, standard deviation; ULN, upper limit of normal; BMI, body mass index; ALT, alanine aminotransferase; AST, aspartate aminotransferase; TBIL, total bilirubin; γ-GT, γ-glutamyl transpeptidase; ALP, alkaline phosphatase; LDH, lactate dehydrogenase; CRP, C-reactive protein; IL-6, interleukin-6; INR, international normalized ratio; PCT, procalcitonin; Hgb, hemoglobin; WBC, white blood cell; PLT, platelet count; ALB, albumin; AIH, autoimmune hepatitis; MAFLD, metabolic associated fatty liver disease.

MATERIALS AND METHODS

Patients

From December 21, 2019, to March 11, 2020, 51 patients with COVID-19 were admitted and treated to the ICU at Zhongnan Hospital of Wuhan University. Epidemiological, clinical, laboratory characteristics, treatment, and outcomes data were acquired from the electronic medical records. This retrospective study was approved by the Research Ethics Commission of Zhongnan Hospital of Wuhan University and the Ethics Committee of Zhejiang Provincial People's Hospital. Due to the retrospective nature of this study, the need for informed consent was waived.

Data Collection

Laboratory investigations included complete blood count, coagulation function, routine biochemical, and liver function tests. Parameters related to patient characteristics included sex, age, and comorbidities (diabetes mellitus, hypertension, coronary heart disease, heart disease, and chronic obstructive pulmonary disease). Parameters related to the episode of HH included cause, supportive therapy (vasopressor agents, mechanical ventilation, and extracorporeal membrane oxygenation), and specific drug use (ribavirin, remdesivir, oseltamivir, glucocorticoid, etc.).

Hypoxic Hepatitis

Patients who met all of the following criteria were diagnosed with HH based on a previous report (10) (i) a massive but transient elevated ALT level [more than 20-fold the upper limit of normal (ULN)], (ii) the presence of respiratory, cardiac or circulatory failure, and (iii) exclusion of other causes of liver injury. Liver biopsy was not required for the diagnosis of HH, in agreement with other studies showing that a histological confirmation is unwarranted and even inadvisable when the criteria listed above are met (11, 12).

Statistical Analysis

Statistical analysis was performed using the SPSS software package (version 21.0, SPSS Inc., IBM, Chicago, IL, USA). Categorical variables were described as frequency and percentages, and continuous variables as means ± standard deviation (SD) or median and interquartile range (IQR). Continuous variables were compared using independent group *t*-tests when the data were normally distributed; otherwise, the Mann-Whitney U test was used. Comparison of categorical variables was done using the chi-square test or the Fisher exact test if the cell counts were small. Dynamic changes of liver

function indicators by the influence of hypoxic hepatitis were presented using locally weighted scatterplot smoothing (LOESS). Survival analysis was performed by the Kaplan-Meier and Log rank test. A *P*-value < 0.05(two-tailed) was considered to indicate significance.

RESULTS

Characteristics of the Patients With COVID-19 in ICU

The 51 patients in ICU with COVID-19 were predominantly male (n = 35,68.63%), and aged ≤65 years (n = 32,62.75%). There underlying medical conditions described in **Table 1**, mainly included hypertension (n = 22,43.14%), diabetes mellitus (DM) (n = 7,13.73%), coronary heart disease (CHD) (n = 12,23.53%), chronic obstructive pulmonary disease (COPD) (n = 2,3.92%). None of the critical patients had a malignant tumor. The proportion of patients with liver impairment on admission was much lower than the hospitalization (n = 39, 76.47% vs. n = 21, 41.18%, $P < 0.001$). Antiviral therapy was performed in 38 (74.51%) patients and antibiotic therapy was performed in 16 (31.4%), while the combination of the two therapies was 11 (21.56%). What's more, the proportion of patients using two or more antiviral drugs is 23.53% (12/51) and glucocorticoid therapy is 82.35% (42/51). Mechanical ventilation was performed in 37 (72.55%) while extracorporeal membrane oxygenation (ECMO) was performed in 3 (5.88%) (**Table 1**).

An ALT level of >20-fold the ULN was found in only three patients, not on admission but during hospitalization. The peak value of ALT was 1665, 1414, and 1140 U/L respectively. The degree of ALT elevation in HH patients was significantly higher than that in non-HH patients with liver impairment (during hospitalization, 1406.33 ± 262.58 vs. 118.23 ± 90.75 U/L, $P < 0.001$). These cases were diagnosed as HH. The incidence of HH in our single-center cohort of ICU patients with COVID-19 was 5.88% (3/51). All cases deteriorated into respiratory failure. Also, viral hepatitis and autoimmune diseases were excluded based on negative results of serum marker tests.

TABLE 1 | Characteristics of the patients with COVID-19 in ICU (n = 51).

Characteristics	Number (%)	
Age		
≤65 years	32 (62.75)	
>65 years	19 (37.25)	
Sex		
Male	35 (68.63)	
Female	16 (31.37)	
BMI>25 (kg/m^2)	16 (31.37)	
Underlying medical conditions		
Hypertension	22 (43.14)	
DM	7 (13.73)	
CHD	12 (23.53)	
COPD	2 (3.92)	
Cerebrovascular disease	5 (9.80)	
Hepatopathy	1 (1.96)	
Hemorrhage of digestive tract	2 (3.92)	
Chronic kidney disease	1 (1.96)	
Renal transplant	1 (1.96)	
Malignant tumor	0	
Liver impairment		Value (mean ± SD) U/L
On admission	21 (41.18)	53.13 ± 65.55
ULN <ALT ≤20-fold ULN	21 (41.18)	53.13 ± 65.55
ALT >20-fold ULN	0	
Hospitalization*	39 (76.47)*	70.54 ± 142.90
ULN <ALT ≤20-fold ULN	36 (70.59)	118.23 ± 90.75
ALT >20-fold ULN	3 (5.88)	1406.33 ± 262.58#
Treatment		
Antibiotic therapy	16 (31.37)	
Antiviral therapy	38 (74.51)	
A combination of antibiotic and antiviral therapy	11 (21.56)	
Multiple antiviral therapies (≥2)	12 (23.53)	
Glucocorticoid therapy	42 (82.35)	
Mechanical ventilation	37 (72.55)	
ECMO	3 (5.88)	

**Liver impairment ratio (hospitalization vs. on admission, P < 0.001).*
#Peak ALT level during hospitalization (HH patients vs. non-HH patients with liver impairment, P < 0.001).
ALT, alanine aminotransferase; BMI, body mass index; CHD, coronary heart disease; COPD, chronic obstructive pulmonary disease; DM, diabetes mellitus; ULN, upper limit of normal; ECMO: extracorporeal membrane oxygenation; SD, standard deviation; HH, hypoxic hepatitis.

Comparison of Clinical Characteristics Between HH and Non-HH Patients

The clinical characteristics of the two groups were shown in **Table 2**. Mean age at diagnosis was (63.33 ± 7.64), which was slightly older than that non-HH group. There was no significant difference in age and sex between the two groups. In our cohort of 51 patients, no children or adolescents were infected. The incidence of hypertension and CHD were 2 (66.67%) and 1 (33.33%), respectively, which were higher than that of 20 (41.67%) and 11 (22.92%) patients without HH. There were no DM and hepatopathy in the HH group, compared with 7/48 (14.58%) cases of DM and 1/48 (2.08%) cases of hepatopathy in the non-HH group. The most common symptoms at the onset of illness were fever (88.23%), cough (64.71%), and dyspnea (52.94%). There was no significant difference in the incidence of myalgia and COPD between the two groups. To get the outcomes of the patients, we followed up to April 5, 2020, 29 (60.42%) patients have been discharged and 19 (39.58%) died in the group of non-HH patients, while 3 (100.00%) patients have all died in the group of HH. Besides, **Figure 1** also showed that the median survival time of the HH group was significantly shorter than the non-HH group ($p < 0.05$). Fitness for discharge was based on abatement of fever for at least 10 days, with the improvement of chest radiographic evidence and viral clearance in respiratory samples from the upper respiratory tract (**Table 2**).

Selected Laboratory Tests of COVID-19 Patients

Table 3 shows that the median values of lymphocytes and PLT were 0.26 (0.20–0.48) and 64.00 (48.25–147.25), respectively, which were significantly lower than those of patients without HH ($P < 0.001$). No significant difference in the level of white blood cells or hemoglobin between the two groups was observed ($P > 0.05$). In indexes of liver enzymes and function, patients with HH had significant degrees of ALB reduction compared with that non-HH group ($P < 0.05$) and the concentration of ALB has reached the level of hypoalbuminemia (ALB<30 g/L). The median levels of ALT, AST, γ-GT, LDH, and AKP in patients with HH were no significant differences between the two groups. Furthermore, ALT, AST, and γ-GT were slightly above normal, while LDH was significantly above normal. No obvious jaundice was observed in any of the patients with HH, even though the median TBIL level in the HH group was significantly higher than that non-HH group ($P < 0.001$). Since the coagulation proteins required for blood coagulation cascade are mainly produced by the liver, and the half-life of coagulation factors is shorter than ALB, INR is often used as the marker of liver synthesis function (13). Patients with HH had higher median INR values compared with those patients without HH (1.26 vs. 1.22), though it presented only a very slight INR elevation. Inflammatory markers among these critically ill patients, including CRP, PCT, D-dimer, and IL-6. The concentration of PCT, CRP, and IL-6 were 5.43 (1.87–20.13), 235.30 (102.80–300.50), and 356.10 (149.70–1622.25), respectively, which were significantly higher than those of patients without HH ($P < 0.001$). Besides, CRP as the indicator of acute inflammation, the levels of CRP in both groups was well above normal. As for the indicator of renal function, the median value of creatinine was 88.50 (71.00–124.55) and 70.00 (52.53–115.70), respectively, which were significantly higher than that non-HH group ($P < 0.05$), although still in the normal range. The levels of myocardial necrosis markers in patients with HH were also higher than those in patients without HH and far above normal.

TABLE 2 | Clinical characteristics of COVID-19 patients.

Characteristics	With HH ($n = 3$)	Without HH ($n = 48$)	*P* value
Age (years)	63.33 ± 7.638	59.94 ± 14.110	0.68
Sex (male)	3 (100.00)	32 (66.67)	0.54
Current smoker (%)	2 (66.67)	9 (18.75)	0.22
Current drinker (%)	1 (33.33)	10 (20.83)	>0.999
Pre-existing conditions (%)			
Hypertension	2 (66.67)	20 (41.67)	0.81
DM	0	7 (14.58)	>0.999
Heart disease	1 (33.33)	11 (22.92)	>0.999
COPD	1 (33.33)	1 (2.08)	0.24
Hepatopathy	0	1 (2.08)	>0.999
Other diseases	3 (100.00)	20 (41.67)	0.09
Comorbidities	3 (100.00)	32 (66.67)	0.543
Symptom (%)			
Fever	3 (100.00)	42 (87.50)	>0.999
Cough	3 (100.00)	30 (62.50)	0.54
Dyspnea	3 (100.00)	24 (50.00)	0.24
Myalgia	3 (33.33)	8 (16.67)	0.25
Chest distress	3 (100.00)	22 (45.83)	0.11
Other	2 (66.67)	17 (35.42)	0.64
Outcome (%)			
Discharge	0	29 (60.42)	0.07
Death	3 (100.00)	19 (39.58)	0.07

Dynamic Changes in Liver Function Indicators in COVID Patients in ICU

To determine the trajectory of liver function indicators in patients enrolled in this study, multiple liver function test results

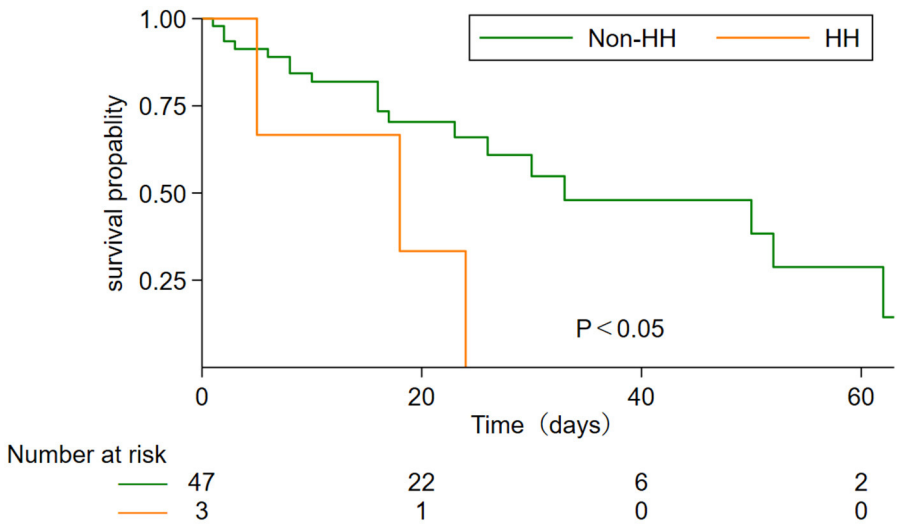

FIGURE 1 | Comparison of survival probability between HH and non-HH group. Group comparisons were performed using the Kaplan-Meier and long-rank test.

TABLE 3 | Selected laboratory data of COVID-19 patients.

Characteristics	With HH (n = 3)	Without HH (n = 48)	P-value
BLOOD COUNTS			
WBC ($\times 10^9$/L)	9.98 (6.19–15.23)	9.32 (6.58–14.10)	0.89
Lymphocyte ($\times 10^9$/L)	0.26 (0.20–0.48)	0.57 (0.34–1.04)	<0.001
Hgb (g/L)	95.95 (83.90–123.70)	111.00 (82.85–126.90)	0.26
PLT ($\times 10^9$/L)	64.00 (48.25–147.25)	151.00 (103.00–219.50)	<0.001
LIVER ENZYMES AND FUNCTION			
ALB (g/L)	28.95 (24.95–31.28)	30.70 (27.80–34.35)	0.02
ALT (U/L)	42.00 (21.00–54.00)	40.00 (26.00–69.00)	0.50
AST (U/L)	40.00 (34.00–61.00)	38.00 (26.00–65.00)	0.23
TBIL (μmol/L)	21.30 (14.50–32.90)	14.20 (10.20–21.10)	<0.001
γ-GT (U/L)	70.50 (43.75–97.00)	45.00 (24.00–111.00)	0.07
ALP (U/L)	100.00 (87.25–120.75)	90.50 (71.00–122.75)	0.13
LDH (U/L)	432.00 (347.25–895.25)	460.50 (322.25–641.75)	0.86
INR	1.26 (1.16–1.43)	1.22 (1.13–1.36)	0.14
ADDITIONAL MARKERS OF ORGAN DAMAGE AND INFLAMMATION			
CRP (mg/L)	235.30 (102.80–300.50)	53.60 (23.58–112.33)	<0.001
PCT (ng/ml)	5.43(1.87–20.13)	0.29(0.06–1.90)	<0.001
D-dimer (μg/L)	935.00 (622.50–2049.00)	1123.00 (578.00–3254.00)	0.61
IL-6 (pg/mL)	356.10 (149.70–1622.25)	45.21 (17.90–103.60)	<0.001
Creatinine (μmol/L)	88.50 (71.00–124.55)	70.00 (52.53–115.70)	0.02

WBC, white blood cell;Hgb, hemoglobin; PLT, platelet count; ALB, albumin; ALT, alanine aminotransferase; AST, aspartate transaminase; TBIL, total bilirubin; γ-GT, γ-glutamyl transpeptidase; ALP, alkaline phosphatase; LDH, lactic dehydrogenase; INR, international normalized ratio; CRP, C-reactive protein; PCT, procalcitonin; IL-6, interleukin-6.

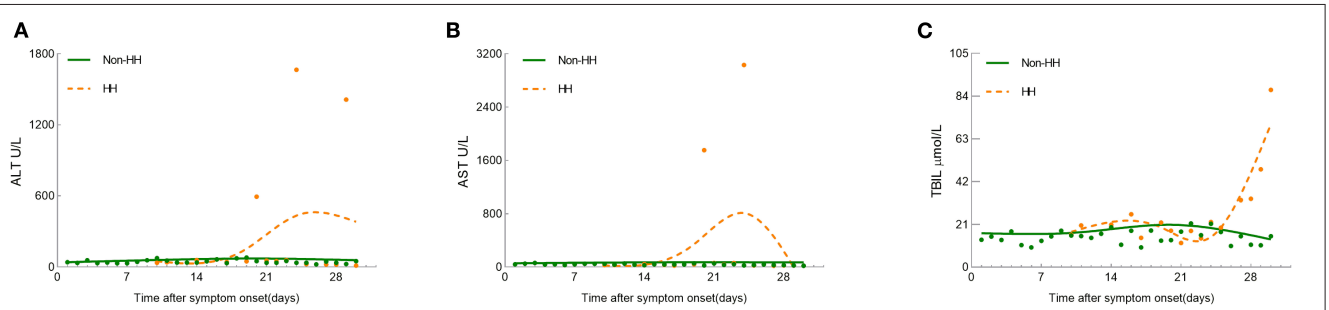

FIGURE 2 | Smooth trajectories and scatters represent the median values **(A)** ALT; **(B)** AST; **(C)** TBIL in the HH and non-HH groups. The ULN in our health care system is defined as 40 U/L for ALT, 40 U/L for AST, and 21 μmol/L for TBIL, respectively.

were recorded during hospitalization. LOESS models illustrated the trajectory of ALT, AST, and TBIL between the two groups (**Figure 2**). From the general trend, the rangeability of the non-HH group was much flatter than that of the HH group. Unlike the non-HH group, the curve of HH started on day 10. **Figure 2A** suggested that the curve of the non-HH group fluctuated roughly in a range of 1–2 times of ULN. ALT began to rise rapidly at the 2nd week and peaked within 3 to 4 weeks after symptom onset in the HH group. Besides, invasive mechanical ventilation was used when ALT levels reached a peak. **Figure 2B** illustrated that the curve of the non-HH group is close to a straight line compared with the HH group. Similar to ALT, AST also increased dramatically at the 2nd week and peaked within 3 to 4 weeks. Subsequently, the curve dropped sharply to a normal level. **Figure 2C** showed that the fluctuation in TBIL levels was mild and normal in the non-HH group. Moreover, TBIL levels were slightly higher than that non-HH group in the 1st week of the curve. Shortly after TBIL slowed down in the next week. However, the curve of TBIL was increased dramatically in the 3rd week. The dynamic changes in indicators suggested potential mechanisms of COVID-19 patients with HH in ICU.

DISCUSSION

HH, as manifested by ALT abrupt and massive elevation, is emerging as a clinical consequence of COVID-19, and often predict a poor outcome. These severely infected patients with HH had a high rate of ARDS and a high risk of death. SARS-CoV-2 infection in humans can cause respiratory diseases, acute kidney injury, myocarditis, thrombosis, and acute liver injury

(14). Most studies reported the prevalence of liver enzyme elevation has ranged from 20 to 30% and severe liver injury was uncommon (5, 15). However, extreme liver impairment (ALT >20-fold the ULN) was not rare in our study ($n = 3$, 5.88%) compared with previous reports (7). What's more, the significant difference of ALT elevation between HH patients and non-HH patients with liver impairment ($P < 0.001$) indicated that HH can be distinguished from other types of liver injury by the sharp increase of ALT level. It is also reported that liver impairment is caused by drug hepatotoxicity (such as remdesivir) (16) and immune-mediated inflammation (17). Thus, it's necessary to distinguish the causes of liver impairment.

DILI can be ruled out because hepatotoxic drugs continue to be used, and ALT also gradually decreases. Autoimmune hepatitis (AIH) was excluded because the score is not up to the diagnostic criteria(include autoantibodies, immunoglobulins, viral markers, and histological findings) proposed by the International Autoimmune Hepatitis Group (18). No imaging evidence suggested hepatic steatosis and no patients met one of the following clinical parameters, such as being overweight, having type 2 diabetes mellitus, or exhibiting metabolic dysregulation (19). Thus, metabolic associated fatty liver disease (MAFLD) was also ruled out. Henrion et al. reported that heart failure, respiratory failure, and septic toxic shock accounted for more than 90% of HH cases and the core mechanism was reduced oxygen supply to the liver (7). The hallmark of COVID-19 is respiratory failure. HH is therefore frequent in severe cases. In our study, 3 HH cases all progressed to respiratory failure, which led to hypoxia of liver tissue and abnormalities of liver function. Moreover, heart failure reduces the output, thereby decreasing the blood flow to the liver and further exacerbating hypoxia in the liver. This is consistent with previous research (7, 8). Although several hemodynamic mechanisms of liver hypoxia are involved, liver ischemia is not the only explanation for HH. On the one hand, previous studies indicated that ALT levels correlate well with markers of inflammation and are likely higher among patients with severe cytokine release syndromes (14, 20, 21). On the other hand, cytokine storm syndromes have been described in COVID-19, and are associated with severe elevations in liver enzymes (22). What's more, IL-6 is significantly increased in severe COVID-19 patients and plays a key role in the so-called "cytokine storm" (23, 24). In our study, the levels of ALT were extremely elevated and the concentrations of inflammatory markers including CRP, D-dimer, and IL-6 were significantly far above normal. Therefore, it suggested that HH may be associated with the immune-mediated inflammatory response.

Ours is the first batch of treatment centers for COVID-19 patients in the world. COVID-19 patients in ICU accounted for 7.02% (51/726) of the total number of patients diagnosed with SARA-CoV-2 infection during our observation. The prevalence of HH in patients with severe SARS-CoV-2 infection in our ICU is 5.88%. Most studies have reported an incidence of 0.9–2.4% (7). This is lower than ours, which indicated that patients with severe SARS-CoV-2 infection in ICU have a higher incidence of HH than that of patients with other causes.

At present, there has been no study on the dynamic changes of liver function in patients with COVID-19 combined with HH, and only a few studies in COVID-19-related liver injury (25, 26). The increase of ALT and AST levels in the early stage of the disease might be related to the immune-mediated inflammation in the liver. However, when ALT and AST showed a downward trend in the late stage of the disease in the HH group, the level of TBIL increased sharply. This may be a result of MOF.

The prognosis of HH is poor. Extensive analysis by Aboelsoud et al. showed that the mortality of HH was 44.1% (27). However, the mortality rate in our study was as high as 100%. MOF contributed heavily to the high mortality. We also observed an elevation in INR, significant hypoalbuminemia, and lymphopenia in patients with HH. Hypoalbuminemia is emerging as a consistent risk factor for severe disease (3, 6, 28) and is linked to poor clinical outcomes for hospitalized patients (29). Besides, increased INR in severe COVID-19 patients indicate damage of liver synthetic function. A study has also shown that lymphopenia may be a key factor related to disease severity and mortality (30). All of these factors can affect the prognosis of HH. In general, severe liver injury was not the direct cause of death. These patients died as a consequence of MOF, but the occurrence of HH had a high impact on the mortality of those critically ill patients.

In conclusion, we report a 5.88% prevalence of HH in COVID-19 patients in ICU, the first study to combine COVID-19 and HH. HH was not a rare condition in ICU, and was frequently accompanied by MOF, with high mortality. Patients with COVID-19 developed MOF accompanied by a sudden and sharp elevation of serum ALT level during hospitalization, which should be considered HH. Attention should also be paid to monitor liver function during the course of COVID-19, especially in patients with higher disease severity.

DATA AVAILABILITY STATEMENT

All data generated or analyzed during this study are included in this manuscript.

ETHICS STATEMENT

The analysis was approved by the Research Ethics Commission of Zhongnan Hospital of Wuhan University and the Ethics Committee of Zhejiang Provincial People's Hospital, and the need for informed consent was waived.

AUTHOR CONTRIBUTIONS

MG and YT designed study and revised the manuscript. HH and XZ analyzed data and prepared the manuscript. HL analyzed data and performed manuscript drafting. SC performed manuscript drafting. XD arranged and filtered data. JW and JZ searched the literature and analyzed data. LS, RY, MW, and JW collect data. HH reviewed the

results and made critical comments on the manuscript. All authors contributed to the article and approved the submitted version.

FUNDING

This study was supported by the Scientific Research Fund of the National Health Commission of China (No. WKJ-ZJ-2102), the General Scientific Research Projects of Zhejiang Education Department (No. Y202044644), the General Scientific Research Projects of Zhejiang Education Department (No. Y202044571).

ACKNOWLEDGMENTS

We received data from the Zhongnan Hospital of Wuhan University. We thank the Zhejiang Provincial People's Hospital for their support. We also appreciate all Zhongnan Hospital of Wuhan University for their elaborate work and patient assistance.

REFERENCES

1. Alexander E, Gorbalenya S, Baker C, Ralph S, Baric J. de Groot R, et al. Severe acute respiratory syndrome-related coronavirus: the species and its viruses - a statement of the Coronavirus Study Group. *bioRxiv*. (2020). doi: 10.1101/2020.02.07.937862
2. Chen N, Zhou M, Dong X, Qu J, Gong F, Han Y, et al. Epidemiological and clinical characteristics of 99 cases of 2019 novel coronavirus pneumonia in Wuhan, China: a descriptive study. *Lancet*. (2020) 395:507–13. doi: 10.1016/S0140-6736(20)30211-7
3. Huang C, Wang Y, Li X, Ren L, Zhao J, Hu Y, et al. Clinical features of patients infected with 2019 novel coronavirus in Wuhan, China. *Lancet*. (2020) 395:497–506. doi: 10.1016/S0140-6736(20)30183-5
4. Guan WJ, Ni ZY, Hu Y, Liang WH, Ou CQ, He JX, et al. Clinical characteristics of coronavirus disease 2019 in China. *N Engl J Med*. (2020) 382:1708–20. doi: 10.1056/NEJMoa2002032
5. Wang D, Hu B, Hu C, Zhu F, Liu X, Zhang J, et al. Clinical characteristics of 138 hospitalized patients with 2019 novel coronavirus-infected pneumonia in Wuhan, China. *JAMA*. (2020). 323:1061–9. doi: 10.1001/jama.2020.1585
6. Wu C, Chen X, Cai Y, Xia J, Zhou X, Xu S, et al. Risk factors associated with acute respiratory distress syndrome and death in patients with coronavirus disease 2019 pneumonia in Wuhan, China. *JAMA Intern Med*. (2020) 180:1–11. doi: 10.1001/jamainternmed.2020.0994
7. Henrion J. Hypoxic hepatitis. *Liver Int*. (2012) 32:1039–52. doi: 10.1111/j.1478-3231.2011.02655.x
8. Dunn GD, Hayes P, Breen KJ, Schenker S. The liver in congestive heart failure: a review. *Am J Med Sci*. (1973). 265:16. doi: 10.1097/00000441-197303000-00001
9. Van den Broecke A, Van Coile L, Decruyenaere A, Colpaert K, Benoit D, Van Vlierberghe H, et al. Epidemiology, causes, evolution and outcome in a single-center cohort of 1116 critically ill patients with hypoxic hepatitis. *Ann Intensive Care*. (2018) 8:15. doi: 10.1186/s13613-018-0356-z
10. Zhang Y, Liu J, Yu L, Zhou N, Ding W, Zheng S, et al. Prevalence and characteristics of hypoxic hepatitis in the largest single-centre cohort of avian influenza A(H7N9) virus-infected patients with severe liver impairment in the intensive care unit. *Emerg Microbes Infect*. (2016) 5:e1. doi: 10.1038/emi.2016.1
11. Kneidinger N, Funk GC, Lindner G, Drolz A, Schenk P, Fuhrmann V. Unmeasured anions are associated with short-term mortality in patients with hypoxic hepatitis. *Wien Klin Wochenschr*. (2013) 125:474–80. doi: 10.1007/s00508-013-0400-9
12. Henrion J, Schapira M, Luwaert R, Colin L, Delannoy A, Heller FR. Hypoxic hepatitis: clinical and hemodynamic study in 142 consecutive cases. *Medicine*. (2003) 82:392–406. doi: 10.1097/01.md.0000101573.54295.bd
13. Northup PG, Caldwell SH. Coagulation in liver disease: a guide for the clinician. *Clin Gastroenterol Hepatol*. (2013) 11:1064–74. doi: 10.1016/j.cgh.2013.02.026
14. Phipps MM, Barraza LH, LaSota ED, Sobieszczyk ME, Pereira MR, Zheng EX, et al. Acute liver injury in COVID-19: prevalence and association with clinical outcomes in a large US cohort. *Hepatology*. (2020). doi: 10.1002/hep.31404. [Epub ahead of print].
15. Lee IC, Huo TI, Huang YH. Gastrointestinal and liver manifestations in patients with COVID-19. *J Chin Med Assoc*. (2020) 83:521–3. doi: 10.1097/JCMA.0000000000000319
16. Leegwater E, Strik A, Wilms EB, Bosma LBE, Burger DM, Ottens TH, et al. Drug-induced liver injury in a COVID-19 patient: potential interaction of remdesivir with P-glycoprotein inhibitors. *Clin Infect Dis*. (2020). doi: 10.1093/cid/ciaa883. [Epub ahead of print].
17. Wu D, Yang XO. TH17 responses in cytokine storm of COVID-19: An emerging target of JAK2 inhibitor fedratinib. *J Microbiol Immunol Infect*. (2020) 53:368–70. doi: 10.1016/j.jmii.2020.03.005
18. Czaja AJ. Diagnosis and management of autoimmune hepatitis: current status and future directions. *Gut Liver*. (2016) 10:177–203. doi: 10.5009/gnl15352
19. Eslam M, Newsome PN, Sarin SK, Anstee QM, Targher G, Romero-Gomez M, et al. A new definition for metabolic dysfunction-associated fatty liver disease: an international expert consensus statement. *J Hepatol*. (2020) 73:202–9. doi: 10.1016/j.jhep.2020.07.045
20. Levi M, Thachil J, Iba T, Levy JH. Coagulation abnormalities and thrombosis in patients with COVID-19. *Lancet Haematol*. (2020) 7:e438–e40. doi: 10.1016/S2352-3026(20)30145-9
21. Zeng JH, Liu YX, Yuan J, Wang FX, Wu WB, Li JX, et al. First case of COVID-19 complicated with fulminant myocarditis: a case report and insights. *Infection*. (2020). doi: 10.20944/preprints202003.0180.v1. [Epub ahead of print].
22. Mehta P, McAuley DF, Brown M, Sanchez E, Tattersall RS, Manson JJ. COVID-19: consider cytokine storm syndromes and immunosuppression. *Lancet*. (2020) 395:1033–4. doi: 10.1016/S0140-6736(20)30628-0
23. Wan S, Yi Q, Fan S, Lv J, Zhang X, Guo L, et al. Characteristics of lymphocyte subsets and cytokines in peripheral blood of 123 hospitalized patients with 2019 novel coronavirus pneumonia (NCP). *J Infect Dis*. (2020) 221:1762–9. doi: 10.1101/2020.02.10.20021832
24. Liu J, Li S, Liu J, Liang B, Wang X, Wang H, et al. Longitudinal characteristics of lymphocyte responses and cytokine profiles in the peripheral blood of SARS-CoV-2 infected patients. *EBioMedicine*. (2020) 55:102763. doi: 10.1016/j.ebiom.2020.102763
25. Lei F, Liu YM, Zhou F, Qin JJ, Zhang P, Zhu L, et al. Longitudinal association between markers of liver injury and mortality in COVID-19 in China. *Hepatology*. (2020). doi: 10.1002/hep.31301. [Epub ahead of print].
26. Bloom PP, Meyerowitz EA, Reinus Z, Daidone M, Gustafson J, Kim AY, et al. Liver biochemistries in hospitalized patients with COVID-19. *Hepatology*. (2020). doi: 10.1002/hep.31326. [Epub ahead of print].
27. Aboelsoud MM, Javaid AI, Al-Qadi MO, Lewis JH. Hypoxic hepatitis - its biochemical profile, causes and risk factors of mortality in critically-ill patients: a cohort study of 565 patients. *J Crit Care*. (2017) 2017:7. doi: 10.1016/j.jcrc.2017.04.040
28. Zhou F, Yu T, Du R, Fan G, Liu Y, Liu Z, et al. Clinical course and risk factors for mortality of adult inpatients with COVID-19 in Wuhan, China: a retrospective cohort study. *Lancet*. (2020) 395:1054–62. doi: 10.1016/S0140-6736(20)30566-3
29. Kim S, McClave SA, Martindale RG, Miller KR, Hurt RT. Hypoalbuminemia and clinical outcomes: what is the mechanism behind the relationship? *Am Surg*. (2017) 83:1220–7. doi: 10.1177/000313481708301123

30. Chen P, Zhou B. Clinical characteristics of COVID-19 in patients with liver injury. *Clin Gastroenterol Hepatol*. (2020) 18:2846–7. doi: 10.1016/j.cgh.2020.04.043

Conflict of Interest: The authors declare that the research was conducted in the absence of any commercial or financial relationships that could be construed as a potential conflict of interest.

frontiers in Medicine

ORIGINAL RESEARCH
published: 11 February 2021
doi: 10.3389/fmed.2020.591736

DHX15 Inhibits Autophagy and the Proliferation of Hepatoma Cells

*Miaomiao Zhao [1,2], Lixiong Ying [3], Rusha Wang [1,2], Jiping Yao [1,2], Liming Zhu [4], Min Zheng [1,2], Zhi Chen [1,2] and Zhenggang Yang [1,2]**

[1] The State Key Laboratory for Diagnosis and Treatment of Infectious Diseases, College of Medicine, The First Affiliated Hospital, Zhejiang University, Hangzhou, China, [2] Collaborative Innovation Center for Diagnosis and Treatment of Infectious Diseases, Hangzhou, China, [3] Pathology Department, College of Medicine, The First Affiliated Hospital, Zhejiang University, Hangzhou, China, [4] Department of Chemotherapy, Zhejiang Cancer Hospital, Hangzhou, China

Autophagy is a highly conserved process by which superfluous or harmful components in eukaryotic cells are degraded by autophagosomes. This cytoprotective mechanism is strongly related to various human diseases, such as cancer, autoimmune diseases, and diabetes. DEAH-box helicase 15 (DHX15), a member of the DEAH box family, is mainly involved in RNA splicing and ribosome maturation. Recently, DHX15 was identified as a tumor-related factor. Although both autophagy and DHX15 are involved in cellular metabolism and cancer progression, their exact relationship and mechanism remain elusive. In this study, we discovered a non-classic function of DHX15 and identified DHX15 as a suppressive protein in autophagy for the first time. We further found that mTORC1 is involved in DHX15-mediated regulation of autophagy and that DHX15 inhibits proliferation of hepatocellular carcinoma (HCC) cells by suppressing autophagy. In conclusion, our study demonstrates a non-classical function of DHX15 as a negative regulator of autophagy related to the mTORC1 pathway and reveals that DHX15-related autophagy dysfunction promotes HCC cell proliferation, indicating that DHX15 may be a target for liver cancer treatment.

Keywords: DEAH-box helicase 15, RNA helicase, autophagy, mTORC1, HCC cells

OPEN ACCESS

Edited by:
Xiaojun Chen,
Nanjing Medical University, China

Reviewed by:
Zhengxiang He,
Icahn School of Medicine at Mount Sinai, United States
Chenyang Wang,
Nanjing University, China

***Correspondence:**
Zhenggang Yang
yangzg@zju.edu.cn

Specialty section:
This article was submitted to Gastroenterology, a section of the journal Frontiers in Medicine

Received: *05 August 2020*
Accepted: *10 December 2020*
Published: *11 February 2021*

Citation:
Zhao M, Ying L, Wang R, Yao J, Zhu L, Zheng M, Chen Z and Yang Z (2021) DHX15 Inhibits Autophagy and the Proliferation of Hepatoma Cells. Front. Med. 7:591736. doi: 10.3389/fmed.2020.591736

INTRODUCTION

Autophagy is a highly conserved mechanism by which redundant cellular components are degraded in double-membrane vesicles called autophagosomes. During this process, the outer membrane of a autophagosome fuses with a lysosome, after which acidic hydrolases degrade autophagic cargo and subsequently recycle the macromolecules (1, 2). Under physiological conditions, basal autophagy helps cells discard damaged organelles, degrade misfolded proteins, resist exogenous microorganisms, and maintain genomic stability, thus protecting the body from chronic damage and inflammation and inhibiting cancer initiation (3, 4). However, under abnormal conditions, long-term, excessive or defective autophagy is harmful and is closely related to the occurrence and development of cancers, autoimmune diseases, heart failure, neurodegenerative diseases and other diseases (5–8). In the case of cancer, autophagy can be used by cancer cells to defend against host immune attack, thus enhancing cancer cell survival, invasion and metastasis (9–11). Therefore, precise regulation of autophagy is extremely important for the maintenance of cellular homeostasis and treatment of several diseases.

DEAH-box 15 (DHX15), an important member of the RNA helicase family, is involved mainly in pre-mRNA splicing and promotion of ribosome maturation (12–14). Most reported studies have concentrated on its splicing function in RNA metabolism (15–17). However, DHX15 exhibits various functions in human tumorigenesis through transcriptional or post-transcriptional regulation independent of its ATPase activity (18, 19) or through interaction with proteins that have a G-patch domain (20). DHX15 enhances androgen receptor (AR) transcriptional activity by stimulating Siah2-mediated ubiquitination, which contributes to the progression of prostate cancer (19). In glioma, DHX15 is an antitumour gene, and its Ia–Ib and III–IV motifs, but not its ATPase activity, play important roles in its growth-inhibitory function (18). Moreover, DHX15 not only dysregulates genes downstream of the NF-kB signaling pathway, an important mechanism of its antitumour function, but also downregulates genes involved in splicing and ribosomal biogenesis in glioma, indicating that DHX15 regulates glioma at the post-transcriptional level (18). The G-patch is a glycine-rich domain that interacts with DEAH helicases to enhance their activity (21–23). For example, the G-patch domain of the GPATCH2 protein interacts with DHX15, which promotes breast cancer cell growth (20). Therefore, DHX15 is a versatile protein that participates in different stages of many types of cancers. In addition, DHX15 has been shown to aid in the diagnosis of acute lymphoblastic leukemia (AML) (24, 25) and to act as a viral RNA sensor in antiviral responses and innate immunity through the MAVS-mediated signaling pathway and the Nlrp6-interferon pathway (26, 27). Recently, DHX15 has been shown to be associated with clinically pathological elements and prognosis in patients with hepatocellular carcinoma (HCC) (28).

Autophagy is a highly conserved mechanism in cells proven to be closely related to the occurrence and progression of tumors. DHX15, a member of RNA helicase family, is also highly conserved in structure and function. Recently, DHX15 has been reported to be a tumor-related factor. However, the relationship between autophagy and DHX15 remains unclear. Nor is it clear whether this relationship plays a role in cancer. In this study, we found the relationship between autophagy and DHX15 and identified DHX15 as an autophagy suppressor for the first time. Knockdown of endogenous DHX15 dramatically induced autophagy independent of the function of DHX15 in regulating RNA metabolism. In addition, downregulation of DHX15 inhibited activation of mTORC1. Furthermore, we found that DHX15 acts as a suppressor of proliferation in hepatoma cells and that this function is dependent on autophagy inhibition. Collectively, these results show that DHX15 inhibits autophagy by activating mTORC1, which is associated with the anti-tumor effect of DHX15.

Abbreviations: DHX15, DEAH box helicase 15; mTORC1, mammalian target of rapamycin complex 1; MAP1LC3 (LC3), microtubule-associated protein 1 light chain 3 beta; p62, Sequestosome-1; AMPK, AMP-activated protein kinase; 70S6K, 70 S6 kinase 1; 4EBP1, eukaryotic translation initiation factor 4E-binding protein 1; 3-MA, 3-methyladenine; GFP, green fluorescent protein; Ki67, marker of proliferation Ki67; ATG, autophagy-associated gene; Baf-A1, bafilomycin A1; CQ, Chloroquine diphosphate.

RESULTS

Downregulation of Endogenous DHX15 Induces Autophagy

To examine the effect of DHX15 on autophagy, we temporarily knocked down endogenous DHX15 in different human cell lines after transfection with small interfering RNA (siRNA) and detected the protein expression of microtubule-associated protein 1 light chain 3 (LC3) and SQSTM/p62, important biomarkers of autophagy. As shown in **Figure 1A**, we first visualized autophagic activity in 293-GFP-LC3 cells (HEK293 cells with stable expression of GFP-LC3) by fluorescence microscopy. Compared with control cells, 293-GFP-LC3 cells in which endogenous DHX15 expression was knocked down exhibited significantly more GFP-LC3 puncta (**Figures 1A,B**). Similarly, DHX15 silencing in both L02 hepatocytes and HepG2 and Huh7 HCC cells significantly promoted LC3-II conversion and SQSTM1/P62 degradation (**Figure 1C** and **Supplementary Figure 1**). In addition to detecting the effect of DHX15 knockdown, we found that overexpression of DHX15 in these cell lines suppressed autophagy under basal conditions (**Figure 1C** and **Supplementary Figure 1**; the data in **Supplementary Figure 1** were obtained from three independent experiments). Data are presented in **Supplementary Figure 1** obtained from three independent experiments. To further confirm this function, autophagosomes were quantified by transmission electron microscopy. Downregulation of DHX15 significantly increased the number of autophagosomes in L02 cells (**Figures 1D,E**). Taken together, these data suggest that downregulation of endogenous DHX15 dramatically induces autophagy and indicate that DHX15 is a suppressor of autophagy.

Knockdown of DHX15 Promotes the Formation of Autophagosomes

Autophagic flux is responsible for the dynamic nature of autophagy and consists of 3 sequential steps: autophagosome generation, autolysosome formation and degradation (29). We hypothesized that increased autophagosome formation and/or decreased autophagic degradation may have been the cause of the DHX15 knockdown-induced GFP-LC3 puncta generation. To determine whether autophagic flux is affected by DHX15, we treated cells with the late-stage autophagy inhibitor bafilomycin A1 (Baf-A1), a vacuolar-type H^+-translocating ATPase inhibitor, after DHX15 silencing. We found that the conversion of LC3-II and the number of GFP-LC3 puncta were significantly augmented by Baf-A1 treatment in cells with knockdown of endogenous DHX15, indicating that DHX15 regulates autophagy by increasing autophagosome formation. **Figure 2A** shows that knockdown of DHX15 dramatically augmented GFP-LC3 puncta formation after treatment with Baf-A1 (**Figures 2A,B**). We also found that the conversion of LC3-II was increased by Baf-A1 treatment after downregulation of DHX15 (**Figure 2C**). As shown in **Figure 2D**, consistent with these findings, SQSTM1/p62 degradation was more obvious in DHX15-knockdown cells than in control cells, and the DHX15 knockdown-induced degradation was inhibit by Baf-A1 treatment (**Figure 2C** and **Supplementary Figure 2**). The similar

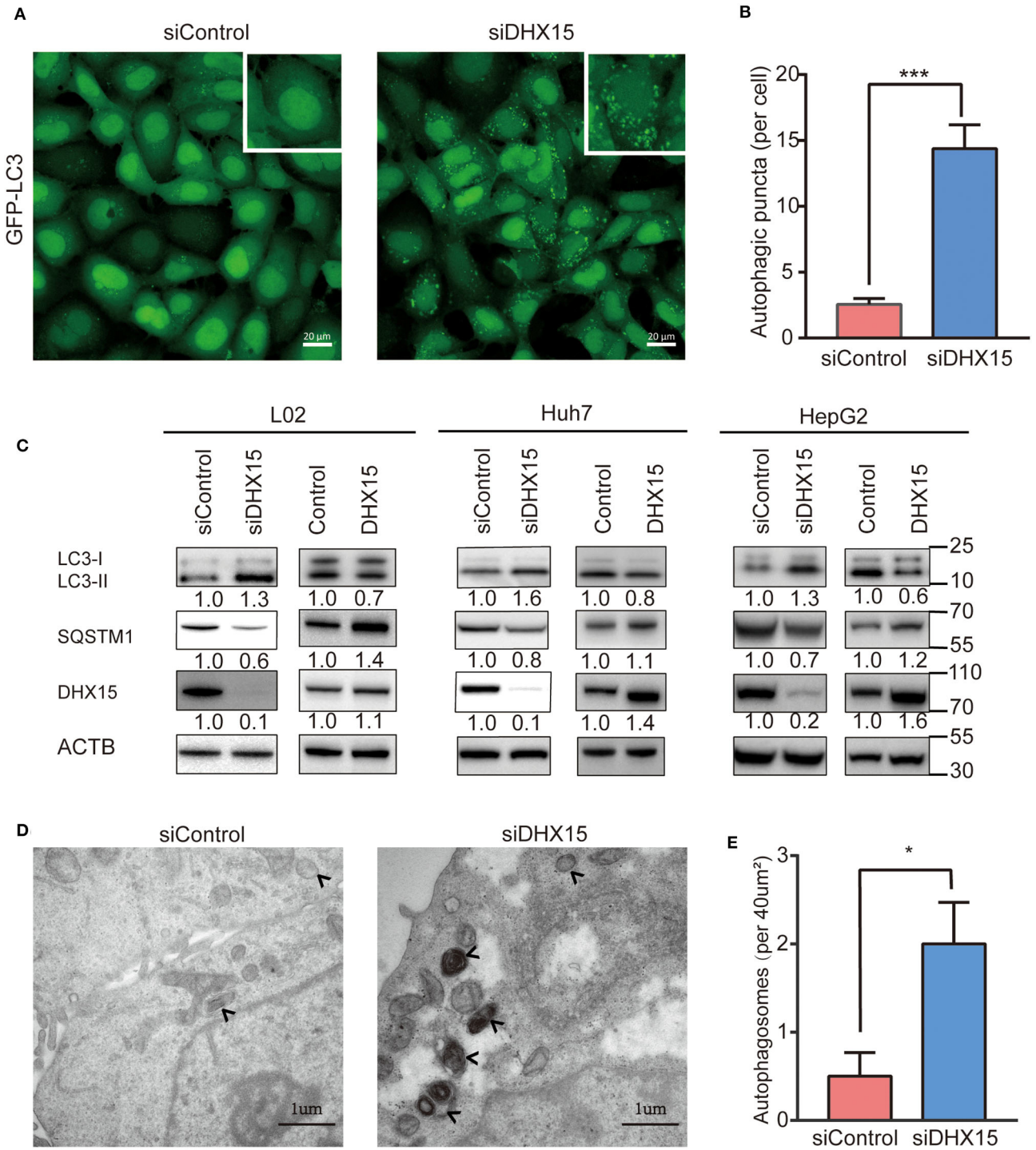

FIGURE 1 | Knockdown of DHX15 induces autophagy. **(A)** GFP-LC3 puncta were analyzed in HEK293 cells stably expressing GFP-LC3 (293-GFP-LC3 cells) after transient transfection with DHX15 siRNA (siDHX15) or a scrambled control (siControl). Representative images were obtained at 600× magnification. Scale bars: 20 μm. **(B)** The number of GFP-LC3 puncta per cell was quantified for each group. The data are presented as the mean ± SEM. Unpaired Student's *t*-test ($n = 5$). ***$P < 0.001$. **(C)** LC3-II conversion and SQSTM/p62 degradation in L02, Huh7, and HepG2 cells that had been transiently transfected with siDHX15 or siControl were detected by western blotting. LC3-II conversion and SQSTM1/p62 degradation in these three cell lines that had been transiently transfected by DHX15 plasmid or control plasmid were detected by western blotting. *$P < 0.05$. **(D)** Autophagosomes in L02 cells were analyzed by transmission electron microscopy. The autophagosomes are indicated by arrows. Scale bars: 1 μm. **(E)** Numbers of autophagosomes per 40 μm^2 as determined from the images. The data are presented as the mean ± SEM. Unpaired Student's *t*-test ($n = 10$). *$P < 0.05$.

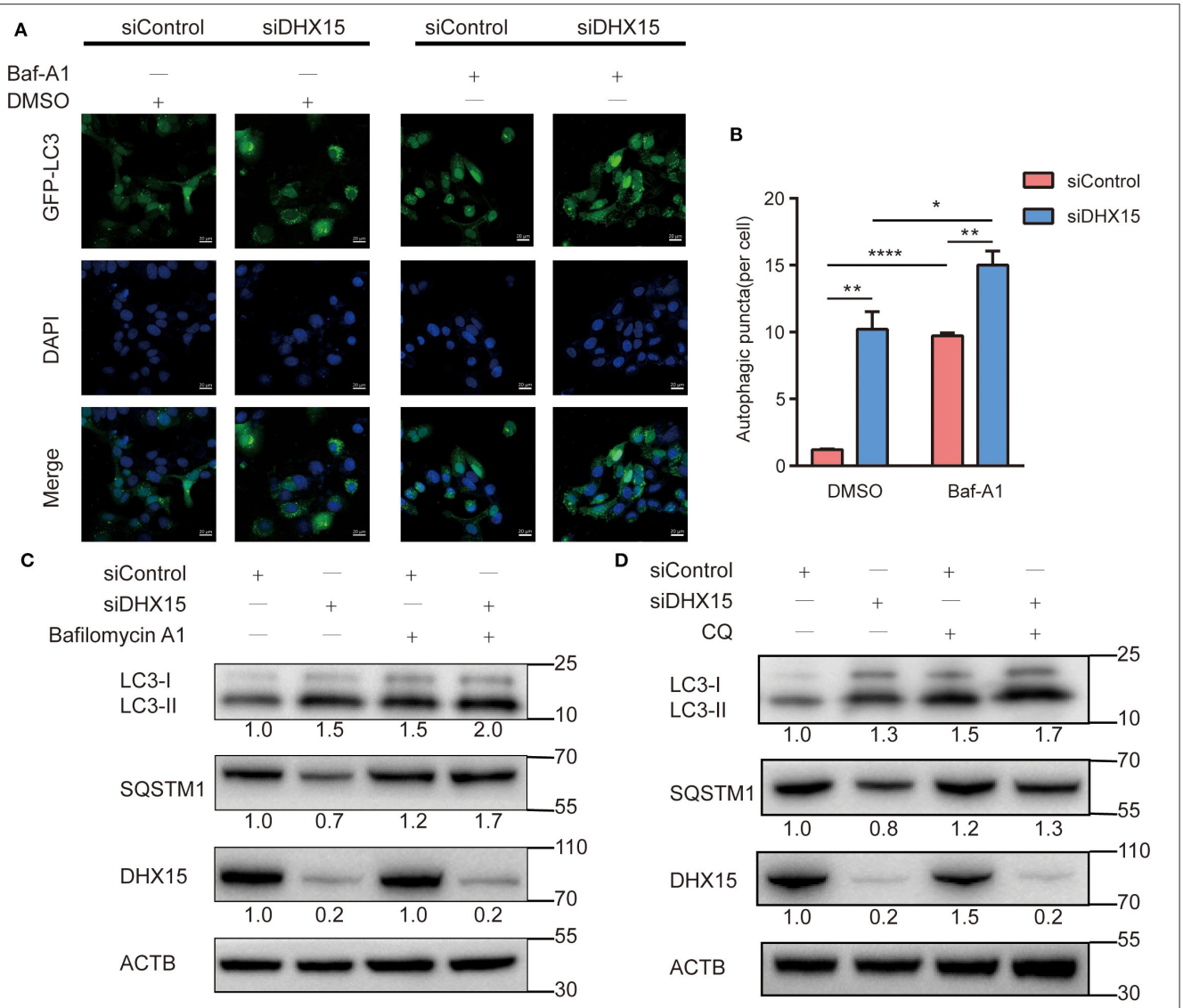

FIGURE 2 | Depletion of DHX15 stimulates autophagosome generation. **(A)** GFP-LC3 puncta were analyzed in Huh7 cells transiently cotransfected with DHX15 siRNA (siDHX15) or scrambled control siRNA (siControl) and GFP-LC3 plasmids with or without Baf-A1 (200 nM) treatment for 6 h. Cellular nuclei were counterstained with DAPI. Representative images were obtained at 600× magnification. Scale bars: 20 μm. **(B)** The number of GFP-LC3 puncta per cell was quantified for each group. The data are presented as the mean ± SEM. Unpaired Student's *t*-test ($n = 5$). $^{*}P < 0.05$, $^{**}P < 0.01$, $^{****}P < 0.0001$. **(C)** The expression of SQSTM1/p62 and LC3B-II in Huh7 cells transiently transfected with siDHX15 or siControl with or without Baf-A1 (200 nM) treatment for 6 h was measured by western blotting. $^{*}P < 0.05$. **(D)** The expression of SQSTM1/p62 and LC3B-II in Huh7 cells transiently transfected with siDHX15 or siControl with or without chloroquine diphosphate(CQ) (20 uM) treatment for 24 h were measured by western blotting.

results also show in chloroquine diphosphate(CQ) treatment (**Figure 2D** and **Supplementary Figure 2**). Collectively, these results indicate that knockdown of DHX15 augments the formation of autophagosomes but does not decrease autophagic degradation, revealing that DHX15 functions in an early step before autophagosome fusion.

DHX15 Regulates Autophagy in a Manner Associated With mTORC1 Activation

MTORC1 is a key upstream inhibitor of autophagy that balances autophagy and other cellular physiological processes, such as cell growth (30). Since DHX15 is also an inhibitor of autophagy, we hypothesized that mTORC1 and DHX15 work together to achieve autophagy regulation. To test this hypothesis, we investigated the phosphorylation statuses of RPS6KB/p70S6K, initiation factor 4E binding protein 1 (4EBP1) and ULK1, which are signaling molecules downstream of mTORC1, after endogenous DHX15 knockdown. We found that p70S6K and p4EBP1 protein levels dramatically declined when DHX15 was knocked down (**Figure 3A**). We further measured the level of ULK1 phosphorylation at residue Ser757, which negatively affects autophagy initiation by disrupting the interaction of AMPK and ULK1 mediated by mTORC1 (31). Consistent with the initial

results, our data showed that the level of ULK1 phosphorylation at Ser757 was decreased by DHX15 depletion (**Figure 3A**). Data quantification of western blots are shown in **Figure 3B** and representative western blots of three independent assays. Autophagy was induced upon Torin1 treatment or siDHX15 treatment (**Figure 3D** and **Supplementary Figure 3**).

Rapamycin is a classic inhibitor of mTOR, and previous research has shown that this inhibitor inhibits growth and angiogenesis in metastatic tumors by reducing VEGF production and blocking VEGF-induced endothelial cell signaling in a CT-26 cell-transplanted tumor model (32). We found that downregulation of DHX15 promoted degradation of both phosphorylation and dephosphorylation substrates of mTORC1 upon rapamycin treatment (**Figure 3C**). In addition, we also examined the autophagy level after siDHX15 and rapamycin treatment. The results showed that depletion of DHX15 promoted rapamycin-induced autophagy (**Supplementary Figure 3**).

These data indicate that DHX15 regulates autophagy involved in mTORC1 pathway. Therefore, DHX15 inhibits autophagy in a manner associated with mTORC1 activation.

DHX15 Inhibits the Proliferation of Hepatoma Cells in an Autophagy-Dependent Manner

RNA helicases have been demonstrated to play vital roles in the growth, invasion, and metastasis of HCC (33, 34) and can be used to closely evaluate the prognoses of HCC patients (35). In recent years, DHX15 has been identified as a crucial tumor related protein (18, 19, 28, 36). In addition, the expression status of DHX15 in HCC patients has been described (28). However, the molecular mechanism by which DHX15 regulates HCC is elusive. To determine whether DHX15 is related to HCC, we knocked down DHX15, which markedly increased the growth of HepG2 cells (**Figure 4A**). Consistent with this finding, DHX15 knockdown also increased the number of puncta positive for Ki67 (a biomarker of cell proliferation) in HepG2 cells (**Figure 4B**). To further confirm this effect, DHX15 plasmid DNA was transfected into HepG2 cells, and the data showed that overexpression of DHX15 attenuated the proliferation and colony formation of HepG2 cells (**Figures 4C,D**).

Some studies have demonstrated that autophagy levels are low in HCC (37, 38). However, recent studies have also revealed that autophagy plays contrasting roles in HCC and hepatoma cells (10, 39, 40). We found that DHX15 is a novel suppressor of autophagy. To determine whether autophagy participates in the process by which DHX15 regulates HCC, we treated cells with Baf-A1 (a late-stage autophagy inhibitor) and 3-methyladenine (3-MA, an early-stage autophagy inhibitor). Depletion of DHX15 promoted HCC cell proliferation, but this effect disappeared after treatment with the inhibitors (**Figures 4A,B**). In addition, we used **Supplementary Figure 5** verified the ATG5 siRNA is effective in HepG2 cells to further verify this effect and obtained a consistent result (**Figures 4A,B**). Moreover, overexpression of DHX15 inhibited HepG2 cell growth; this effect was also inhibited by autophagy inhibitor treatment and ATG5 siRNA transfection (**Figures 4C,D**). In addition, we also detect the expression of DHX15 in human liver cancer tissues. The data showed that the levels of DHX15 (mainly distributed in the cytoplasm) were higher in adjacent normal tissues than in tumor tissues (15 of the 20 sample pairs, **Figures 5A,B**). These findings indicate that DHX15 inhibits the proliferation of HCC cells in an autophagy-dependent manner.

DISCUSSION

In the present study, we found, for the first time, that the RNA helicase DHX15 is a negative regulator of autophagy and that MTORC1 is involved in the process by which DHX15 regulates autophagy. Moreover, we found that DHX15 silencing prominently increases HCC cell proliferation and that this effect can be suppressed by autophagy inhibition.

The DEAD/H box helicase family includes various members, and emerging studies have reported the mechanisms of DEAD/H box helicases in autophagy. For example, a recent study demonstrated that DDX5 positively regulates autophagy by interacting with p62 to suppress HCC tumorigenesis (41). The authors also found that DDX5 disrupts the binding of p62 and TRAF6 (a tumor-related protein) and inhibits the activation of mTORC1 (41). Another study has revealed that DDX6 negatively regulates autophagy (6). DDX6 has been shown to bind the decapping enzyme Dcp2, leading to the degradation of autophagic gene mRNA (6). In this study, DHX15 suppressed autophagy in a manner associated with the activation of mTORC1; this mechanism is different from the mechanism by which DDX5 regulates autophagy. We also found that DHX15 did not influence autophagic gene mRNA levels. Consistent with previous work (6), our study revealed that downregulation of DDX6 in HepG2 cells enhanced the mRNA expression of autophagy genes (**Supplementary Figure 4**); however, the mRNA expression profile in our study differed from that in the previous work, possibly because of the different species and cell lines used. These results indicate that DHX15 inhibits autophagy in other ways, such as by regulating other mRNA molecules or by interacting with other proteins such as G-patch proteins. Therefore, we have identified DHX15 as a novel inhibitor of autophagy that associates with mTORC1 and does not affect the mRNA expression of autophagy genes.

Autophagy dysfunction leads to many human pathologies, such as neurodegenerative diseases (8), liver injury (42) and cancer (37). Basal autophagy maintains genomic stability, protects the body from chronic diseases, and inhibits excessive inflammation under physiological conditions (4). Under pathological conditions, however, autophagy helps cancer cells resist host immune attack or other stressful conditions (9–11). Therefore, precise autophagy regulation is crucial. Autophagy inhibition, which takes place under many conditions, such as viral infection (43), post-prandial lipid assimilation in hepatic cells (44), and neurodegenerative diseases and cancer (45), is an essential part of autophagy regulation. In this study, DHX15 was identified as an autophagy suppressor. MTORC1 is the most important upstream suppressor of autophagy, and we found that

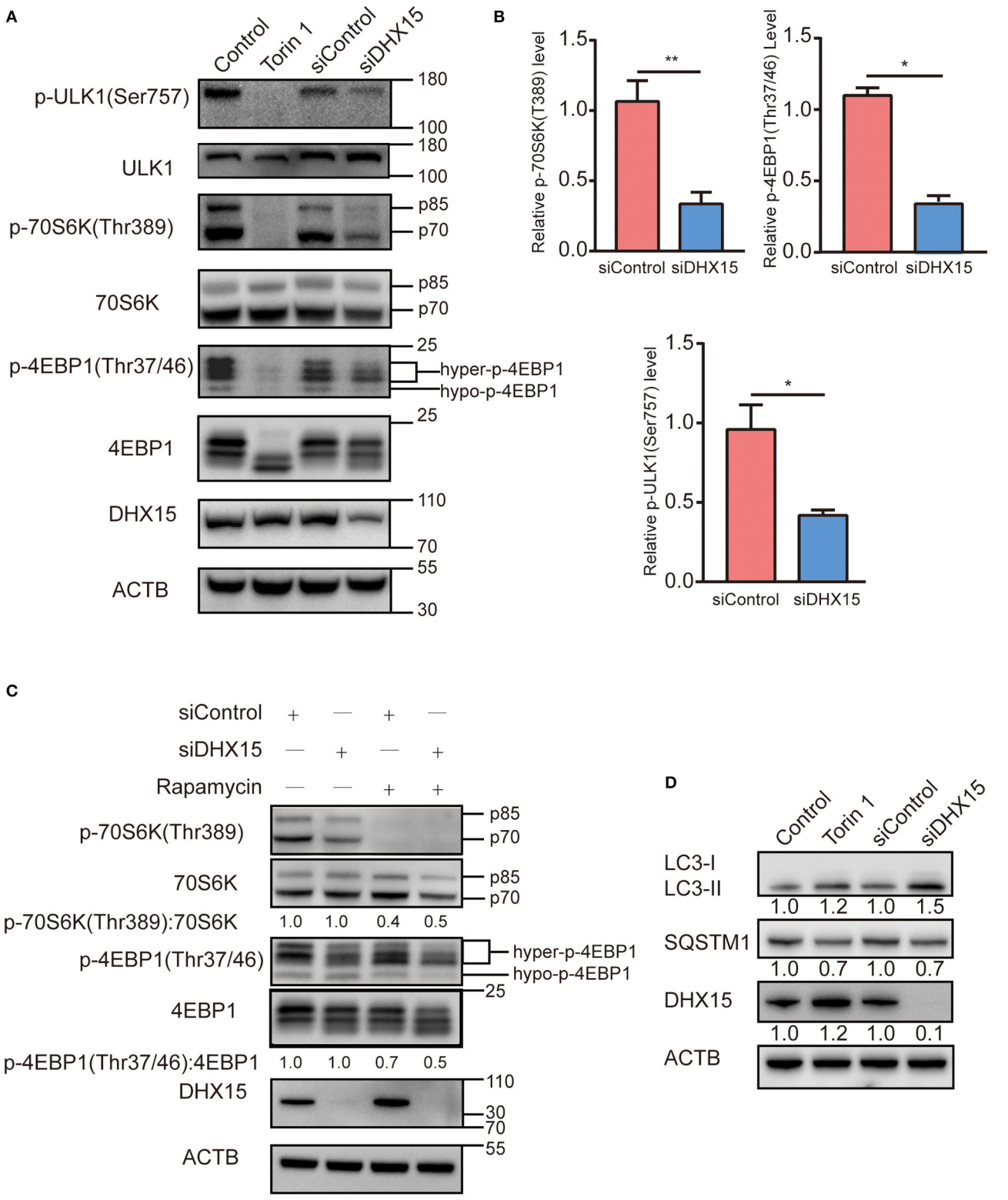

FIGURE 3 | Depletion of DHX15 induces autophagy associated with suppressing mTORC1. **(A)** The levels of phosphorylated substrates of the mTORC1 complex in HepG2 cells transiently transfected with DHX15 siRNA (siDHX15) or scrambled control siRNA (siControl) were analyzed by western blotting. Treatment with Torin 1 (250 nM) for 6 h was used as a positive control. Treatment with DMSO was used as a negative control. β-Actin was used as a loading control. $^{*}P < 0.05$. **(B)** Data are representative western blots of three independent assays. $^{*}P < 0.05$, $^{**}P < 0.001$ **(C)** HepG2 cells transiently transfected with siDHX15 or siControl were treated with

(Continued)

FIGURE 3 | 200 nM rapamycin for 2 h and harvested for western blotting. Treatment with DMSO was used as a negative control. β-Actin was used as a loading control. *$P < 0.05$. **(D)** LC3 and SQSTM1/p62 levels in HepG2 cells transiently transfected with siDHX15 or siControl were measured by western blotting. Treatment with Torin 1 (250 nM) for 6 h was used as a positive control. *$P < 0.05$.

DHX15 negatively regulates autophagy in a manner associated with mTORC1 activation (**Figure 3**). More importantly, we found that depletion of DHX15 increased hepatoma cell proliferation in a manner dependent on the DHX15-mediated regulation of autophagy. These results indicate the existence of a relationship between DHX15 and autophagy inhibition that is related to the antitumour effect of DHX15.

Autophagy is a key process in the maintenance of cellular homeostasis. Factors that disrupt autophagy balance can lead to many human diseases, such as cancer. However, autophagy is a double-edged sword, and its role in cancer is complicated (46). Autophagy participates in many types of cancers but exerts completely opposite effects on tumor progression (47, 48). The dynamic and complex conditions under which cancer cells survive are determined by the microenvironment. Although much about the relationship between autophagy and cancer remains unknown, it is clear that restoration of aberrant autophagy is a new target for disease treatment. In general, DHX15 is thought to regulate RNA metabolism. We found that depletion of DHX15 markedly induced autophagy, which suggests that DHX15 plays an essential role in maintaining the homeostasis of the cellular environment that is independent of its classical function in regulating RNA metabolism. We also detected the expression of DHX15 in human liver tissues (**Figure 5A**) which suggested DHX15 may be a vital factor in liver cancer. Overall, this study has identified a non-classic function of the RNA helicase DHX15 as a suppressor of autophagy and liver cancer, and the findings suggest that DHX15 may be a potential therapeutic element for liver cancer and autophagy-related diseases. And the mechanism between DHX15 and autophagy maybe the potential prognostic indicator in cancer therapy. In contrast, DHX15 may be a new clinical indicator of liver cancer progression and outcome. However, the precise mechanism of the antitumour effect of DHX15 is not further discussed in this study. Moreover, identification of the precise target by which DHX15 regulates autophagy, which may contribute to further exploration of the role of DHX15 in liver cancer, remains to be identified. In addition, although we have revealed the role of DHX15 in some human liver cancer tissues, an examination of more samples is required to fully demonstrate its role, and the clinic outcome of liver cancer patients should be examined.

MATERIALS AND METHODS

Cell Culture and Treatments

Hepatocyte lines (Huh7 and HepG2) and HEK293 cells with stable LC3-GFP expression were cultured in Dulbecco's modified Eagle's medium (DMEM) with 10% fetal bovine serum (FBS), and L02 cells were grown in RPMI 1640 medium with 10% FBS at 37°C in 5% CO_2. 293-GFP-LC3 cell line and LC3-GFP plasmid were gifts from Professor Liu Wei in Zhejiang University (49). Transient transfection for knockdown was carried out with Lipofectamine RNAiMAX (Invitrogen, 13778-015) according to the manufacturer's instructions. Transient transfection for overexpression was carried out with Lip3000 (Invitrogen, L3000015).

Reagents, Antibodies, and Plasmids

Baf-A1 (s1413), Torin 1 (s2827), 3-MA (s2767), and Chloroquine diphosphate(CQ, s4157)were purchased from Selleck. The following antibodies were used: anti-LC3 (Sigma, L7645), anti-ACTB/β-actin (Cell Signaling, A5316), anti-phospho-p70 S6 kinase (Thr389) (Cell Signaling, 9234), anti-phospho-4E-BP1 (Thr37/46) (Cell Signaling, 2855), anti-SQSTM1/p62 (MBL PM045), anti-DHX15 (Abcam, ab70454), anti-Ki67 (Cell Signaling, 9449), anti-ULK1 (Cell Signaling, 8054), anti-phospho-ULK1(Ser757) (Cell Signaling, 14202), anti -p70 S6 kinase (Cell Signaling, 2708), anti-4E-BP1 (Cell Signaling, 9452) and CoraLite488–conjugated Affinipure goat anti-mouse IgG (H+L) (Proteintech, SA00013-1). DHX15-Flag was created in the CV702 by standard subcloning. DHX15 plasmid and its negative control were purchased from Genechem (Shanghai, China).

Protein Extraction and Western Blotting

Ice-cold phosphate-buffered saline (PBS) was used to wash cells three times, and the total proteins were then extracted using extraction reagent (Thermo Fisher, 78501) according to the manufacturer's protocol. After quantification using a BCA Protein Assay Kit (Thermo Fisher, 23227), samples containing equal amounts of protein were loaded onto gels and separated by sodium dodecyl sulfate-polyacrylamide gel electrophoresis (SDS-PAGE). Afterwards, the proteins were transferred to 0.2 μm PVDF membranes and blocked in TBS-T [150 mM NaCl, 10 mM Tris-HCl (pH 7.5), and 0.1% Tween 20] containing 5% bovine serum albumin (BSA) or skim milk powder for 1 h. Then, the corresponding primary antibodies were added, and the membranes were incubated overnight at 4°C. The membranes were incubated with secondary antibodies for 1 h at room temperature. Data are representative western blots of three independent assays.

RNA Interference

All siRNAs used in this study were purchased from RiBo Biology (Guangzhou, China). The following siRNAs were used: siDHX15 (stB0006121A), 5′-GGGCATTACTTAACTGTGA-3′;

siATG5 (siG10726164423), 5′-GTGAGATATGGTTTGAATA-3″; and a negative control siRNA. Cells were transfected with siRNAs (at a final concentration of 100 nM) using Lipofectamine RNAiMAX reagent. After 48 or 72 h, the cells were analyzed for target expression, autophagy, DHX15 expression, and DHX15 knockdown-mediated changes in cell proliferation.

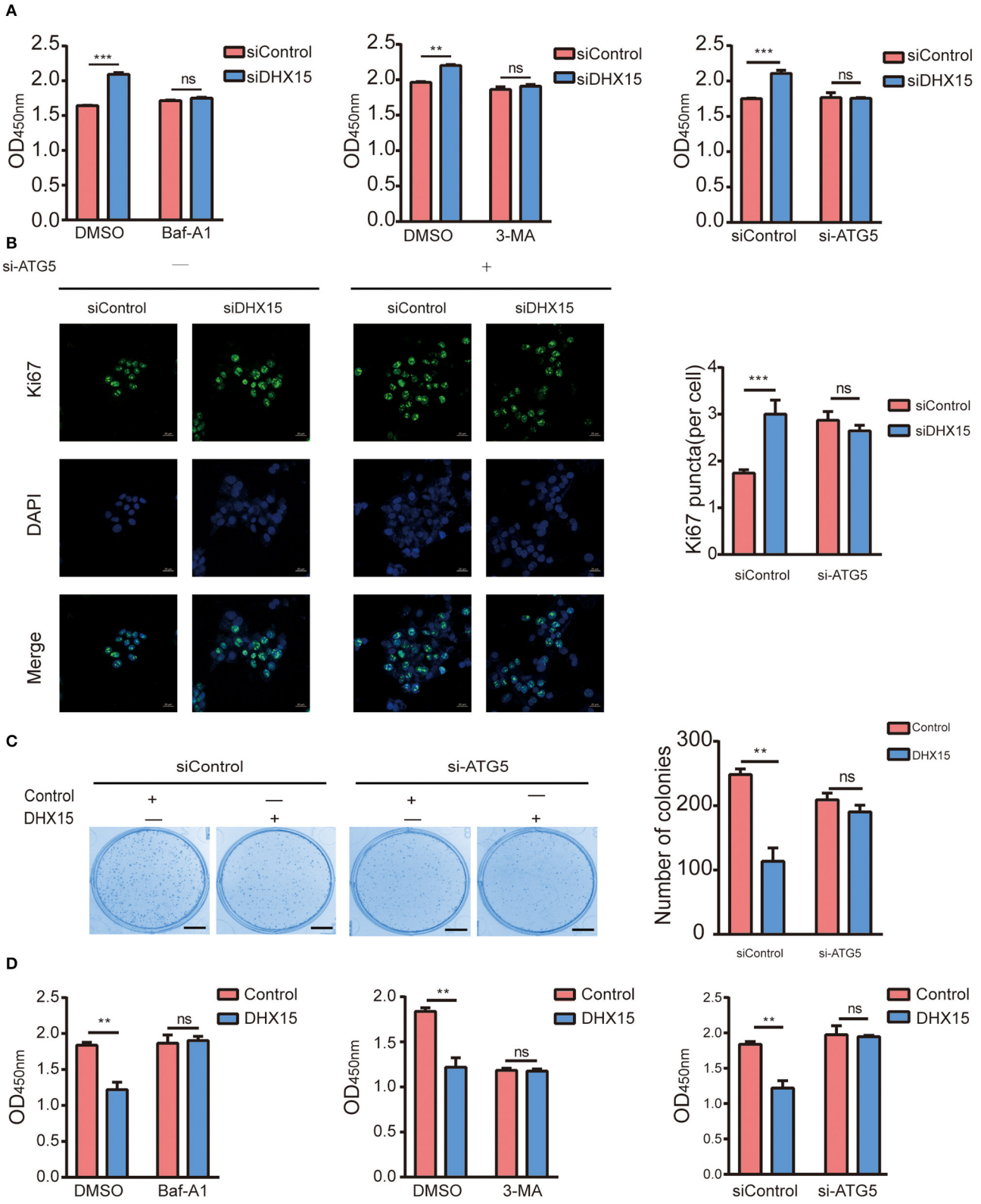

FIGURE 4 | DHX15 suppresses the growth of HCC cells by inhibiting autophagy. **(A)** The relative viability of DHX15-knockdown cells with or without autophagy inhibition was measured by CCK-8 assay. The data are presented as the mean ± SEM ($n = 3$). ***$P < 0.001$. **(B)** The Ki67-positive puncta in DHX15-knockdown HepG2 cells with or without ATG5 siRNA (si-ATG5) treatment were analyzed by immunofluorescence. Cellular nuclei were counterstained with DAPI. Representative images were obtained at 600× magnification. Scale bars: 20 μm. The graph shows the results of statistical analysis of the numbers of Ki67-positive puncta per cell.

(Continued)

FIGURE 4 | The data are presented as the mean ± SEM ($n = 10$). ***$P < 0.001$. **(C)** After HepG2 cells had been cotransfected with or without DHX15 and si-ATG5 and incubated for 12 days, colonies were stained with Coomassie brilliant blue and counted (scale bar: 5 mm). The data are the mean ± SEM ($n = 3$). **$P < 0.01$. **(D)** The relative viability of cells overexpressing DHX15 with or without autophagy inhibition was measured by CCK-8 assay. The data are presented as the mean ± SEM ($n = 3$). **$P < 0.01$.

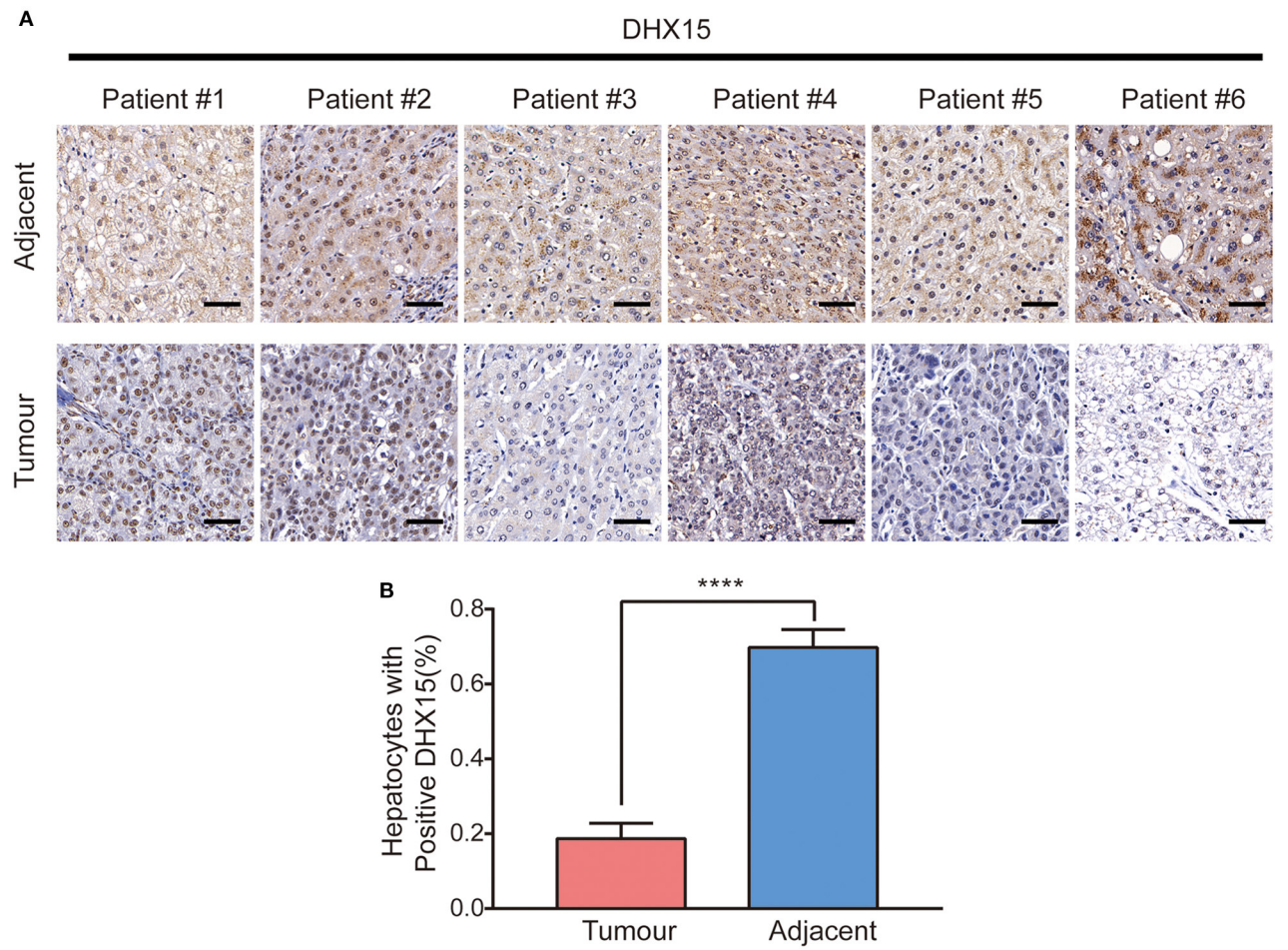

FIGURE 5 | Expression of DHX15 in human liver cancer tissues. **(A)** Expression of DHX15 was detected with immunohistologic staining in tumor tissues and adjacent non-tumor tissues of the representative liver cancer patients. Scale bars: 50 um. **(B)** Plots of percentage of DHX15 positive cells to total cells in human liver cancer tissues. The data are presented as the mean ± SEM. Unpaired Student's *t*-test ($n = 20$). ****$P < 0.0001$.

Confocal Microscopy

After 48 h of transfection, cells were washed with PBS three times. After treatment with 4% paraformaldehyde (PFA) for 15 min, the cells were washed with PBS three times. The cellular nuclei were counterstained with DAPI. A Carl Zeiss LSM 880 fluorescence microscope was used to capture images showing the cellular localization of LC3B puncta. All of the puncta were analyzed with ImageJ software. The numbers of fluorescent LC3B puncta were determined by counting in more than 100 cells in triplicate.

Transmission Electron Microscopy

After 48 h of siRNA transfection, L02 cells were fixed in 2.5% glutaraldehyde in 0.2 M HEPES (pH 7.4) and post-fixed in aqueous 1% OsO_4 followed by 2% uranyl acetate. After ethanol and propylene oxide dehydration and embedding in Polybed 812 resin, ultrathin (80 nm) sections were post-stained with 2% uranyl acetate followed by 0.3% lead citrate. Sections were imaged using an H-7650 transmission electron microscope (Hitachi Company) at 80 kV. For autophagic vacuole quantification, 10 micrographs at a primary magnification of 25,000× were obtained with systematic random sampling of each sample.

RNA Extraction and Expression Analysis

TRIzol reagent was used for RNA extraction following the manufacturer's instructions. Purified RNA was converted to cDNA using a reverse transcription kit (Takara), and quantitative PCR (qPCR) was performed on an ABI 7900 real-time PCR

system using FAST SYBR Master mix (all from Takara). GAPDH expression was used to normalize gene expression.

Autophagy-Related Treatments

For Torin 1 treatment, cells were cultured with 250 nM Torin 1 for 6 h. Baf-A1 at 200 nM was used to treat cells for 4 h. 3-MA at 5 mM was used to treat cells for 2 h.

Immunofluorescence

After 48 h of transfection, cells were washed with PBS three times. After 15 min of treatment with 4% PFA, the cells were washed with PBS three times for 5 min each. Then, the cells were permeabilized in 0.5% Triton X-100 for 20 min at room temperature. After blocking in 3% BSA for 30 min at room temperature, the cells were incubated with primary antibodies diluted in blocking buffer overnight at 4°C. The cells were then incubated with secondary antibodies diluted in blocking buffer at room temperature for 1 h in the dark. PBS was used to wash the cells three times for 5 min each. The nuclei were counterstained with DAPI. The stained cells were observed with an inverted fluorescence light microscope (Carl Zeiss LSM 880). The numbers of fluorescent Ki67-positive puncta were determined by counting in more than 100 cells in triplicate.

Cell Viability Assay

Cells were counted and seeded in 96-well plates with 100 μl of cell suspension per well. After transfection for 48 h, Cell Counting Kit-8 (CCK-8) solution was added to each well. The 96-well plates containing CCK-8 solution were incubated for 1–3 h. The absorbance (450 nm) of the samples was measured, and the relative cell viability was calculated.

Colony Formation Assay

HepG2 cells were seeded at a density of 1,000 cells/well in six-well plates. The cells were transfected with each siRNA and incubated in DMEM with 10% FBS at 37°C in 5% CO_2 for 12 days. After 15 min of treatment with 4% PFA, the cells were washed with PBS three times. Then, the colonies were stained with Coomassie brilliant blue for 35 min. Finally, the staining solution was washed away with distilled water. The total number of colonies was determined.

Human Samples

Human liver cancer tissues were taken from the First Affiliated Hospital, Zhejiang University School of Medicine. Twenty pairs of tumor liver tissues and their adjacent non-tumor tissues were collected from HCC patients after surgical resection. All the diagnoses of 20 patients were based on clinical and pathological examination. The clinicopathological characteristics of the 20 patients are summarized in **Supplementary Table 1**. All the human tissues were taken with written informed consent and with the approval of the Medical Ethical Committee of the First Affiliated Hospital, Zhejiang University School of Medicine.

Immunohistochemistry

In vivo DHX15 expression was detected by immunohistochemistry using 20 pairs of cancer tissues and adjacent normal-tissues (santa cruz, sc-271686). Immunohistochemistry was performed according to standard protocols, the sections were scanned, and the images were then digitalized. The integrated optical density of DHX15 was calculated using Image-J. The clinicopathological characteristics of the 20 patients are summarized in **Supplementary Table 1**.

Statistical Analysis

All measurements were performed at least in triplicate. The data are presented as the mean ± SEM or SD. Student's *t*-test was used to evaluate differences between groups. $P < 0.05$ indicated statistical significance.

DATA AVAILABILITY STATEMENT

The original contributions presented in the study are included in the article/**Supplementary Material**, further inquiries can be directed to the corresponding author/s.

ETHICS STATEMENT

The studies involving human participants were reviewed and approved by the Medical Ethical Committee of the First Affiliated Hospital, Zhejiang University School of Medicine. The patients provided their written informed consent to participate in this study.

AUTHOR CONTRIBUTIONS

MZha wrote the manuscript and prepared the figures. LY collected and analyzed the human samples. JY and RW amended the grammar of the manuscript. LZ provided some technical advice. ZY, MZhe, and ZC provided expert comments and edits. All authors read and approved the final manuscript.

FUNDING

This work was supported by the States S&T Projects of the 13th Five Year Plan (2018ZX10302206), the National Key Research and Development Program (2017YFA0503402), and Zhejiang Provincial Medicine and Health Science Fund (2015KYA031). Independent Project Fund of the State Key Laboratory for Diagnosis and Treatment of Infectious Disease.

ACKNOWLEDGMENTS

We appreciate the excellent experimental support from the Public Platform of Medical Research Center, Academy of Chinese Medical Science, Zhejiang Chinese Medical University.

SUPPLEMENTARY MATERIAL

The Supplementary Material for this article can be found online at: https://www.frontiersin.org/articles/10.3389/fmed.2020.591736/full#supplementary-material

REFERENCES

1. Wen X, Klionsky DJ. An overview of macroautophagy in yeast. *J Mol Biol.* (2016) 428 (9 Part A):1681–99. doi: 10.1016/j.jmb.2016.02.021
2. Yang Z, Klionsky DJ. Mammalian autophagy: core molecular machinery and signaling regulation. *Curr Opinion Cell Biol.* (2010) 22:124–31. doi: 10.1016/j.ceb.2009.11.014
3. Takamura A, Komatsu M, Hara T, Sakamoto A, Kishi C, Waguri S, et al. Autophagy-deficient mice develop multiple liver tumors. *Genes Dev.* (2011) 25:795–800. doi: 10.1101/gad.2016211
4. Guo JY, Xia B, White E. Autophagy-mediated tumor promotion. *Cell.* (2013) 155:1216–9. doi: 10.1016/j.cell.2013.11.019
5. Mizushima N, Levine B, Cuervo AM, Klionsky DJ. Autophagy fights disease through cellular self-digestion. *Nature.* (2008) 451:1069–75. doi: 10.1038/nature06639
6. Hu G, McQuiston T, Bernard A, Park YD, Qiu J, Vural A, et al. A conserved mechanism of TOR-dependent RCK-mediated mRNA degradation regulates autophagy. *Nat Cell Biol.* (2015) 17:930–42. doi: 10.1038/ncb3189
7. Levine B, Kroemer G. Autophagy in the pathogenesis of disease. *Cell.* (2008) 132:27–42. doi: 10.1016/j.cell.2007.12.018
8. Hara T, Nakamura K, Matsui M, Yamamoto A, Nakahara Y, Suzuki-Migishima R, et al. Suppression of basal autophagy in neural cells causes neurodegenerative disease in mice. *Nature.* (2006) 441:885–9. doi: 10.1038/nature04724
9. Kaminskyy VO, Piskunova T, Zborovskaya IB, Tchevkina EM, Zhivotovsky B. Suppression of basal autophagy reduces lung cancer cell proliferation and enhances caspase-dependent and -independent apoptosis by stimulating ROS formation. *Autophagy.* (2012) 8:1032–44. doi: 10.4161/auto.20123
10. Peng YF, Shi YH, Ding ZB, Ke AW, Gu CY, Hui B, et al. Autophagy inhibition suppresses pulmonary metastasis of HCC in mice via impairing anoikis resistance and colonization of HCC cells. *Autophagy.* (2013) 9:2056–68. doi: 10.4161/auto.26398
11. Zhan Z, Xie X, Cao H, Zhou X, Zhang XD, Fan H, et al. Autophagy facilitates TLR4- and TLR3-triggered migration and invasion of lung cancer cells through the promotion of TRAF6 ubiquitination. *Autophagy.* (2014) 10:257–68. doi: 10.4161/auto.27162
12. Arenas JE, Abelson JN. Prp43: an RNA helicase-like factor involved in spliceosome disassembly. *Proc Natl Acad Soc USA.* (1997). 94:11798–802. doi: 10.1073/pnas.94.22.11798
13. Combs DJ, Nagel RJ, Ares M, Stevens SW. Prp43p is a DEAH-box spliceosome disassembly factor essential for ribosome biogenesis. *Mol Cell Biol.* (2006) 26:523–34. doi: 10.1128/MCB.26.2.523-534.2006
14. Tanaka N, Aronova A, Schwer B. Ntr1 activates the Prp43 helicase to trigger release of lariat-intron from the spliceosome. *Genes Dev.* (2007) 21:2312–25. doi: 10.1101/gad.1580507
15. Koodathingal P, Novak T, Piccirilli JA, Staley JP. The DEAH box ATPases Prp16 and Prp43 cooperate to proofread 5' splice site cleavage during pre-mRNA splicing. *Mol Cell.* (2010) 39:385–95. doi: 10.1016/j.molcel.2010.07.014
16. Walbott H, Mouffok S, Capeyrou R, Lebaron S, Humbert O, van Tilbeurgh H, et al. Prp43p contains a processive helicase structural architecture with a specific regulatory domain. *EMBO J.* (2010) 29:2194–204. doi: 10.1038/emboj.2010.102
17. Fourmann JB, Schmitzova J, Christian H, Urlaub H, Ficner R, Boon KL, et al. Dissection of the factor requirements for spliceosome disassembly and the elucidation of its dissociation products using a purified splicing system. *Genes Dev.* (2013) 27:413–28. doi: 10.1101/gad.207779.112
18. Ito S, Koso H, Sakamoto K, Watanabe S. RNA helicase DHX15 acts as a tumour suppressor in glioma. *Br J Cancer.* (2017) 117:1349–59. doi: 10.1038/bjc.2017.273
19. Jing Y, Nguyen MM, Wang D, Pascal LE, Guo W, Xu Y, et al. DHX15 promotes prostate cancer progression by stimulating Siah2-mediated ubiquitination of androgen receptor. *Oncogene.* (2018) 37:638–50. doi: 10.1038/onc.2017.371
20. Lin ML, Fukukawa C, Park JH, Naito K, Kijima K, Shimo A, et al. Involvement of G-patch domain containing 2 overexpression in breast carcinogenesis. *Cancer Sci.* (2009) 100:1443–50. doi: 10.1111/j.1349-7006.2009.01185.x
21. Studer MK, Ivanovic L, Weber ME, Marti S, Jonas S. Structural basis for DEAH-helicase activation by G-patch proteins. *Proc Natl Acad Sci USA.* (2020) 117:7159–70. doi: 10.1073/pnas.1913880117
22. Hamann F, Schmitt A, Favretto F, Hofele R, Neumann P, Xiang S, et al. Structural analysis of the intrinsically disordered splicing factor Spp2 and its binding to the DEAH-box ATPase Prp2. *Proc Natl Acad Sci USA.* (2020) 117:2948–56. doi: 10.1073/pnas.1907960117
23. Robert-Paganin J, Rety S, Leulliot N. Regulation of DEAH/RHA helicases by G-patch proteins. *Biomed Res Int.* (2015) 2015:931857. doi: 10.1155/2015/931857
24. Farrar JE, Schuback HL, Ries RE, Wai D, Hampton OA, Trevino LR, et al. Genomic profiling of pediatric acute myeloid leukemia reveals a changing mutational landscape from disease diagnosis to relapse. *Cancer Res.* (2016) 76:2197–205. doi: 10.1158/0008-5472.CAN-15-1015
25. Chen XL, Cai YH, Liu Q, Pan LL, Shi SL, Liu XL, et al. ETS1 and SP1 drive DHX15 expression in acute lymphoblastic leukaemia. *J Cell Mol Med.* (2018) 22:2612–21. doi: 10.1111/jcmm.13525
26. Wang P, Zhu S, Yang L, Cui S, Pan W, Jackson R, et al. Nlrp6 regulates intestinal antiviral innate immunity. *Science.* (2015) 350:826–30. doi: 10.1126/science.aab3145
27. Mosallanejad K, Sekine Y, Ishikura-Kinoshita S, Kumagai K, Nagano T, Matsuzawa A, et al. The DEAH-box RNA helicase DHX15 activates NF-kappaB and MAPK signaling downstream of MAVS during antiviral responses. *Sci Signal.* (2014) 7:ra40. doi: 10.1126/scisignal.2004841
28. Xie C, Liao H, Zhang C, Zhang S. Overexpression and clinical relevance of the RNA helicase DHX15 in hepatocellular carcinoma. *Hum Pathol.* (2019) 84:213–20. doi: 10.1016/j.humpath.2018.10.006
29. Glick D, Barth S, Macleod KF. Autophagy: cellular and molecular mechanisms. *J Pathol.* (2010) 221:3–12. doi: 10.1002/path.2697
30. Jung CH, Ro SH, Cao J, Otto NM, Kim DH. mTOR regulation of autophagy. *FEBS Lett.* (2010) 584:1287–95. doi: 10.1016/j.febslet.2010.01.017
31. Kim J, Kundu M, Viollet B, Guan KL. AMPK and mTOR regulate autophagy through direct phosphorylation of Ulk1. *Nat Cell Biol.* (2011) 13:132–41. doi: 10.1038/ncb2152
32. Kenerson HL, Aicher LD, True LD, Yeung RS. Activated mammalian target of rapamycin pathway in the pathogenesis of tuberous sclerosis complex renal tumors. *Cancer Res.* (2002) 62:5645–50.
33. Zhang T, Ma Z, Liu L, Sun J, Tang H, Zhang B, et al. DDX39 promotes hepatocellular carcinoma growth and metastasis through activating Wnt/beta-catenin pathway. *Cell Death Dis.* (2018) 9:675. doi: 10.1038/s41419-018-0591-0
34. Chang PC, Chi CW, Chau GY, Li FY, Tsai YH, Wu JC, et al. DDX3, a DEAD box RNA helicase, is deregulated in hepatitis virus-associated hepatocellular carcinoma and is involved in cell growth control. *Oncogene.* (2006) 25:1991–2003. doi: 10.1038/sj.onc.1209239
35. Hou J, Zhou Y, Zheng Y, Fan J, Zhou W, Ng IOL, et al. Hepatic RIG-I predicts survival and interferon-α therapeutic response in hepatocellular carcinoma. *Cancer cell.* (2014) 25:49–63. doi: 10.1016/j.ccr.2013.11.011
36. Niu Z, Jin W, Zhang L, Li X. Tumor suppressor RBM5 directly interacts with the DExD/H-box protein DHX15 and stimulates its helicase activity. *FEBS Lett.* (2012) 586:977–83. doi: 10.1016/j.febslet.2012.02.052
37. Rautou PE, Mansouri A, Lebrec D, Durand F, Valla D, Moreau R. Autophagy in liver diseases. *J Hepatol.* (2010) 53:1123–34. doi: 10.1016/j.jhep.2010.07.006
38. Mathew R, Karp CM, Beaudoin B, Vuong N, Chen G, Chen HY, et al. Autophagy suppresses tumorigenesis through elimination of p62. *Cell.* (2009) 137:1062–75. doi: 10.1016/j.cell.2009.03.048
39. Liu H, Ma Y, He HW, Zhao WL, Shao RG. SPHK1 (sphingosine kinase 1) induces epithelial-mesenchymal transition by promoting the autophagy-linked lysosomal degradation of CDH1/E-cadherin in hepatoma cells. *Autophagy.* (2017) 13:900–13. doi: 10.1080/15548627.2017.1291479
40. Luo T, Fu J, Xu A, Su B, Ren Y, Li N, et al. PSMD10/gankyrin induces autophagy to promote tumor progression through cytoplasmic interaction with ATG7 and nuclear transactivation of ATG7 expression. *Autophagy.* (2016) 12:1355–71. doi: 10.1080/15548627.2015.1034405
41. Zhang H, Zhang Y, Zhu X, Chen C, Zhang C, Xia Y, et al. DEAD box protein 5 inhibits liver tumorigenesis by stimulating autophagy via interaction with p62/SQSTM1. *Hepatology.* (2019) 69:1046–63. doi: 10.1002/hep.30300
42. Wang K. Autophagy and apoptosis in liver injury. *Cell Cycle.* (2015) 14:1631–42. doi: 10.1080/15384101.2015.1038685

43. Chen D, Feng C, Tian X, Zheng N, Wu Z. Promyelocytic leukemia restricts enterovirus 71 replication by inhibiting autophagy. *Front Immunol.* (2018) 9:1268. doi: 10.3389/fimmu.2018.01268
44. Byun S, Kim YC, Zhang Y, Kong B, Guo G, Sadoshima J, et al. A postprandial FGF19-SHP-LSD1 regulatory axis mediates epigenetic repression of hepatic autophagy. *EMBO J.* (2017) 36:1755–69. doi: 10.15252/embj.201695500
45. Goiran T, Duplan E, Rouland L, El Manaa W, Lauritzen I, Dunys J, et al. Nuclear p53-mediated repression of autophagy involves PINK1 transcriptional down-regulation. *Cell Death Differ.* (2018) 25:873–84. doi: 10.1038/s41418-017-0016-0
46. White E, DiPaola RS. The double-edged sword of autophagy modulation in cancer. *Clin Cancer Res.* (2009) 15:5308–16. doi: 10.1158/1078-0432.CCR-07-5023
47. Kenific CM, Debnath J. Cellular and metabolic functions for autophagy in cancer cells. *Trends Cell Biol.* (2015) 25:37–45. doi: 10.1016/j.tcb.2014.09.001
48. Ueno T, Komatsu M. Autophagy in the liver: functions in health and disease. *Nat Rev Gastroenterol Hepatol.* (2017) 14:170–84. doi: 10.1038/nrgastro.2016.185
49. Huang R, Xu Y, Wan W, Shou X, Qian J, You Z, et al. Deacetylation of nuclear LC3 drives autophagy initiation under starvation. *Mol Cell.* (2015) 57:456–66. doi: 10.1016/j.molcel.2014.12.013

Conflict of Interest: The authors declare that the research was conducted in the absence of any commercial or financial relationships that could be construed as a potential conflict of interest.

frontiers in Medicine

ORIGINAL RESEARCH
published: 08 March 2021
doi: 10.3389/fmed.2021.626948

Circular RNA Microarray Analyses in Hepatic Ischemia-Reperfusion Injury With Ischemic Preconditioning Prevention

Xinyao Tian[1,2†], *Yan Hu*[3†], *Yuanxing Liu*[1], *Zhe Yang*[4], *Haiyang Xie*[2*], *Lin Zhou*[2*] and *Shusen Zheng*[1,2,4*]

[1] Division of Hepatobiliary and Pancreatic Surgery, Department of Surgery, The First Affiliated Hospital, Zhejiang University School of Medicine, Hangzhou, China, [2] Key Laboratory of Combined Multi-organ Transplantation, National Health Commission of PRC, Hangzhou, China, [3] Department of Pharmacy, Second Affiliated Hospital of Dalian Medical University, Dalian, China, [4] Department of Hepatobiliary and Pancreatic Surgery, Department of Liver Transplantation, Shulan (Hangzhou) Hospital, Hangzhou, China

OPEN ACCESS

Edited by:
Chao Yan,
Xuzhou Medical University, China

Reviewed by:
Hakan Akin,
Marmara University, Turkey
Roberto Gramignoli,
Karolinska Institutet (KI), Sweden

***Correspondence:**
Shusen Zheng
shusenzheng@zju.edu.cn
Lin Zhou
linzhou19@163.com
Haiyang Xie
xiehy@zju.edu.cn

†These authors have contributed equally to this work

Specialty section:
This article was submitted to Gastroenterology, a section of the journal Frontiers in Medicine

Received: 07 November 2020
Accepted: 25 January 2021
Published: 08 March 2021

Citation:
Tian X, Hu Y, Liu Y, Yang Z, Xie H, Zhou L and Zheng S (2021) Circular RNA Microarray Analyses in Hepatic Ischemia-Reperfusion Injury With Ischemic Preconditioning Prevention. Front. Med. 8:626948. doi: 10.3389/fmed.2021.626948

Ischemic preconditioning (IPC) represents an effective intervention to relieve hepatic ischemia-reperfusion injury (IRI). Systematic detection of circRNA expression revealing the protection effect of IPC still remains to be elucidated. Here, we applied a microarray to detect circRNA and mRNA expression in ischemic liver with and without IPC (n = 3 in each group). Compared with the sham group, there were 39 circRNAs and 432 mRNAs increased and 38 circRNAs and 254 mRNAs decreased (fold change $\geq$1.5, $P < 0.05$) in the group of hepatic IRI. As the result of IPC intervention, 43 circRNAs and 64 mRNAs were increased, and 7 circRNAs and 31 mRNAs were decreased in the IPC group when compared with IRI. We then identified circRNA_017753 as the most possible target that may closely relate to IPC protective signaling and predicted Jade1 as the target related to circRNA_017753. Three possible circRNA–miRNA–mRNA axes were constructed that may play a vital role in protective mechanisms in IPC. The study for the first time systematically detects the dysregulated circRNAs and mRNAs in response to hepatic IRI and IPC intervention. Our profile and bioinformatic analysis provide numerous novel clues to understanding the pathophysiologic mechanism of IPC protection against hepatic IRI.

Keywords: circular RNA, ischemia-reperfusion injury, ischemic preconditioning, microarray analyses, high-throughput sequencing

INTRODUCTION

Hepatic ischemia-reperfusion injury (IRI) occurs in clinical circumstances, including hepatic resection, transplantation, liver trauma, or septic shock (1). The reperfusion aggravates hepatic injury after ischemia. Concerning mechanisms involve microcirculatory failure, inflammatory cytokine release, and reactive oxygen species accumulation (2, 3). Especially in the surgical procedures of hepatic resections and liver transplantation, IRI not only contributes to organ damage, but also reduces the long-term survival rates. Therefore, strategies to reduce hepatic IRI and improve patient outcomes is clinically important at any point.

Ischemic preconditioning (IPC) refers to an intrinsic procedure in the form of repeated short episodes of ischemia that increase the resistance of organs against IRI. This powerful intervention for protection against IRI was first reported in 1986 by Murry et al. (4). Though, today, the surgical techniques and clinical conditions improve rapidly concerning the intervention of IPC, the precise molecular mechanisms behind IRI and the protection effect of IPC still remain an important problem. Moreover, recent studies comparing different protective methods of IRI have demonstrated variable protective mechanisms in IPC and ischemic postconditioning (IPostC) (5, 6). The mechanism of comparative and collaborative research on IPC and IPostC are of great significance in the research on IRI.

Nowadays, high-throughput RNA sequencing and microarray of gene files have been widely applied among different species and diseases. Such transcriptome research can not only testify to gene functions and structures comprehensively, but also disclose the specific pathophysiologic mechanism underlying disease. However, a majority of the existing research remains limited to the coding RNA. On its rising slope, the quantity and quality of research on ncRNAs remains insufficient. Circular RNAs (circRNAs), the novel type of endogenous ncRNAs, has widely attracted scientists' attention lately (7). Compared with linear RNAs, the structure of covalently closed loops determines the stability of circRNAs by providing resistance to the exonuclease (8). With the development of this technique, an increasing amount of research has revealed the features of a majority of circRNAs in mammalian cells. They are endogenous, conserved, stable, and abundant, making them ideal therapeutic targets or potential biomarkers for the future (9–12).

A previous study applying microRNA microarrays has detected several miRNAs with significant expressive changes upon hepatic IPC following IRI (13). Moreover, a recent study conducted by Ye Z et al. investigated differentially expressed cirRNAs in liver IRI (14). Using a microarray, Zhang P et al. went further, comparing cirRNAs in hepatic IRI with or without IPostC and regarded mmu_circRNA_005186 as having a potential protective role in IPostC (15). However, systematic detection of the dysregulated circRNAs and mRNAs in response to IPC intervention still remains to be elucidated. Here, we suppose that the expressive alteration of circRNAs may closely relate to the pathophysiologic mechanism of hepatic IRI and may contribute to IPC-mediated protection against hepatic IRI. Comprehensive application of microarray, quantitative real-time PCR (qRT-PCR), and a progressive analysis were applied to reveal the expressive changes of circRNAs in the model of hepatic IRI with or without IPC and to investigate the protective circRNAs related to hepatic IPC intervention. Our data may offer a new understanding of the mechanical basis of IPC and may provide a possible research target for prospective studies.

MATERIALS AND METHODS

Experimental Animals

C57BL/6 male mice were obtained for our study. Each mouse weighed from 18 to 22 g and was fostered in a temperature-constant room and nourished by a standard chow pellet diet. Preoperative fasting was performed 12 h before the surgical procedure without water prohibition. The experiments were performed in accordance with the Institutional Animal Committee guidelines. All animal protocols were approved by the Institutional Ethics Committee.

Model Construction and Experimental Groups

The hepatic IRI model was established by hepatic artery occlusion with clips as described previously (16). Briefly, after being anesthetized by pentobarbital (50 mg/kg body weight) and laparotomy, the mouse's portal vein and hepatic artery were isolated and temporarily clipped by atraumatic microvascular clip. After 1 h of ischemia to 70% of the liver, the vascular clip was wiped off to allow 6 h hepatic reperfusion. The ischemia extent was assessed by pale color of liver or pulselessness. Also, the recovery of the pale color and the pulse were considered to confirm valid hepatic reperfusion.

Three groups of the mouse model were constructed ($n = 8$ in each group): (1) sham group: sham model underwent portal vein and hepatic artery isolation with no occlusion; (2) IRI group: IRI model underwent IRI surgery without IPC; (3) IPC group: IPC was induced by 10 min of ischemia and 10 min of reperfusion before the intervention of IRI as reported previously (17). All the mice were sacrificed, and blood and organ samples were obtained at the end.

Histological Analysis

To achieve hepatic injury, we collected hepatic samples from the different groups of mice and embedded them in paraffin. Then, 5 μm thickness consecutive sections were stained separately with hematoxylin and eosin (H&E), immunohistochemistry of F4/80, and Ly6G + and evaluated by microscopy.

Analyses of Hepatic Injury and Cytokine Levels

Serum levels of alanine aminotransferase (ALT) and aspartate aminotransferase (AST) levels were tested using assay kits following the manufacturer's instructions (Nanjing Jiancheng). The levels of interleukin (IL)-6 and tumor necrosis factor (TNF)-α were measured using immunosorbent assay kits from the ENGTON Bio-engineering Limited Company (Shanghai, China) following the kit instructions.

RNA Extraction

Tissue RNA was extracted from each hepatic sample using Trizol (Invitrogen, Carlsbad, CA, USA) following the instructions. The concentration and purity of RNA were accessed by a NanoDrop 2000 spectrophotometer (Thermo Scientific, MA, USA). Genomic DNA (gDNA) residual and RNA integrity were measured by denaturing agarose gel electrophoresis.

Labeling and Hybridization

We selected three samples randomly from each group for microarray studies. RNA labeling and hybridization were done following the Agilent One-Color Microarray-Based Gene Expression Analysis construction. The microarray hybridization

TABLE 1 | Primer sequences used for qRT-PCR analysis of circRNA and mRNA levels.

Name	Primer F (5′–3′)	Primer R (5′–3′)
mmu_circRNA_007095	CTATCTCTCAGAGGCAGGGG	TGGGTTTGAAGACAGCAACG
mmu_circRNA_017753	CGCAAGGTCACTGGAGGAAT	TCTTAACTGCCACACGATGC
mmu_circRNA_010415	AACTGGGCCGTGGCAATC	CACTGACACTCTTTCCCTCTGG
mmu_circRNA_000895	CTTGTCAGCCTCAGTGGGA	CTCAGAGGTCGTTTAGCTTGG
mmu_circRNA_001946	TCGGCGTTTTGACATTCAGG	GGAAGACCTTGGTACTGGCA
mmu_circRNA_027197	TGTTTGTGACCTCCCTCTCC	CAGAATCACGCCACACACTT
mmu_circRNA_010498	TGATTTCTTCTGTTATGGTGGCG	TGCATAGTCGTTGAAGAAGGC
Gclc	AGCCCTACGGAGGAACGA	CCTCTGGGTTGGGTCTGTG
Krt18	CTTGCCGCCGATGACTTT	TGCAGCCTTGTGATGTTGG
Hacl1	TCCCTCCAATGTGCCTCTT	CCTGCCTCAGCGAGTGTTG
Stim1	GCTGGCAAGAAGGCAATG	AAAGAAAGGAAGGGAGGTGAA
Phc3	TCGGGATGTGAGGATTAGGA	CGGGCAAAGAATGGATGAA
β-actin	AGAGGGAAATCGTGCGTGAC	CAATAGTGATGACCTGGCCGT

was applied following the manufacturer's instructions; five probes were used to increase the confidence of each transcript. To enrich circRNAs, total RNA of each sample was soaked with RNase R (Epicentre, Madison, WI, USA) to remove linear RNAs. Then, the Arraystar Labeling Kit (Arraystar, Rockville, USA) was used to transcribe circRNAs into fluorescent cRNA. Such cRNAs were then hybridized to the Arraystar circRNA array V_2.0 (8x15K). The Agilent Scanner was applied to detect the arrays following washing the slides. In the mRNA study, the whole mRNA microarray (Agilent Technology, CA, USA) was conventionally applied.

Microarray Information Analyses

Array data was processed by Agilent Feature Extraction software (version 11.0.1.1) and R software limma package. Low-intensity filtering was then applied after quantile normalization. The prominent different expressive circRNAs/mRNAs were sorted following the fold-change cutoff (fold change $\geq$ 1.5) or using volcano plot filtering. Distinctive circRNA/mRNA expression patterns were shown by hierarchical clustering.

Pathway Analyses

Gene Ontology (GO) analyses (http://www.geneontology.org) were conducted to set up gene annotation built upon different organisms. Gene functions include cellular components (CC), biological processes (BP), and molecular functions (MF). The -log10 (*P*-value) represented GO score, denoting the abundance in different genes. Also, pathway clusters were harvested using Kyoto Encyclopedia of Genes and Genomes (KEGG) pathway analyses relying on existing molecular networks from various gene data. The -log10 (*P*-value) indicated the KEGG score, denoting the significant relationship with the putative pathway.

Quantitative Real-Time Polymerase Chain Reaction (qRT-PCR)

The HiScript RT SuperMix for qPCR (+gDNA wiper) (Vazyme, Nanjing, China) was applied to reverse transcribe the total RNAs of each group following the protocol. QPCR using the SYBR Green kit (TaKaRa, Dalian, China) was applied to evaluate the expression levels of the circRNAs and mRNAs. Primers for mRNAs were routinely used. To amplify the circRNA junctions, we designed specific divergent primers based on the sequence obtained from the database "circBase" (http://www.circbase.org/). By using the 2-ΔΔCt method that normalizes against the expression of the β-actin gene, the circRNA and mRNA relative expressions were calculated. GenePharma (Shanghai, China) was applied to design, verify, and synthesize all primers. All sequences are as in **Table 1**.

Prediction of circRNA/miRNA Coactions

Arraystar's commercial miRNA coaction prediction software was applied to predict the circRNA/miRNA coaction. The database is based upon the existing online informatics tools miRanda (http://www.microrna.org/) and TargetScan (http://www.targetscan.org/). The Arraystar's miRNA scores of support vector regression (mirSVR) were used as a basis to rank miRNAs, and the miRNAs ranking the highest were considered for further analysis.

circRNA–miRNA–mRNA Pathway Prediction

Arraystar's software was applied to search circRNA_017753 MERs and select top potential target miRNAs based on match sequences. Then, top target miRNAs for the circRNA were selected according to the databases miRDB (http://mirdb.org/) and TargetScan. Based on the ceRNA theory, the direction of circRNA and mRNA changes in the same orientation. To reveal the beneficial mechanisms of the circRNA_017753 in hepatic IPC, we identified predicted downstream mRNA targets in the IRI group and elevated in the IPC group and constructed a Venn diagram. In the end, we selected the overlaying mRNAs and constructed the circRNA–miRNA–mRNA pathway.

Statistics

In the microarray data, a circRNA/mRNA fold change $\geq$ 1.5 was selected, and $P < 0.05$ was conventionally regarded as significant.

GraphPad Prism 5.0 (GraphPad Software, CA, USA) was applied to analyze other data, and all data were indicated as the mean ± standard deviation. One-way analysis of variance followed by the Student–Newman–Keuls test were applied to compare data with normal distribution. The Kruskal–Wallis test and the Wilcoxon rank sum test with Bonferroni adjustments were used to compare data with nonnormal distributions. Means between two groups were compared by a two-tailed Student *t*-test. $P < 0.05$ was regarded as significant.

RESULTS

Evaluation of Hepatic IRI and Hepatic Protection by IPC

The blood index of hepatic injury after hepatic IRI with or without IPC were tested to identify the beneficial effect of IPC in the study. As presented in our H&E staining, liver IRI induced a marked hepatocellular necrosis. In contrast, mice with IPC presented with only minor signs of ischemic congestion and necrosis. Our histochemical evaluation of F4/80 showed an intense inflammatory process occurring in ischemic parenchyma and alleviated levels in IPC. Also, the immunohistochemistry of Ly6G + showed a decreased level of infiltrating Ly6G + cells (a neutrophil plasma membrane biomarker) comparing the IPC and IRI groups (**Figure 1A**). The hepatic injury by IRI and the beneficial effect of IPC were further identified by serum examination. Serum ALT and AST were upregulated after hepatic IRI, and IPC remarkably decreased serum transaminase levels (**Figure 1B**). In addition, IPC ameliorated the TNF-α and IL-6 increase caused by IRI (**Figure 1C**). The results indicate that the current IPC intervention is effective enough to protect the liver against IRI. Hence, the model is suitable for comparing the circRNAs among IRI with or without IPC intervention.

Comparison of circRNA and mRNA in Hepatic IRI and IPC

To compare circRNA expression in the (1) sham, (2) IRI, and (3) IRI + IPC groups, we applied microarray analysis for circRNA and mRNA expression profiles of three samples in each. About 10,535 circRNA and 10,654 mRNA targets in the liver were spotted by microarray. Among them, 77 circRNAs and 686 mRNAs in the IRI group altered more than 1.5-fold compared with those in the sham group ($P < 0.05$). To be precise, 39 circRNAs and 432 mRNAs were increased, and 38 circRNAs and 254 mRNAs were decreased compared with the sham group (**Figures 2A**, **3A**). Moreover, as a result of IPC intervention, a total of 50 circRNA and 95 mRNA alterations with significance (fold change ≥ 1.5, $P < 0.05$) were detected, in which 43 circRNAs and 64 mRNAs increased, 7 circRNAs and 31 mRNAs decreased in the IPC group when compared with IRI (**Figures 2B**, **3B**). Based on fold change, we summarize the top 10 altered circRNAs in **Table 2** and the top 10 altered mRNAs in **Table 3**. We then classified the significant altered circRNAs into various groups. Comparing the altered circRNAs in the IRI and sham groups, there were 77 exonic, 14 sense overlapping, 3 intronic, 5 antisense, and 1 intergenic and 74 exonic, 12 sense overlapping, 4 intronic, 6 antisense, and 4 intergenic when comparing the IPC and IRI groups (**Figure 2C**). Also, by using hierarchical clustering, we were able to cluster the differentially altered circRNAs and mRNAs of comparison groups and visualize the expression profiles. As indicated by the data, circRNAs and mRNAs in the IRI group were dramatically different from those of the sham group although IPC intervention significantly altered the IRI-induced expressions (**Figures 2D**, **3C**).

circRNA and mRNA qRT-PCR Verification

qRT-PCR was further applied to confirm the microarray results. Seven circRNAs and five mRNAs were selected considering their fold change, *P*-value, and raw data. As qRT-PCR results show in **Figure 4**, the expression of circRNA_007095, Gclc, and Krt18 increased, and the circRNA_017753, circRNA_010415, circRNA_000895, circRNA_001946, and Hacl1 decreased enormously after hepatic IRI compared with the sham group. Otherwise, compared with IRI, IPC intervention remarkably elevated the expression of circRNA_027197, circRNA_010498, and Stim1, whereas Phc3 were reduced. The verified results are accordant with the data, indicating the dependability of our microarray profile.

Analysis of Variously Expressed mRNAs

Concerning that biologically similar genes share the same patterns of change, we decided to excavate the variations of coding gene expression among the IRI and IPC groups to reveal the behavior of these variously expressed circRNAs. GO enrichment analysis was used first for variously expressed mRNAs. In response to hepatic IRI, upregulated mRNAs were most related with response to organic substance and cellular response to chemical stimulus, and the downregulated mRNAs were most related to small molecule metabolic and organic acid metabolic processes (**Figure 5A**). Compared with the IRI, IPC mostly elevated the mRNAs related with response to hormone and regulation of signal transduction; meanwhile the downregulated mRNAs of IPC were most involved in regulation of cellular metabolic processes and organic cyclic compound metabolic processes (**Figure 5B**).

Applying the pathway analysis of KEGG, we found that fluid shear stress and atherosclerosis and protein processing in the endoplasmic reticulum were involved in the upregulated mRNAs, whereas the pathways of phenylalanine metabolism and peroxisome were most involved in the decreased mRNAs in the IRI group (**Figure 6A**). Notably, pathways related to the inflammatory process and apoptosis were the most involved in the IRI process as listed, such as pathways of PI3K-AKT, NF-Kappa B, IL-17 signaling, and apoptosis. Moreover, compared with the IRI group, IPC can significantly upregulate mRNAs involved in the pathways of ovarian steroidogenesis and lysine degradation and downregulate the mRNAs related with drug metabolism-cytochrome p450 and chemical carcinogenesis pathways (**Figure 6B**). Our computational analysis results may contribute dramatically to the pathogenesis of hepatic IRI and IPC intervention.

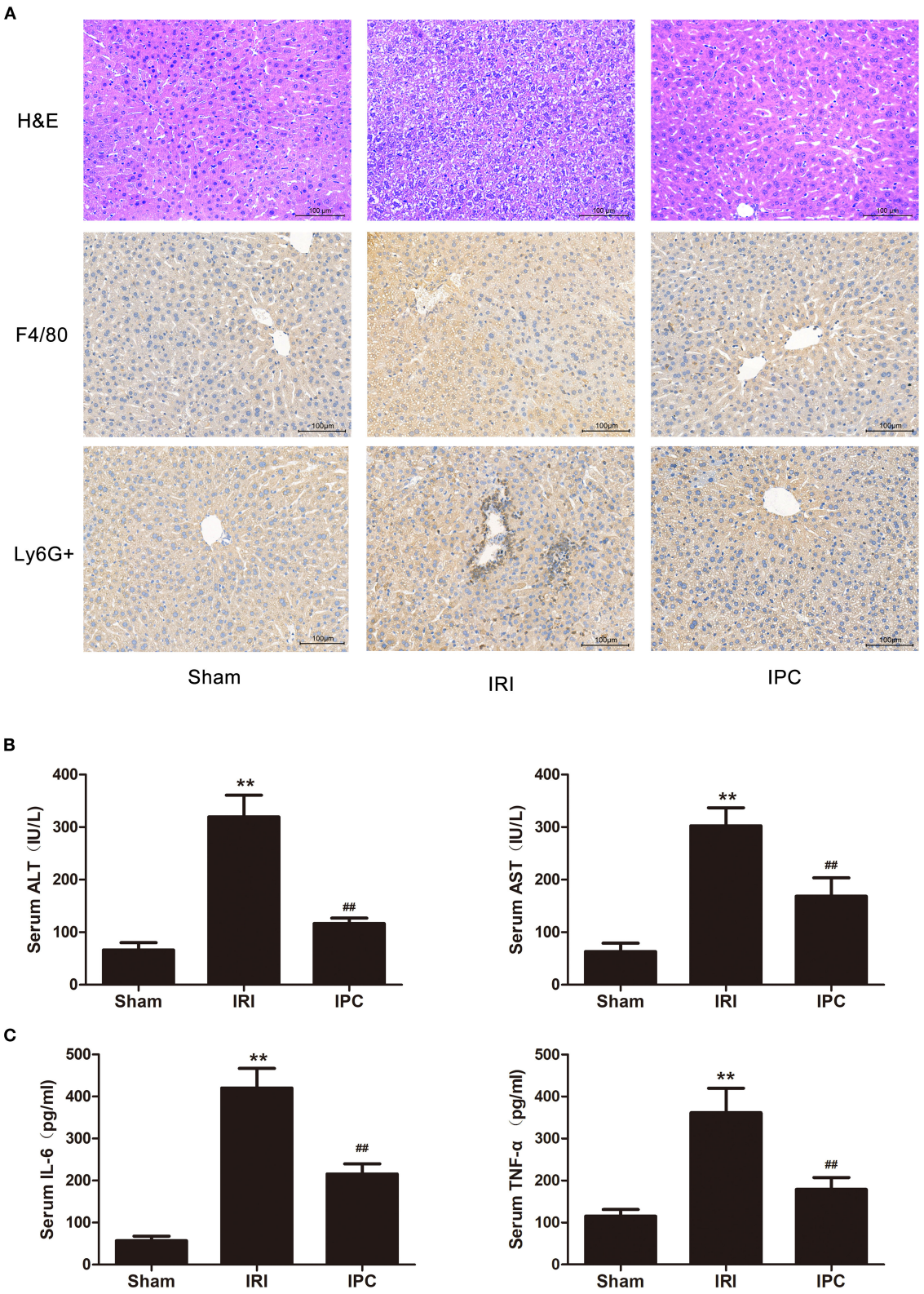

FIGURE 1 | The IPC model is suitable for investigating mechanisms of protecting the liver against IRI. **(A)** H&E staining (up), immunohistochemistry of F4/80 (middle), and Ly6G + (down) images are shown for the hepatic histopathological alteration (magnification × 200). **(B)** Serum levels of ALT and AST. **(C)** Serum levels of IL-6 and TNF-α. Data are expressed as the means ± SD, $n = 8$. $^{**}P < 0.01$ compared with the sham group; $^{\#\#}P < 0.01$ compared with the IRI group.

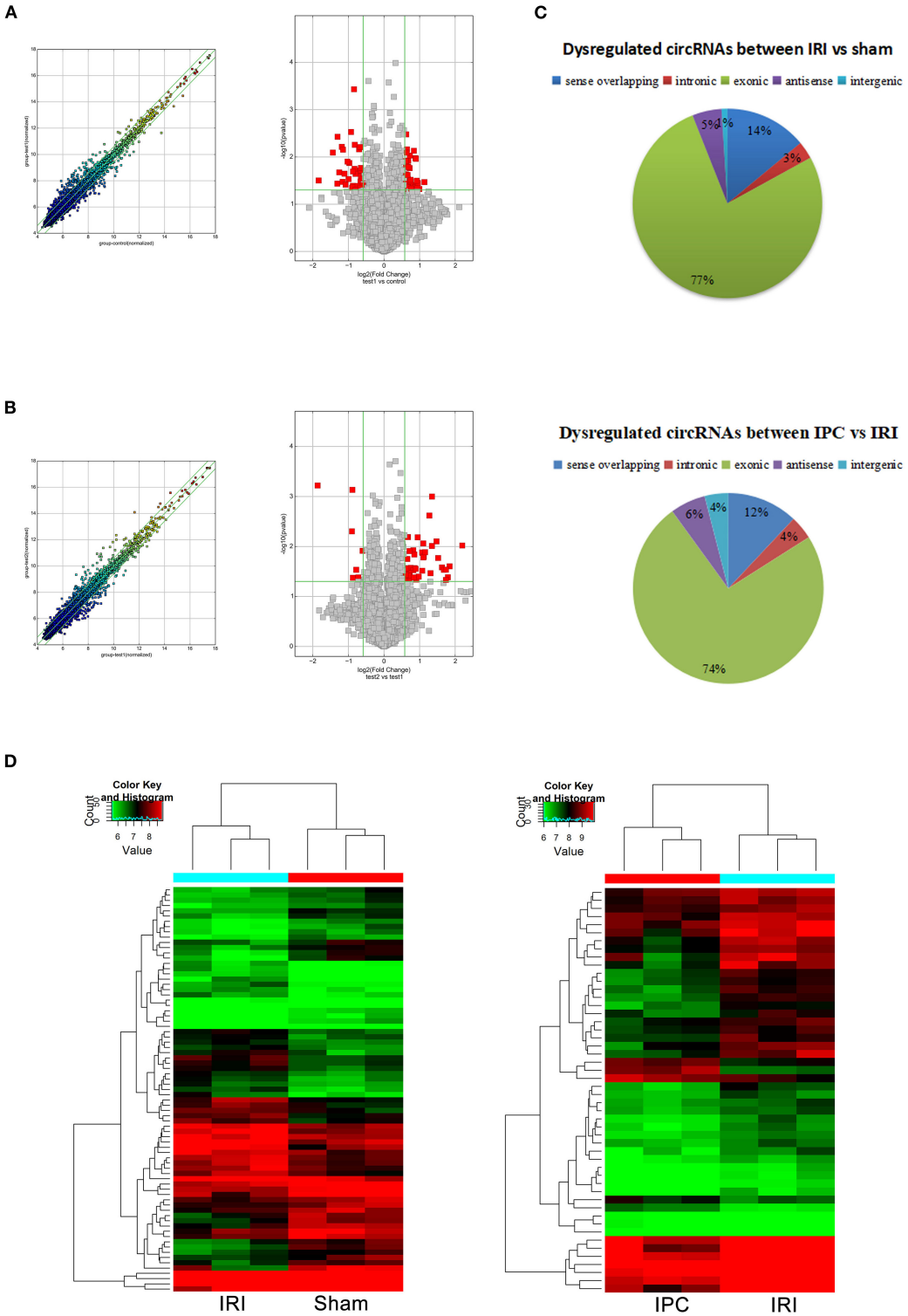

FIGURE 2 | CircRNAs comparing the IRI and sham groups and between the IPC and IRI groups. The left (scatterplots) and right (volcano plots) show the alteration of circRNA expression between IRI and sham groups **(A)** and between IPC and IRI groups **(B)**. In the scatterplot, the values on the *X*- and *Y*-axes are the log2 scaled signals of samples. Fold change is represented by the green lines. The circRNAs outside the range formed by the upper and lower green lines are those with the fold change ≥ 1.5 between the compared groups. In the volcano plot, the vertical green lines represent a 1.5-fold change although the horizontal green line corresponds to a *P*-value of 0.05. The red points in the volcano plot represent the significantly altered circRNAs with *P*-value <0.05. **(C)** Different subgroups of significantly altered circRNAs according to their effects and position. **(D)** Heat maps of circRNA profiles from the microarray data. The color scales represent expression values. Red represents high expression, and green indicates low relative expression. Each row of colored boxes indicates a single circRNA, each column indicates a single sample.

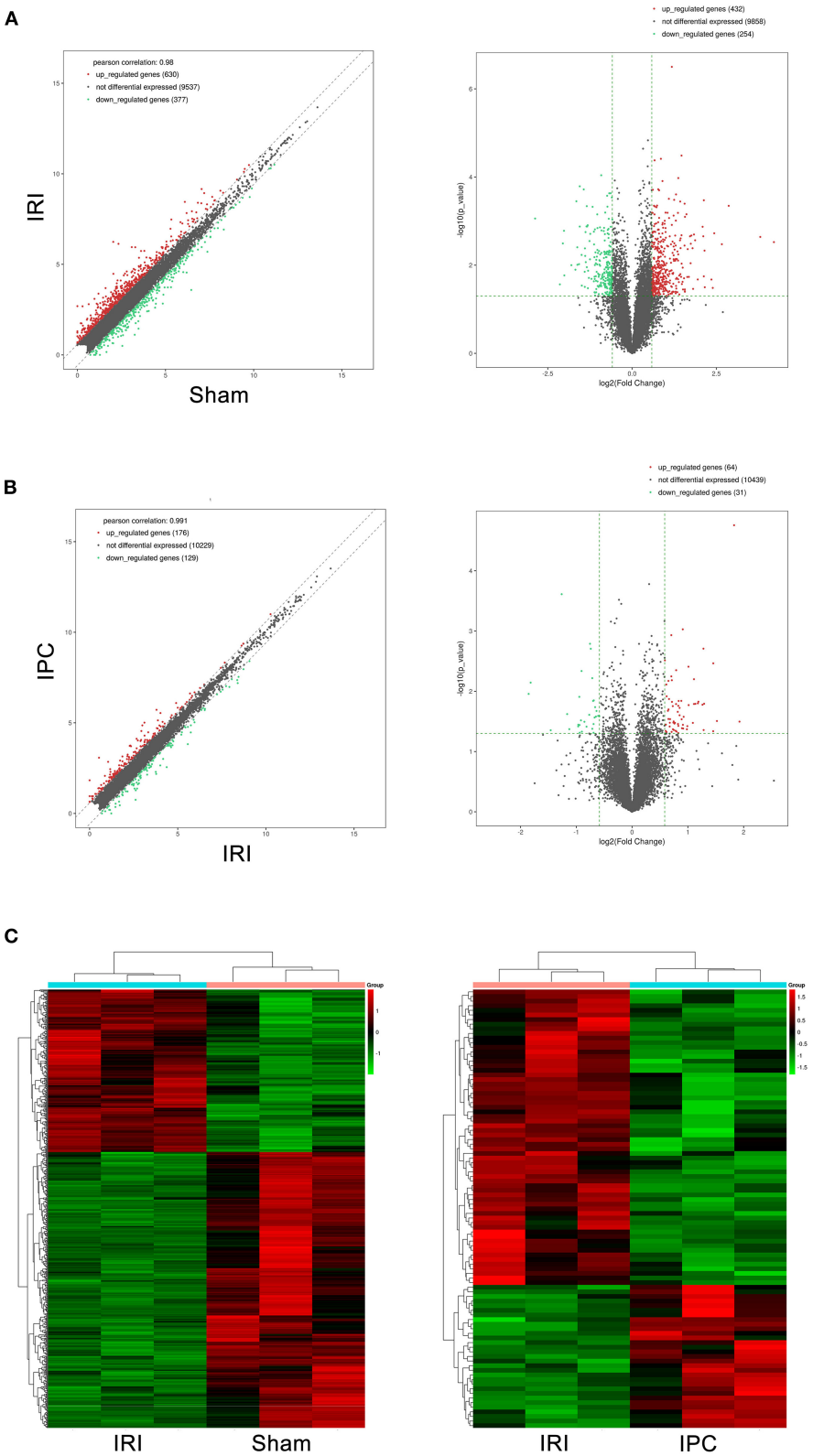

FIGURE 3 | mRNAs comparing the IRI and sham groups and between the IPC and IRI groups. The left (scatterplots) and right (volcano plots) show the alteration of mRNA expression between IRI and sham groups **(A)** and between IPC and IRI groups **(B)**. In the plot, red and green points represent significant altered mRNAs (fold change $\geq$ 1.5, *P*-value $<$ 0.05), respectively. **(C)** Heat maps of mRNA profiles from the microarray data. The color scales represent expression values. Red represents high expression, and green indicates low relative expression. Each row of colored boxes indicates single circRNA; each column indicates single sample.

TABLE 2 | Top 10 significantly dysregulated circRNAs and mRNAs ranked by fold change between I/R and sham groups.

CircRNA

Name	circRNA_type	GeneSymbol	Fold Change	Regulation	*P*-value
mmu_circRNA_29990	Exonic	Bach1	2.195	Up	0.034
mmu_circRNA_29992	Exonic	Bach1	1.987	Up	0.048
mmu_circRNA_32165	Exonic	Chka	1.933	Up	0.035
mmu_circRNA_22310	Exonic	Slc41a2	1.906	Up	0.043
mmu_circRNA_35001	Exonic	B4galt5	1.892	Up	0.032
mmu_circRNA_39714	Exonic	Wdr95	3.566	Down	0.031
mmu_circRNA_34157	Exonic	Qser1	2.707	Down	0.008
mmu_circRNA_000113	Antisense	Rian	2.482	Down	0.037
mmu_circRNA_29383	Exonic	Prodh	2.469	Down	0.004
mmu_circRNA_011844	Exonic	Inpp5a	2.390	Down	0.021

mRNA

Gene Name	Fold Change	Regulation	*P*-value
Gm3776	18.449	Up	0.003
Gsta1	13.939	Up	0.002
Serpina7	7.287	Up	4.50191E-04
Plscr1	6.328	Up	0.003
Tubb6	5.410	Up	0.002
G0s2	7.339	Down	0.001
Ppp1r3g	4.412	Down	0.027
Sftpa1	4.150	Down	0.003
Usp2	4.054	Down	0.002
Ppp1r3b	4.025	Down	0.017

Identification of circRNAs Related to Hepatic Protection by IPC

Concerning the protection effect of IPC intervention against IRI, we compared the circRNA alteration and direction of alterations of the three groups to reveal the potential relevance between circRNA changes and IPC protection. As a result, we sorted circRNAs that showed up with opposite alteration directions between the comparison groups (sham vs. IRI and IRI vs. IPC). Following this method, we selected three circRNAs that were upregulated in IRI but downregulated in the IPC group and 12 circRNAs that showed a completely opposite direction (**Figure 7A**). Concerning the type of circRNAs and data sources of circRNAs, we then selected only one circRNA, circRNA_017753, that was considered significatively related to the IPC protective effect. The gnomic locus of circRNA_017753 is on chromosome 17, and it is spliced from Mapk14. The circRNA_017753 expression level was then confirmed by qRT-PCR; IPC intervention can significantly restore the downregulation caused by hepatic IRI. Our data indicate that circRNA_017753 may play a protective role in hepatic IRI that arouses our desire to learn the potential role of circRNA_017753. In addition, we also compared our data with the microarray data of hepatic IPostC intervention in IRI (GSE117524) (15). Though circRNA_010498 does not show a comparative fold change to circRNA_017753 in our data, the intersection of research (fold change $\geq$ 1.5, *P*-value$<$0.05) indicates its potential significant protective effect in both IPC and IPostC intervention and is worth further study (**Supplementary Figure 1**).

Prediction of miRNA and CircRNA–miRNA–mRNA Pathway for CircRNA_017753

It is well-known that circRNA regulates miRNAs by interacting with miRNA response elements (MREs). Such way of interaction can competitively suppress miRNAs' activity and is, thus, called miRNA sponges. To figure out the function of circRNA_017753, we applied Arraystar's prediction software, which combined TargetScan and miRanda databases. We predict and list the five highest ranking target miRNAs of circRNA_017753 and annotation of their circRNA/miRNA interactions (**Table 4**, **Figure 8A**).

To further investigate the potential mechanisms of circRNA_017753 in IPC, we construct the possible circRNA_017753–miRNA–mRNA pathways. Applying Arraystar's miRNA prediction software, 119 genes were selected related to the 5 miRNAs mentioned (**Supplementary Table 1**). Because of the widely accepted ceRNA concept that circRNAs may positively regulate mRNAs, we paid more attention to the mRNAs downregulated in IRI but significantly inhibited by IPC. By establishing the intersections of 65 mRNAs significantly increased by IPC and 119 predicted mRNA targets connected to circRNA_017753,

TABLE 3 | Top 10 significantly dysregulated circRNAs and mRNAs ranked by fold change between IPC and I/R groups.

CircRNA

Name	circRNA_type	GeneSymbol	Fold Change	Regulation	*P*-value
mmu_circRNA_31583	Exonic	Sil1	4.585	Up	0.010
mmu_circRNA_000113	Antisense	Rian	3.586	Up	0.025
mmu_circRNA_37852	Exonic	Igsf21	3.465	Up	0.041
mmu_circRNA_19765	Exonic	Fam135a	3.335	Up	0.046
mmu_circRNA_38137	Exonic	Sema3c	3.334	Up	0.029
mmu_circRNA_38159	Exonic	Magi2	3.638	Down	0.001
mmu_circRNA_19091	Sense overlapping	Cdyl	1.866	Down	0.005
mmu_circRNA_41223	Exonic	Grik5	1.851	Down	0.001
mmu_circRNA_003780	Exonic	Cdyl	1.832	Down	0.042
mmu_circRNA_43573	Exonic	Banp	1.718	Down	0.029

mRNA

Gene Name	Fold Change	Regulation	*P*-value
Hist1h1c	3.800	Up	0.032
Kctd12	3.553	Up	1.75414E-05
Rab30	2.871	Up	0.031
Ankrd33b	2.743	Up	0.003
Ldlr	2.740	Up	0.046
Ppp1r3c	3.617	Down	0.011
Cyp2b10	3.529	Down	0.007
Nrg4	2.750	Down	0.044
Phc3	2.399	Down	2.44694 E-04
Ddit4	2.241	Down	0.024

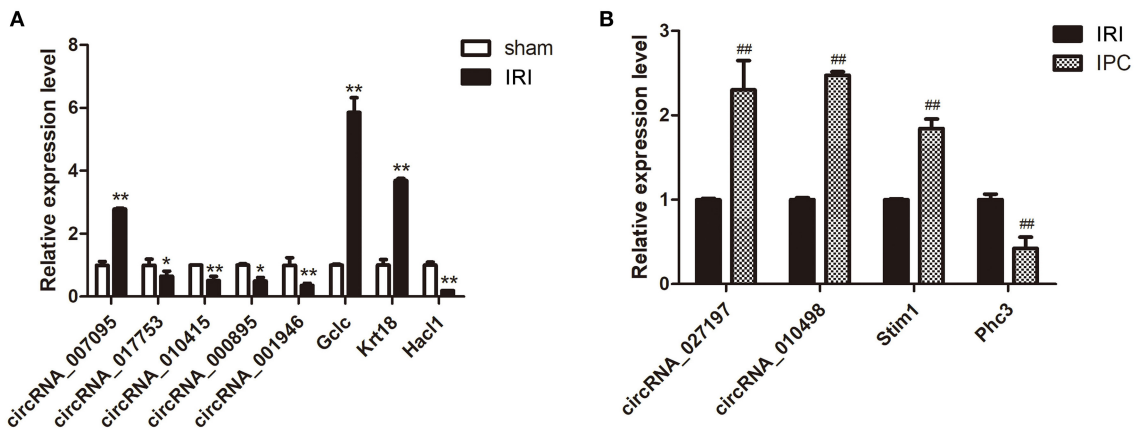

FIGURE 4 | Selected circRNA and mRNA qRT-PCR verification between the IRI and sham groups **(A)** and between the IPC and IRI groups **(B)**. Data are expressed as the means ± SD, $n = 6$. $^{*}P < 0.05$ compared with the sham, and $^{**}P < 0.01$ compared with the sham group; $^{\#\#}P < 0.01$ compared with the IRI group.

we identified only one overlapping mRNA, Jade1, and predicted three following circRNA–miRNA–mRNA signals: circRNA_017753–miR-218-5p–Jade1, circRNA_017753–miR-7002-3p–Jade1, and circRNA_017753–miR-7008-3p–Jade1. These regulatory ceRNA signaling pathways may play important roles in the mechanisms of IPC protection and deserve further study.

DISCUSSION

Hepatic IRI contributes significantly to organ damage in the surgical procedures of hepatic resections and liver transplantation. Such injury possesses a high mortality rate caused by an intense inflammatory process occurring in the ischemic liver. As presented in our research, not only did serum

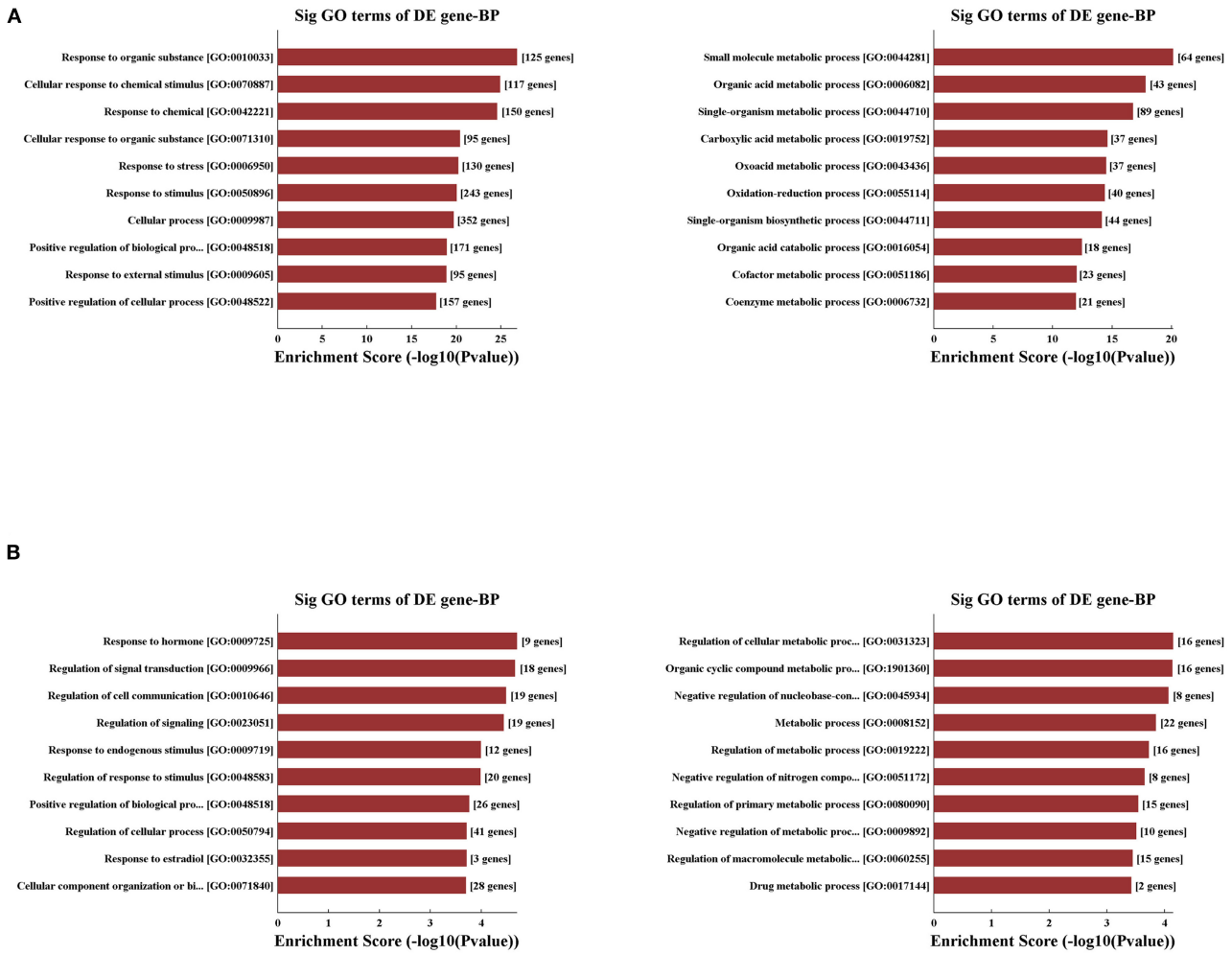

FIGURE 5 | Variously expressed mRNA GO analysis. GO analysis between the IRI and sham groups **(A)** and between the IPC and IRI groups **(B)**. Top 10 up- (left) and downregulated (right) mRNAs were analyzed by GO analysis concerning biological processes.

TNF-α and IL-6 increase in the IRI group, the evaluation of F4/80 and infiltrating of Ly6G + staining demonstrated an intense inflammatory process in IRI. IPC has been most investigated in the past decades as a life-saving intervention. Though widely applied clinically, the exact molecular mechanisms behind the protection effect of IPC still remain largely unclear. A majority of the existing research mainly focuses on protein-coding RNA while research on ncRNAs (long ncRNAs and circRNAs) remain insufficient. It was not until the mechanism of powerful miRNA sponges revealed circRNAs as a potential target for treatment and diagnosis scientists' attention was widely attracted. In our research, by utilizing circRNA microarray analysis, we first report circRNA alteration profiles induced by hepatic IRI and the protection intervention of IPC systematically. More importantly, through bioinformatic comparison of circRNA alteration and the direction of alteration, we identified one possible circRNA, circRNA_017753, related with hepatic protection by IPC intervention. By comparing the data with the previous microarray data of hepatic IPostC, we identified one possible circRNA, circRNA_010498, that may have a potential protective effect in both IPC and IPostC. Also, by integrated application of TargetScan and miRanda databases, we predicted three circRNA–miRNA–mRNA pathways that may take effect in the mechanisms of IPC protection against hepatic IRI.

In our research, the microarray profiles identified 77 circRNAs that were significantly altered (39 up- and 38 downregulated) after hepatic IRI, whereas a total of 50 circRNAs altered significantly due to the IPC intervention (43 up- and 7 downregulated). As previously reported, the majority of circRNAs arise from exons; our profiles identified that about 2/3 altered circRNAs were exonic (18). Though none of the circRNAs in our top dysregulated list have been reported before as the reason for nascent circRNA functional study, it is encouraging to see some mRNAs regarded as alternative transcripts of these circRNAs reported to take effect in different

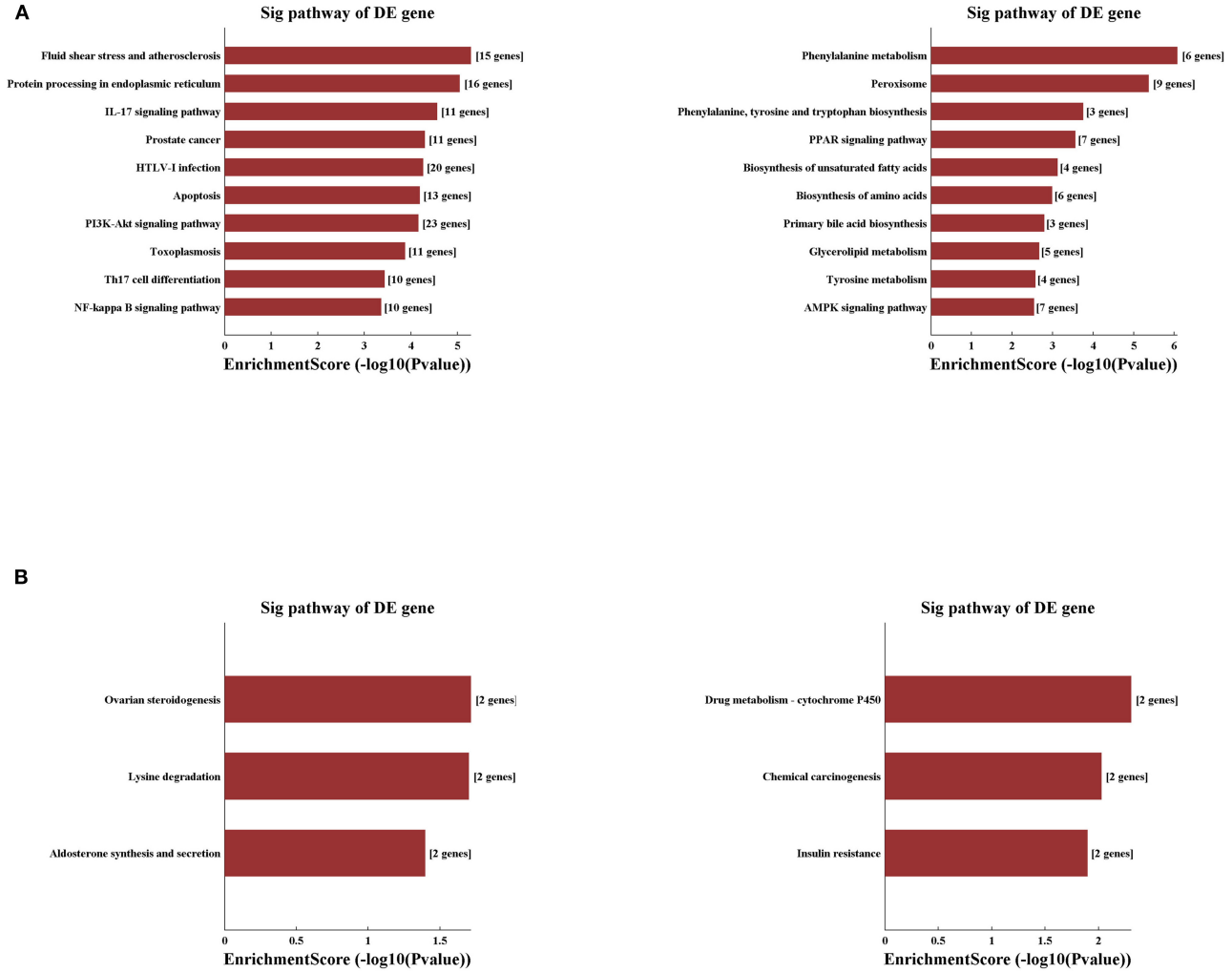

FIGURE 6 | Variously expressed mRNAs KEGG pathway analysis. KEGG pathway analysis between the IRI and sham groups **(A)** and between the IPC and IRI groups **(B)**. Top 10 up- (left) and downregulated (right) mRNAs were analyzed by KEGG analysis.

physiopathologic mechanisms related to the IRI process. For example, Bach1 is the alternative transcript of circRNA_29990 and circRNA_29992 (2 of the top 5 upregulated circRNAs in hepatic IRI), and its protein inhibits the transcription of HO-1 and related genes involved in the oxidative stress response by binding to Maf genome recognition elements (19). Bach1 deficiency may increase resistance to ischemic stresses by elevating HO-1 expression (20, 21). Several studies also reveal its important role in ischemic or oxidative damage (22–24). More importantly, Bach1 is identified to repress Wnt/β-Catenin signaling and angiogenesis in peripheral ischemic injury in a recent study (25). Magi2 is the transcript of circRNA_38159 (one of the top five downregulated circRNAs listed in IPC); it encodes scaffolding proteins binding to PTEN and is identified an important element in the ischemic injury of the central nervous system. As it is well-known that circRNAs may regulate its linear counterparts (26), the circRNAs listed may play crucial roles in hepatic IRI and IPC by regulating the transcription of the parent genes.

The data on dysregulated mRNAs are also inspiring. In the list of top 10 dysregulated mRNAs in hepatic IRI, G0s2 (G0/G1 switch gene 2) decreased the most among all downregulated mRNAs and is widely recognized as a direct activator of oxidative phosphorylation at the early phase of hypoxia (27, 28). A recent study just identified that its overexpression can alleviate ATP decrease in myocardial cells and increase their hypoxic resistance during ischemia (29), suggesting its crucial role in hepatic IRI. Also, we can identify some new clues on the protection mechanisms of IPC in our profile of dysregulated mRNAs between IPC and I/R groups. For instance, Ddit4 (DNA-damage inducible transcript 4), widely recognized as an autophagy regulator by negatively regulating mTORC1, is found downregulated in the IPC group (30). Our result is consistent with the previous research that Ddit4 is a novel protection

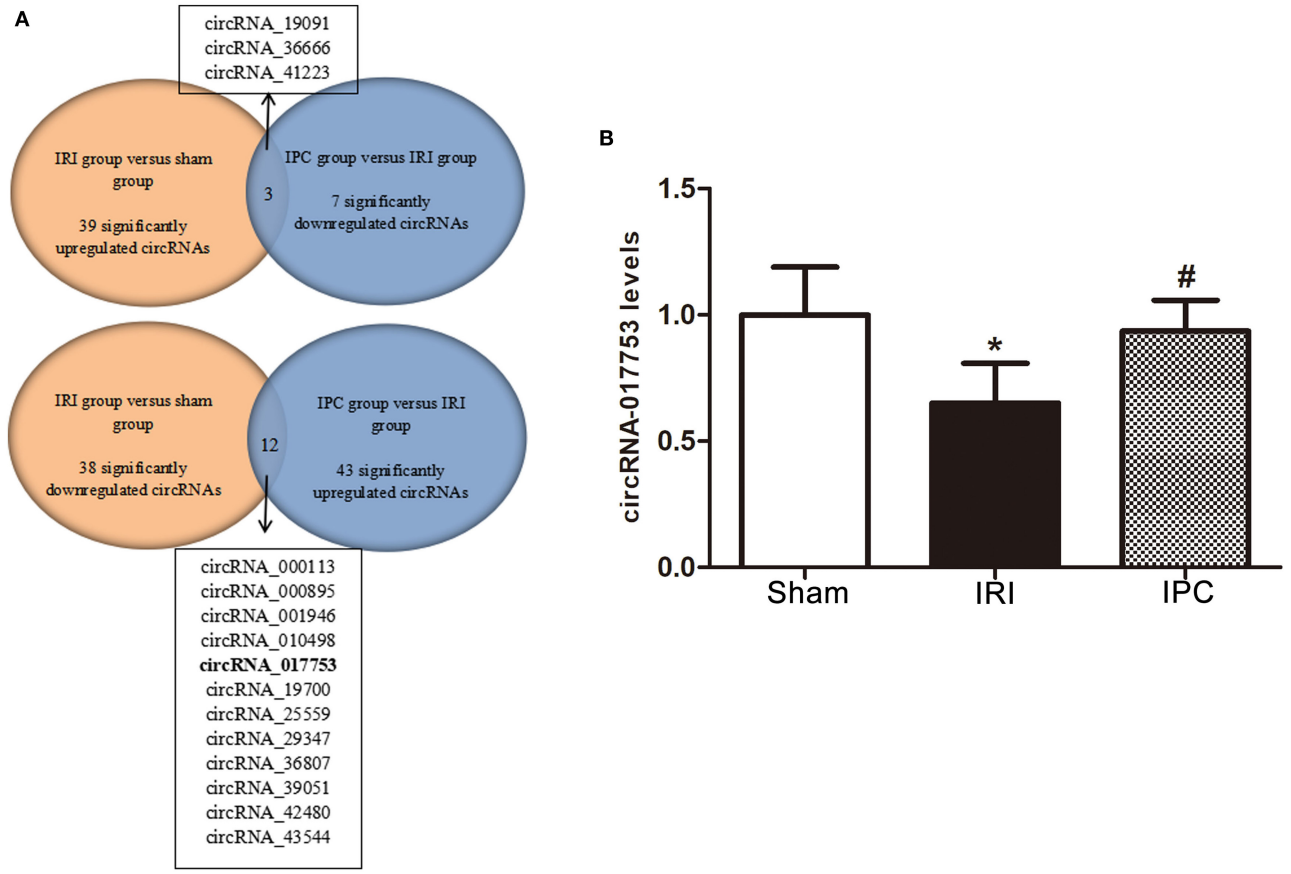

FIGURE 7 | Identification of circRNAs related to hepatic protection by IPC and qRT-PCR validation. **(A)** The Venn diagram shows the circRNAs with an opposite direction of the alterations between the two comparison groups (sham vs. IRI and IRI vs. IPC). **(B)** qRT-PCR detected expression levels of circRNA_017753 in mouse liver among the three groups. Data are expressed as the means ± SD, $n = 6$. $^{*}P < 0.05$ compared with the sham group; $^{\#}P < 0.05$ compared with the IRI group.

TABLE 4 | The identified circRNAs and its predicted miRNA response elements (MREs).

CircRNAs	Alias (circBase)	Chrom	Gene Symbol	MRE1	MRE2	MRE3	MRE4	MRE5
mmu_circRNA_017753	mmu_circ_0000737	Chr17 +	Mapk14	mmu-miR-103-2-5p	mmu-miR-103-1-5p	mmu-miR-196b-3p	mmu-miR-7675-3p	mmu-miR-6409

molecule that prevents ischemic injury in hepatocytes (31). Also, the protective effect of Ddit4 is found to be vital in cardiac and cerebral IRI (32–34). All these consistencies prove the reliability of our profile and provide us the credibility of other listed mRNAs in the mechanisms of IPC protection against hepatic IRI, thus making it worth further study.

We can also profit from GO and KEGG pathway analysis of altered mRNAs, which may reveal the key processes of hepatic IRI pathogenesis. The data emphasize the crucial roles of the inflammatory process and apoptosis in the IRI process, such as pathways of PI3K-AKT, NF-Kappa B, IL-17 signaling, and apoptosis. Moreover, the pathways of the metabolic process and regulation of signaling are prominent when comparing the IPC and IRI groups, indicating that related genes may play vital roles in IPC protection mechanisms. Our observation was partially consistent with a previous study revealing the relationship with metabolic process and the IPC protective mechanism (35).

It is worth mentioning that, in our data, only one circRNA, circRNA_017753, was selected to have a relationship with the protective mechanisms of IPC with the most possibility. Our data on the microarray and qRT-PCR both confirm its decrease in the IRI group and upregulation with IPC intervention. We speculate that the decreased level of circRNA_017753 may reflect hepatic dysfunction during IRI, and IPC may alleviate the hepatic dysfunction by the circRNA adjustment. Thus, circRNA_017753 may play a crucial role in the protective mechanism of hepatic IRI and may be a possible therapeutic target of hepatic injury.

To make the analysis more comprehensive, we also compared our data with previous data on hepatic IRI and IPostC prevention (14, 15). Because of different experimental environments and

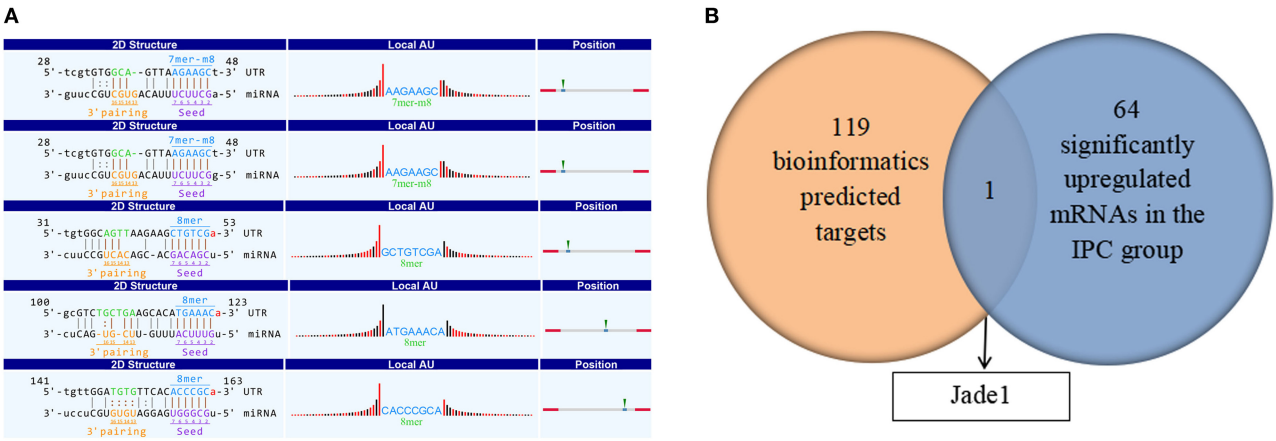

FIGURE 8 | (A) Prediction of MiRNA and the circRNA–miRNA–mRNA pathway. Detailed structure of circRNA/miRNA interactions. The MRE sequence, miRNA seed type, precise base positions and target miRNA nucleotides are presented as annotation in 2-D structure column. Thirty nucleotides downstream and upstream the seed sequence are presented in "local AU." Red bars present A/U, and black bars present G/C. The most likely relative MRE position are presented in position column. **(B)** Overlap of the predicted mRNA target related to circRNA_017753 and significantly upregulated mRNAs caused by IPC intervention.

model construction methods (such as reperfusion 4 h after ischemia 1 h by Zhang P et al.), though reported circRNAs, such as circRNA_005186, exhibit the same alteration trend in our study in both IRI and prevention, the fold change of these circRNAs does not meet our screening criteria (fold change ≥ 1.5, P-value<0.05). However, it is worth noting that, by constructing the intersection of our data and GSE117524, circRNA_010498 shows sufficient significance as a protective factor in both IPC and IPostC intervention.

It is widely recognized today that circRNAs regulate gene expression by serving as miRNA sponges. Based on sequence comparing and bioinformatic methods, we predicted the five potential candidate miRNAs for circRNA_017753 with the most possibility. Then, by applying prediction software that combines TargetScan and miRanda databases, we are able to construct three circRNA–miRNA–mRNA regulatory axes that may have a protective effect in IPC intervention. Even though three circRNA–miRNA–mRNA axes have not been previously reported, the predicted molecule of Jade1 was found to have a huge possibility to play a part in the hepatic IPC protection mechanism. As a component of the HBO1 complex, Jade1 was identified as a key regulator of apoptosis (36). In previous study, by promoting acetylation of histones, it functioned as a key regulator of cycle progression and redifferentiation in renal tubule regeneration after IRI (37). Further studies on Jade1 and related circRNA–miRNA–mRNA axes are in progress in our laboratory.

The current study has some limitations that should be admitted. First, our data was obtained in an animal model and may not fully represent human pathological pathways. However, there is a high degree of similarity between human and mouse research in circRNAs. As it is demonstrated in previous research that most circRNAs present to be conserved between mouse and human (38), most of the circRNAs detected in our microarray data are conserved and of great interest for human research. Second, our research focuses on integral hepatic parenchyma injury and IPC prevention, thus less consideration was put into the design of circRNA profiling in different hepatic zones. In the development of spatial transcriptomics and microarray methods, specific profiling for circRNA expression in different hepatic zones would be of great interest and worth further study.

CONCLUSION

Our study for the first time delineates the expression data of dysregulated circRNAs and mRNAs in response to hepatic IRI and IPC intervention. Our profile and bioinformatic analyses provide numerous novel clues on the pathophysiologic mechanism of IPC protection. Several potential circRNA–miRNA–mRNA axes we predicted may offer promising targets for hepatic ischemic prevention and treatment.

DATA AVAILABILITY STATEMENT

The datasets presented in this study can be found in online repositories. The names of the repository/repositories and accession number(s) can be found below: GSE164367, https://www.ncbi.nlm.nih.gov/geo/query/acc.cgi?acc=GSE164367.

ETHICS STATEMENT

The animal study was reviewed and approved by The First Affiliated Hospital, Zhejiang University School of Medicine.

AUTHOR CONTRIBUTIONS

XT, HX, LZ, and SZ designed the study. XT and YH performed most of the experiments. YL and ZY performed part of the experiments. XT, YH, and ZY analyzed the data. XT prepared and

wrote the manuscript. All authors contributed to the article and approved the submitted version.

FUNDING

The research was supported by the National Natural Science Foundation of China (Grant No. 81970543) and National Natural Science Foundation of China (Grant No. 81570591).

SUPPLEMENTARY MATERIAL

The Supplementary Material for this article can be found online at: https://www.frontiersin.org/articles/10.3389/fmed.2021.626948/full#supplementary-material

Supplementary Figure 1 | Identification of circRNAs related to hepatic protection by IPC and IPostC. The Venn diagram shows the possible protective circRNAs intersection of our data and GSE117524. (fold change≥1.5, *P*-value<0.05).

REFERENCES

1. Sakai N, Van Sweringen HL, Schuster R, Blanchard J, Burns JM, Tevar AD, et al. Receptor activator of nuclear factor-κB ligand (RANKL) protects against hepatic ischemia/reperfusion injury in mice. *Hepatology.* (2012) 55:888–97. doi: 10.1002/hep.24756
2. Walsh KB, Toledo AH, Rivera-Chavez FA, Lopez-Neblina F, Toledo-Pereyra LH. Inflammatory mediators of liver ischemia-reperfusion injury. *Exp Clin Transplant.* (2009) 7:78–93. Available online at: https://apps.webofknowledge.com/full_record.do?product=UA&search_mode=GeneralSearch&qid=1&SID=5FlwRUV3HJhawCTnGz3&page=1&doc=4
3. Perry BC, Soltys D, Toledo AH, Toledo-Pereyra LH. Tumor necrosis factor-α in liver ischemia/reperfusion injury. *J Invest Surg.* (2011) 24:178–88. doi: 10.3109/08941939.2011.568594
4. Murry CE, Jennings RB, Reimer KA. Preconditioning with ischemia: a delay of lethal cell injury in ischemic myocardium. *Circulation.* (1986) 74:1124–36. doi: 10.1161/01.cir.74.5.1124
5. Shawky HM, Younan SM, Rashed LA, Shoukry H. Effect of recombinant erythropoietin on ischemia-reperfusion-induced apoptosis in rat liver. *J Physiol Biochem.* (2012) 68:19–28. doi: 10.1007/s13105-011-0114-2
6. Knudsen AR, Kannerup AS, Grønbæk H, Dutoit SH, Nyengaard JR, Funch-Jensen P, et al. Quantitative histological assessment of hepatic ischemia-reperfusion injuries following ischemic pre- and post-conditioning in the rat liver. *J Surg Res.* (2013) 180:e11–20. doi: 10.1016/j.jss.2012.03.036
7. Qu S, Yang X, Li X, Wang J, Gao Y, Shang R, et al. Circular RNA: a new star of noncoding RNAs. *Cancer Lett.* (2015) 365:141–8. doi: 10.1016/j.canlet.2015.06.003
8. Kristensen LS, Andersen MS, Stagsted LVW, Ebbesen KK, Hansen TB, Kjems J. The biogenesis, biology and characterization of circular RNAs. *Nat Rev Genet.* (2019) 20:675–91. doi: 10.1038/s41576-019-0158-7
9. Salzman J, Gawad C, Wang PL, Lacayo N, Brown PO. Circular RNAs are the predominant transcript isoform from hundreds of human genes in diverse cell types. *PLoS ONE.* (2012) 7:e30733. doi: 10.1371/journal.pone.0030733
10. Jeck WR, Sorrentino JA, Wang K, Slevin MK, Burd CE, Liu J, et al. Circular RNAs are abundant, conserved, and associated with ALU repeats. *RNA.* (2013) 19:141–57. doi: 10.1261/rna.035667.112
11. Memczak S, Jens M, Elefsinioti A, Torti F, Krueger J, Rybak A, et al. Circular RNAs are a large class of animal RNAs with regulatory potency. *Nature.* (2013) 495:333–8. doi: 10.1038/nature11928
12. Salzman J, Chen RE, Olsen MN, Wang PL, Brown PO. Cell-type specific features of circular RNA expression. *PLoS Genet.* (2013) 9:e1003777. doi: 10.1371/journal.pgen.1003777
13. Xu CF, Yu CH, Li YM. Regulation of hepatic microRNA expression in response to ischemic preconditioning following ischemia/reperfusion injury in mice. *Omics.* (2009) 13:513–20. doi: 10.1089/omi.2009.0035
14. Ye Z, Kong Q, Han J, Deng J, Wu M, Deng H. Circular RNAs are differentially expressed in liver ischemia/reperfusion injury model. *J Cell Biochem.* (2018) 119:7397–405. doi: 10.1002/jcb.27047
15. Zhang P, Ming Y, Ye Q, Niu Y. Comprehensive circRNA expression profile during ischemic postconditioning attenuating hepatic ischemia/reperfusion injury. *Sci Rep.* (2019) 9:264. doi: 10.1038/s41598-018-36443-8
16. Kuroda S, Tashiro H, Igarashi Y, Tanimoto Y, Nambu J, Oshita A, et al. Rho inhibitor prevents ischemia-reperfusion injury in rat steatotic liver. *J Hepatol.* (2012) 56:146–52. doi: 10.1016/j.jhep.2011.04.029
17. Nakayama H, Yamamoto Y, Kume M, Yamagami K, Yamamoto H, Kimoto S, et al. Pharmacologic stimulation of adenosine A2 receptor supplants ischemic preconditioning in providing ischemic tolerance in rat livers. *Surgery.* (1999) 126:945–54. doi: 10.1016/s0039-6060(99)70037-1
18. Ashwal-Fluss R, Meyer M, Pamudurti NR, Ivanov A, Bartok O, Hanan M, et al. circRNA biogenesis competes with pre-mRNA splicing. *Mol Cell.* (2014) 56:55–66. doi: 10.1016/j.molcel.2014.08.019
19. Ogawa K, Sun J, Taketani S, Nakajima O, Nishitani C, Sassa S, et al. Heme mediates derepression of Maf recognition element through direct binding to transcription repressor Bach1. *Embo J.* (2001) 20:2835–43. doi: 10.1093/emboj/20.11.2835
20. Omura S, Suzuki H, Toyofuku M, Ozono R, Kohno N, Igarashi K. Effects of genetic ablation of bach1 upon smooth muscle cell proliferation and atherosclerosis after cuff injury. *Genes Cells.* (2005) 10:277–85. doi: 10.1111/j.1365-2443.2005.00832.x
21. Yano Y, Ozono R, Oishi Y, Kambe M, Yoshizumi M, Ishida T, et al. Genetic ablation of the transcription repressor Bach1 leads to myocardial protection against ischemia/reperfusion in mice. *Genes Cells.* (2006) 11:791–803. doi: 10.1111/j.1365-2443.2006.00979.x
22. Tanimoto T, Hattori N, Senoo T, Furonaka M, Ishikawa N, Fujitaka K, et al. Genetic ablation of the Bach1 gene reduces hyperoxic lung injury in mice: role of IL-6. *Free Radic Biol Med.* (2009) 46:1119–26. doi: 10.1016/j.freeradbiomed.2009.01.017
23. Warnatz HJ, Schmidt D, Manke T, Piccini I, Sultan M, Borodina T, et al. The BTB and CNC homology 1 (BACH1) target genes are involved in the oxidative stress response and in control of the cell cycle. *J Biol Chem.* (2011) 286:23521–32. doi: 10.1074/jbc.M111.220178
24. Kondo K, Ishigaki Y, Gao J, Yamada T, Imai J, Sawada S, et al. Bach1 deficiency protects pancreatic β-cells from oxidative stress injury. *Am J Physiol Endocrinol Metab.* (2013) 305:E641–648. doi: 10.1152/ajpendo.00120.2013
25. Jiang L, Yin M, Wei X, Liu J, Wang X, Niu C, et al. Bach1 represses Wnt/β-catenin signaling and angiogenesis. *Circ Res.* (2015) 117:364–75. doi: 10.1161/circresaha.115.306829
26. Li Z, Huang C, Bao C, Chen L, Lin M, Wang X, et al. Exon-intron circular RNAs regulate transcription in the nucleus. *Nat Struct Mol Biol.* (2015) 22:256–64. doi: 10.1038/nsmb.2959
27. Kioka H, Kato H, Fujikawa M, Tsukamoto O, Suzuki T, Imamura H, et al. Evaluation of intramitochondrial ATP levels identifies G0/G1 switch gene 2 as a positive regulator of oxidative phosphorylation. *Proc Natl Acad Sci USA.* (2014) 111:273–8. doi: 10.1073/pnas.1318547111
28. Hayashi T, Asano Y, Shintani Y, Aoyama H, Kioka H, Tsukamoto O, et al. Higd1a is a positive regulator of cytochrome c oxidase. *Proc Natl Acad Sci USA.* (2015) 112:1553–8. doi: 10.1073/pnas.1419767112
29. Kamikubo K, Kato H, Kioka H, Yamazaki S, Tsukamoto O, Nishida Y, et al. A molecular triage process mediated by RING finger protein 126 and BCL2-associated athanogene 6 regulates degradation of G(0)/G(1) switch gene 2. *J Biol Chem.* (2019) 294:14562–73. doi: 10.1074/jbc.RA119.008544
30. Dennis MD, McGhee NK, Jefferson LS, Kimball SR. Regulated in DNA damage and development 1 (REDD1) promotes cell survival during serum deprivation by sustaining repression of signaling through the mechanistic target of rapamycin in complex 1 (mTORC1). *Cell Signal.* (2013) 25:2709–16. doi: 10.1016/j.cellsig.2013.08.038
31. Cho SS, Kim KM, Yang JH, Kim JY, Park SJ, Kim SJ, et al. Induction of REDD1 via AP-1 prevents oxidative stress-mediated injury in hepatocytes. *Free Radic Biol Med.* (2018) 124:221–31. doi: 10.1016/j.freeradbiomed.2018.06.014

32. Chen Q, Zhou Y, Richards AM, Wang P. Up-regulation of miRNA-221 inhibits hypoxia/reoxygenation-induced autophagy through the DDIT4/mTORC1 and Tp53inp1/p62 pathways. *Biochem Biophys Res Commun.* (2016) 474:168–74. doi: 10.1016/j.bbrc.2016.04.090
33. Park KM, Teoh JP, Wang Y, Broskova Z, Bayoumi AS, Tang Y, et al. Carvedilol-responsive microRNAs, miR-199a-3p and−214 protect cardiomyocytes from simulated ischemia-reperfusion injury. *Am J Physiol Heart Circ Physiol.* (2016) 311:H371–383. doi: 10.1152/ajpheart.00807.2015
34. Park JA, Lee CH. Time-course change of redd1 expressions in the hippocampal CA1 region following chronic cerebral hypoperfusion. *Cell Mol Neurobiol.* (2017) 37:563–9. doi: 10.1007/s10571-016-0385-9
35. Zhang XJ, Cheng X, Yan ZZ, Fang J, Wang X, Wang W, et al. An ALOX12-12-HETE-GPR31 signaling axis is a key mediator of hepatic ischemia-reperfusion injury. *Nat Med.* (2018) 24:73–83. doi: 10.1038/nm.4451
36. Zhou MI, Foy RL, Chitalia VC, Zhao J, Panchenko MV, Wang H, et al. Jade-1, a candidate renal tumor suppressor that promotes apoptosis. *Proc Natl Acad Sci USA.* (2005) 102:11035–40. doi: 10.1073/pnas.0500757102
37. Havasi A, Haegele JA, Gall JM, Blackmon S, Ichimura T, Bonegio RG, et al. Histone acetyl transferase (HAT) HBO1 and JADE1 in epithelial cell regeneration. *Am J Pathol.* (2013) 182:152–62. doi: 10.1016/j.ajpath.2012.09.017
38. Rybak-Wolf A, Stottmeister C, GlaŽar P, Jens M, Pino N, Giusti S, et al. Circular RNAs in the mammalian brain are highly abundant, conserved, and dynamically expressed. *Mol Cell.* (2015) 58:870–85. doi: 10.1016/j.molcel.2015.03.027

Conflict of Interest: The authors declare that the research was conducted in the absence of any commercial or financial relationships that could be construed as a potential conflict of interest.

frontiers in Medicine

ORIGINAL RESEARCH
published: 05 May 2021
doi: 10.3389/fmed.2021.620988

Clonal Evolution Dynamics in Primary and Metastatic Lesions of Pancreatic Neuroendocrine Neoplasms

Zhou Tong[1†], Lin Wang[2†], Weiwei Shi[3], Yanwu Zeng[3], Hangyu Zhang[1], Lulu Liu[1], Yi Zheng[1], Chunlei Chen[4], Weiliang Xia[5], Weijia Fang[1,2] and Peng Zhao[1]*

[1] Department of Medical Oncology, The First Affiliated Hospital, Zhejiang University School of Medicine, Hangzhou, China, [2] Zhejiang Provincial Key Laboratory of Pancreatic Disease, The First Affiliated Hospital, Zhejiang University School of Medicine, Hangzhou, China, [3] OrigiMed, Shanghai, China, [4] State Key Laboratory for Diagnosis and Treatment of Infectious Disease, Collaborative Innovation Center for Diagnosis and Treatment of Infectious Diseases, The First Affiliated Hospital, Zhejiang University School of Medicine, Hangzhou, China, [5] Division of Hepatobiliary and Pancreatic Surgery, Department of Surgery, The First Affiliated Hospital, Zhejiang University School of Medicine, Hangzhou, China

OPEN ACCESS

Edited by:
Jianpeng Sheng, Nanyang Technological University, Singapore

Reviewed by:
Hong-Kun Wu, Zhejiang University, China
Yanfang Wang, Ludwig Maximilian University of Munich, Germany

***Correspondence:**
Peng Zhao
zhaop@zju.edu.cn

[†] These authors have contributed equally to this work

Specialty section:
This article was submitted to Gastroenterology, a section of the journal Frontiers in Medicine

Received: *24 October 2020*
Accepted: *06 April 2021*
Published: *05 May 2021*

Citation:
Tong Z, Wang L, Shi W, Zeng Y, Zhang H, Liu L, Zheng Y, Chen C, Xia W, Fang W and Zhao P (2021) Clonal Evolution Dynamics in Primary and Metastatic Lesions of Pancreatic Neuroendocrine Neoplasms. Front. Med. 8:620988. doi: 10.3389/fmed.2021.620988

Background: Data on inter-tumoral heterogeneity and clonal evolution of pancreatic neuroendocrine neoplasms (panNENs) with liver metastasis are limited. The aim of this study was to explore different patterns of clonal evolution of pancreatic neuroendocrine neoplasms with liver metastasis and the possible distinctive signaling pathways involved between G2 neuroendocrine tumors (NETs) and neuroendocrine carcinomas (NECs).

Methods: Tumor tissues of five patients (10 samples) with pancreatic neuroendocrine neoplasms with synchronous liver metastasis were analyzed using next-generation sequencing. PyClone, Gene Ontology, and Reactome pathway enrichment analysis were also applied.

Results: Mutated genes varied in individuals, reflecting the inter-tumoral heterogeneity of panNENs. The distribution of subclones varied during tumor metastasis, and different clonal evolution patterns were revealed between NETs and NECs. Gene Ontology and Reactome analyses revealed that in both NETs and NECs, signaling pathways and biological processes shared similarities and differences in the primary and metastatic lesions. In addition, the signaling pathway features were different between NETs and NECs. In the primary lesions, epigenetic changes and post-transcriptional modifications participated in NETs, while FGFR signaling, EGFR signaling, and NTRK2 signaling were largely involved in NECs. Although DNA repair and TP53 regulation were both involved in the metastatic lesions, most of the signaling pathways and biological processes disrupted by the mutated genes were different.

Conclusions: Our study revealed spatial inter-tumoral heterogeneity and temporal clonal evolution in PanNENs, providing potential therapeutic targets for further prospective clinical trials.

Keywords: clonal evolution, pancreatic neuroendocrine neoplasms, heterogeneity, liver metastasis, next-generation sequencing

INTRODUCTION

Pancreatic neuroendocrine neoplasms (panNENs) are heterogeneous tumors with distinct clinical syndromes and malignant potential. Unfortunately, the worldwide incidence and prevalence of panNENs have recently increased (1, 2). A subset of primary panNENs are aggressive and have a potential to metastasize. The 2019 World Health Organization (WHO) classification divides gastroenteropancreatic NENs into six groups—well-differentiated NETs G1, well-differentiated NETs G2, well-differentiated NETs G3, poorly-differentiated NECs—according to mitotic count and Ki-67 proliferation index, MiNEN and tumor-like lesions. Increased mitotic rate and high Ki-67 index are associated with a more aggressive clinical course and poorer prognosis (3, 4). Many studies have shown that distant metastases are related to poor overall survival in PanNENs (5, 6); however, the potential mechanisms of metastasis are poorly investigated and remain unclear.

Tumors progress and metastasize under Darwinian selection and evolution (7), and diverse genetic alterations create intra- and inter-tumoral heterogeneity. Difficulties with treatment, including drug resistance due to inter-tumoral heterogeneity and clonal evolution dynamics, are common. Some studies have shown concordance in mutational status between primary and distant metastases, where others do not (8, 9). Recent studies of breast cancer lung metastasis in mice showed that metastatic lesions were polyclonal, while omental metastases of high grade serous human ovarian cancer predominantly exhibited a single phylogenetic clade (10, 11). However, there are few studies investigating the clonal variation between primary and metastatic lesions of panNENs, or the different metastatic mechanisms among different grades. Studies of inter-tumoral heterogeneity in primary and metastatic lesions of panNENs are of great importance and could lead to more accurate clinical strategies for treatment.

The advent of next-generation sequencing (NGS) has increased understanding of tumor heterogeneity and clonal evolution (12, 13). In our study, we used a 450 oncogene sequencing panel to sequence pairs of primary tumors and hepatic metastases from synchronously metastasized panNENs from five patients. PyClone was applied to analyze the clonal populations and demonstrate the clonal distribution variation of primary and metastatic lesions. In addition, GO (Gene Ontology) and pathway enrichment analysis revealed distinct biological pathways that participated in primary and metastatic lesions in G2 neuroendocrine tumors (NETs) and neuroendocrine carcinomas (NECs).

MATERIALS AND METHODS

Patients

Five panNEN patients with synchronous liver metastasis were included. Fresh tumor specimens were collected at the time of synchronous resection of primary tumors and liver metastases. Primary tissue samples, metastatic tissue samples, and adjacent normal tissue samples were collected. Our research was permitted by the Ethics Committee of the First Affiliated Hospital of Zhejiang University and the patients were informed of and gave consent to the use of tumor tissues for this research. All methods were performed in accordance with the declaration of Helsinki. Patient characteristics including patient demographics, pathologic TNM staging, histology stage, tumor thrombus, functional status, surgical approach, disease free survival (DFS), and patient status were obtained. TNM staging was adopted according to the 8th AJCC cancer staging system for neuroendocrine tumors of the pancreas. Grade was adopted according to the new WHO 2019 grading classifications.

Hematoxylin and Eosin and Immunohistochemistry

Hematoxylin and eosin (HE) staining and immunohistochemistry against Ki67 were carried out on each sample to confirm diagnosis and to determine the histological subtype. Briefly, the tumor samples were fixed in 4% neutral paraformaldehyde, dehydrated via a gradient ethanol, and embedded within paraffin blocks. Then, the histological sections (5 um) were prepared, deparaffinized, hydrated, and subjected to HE staining and immunohistochemistry (IHC). For IHC, the hydrated sections were first heated in antigen retrieval buffer, permeabilized with PBS containing 0.1% Triton X-100, and then blocked with 1% bovine serum albumin (BSA). Then, the sections were incubated with a Ki67 primary antibody at 4°C overnight and treated with 3% H_2O_2 to inhibit endogenous peroxidases. Then, sections were incubated with an HRP-linked secondary antibody for 1 h at room temperature; 3,30-diaminobenzidine was used as a chromogenic agent. Finally, the nuclei were stained with hematoxylin before dehydration and mounting.

Hybrid Selection and Sequencing

A custom hybridization capture panel including over 23,660 individually synthesized 5′-biotinylated DNA 120 bp oligonucleotides was used to target ∼2.6 Mb of the human genome, including most exons of cancer-related genes and select introns of genes frequently rearranged in cancer (a 450 oncogene sequencing panel was used; gene names are listed in **Supplementary Table 1**). Hybridization capture employed xGen® Lockdown® Probes and Reagents (Integrated DNA Technologies, Version 3). Post-capture libraries were mixed, denatured, diluted, and then sequenced. For estimation of sequencing error rate, a PhiX spike-in was added as an external control to measure the percentage of reads with 0–4 mismatches, following the method described by Manley et al. (14). The average sequencing depth was 1000X for tissue-based deep sequencing.

Bioinformatics Pipeline for SNV and Short Indels

Alignment of raw reads to the human genome reference sequence (hg19) was done with the Burrows-Wheeler Aligner (BWA, v0.6.2), followed by PCR duplicate removal using the MarkDuplicates algorithm from Picard (version 1.47, http://picard.sourceforge.net/). Local realignment and base quality recalibration for single nucleotide variants (SNV) were performed using GATK (v3.1-1) and subsequently culled by MUTECT (v1.7).

Bioinformatics Pipeline for Copy Number Alternations

To identify CNA, aligned reads were first normalized within each bed by EXCAVATOR (version v2.2, http://sourceforge.net/projects/excavatortool/). Log ratio of read depths for each gene from tumor tissue and its matched normal blood control was then calculated. Tumor cellularity was estimated by allele frequencies of 4,088 sequenced SNPs (single nucleotide polymorphism), following the method in ASCAT.

Bioinformatics Pipeline for Gene Rearrangement

For detection of gene rearrangement, aligned reads with abnormal insert size of over 2,000 or zero bp were collected and used as discordant reads, i.e., paired-end reads that could not be closely mapped to a genome reference, with each read of paired-reads aligned to the same chromosomes or different chromosomes. Originally, the discordant reads with the distance $<$ 500 bp formed clusters were further assembled by fermi-lite (https://github.com/lh3/fermi-lite) to identify potential rearrangement breakpoints. The breakpoints were double-confirmed by BLAT and the resulted chimeric gene candidates were annotated.

Tumor Mutation Burden and Microsatellite Instability

Tumor mutation burden (TMB) was estimated by counting somatic mutations, including coding SNVs and indels per megabase of the sequence examined. Driver mutations and known germline alterations in dbSNP were not counted. MSI status was inferred based on MANTIS (15) score, and microsatellite regions were manually reviewed in Integrated Genomics Viewer (IGV) (16) for confirmation.

PyClone

A Bayesian clustering method, PyClone, was used to infer clonal population structures present in the tumor as previously described (17). Briefly, given the mutation allele frequencies for each sample, PyClone estimates cellular prevalence for each cluster in each sample. PyClone is freely available for academic use at https://github.com/Roth-Lab/pyclone.

GO and Reactome Pathway Enrichment Analysis

Related genes were selected using the Cytoscape GeneMANIA plugin (18). Genes from NEC and NET samples were combined separately and enrichment analysis for Biological Process was performed using the R software clusterProfiler (19) package with the pvalueCutoff set as 0.05. Reactome pathway enrichment analysis was performed using the ReactomePA package (20) with the p-value cutoff set as 0.05. Only the top 20 entries with a minimum adjusted p-value for primary and metastatic sites were included in the dotplot.

RESULTS

Patient Demographics

Five panNEN patients with synchronous liver metastasis were included. All patients received synchronous resection of primary and liver metastases. The pathology of patients 1 and 2 was NEC. In the primary and metastatic lesions, the cells were poorly differentiated, composed of highly atypical neoplastic cells, with a mitotic rate $>$ 20/10 high-power fields, and ki67 $>$ 20%. Patient 3, patient 4, and patient 5 were G2 NET. The cells were arranged in nests and glandular tubes, were trabecular, had a mitotic rate of 2–20/10 high-power fields, and ki67 3–20%. All tumors were positive for Synaptophysin and Chromogranin A. Representative hematoxylin- and eosin-stained sections and IHC against ki67 in primary tumors and metastases are shown in **Figure 1**. TNM stage is also listed. All tumors were non-functioning. The tumors of patients 1 and 2 exhibited perineural invasion, and patient 5 was confirmed to have tumor thrombus. Among the surgical choices for these patients, four patients were treated with distal pancreatectomy and one by pancreaticoduodenectomy. Liver tumor resection was performed in all cases. Mean follow-up time was 51.7 months (46.9–54.6 months). Patient characteristics are listed in **Table 1**.

Sequencing

All primary and metastatic lesions of the five patients were sequenced (**Figure 2**, **Supplementary Table 2**) using a 450 oncogene sequencing panel. In patient 1, EPHA2, KRAS, SMARCB1, APC, and SPINK1 were altered in both primary and metastatic lesions, whereas RNF43 and AXIN2 were altered only in metastatic lesions. The VAF of EPHA2, KRAS, SMARCB1, APC all arose in metastatic lesion. In patient 2, TP53 and MEN1 were altered in both samples. Alteration of PIK3CA, RARA, CARD11, TET1, and PRSS1 were found only in the primary lesion while PRSS8 and PLA2G1B were found only in the metastatic lesion. The VAF of TP53 and MEN1 decreased in metastatic lesion. In patient 3, ETV1 was altered in the primary lesion and FGFR3 was altered in the metastatic lesion. In patient 4, MEN1, TSC2, and SIK1 were altered in both lesions and the VAF of TSC2 and MEN1 decreased in metastatic lesion. In patient 5, ATRX and MEN1 were altered in the primary and metastatic lesions. SMAD4 and TSC2 were altered in the primary lesion while FANCM was altered in the metastatic lesion. The VAF of ATRX arose from 0.53 to 0.57 in metastatic lesion while VAF of MEN1 decreased from 0.42 to 0.38. Mutated genes varied in the individuals, reflecting the heterogeneity of NETs and NECs. Compared with NETs, more mutations were revealed in NECs (more than five alterations in both primary lesions and metastatic lesions). And in NETs, gene alterations were less than four. After metastasis, the VAF elevated in one NEC patient, while the increasing VAF were hardly seen in NETs. In addition, in each patient, most of the mutated genes in the primary and metastatic lesions were common (except for patient 3). The TMB value varied from 1.6 to 6.4 mut/Mb in the five patients. All patients were classified as microsatellite stable (MSS).

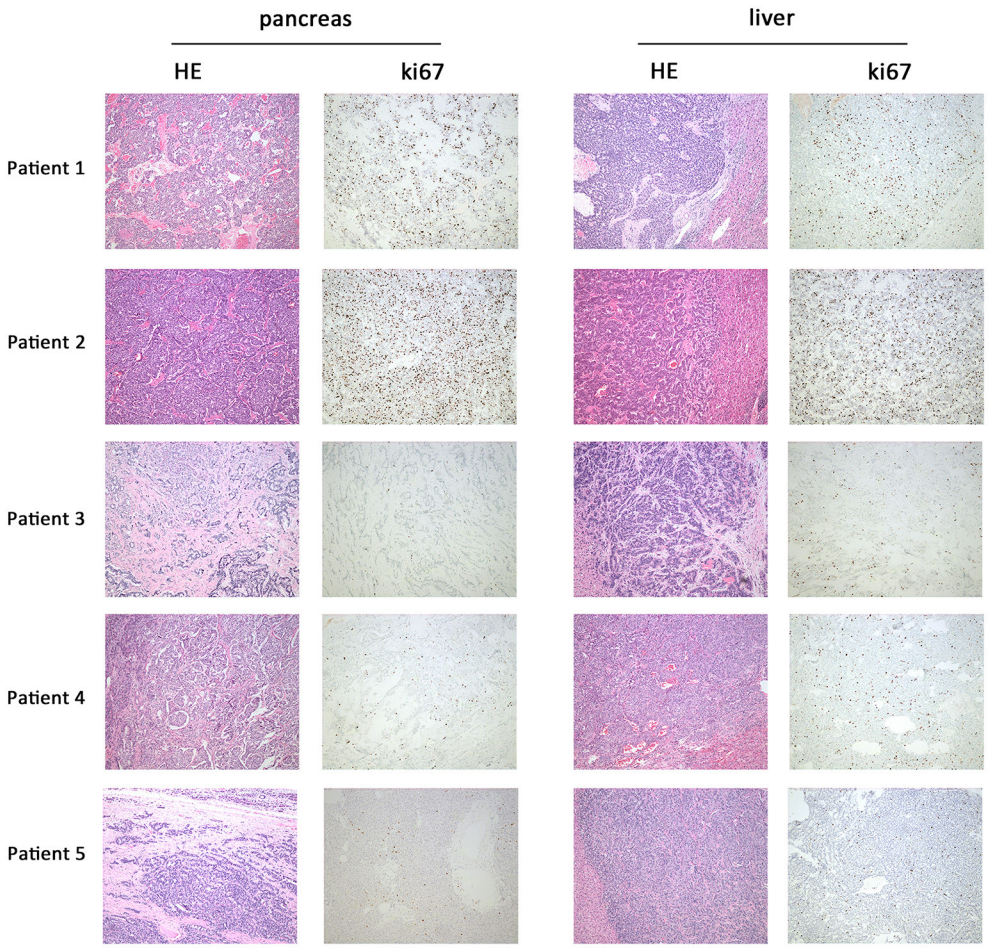

FIGURE 1 | Representative hematoxylin and eosin and immunohistochemistry against ki67 in primary and metastatic lesions. In patient 1 and patient 2, HE staining of primary (pancreas) and metastatic lesions (liver) showed a mitotic count >20/10 HPF; the cells were poorly differentiated and composed of highly atypical neoplastic cells. Ki67 of patient 1 was 30–40%; patient 2 was 25–30%. In patients 3, 4, and 5, HE staining showed a mitotic count of 2–20/10 HPF. The cells were arranged in nests, glandular tubes, and were trabecular. Ki67 of patient 3 was 10–20%, patient 4 was 5–10%, and patient 5 was 8–10%. Magnification: 100x.

PyClone

Based on variations identified using Bayesian clustering with PyClone, we identified three clusters in patients 1 and 2 (**Figures 3A,B**), one cluster in patient 3, and two clusters in patients 4 and 5 (**Figures 3C–E**); one cluster represents one subclone. Inter-tumoral heterogeneity was observed between the primary tumor samples and the metastases. The distribution of subclones changed, reflecting the evolution of tumors from primary to metastatic lesions. All tumor samples except for those of patient 3 showed evidence of subclonal structure.

NEC patients had three clonal populations in the primary lesions, while two clonal populations were identified in patient 1 and only one clonal population in patient 2. In addition, fewer clonal populations were found in G2 NETs and only one clonal population was identified in the metastatic lesions. Different clonal evolution patterns were identified between NETs and NECs.

GO Term and Reactome Analysis

We performed Gene Ontology (GO) enrichment analysis and Reactome analysis on sets of genes mutated in NETs and NECs. Mutated genes in the primary lesions of NET participated in sets of epigenetic changes and post-transcriptional modifications, such as histone methylation, chromatin modification, and macromolecule and protein methylation. In addition, the Reactome analysis showed that chromatin organization, SUMOylation, and the RUNX1 and NOTCH signaling pathways were most involved in the primary lesion. In the metastatic lesions of NETs, however, both Reactome and GO analysis showed that the mutated genes were prone to participation in histone and chromatin modification, DNA structure changes, DNA repair, and TP53 regulation. Histone and chromatin modification, DNA repair, and the regulation of TP53 and RUNX1 were involved in the primary and metastatic lesions in NET, whereas most other pathways were different (**Figures 4A,B**).

TABLE 1 | Characteristics of the five patients.

	Age	Gender	Grade	Differentiated	T	N	M	Perineural invasion	Tumor thrombus	Surgical approaches	Function	DFS (mo)	Status	OS (mo)
Patient 1	48	Male	G3	Poorly-differentiated	3	0	1	Yes	No	Pancreaticoduodenectoy + liver tumor resection	No	1.47	Deceased	51.8
Patient 2	61	Male	G3	Poorly-differentiated	3	1	1	Yes	No	Distal pancreatectomy + liver tumor resection	No	7.97	Deceased	45.9
Patient 3	70	Female	G2	Well-differentiated	4	0	1	No	No	Distal pancreatectomy + liver tumor resection	No	1.20	Alive	>53.8
Patient 4	59	Male	G2	Well-differentiated	2	0	1	No	No	Distal pancreatectomy + liver tumor resection	No	17.00	Alive	>50.1
Patient 5	71	Male	G2	Well-differentiated	3	1	1	No	Yes	Distal pancreatectomy + liver tumor resection	No	1.20	Alive	>53.4

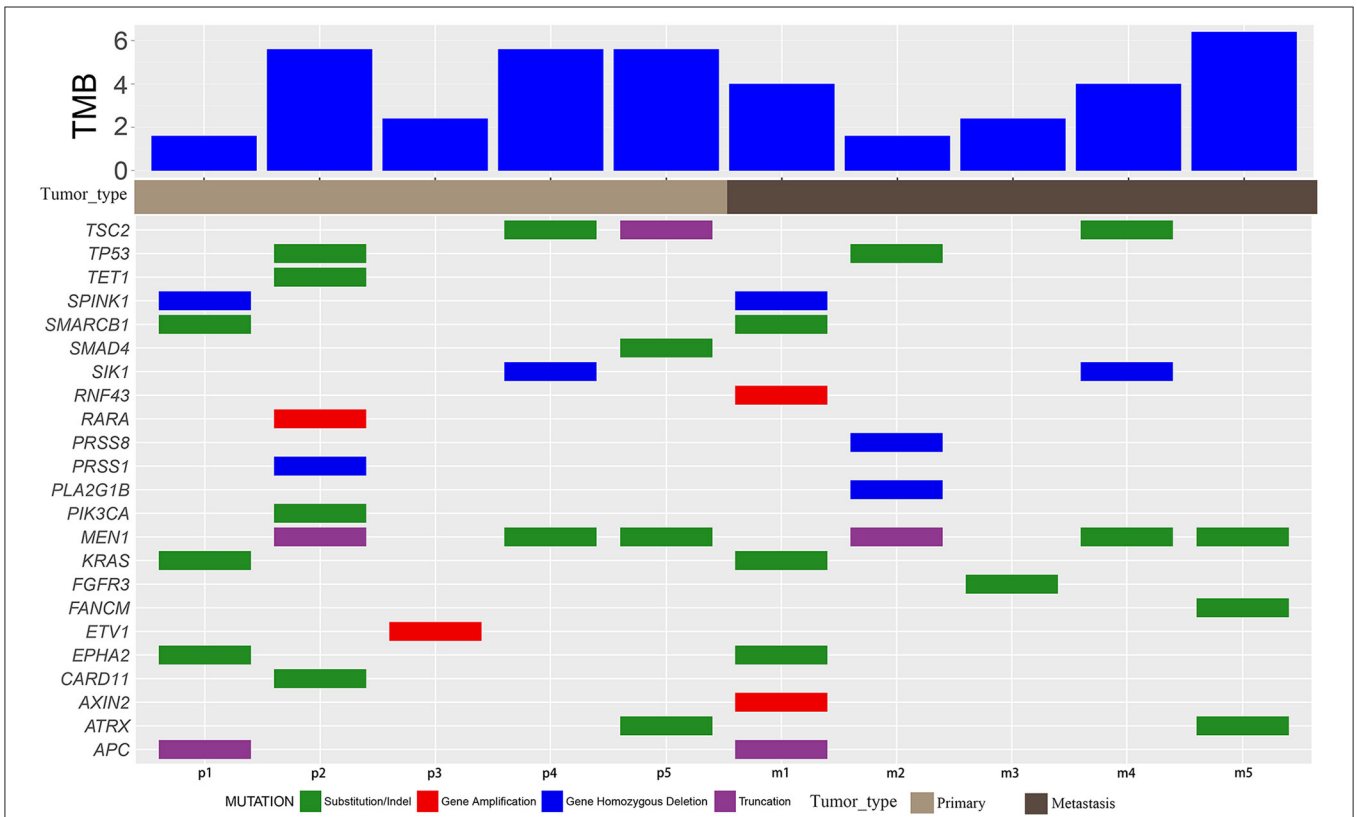

FIGURE 2 | Mutation characteristics and TMB. Mutation details of primary (p) and metastatic (m) samples of patients 1–5. Green blocks represent substitution/indel. Red blocks represent gene amplification. Blue blocks represent homozygous gene deletion. Purple blocks represent truncation.

In the primary lesions of NECs, GO analysis revealed that the mutated genes were most related to radiation response, cellular response to peptides and hormones, and transcription factor activity regulation. The Reactome analysis found that FGFR signaling, EGFR signaling, and NTRK2 signaling were largely involved in the NEC primary lesions. In the metastatic lesions of NECs, GO analysis showed that the mutated genes largely participated in organ development and differentiation processes. Reactome analysis revealed that mutated genes influenced DNA repair, chromatin modification, SUMOylation, WNT signaling, and the regulation of transcription and activity of TP53 and RUNX1. The common pathways between the primary and metastatic lesions in NECs were rare except for radiation response (**Figures 5A,B**).

These data revealed that in both NETs and NECs, signaling pathways and biological processes shared similarities and differences in the primary and metastatic lesions. However, the signaling pathways and biological process patterns were different between NETs and NECs. In the primary lesion, epigenetic changes and post-transcriptional modification participated in NETs, while FGFR signaling, EGFR signaling, and NTRK2 signaling were largely involved in NECs. In the metastatic lesions,

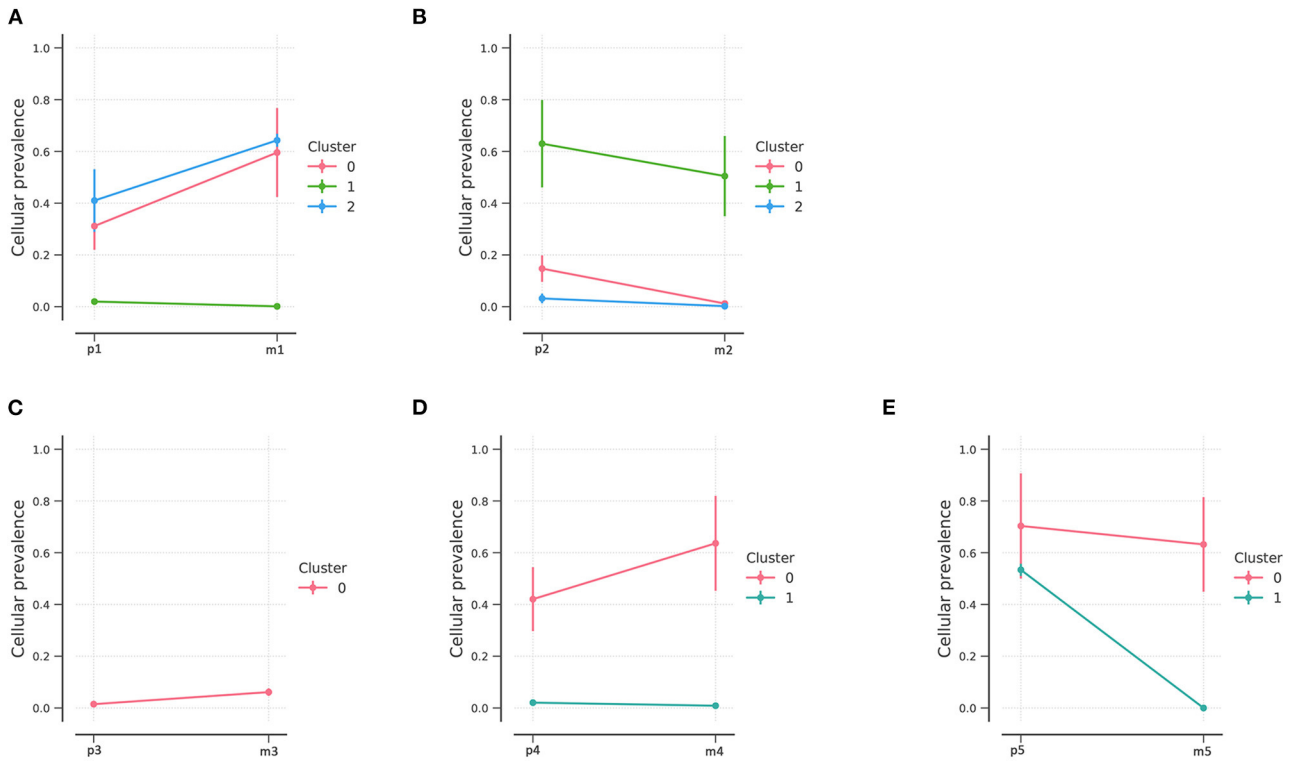

FIGURE 3 | PyClone analysis of the five patients. PyClone quantification of clonal populations in sequenced mutations of patients 1–5 (**A–E**, respectively). Cellular prevalence of clonal populations is the mean value of the cellular prevalence of mutations in the cluster. The predicted cellular frequencies represent the proportion of cancer cells in each set of clonal mutation.

although DNA repair and TP53 regulation were both involved, most of the signaling pathways and biological process disrupted by the mutated genes were different between NETs and NECs.

DISCUSSION

Clonal evolution is defined by tumor heterogeneity over both space and time (21). Clonal evolutionary processes have been observed in many tumor types including pancreatic cancer (22), leukemia (23), and renal-cell carcinoma (24). Several large-scale genomic studies have characterized panNET genomes, including hundreds of somatic mutations and copy number variations, and reported that significantly mutated genes such as MEN1, DAXX, ATRX contribute to the mutagenic processes (25–27). Most panNECs harbor TP53 and RB1 alterations and lack neuroendocrine-related genetic changes (28). However, few researchers have studied the relationship between primary and metastatic lesions of individual panNENs from the perspective of clonal evolution. Our study performed NGS on five pairs of tumor lesions, revealing a comprehensive analysis of the course of tumor genomic evolution from primary lesion to metastatic lesion.

Tumors progress under Darwinian evolution, in which genetic variation alters molecular phenotypes in individual cells (29). Consequently, tumors often consist of multiple genes and different cell populations. These populations, known as clones, undergo selection in response to different tumor microenvironments or therapeutic interventions (30). Identifying dynamic clonal population structures can aid in predicting metastatic potential and chemotherapeutic resistance (17). PyClone is a Bayesian clustering method for grouping sets of somatic mutations into clonal clusters (17). PyClone was performed in the current study and identified three mutant clonal populations of primary lesions of panNEC and two clonal populations of panNET. Through the clone analysis, the sub-clones in each patient were identified, and the distribution of sub-clones reflected the evolutionary process of the tumors. Some clonal populations diminished, and some clonal populations expanded, which is one of the features of clonal evolution. Interestingly, metastatic lesions in NET patients tended to be from a single clone, which suggests monoclonal seeding from pancreatic lesion to liver and suggests a distinct clonal evolution mode from NEC. More importantly, the result should be confirmed by multiple lesion biopsies and NGS. It has been reported that panNETs exhibit a lower mutation burden (25), which may account for the small number of clonal populations in panNETs.

The failure of therapy and drug resistance is partially caused by intratumor heterogeneity, which provides diverse genetic material under evolutionary selection. In these five patients, the mutated genes varied in the individuals. The data from our study support the notion that pancreatic neuroendocrine

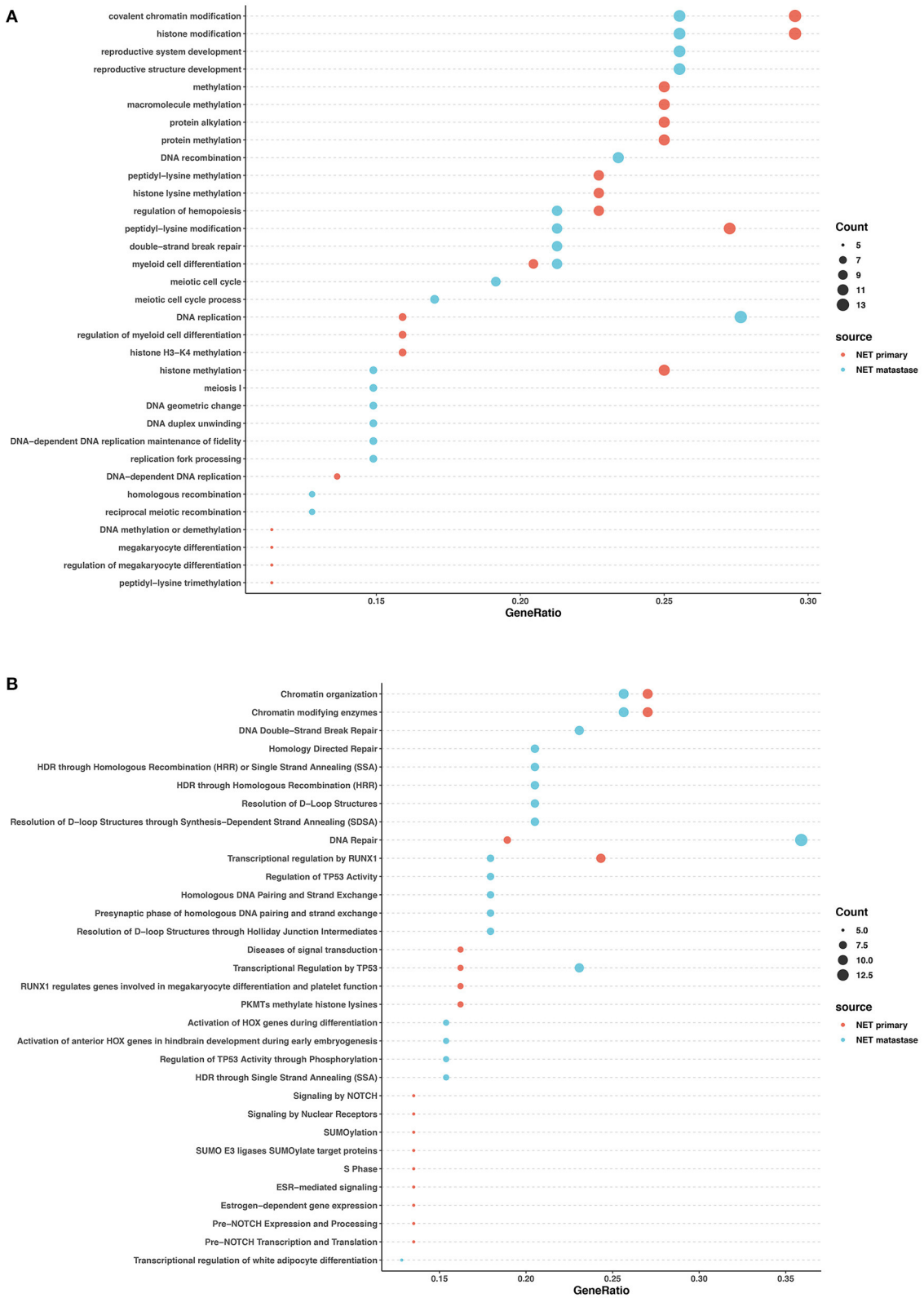

FIGURE 4 | GO and pathway enrichment analysis of mutated genes involved in G2 NETs. GO enrichment analysis of biological process in mutated genes in NETs **(A)**. Reactome pathway enrichment analysis in NETs **(B)**. Dot size corresponds to number of genes; gene ratio is defined as percentage of genes in certain pathways compared with all genes in the samples.

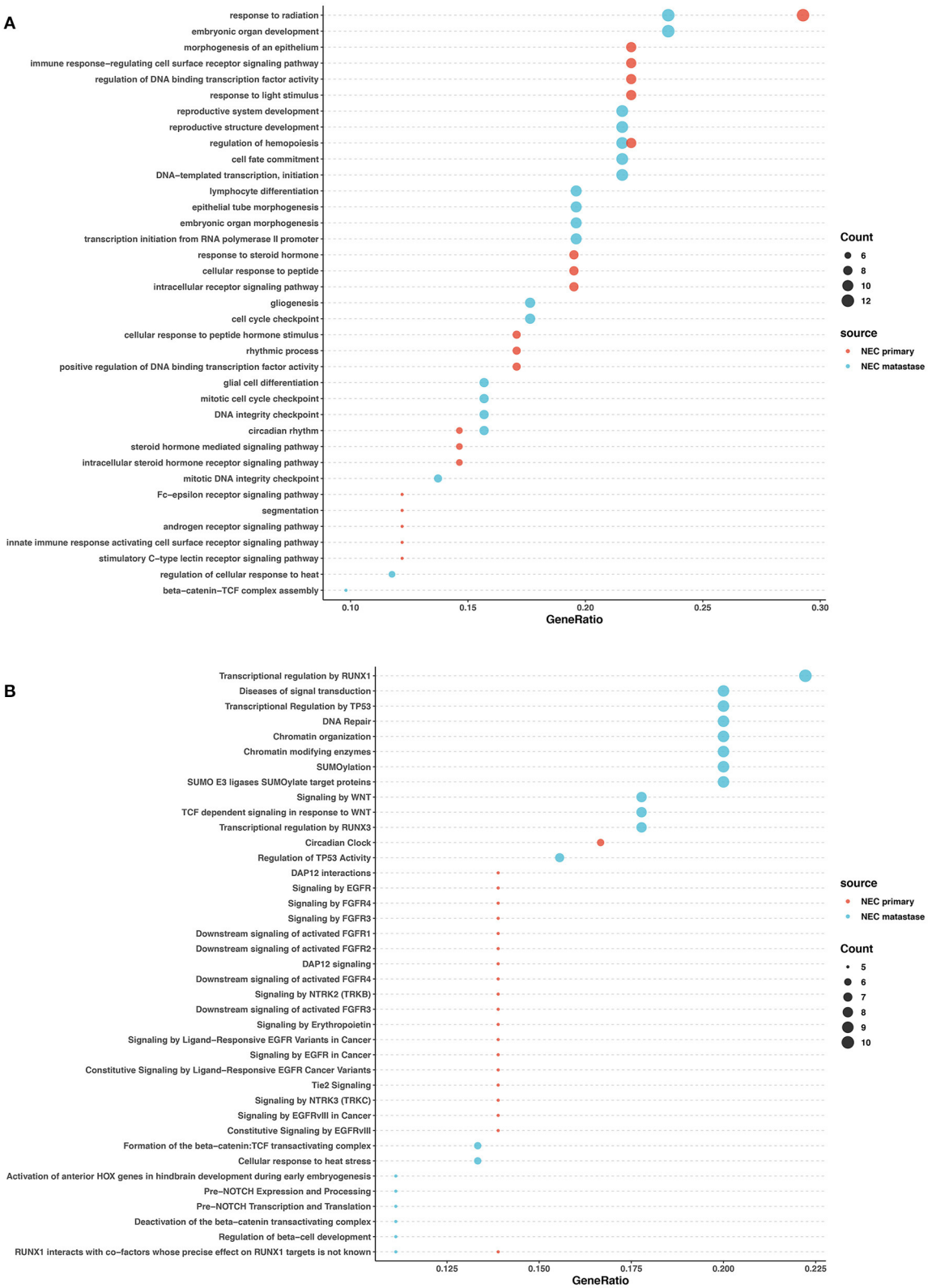

FIGURE 5 | GO and pathway enrichment analysis of mutated genes involved in NECs. GO enrichment analysis of biological processes in mutated genes in NECs **(A)**. Reactome pathway enrichment analysis in NEC **(B)**. Dot size corresponds to number of genes; gene ratio is defined as the percentage of genes in certain pathways compared with all genes in the samples.

carcinomas are fundamentally discordant from neuroendocrine tumors. Apart from their clinicopathological features, including histologic architecture, hormone production, and malignancy, the genetic profile differed. In patient 2, with the shortest overall survival, 45.9 months, TP53 was mutated in both the primary and metastatic lesions. It has been reported that in panNEC, ∼70% of the tumors harbor TP53 mutations (28, 31, 32). Alternatively, in well-differentiated neuroendocrine neoplasms of the pancreas, TP53 mutations rarely occur. TP53 mutations, have been consistently associated with poor prognosis in cancers (33). Consistent with the literature, deleterious TP53 mutations were uncommon in panNET in our study. KRAS mutation was observed in one NEC patient and mutations in KRAS codon 12 were independently associated with a worse survival vs. wild-type KRAS (34). Somatic mutations of MEN1 occur in 30–44% of panNETs (25, 35, 36). In our study, patients 4 and 5 carried MEN1 mutations and patient 5 had a mutation of ATRX. DAXX and ATRX are mutually exclusive inactivating mutations, and no tumor with a mutation in ATRX had a mutation in DAXX. It has been reported that mutations in the MEN1 and the DAXX/ATRX genes are associated with prolonged survival compared with patients with tumors that lack these mutations (35). However, Fei Yuan et al. (37) and Marinoni et al. (38) reported that mutations of DAXX/ATRX were associated with a shortened survival. TSC2 mutations, which inhibit the mTOR signaling pathway and are mutually exclusive of mutations of PTEN, were revealed in patients 4 and 5. It has been reported that mTOR pathway genes (PTEN and TSC2) did not predict the pNET patients' survival (37). In addition, we observed high rates of common mutations in the primary and metastatc samples in these patients, except for patient 3. Recent studies on malignancies such as head and neck squamous cell carcinoma, non-small cell lung cancer, endometrial cancer, and small cell lung cancer all observed high rates of common mutations in primary and metastatic lesions (39–41).

Clonal evolution has two patterns, linear evolution or branched evolution. The linear model states that tumor cells acquire mutations over time, and that the strongest tumor becomes dominant. The branching evolution model states that parallel tumor cell clones acquire different genomic mutations over time (42, 43). In our study, both NEC and NET patients shared similar mutations in the primary and metastatic lesions, indicating the tumors were homogeneous at different locations and revealing a probable linear evolution model in PanNENs. This result should be confirmed by multiple biopsy analysis.

The mutated genes in the primary and metastatic lesions of NETs and NECs were analyzed via GO and Reactome analysis to explore the affected biological processes and pathways. The results revealed that the involved biological process and pathways were largely different among the primary and metastatic lesions of NETs and NECs. In NEC primary lesions, the EGFR, FGFR, and NTRK3 pathways were also involved. EGFR, FGFR, and NTRK3 targeted therapy may therefore be new options for NEC patients; however, clinical trials are required to validate this hypothesis. Further, mutated genes in the primary lesions of NETs exhibited sets of epigenetic changes, raising the intriguing possibility of epigenetic inhibitor treatment. Interestingly, though TP53 mutation was not detected in both primary and metastatic lesions in NETs, the Reactome analysis demonstrated that transcriptional regulation of TP53 was involved in NET primary lesions, whereas both the transcriptional regulation and activity regulation of TP53 were involved in NET metastasis. These results indicated that TP53 dysregulation may also play an important role in NET carcinogenesis and metastasis. In addition, we found that the DNA repair pathway participated in both NET and NEC metastasis. It has been reported that failed DNA repair can lead to carcinogenesis and tumor genome instability (44). And defects in DNA repair pathways may indicate a potential vulnerability to DNA-damaging therapies such as platinum (45). Additionally, oxaliplatin-based chemotherapy also shows a relatively high response rate in NETs (46). These findings not only provide better understanding of the mechanisms of NEC and NET carcinogenesis and metastasis, partially explaining the different clonal evolution patterns, but also give new insight into potential therapeutic approaches.

Immune checkpoint inhibitors have recently gained the attention of oncologists. PD-1/PD-L1 expression, tumor mutation burden, and DNA mismatch repair deficiency (dMMR) have been demonstrated as three potential biomarkers for the use of immune checkpoint inhibitors (47–50). Our results showed low TMB and MSS in both primary and metastatic lesions, which is consistent with other reports showing that neuroendocrine tumors have a relatively low mutation burden compared with other tumors (51) and may not benefit from immunotherapy.

This is the first study comparing primary and metastatic lesions of panNENs within the same person using NGS. Our study showed the mutation variation of primary and metastatic lesions and revealed clonal evolution dynamics in panNENs. We further detected different signaling pathways involved in the clonal evolution of NETs and NECs. However, our study had some limitations. The sample size was limited mostly due to the low incidence of PanNENs, and further studies including whole genome sequencing and other experimental studies are needed to verify the results. Our study does shed light on potential novel approaches for predicting and treating panNEN patients with synchronous liver metastasis.

CONCLUSIONS

Our study revealed spatial inter-tumoral heterogeneity and temporal clonal evolution in PanNENs, which provides potential therapeutic targets for further prospective clinical trials.

DATA AVAILABILITY STATEMENT

According to national legislation/guidelines, specifically the Administrative Regulations of the People's Republic of China on Human Genetic Resources (http://www.gov.cn/zhengce/content/2019-06/10/content_5398829.htm, http://english.www.gov.cn/policies/latest_releases/2019/06/10/content_281476708945462.htm), no additional raw data is available at this time. Data of this project can be accessed after an approval application to the China

National Genebank (CNGB, https://db.cngb.org/cnsa/). Please refer to https://db.cngb.org/, or email: CNGBdb@cngb.org for detailed application guidance. The accession code CNP0001685 should be included in the application.

ETHICS STATEMENT

The studies involving human participants were reviewed and approved by Research Ethics Committee of the First Affiliated Hospital, College of Medicine, Zhejiang University (2017-778). The patients/participants provided their written informed consent to participate in this study.

AUTHOR CONTRIBUTIONS

ZT wrote the manuscript. LW, WS, and YZe analyzed the data. HZ and LL collected the clinical and pathological information from the cancer patients. YZh and CC designed the study. WF, WX, and PZ revised the manuscript. All authors contributed to the article and approved the submitted version.

FUNDING

This work was supported by National Natural Science Foundation of China (81472346), Natural Science Foundation of Zhejiang Province (LY15H030012). The funding source had no role in the design of the study, data collection, data analysis, or manuscript writing.

SUPPLEMENTARY MATERIAL

The Supplementary Material for this article can be found online at: https://www.frontiersin.org/articles/10.3389/fmed.2021.620988/full#supplementary-material

REFERENCES

1. Yao JC, Hassan M, Phan A, Dagohoy C, Leary C, Mares JE, et al. One hundred years after "carcinoid": epidemiology of and prognostic factors for neuroendocrine tumors in 35,825 cases in the United States. *J Clin Oncol.* (2008) 26:3063–72. doi: 10.1200/JCO.2007.15.4377
2. Metz DC, Jensen RT. Gastrointestinal neuroendocrine tumors: pancreatic endocrine tumors. *Gastroenterology.* (2008) 135:1469–92. doi: 10.1053/j.gastro.2008.05.047
3. Panzuto F, Boninsegna L, Fazio N, Campana D, Pia Brizzi M, Capurso G, et al. Metastatic and locally advanced pancreatic endocrine carcinomas: analysis of factors associated with disease progression. *J Clin Oncol.* (2011) 29:2372–7. doi: 10.1200/JCO.2010.33.0688
4. Pape UF, Jann H, Muller-Nordhorn J, Bockelbrink A, Berndt U, Willich SN, et al. Prognostic relevance of a novel TNM classification system for upper gastroenteropancreatic neuroendocrine tumors. *Cancer.* (2008) 113:256–65. doi: 10.1002/cncr.23549
5. Birnbaum DJ, Turrini O, Ewald J, Barbier L, Autret A, Hardwigsen J, et al. Pancreatic neuroendocrine tumor: a multivariate analysis of factors influencing survival. *Eur J Surg Oncol.* (2014) 40:1564–71. doi: 10.1016/j.ejso.2014.06.004
6. Li Z, Du S, Feng W, Zhang W, Li G, Wei J, et al. Competing risks and cause-specific mortality in patients with pancreatic neuroendocrine tumors. *Eur J Gastroenterol Hepatol.* (2019) 31:749–55. doi: 10.1097/MEG.0000000000001350
7. McGranahan N, Swanton C. Clonal heterogeneity and tumor evolution: past, present, and the future. *Cell.* (2017) 168:613–28. doi: 10.1016/j.cell.2017.01.018
8. Brannon AR, Vakiani E, Sylvester BE, Scott SN, McDermott G, Shah RH, et al. Comparative sequencing analysis reveals high genomic concordance between matched primary and metastatic colorectal cancer lesions. *Genome Biol.* (2014) 15:454. doi: 10.1186/s13059-014-0454-7
9. Sebagh M, Allard MA, Bosselut N, Dao M, Vibert E, Lewin M, et al. Evidence of intermetastatic heterogeneity for pathological response and genetic mutations within colorectal liver metastases following preoperative chemotherapy. *Oncotarget.* (2016) 7:21591–600. doi: 10.18632/oncotarget.7809
10. McPherson A, Roth A, Laks E, Masud T, Bashashati A, Zhang AW, et al. Divergent modes of clonal spread and intraperitoneal mixing in high-grade serous ovarian cancer. *Nat Genet.* (2016) 48:758–67. doi: 10.1038/ng.3573
11. Cheung KJ, Padmanaban V, Silvestri V, Schipper K, Cohen JD, Fairchild AN, et al. Polyclonal breast cancer metastases arise from collective dissemination of keratin 14-expressing tumor cell clusters. *Proc Natl Acad Sci USA.* (2016) 113:E854–63. doi: 10.1073/pnas.1508541113
12. Zhao B, Hemann MT, Lauffenburger DA. Modeling tumor clonal evolution for drug combinations design. *Trends Cancer.* (2016) 2:144–58. doi: 10.1016/j.trecan.2016.02.001
13. Ding L, Raphael BJ, Chen F, Wendl MC. Advances for studying clonal evolution in cancer. *Cancer Lett.* (2013) 340:212–9. doi: 10.1016/j.canlet.2012.12.028
14. Manley LJ, Ma D, Levine SS. Monitoring error rates in illumina sequencing. *J Biomol Tech.* (2016) 27:125–8. doi: 10.7171/jbt.16-2704-002
15. Kautto EA, Bonneville R, Miya J, Yu L, Krook MA, Reeser JW, et al. Performance evaluation for rapid detection of pan-cancer microsatellite instability with MANTIS. *Oncotarget.* (2017) 8:7452. doi: 10.18632/oncotarget.13918
16. Robinson JT, Thorvaldsdóttir H, Winckler W, Guttman M, Lander ES, Getz G, et al. Integrative genomics viewer. *Nat Biotechnol.* (2011) 29:24–6. doi: 10.1038/nbt.1754
17. Roth A, Khattra J, Yap D, Wan A, Laks E, Biele J, et al. PyClone: statistical inference of clonal population structure in cancer. *Nat Methods.* (2014) 11:396–8. doi: 10.1038/nmeth.2883
18. Montojo J, Zuberi K, Rodriguez H, Bader GD, Morris Q. GeneMANIA: fast gene network construction and function prediction for Cytoscape. *F1000Res.* (2014) 3:153. doi: 10.12688/f1000research.4572.1
19. Yu G, Wang LG, Han Y, He QY. clusterProfiler: an R package for comparing biological themes among gene clusters. *OMICS.* (2012) 16:284–7. doi: 10.1089/omi.2011.0118
20. Yu G, He QY. ReactomePA: an R/Bioconductor package for reactome pathway analysis and visualization. *Mol Biosyst.* (2016) 12:477–9. doi: 10.1039/C5MB00663E
21. Amirouchene-Angelozzi N, Swanton C, Bardelli A. Tumor evolution as a therapeutic target. *Cancer Discov.* (2017) 7:805–17. doi: 10.1158/2159-8290.CD-17-0343
22. Yachida S, Jones S, Bozic I, Antal T, Leary R, Fu B, et al. Distant metastasis occurs late during the genetic evolution of pancreatic cancer. *Nature.* (2010) 467:1114–7. doi: 10.1038/nature09515
23. Anderson K, Lutz C, van Delft FW, Bateman CM, Guo Y, Colman SM, et al. Genetic variegation of clonal architecture and propagating cells in leukaemia. *Nature.* (2011) 469:356–61. doi: 10.1038/nature09650
24. Gerlinger M, Rowan AJ, Horswell S, Math M, Larkin J, Endesfelder D, et al. Intratumor heterogeneity and branched evolution revealed by multiregion sequencing. *N Engl J Med.* (2012) 366:883–92. doi: 10.1056/NEJMoa1113205
25. Scarpa A, Chang DK, Nones K, Corbo V, Patch AM, Bailey P, et al. Whole-genome landscape of pancreatic neuroendocrine tumours. *Nature.* (2017) 543:65–71. doi: 10.1038/nature21063
26. Pea A, Yu J, Marchionni L, Noe M, Luchini C, Pulvirenti A, et al. Genetic analysis of small well-differentiated pancreatic neuroendocrine tumors

identifies subgroups with differing risks of liver metastases. *Ann Surg.* (2020) 271:566–73. doi: 10.1097/SLA.0000000000003022
27. Chan CS, Laddha SV, Lewis PW, Koletsky MS, Robzyk K, Da Silva E, et al. ATRX, DAXX or MEN1 mutant pancreatic neuroendocrine tumors are a distinct alpha-cell signature subgroup. *Nat Commun.* (2018) 9:4158. doi: 10.1038/s41467-018-06498-2
28. Konukiewitz B, Jesinghaus M, Steiger K, Schlitter AM, Kasajima A, Sipos B, et al. Pancreatic neuroendocrine carcinomas reveal a closer relationship to ductal adenocarcinomas than to neuroendocrine tumors G3. *Hum Pathol.* (2018) 77:70–9. doi: 10.1016/j.humpath.2018.03.018
29. Gonzalgo ML, Jones PA. Mutagenic and epigenetic effects of DNA methylation. *Mutat Res.* (1997) 386:107–18. doi: 10.1016/S1383-5742(96)00047-6
30. Aparicio S, Caldas C. The implications of clonal genome evolution for cancer medicine. *N Engl J Med.* (2013) 368:842–51. doi: 10.1056/NEJMra1204892
31. Konukiewitz B, Schlitter AM, Jesinghaus M, Pfister D, Steiger K, Segler A, et al. Somatostatin receptor expression related to TP53 and RB1 alterations in pancreatic and extrapancreatic neuroendocrine neoplasms with a Ki67-index above 20. *Modern Pathol.* (2017) 30:587–98. doi: 10.1038/modpathol.2016.217
32. Yachida S, Vakiani E, White CM, Zhong Y, Saunders T, Morgan R, et al. Small cell and large cell neuroendocrine carcinomas of the pancreas are genetically similar and distinct from well-differentiated pancreatic neuroendocrine tumors. *Am J Surg Pathol.* (2012) 36:173–84. doi: 10.1097/PAS.0b013e3182417d36
33. Olivier M, Hollstein M, Hainaut P. TP53 mutations in human cancers: origins, consequences, and clinical use. *Cold Spring Harbor Perspect Biol.* (2010) 2:a001008. doi: 10.1101/cshperspect.a001008
34. Hayama T, Hashiguchi Y, Okamoto K, Okada Y, Ono K, Shimada R, et al. G12V and G12C mutations in the gene KRAS are associated with a poorer prognosis in primary colorectal cancer. *Int J Colorectal Dis.* (2019) 34:1491–6. doi: 10.1007/s00384-019-03344-9
35. Jiao Y, Shi C, Edil BH, de Wilde RF, Klimstra DS, Maitra A, et al. DAXX/ATRX, MEN1, and mTOR pathway genes are frequently altered in pancreatic neuroendocrine tumors. *Science.* (2011) 331:1199–203. doi: 10.1126/science.1200609
36. Corbo V, Dalai I, Scardoni M, Barbi S, Beghelli S, Bersani S, et al. MEN1 in pancreatic endocrine tumors: analysis of gene and protein status in 169 sporadic neoplasms reveals alterations in the vast majority of cases. *Endocr Relat Cancer.* (2010) 17:771–83. doi: 10.1677/ERC-10-0028
37. Yuan F, Shi M, Ji J, Shi H, Zhou C, Yu Y, et al. KRAS and DAXX/ATRX gene mutations are correlated with the clinicopathological features, advanced diseases, and poor prognosis in Chinese patients with pancreatic neuroendocrine tumors. *Int J Biol Sci.* (2014) 10:957–65. doi: 10.7150/ijbs.9773
38. Marinoni I, Kurrer AS, Vassella E, Dettmer M, Rudolph T, Banz V, et al. Loss of DAXX and ATRX are associated with chromosome instability and reduced survival of patients with pancreatic neuroendocrine tumors. *Gastroenterology.* (2014) 146:453–60.e455. doi: 10.1053/j.gastro.2013.10.020
39. Saber A, Hiltermann TJN, Kok K, Terpstra MM, de Lange K, Timens W, et al. Mutation patterns in small cell and non-small cell lung cancer patients suggest a different level of heterogeneity between primary and metastatic tumors. *Carcinogenesis.* (2017) 38:144–51. doi: 10.1093/carcin/bgw128
40. Gibson WJ, Hoivik EA, Halle MK, Taylor-Weiner A, Cherniack AD, Berg A, et al. The genomic landscape and evolution of endometrial carcinoma progression and abdominopelvic metastasis. *Nat Genet.* (2016) 48:848–55. doi: 10.1038/ng.3602
41. Hedberg ML, Goh G, Chiosea SI, Bauman JE, Freilino ML, Zeng Y, et al. Genetic landscape of metastatic and recurrent head and neck squamous cell carcinoma. *J Clin Investig.* (2016) 126:1606. doi: 10.1172/JCI86862
42. Polyak K. Is breast tumor progression really linear? *Clin Cancer Res.* (2008) 14:339–341. doi: 10.1158/1078-0432.CCR-07-2188
43. Yates LR, Campbell PJ. Evolution of the cancer genome. *Nat Rev Genet.* (2012) 13:795–806. doi: 10.1038/nrg3317
44. Bouwman P, Jonkers J. The effects of deregulated DNA damage signalling on cancer chemotherapy response and resistance. *Nat Rev Cancer.* (2012) 12:587–98. doi: 10.1038/nrc3342
45. Bever KM, Le DT. DNA repair defects and implications for immunotherapy. *J Clin Investig.* (2018) 128:4236–42. doi: 10.1172/JCI122010
46. Kunz PL, Balise RR, Fehrenbacher L, Pan M, Venook AP, Fisher GA, et al. Oxaliplatin-fluoropyrimidine chemotherapy plus bevacizumab in advanced neuroendocrine tumors: an analysis of 2 phase II trials. *Pancreas.* (2016) 45:1394–400. doi: 10.1097/MPA.0000000000000659
47. Rosenberg JE, Hoffman-Censits J, Powles T, van der Heijden MS, Balar AV, Necchi A, et al. Atezolizumab in patients with locally advanced and metastatic urothelial carcinoma who have progressed following treatment with platinum-based chemotherapy: a single-arm, multicentre, phase 2 trial. *Lancet.* (2016) 387:1909–20. doi: 10.1016/S0140-6736(16)00561-4
48. Le DT, Uram JN, Wang H, Bartlett BR, Kemberling H, Eyring AD, et al. PD-1 blockade in tumors with mismatch-repair deficiency. *N Engl J Med.* (2015) 372:2509–20. doi: 10.1056/NEJMoa1500596
49. Hodges TR, Ott M, Xiu J, Gatalica Z, Swensen J, Zhou S, et al. Mutational burden, immune checkpoint expression, and mismatch repair in glioma: implications for immune checkpoint immunotherapy. *Neurooncology.* (2017) 19:1047–57. doi: 10.1093/neuonc/nox026
50. Teng F, Meng X, Kong L, Yu J. Progress and challenges of predictive biomarkers of anti PD-1/PD-L1 immunotherapy: a systematic review. *Cancer Lett.* (2018) 414:166–73. doi: 10.1016/j.canlet.2017.11.014
51. Cunha LL, Marcello MA, Rocha-Santos V, Ward LS. Immunotherapy against endocrine malignancies: immune checkpoint inhibitors lead the way. *Endocr Relat Cancer.* (2017) 24:T261–81. doi: 10.1530/ERC-17-0222

Conflict of Interest: WS and YZe were employed by the company OrigiMed.

The remaining authors declare that the research was conducted in the absence of any commercial or financial relationships that could be construed as a potential conflict of interest.

The reviewer H-KW declared a shared affiliation, though no other collaboration, with several of the authors, ZT, LW, HZ, LL, YZh, CC, WX, WF, and PZ to the handling editor.

frontiers in Medicine

SYSTEMATIC REVIEW
published: 08 June 2021
doi: 10.3389/fmed.2021.608760

High SVR12 With 8-Week Course of Direct-Acting Antivirals in Adolescents and Children With Chronic Hepatitis C: A Comprehensive Analysis

Zuqiang Fu[1,2†], Chen Dong[3†], Zhijun Ge[4], Chunhui Wang[2], Yun Zhang[1,2], Chao Shen[1,2], Jun Li[5], Chuanlong Zhu[5], Yan Wang[1], Peng Huang[1,2] and Ming Yue[5*]*

[1] Department of Epidemiology, School of Public Health, Nanjing Medical University, Nanjing, China, [2] Eastern Theater Command Centers for Disease Control and Prevention, Institute of Epidemiology and Microbiology, Nanjing, China, [3] Department of Epidemiology and Statistics, School of Public Health, Medical College of Soochow University, Suzhou, China, [4] Department of Critical Care Medicine, The Affiliated Yixing Hospital of Jiangsu University, Yixing, China, [5] Department of Infectious Diseases, The First Affiliated Hospital of Nanjing Medical University, Nanjing, China

OPEN ACCESS

Edited by:
Jianpeng Sheng,
Nanyang Technological University, Singapore

Reviewed by:
Xiaomei Ma,
Henan, China
Mingwang Shen,
Xi'an Jiaotong University, China

***Correspondence:**
Peng Huang
huangpeng@njmu.edu.cn
Ming Yue
yueming@njmu.edu.cn

†These authors have contributed equally to this work and share first authorship

Specialty section:
This article was submitted to Gastroenterology, a section of the journal Frontiers in Medicine

Received: 21 September 2020
Accepted: 30 April 2021
Published: 08 June 2021

Citation:
Fu Z, Dong C, Ge Z, Wang C, Zhang Y, Shen C, Li J, Zhu C, Wang Y, Huang P and Yue M (2021) High SVR12 With 8-Week Course of Direct-Acting Antivirals in Adolescents and Children With Chronic Hepatitis C: A Comprehensive Analysis. Front. Med. 8:608760. doi: 10.3389/fmed.2021.608760

Direct-acting antiviral (DAA) treatment for 8 weeks has a sustained virological response rate in adults with chronic hepatitis C. We have conducted a systematic review and meta-analysis to compare the efficacy and safety of the 8-week vs. 12/24-week DAA treatment in adolescents and children with CHC. The PubMed, Web of Science, and Cochrane databases were searched for the relevant articles from January 1, 2017 to August 28, 2020 and further screened for literature reviews on April 1, 2021. Pool proportions with 95% CIs for SVR12 were summarized with fixed/random effects models using Freeman–Tukey double arcsine transformation. Subgroup analysis was used to explore the source of heterogeneity. Thirty-six relevant publications were identified. For adolescents aged 12–17 years old, the pooled SVR12 and AE rate were 99.4% (95% CI: 98.7–99.9) and 34.7% (95% CI: 31.9–37.6). No one discontinued treatment due to drug intolerance. In addition, the SVR12 adolescents treated for 12 and 8/24 weeks were 99.3% (95% CI: 98.4–99.9) and 100%, respectively. The pooled SVR12 rate, AEs, and SAEs for children younger than 12 years were 98.9% (95% CI: 97.3–99.8), 51.6% (95% CI: 47.0–56.2), and 1.1% (95% CI: 0.4–2.5), respectively. The most common AE was fatigue (28.4%). The SVR12 was 98.8% (95% CI: 97.1–99.8) and 100% for the pediatric patients treated for 12 weeks and 8/24 weeks, respectively. Taken together, DAAs are generally effective against CHC and well-tolerated by the adolescents and children. A treatment duration of 8 weeks is equally effective and safe as 12/24 weeks in this demographic group.

Keywords: hepatitis C virus, direct-acting antivirals regimens, adolescents and children, sustained virological response, treatment duration

INTRODUCTION

Hepatitis C is caused by hepatitis C virus (HCV) infection and afflicted 71.7 million people or 1% of the global population in 2015 (1, 2), of which 13.2 (11.5–21.2) million were children and adolescents aged 1–15 years (3). Only 1.76 million (13%) of the patients received treatment, and 86% (1.51 million) were treated with direct-acting antivirals (DAAs) (1, 2).

Vertical HCV infection is cleared spontaneously without treatment in 20% of the pediatric patients, while the remaining 80% develop chronic infection in the first 4 years of life that usually persists into adulthood (4–6). Early diagnosis and treatment at younger age can reduce the prevalence of chronic infection in adulthood, and therefore reduce the global burden of HCV (7). However, although 5.5 million people with chronic HCV have been treated so far, most of these patients are adults that received the less effective interferon-based regimens (2).

The Food and Drug Administration (FDA) approved supplemental administration of sofosbuvir (SOF) and a combination of sofosbuvir and ledipasvir (SOF+LDV) in April 2017 to treat HCV in adolescents aged 12–17 years (8). In addition, several single-arm clinical trials conducted in the last 2 years have shown that DAAs are highly effective in pediatric CHC patients aged 6–12 years (9, 10). However, most of these studies have only analyzed the efficacy of DAAs on specific pediatric patient populations, such as those infected with HCV genotype 4 (GT) (11, 12), or the treatment experienced (TE) or treatment-naïve (TN) patients (13). The efficacy of short-duration (8 weeks) DAA treatment in adolescents and children with HCV infection has not been summarized so far.

The aim of this study was to comprehensively evaluate the efficacy and safety of 8-week vs. 12/24-week DAA regimens in adolescents and children with HCV infection using data from published studies. Our findings provide valuable information for medical professionals and researchers.

MATERIALS AND METHODS

This systematic review and meta-analysis was conducted according to the preferred reporting items for systematic review and meta-analyses (PRISMA) statement (**Supplementary Table 1**) (14).

Literature Search

PubMed, Cochrane Library, and Web of Science databases were searched for the relevant articles from January 1, 2017 to August 28, 2020. Literature reviews were searched on April 1, 2021. There were no restrictions on the year of publication and language. To avoid missing any study, several keywords were replaced with their synonyms. The following search terms were applied: "hepatitis C virus" (e.g., "HCV"; "CHC"; "hepatitis c"); "direct-acting antiviral" (e.g., "DAA"; "Sofosbuvir"; "Dasabuvir"; "Daclatasvir"; "Ledipasvir"; "Ombitasvir"; "Elbasvir"; "Velpatasvir"; "Boceprevir"; "Telaprevir"; "Simeprevir"; "Asunaprevir"; "Paritaprevir"; "Grazoprevir"); "pediatric" (e.g., "paediatr"; "pediatr"); and "children" (e.g., "child"; "teenager"; "kid"; "adolescent"; "youngster"; "juvenile") (**Supplementary Table 2**). All types of studies were collated initially. The procedure is outlined in **Figure 1**.

Inclusion and Exclusion Criteria

Studies that met the following criteria were included: (i) HCV infection (HCV RNA positive in blood) (8), (ii) adolescents (12–17 years) or pediatric (<12 years of age) patients, (iii) DAA treatment regimen, (iv) all HVC genotypes, (v) definite outcome variables (SVR12), (vi) TN or TE patients, and (vii) informed consent.

The exclusion criteria of the studies were as follows: (i) co-infection with HBV or HIV, (ii) evidence of HCC or other malignancy, (iii) history of solid organ or bone marrow transplantation, (iv) decompensated liver disease or chronic liver disease of a non-HCV etiology, (v) review, case report, or articles with >10 subjects, and (vi) not treated with any DAA-containing regimens.

Study Selection

The duplicate studies were first eliminated using Endnote software, and the unrelated studies were excluded by browsing through the titles and abstracts. Studies with only adult subjects or lacking DAAs in the treatment regimens were excluded, and those reporting on the efficacy or safety of DAA treatment in children were retained. The bibliographies of the most recent relevant literature reviews were manually inspected to obtain additional articles. To avoid selection bias caused by one person, two reviewers (Mr. Fu and Miss Yue) evaluated all abstracts and selected the relevant studies for full-text reading. Any disagreement was resolved by consensus among all authors.

Research Outcomes

The primary outcome was the efficacy of DAA regimens in adolescents and children, which was defined as the percentage of patients with SVR12 [HCV RNA < the lower limit of quantitation (LLOQ) at 12 weeks after cessation of therapy]. The SVR12 in this meta-analysis was the intention-to-treat (ITT) SVR12. The second outcome was the percentage of patients with adverse events (AEs) and serious AEs (SAEs). The AEs were defined as any unfavorable medical event reported by patients or any aberrations observed by the clinicians from the baseline laboratory indices after administration of the first dose until 30 days after the last dose. Common AEs included fatigue, nausea, and so on. The SAEs were defined as any event causing disability, congenital malformation, or death (8, 15–17). The worsening of laboratory test values from baseline was graded using the National Cancer Institute Common Terminology Criteria for Adverse Events (18). The safety of DAA regimen for HCV-infected patients was evaluated by the rate of drug-related AEs, SAEs, discontinuation, and laboratory abnormalities (19).

Data Extraction and Quality Evaluation

All relevant data including SVR12 (the primary endpoints of interest), side effects, study characteristics (e.g., study author, publication date, study type, and study sites), patient characteristics at baseline (e.g., age, sex rate, genotype, and

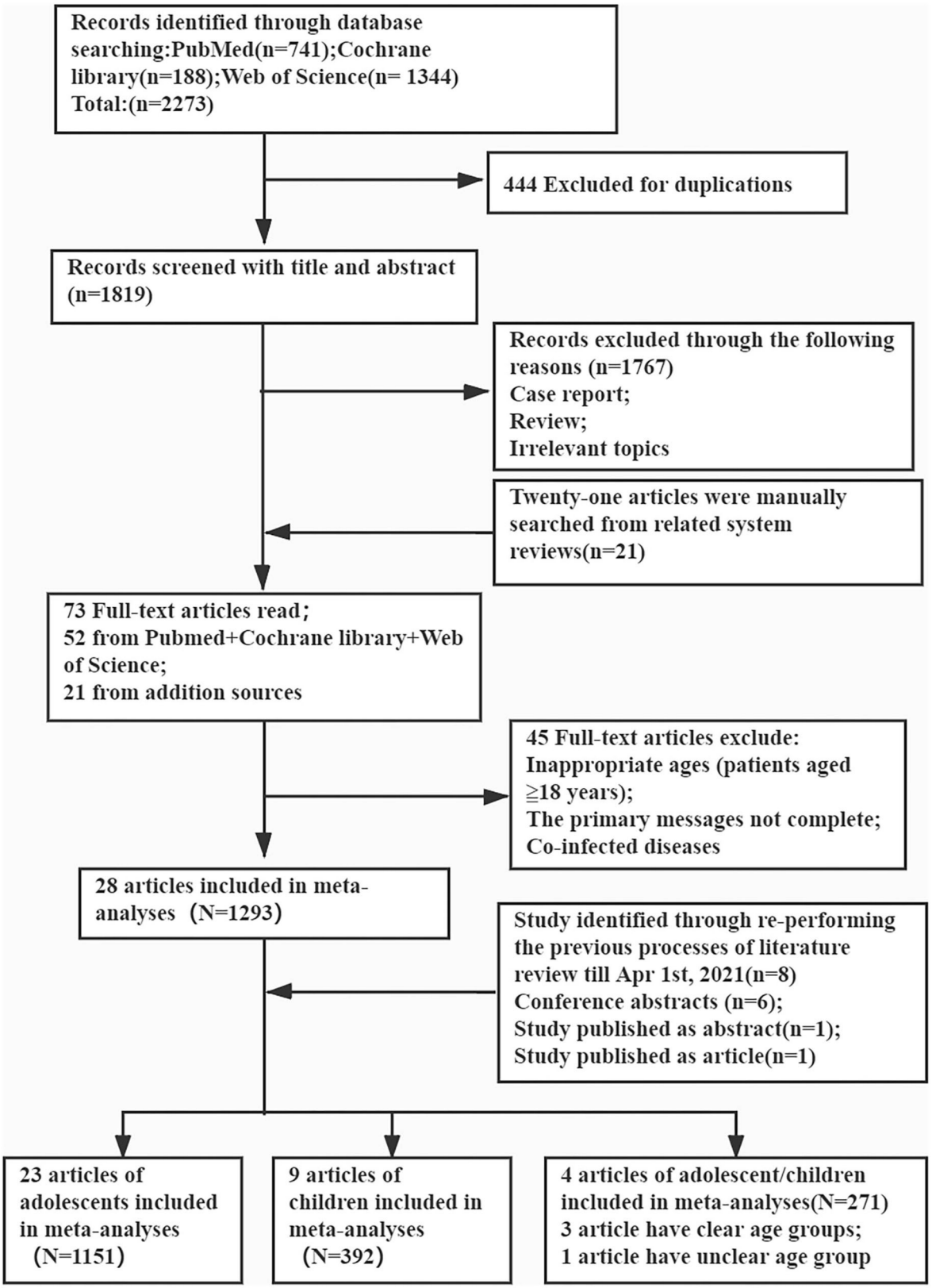

FIGURE 1 | Preferred reporting items for the review flow diagram for identification of relevant studies.

treatment regimen/duration), and possible factors that affect the outcomes of treatment were extracted from the articles. The study subjects were divided into the adolescents (12–17 years) and children (<12 years of age) groups.

All studies were assessed for methodological quality using the tool of Review Manager 5.2. The items of evaluation refer to a National Institutes of Health quality assessment tool: the tool for "Before-After (Pre-Post) Studies With No Control Group" (https://www.nhlbi.nih.gov/health-topics/study-quality-assessment-tools) (**Supplementary Table 3**). Each criterion was graded as "yes," "no," or "unclear," which corresponded to "low bias risk," "high bias risk," and "unclear risk of bias," respectively.

Statistical Analyses

R x64-3.6.1 software (The R Foundation for Statistical Computing) was used for the meta-analysis. Pool proportions with 95% CIs for SVR were summarized with fixed effects models using Freeman–Tukey double arcsine transformation (20). Fixed/random effects models were used in all analyses, and statistical heterogeneity was calculated with the I^2 method and subgroup differences using the Q-test. I^2 was calculated as follows: I^2 (%) $= 100 \times$ (Q − df)/Q, where Q is Cochrane's heterogeneity statistic and df indicates the degree of freedom. Negative values for I^2 were set to zero, and an $I^2 \geq 50\%$ was considered to have substantial heterogeneity. Publication bias was analyzed by Funnel plots. $P < 0.05$ was considered statistically significant.

RESULTS

A total of 741, 1,344, and 188 studies were initially identified in the PubMed, Web of Science, and Cochrane Library databases, respectively, of which 444 duplicate articles were excluded. After screening the titles and abstracts, 1,767 articles were further excluded. After including 21 additional articles from manual search of the reference lists, a total of 73 papers were eligible for full-text screening, of which 45 were excluded for incomplete data and/or inappropriate age groups (patients aged ≥18 years) and 7 for patients with co-morbidities. Another eight articles were included after the later literature search. Finally, 36 articles were included for further review, except for one that included both children and adolescents (**Figure 1**).

Studies and Patients' Characteristics

The main characteristics of the patients and studies are summarized in **Table 1**. A total of 28 studies were included, of which 18 were from Egypt, 7 from the United States, 4 from India, and 5 from multiple or other countries. All studies were observational, and 14 were multi-center studies. Except for three studies that did not specify the age groups, a total of 1,718 patients (1,253 adolescents and 465 children) were included in the studies, of which 792 were infected with HCV GT4, 545 with HCV GT1, 156 with GT3, 43 with HCV GT2, 1 with HCV GT5, and 213 with unknown GTs. Apart form 267 patients with unavailable treatment history, 1,216 were TN and 272 were TE. The majority of the patients (59%, 951/1,612) were males.

The methodological quality of each study is shown in **Supplementary Figures 1, 2**. The quality assessment criteria according to the National Institute of Health quality assessment tools are listed in **Supplementary Table 3** (https://www.nhlbi.nih.gov/health-topics/study-quality-assessment-tools). As shown in **Supplementary Figure 2**, most items had good level of research quality except for Q5, which was the result of patient specificity.

Efficacy Analysis of DAAs in Adolescents With CHC

A total of 24 studies including 1,253 adolescents patients were included for evaluating SVR12. The fixed-effect model showed that the pooled SVR12 rate was 99.4% (837/1,253, 95% CI: 98.7–99.9) (12, 15, 16, 18, 22, 23, 27–32, 34–36, 38, 39, 42–48). There was no significant heterogeneity ($I^2 = 0\%$, $P = 0.83$) (**Figure 2A**) or publication bias ($t = 0.22$, $P = 0.828$) (**Supplementary Figure 3A**) among these studies. There were three different treatment cycles of 8, 12, and 24 weeks. As shown in **Table 2**, the SVR12 rate was 100% (193/194, 95% CI: 98.7–100) for patients treated for 8 weeks, 99.3% (998/1,015, 95% CI: 98.4–99.9) for those treated for 12 weeks, and 100% (43/44, 95% CI: 98.9–100) for those treated for 24 weeks. The pooled SVR12 rate was 100% (95% CI: 100.0–100.0) (**Supplementary Figure 4A**), with litter heterogeneity among the three groups ($P = 0.398$). In addition, there were no significant differences in the pooled SVR12 rates when analyzed for the genotype, treatment history, and treatment regimen subgroups (**Supplementary Figures 6A–8A**).

Safety Analysis of DAAs in Adolescents With CHC

As shown in **Table 3** and **Supplementary Figure 5A**, the AE rate was 31, 36.1, and 41.7% among adolescents treated with DAAs for 8, 12, and 24 weeks, respectively. No significant heterogeneity was observed among three groups (31.0 vs. 36.1 vs. 41.7%, $P = 0.918$). Furthermore, the pooled AE rate for the adolescents aged 12–17 years was 34.7% (385/1,109, 95% CI: 31.9–37.6) and the SAE rate was 0.2% (95% CI: 0–0.6). The top AEs in adolescents were headache (22.6%, 206/910), abdominal pain (21.1%, 118/560), fatigue (15.5%, 129/832), nausea (15.4%, 90/585), and diarrhea (15.0%, 104/695).

Efficacy Analysis of DAAs in Children With CHC

A total of nine studies including 465 pediatric patients were included for SVR12 evaluation, and the fixed-effect model showed that the pooled SVR12 rate was 98.9% (454/465, 95% CI: 97.3–99.8) (10, 11, 13, 17, 21, 24–26, 37, 46). There was little heterogeneity among these studies ($I^2 = 35\%$, $P = 0.13$) (**Figure 2B**), and no significant publication bias was observed as per the funnel plot ($t = -0.68$, $P = 0.519$) (**Supplementary Figure 3B**). Eight of these studies reported the efficacy of 12-week treatment, two studies reported the efficacy of 8-week treatment, and only one study observed the outcomes

TABLE 1 | Main characteristics of the studies and patients included in this review.

References	Study design	Study sites	Genotype (n)	Treatment history (TN/TE)	Man (n, %)	Age (median)	Treatment regimen	Treatment duration (weeks)	Total (N)	Primary events, SVR (%, n/N)
Rosenthal et al. (21)**	Multicenter, open-label	USA	G1 (26)	26/0	9 (35)	7.5 (3.0–11.0)	OBV/PTV/R +DSV+RBV	12	26	SVR12, 96.0 (25/26)
Fouad et al. (22)	Single-arm	Egypt	NA	36/8	28 (60.9)	13.5 (12–17)	SOF+LDV	12	46	SVR12, 100.0 (46/46)
Makhlouf et al. (23)	Open-label	Egypt	G4 (50)	6/44	36 (72.0)	13.6 (12–17)	SOF+LDV	12	50	SVR12, 100.0 (50/50)
Jonas et al. (18)	Open-label	USA	G1 (37), G2 (3), G3 (1), G4 (3)	36/8	21 (47.7)	14 (12–17)	G+P	8	44	SVR12, 100.0 (44/44)
Behairy et al. (13)	Single-arm	Egypt	G4 (30)	30/0	20 (66.7)	6.7 (4–10)	SOF+LDV	8	30	SVR12, 100.0 (30/30)
Schwarz et al. (24)	Multicenter, open-label	USA, UK, and Australia	G1 (33), G4 (1)	33/1	24 (71.0)	5 (3–5)	SOF+LDV	12	34	SVR12, 97.1 (33/34)
Kamal et al. (25)	Multicenter	Egypt	G4	22/0	19 (86.0)	4.8 (3–6)	SOF+LDV	8;12	22	SVR12, 100.0 (22/22)
Rosenthal et al. (26)**	Multicenter, open-label	USA	G2 (18), G3 (36)	53/1	14 (25.9)	6.5 (3–11)	SOF+RBV	12	54	SVR12, 98.2 (53/54)
Serranti et al. (27)	Multicenter open-label	Italian	G1 (14)	14/10	6 (42.9)	16.5 (12–7)	SOF+LDV	8	14	SVR12, 100.0 (40/40)
Dhiman et al. (28)	Multicenter open-label	India	G1 (9), G3 (24), G4 (2), G5 (1), unknown (21)	57/0	40 (69.3)	15.8 (12–17)	SOF+LDV; SOF+DCV ± RBV	12;24	57	SVR12, 98.3 (56/57)
Abdel Ghaffar et al. (29)	Open-label	Egypt	G4 (40)	40/0	25 (62.5)	12.27 (8–17.58)*	SOF+DCV	12	40	SVR12, 97.5 (39/40)
Fouad et al. (30)	Observational	Egypt	G4a (51)	35/16	32 (62.7)	14.7 (11–17.5)	SOF+LDV	12	51	SVR12, 100.0 (51/51)
El-Khayat et al. (15)	Cross-sectional	Egypt	G4 (157)	63/94	97 (62.0)	14 (12–17)	SOF+LDV	8;12	157	SVR12, 98.1 (154/157)
Nagral et al. (31)	Single-arm	India	G1 (12), G3 (5), unknown (1)	17/1	9 (50.0)	15.1 (12–17)	SOF+LDV; SOF+DCV ± RBV	12;24	18	SVR12, 88.9 (16/18)
El-Araby et al. (11)	Observational	Egypt	G4	80/20	66 (66.0)	13.8 (9–12)	SOF+LDV	12	100	SVR12, 100.0 (100/100)
Padhi (10)	Observational	India	G3 (14)	14/0	12 (85.7)	9.5 (7–13)	SOF+DCV	12	14	SVR12, 100.0 (14/14)
Mehta et al. (32)	Observational	India	G3 (10)	10/0	10 (100)	13 (11–17)	SOF+DCV	12	10	SVR12, 100.0 (10/10)
Alkaaby et al. (33)	Observational	Iraq	G1 (10), G4 (2), unknown (10)	15/7	14 (63.6)	12.5 (7–17)*	SOF+LDV	12	22	SVR12, 90.9 (20/22)
El-Karaksy et al. (34)	Observational	Egypt	G4 (40)	30/10	26 (65.0)	13.9 (11.5–17.5)	SOF+LDV	12	40	SVR12, 100.0 (40/40)
Yakoot et al. (35)	Multicenter, open-label	Egypt	G4 (30)	NA	17 (56.7)	12.567 (12–17)	SOF+DCV	12	30	SVR12, 96.7 (29/30)
Murray et al. (17)	Multicenter, open-label	USA	G1 (88), G3 (2), G4 (2)	72/20	84 (91.5)	9 (6–11)	SOF+LDV ± RBV	12; 24	92	SVR12, 98.9 (91/92)
Leung et al. (36)	Multicenter, open-label	USA	G1 (31), G4 (7)	25/13	13 (34.0)	15 (12–17)	OBV/PTV/R ± DSV ± RBV	12; 24	38	SVR12, 100.0 (38/38)
El-Shabrawi et al. (37)	Single-arm, multicenter	Egypt	G4 (20)	17/3	11 (55.0)	9.1 (6–12)	SOF+LDV	12	20	SVR12, 95.0 (19/20)
El-Shabrawi et al. (38)	Open-label	USA	NA	9/1	5 (50.0)	15.5 (13–17)	SOF+DCV	8	10	SVR12, 100.0 (10/10)
El-Khayat et al. (12)	Multicenter, open-label	Egypt	G4 (144)	128/16	99 (69.0)	14 (12–17)	SOF+LDV	12	144	SVR12, 98.6 (142/144)
Wirth et al. (39)	Multicenter, open-label	USA	G2 (13), G3 (39)	43/9	31 (60.0)	15 (12–17)	SOF+RBV	12; 24	52	SVR12, 98.1 (51/52)

(Continued)

TABLE 1 | Continued

References	Study design	Study sites	Genotype (n)	Treatment history (TN/TE)	Man (n, %)	Age (median)	Treatment regimen	Treatment duration (weeks)	Total (N)	Primary events, SVR (%, n/N)
Balistreri et al. (16)	Multicenter, open-label	USA, UK, and Australia	G1 (100)	80/20	37 (37.0)	15 (12–17)	SOF+LDV	12	100	SVR12, 98.0 (98/100)
Hashmi et al. (40)	Open-label	Pakistan	G3 (27), G1 (6), unknown (2)	35/0	22 (62.9)	10.2 (5–17)*	SOF+RBV	24	35	SVR12, 97.1 (30/35)
El-Shabrawi et al. (41)	Single-center	Egypt	NA	39/0	NA	16.5 (6–17)*	SOF+LDV/ SOF+DCV	8; 12	39	SVR12, 100.0 (39/39)
Ahmed et al. (42)	NA	Egypt	NA	NA	NA	NA (10–17)	SOF+LDV/ SOF+DCV	12	40	SVR12, 100.0 (40/40)
El-Sayed et al. (43)	Prospective pilot study	Egypt	NA	NA	NA	16 (15–17)	SOF+DCV ± RBV	12	13	SVR12, 100.0 (13/13)
El-Sayed et al. (44)	Open-label, phase 2 study	Egypt	G4 (13)	13/0	11 (85.0)	NA (12–17)	SOF+LDV	12	13	SVR12, 100.0 (13/13)
Isakov et al. (45)	NA	Egypt	NA	NA	27 (50.9)	12.5 (10–17)	SOF+LDV	8	53	SVR12, 100.0 (53/53)
Jonas et al. (46)	Open-label	NA	G1 (131), G2 (9), G3 (23), G4 (5), G6 (5)	149/26	86 (49.0)	102 (12–17); 73 (6–12)	SOF+VEL	12	102;73	SVR12, 95.0 (97/102); 92.0 (67/73)
Sheha et al. (47)	Single-center	Egypt	G4	NA	NA	NA (12–17)	SOF+LDV	12	53	SVR12, 100.0 (53/53)
Serranti et al. (48)	Multi-center study	NA	G1 (64), G3 (2), G4 (12)	NA	36 (46.2)	15.2 (12–17)	SOF+LDV	12	78	SVR12, 98.7 (77/78)

*SOF, sofosbuvir; LDV, ledipasvir; OBV, ombitasvir; PTV, paritaprevir; r, ritonavir; RBV, ribavirin; DCV, daclatasvir; DSV, dasabuvir; G, glecaprevir; P, pibrentasvir; VEL, velpatasvir. *The distribution of age for subjects was undefined; **Different articles form the same first author.*

of 24-week treatment. The SVR12 rates were 100% (41/41, 95% CI: 95.9–100), 98.8% (410/421, 95% CI: 97.1–99.8), and 100% (3/3, 95% CI: 50.0–100.0) for patients treated for 8, 12, and 24 weeks, respectively (**Supplementary Figure 4B**). No distinct heterogeneity was observed among these groups ($P = 0.676$). Moreover, the pooled SVR12 rate for children with CHC was independent of HCV genotypes, treatment history, and treatment regimens (**Supplementary Figures 6B–8B**).

Safety Analysis of DAAs in Children With CHC

As shown in **Table 3**, the AE rates in pediatric patients treated with DAAs for 8, 12, and 24 weeks were 57.8, 45.1, and 98.7%, respectively (**Supplementary Figure 5B**). Thus, the AE rate increased significantly when the treatment was continued for 24 weeks (98.7 vs. 57.8/45.1%, $P < 0.001$). The pooled AE rate was 51.6% (240/465, 95% CI: 47.0–56.2) and the SAE rate was 1.1% (5/465, 95% CI: 0.4–2.5) for children (<12 years of age), and the most common AEs were fatigue (28.4%, 80/282), headache (27.6%, 82/297), vomiting (21.1%, 51/242), cough (15.4%, 35/228), and fever (14.9%, 34/228) (**Table 4**).

DISCUSSION

Compared to adult patients, there are significant gaps regarding the data of adolescents and children with HCV infection. Although several DAAs are effective and safe in adolescents with hepatitis C (8, 49), it is unclear whether a shorter 8-week treatment cycle would achieve similar outcomes as the 12-week or even 24-week cycles. To this end, we systematically analyzed the studies published so far on the therapeutic efficacy of DAA-containing regimens in children and adolescents with HCV infection.

Prior to the regulatory approval of DAAs for pediatric patient, the standard treatment for adolescents and children infected with HCV was 24 weeks of pegIFN and RBV for GT 2 and 3, and 48 weeks for GT 1 and 4 (50–58). This combination resulted in an SVR of around 52% in patients infected with HCV GT 1 and 4, and 89% in those infected with HCV GT 2 and 3, but was associated with significant side effects (54–56, 58). Compared to IFN-based regimens, DAAs not only are more efficient but also have fewer side effects (10–12, 15–17, 22, 24–26, 28, 29, 31, 34–39). We found that the overall SVR12 rate for the adolescents and children treated with DAAs was 99.4 and 98.9%, respectively, although the frequency of AEs was substantial (34.7 and 51.6%). Nevertheless, SAEs were rare (0.2 and 1.1%) and no adolescent patients discontinued treatment due to the AEs since most were tolerable, such as headaches (22.6%), abdominal pain (21.1%), and fatigue (15.5%). Moreover, children were more likely to experience side effects compared to teenagers (51.6 vs. 34.7%). The most common AE among children was fatigue (28.4%), most likely due to "abnormal drug taste" (24, 26). Thus, DAAs are relatively well-tolerated by both children and adolescents.

Apart from efficacy and safety, cost-effectiveness is also an important issue for any drug regimen (59). Kohli et al.

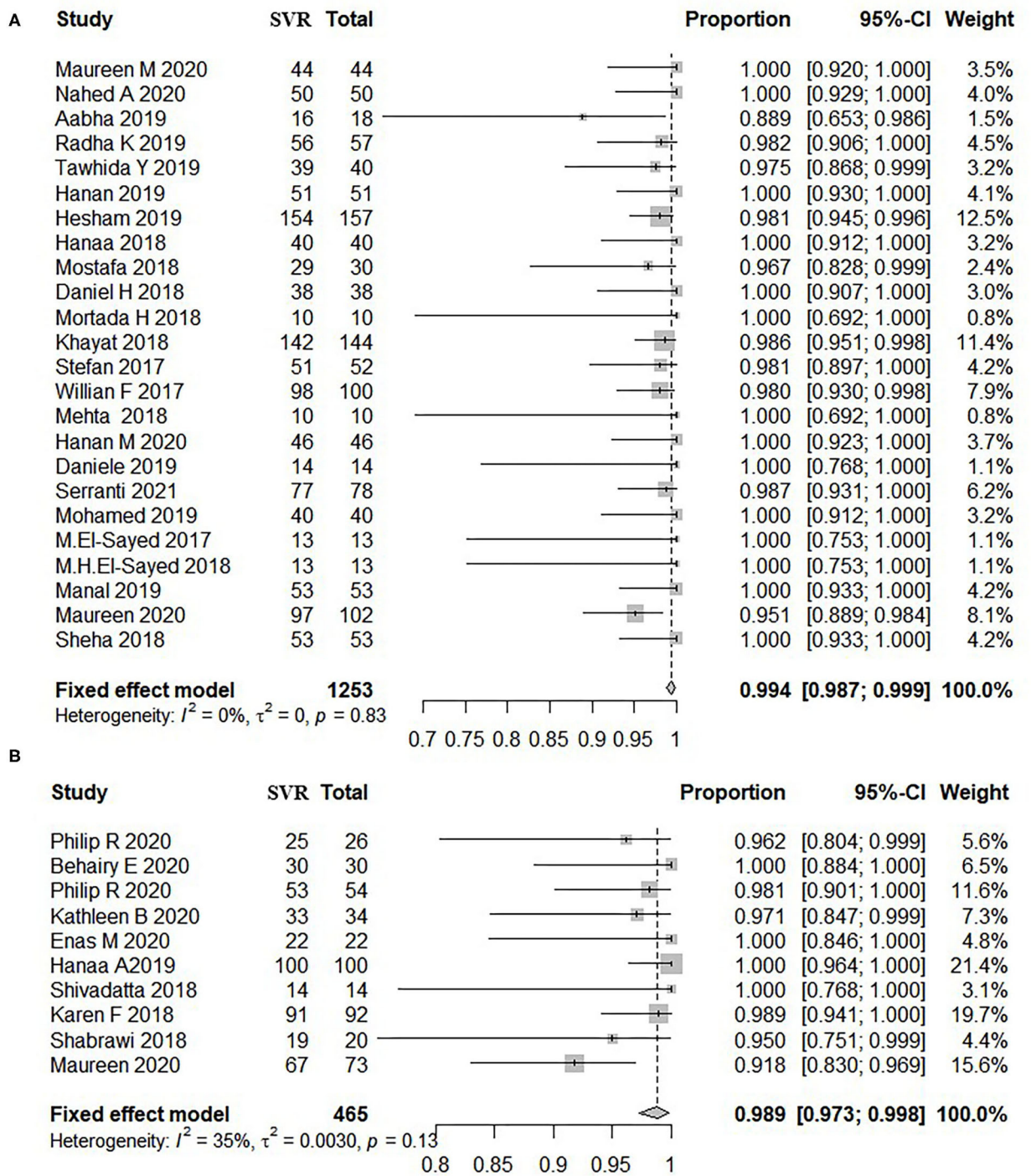

FIGURE 2 | Overall rate of SVR12 in patients treated by DAAs. **(A)** Patients aged 12–17 years old. **(B)** Patients below 12 years old. The size of the square represents the weight of the study in the meta-analysis; the line width represents the 95% confidence interval of the study; the vertical line represents the "no effect line"; the diamond-shaped block represents the combined effect estimate of each study (fixed effect model or random effects model). **(A)** Patients aged 12–17 years old. **(B)** Patients below 12 years old. SVR, sustained virological response; DAAs, direct-acting antivirals; CI, confidence interval; Total, sum of patients treated by DAA.

(60), Latt et al. (61), and Kattakuzhy et al. (62) analyzed the outcomes of HCV treatment shorter than 12 weeks and reported ambiguous results. A recent review has shown that 8 weeks of glecaprevir/pibrentasvir (G/P) is equally effective in treatment-naive non-cirrhotic adults (63). We did not detect any significant differences between the various treatment durations

TABLE 2 | Rate of SVR12 after different durations of treatment in children and adolescents.

	Adolescents group (12–17 years)						Children group (<12 years)					
Subgroups	**Studies (n)**	**SVR12 (*N* = 831)**		**Heterogeneity**		**P^b**	**Studies (n)**	**SVR12 (*N* = 392)**		**Heterogeneity**		**P^d**
		Total, n/N	**Rate% (95% CI)**	**I^2 (%)**	**P^a**			**Total, n/N**	**Rate% (95% CI)**	**I^2 (%)**	**P^c**	
By the durations of treatment						0.398						0.716
8 weeks	5	193/194	100.0 (98.7–100.0)	0	0.92		2	41/41	100.0 (95.9–100.0)	0	0.75	
12 weeks	20	998/1,015	99.3 (98.4–99.9)	0	0.78		9	410/421	98.8 (97.1–99.8)	38	0.11	
24 weeks	4	43/44	100.0 (98.9–100.0)	0	0.93		1	3/3	100.0 (50.0–100.0)	NA	NA	

SVR, sustained virological response; CI, confidence interval; I^2, I-square; NA, not applicable. [a]Test of heterogeneity in adolescents group; [b]Test for subgroup differences in adolescents group; [c]Test of heterogeneity in children group; [d]Test for subgroup differences in children group.

TABLE 3 | AEs after different treatment durations in children and adolescents.

	Adolescents group (12–17 years)						Children group (<12 years)					
Variables	**Studies (n)**	**AE**		**Heterogeneity**		**P^b**	**Studies (n)**	**AE**		**Heterogeneity**		**P^d**
		Total, n/N	**Rate% (95% CI)**	**I^2 (%)**	**P^a**			**Total, n/N**	**Rate% (95% CI)**	**I^2 (%)**	**P^c**	
Durations of treatment						0.918						<0.001
8 weeks	5	55/194	31.0 (0–79.2)	98.0	<0.01		2	29/41	57.8 (0–100.0)	95.0	<0.01	
12 weeks	17	297/871	36.1 (23.3–49.9)	94.0	<0.01		8	174/385	45.1 (24.4–66.8)	94.0	<0.01	
24 weeks	4	31/44	41.7 (0–94.2)	63.0	0.05		2	37/39	98.7 (88.9–100.0)	0	1.00	

AE, adverse event. [a]Test of heterogeneity in adolescents group; [b]Test for subgroup differences in adolescents group; [c]Test of heterogeneity in children group; [d]Test for subgroup differences in children group.

TABLE 4 | Rate of AEs, SAEs, discontinuation, and the common AEs among children and adolescents.

Response	**Adolescents group (12–17 years)**		**Children group (<12 years)**	
	Total, n/N	**Rate% (95% CI)**	**Total, n/N**	**Rate% (95% CI)**
Total AEs (not including SAEs)	385/1,109	34.7 (31.9–37.6)	240/465	51.6 (47.0–56.2)
SAEs	2/1,122	0.2 (0–0.6)	5/465	1.1 (0.4–2.5)
AEs leading to discontinuation	0/1,253	0 (0–0.3)	2/465	0.4 (0.1–1.5)
Headache	206/910	22.6 (20.0–25.5)	82/297	27.6 (22.6–33.1)
Fatigue	129/832	15.5 (13.1–18.1)	80/282	28.4 (23.2–34.0)
Diarrhea	104/695	15.0 (12.4–17.8)	–	–
Abdominal pain	118/560	21.1 (17.8–24.7)	–	–
Nausea	90/585	15.4 (12.6–18.6)	–	–
Vomiting	–	–	51/242	21.1 (16.1–26.8)
Cough	–	–	35/228	15.4 (10.9–20.7)
Fever	–	–	34/228	14.9 (10.6–20.2)

AE, adverse event; SAE, severe adverse event.

in terms of efficacy in adolescents or children ($P_b = 0.398$, $P_d = 0.716$). Hesham et al. also found that 8 weeks of treatment with the SOF/LDV combination was as effective and safe as the 12-week regimen in adolescent GT4 patients (15). Similar results were reported by Mortada et al. (38). As for the treatment cycle of 24 weeks, most just appeared in RBV-based regimen in children, because SOF+RBV was also a suboptimal regimen for persons with GT 3 infection, especially if they have liver cirrhosis (8). We found that both 8-week and 12/24-week treatment courses were well-tolerated in adolescents (31 vs. 36.1%/41.7%, $P = 0.918$), whereas the AE rate at 24 weeks was greater than that at 8/12 weeks (98.7 vs. 57.8%/45.1%, $P < 0.001$) in children with CHC. This can be attributed to RBV intolerance, as well as the fact that a longer treatment duration would also increase the chances of detecting AEs that manifest late. The correlation between treatment duration and AEs needs to be studied further.

Given the underdeveloped immune system of children and the limited time for which DAAs have been administered to

this group, our findings should be interpreted with caution. In addition, we only evaluated the efficacy of DAAs in terms of SVR12, and some subgroups did not have a corresponding control due to ethical reasons. Secondly, stratified analysis of SVR showed that the heterogeneity within the three treatment cycles was somewhat large, but the inter-group heterogeneity was not statistically significant. Lastly, only the FDA-approved DAAs were analyzed in the review. Therefore, the treatment outcomes of novel DAAs will have to be continuously monitored in children.

In conclusion, DAAs are overall effective and well-tolerated in adolescents and children with chronic hepatitis C. The 8-week treatment course is as effective as 12/24 weeks in both adolescents and children.

DATA AVAILABILITY STATEMENT

The original contributions presented in the study are included in the article/**Supplementary Material**, further inquiries can be directed to the corresponding author/s.

AUTHOR CONTRIBUTIONS

ZF and MY: study design and protocol, searches, title, abstract, full-text screening, data abstraction, statistical analyses, interpretation of the data, and drafting the article. ZG and CW: data verification and statistical analyses. CS and YW: statistical analyses and interpretation of the data. JL and CZ: interpretation of the data. PH, CD, and YZ: study design and protocol, interpretation of the data, and drafting the article. ZF, CD, PH, and MY: manuscript revision and question answer. All authors contributed to the article and approved the submitted version.

FUNDING

This study was supported by the National Natural Science Foundation of China (81703273 and 81773499), the Natural Science Foundation of Jiangsu Province of China (BK20171054), the Science Foundation for Distinguished Young Scholars of Jiangsu Province (BK20190106), Jiangsu Program for Young Medical Talents (QNRC2016616), and the Key Project of Yunnan Province Applied Basic Research Program (2019FA005).

SUPPLEMENTARY MATERIAL

The Supplementary Material for this article can be found online at: https://www.frontiersin.org/articles/10.3389/fmed.2021.608760/full#supplementary-material

REFERENCES

1. Spearman CW, Dusheiko GM, Hellard M, Sonderup M. Hepatitis C. *Lancet.* (2019) 394:1451–66. doi: 10.1016/S0140-6736(19)32320-7
2. WHO. *Global Hepatitis Report*. Geneva World Health Organization (2018).
3. El-Sayed MH, Razavi H. Global estimate of HCV infection in the pediatric and adolescent population. *J Hepatol.* (2015) 62:S831–2. doi: 10.1016/S0168-8278(15)31458-6
4. Bortolotti F, Verucchi G, Camma C, Cabibbo G, Zancan L, Indolfi G, et al. Long-term course of chronic hepatitis C in children: from viral clearance to end-stage liver disease. *Gastroenterology.* (2008) 134:1900–7. doi: 10.1053/j.gastro.2008.02.082
5. Network. The European Paediatric Hepatitis C Virus Three broad modalities in the natural history of vertically acquired hepatitis C virus infection. *Clin Infect Dis.* (2005) 41:45–51. doi: 10.1086/430601
6. Resti M, Jara P, Hierro L, Azzari C, Giacchino R, Zuin G, et al. Clinical features and progression of perinatally acquired hepatitis C virus infection. *J Med Virol.* (2003) 70:373–7. doi: 10.1002/jmv.10405
7. Modin L, Arshad A, Wilkes B, Benselin J, Lloyd C, Irving WL, et al. Epidemiology and natural history of hepatitis C virus infection among children and young people. *J Hepatol.* (2019) 70:371–8. doi: 10.1016/j.jhep.2018.11.013
8. World Health Organisation. *Guidelines for the Care and Treatment of Persons Diagnosed With Chronic Hepatitis C Virus Infection*. Geneva: World Health Organisation (2018).
9. Thorne C, Indolfi G, Turkova A, Giaquinto C, Nastouli E. Treating hepatitis C virus in children: time for a new paradigm. *J Virus Erad.* (2015) 1:203–5. doi: 10.1016/S2055-6640(20)30500-8
10. Padhi S, Maharshi S, Gupta GK, Garg KS. Nijhawan efficacy and safety of direct acting antiviral therapy for chronic hepatitis C in thalassemic children. *J Pediatr Hematol Oncol.* (2018) 40:511–4. doi: 10.1097/MPH.0000000000001217
11. El-Araby HA, Behairy BE, El-Guindi MA, Adawy NM, Allam AA, Sira AM, et al. Generic sofosbuvir/ledipasvir for the treatment of genotype 4 chronic hepatitis C in Egyptian children (9-12 years) and adolescents. *Hepatol Int.* (2019) 13:706–14. doi: 10.1007/s12072-019-09985-w
12. El-Khayat HR, Kamal EM, El-Sayed MH, El-Shabrawi M, Ayoub H, Riz KA, et al. The effectiveness and safety of ledipasvir plus sofosbuvir in adolescents with chronic hepatitis C virus genotype 4 infection: a real-world experience. *Aliment Pharmacol Ther.* (2018) 47:838–44. doi: 10.1111/apt.14502
13. Behairy BE, El-Araby HA, El-Guindi MA, Basiouny HM, Fouad OA, Ayoub BA, et al. Safety and EFFICACY of 8 weeks Ledipasvir/Sofosbuvir for chronic hepatitis C genotype 4 in children aged 4-10 years. *J Pediatr.* (2020) 219:106–10. doi: 10.1016/j.jpeds.2019.12.034
14. Moher D, Liberati A, Tetzlaff J, Altman DG. Preferred reporting items for systematic reviews and meta-analyses: the PRISMA statement. *Ann Intern Med.* (2009) 151:264–9. doi: 10.7326/0003-4819-151-4-200908180-00135
15. El-Khayat H, Kamal EM, Yakoot M, Gawad MA, Kamal N, El Shabrawi M, et al. Effectiveness of 8-week sofosbuvir/ledipasvir in the adolescent chronic hepatitis C-infected patients. *Eur J Gastroenterol Hepatol.* (2019) 31:1004–9. doi: 10.1097/MEG.0000000000001360
16. Balistreri WF, Murray KF, Rosenthal P, Bansal S, Lin CH, Kersey K, et al. The safety and effectiveness of ledipasvir-sofosbuvir in adolescents 12-17 years old with hepatitis C virus genotype 1 infection. *Hepatology.* (2017) 66:371–8. doi: 10.1002/hep.28995
17. Murray KF, Balistreri WF, Bansal S, Whitworth S, Evans HM, Gonzalez-Peralta RP, et al. Safety and efficacy of Ledipasvir-Sofosbuvir with or without ribavirin for chronic hepatitis C in children ages 6-11. *Hepatology.* (2018) 68:2158–66. doi: 10.1002/hep.30123
18. Jonas MM, Squires RH, Rhee SM, Lin CW, Bessho K, Feiterna-Sperling C, et al. Pharmacokinetics safety, and efficacy of Glecaprevir/Pibrentasvir in adolescents with chronic hepatitis C virus: part 1 of the DORA study. *Hepatology.* (2020) 71:456–62. doi: 10.1002/hep.30840
19. Wang X, Fan X, Deng H, Zhang X, Zhang K, Li N, et al. Efficacy and safety of glecaprevir/pibrentasvir for chronic hepatitis C virus genotypes 1-6 infection: a systematic review and meta-analysis. *Int J Antimicrob Agents.* (2019) 54:780–9. doi: 10.1016/j.ijantimicag.2019.07.005

20. Miller John J. The inverse of the freeman – Tukey double arcsine transformation. *Am Statist.* (1978) 32:138. doi: 10.1080/00031305.1978.10479283
21. Rosenthal P, Narkewicz MR, Yao BB, Jolley CD, Lobritto SJ, Wen J, et al. Ombitasvir, paritaprevir, ritonavir, and dasabuvir mini-tabs plus ribavirin for children aged 3-11 years with hepatitis C genotype 1a. *Adv Ther.* (2020) 37:3299–310. doi: 10.1007/s12325-020-01389-9
22. Fouad HM, Ahmed Mohamed A, Sabry M, Abdel Aziz H, Eysa B, Rabea M. The effectiveness of Ledipasvir/Sofosbuvir in youth with genotype 4 hepatitis C virus: a single egyptian center study. *Pediatr Infect Dis J.* (2019) 38:22–5. doi: 10.1097/INF.0000000000002189
23. Makhlouf NA, Abdelmalek MO, Ibrahim ME, Abu-Faddan NH, Kheila AE, Mahmoud AA. Ledipasvir/Sofosbuvir in adolescents with chronic hepatitis C genotype with and without hematological disorders: virological efficacy and impact on liver stiffness. *J Pediatric Infect Dis Soc.* (2020) 4:7–13. doi: 10.1093/jpids/piaa006
24. Schwarz KB, Rosenthal P, Murray KF, Honegger JR, Hardikar W, Hague R, et al. Ledipasvir-Sofosbuvir for 12 weeks in children 3 to <6 years old with chronic hepatitis C. *Hepatology.* (2019) 71:422–30. doi: 10.1002/hep.30830
25. Kamal EM, El-Shabrawi M, El-Khayat H, Yakoot M, Sameh Y, Fouad Y, et al. Effects of sofosbuvir/ledipasvir therapy on chronic hepatitis C virus genotype 4, infected children of 3-6 years of age. *Liver Int.* (2019) 40:319–23. doi: 10.2139/ssrn.3429908
26. Rosenthal P, Schwarz KB, Gonzalez-Peralta RP, Lin CH, Kelly DA, Nightingale S, et al. Ribavirin therapy for children aged 3 to <12 years with hepatitis C virus genotype 2 or 3 infection. *Hepatology.* (2019) 71:31–43. doi: 10.1002/hep.30821
27. Serranti D, Dodi I, Nicastro E, Cangelosi AM, Riva S, Ricci S, et al. Shortened 8-week course of Sofosbuvir/Ledipasvir therapy in adolescents with chronic hepatitis C infection. *J Pediat Gastroenterol Nutr.* (2019) 69:595–8. doi: 10.1097/MPG.0000000000002449
28. Dhiman RK, Grover GS, Premkumar M, Taneja S, Duseja A, Rathi S, et al. Direct-acting antiviral therapy is safe and effective in pediatric chronic hepatitis C: the public health perspective. *J Pediatr Gastroenterol Nutr.* (2019) 68:74–80. doi: 10.1097/MPG.0000000000002139
29. Abdel Ghaffar TY, El Naghi S, Abdel Gawad M, Helmy S, Abdel Ghaffar A, Yousef M. Safety and efficacy of combined sofosbuvir/daclatasvir treatment of children and adolescents with chronic hepatitis C Genotype 4. *J Viral Hepat.* (2019) 26:263–70. doi: 10.1111/jvh.13032
30. Fouad HM, Sabry MA, Ahmed A, Hassany M, Al Soda MF, Abdel Aziz H. Generic Ledipasvir-Sofosbuvir treatment for adolescents with chronic hepatitis C virus infection. *J Pediatric Infect Dis Soc.* (2020) 9:386–9. doi: 10.1093/jpids/piz041
31. Nagral A, Jhaveri A, Sawant S, Parikh NS, Nagral N, Merchant R, et al. Treatment of chronic hepatitis C infection with direct acting antivirals in adolescents with thalassemia major. *Ind J Pediatr.* (2019) 86:148–53. doi: 10.1007/s12098-018-2752-7
32. Mehta R, Kabrawala M, Nandwani S, Desai P, Bhayani V, Patel S, et al. Safety and efficacy of sofosbuvir and daclatasvir for hepatitis C virus infection in patients with beta-thalassemia major. *J Clin Exp Hepatol.* (2018) 8:3–6. doi: 10.1016/j.jceh.2017.06.002
33. Alkaaby BA, Al-Ethawi AE. The effectiveness of oral antiviral (Sofosbuvir/Ledipasvir) in treating children with HCV infection. *Pak J Med Sci.* (2018) 34:1353–6. doi: 10.12669/pjms.346.15722
34. El-Karaksy H, Mogahed EA, Abdullatif H, Ghobrial C, El-Raziky MS, El-Koofy N, et al. Sustained viral response in genotype 4 chronic hepatitis C virus-infected children and adolescents treated with Sofosbuvir/Ledipasvir. *J Pediatr Gastroenterol Nutr.* (2018) 67:626–30. doi: 10.1097/MPG.0000000000002101
35. Yakoot M, El-Shabrawi MH, AbdElgawad MM, Mahfouz AA, Helmy S, Abdo AM, et al. Dual Sofosbuvir/Daclatasvir therapy in adolescent patients with chronic hepatitis C infection. *J Pediatr Gastroenterol Nutr.* (2018) 67:86–9. doi: 10.1097/MPG.0000000000001968
36. Leung DH, Wirth S, Yao BB, Viani RM, Gonzalez-Peralta RP, Jonas MM, et al. Ombitasvir/Paritaprevir/Ritonavir with or without dasabuvir and with or without ribavirin for adolescents with HCV genotype 1 or 4. *Hepatol Commun.* (2018) 2:1311–9. doi: 10.1002/hep4.1250
37. El-Shabrawi MHF, Kamal NM, El-Khayat HR, Kamal EM, AbdElgawad M. A pilot single arm observational study of sofosbuvir/ledipasvir (200 + 45 mg) in 6- to 12- year old children. *Aliment Pharmacol Ther.* (2018) 47:1699–704. doi: 10.1111/apt.14677
38. El-Shabrawi MH, Abdo AM, El-Khayat HR, Yakoot M. Shortened 8 weeks course of dual Sofosbuvir/Daclatasvir therapy in adolescent patients, with chronic hepatitis C infection. *J Pediatr Gastroenterol Nutr.* (2018) 66:425–7. doi: 10.1097/MPG.0000000000001838
39. Wirth S, Rosenthal P, Gonzalez-Peralta RP, Jonas MM, Balistreri WF, Lin CH, et al. Sofosbuvir and ribavirin in adolescents 12-17 years old with hepatitis C virus genotype 2 or 3 infection. *Hepatology.* (2017) 66:1102–10. doi: 10.1002/hep.29278
40. Hashmi M. A.,Cheema H. A. Effectiveness and Safety of Sofosbuvir in Treatment-NäiveChildren with Hepatitis C Infection. *J Coll Physicians Surg Pak.* (2017) 27:423–6.
41. El-Shabrawi M, Baroudy S, Hassanin F, Behairy AS, Yakoot M, Ahmed A. Follow-up of chronic paediatric hepatitis C virus in a low-/middle-income country. *Acta Paediatr.* (2020) 109:2699–705. doi: 10.1111/apa.1533310.1111/apa.15333
42. Ahmed M, Hanno A, Hamouda S, Abdelgawad M, Abouelkhier H. THU-113-comparison between safety and efficacy of two treatment regimens for pediatric patients with chronic hepatitis C virus: Sofosbuvir/ledipasvir versus sofosbuvir/daclatasvir regimen. *J Hepatol.* (2019) 70(Suppl. 1):e208. doi: 10.1016/S0618-8278(19)30388-3
43. El-Sayed M, Hassany M, Asem N. THU-412 - A pilot study for safety and efficacy of 12 weeks sofosbuvir plus daclatasvir with or without ribavirin in egyptian adolescents with chronic hepatitis C virus Infection. *J Hepatol.* (2017) 66:S178. doi: 10.1016/S0168-8278(17)30642-6
44. El-Sayed MH, Ebeid FSES, Zekri AR, Massetto B, Kersey K, Osinusi A, et al. Ledipasvir/Sofosbuvir for 12 weeks is safe and effective in adolescents with chronic hepatitis C virus infection and hematological malignancies undergoing chemotherapy. *J Hepatol.* (2018) 68:S515. doi: 10.1016/S0168-8278(18)31278-9
45. Isakov V, Gankina N, Morozov V, Kersey K, Lu S, Osinusi A, et al. THU-136-Ledipasvir/sofosbuvir for 8 weeks cures genotype 4 chronic hepatitis C in non-cirrhotic children and adolescents. *J Hepatol.* (2019) 70:e221. doi: 10.1016/S0618-8278(19)30411-6
46. Jonas M, Romero R, Sokal E, Rosenthal P, Verucchi G, Lin H, et al. IDDF2020-ABS-0059 Safety and efficacy of sofosbuvir/velpatasvir (SOF/VEL) in pediatric patients 6 to < 18 years old with chronic hepatitis C (CHC) infection. *Gut.* (2020) 69:1832–40. doi: 10.1136/gutjnl-2020-IDDF.142
47. Sheha G, Elsayed R, Elbasiony M, Mikhail N. Ledipasvir 90 mg/sofosbuvir 400 mg for treatment of children with CHC genotype 4: single centre experience. *J Hepatol.* (2018) 68:S267. doi: 10.1016/S0168-8278(18)30748-7
48. Serranti D, Nebbia G, Cananzi M, Nicastro E, Di Dato F, Nuti F, et al. Efficacy of Sofosbuvir/Ledipasvir in adolescents with chronic hepatitis C genotypes 1, 3, and 4: a real-world study. *J Pediatr Gastroenterol Nutr.* (2021) 72:95–100. doi: 10.1097/MPG.0000000000002900
49. Indolfi G, Giometto S, Serranti D, Bettiol A, Bigagli E, De Masi S, et al. Systematic review with meta-analysis: the efficacy and safety of direct-acting antivirals in children and adolescents with chronic hepatitis C virus infection. *Aliment Pharmacol Ther.* (2020) 52:1125–33. doi: 10.1111/apt.16037
50. Baker RD, Dee D, Baker SS. Response to pegylated interferon alpha-2b and ribavirin in children with chronic hepatitis C. *J Clin Gastroenterol.* (2007) 41:111–4. doi: 10.1097/MCG.0b013e31802dd2f6
51. Jara P, Hierro L, de la Vega A, Diaz C, Camarena C, Frauca E, et al. Efficacy, safety of peginterferon-alpha2b ribavirin combination therapy in children with chronic hepatitis C infection. *Pediatr Infect Dis J.* (2008) 27:142–8. doi: 10.1097/INF.0b013e318159836c
52. Tajiri H, Inui A, Kiyohara Y, Suzuki M, Kagimoto S, Etani Y, et al. Peginterferon alpha-2b and ribavirin for the treatment of chronic hepatitis C in Japanese pediatric and young adult patients: a survey of the Japan society of pediatric hepatology. *Eur J Gastroenterol Hepatol.* (2009) 21:1256–60. doi: 10.1097/MEG.0b013e32832a4e97
53. Sokal EM, Bourgois A, Stephenne X, Silveira T, Porta G, Gardovska D, et al. Peginterferon alfa-2a plus ribavirin for chronic hepatitis C virus infection in children and adolescents. *J Hepatol.* (2010) 52:827–31. doi: 10.1016/j.jhep.2010.01.028

54. Wirth S, Ribes-Koninckx C, Calzado MA, Bortolotti F, Zancan L, Jara P, et al. High sustained virologic response rates in children with chronic hepatitis C receiving peginterferon alfa-2b plus ribavirin. *J Hepatol.* (2010) 52:501–7. doi: 10.1016/j.jhep.2010.01.016
55. Mack CL, Gonzalez-Peralta RP, Gupta N, Leung D, Narkewicz MR, Roberts EA, et al. NASPGHAN practice guidelines: diagnosis and management of hepatitis C infection in infants, children, and adolescents. *J Pediatr Gastroenterol Nutr.* (2012) 54:838–55. doi: 10.1097/MPG.0b013e318258328d
56. Druyts E, Thorlund K, Wu P, Kanters S, Yaya S, Cooper CL, et al. Efficacy and safety of pegylated interferon alfa-2a or alfa-2b plus ribavirin for the treatment of chronic hepatitis C in children and adolescents: a systematic review and meta-analysis. *Clin Infect Dis.* (2013) 56:961–7. doi: 10.1093/cid/cis1031
57. Indolfi G, Nebbia G, Cananzi M, Maccabruni A, Zaramella M, D'Antiga L, et al. Kinetic of virologic response to pegylated interferon ribavirin in children with chronic hepatitis C predicts the effect of treatment. *Pediatr Infect Dis J.* (2016) 35:1300–3. doi: 10.1097/INF.0000000000001325
58. Wirth S, Pieper-Boustani H, Lang T, Ballauff A, Kullmer U, Gerner P, et al. Peginterferon alfa-2b plus ribavirin treatment in children and adolescents with chronic hepatitis C. *Hepatology.* (2005) 41:1013–8. doi: 10.1002/hep.20661
59. Rosenthal ES, Graham CS. Price and affordability of direct-acting antiviral regimens for hepatitis C virus in the United States. *Infect Agent Cancer.* (2016) 11:24. doi: 10.1186/s13027-016-0071-z
60. Kohli A, Kattakuzhy S, Sidharthan S, Nelson A, McLaughlin M, Seamon C, et al. Four-week direct-acting antiviral regimens in noncirrhotic patients with hepatitis C virus genotype 1 infection: an open-label, nonrandomized trial. *Ann Intern Med.* (2015) 163:899–907. doi: 10.7326/M15-0642
61. Latt NL, Yanny BT, Gharibian D, Gevorkyan R, Sahota AK. Eight-week ledipasvir/sofosbuvir in non-cirrhotic, treatment-naïve hepatitis C genotype-1 patients with hepatitis C virus-RNA < 6 million: single center, real world effectiveness and safety. *World J Gastroenterol.* (2017) 23:4759–66. doi: 10.3748/wjg.v23.i26.4759
62. Kattakuzhy S, Wilson E, Sidharthan S, Sims Z, McLaughlin M, Price A, et al. Moderate sustained virologic response rates with 6-week combination directly acting anti-hepatitis C virus therapy in patients with advanced liver disease. *Clin Infect Dis.* (2016) 62:440–7. doi: 10.1093/cid/civ897
63. Abutaleb A, Kottilil S, Wilson E. Glecaprevir/pibrentasvir expands reach while reducing cost and duration of hepatitis C virus therapy. *Hepatol Int.* (2018) 12:214–22. doi: 10.1007/s12072-018-9873-y

Conflict of Interest: The authors declare that the research was conducted in the absence of any commercial or financial relationships that could be construed as a potential conflict of interest.

frontiers in Medicine

REVIEW
published: 28 September 2021
doi: 10.3389/fmed.2021.725390

Molecular and Cellular Mediators of the Gut-Liver Axis in the Progression of Liver Diseases

*Alix Bruneau, Jana Hundertmark, Adrien Guillot and Frank Tacke**

Department of Hepatology & Gastroenterology, Charité Universitätsmedizin Berlin, Campus Virchow-Klinikum (CVK) and Campus Charité Mitte (CCM), Berlin, Germany

The gut-liver axis covers the bidirectional communication between the gut and the liver, and thus includes signals from liver-to-gut (e.g., bile acids, immunoglobulins) and from gut-to-liver (e.g., nutrients, microbiota-derived products, and recirculating bile acids). In a healthy individual, liver homeostasis is tightly controlled by the mostly tolerogenic liver resident macrophages, the Kupffer cells, capturing the gut-derived antigens from the blood circulation. However, disturbances of the gut-liver axis have been associated to the progression of varying chronic liver diseases, such as non-alcoholic fatty liver disease, non-alcoholic steatohepatitis, and primary sclerosing cholangitis. Notably, changes of the gut microbiome, or intestinal dysbiosis, combined with increased intestinal permeability, leads to the translocation of gut-derived bacteria or their metabolites into the portal vein. In the context of concomitant or subsequent liver inflammation, the liver is then infiltrated by responsive immune cells (e.g., monocytes, neutrophils, lymphoid, or dendritic cells), and microbiota-derived products may provoke or exacerbate innate immune responses, hence perpetuating liver inflammation and fibrosis, and potentiating the risks of developing cirrhosis. Similarly, food derived antigens, bile acids, danger-, and pathogen-associated molecular patterns are able to reshape the liver immune microenvironment. Immune cell intracellular signaling components, such as inflammasome activation, toll-like receptor or nucleotide-binding oligomerization domain-like receptors signaling, are potent targets of interest for the modulation of the immune response. This review describes the current understanding of the cellular landscape and molecular pathways involved in the gut-liver axis and implicated in chronic liver disease progression. We also provide an overview of innovative therapeutic approaches and current clinical trials aiming at targeting the gut-liver axis for the treatment of patients with chronic liver and/or intestinal diseases.

Keywords: microbiota, liver diseases, immune cells, gut-liver axis, TLRs (Toll-like receptors), NAFLD (non-alcoholic fatty liver disease), NASH, PSC

OPEN ACCESS

Edited by:
Chao Yan,
Xuzhou Medical University, China

Reviewed by:
Stefano Fiorucci,
University of Perugia, Italy
Huikuan Chu,
Huazhong University of Science and Technology, China

****Correspondence:***
Frank Tacke
frank.tacke@charite.de

Specialty section:
This article was submitted to Gastroenterology, a section of the journal Frontiers in Medicine

Received: *15 June 2021*
Accepted: *01 September 2021*
Published: *28 September 2021*

Citation:
Bruneau A, Hundertmark J, Guillot A and Tacke F (2021) Molecular and Cellular Mediators of the Gut-Liver Axis in the Progression of Liver Diseases. Front. Med. 8:725390. doi: 10.3389/fmed.2021.725390

INTRODUCTION

The liver is a highly vascularized organ that receives ∼75% of its blood supply from the enterohepatic circulation, delivering nutrients from the intestines, together with recirculating bile acids and gut microbiota-derived products. In turn, the liver provides signals to the gut by secreting bile, antimicrobial molecules in the bile ducts. The liver vasculature is made

of fenestrated capillaries formed by liver sinusoidal cells, with intense biomolecule exchange between the blood compartment and the hepatic parenchymal cells. Liver resident macrophages, termed Kupffer cells (KCs), reside in these capillaries and play the roles of sentinels, sensing their microenvironment and catching cellular residues and microorganisms, thus maintaining homeostasis and an immunotolerant environment (1, 2). The intestinal mucosal and vascular barriers contribute to the communication between the gut and the liver, because they prevent microbiota and their metabolites from excessively spreading through the portal circulation in healthy conditions. The gastrointestinal tract shelters an ensemble of microorganisms including bacteria, fungi, archaea, viruses, and their genomes, all regrouped under the term of microbiome (3). Microbiota is a fundamental part of the gut, playing an essential role in digestion and bile metabolism, but also able to release a wide number of metabolites, peptides, and hormones capable of activating immune cells, thus continually shaping host immunity and metabolism (3, 4). The integrity of the gastrointestinal mucosa is then crucial to protect liver cells from exposure to gut-derived pathogen-associated molecular pattern molecules (PAMPs, e.g., bacteria and bacterial products), fatty acids and carbohydrates or modified bile composition (5).

The gut-liver axis is therefore an anatomical and functional connection existing through blood and bile circulation, integrating signals generated from environmental factors, diet, or microbiota (6). A healthy microbiota exerts protective effects (7, 8), highlighting the importance of considering therapeutic interventions targeting patients microbiota to slow down the progression of chronic liver diseases. However, growing evidence from clinical studies and experimental models show the involvement of gut-derived signals in the modulation of numerous liver diseases, including non-alcoholic fatty liver disease (NAFLD), non-alcoholic steatohepatitis (NASH), alcohol-associated hepatitis, cholestatic liver diseases, and in the progression to cirrhosis and hepatocellular carcinoma (HCC) (5, 6, 9, 10).

In a healthy liver, PAMPs are usually not harmful, since they are eliminated by KCs (1). However, in the context of acute or chronic liver inflammation, liver cell injury may induce cell death, releasing pro-inflammatory cytokines and chemoattractants, damage-associated molecular patterns (DAMPs), thus fueling chronic inflammation and innate immune cell recruitment (1). Furthermore, increased intestinal permeability associated with dysbiosis could result in bacteria translocation and higher presence of PAMPs or toxic bile acids, and increased fatty acid concentrations within the liver. Recognition of environmental immune signals, such as PAMPs, DAMPs, and gut-derived microorganisms by pattern-recognition receptors (PRRs) contributes to shaping myeloid immune cell phenotypes, thus participating in the progression of liver diseases (11). Hence, gut-derived signals can be aggravating factors of an innate immune response, most notably characterized by a potent infiltration of neutrophils and monocyte-derived macrophages, key in the orchestration of inflammatory response in acute and chronic liver diseases (6).

The liver also affects gut homeostasis. Indeed, bile acids and immunoglobulin A (IgA) secreted by the liver act as regulators of the gut microbiota (12) and immunity (13), for instance by preventing the colonization of pathogenic species and reshaping immune cell phenotypes in the gut. Thus, upon liver injury, a modified bile acid pool might in turn affect microbiota composition and gastrointestinal inflammation (**Figure 1**).

For all these reasons, deciphering the molecular mechanisms involved in immune cell recruitment and activation in the liver and the intestine is of great interest in developing promising therapeutic approaches. In this review, we summarize the current knowledge about molecular and cellular mediators of the gut-liver axis and their involvement in the progression of liver diseases. We also detail the most recent therapeutic options and perspectives to treat patients suffering from various liver diseases, by focusing on targeting actors of the gut-liver axis.

INVOLVEMENT OF THE GUT-MICROBIOTA IN LIVER DISEASES

Our understanding of the composition and functions of the gut microbiota in physiological conditions is in constant evolution. Several national or multinational studies contributed to the identification of three main enterotypes (14) present through all populations and continents, *Bacteroides*, *Prevotella*, *Ruminococcus*, comprising the main bacterial phyla: *Firmicutes*, *Bacteroidetes*, *Actinobacteria*, *Proteobacteria*, and *Verrucomicrobia* (15). The gut microbiome is highly variable among individuals and depends on many elements, including age, birth mode, diet, geography, exercise, and other lifestyle factors, such as alcohol consumption and exposure to antibiotics (3, 16). Over the last decade, many research articles highlighted the role of dysbiosis in liver diseases (**Table 1**). As discussed below, disruption in gut microbiota homeostasis can affect bile acid metabolism, intestinal permeability, short chain fatty acids (SCFAs) availability and consequently alter alcohol, glucose and lipid metabolism, dietary energy utilization, along with promoting liver injury, and inflammation. However, whether intestinal dysbiosis is part of the causes or a result of liver diseases remains an unanswered question in many cases.

Cholangiopathies

Cholestatic diseases or cholangiopathies encompass several conditions, from pediatric genetic liver diseases, e.g., progressive familial intrahepatic cholestasis (PFIC), to adult idiopathic or genetic diseases including primary biliary cholangitis (PBC), and primary sclerosing cholangitis (PSC).

Abbreviations: BDL, Bile duct ligation; CDAA, Choline-deficient L-amino-defined; DAMPs, Danger-associated molecular patterns; DCs, Dendritic cells; DSS, Dextran sodium sulfate; FMT, Fecal microbiota transfer; FXR, Farnesoid X Receptor; HCC, Hepatocellular carcinoma; HFD, High fat-diet; IBD, Inflammatory bowel disease; IFN, Interferon; IL, Interleukin; KCs, Kupffer cells; LPS, Lipopolysaccharide; NAFLD, Non-alcoholic fatty liver disease; NASH, Non-alcoholic steatohepatitis; PAMPs, Pathogen-associated molecular patterns; PBC, Primary biliary cholangitis; PRRs, Pattern-recognition receptors; PSC, Primary sclerosing cholangitis; SCFAs, Short-chain fatty acids; TLRs, Toll-like receptors; TNF, Tumor necrosis factor.

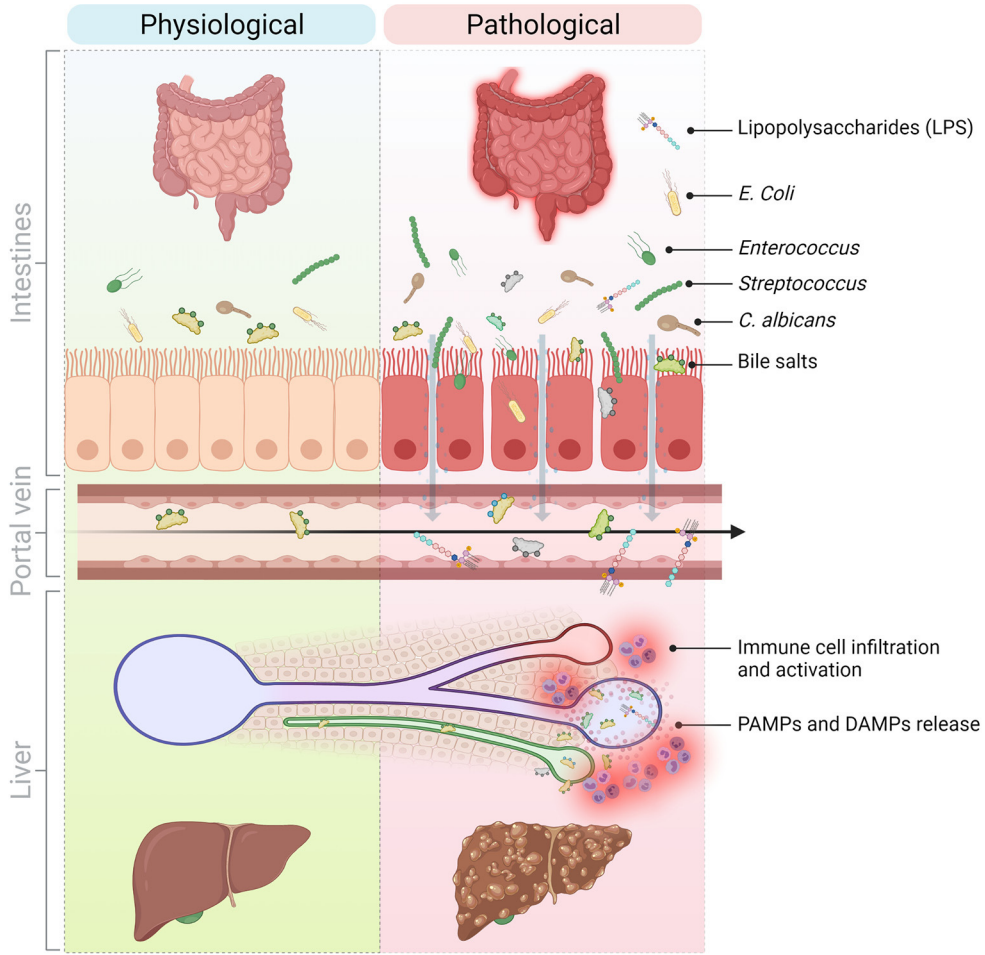

FIGURE 1 | Molecular and cellular mediators of the gut-liver axis implicated in the progression of liver inflammation in chronic liver diseases. The communication between the liver and the gut is bidirectional. The liver secretes primary bile acids and antimicrobial peptides in the bile ducts while the gut contains host-, food-, and microbiota-derived antigens and metabolites. In normal conditions, these signals contribute to maintain physiological immune cell populations in the gut and are well-tolerated by the liver. However, in pathological conditions and because of a perturbed intestinal barrier (e.g., in NASH, NAFLD, PSC), DAMPs and PAMPs originating from the intestines translocate to the liver via the hepatic portal vein and thus, promote liver injury and inflammation and sustain liver disease progression. DAMPs, Danger-associated molecular patterns; LPS, Lipopolysaccharide; NAFLD, Non-alcoholic fatty liver disease; NASH, Non-alcoholic steatohepatitis; PAMPs, Pathogen-associated molecular patterns; PSC, Primary sclerosing cholangitis. Created with Biorender.

Notable changes in the composition of the gut microbiota in patients with PSC and PBC have been reported, suggesting a role of microbiota in their pathogenesis (41). Enriched amounts of some species, including *Veillonella*, *Streptococcus*, and *Enterococcus* or depletion in *Clostridiales II* have been described in feces or mucosal biopsies of patients in several cohorts (18–20, 22). Moreover, the strong association of Inflammatory Bowel Disease (IBD) and PSC is well-known, in particular in the Northern European population with ∼80% of PSC patients suffering from IBD (42). It is plausible that dysbiosis and liver inflammation are functionally linked, as proposed by the leaky gut hypothesis. Indeed, supporting this hypothesis, a recent study showed an increased recruitment of $CD11b^{+}CD11c^{-}Ly6C^{+}$ macrophages in the liver, associated with bacteria homing after induction of colitis in PSC mouse models (43). However, the gut-liver axis is bidirectional, and thus an impaired bile acid flux or modified bile acid composition could very well alter the microbiota in return (e.g., by promoting the colonization of invasive bacterial populations) and may thereby provoke a much more harmful translocation of PAMPs to the liver, thus aggravating liver injury in a negative feedback loop. The $Mdr2^{-/-}$ mouse model is commonly used as a model for PSC. As these mice lack phospholipids in its bile, toxic free bile acids and cholesterol crystals will trigger cholangiocyte injury. Tedesco et al. demonstrated that these mice spontaneously display an increased intestinal permeability and dysbiosis with an enrichment in *Lactobacillus sp.* associated with increased IL-17 in the serum (44).

Recently, different studies demonstrated that besides bacteria dysbiosis, PSC patients also suffer from fungi dysbiosis.

TABLE 1 | Summary of studies analyzing microbiota in chronic liver diseases.

Disease	Characteristic changes in the gut microbiota (dysbiosis)	Sample	References
PBC	↓ *Sutterella, Oscillospira* and *Faecalibacterium* and ↑ *Haemophilus, Veillonella, Clostridium, Lactobacillus, Streptococcus, Pseudomonas, Klebsiella*	Stool	(17)
PSC	↑*Veilloneilla*	Stool	(18)
	↑*Escherichia*, *Lachnospiraceae*, *Megasphera* and ↓*Clostridiales II*	Colon biopsies	(19) (20)
	↓*Clostridiales II*	Colon + Ileum	(21)
	↑Ruminococcus and Fusobacterium, ↓ Dorea, Veillonella, Lachnospira, Blautia, and Roseburia	Stool	(22)
	↑ *Enterococcus*, *Streptococcus*, *Lactobacillus*	Stool	(23)
	↑*Rothia*, *Enterococcus*, *Streptococcus*, *Veillonella*,	Stool	(24)
	↑ *Trichocladium griseum*, *Candida spp.*	Stool	(25)
	↓ *Firmicutes spp.* (*Faecalibaterium* and *Ruminococcus*) except ↑ of *Veilloneilla,* ↑ Proteobacteria; ↓ *S. cerevisiae* and ↑ *Exophiala*	Stool	
ALD	↑ *Candida*, ↓ *Epicoccum,* ↓ *Galactomyces*	Stool	(26)
	↑ *Bifidobacterium, Streptococcus spp, Lactobacillus spp* ↓ Prevotella, Paraprevotella, and Alistipes	Stool	(27)
NAFLD	↑ Escherichia coli and Bacteriodes vulgatus, ↓ *Ruminococcus spp.*, *Eubacterium rectale*, *Faecalibacterium prausnitzii*	Stool	(28)
	↓ virus and bacteriophage diversity, ↑ *Escherichia, Enterobacteria,* and *Lactobacillus* phage	Stool	(29)
	↑ *Gemmiger*, ↓ Faecalibacterium, Bacteroides and Prevotella	Stool	(30)
	↑ *Gemmiger*, ↓ *Bacteroides*	Stool	(31)
NASH	↑ *Bacteroides,* ↓ *Prevotella*	Stool	(32)
	↓ *Firmicutes* and *Clostridiales* (*Faecalibacterium* and *Anaerosporobacte),* ↑ *Bacteroidetes* (*Parabacteroides* and *Allisonella)*	Stool	(33)
	↑ Proteobacteria, *Bacteroidetes*, ↓ *Actinobacteria*, *Firmicutes*	Stool	(34)
Cirrhosis	↑ *Veillonella spp.* and *Streptococcus spp.*, ↓ *Bacteroidetes* and *Firmicutes*	Stool	(9)
	↓ *Lachnospiraceae, Ruminococcaceae* and *Blautia*	Stool	(35)
	↑ *Staphylococcaeae*, *Enterobacteriaceae, Enterococcaceae* and *Enterococcaceae,* ↓ *Lachnospiraceae*, *Ruminococcaceae* and *Clostridiales XIV*	Stool	(36)
	↑ *Candida spp.*	Duodenal fluid	(37)
HCC	↑ *Bacteroide,* ↓ *Bifidobacterium, Blautia*	Stool	(38)
	↑ *Escherichia coli*	Stool	(39)
	Presence of *H. pylori*	Liver	(40)

ALD, Alcohol-related liver disease; HCC, Hepatocellular carcinoma; NAFLD, Non-alcoholic fatty liver disease; NASH, Non-alcoholic steatohepatitis; PBC, Primary biliary cholangitis; PSC, Primary sclerosing cholangitis; Underlined: fungi. ↓ decrease ↑ increase.

According to a French study by Lemoinne et al., PSC patients with associated IBD display a specific signature different from PSC patients without IBD or patients with IBD only (25). On the contrary, in a German cohort, no differences were found between PSC patients suffering colitis or not. However, they confirmed Lemoinne et al. data concerning an increase of *Candida* species and of the fungal class *Sordariomycetes* for all PSC patients compared to the healthy group (24).

Non-alcoholic Fatty Liver Disease and Non-alcoholic Steatohepatitis

NAFLD is the most frequent cause of chronic liver disease worldwide. NAFLD is commonly associated to metabolic syndrome, insulin resistance, type 2 diabetes, and obesity. The term NAFLD refers to a wide spectrum of conditions, from simple liver steatosis to NASH. NASH is characterized by chronic inflammation, fibrosis, hepatocellular injury, and can progress to cirrhosis and HCC (45).

There is evidence for the involvement of several components of the gut-liver axis, e.g., microbiota dysbiosis, modification in the gut barrier permeability, bile acid metabolism changes, and SCFAs in the progression of the NAFLD and NASH (46).

The first report suggesting an impact of gut microbiota in human NAFLD dates back to the 80s (47). Consequently, other studies explored the roles of gut microbiome in patients with NASH. Small intestinal bacterial overgrowth (SIBO) in NASH groups compared to controls has been reported by Wigg et al. (48) as well as Shanab et al. (49), while several studies characterized dysbiosis in more detail. An increase in *Bacteroidetes* phylum, colonization by pro-inflammatory *Proteobacteria*, *Enterobacteriaceae*, and *Escherichia* and decrease in *Firmicutes* (including *Prevotella*, *Faecalibacterium* species) are the most common changes observed in NAFLD and NASH patients (32–34). Boursier et al. were able to link fecal microbiota alterations with the severity of NAFLD lesions, based on changes in *Bacteroides* and *Ruminococcus* abundance (32). Serum and hepatic bile acid concentrations can be modified in NASH patients, and the latter could have an effect on the progression of fibrosis (50).

An increase of the gut barrier permeability as a result of dysbiosis leads to higher bacterial translocation and elevated levels of LPS reaching the liver, leading to PRR activation and immune cell recruitment, thus sustaining liver inflammation.

Alcohol-Related Liver Diseases

Excessive alcohol drinking is a major cause of liver damage and deaths worldwide (51). Involvement of gut dysbiosis in the severity of liver injury in alcohol-related liver diseases has long been emphasized in both patients and animal models (52). Following 6 weeks of alcohol feeding, mice have a loss of bacterial diversity characterized by a shift in phyla with more *Proteobacteria, but* less *Bacteroidetes*, *Firmicutes*, and *Lactobacillus* (53). Accordingly, in a mouse model, 3 weeks of alcohol exposure were sufficient to observe an increase in plasma LPS. In the same study, the authors observed bacteria overgrowth, which they attributed to a downregulation of mouse antimicrobial proteins Reg3b and Reg3g (54). Ethanol-induced gut microbiota alterations were also associated with changes in metabolic profiles, including an increase in intestinal levels of SCFAs. This mouse data has been confirmed in patient cohorts, showing that alcohol is one of the main factors contributing to modifications in the gut microbiota. For instance, an enrichment in pro-inflammatory *Enterobacteria* such as *Escherichia* and *Klebsiella* and a decreased abundance in butyrate-producing species which have an anti-inflammatory protective effect were reported (27, 55). 16S sequencing from patients with alcohol-associated hepatitis highlighted a drastic increase of *Enterococcus faecalis* in stool samples compared with controls. Duan et al. identified cytolysin, a bacterial toxin secreted by *E. faecalis*, in stool samples of these patients and showed that its presence is associated with a worse clinical outcome and a higher death rate. Moreover, they demonstrated that in a mouse model infected with a cytolitic *E. faecalis* strain followed by an ethanol diet *E. faecalis* can be detected in the liver and is associated with increased liver inflammation. *In vitro*, the cytolitic *E. faecalis* promotes primary hepatocytes cell death, offering a possible explanation for the ethanol-liver injury induced by this bacteria strain (56).

Fungi also play a role in the development of alcohol-related liver disease. Indeed, Yang et al. showed that chronic ethanol administration is responsible for a fungal dysbiosis and elevated plasma levels of β-glucan in mice (26). They presented evidence for similar modifications in the composition of fecal mycobiome for patients with chronic alcohol abuse. The diversity and richness of fungal species is reduced in alcohol-dependent patients compared to healthy controls. Additionally, an overgrowth of *Candida* species, mainly *Candida albicans* is observed (26).

Cirrhosis

Cirrhosis is the end-stage of chronic liver diseases and is associated with dysbiosis and a disruption of the intestinal barrier, partly due to portal hypertension. Portal hypertension does not only promote neo-angiogenesis and intestinal permeability, but also increases intercellular spaces between enterocytes and affects microvilli density in patients with cirrhosis (57), thus allowing PAMPs to easily reach the liver and accelerate the pre-existing hepatic inflammation.

The gut microbiome of a Chinese cohort of 98 patients has been sequenced from stool samples and the authors found out that species decreasing the most belong to *Bacteroidetes* and *Firmicutes* phyla, while *Streptococcus* and *Veillonella spp.* have the greatest increase (9). They propose a patient discrimination index (PDI) relying on 15 gene markers, all related to gut microbiota, which could be used to diagnose liver cirrhosis in a non-invasive way. Bajaj et al. obtained similar results in patients with varying cirrhosis severity: an enrichment in pathogenic taxa, *Staphylococcaceae*, *Enterobacteriaceae*, and *Enterococcaceae* along with a decrease in *Lachnospiraceae*, *Ruminococcaceae*, and *Clostridiales XIV* (35, 36). By calculating a cirrhosis dysbiosis ratio (CDR), the same authors correlated the severity of cirrhosis with the changes in patient's microbiota. The reduced species are important for the production of SCFAs, thus reducing the intestinal inflammation and protecting the mucosa. A lower amount of SCFAs might also explain the disruption of the intestinal barrier as well as the release and translocation of PAMPs (including LPS) to the liver, and thereby contribute contribute to the disease severity and occurrence of complications in patients (36). Moreover, this dysbiosis is responsible for modifications in the bile acid pool in the gut, caused by a depletion in certain bacteria species involved in the regulation of primary bile acids conversion (35).

A clear correlation exists between fungal infection, higher inflammation, and increased mortality rate in patients with end stage liver disease (58). Several *Candida* species were detected with 18S rRNA gene-based PCR method in a cohort of patients with cirrhosis (37). A more recent study linked fungal infections in cirrhotic patients with a weakened ability of their neutrophils to kill *C. albicans* (59). Mechanisms involved in the progression of cirrhosis or complications in patients following fungal dysbiosis remain mostly unexplored but are of interest to develop innovative and efficient therapies.

Hepatocellular Carcinoma

Hepatocellular carcinoma (HCC) represents about 80% of primary liver cancer cases worldwide (60). Increased intestinal permeability and significant modifications in the microbiota profile of HCC patients strongly advocate for a role of the gut-liver axis in the progression of HCC (38). Along with a disturbed intestinal mucosa, LPS was shown to be increased in HCC patient serum, and there has been evidence of bacterial translocation, which correlate with chronic inflammation characterized by more $CD14^{+}PD\text{-}L1^{+}$ circulating monocytes and a specific cytokine and chemokine signature in the HCC group. The deficit in anti-inflammatory species *Bifidobacterium* or *Blautia* could explain this enhanced intestinal and hepatic inflammation (38). Depending on the studies, the dysbiosis is characterized by increased *Escherichia coli* (39), increased *Bacteroides* (38), and *H. pylori* presence has even been detected in liver samples from HCC patients (40). Rao et al. suggested using patient's microbiota signature from tongue swab as a non-invasive tool for HCC diagnosis (10).

Several studies using animal models relate to this clinical data: in a diethylnitrosamine (DEN) model of rat HCC, authors noticed a decrease in *Bifidobacterium*, *Enterococcus*, and *Lactobacillus* species in the gut (61). Moreover, colonization of the gut with *Helicobacter hepaticus* in aflatoxin B1 (AFB1)-induced liver cancer mouse model is linked with a poor

prognosis and the severity of inflammation, thus promoting carcinogenesis (62).

GUT-DERIVED METABOLITES AND MOLECULAR PATHWAYS

Microbial metabolites and bile acids shape immune cell maturation and homeostasis and contribute to maintain intestinal barrier integrity. Thus, modifications in the microbiota or their metabolite profiles can alter immune response and trigger inflammation in the gut and in the liver. Furthermore, modifications in bile acids, SCFAs or tryptophan metabolites have been described in the pathogenesis of several chronic liver diseases.

Molecular Mediators in the Gut-Liver Axis

Bile Acids

Bile acids have a key role in homeostasis as they contribute to the absorption of dietary fats and liposoluble vitamins and prevent commensal bacteria over-growth or colonization of the intestines by pathogenic bacteria species (63). Bile acids are secreted by hepatocytes through the ATP-dependent transporter called ABCB11, and are derived from two different origins; primary bile acids (5% of total bile acids) are *de novo* synthesized from cholesterol and secondary bile acids (95%), which are deconjugated by gut microbiota and recycled daily after ileal reabsorption through the entero-hepatic circulation (12). In homeostatic situations, the ratio between glyco-conjugated and tauro-conjugated bile acids synthesized in the liver is tightly regulated. Similarly, the deconjugation of bile acids in the colon by anaerobic bacteria is under strict control since secondary bile acids are more hydrophobic and thus more toxic for the intestinal and hepatic epithelial cells (63, 64). Thus, (1) a modification in the ratio of synthesized bile acids could change the antimicrobial properties of bile and alter the gut microbiota as well as having a deleterious effect on hepatocytes and cholangiocytes membrane, generating apoptosis, and inflammation in the liver; and (2) an intestinal dysbiosis might be responsible for the increased generation of toxic bile acids by bacteria (12).

Modifications of the bile acid profile in the plasma of PSC patients have been evidenced and are clinically associated with hepatic decompensation (65). Torres et al. were able to demonstrate a relationship between stool bile acids profile and microbiota composition in patients with PSC associated to IBD compared to patients suffering from IBD alone, thus suggesting an effect of bile acids on the microbiota composition of PSC patients (21). Similar findings have been made with circulating bile acids from NAFLD and NASH patients (66, 67). Moreover, in a mouse model of high fat-diet (HFD), the presence of hydrophobic bile acids is correlated with liver inflammation and bacteria dysbiosis, and promotes carcinogenesis (68). Along with dysbiosis and stronger colon inflammation, Xie et al. have reported increased expression of several genes involved in bile synthesis in a model of alcohol-related liver disease (68), while others indicate higher concentrations of total fecal bile acids as well as modifications in the primary to secondary bile acids ratio in patients actively drinking (69).

Bile acids are recognized by several receptors in a wide variety of cells and can regulate bile acid synthesis and immune cell activation. Bile acids can directly bind the Farnesoid X Receptor (FXR) which will then be translocated to the nuclei and inhibit bile acids synthesis. FXR is expressed in hepatocytes, enterocytes, and regulates lipid metabolism, glucose metabolism, and inflammation on top of bile acids synthesis (70). Targeted inhibition of intestinal FXR helped reducing hepatic lipid droplets in a HFD model, thus protecting mice from hepatic steatosis. Moreover, authors showed an overexpression of FXR and its downstream effectors in the intestine of obese humans compared with lean controls, thus suggesting a role of FXR in the pathogenesis of metabolic syndromes in patients (71). Indeed, modified bile acid composition and elevated plasma bile acids levels in NAFLD patients negatively influence FXR signaling, which impacts bile acid synthesis, lipid and glucose metabolism, and inflammation, thus potentially contributing to hepatic injury. Additionally, expression of downstream effectors of intestinal FXR is decreased in NAFLD and NASH patient biopsies (72). In rodents fed with HFD, intestinal FXR is downregulated and the use of an FXR agonist, obeticholic acid (OCA), helped preserve the gut barrier integrity, thus decreasing PAMPs amount in the liver (73). Decreased FXR expression also correlates with fibrosis and NAFLD activity score (74). Moreover, Pathak et al. showed that intestinal FXR activation is responsible for microbiota composition modifications, which will in return activate TGR5 signaling, improving glucose and lipid metabolism in an obesity mouse model, thus suggesting a role in NAFLD and NASH pathogenesis (75).

TGR5 is a plasma membrane associated protein expressed by cholangiocytes, immune cells -including KCs- and hepatic stellate cells (HSC), mostly activated by hydrophobic bile acids. In reaction to LPS, TGR5 represses the secretion of pro-inflammatory cytokines by macrophages through an NF-κB dependent pathway (**Figure 2**) (70). Leonhardt et al. showed that patients with liver failure display a specific serum bile acids profile responsible for TGR5 activation in monocytes and correlated with increased mortality. Indeed, monocytes from healthy controls treated with TGR5-activating bile acids that were then stimulated with LPS, exhibit a drastically diminished pro-inflammatory phenotype (76). In a *Tgr5*$^{-/-}$ mouse model fed with alcohol, Spatz et al. observed increased liver injury, inflammation and steatosis compared to WT mice fed with alcohol. Those mice also display increased dysbiosis, independent from the alcohol uptake, massive macrophage infiltration (77). Moreover, TGR5 is downregulated in PSC patients and *Mdr2*$^{-/-}$ mice cholangiocytes, which promotes biliary injury and liver inflammation. Norursodeoxycholic acid (norUDCA) treatment can increase TGR5 expression, and thus attenuate biliary inflammation phenotype in *Mdr2*$^{-/-}$ mice (78). The treatment of HFD model with TGR5 agonists is able to reverse steatohepatitis in mouse and to generally improve liver histology (79, 80). In general, studies in animal models suggest that those receptors may be downregulated by ethanol consumption (81), liver inflammation, gut dysbiosis, or activation of NF-κB (82), and

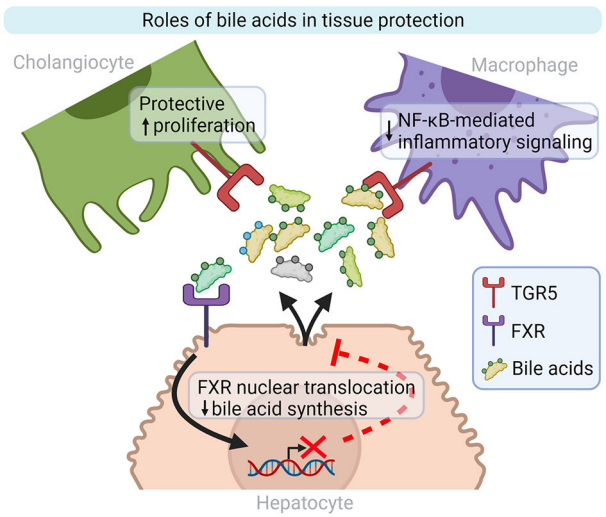

FIGURE 2 | Bile acid roles in inflammation and tissue repair modulation. TGR5 and FXR are two well-characterized bile acid receptors implicated in liver homeostasis. TGR5 activation on cholangiocytes and macrophages stimulates cell proliferation and decreases inflammatory signaling, respectively. Bile acid synthesis by hepatocytes is repressed by FXR activation. FXR, Farnesoid X-Activated Receptor; NF-κB, Nuclear factor kappa-light-chain-enhancer of activated B cells; TGR5, also known as GPBAR1, G-protein-coupled bile acid receptor. Created with Biorender.

that the use of TGR5 and FXR agonists could be beneficial for patients (83–85).

Bacterial and Fungi Products

Innate immune cells can recognize a wide variety of PAMPs released by bacteria, viruses or fungi. Among them, LPS (from Gram-negative bacteria), bacterial flagellin, bacterial/viral nucleic acids (ssRNA, dsRNA, CpG DNA), peptidoglycans (Gram-positive bacteria) β-glucans from fungi can all be recognized by PRRs and involved in the progression of liver diseases (6). As stated above, elevated serum levels of LPS or LPS-binding protein have been described in nearly all liver diseases: Alcohol-related liver diseases (6), NAFLD and NASH (46, 86), HCC (38, 61), PSC (87), indicating an increase of intestinal permeability and suggesting that signals derived from a diseased liver (e.g., modified bile acids, pro-inflammatory cytokines) affect the intestinal barrier integrity.

Bacteria can also interact with the host via secretion of metabolites, either derived from bacteria metabolism like tryptophan, or host molecules modified by bacteria such as bile acids (see above). The gastrointestinal tract is a central place for tryptophan metabolism, where it can directly and indirectly be metabolized to indoles and their derivatives by microbiota. Indoles are able to decrease macrophage production of pro-inflammatory cytokines and inhibit macrophage migration (86). Discovery of a perturbed tryptophan metabolism in patients suffering from IBD or colitis suggests common mechanisms for patients suffering of liver diseases associated with intestinal dysbiosis (88). In mice that were subjected to a model of alcohol-related liver disease and transplanted with patient's microbiota, targeting the tryptophan pathway was effective in reducing liver injury (89). Moreover, in order to determine a microbial signature in HCC, patient's stool microbiota was sequenced. Albhaisi et al. found no differences in the overall microbial diversity for cirrhotic patients who would develop HCC. However, specific changes in species involved in tryptophan metabolism were detected (90). Even though, research for new biomarkers in patients or animal models highlight the involvement of tryptophan and its metabolites in the pathogenesis of PSC (91) and NASH (92), the causal link with microbiota dysbiosis yet remains to be demonstrated.

In the past years, the interest for the mycobiome has been rising. Despite being at lower abundance compared to bacteria, commensal fungi are essential for tissue homeostasis and regulate many physiological processes (93). Fungal dysbiosis has been observed in several liver diseases as NASH (93), PSC (24, 25), alcohol-related liver diseases and cirrhosis (37, 58). Fungal dysbiosis occurs following chronic ethanol administration in mouse and is responsible for elevated plasma levels of β-glucan, and hepatocyte damage. It could activate liver resident macrophages through chitin or β-glucan (26, 93).

Short-Chain Fatty Acids

SCFAs produced by gut microbiota, in particular by *Firmicutes*, are essential actors in the maintenance of gut homeostasis through strong anti-inflammatory and anti-proliferative effects (94). Several SCFAs are generated by bacteria from dietary fibers, the predominant ones are butyrate, acetate and propionate (94). In patients with ulcerative colitis as well as colitis mouse models, changes in SCFAs concentration (in particular butyrate) are responsible for the activation of several pro-inflammatory pathways, including activation of the inflammasome (NLRP3) pathway with increased IL-18 secretion, increased production of pro-inflammatory cytokines like IFN-γ, IL-5, IL-8, IL-10, and IL-13 but also downregulation of NF-κB signaling, all of which have been linked to gut microbiota changes (4, 95). Dysbiosis observed in patients with chronic liver disease is often associated with a loss of bacterial species producing butyrate, thus explaining a reduction in SCFAs in several patient cohorts (27, 96). There is growing evidence that T-cell immunity can be regulated by gut-microbiota through SCFAs. On one hand, SCFAs can induce IL-10 secretion by $CD4^+$ Th1 cells, hence protecting mice from colitis (97), but on another hand, *in vitro*, SCFAs have been shown to affect the balance between Th17 and Treg cells by affecting peripheral blood mononuclear cells (PBMCs) production of cytokines involved in T cell differentiation (98).

Increase in SCFAs can also be deleterious. Indeed, in NAFLD-HCC patients, dysbiosis has been associated with an enrichment of five bacteria species, all linked to an elevated SCFAs production compared to control or NAFLD-cirrhosis groups. Behary et al. connected this specific bacteria profile of NAFLD-HCC patients, with elevated SCFAs concentration and T cell response, with an expansion of IL-10^+ Treg cells and a reduction of cytotoxic $CD8^+$ T cells in an *ex vivo* model (99). Involvement of SCFAs in the pathogenesis of cholestatic liver cancer has been highlighted by Singh et al. in a model of gut dysbiosis in mice fed with

enriched amounts of SCFAs. They showed that feeding with increased SCFAs is responsible for an even stronger intestinal dysbiosis in these mice as well as increased cholestatic liver injury, leading to HCC after 6 months. After 2 weeks of feeding, the mice displayed elevated bile acids in the serum, and at 4 weeks, hepatocyte apoptosis was elevated and triggered a massive neutrophils infiltration (100). A recent study correlated the presence of SCFAs with fibrosis in PBC patients, however the molecular roles of SCFAs in the pathogenesis of PBC have not been studied to this day (101).

Micro-RNA (miRNA)

Perturbation of the gut-liver axis can be responsible for changes in the expression of miRNAs. miRNAs are small single-stranded, non-coding RNAs involved in the silencing of protein-coding messenger RNAs (mRNAs) through translational repression and mRNA degradation (102). Modifications of miRNAs expression is connected with several chronic liver diseases, including NAFLD (103, 104), alcohol-related liver disease (105), cirrhosis, and HCC (106). Moreover, the impact of diet or gut-microbiota derived metabolites in the regulation of miRNAs expression in the gut and in the liver was demonstrated by multiple studies (106–109).

miR-22 expression is known to be down-regulated in HCC patients (109). A loss of butyrate-producing bacteria has been described in several HCC cohorts and may explain the link between intestinal dysbiosis and hepatic miR-22 down-regulation in those patients (108, 109). *In vitro*, butyrate induces miR-22 expression in the Huh7 hepatoma cell line. Moreover, Pant et al. showed that following miR-22 activation by butyrate, a SCFA produced by bacteria, ROS production is increased, cells undergo apoptosis and cell proliferation is inhibited (109).

In a rat model of NASH, gut dysbiosis, and increased intestinal permeability aggravates liver inflammation, and the authors observed modifications in miRNAs expression. For example, miR-122 expression is increased in the serum of NASH and NAFLD patients, while its hepatic expression is decreased. On the contrary, miR-146b expression is reduced in NASH patient serum and increased in tissue. Those two miRNAs are known for acting on the hepatic stellate cells, promoting fibrosis (110, 111). In a HFD model, the authors observed that HFD induces a microbiota dysbiosis and a hepatic downregulation of miR-122 and upregulation of miR34a as compared to mice fed with standard diet (112). A correlation analysis in HFD induced NAFLD mouse model, showed that miR-34a was associated with alterations in the gut microbiota, in particular with modifications in Firmicutes (113). Santos et al. used a mouse model lacking miR-21 and showed that when challenged with bile duct ligation (BDL), the absence of miR-21 protects those mice from liver injury and fibrosis (114). Those results are similar to those from Blasco-Baque et al., who used the same miR-21 KO mouse and demonstrated that they are protected from NASH with significant reduction of steatosis, fibrosis and inflammation (115). In both cases, the authors were able to link the hepatic expression of miR-21 and other miRNAs with gut microbiota changes. Indeed, LPS regulates the expression of miR-21, miR-181a, and miR-666 in a dose-dependent manner (115). Moreover, miR-21 deletion is responsible for gut microbiota modifications, which seem to have a protective effect in mice and to prevent a detrimental macrophage pro-inflammatory phenotype in the gut (114). A direct relationship also exists between LPS concentration and miR-146a-5p expression in the progression of liver fibrosis, indicating once again an indirect link between miRNAs and gut microbiota (116). Several miRNAs induce macrophage activation and contribute to inflammation and progression in liver diseases (117).

Also, in female mice, dysbiosis is not as severe as in male mice, leading to less toxic modification in the bile acids profile, which is likely due to protective role of estrogens (118). Furthermore, female mice have higher levels of the bile acid receptor FXR compared to male, which seems to increase the expression or miR-26a and miR-122, known to have tumor-suppressive effects in a murine NASH model (118). miRNAs are also known to be regulators of TLRs in immune cells (119), a family of receptors involved in the recognition of PAMPs as detailed in this review.

Recognition and Processing of Gut-Derived Signal in Hepatic and Immune Cells

Pattern Recognition Receptors and Signaling Pathways

With 10 members identified in humans, Toll-like receptors constitute the main family of PRRs. They have a fundamental role in the recognition of pathogens and pathogen-derived motifs (i.e., PAMPs). TLRs are expressed by hepatic stellate cells, liver parenchymal cells such as hepatocytes, cholangiocytes, as well as a wide variety of immune cells, including resident and circulating macrophages, dendritic cells (DCs) and neutrophils (**Figure 3**) (5). TLR signaling pathways are involved in maintaining homeostasis, and dysregulations of those pathways are involved in aberrant inflammatory reactions and autoimmune diseases. TLR1 (binding bacterial lipoproteins), TLR2 (bacterial and fungi lipoproteins), TLR4 (LPS), TLR5 (flagellin), and TLR6 (bacterial lipoproteins), are plasma membrane localized TLRs while TLR3 (dsRNA), TLR7, and TLR8 (ssRNA) TLR9 (unmethylated CpG containing ssDNA) and TLR13 (bacterial ribosomal DNA) are found in endosomes. Despite different cellular localizations, they share common signal transduction pathways. Upon TLR activation, two main molecular pathways can be induced: one mediated by TRIF (TLR3, TLR4) and another one involving Myd88 (all TLRs but TLR3) (120). They will both lead to the activation of transcriptional factors NF-κB, AP-1, and IRF3 thus promoting the expression and release of several pro-inflammatory cytokines: TNF-α, IL-1β, IL-6 as well as IFNs. TRIF can also promote RIPK3-dependent necroptosis (120). Isolated KCs strongly express all TLRs except TLR5, and KCs respond to all TLR ligands mainly by secreting TNF-α and IL-6 (121). Activated HSCs express TLR2, 4, and 9. Murine hepatic DCs express all TLRs at various levels and IFN-α, IFN-β and TNF-α are released after activation with TLR3 agonists, TLR3,−4,−7,−8, and−9 and all TLR agonists (121).

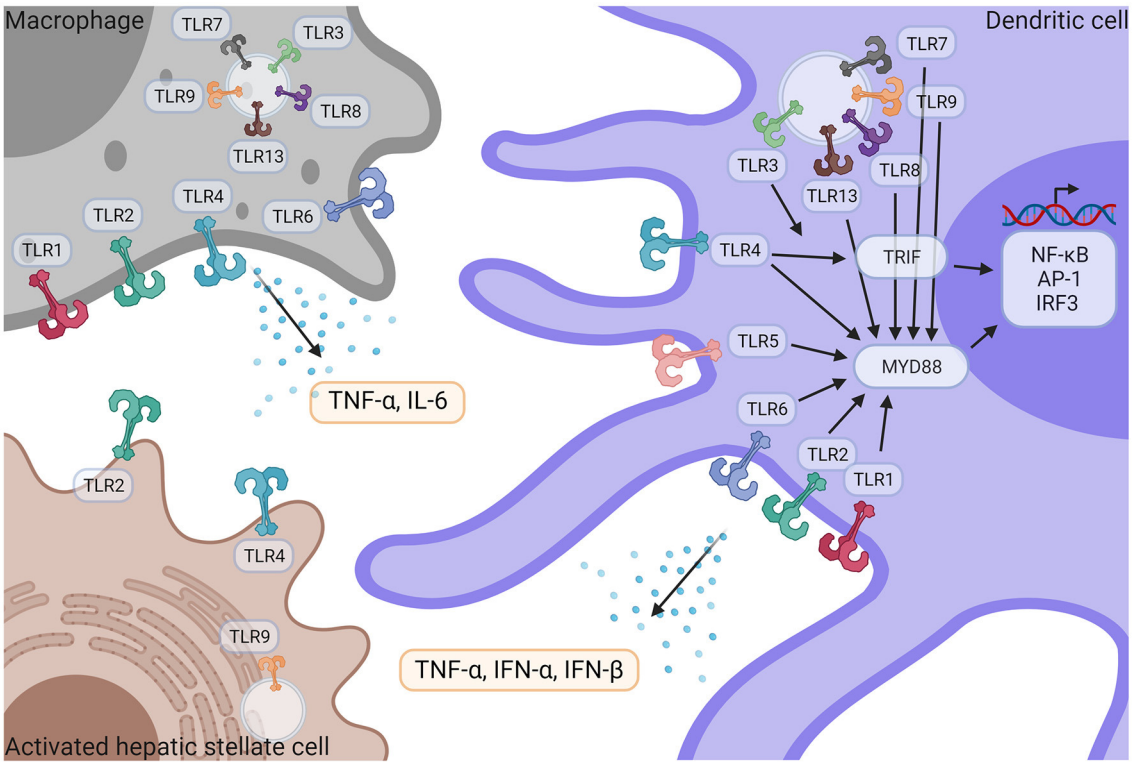

FIGURE 3 | TLR signaling in liver immune pathogenesis. Macrophages and DCs express TLR1,−2−3−4−6−7−8−9−13 and TLR5 is only expressed in DCs. HSCs express TLR2, TLR4, and TLR9. Following activation by their respective ligands, TLRs induce TRIF and/or MyD88 signaling pathways, leading to the activation of NF-κB, AP-1, and IRF3 transcriptional factors, followed by the release of pro-inflammatory cytokines such as TNF-α, IFN- α, IFN-β and IL-6. IFN-α, Interferon α; IFN-β, Interferon β; IL-6, Interleukin 6; NF-κB, nuclear factor kappa-light-chain-enhancer of activated B cells; TNF-α, Tumor necrosis factor α; TLR, Toll like receptor. Created with Biorender.

Cholangiopathies

Several groups demonstrated that mouse and human cholangiocytes express TLR2, 4, and 5, allowing them to recognize the PAMPs present in bile. Upon stimulation with bacterial components, cholangiocytes are able to trigger NF-κB pathway activation and release of IL-6 *in vitro* (122). The role of TLRs has been demonstrated in cholangiocytes for PSC and PBC patients, but little is known concerning their activation in immune cells and their role in the pathogenesis of these cholangiopathies (5).

Alcohol-Related Liver Disease

It is well-known that serum LPS levels are elevated in alcohol-related liver disease patients and are correlated with liver injury (52).

Expression levels of TLR2 and TLR4 were assessed in peripheral blood monocytes of patients suffering from alcohol-related liver disease. Even though no significant difference was detected between the groups, the authors described a diminution of TLR2-mediated immune response in the alcohol-related liver disease group compared to controls following stimulation of the cells with bacterial products (123). In another study, overexpression of TLR2, 4, and 9 has been associated with neutrophil dysfunction for patients suffering from alcohol-associated hepatitis (124).

Mice fed with ethanol for 10 days display an overexpression of liver TLR1, 2, 4, 6, 7, 8, and 9 at the mRNA level, resulting in an upregulation of TNF-α (125). KCs from rats exposed to ethanol upregulate TLR2 and TLR4 compared to control groups (126).

Feeding of WT mice with ethanol and unsaturated fat has a negative impact on liver injury and steatosis compared to ethanol and saturated fat feeding. This combination clearly damages the intestinal barrier, thus increasing LPS levels in mouse serum, which aggravates hepatic inflammation, characterized by a massive macrophage infiltration but also upregulation of all TLRs in the liver. It is unfortunate that the cell types overexpressing TLRs have not been characterized in this study (127). In a recent study, depletion of *Roseburia spp.* was associated with alcohol consumption and modifications in fecal SCFAs in patients, while *Roseburia spp.* supplementation in ethanol-fed mouse group could weaken hepatic inflammation. The mechanisms responsible for this amelioration are multiple: increased Muc2 and occluding expression in the gut barrier, indicating recovery of the barrier integrity, and decreased LPS serum levels and TLR4 expression in the liver. The authors

suggest that this amelioration due to *Roseburia spp.* is mediated by TLR5 (128).

Animal models of alcohol-induced liver injury indicate that TLR2/Myd88 and TLR9/Myd88 signaling in hepatocytes is indispensable for neutrophil infiltration and liver injury. Following depletion of KCs, infiltration of neutrophils is not prevented, however ALT levels and the gene expression of proinflammatory cytokines, such as *Il1b*, *Il6*, and *Tnfa* is decreased in KC-depleted mice compared with controls. This study suggests that dysbiosis in alcohol-related liver disease could increase hepatic presence of TLR2 and TLR9 ligands, thus contributing to liver inflammation (129). The activation of TLR2 pathway in KCs seems to be equally deleterious in the progression of alcohol-related liver disease and its deletion was beneficial for mice, due to a decreased activation of the NF-κB pathway and increased release of the anti-inflammatory cytokine IL-10 (130).

Activation of KCs via LPS-TLR4 pathways seems to be essential in the pathogenesis of alcohol-related liver diseases by activating a TRIF-dependent pathway and upregulating TNF-α (131). Bala et al. partly explain this by the increased activation of miR-155 in KCs following alcohol diet in mice. When induced, miR-155 negatively regulates inhibitors of the LPS-TLR4 pathway, thus enhancing KCs response to LPS (132).

NAFLD and NASH

Several studies in human or animal models have shown an association between changes in the gut microbiota and activation of TLRs signaling pathways in the liver (133, 134). TLR2, 4, 5, and 9 have been particularly associated with the progression of NAFLD and NASH, studies are summarized in **Table 2**.

Mridha et al. observed increased TLR4 and TLR9 mRNA in NASH patient biopsies compared to steatotic or control livers. Those results were confirmed in two murine NASH models, leading the authors to use *Tlr9*$^{-/-}$ mice. They showed that these mouse liver exhibit steatosis in the same way WT mouse do under HFD, however they seem to be more protected toward liver inflammation and fibrosis. Characterization of the inflammation revealed that liver from *Tlr9*$^{-/-}$ mice have a diminution in NF-κB and JNK activation and less macrophage and neutrophil recruitment compared to WT when fed with a high sucrose (atherogenic) diet. Moreover, evidence indicate that bone marrow derived cells expressing TLR9 are responsible for macrophage and neutrophil recruitment in a NASH model and that *Tlr9* deletion allows a reduction of hepatic inflammation (142).

TLR6 implication in the pathogenesis of liver diseases is mostly unexplored. In a NAFLD cohort, Arias-Loste et al. observed an overexpression of TLR6 in monocytes isolated from NAFLD patients compared to controls and a similar overexpression in monocytes, T cells and B cells of NASH patients compared to NAFLD. Following *in vitro* stimulation with TLR2 and TLR6 agonists, those isolated monocytes produce more pro-inflammatory cytokines like IL-1β, TNF-α, and IL-6. Furthermore, TLR6 expression is also increased in the liver biopsies of NAFLD and NASH patients. These results suggest a role of TLR6 in the progression of NAFLD to NASH and its potential use as a new marker in patient blood samples (144).

TABLE 2 | TLRs involvement in the progression of NAFLD and NASH.

	NAFLD	NASH
TLR2	↗ in HFD mouse KCs (135)	CDAA, expression by KCs increases inflammation and fibrosis, TLR2 activation is followed by inflammasome activation IL1α and IL1β (136)
TLR4	↗ in HFD mouse KCs (135) ↗ in patients biopsies (135)	↗ in patients biopsies ↗ in patients serum (137) ↗ liver expression after DSS treatment in a NASH model (138) ↗ liver expression in a NASH model (108)
TLR5	Activated in hepatocytes and adipocytes in HFD model (139) ↗ in NAFLD patients	Expression in hepatocytes has a protecting role in NASH model (140, 141)
TLR9		↗ in patients biopsies (142) ↗ liver expression after DSS treatment (138) Expression by KCs neutrophils and DCs is involved in NASH progression (143) Deletion has a protective effect in a HFD model (143)

CDAA, Choline deficient amino acid; DCs, Dendritic cells; DSS, Dextran sodium sulfate; HFD, High fat-diet; IL, Interleukin; KCs, Kupffer cells; NAFLD, Non-alcoholic fatty liver disease; NASH, Non-alcoholic steatohepatitis; TLRs, Toll like receptors; ↗, Overexpression.

HFD in a mouse model is responsible for an increase of flagellin producing bacteria species in the gut, which causes an increase in serum LPS and hepatic flagellin presence. Flagellin in the liver activates TLR5/Myd88/NF-κB pathway in hepatocytes, then responsible for elevated HDL cholesterol levels (145). Moreover, activation or TLR5 in hepatocytes by flagellin increases intrahepatic $CD8^+$ T cell response, possibly through secretion of IFN-γ (146). Munakka et al. previously demonstrated that flagellin induced TLR5 in adipocytes was responsible for accumulation of fat in hepatocytes of mouse fed with HFD. Moreover, they showed that adipose tissue TLR5 expression correlated closely with liver fat content in NAFLD patients (139).

Cirrhosis

TLR2 is upregulated in PBMCs of cirrhotic patients displaying high serum LPS levels (147). In order to mimic cirrhotic patient's tendency to develop bacterial infections, Hackstein et al. used a combination of BDL and carbon tetrachloride (CCl_4) as a cirrhosis model to observe the anti-microbial capacity of immune cells when they induced bacterial infections. Under these conditions, they demonstrated that immune cells, in particular liver-resident macrophages, are unable to control bacterial infection compared to control mice. The authors observed a decreased expression of IL-1β, IL-12, and IFN-γ, known for their anti-microbial properties and increased production of TNF. Moreover, following bacterial translocation to the liver, IFN-β expression is enhanced in the livers of cirrhotic patients vs. healthy controls and in macrophages and DCs of BDL mice

compared to sham. *In vitro*, this overexpression occurs following activation or TLR2, 4, and 9 pathways, which will trigger IL-10 secretion by isolated macrophages (148).

HCC

In an HCC mouse model, TLR4 deficiency slows down the progression of hepatic tumors and decrease $F4/80^{+}$ immune cell infiltration. Those immune cells were characterized as hepatic macrophages, and when stimulated with LPS through TLR4 signaling, they will produce pro-inflammatory cytokines such as IL-6 and TNF-α, thus contributing to tumors growth. Hepatic macrophages involvement in the progression of HCC in this mouse model was further demonstrated by the fact that depletion of those macrophages suppressed tumor growth (149). The downregulation of miR-143 in HCC tumors from patients is responsible for an increased proliferation of cancer cells associated with less apoptosis. Authors suggest that this loss miR-143 is causing the overexpression of TLR2 in tumors and thus the activation of the NF-κB pathway (150).

Mularczyck et al. recently showed the role of Fetuin-A (Fet-A), an α2-Heremans-Schmid glycoprotein (AHSG), in the activation of the TLR4-JNK-NF-κB pathway in human hepatocarcinoma cell line (151). Once activated, this TLR4 pathway will aggravate insulin resistance and participate to NAFLD progression. In this study, the established a protective effect of probiotics emulsion against lipotoxicity and apoptosis in HepG2 cell lines. Authors showed that this protective effect is mediated through the regulation of Fetuin-A-TLR4-JNK-NF-κB axis thus preventing an increase of insulin resistance.

Other Non-TLRs Members of the PRR Family

Dectin-1/Clec7a is a C-type lectin receptor member of the PRR family and recognizes β-glucans from pathogenic fungi. Dectin-1 is expressed by myeloid cells including NK cells, macrophages, DCs and neutrophils, where it can induce the secretion of several pro-inflammatory cytokines and chemokines and modulate inflammation *in vivo* (152). Dectin-1 is overexpressed in human and mouse liver fibrosis. In a CCl_4 mouse model, the upregulation of Dectin-1 in hepatic DCs and macrophages is responsible for the downregulation of TLR4 and CD14, which negatively regulates liver fibrosis, inflammation, and HCC development (153). Indeed, following deletion of Dectin-1 mice are more prone to develop liver fibrosis and tumors. The authors observed a massive infiltration of leukocytes, neutrophils and bone marrow derived macrophages compared to control group. Furthermore, higher levels of IL-6 and TNF-α are detected in the KO mice (153). Yang et al. described fungal overgrowth and increased plasma levels of β-glucan in mice fed with ethanol. The use of antifungal treatments decreases liver injury and steatosis following ethanol feeding. The authors demonstrated that elevated β-glucan levels are responsible for the Dectin-1 dependent secretion of IL-1β by Kupffer cells and activation of NRLP3 pathway (26). Increased presence of *Candida* species in PSC patients bile suggest a role for Dectin-1 in the progression of the disease (154).

Galectin 3 is a member of the galectin family who recognize a variety of microbial pathogens (viruses, bacteria, fungi) and is expressed by neutrophils, macrophages, DCs. Galectin 3 specifically binds to β-1,2-mannans from *C. albicans* and can induce its death alone *in vitro* (155) but galectin-3 can also be secreted by neutrophils, link to pathogens and induce their phagocytosis by neutrophils. Primary macrophages expressing TLR4 and CD14 secrete galectin-3, which binds to LPS and negatively regulates LPS-driven inflammatory cytokines (IL-12, IL-6, and TNF-α) release (156). Besides, Jouault et al. showed that co-expression of TLR2 and galectin-3 is required for the endocytosis of *C. albicans* and the release on TNF-α by macrophages (157).

Pro-inflammatory IL-1β can be produced following TLRs pathway activation but also after the NOD-like receptor NLRP3 activation. Inflammasome expression is found in innate immune cells including monocytes, macrophages, neutrophils, and dendritic cells, NLRP3 inflammasome remains the most studied and has been involved in the progression of several chronic liver diseases (158). IL-1β secreted by KCs in alcohol-related liver disease mouse models aggravates steatosis and fibrosis. However, in a similar alcohol-related liver diseases mouse model with a deficiency for NLRP3, steatosis, inflammation, IL-1β expression, and number of activated natural killer T cells are all decreased, highlighting NLRP3 role in the pathogenesis of alcohol-related liver disease. Activation of both NLRP3 and NLRP6 contribute to dysbiosis, liver inflammation, and fibrosis via its effector IL-18 has also been demonstrated in several NASH studies. However, whether they display a protective or aggravating role remains unclear (159–162). NLRP3 expression is enhanced in NASH patients' liver, and seems to play a pro-inflammatory role in the progression from NAFLD to NASH in an animal model (163).

NOD1 and NOD2, two cytoplasmic receptors activated by fungi and bacterial peptidoglycan, are involved in the progression of liver inflammation by activating NF-κB and pro-inflammatory cytokines secretion in animal models, but their role in human liver diseases is mostly unexplored (164).

Serotonin

The involvement of serotonin and the nervous system has been highlighted in a recent study conducted by Ko and co-authors. Indeed, by using a neural blockade approach they demonstrated that neural signal transduction from the liver via the visceral nerve is responsible for liver and body weight increase in HFD-fed mice and liver weight gain in CDAA-fed mice (165). They showed that nerve blockade could have anti-steatotic and anti-fibrotic effects in 4 week CDAA- and HFD NASH models. The authors suggest that these effects are mediated byan increase of Claudin-1 expression in intestine, as well through nerve blockade that potentially influences microbiota diversity and composition of SCFAs possibly slowing down progression of NAFLD. Moreover, they provide direct evidence that the nerve blockade decreases the expression of serotonin, a gastrointestinal hormone known for its regulating role in hepatic regeneration, thus suggesting that the influence of the visceral nerve on NAFLD progression in HFD and CDAA-fed mice models is partially a result of serotonin effect (165).

THERAPEUTIC INTERVENTIONS TARGETING THE GUT-LIVER-AXIS

As stated above, the consistently growing understanding of the crosstalk between the gut microbiota and the liver offers multiple opportunities for novel treatment strategies (6). Currently, many therapeutic strategies to restore gut-liver axis homeostasis, rely on the modulation of the gut microbiome. Traditionally, this has been mainly achieved by using antibiotics, prebiotics, probiotics and fecal microbiota transfer (FMT), but intensive research over the last years has also resulted in a number of new approaches, including but not limited to managing alterations of bile composition.

Application of Antibiotics

Treatment with antibiotics is the most common approach to modulate the intestinal microbiota and decrease bacterial infections. Due to their bactericidal action, non-absorbable antibiotics that mainly remain within the gut are often used to reduce the number of bacteria (and their metabolites). Especially in the context of small bacterial overgrowth, treatment with antibiotics provides an effective solution. Rifaximin is a broad-spectrum antibiotic and is currently widely used in patients with liver cirrhosis to prevent hepatic encephalopathy (166). In addition, it has been suggested that Rifaximin might also have beneficial effects on the gut microbiome and reduces intestinal permeability thereby protecting from the progression of cirrhosis via the gut-liver axis (166). Fujinaga et al. could recently show that the combination of Rifaximin with Angiotensin-II receptor blockers suppressed hepatic fibrosis in a mouse NASH model (167). In addition, a combined use of different antibiotics (e.g., Polymyxin B and Neomycin) was shown to prevent fructose-induced hepatic lipid accumulation in mice (168). Some antibiotics may also induce eubiotic changes and promote the growth of beneficial bacteria (e.g., *Bifidobacteria* and *Lactobacilli*) making them an attractive therapeutic option (169).

Promising preclinical data has resulted in numerous clinical trials focusing on the use of antibiotics for the treatment of liver diseases (see **Table 3**).

Fecal Microbiota Transfer

Fecal microbiota transfer (or transplantation, FMT) is a method to restore homeostasis of the gut microbiome by recolonizing the intestine with fecal bacteria from a healthy individual that has been studied extensively in infections with *Clostridioides difficile*. Several animal studies have also suggested beneficial effects of FMT in the progression of liver diseases (181). FMT could further prevent intestinal dysbiosis and alcohol- induced liver injury in mice and additional analysis showed an association with several species as *Bacteroidales*, *Clostridiales*, and *Enterobacterialis* (182). However, due to a mixed and individual composition of fecal microbiota, heterogeneous results have been reported so far. Nonetheless, currently multiple clinical trials focus on the use of FMT for the treatment of liver disease (see **Table 3**). In patients with metabolic syndrome, FMT from metabolic syndrome donors temporarily decreased insulin sensitivity, whereas after FMT from healthy donors, insulin sensitivity was not altered. Those findings were accompanied by alterations in intestinal transit time, inflammatory markers, fecal bile acid composition as well as changes in several intestinal microbiota taxa (183). Also in PSC patients, a recent clinical trial could demonstrate an improvement of microbial diversity in line with a reduction of alkaline phosphatase levels after FMT from a healthy donor (184). In a small but randomized controlled pilot study, Bajaj et al. further found beneficial effects of FMT on patients with cirrhosis and alcohol use disorder. FMT significantly reduced alcohol craving, and a reduction of serum IL-6 and LPS-binding protein could be observed (185).

Prebiotics, Probiotics, Synbiotics

As opposed to antibiotics and FMT that aim to reshape the entire gut microbiome, specific changes in the microbiota can also be achieved through pro- and prebiotics or a combination of both (synbiotics). Probiotics are living microorganisms contained in food or supplements that may provide numerous health benefits (e.g., by promoting anti-inflammatory effects of the gut microbiota). In mice, the administration of probiotics (namely *Bifidobacteria*, *Lactobacilli*, and *Streptococcus thermophilus*) could reduce HFD-induced hepatic steatosis and insulin resistance and resulted in increasing hepatic NKT cells (186). Interesting *in vitro* studies with human hepatocarcinoma cells further suggested protective effects of probiotics against inflammation and obesity via reduction of Fetuin-A/TLR4-JNK-NF-κB pathway activation (151). Probiotic mixtures were also reported to reduce HCC growth in mice by modulating gut microbiota and resulting in a decrease of Th17 cells in the tumor (187). In a model of alcoholic steatohepatitis, it was shown that colonization with *Akkermansia muciniphila* was able to enhance expression of tight junctions in intestinal epithelial cells, thus decreasing intestinal permeability and systemic LPS levels (188). Those findings are in line with a recent clinical study, in which the supplementation with *A. muciniphila* led to an improvement in blood lipids and insulin sensitivity in obese patients (175). Supplementation with probiotic bacteria was also shown to improve the response to immunotherapy in cancer patients (189). However, the precise mechanisms involved in the beneficial effects of probiotics on HCC patients need to be elucidated.

Prebiotics are indigestible or low digestible fibers that can improve gut peristaltic and promote growth of beneficial bacteria. Prebiotics for example include oligosaccharides, polyunsaturated fatty acids or polyphenols. In mice, the treatment with pectin was shown to introduce major modifications of the intestinal microbiota and prevented steatosis and liver inflammation in alcohol-induced liver injury (182). Moreover, the administration of Inulin was found to prevent NAFLD via modulation of the gut microbiota (e.g., increase of *Akkermansia* and *Bifidobacterium*) and reduction of hepatic macrophages (190).

Due to the many beneficial effects of pre- and probiotics, novel studies suggest their combined use. Hadi et al. suggested that the consumption of synbiotics may improve plasma lipid concentrations and thus may have beneficial effects in the treatment of metabolic liver disease (191). As the treatment with pre- and probiotics is simple and has limited side effects, many

TABLE 3 | Selected clinical trials targeting the gut-liver-axis for the treatment of liver diseases.

Intervention	Study description	Results	Identification
Antibiotics	Administration of Rifaximin in NAFLD patients	Reduction of serum endotoxin levels and improvement of insulin resistance, proinflammatory cytokines, and NAFLD-liver fat score (170)	NCT02884037
	Rifaximin + different doses of Simvastatin in patients with decompensated cirrhosis (Phase II)	No significant differences. 20 mg/day Simvastatin plus Rifaximin is recommended (171)	NCT03150459
FMT	FMT for the treatment of PSC (Phase I/II)	Increased diversity of the microbiome	NCT02424175
	Effect of FMT on NAFLD (Phase IV)	No results yet	NCT04465032
	FMT in cirrhosis (Phase I)	Reduced systemic inflammation and improvement of cirrhosis (172)	NCT03152188
	FMT for alcohol misuse in cirrhosis (Phase I)	FMT is safe and was associated with reduction in alcohol craving and favorable microbial changes	NCT03416751
Prebiotics	Supplementation with oligofructose in NASH patients	Improvement of liver steatosis (173)	NCT03184376
Probiotics	Multi-strain probiotic in NAFLD patients	Reduction of liver fat, serum AST and cytokine levels (174)	NCT03434860
	Effects of the Administration of *A. Muciniphila* on Parameters of Metabolic Syndrome	*A. muciniphila* improved insulin sensitivity and plasma total cholesterol (175)	NCT02637115
Synbiotics	Fructo-oligosaccharide + 4 bacteria in NASH (Phase II/III)	Reduction in hepatic steatosis and fibrosis	NCT02530138
	Supplementation with *Bifidobacterium animalis* and inulin in NAFLD patients	Improved liver enzyme concentrations and hepatic steatosis (176)	NCT02568605
Bile acid regulation	REGENERATE, OCA in NASH patients (Phase III)	OCA significantly improved fibrosis and key components of NASH (177)	NCT02548351
	Aramchol (fatty acid-bile acid conjugate) in NAFLD patients (Phase II)	Aramchol is safe, tolerable, and significantly reduces liver fat content in patients with NAFLD (178)	NCT01094158
	norUDCA in the treatment of PSC (Phase II)	Reduction of alkaline phosphatase levels	NCT01755507
	norUDCA in the treatment of NASH	Reduction of serum ALT (179)	not available
Duodenal mucosal resurfacing	DMR in the treatment of Type 2 Diabetes/NAFLD	Improvement of glycaemic control and reduction of liver fat content (180)	NCT02879383
	DMR in the Treatment of NASH patients	No results yet	NCT03536650
Carbon nanoparticles	Yaq-001 in patients with NAFLD	No results yet	NCT03962608
	Yaq-001 in patients with cirrhosis	No results yet	NCT03202498
Engineered probiotic	SYNB1020 in hepatic insufficiency and cirrhosis patients (Phase I/II)	Terminated due to a lack of efficacy	NCT03447730
Postbiotics	Supplementation with SCFA and physical activity in liver cirrhosis	No results yet	NCT03892070

ALT, Alanin-aminotransferase; AST, Aspartate-aminotransferase; DMR, Duodenal mucosal resurfacing; FMT, Fecal microbiota transfer; NAFLD, Non-alcoholic fatty liver disease; NASH, Non-alcoholic steatohepatitis; norUDCA, 24-norursodeoxycholic acid; PSC, Primary sclerosing cholangitis; SCFA, Short chain fatty acids; OCA, obeticholic acid.

clinical studies focus on their use in therapy for different liver diseases (**Table 3**).

Bile Acid Related Therapies

Due to the diverse effects of bile acids on metabolism and the immune system, modulation of bile acid signaling is an attractive therapeutic option. Several FXR and TGR5 agonists as well as synthetic bile acids are currently under investigation to treat liver diseases. For example, obeticholic acid, a potent FXR agonist is currently used to treat PBC and has also shown many beneficial effects in the treatment of NAFLD/NASH and PSC (192, 193). In cirrhotic mice, treatment with FXR agonists appeared to improve intestinal barrier function by an increased expression of tight junction proteins and an increase of goblet cells (194). Currently, various agonists of the FXR receptor are in clinical phase II and phase III trials to test their efficiency in different liver diseases (**Table 3**).

Especially in PSC and PBC patients, the use of synthetic bile acids, as ursodeoxycholic acid (UDCA) is a well-established treatment strategy (195). Treatment with UDCA has also been shown to resolve intestinal dysbiosis in PBC patients (17). Moreover, norUDCA, a new homolog of UDCA, has shown promising results in the treatment of PSC as well as NAFLD patients (179, 195).

Alternative Approaches Under Development

Novel upcoming therapeutic approaches to target the gut-liver-axis have recently been reviewed by Albillos et al. (6). Direct PRR targeting also holds promises for the development of future therapeutic options. Preclinical evidence suggests that small molecule inhibitors for TLR4 ameliorate liver failure in rodent models (196). In mice, Eritoran, a TLR4 antagonist, was further shown to attenuate hepatic inflammation and fibrosis

(197). However, the relevance and potential side-effects of PRR targeting for liver disease treatment must be further investigated. Another promising approach consists of using adsorbant carbon nanoparticles that can ameliorate liver injury through absorption of gut-derived toxins and other bacterial products. In rodents with NAFLD, administration of a novel carbon nanoparticle, Yaq-001, resulted in a significant reduction of serum ALT and hepatic TLR4 expression (198). Yaq-001 is currently evaluated for safety and tolerability in patients with NAFLD and cirrhosis (NCT03962608 and NCT03202498).

Further preclinical investigations suggest that bacteriophages targeting specific bacteria may serve as a method to modulate the intestinal microbiota in a targeted manner. A recent study found that bacteriophages were able to specifically target intestinal bacteria and thereby attenuate alcohol-related liver disease (56). However, bacteriophage treatment is still in the explorative stage and further investigations are necessary, notably to evaluate its biosafety.

Metabolic diseases can further be treated by duodenal mucosal resurfacing (DMR), an endoscopic technique to ablate the duodenal mucosa and thereby improve glycemic and weight control (180). As studies have further reported an improvement of glucose homeostasis and transaminase levels, a possible improvement of NASH is also assumed. The effect of DMR to treat NASH is currently evaluated (NCT03536650).

Moreover, a lot of the recent research focuses on the identification of microbial metabolites that may have beneficial effects on intestinal barrier function (199). Postbiotics comprise all active compounds produced by intestinal bacteria, and include for example SCFAs, proteins, extracellular polysaccharides or organic acids. Recently, a novel postbiotic from *Lactobacillus rhamnosus* could show beneficial effects on intestinal barrier function and also potential protection of liver injury (200). Another recently published study evaluated the anti-inflammatory effects of *E. coli Nissle1917* derived metabolites and found TNF-α production as well as TLR signaling pathways to be reduced (201).

Further promising preclinical approaches to target the gut-liver axis include the application of engineered probiotics (e.g., SYNB1020) or synthetic live bacterial therapeutics (202, 203). Engineered and optimized bacteria were shown to be able to reduce ethanol-induced liver disease in mice (204).

CONCLUSIONS AND FUTURE PERSPECTIVES

Cumulating evidence from the past years or decades indicate that the gut-liver axis is a promising therapeutic target to treat patients suffering from chronic liver diseases. Indeed, in a pathological context, gut-derived PAMPs and recirculating modified bile acids reach the liver, where hepatic and immune cells can recognize them through PRRs and thus exacerbate a pre-existing hepatic inflammation. Traditional approaches such as pre- and probiotics, FMT, antibiotics, and FXR agonists have already been or are being evaluated in numerous clinical trials. Further translational research will be necessary to transfer the new insights from innovative preclinical approaches to a clinical setting. Finally, approaches aiming at specifically altering targeted gut microbiota species, bile acids, cytokines and chemokines, will advance our understanding of the mechanisms involved in disease progression or resolution, and greatly advance therapeutic options.

AUTHOR CONTRIBUTIONS

AB and JH wrote the manuscript. AG designed the figures. AG and FT revised the manuscript. All authors approved the final manuscript.

FUNDING

AB, JH, and FT were supported by the German Research Foundation, Grant Number DFG Project-ID 403224013, SFB 1382, and CRC/TR 296. AG is a recipient of a Humboldt Research Fellowship for Postdoctoral Researchers (Alexander von Humboldt Foundation).

REFERENCES

1. Guillot A, Tacke F. Liver macrophages: old dogmas and new insights. *Hepatol Commun.* (2019) 3:730–43. doi: 10.1002/hep4.1356
2. Surewaard BG, Deniset JF, Zemp FJ, Amrein M, Otto M, Conly J, et al. Identification and treatment of the *Staphylococcus aureus* reservoir *in vivo*. *J Exp Med.* (2016) 213:1141–51. doi: 10.1084/jem.20160334
3. Sommer F, Backhed F. The gut microbiota–masters of host development and physiology. *Nat Rev Microbiol.* (2013) 11:227–38. doi: 10.1038/nrmicro2974
4. Michaudel C, Sokol H. The gut microbiota at the service of immunometabolism. *Cell Metab.* (2020) 32:514–23. doi: 10.1016/j.cmet.2020.09.004
5. Miyake Y, Yamamoto K. Role of gut microbiota in liver diseases. *Hepatol Res.* (2013) 43:139–46. doi: 10.1111/j.1872-034X.2012.01088.x
6. Albillos A, de Gottardi A, Rescigno M. The gut-liver axis in liver disease: pathophysiological basis for therapy. *J Hepatol.* (2020) 72:558–77. doi: 10.1016/j.jhep.2019.10.003
7. Rosshart SP, Herz J, Vassallo BG, Hunter A, Wall MK, Badger JH, et al. Laboratory mice born to wild mice have natural microbiota and model human immune responses. *Science.* (2019) 365:aaw4361. doi: 10.1126/science.aaw4361
8. Rosshart SP, Vassallo BG, Angeletti D, Hutchinson DS, Morgan AP, Takeda K, et al. Wild mouse gut microbiota promotes host fitness and improves disease resistance. *Cell.* (2017) 171:1015–28 e13. doi: 10.1016/j.cell.2017.09.016
9. Qin N, Yang F, Li A, Prifti E, Chen Y, Shao L, et al. Alterations of the human gut microbiome in liver cirrhosis. *Nature.* (2014) 513:59–64. doi: 10.1038/nature13568
10. Rao BC, Lou JM, Wang WJ, Li A, Cui GY, Yu ZJ, et al. Human microbiome is a diagnostic biomarker in hepatocellular carcinoma. *Hepatobiliary Pancreat Dis Int.* (2020) 19:109–15. doi: 10.1016/j.hbpd.2020.01.003
11. Hundertmark J, Krenkel O, Tacke F. Adapted immune responses of myeloid-derived cells in fatty liver disease. *Front Immunol.* (2018) 9:2418. doi: 10.3389/fimmu.2018.02418
12. Begley M, Gahan CG, Hill C. The interaction between bacteria and bile. *FEMS Microbiol Rev.* (2005) 29:625–51. doi: 10.1016/j.femsre.2004.09.003

13. Chen ML, Takeda K, Sundrud MS. Emerging roles of bile acids in mucosal immunity and inflammation. *Mucosal Immunol.* (2019) 12:851–61. doi: 10.1038/s41385-019-0162-4
14. Arumugam M, Raes J, Pelletier E, Le Paslier D, Yamada T, Mende DR, et al. Enterotypes of the human gut microbiome. *Nature.* (2011) 473:174–80. doi: 10.1038/nature09944
15. Tremaroli V, Backhed F. Functional interactions between the gut microbiota and host metabolism. *Nature.* (2012) 489:242–9. doi: 10.1038/nature11552
16. Conlon MA, Bird AR. The impact of diet and lifestyle on gut microbiota and human health. *Nutrients.* (2014) 7:17–44. doi: 10.3390/nu7010017
17. Tang R, Wei Y, Li Y, Chen W, Chen H, Wang Q, et al. Gut microbial profile is altered in primary biliary cholangitis and partially restored after UDCA therapy. *Gut.* (2018) 67:534–41. doi: 10.1136/gutjnl-2016-313332
18. Kummen M, Holm K, Anmarkrud JA, Nygard S, Vesterhus M, Hoivik ML, et al. The gut microbial profile in patients with primary sclerosing cholangitis is distinct from patients with ulcerative colitis without biliary disease and healthy controls. *Gut.* (2017) 66:611–9. doi: 10.1136/gutjnl-2015-310500
19. Quraishi MN, Sergeant M, Kay G, Iqbal T, Chan J, Constantinidou C, et al. The gut-adherent microbiota of PSC-IBD is distinct to that of IBD. *Gut.* (2017) 66:386–8. doi: 10.1136/gutjnl-2016-311915
20. Rossen NG, Fuentes S, Boonstra K, D'Haens GR, Heilig HG, Zoetendal EG, et al. The mucosa-associated microbiota of PSC patients is characterized by low diversity and low abundance of uncultured Clostridiales II. *J Crohns Colitis.* (2015) 9:342–8. doi: 10.1093/ecco-jcc/jju023
21. Torres J, Palmela C, Brito H, Bao X, Ruiqi H, Moura-Santos P, et al. The gut microbiota, bile acids and their correlation in primary sclerosing cholangitis associated with inflammatory bowel disease. *United European Gastroenterol J.* (2018) 6:112–22. doi: 10.1177/2050640617708953
22. Sabino J, Vieira-Silva S, Machiels K, Joossens M, Falony G, Ballet V, et al. Primary sclerosing cholangitis is characterised by intestinal dysbiosis independent from IBD. *Gut.* (2016) 65:1681–9. doi: 10.1136/gutjnl-2015-311004
23. Bajer L, Kverka M, Kostovcik M, Macinga P, Dvorak J, Stehlikova Z, et al. Distinct gut microbiota profiles in patients with primary sclerosing cholangitis and ulcerative colitis. *World J Gastroenterol.* (2017) 23:4548–58. doi: 10.3748/wjg.v23.i25.4548
24. Ruhlemann MC, Solovjeva MEL, Zenouzi R, Liwinski T, Kummen M, Lieb W, et al. Gut mycobiome of primary sclerosing cholangitis patients is characterised by an increase of *Trichocladium griseum* and Candida species. *Gut.* (2020) 69:1890–2. doi: 10.1136/gutjnl-2019-320008
25. Lemoinne S, Kemgang A, Ben Belkacem K, Straube M, Jegou S, Corpechot C, et al. Fungi participate in the dysbiosis of gut microbiota in patients with primary sclerosing cholangitis. *Gut.* (2020) 69:92–102. doi: 10.1136/gutjnl-2018-317791
26. Yang AM, Inamine T, Hochrath K, Chen P, Wang L, Llorente C, et al. Intestinal fungi contribute to development of alcoholic liver disease. *J Clin Invest.* (2017) 127:2829–41. doi: 10.1172/JCI90562
27. Dubinkina VB, Tyakht AV, Odintsova VY, Yarygin KS, Kovarsky BA, Pavlenko AV, et al. Links of gut microbiota composition with alcohol dependence syndrome and alcoholic liver disease. *Microbiome.* (2017) 5:141. doi: 10.1186/s40168-017-0359-2
28. Loomba R, Seguritan V, Li W, Long T, Klitgord N, Bhatt A, et al. Gut microbiome-based metagenomic signature for non-invasive detection of advanced fibrosis in human nonalcoholic fatty liver disease. *Cell Metab.* (2017) 25:1054–62 e5. doi: 10.1016/j.cmet.2017.04.001
29. Lang S, Demir M, Martin A, Jiang L, Zhang X, Duan Y, et al. Intestinal virome signature associated with severity of nonalcoholic fatty liver disease. *Gastroenterology.* (2020) 159:1839–52. doi: 10.1053/j.gastro.2020.07.005
30. Lang S, Martin A, Zhang X, Farowski F, Wisplinghoff H, M JGTV, et al. Combined analysis of gut microbiota, diet and PNPLA3 polymorphism in biopsy-proven non-alcoholic fatty liver disease. *Liver Int.* (2021) 41:1576–91. doi: 10.1111/liv.14899
31. Lang S, Martin A, Farowski F, Wisplinghoff H, Vehreschild M, Liu J, et al. High protein intake is associated with histological disease activity in patients with NAFLD. *Hepatol Commun.* (2020) 4:681–95. doi: 10.1002/hep4.1509
32. Boursier J, Mueller O, Barret M, Machado M, Fizanne L, Araujo-Perez F, et al. The severity of nonalcoholic fatty liver disease is associated with gut dysbiosis and shift in the metabolic function of the gut microbiota. *Hepatology.* (2016) 63:764–75. doi: 10.1002/hep.28356
33. Wong VW, Tse CH, Lam TT, Wong GL, Chim AM, Chu WC, et al. Molecular characterization of the fecal microbiota in patients with nonalcoholic steatohepatitis–a longitudinal study. *PLoS ONE.* (2013) 8:e62885. doi: 10.1371/journal.pone.0062885
34. Zhu L, Baker SS, Gill C, Liu W, Alkhouri R, Baker RD, et al. Characterization of gut microbiomes in nonalcoholic steatohepatitis (NASH) patients: a connection between endogenous alcohol and NASH. *Hepatology.* (2013) 57:601–9. doi: 10.1002/hep.26093
35. Kakiyama G, Pandak WM, Gillevet PM, Hylemon PB, Heuman DM, Daita K, et al. Modulation of the fecal bile acid profile by gut microbiota in cirrhosis. *J Hepatol.* (2013) 58:949–55. doi: 10.1016/j.jhep.2013.01.003
36. Bajaj JS, Heuman DM, Hylemon PB, Sanyal AJ, White MB, Monteith P, et al. Altered profile of human gut microbiome is associated with cirrhosis and its complications. *J Hepatol.* (2014) 60:940–7. doi: 10.1016/j.jhep.2013.12.019
37. Krohn S, Zeller K, Bohm S, Chatzinotas A, Harms H, Hartmann J, et al. Molecular quantification and differentiation of Candida species in biological specimens of patients with liver cirrhosis. *PLoS ONE.* (2018) 13:e0197319. doi: 10.1371/journal.pone.0197319
38. Ponziani FR, Bhoori S, Castelli C, Putignani L, Rivoltini L, Del Chierico F, et al. Hepatocellular carcinoma is associated with gut microbiota profile and inflammation in nonalcoholic fatty liver disease. *Hepatology.* (2019) 69:107–20. doi: 10.1002/hep.30036
39. Grat M, Wronka KM, Krasnodebski M, Masior L, Lewandowski Z, Kosinska I, et al. Profile of gut microbiota associated with the presence of hepatocellular cancer in patients with liver cirrhosis. *Transplant Proc.* (2016) 48:1687–91. doi: 10.1016/j.transproceed.2016.01.077
40. Huang Y, Fan XG, Wang ZM, Zhou JH, Tian XF, Li N. Identification of helicobacter species in human liver samples from patients with primary hepatocellular carcinoma. *J Clin Pathol.* (2004) 57:1273–7. doi: 10.1136/jcp.2004.018556
41. Li Y, Tang R, Leung PSC, Gershwin ME, Ma X. Bile acids and intestinal microbiota in autoimmune cholestatic liver diseases. *Autoimmun Rev.* (2017) 16:885–96. doi: 10.1016/j.autrev.2017.07.002
42. Ali AH, Carey EJ, Lindor KD. The Microbiome And Primary Sclerosing Cholangitis. *Semin Liver Dis.* (2016) 36:340–8. doi: 10.1055/s-0036-1594007
43. Mathies F, Steffens N, Kleinschmidt D, Stuhlmann F, Huber FJ, Roy U, et al. Colitis promotes a pathological condition of the liver in the absence of Foxp3(+) Regulatory T cells. *J Immunol.* (2018) 201:3558–68. doi: 10.4049/jimmunol.1800711
44. Tedesco D, Thapa M, Chin CY, Ge Y, Gong M, Li J, et al. Alterations in intestinal microbiota lead to production of interleukin 17 by intrahepatic gammadelta T-Cell receptor-positive cells and pathogenesis of cholestatic liver disease. *Gastroenterology.* (2018) 154:2178–93. doi: 10.1053/j.gastro.2018.02.019
45. Younossi ZM, Marchesini G, Pinto-Cortez H, Petta S. Epidemiology of nonalcoholic fatty liver disease and nonalcoholic steatohepatitis: implications for liver transplantation. *Transplantation.* (2019) 103:22–7. doi: 10.1097/TP.0000000000002484
46. Di Ciaula A, Baj J, Garruti G, Celano G, De Angelis M, Wang HH, et al. Liver steatosis, gut-liver axis, microbiome and environmental factors. a never-ending bidirectional cross-talk. *J Clin Med.* (2020) 9:2648. doi: 10.3390/jcm9082648
47. Safari Z, Gerard P. The links between the gut microbiome and non-alcoholic fatty liver disease (NAFLD). *Cell Mol Life Sci.* (2019) 76:1541–58. doi: 10.1007/s00018-019-03011-w
48. Wigg AJ, Roberts-Thomson IC, Dymock RB, McCarthy PJ, Grose RH, Cummins AG. The role of small intestinal bacterial overgrowth, intestinal permeability, endotoxaemia, and tumour necrosis factor alpha in the pathogenesis of non-alcoholic steatohepatitis. *Gut.* (2001) 48:206–11. doi: 10.1136/gut.48.2.206
49. Shanab AA, Scully P, Crosbie O, Buckley M, O'Mahony L, Shanahan F, et al. Small intestinal bacterial overgrowth in nonalcoholic steatohepatitis: association with toll-like receptor 4 expression and plasma levels of interleukin 8. *Dig Dis Sci.* (2011) 56:1524–34. doi: 10.1007/s10620-010-1447-3

50. Ferslew BC, Xie G, Johnston CK, Su M, Stewart PW, Jia W, et al. Altered bile acid metabolome in patients with nonalcoholic steatohepatitis. *Dig Dis Sci.* (2015) 60:3318–28. doi: 10.1007/s10620-015-3776-8
51. Collaborators GBDA. Alcohol use and burden for 195 countries and territories, 1990-2016: a systematic analysis for the Global Burden of Disease Study 2016. *Lancet.* (2018) 392:1015–35. doi: 10.1016/S0140-6736(18)31310-2
52. Parlesak A, Schafer C, Schutz T, Bode JC, Bode C. Increased intestinal permeability to macromolecules and endotoxemia in patients with chronic alcohol abuse in different stages of alcohol-induced liver disease. *J Hepatol.* (2000) 32:742–7. doi: 10.1016/S0168-8278(00)80242-1
53. Bull-Otterson L, Feng W, Kirpich I, Wang Y, Qin X, Liu Y, et al. Metagenomic analyses of alcohol induced pathogenic alterations in the intestinal microbiome and the effect of *Lactobacillus rhamnosus* GG treatment. *PLoS ONE.* (2013) 8:e53028. doi: 10.1371/journal.pone.0053028
54. Yan AW, Fouts DE, Brandl J, Starkel P, Torralba M, Schott E, et al. Enteric dysbiosis associated with a mouse model of alcoholic liver disease. *Hepatology.* (2011) 53:96–105. doi: 10.1002/hep.24018
55. Mutlu EA, Gillevet PM, Rangwala H, Sikaroodi M, Naqvi A, Engen PA, et al. Colonic microbiome is altered in alcoholism. *Am J Physiol Gastrointest Liver Physiol.* (2012) 302:G966–78. doi: 10.1152/ajpgi.00380.2011
56. Duan Y, Llorente C, Lang S, Brandl K, Chu H, Jiang L, et al. Bacteriophage targeting of gut bacterium attenuates alcoholic liver disease. *Nature.* (2019) 575:505–11. doi: 10.1038/s41586-019-1742-x
57. Simbrunner B, Mandorfer M, Trauner M, Reiberger T. Gut-liver axis signaling in portal hypertension. *World J Gastroenterol.* (2019) 25:5897–917. doi: 10.3748/wjg.v25.i39.5897
58. Hassan EA, Abd El-Rehim AS, Hassany SM, Ahmed AO, Elsherbiny NM, Mohammed MH. Fungal infection in patients with end-stage liver disease: low frequency or low index of suspicion. *Int J Infect Dis.* (2014) 23:69–74. doi: 10.1016/j.ijid.2013.12.014
59. Knooihuizen SAI, Alexander NJ, Hopke A, Barros N, Viens A, Scherer A, et al. Loss of coordinated neutrophil responses to the human fungal pathogen, candida albicans, in patients with cirrhosis. *Hepatol Commun.* (2021) 5:502–15. doi: 10.1002/hep4.1645
60. Yang JD, Hainaut P, Gores GJ, Amadou A, Plymoth A, Roberts LR. A global view of hepatocellular carcinoma: trends, risk, prevention and management. *Nat Rev Gastroenterol Hepatol.* (2019) 16:589–604. doi: 10.1038/s41575-019-0186-y
61. Zhang HL, Yu LX, Yang W, Tang L, Lin Y, Wu H, et al. Profound impact of gut homeostasis on chemically-induced pro-tumorigenic inflammation and hepatocarcinogenesis in rats. *J Hepatol.* (2012) 57:803–12. doi: 10.1016/j.jhep.2012.06.011
62. Fox JG, Feng Y, Theve EJ, Raczynski AR, Fiala JL, Doernte AL, et al. Gut microbes define liver cancer risk in mice exposed to chemical and viral transgenic hepatocarcinogens. *Gut.* (2010) 59:88–97. doi: 10.1136/gut.2009.183749
63. Monte MJ, Marin JJ, Antelo A, Vazquez-Tato J. Bile acids: chemistry, physiology, and pathophysiology. *World J Gastroenterol.* (2009) 15:804–16. doi: 10.3748/wjg.15.804
64. Bernstein C, Holubec H, Bhattacharyya AK, Nguyen H, Payne CM, Zaitlin B, et al. Carcinogenicity of deoxycholate, a secondary bile acid. *Arch Toxicol.* (2011) 85:863–71. doi: 10.1007/s00204-011-0648-7
65. Mousa OY, Juran BD, McCauley BM, Vesterhus MN, Folseraas T, Turgeon CT, et al. Bile acid profiles in primary sclerosing cholangitis and their ability to predict hepatic decompensation. *Hepatology.* (2020) 74, 281–295. doi: 10.1002/hep.31652
66. Mouzaki M, Wang AY, Bandsma R, Comelli EM, Arendt BM, Zhang L, et al. Bile acids and dysbiosis in non-alcoholic fatty liver disease. *PLoS ONE.* (2016) 11:e0151829. doi: 10.1371/journal.pone.0151829
67. Nimer N, Choucair I, Wang Z, Nemet I, Li L, Gukasyan J, et al. Bile acids profile, histopathological indices and genetic variants for non-alcoholic fatty liver disease progression. *Metabolism.* (2021) 116:154457. doi: 10.1016/j.metabol.2020.154457
68. Xie G, Wang X, Huang F, Zhao A, Chen W, Yan J, et al. Dysregulated hepatic bile acids collaboratively promote liver carcinogenesis. *Int J Cancer.* (2016) 139:1764–75. doi: 10.1002/ijc.30219
69. Kakiyama G, Hylemon PB, Zhou H, Pandak WM, Heuman DM, Kang DJ, et al. Colonic inflammation and secondary bile acids in alcoholic cirrhosis. *Am J Physiol Gastrointest Liver Physiol.* (2014) 306:G929–37. doi: 10.1152/ajpgi.00315.2013
70. de Aguiar Vallim TQ, Tarling EJ, Edwards PA. Pleiotropic roles of bile acids in metabolism. *Cell Metab.* (2013) 17:657–69. doi: 10.1016/j.cmet.2013.03.013
71. Jiang C, Xie C, Lv Y, Li J, Krausz KW, Shi J, et al. Intestine-selective farnesoid X receptor inhibition improves obesity-related metabolic dysfunction. *Nat Commun.* (2015) 6:10166. doi: 10.1038/ncomms10166
72. Radun R, Trauner M. Role of FXR in bile acid and metabolic homeostasis in NASH: pathogenetic concepts and therapeutic opportunities. *Semin Liver Dis.* (2021) doi: 10.1055/s-0041-1731707. [Epub ahead of Print].
73. Mouries J, Brescia P, Silvestri A, Spadoni I, Sorribas M, Wiest R, et al. Microbiota-driven gut vascular barrier disruption is a prerequisite for non-alcoholic steatohepatitis development. *J Hepatol.* (2019) 71:1216–28. doi: 10.1016/j.jhep.2019.08.005
74. Puri P, Daita K, Joyce A, Mirshahi F, Santhekadur PK, Cazanave S, et al. The presence and severity of nonalcoholic steatohepatitis is associated with specific changes in circulating bile acids. *Hepatology.* (2018) 67:534–48. doi: 10.1002/hep.29359
75. Pathak P, Xie C, Nichols RG, Ferrell JM, Boehme S, Krausz KW, et al. Intestine farnesoid X receptor agonist and the gut microbiota activate G-protein bile acid receptor-1 signaling to improve metabolism. *Hepatology.* (2018) 68:1574–88. doi: 10.1002/hep.29857
76. Leonhardt J, Haider RS, Sponholz C, Leonhardt S, Drube J, Spengler K, et al. Circulating bile acids in liver failure activate TGR5 and induce monocyte dysfunction. *Cell Mol Gastroenterol Hepatol.* (2021) 12:25–40. doi: 10.1016/j.jcmgh.2021.01.011
77. Spatz M, Ciocan D, Merlen G, Rainteau D, Humbert L, Gomes-Rochette N, et al. Bile acid-receptor TGR5 deficiency worsens liver injury in alcohol-fed mice by inducing intestinal microbiota dysbiosis. *JHEP Rep.* (2021) 3:100230. doi: 10.1016/j.jhepr.2021.100230
78. Reich M, Spomer L, Klindt C, Fuchs K, Stindt J, Deutschmann K, et al. Downregulation of TGR5 (GPBAR1) in biliary epithelial cells contributes to the pathogenesis of sclerosing cholangitis. *J Hepatol.* (2021) 75:634–46. doi: 10.1016/j.jhep.2021.03.029
79. Carino A, Cipriani S, Marchiano S, Biagioli M, Scarpelli P, Zampella A, et al. Gpbar1 agonism promotes a Pgc-1alpha-dependent browning of white adipose tissue and energy expenditure and reverses diet-induced steatohepatitis in mice. *Sci Rep.* (2017) 7:13689. doi: 10.1038/s41598-017-13102-y
80. Carino A, Marchiano S, Biagioli M, Bucci M, Vellecco V, Brancaleone V, et al. Agonism for the bile acid receptor GPBAR1 reverses liver and vascular damage in a mouse model of steatohepatitis. *FASEB J.* (2019) 33:2809–22. doi: 10.1096/fj.201801373RR
81. Manley S, Ding W. Role of farnesoid X receptor and bile acids in alcoholic liver disease. *Acta Pharm Sin B.* (2015) 5:158–67. doi: 10.1016/j.apsb.2014.12.011
82. Jia W, Xie G, Jia W. Bile acid-microbiota crosstalk in gastrointestinal inflammation and carcinogenesis. *Nat Rev Gastroenterol Hepatol.* (2018) 15:111–28. doi: 10.1038/nrgastro.2017.119
83. Chavez-Talavera O, Tailleux A, Lefebvre P, Staels B. Bile acid control of metabolism and inflammation in obesity, type 2 diabetes, dyslipidemia, and nonalcoholic fatty liver disease. *Gastroenterology.* (2017) 152:1679–94 e3. doi: 10.1053/j.gastro.2017.01.055
84. Guillot A, Guerri L, Feng D, Kim SJ, Ahmed YA, Paloczi J, et al. Bile acid-activated macrophages promote biliary epithelial cell proliferation through integrin alphavbeta6 upregulation following liver injury. *J Clin Invest.* (2021) 131:e132305. doi: 10.1172/JCI132305
85. Pathak P, Liu H, Boehme S, Xie C, Krausz KW, Gonzalez F, et al. Farnesoid X receptor induces Takeda G-protein receptor 5 cross-talk to regulate bile acid synthesis and hepatic metabolism. *J Biol Chem.* (2017) 292:11055–69. doi: 10.1074/jbc.M117.784322
86. Zhou D, Fan JG. Microbial metabolites in non-alcoholic fatty liver disease. *World J Gastroenterol.* (2019) 25:2019–28. doi: 10.3748/wjg.v25.i17.2019
87. Dhillon AK, Kummen M, Troseid M, Akra S, Liaskou E, Moum B, et al. Circulating markers of gut barrier function associated with disease

severity in primary sclerosing cholangitis. *Liver Int.* (2019) 39:371–81. doi: 10.1111/liv.13979
88. Agus A, Planchais J, Sokol H. Gut microbiota regulation of tryptophan metabolism in health and disease. *Cell Host Microbe.* (2018) 23:716–24. doi: 10.1016/j.chom.2018.05.003
89. Wrzosek L, Ciocan D, Hugot C, Spatz M, Dupeux M, Houron C, et al. Microbiota tryptophan metabolism induces aryl hydrocarbon receptor activation and improves alcohol-induced liver injury. *Gut.* (2020) 70:1299–308. doi: 10.1136/gutjnl-2020-321565
90. Albhaisi S, Shamsaddini A, Fagan A, McGeorge S, Sikaroodi M, Gavis E, et al. Gut microbial signature of hepatocellular cancer in men with cirrhosis. *Liver Transpl.* (2021) 27:629–40. doi: 10.1002/lt.25994
91. Dhillon AK, Rupp C, Bergquist A, Voitl R, Folseraas T, Troseid M, et al. Associations of neopterin and kynurenine-tryptophan ratio with survival in primary sclerosing cholangitis. *Scand J Gastroenterol.* (2021) 56:443–52. doi: 10.1080/00365521.2021.1880627
92. Qi S, Huang S, Chen X, Huo Q, Xie N, Xia J. Liver tissue metabolic profiling and pathways of non-alcoholic steatohepatitis in rats. *Hepatol Res.* (2017) 47:1484–93. doi: 10.1111/hepr.12876
93. Li XV, Leonardi I, Iliev ID. Gut mycobiota in immunity and inflammatory disease. *Immunity.* (2019) 50:1365–79. doi: 10.1016/j.immuni.2019.05.023
94. den Besten G, van Eunen K, Groen AK, Venema K, Reijngoud DJ, Bakker BM. The role of short-chain fatty acids in the interplay between diet, gut microbiota, and host energy metabolism. *J Lipid Res.* (2013) 54:2325–40. doi: 10.1194/jlr.R036012
95. Trapecar M, Communal C, Velazquez J, Maass CA, Huang YJ, Schneider K, et al. Gut-liver physiomimetics reveal paradoxical modulation of IBD-related inflammation by short-chain fatty acids. *Cell Syst.* (2020) 10:223–39 e9. doi: 10.1016/j.cels.2020.02.008
96. Effenberger M, Tilg H. The intestinal microbiota and hepatocellular carcinoma. *Memo-Mag Eur Med Onc.* (2020) 13:223–6. doi: 10.1007/s12254-020-00597-x
97. Sun M, Wu W, Chen L, Yang W, Huang X, Ma C, et al. Microbiota-derived short-chain fatty acids promote Th1 cell IL-10 production to maintain intestinal homeostasis. *Nat Commun.* (2018) 9:3555. doi: 10.1038/s41467-018-05901-2
98. Asarat M, Apostolopoulos V, Vasiljevic T, Donkor O. Short-chain fatty acids regulate cytokines and Th17/Treg cells in human peripheral blood mononuclear cells *in vitro*. *Immunol Invest.* (2016) 45:205–22. doi: 10.3109/08820139.2015.1122613
99. Behary J, Amorim N, Jiang XT, Raposo A, Gong L, McGovern E, et al. Gut microbiota impact on the peripheral immune response in non-alcoholic fatty liver disease related hepatocellular carcinoma. *Nat Commun.* (2021) 12:187. doi: 10.1038/s41467-020-20422-7
100. Singh V, Yeoh BS, Chassaing B, Xiao X, Saha P, Aguilera Olvera R, et al. Dysregulated microbial fermentation of soluble fiber induces cholestatic liver cancer. *Cell.* (2018) 175:679–94 e22. doi: 10.1016/j.cell.2018.09.004
101. Lammert C, A SS, Xu H, Hemmerich C, T MOC, Chalasani N. Short-chain fatty acid and fecal microbiota profiles are linked to fibrosis in primary biliary cholangitis. *FEMS Microbiol Lett.* (2021) 368:fnab0386. doi: 10.1093/femsle/fnab038
102. Chong MM, Zhang G, Cheloufi S, Neubert TA, Hannon GJ, Littman DR. Canonical and alternate functions of the microRNA biogenesis machinery. *Genes Dev.* (2010) 24:1951–60. doi: 10.1101/gad.1953310
103. Ferreira DM, Simao AL, Rodrigues CM, Castro RE. Revisiting the metabolic syndrome and paving the way for microRNAs in non-alcoholic fatty liver disease. *FEBS J.* (2014) 281:2503–24. doi: 10.1111/febs.12806
104. Torres JL, Novo-Veleiro I, Manzanedo L, Alvela-Suarez L, Macias R, Laso FJ, et al. Role of microRNAs in alcohol-induced liver disorders and non-alcoholic fatty liver disease. *World J Gastroenterol.* (2018) 24:4104–18. doi: 10.3748/wjg.v24.i36.4104
105. McDaniel K, Herrera L, Zhou T, Francis H, Han Y, Levine P, et al. The functional role of microRNAs in alcoholic liver injury. *J Cell Mol Med.* (2014) 18:197–207. doi: 10.1111/jcmm.12223
106. Schueller F, Roy S, Vucur M, Trautwein C, Luedde T, Roderburg C. The role of miRNAs in the pathophysiology of liver diseases and toxicity. *Int J Mol Sci.* (2018) 19:261. doi: 10.3390/ijms19010261
107. Feng Q, Chen WD, Wang YD. Gut microbiota: an integral moderator in health and disease. *Front Microbiol.* (2018) 9:151. doi: 10.3389/fmicb.2018.00151
108. Longo L, Tonin Ferrari J, Rampelotto PH, Hirata Dellavia G, Pasqualotto A, C PO, et al. Gut dysbiosis and increased intestinal permeability drive microRNAs, NLRP-3 inflammasome and liver fibrosis in a nutritional model of non-alcoholic steatohepatitis in adult male sprague dawley rats. *Clin Exp Gastroenterol.* (2020) 13:351–68. doi: 10.2147/CEG.S262879
109. Pant K, Yadav AK, Gupta P, Islam R, Saraya A, Venugopal SK. Butyrate induces ROS-mediated apoptosis by modulating miR-22/SIRT-1 pathway in hepatic cancer cells. *Redox Biol.* (2017) 12:340–9. doi: 10.1016/j.redox.2017.03.006
110. Sulaiman SA, Muhsin NIA, Jamal R. Regulatory non-coding RNAs network in non-alcoholic fatty liver disease. *Front Physiol.* (2019) 10:279. doi: 10.3389/fphys.2019.00279
111. Wang XL, He Y, Mackowiak B, Gao B. MicroRNAs as regulators, biomarkers and therapeutic targets in liver diseases. *Gut.* (2021) 70:784–95. doi: 10.1136/gutjnl-2020-322526
112. Cossiga V, Lembo V, Nigro C, Mirra P, Miele C, D'Argenio V, et al. The combination of berberine, tocotrienols and coffee extracts improves metabolic profile and liver steatosis by the modulation of gut microbiota and hepatic miR-122 and miR-34a expression in mice. *Nutrients.* (2021) 13:1281. doi: 10.3390/nu13041281
113. Jia N, Lin X, Ma S, Ge S, Mu S, Yang C, et al. Amelioration of hepatic steatosis is associated with modulation of gut microbiota and suppression of hepatic miR-34a in Gynostemma pentaphylla (Thunb.) Makino treated mice. *Nutr Metab.* (2018) 15:86. doi: 10.1186/s12986-018-0323-6
114. Santos AA, Afonso MB, Ramiro RS, Pires D, Pimentel M, Castro RE, et al. Host miRNA-21 promotes liver dysfunction by targeting small intestinal Lactobacillus in mice. *Gut Microbes.* (2020) 12:1–18. doi: 10.1080/19490976.2020.1840766
115. Blasco-Baque V, Coupe B, Fabre A, Handgraaf S, Gourdy P, Arnal JF, et al. Associations between hepatic miRNA expression, liver triacylglycerols and gut microbiota during metabolic adaptation to high-fat diet in mice. *Diabetologia.* (2017) 60:690–700. doi: 10.1007/s00125-017-4209-3
116. Zou Y, Cai Y, Lu D, Zhou Y, Yao Q, Zhang S. MicroRNA-146a-5p attenuates liver fibrosis by suppressing profibrogenic effects of TGFbeta1 and lipopolysaccharide. *Cell Signal.* (2017) 39:1–8. doi: 10.1016/j.cellsig.2017.07.016
117. Liu XL, Pan Q, Cao HX, Xin FZ, Zhao ZH, Yang RX, et al. Lipotoxic hepatocyte-derived exosomal MicroRNA 192-5p activates macrophages through rictor/Akt/Forkhead box transcription factor O1 signaling in nonalcoholic fatty liver disease. *Hepatology.* (2020) 72:454–69. doi: 10.1002/hep.31050
118. Xie G, Wang X, Zhao A, Yan J, Chen W, Jiang R, et al. Sex-dependent effects on gut microbiota regulate hepatic carcinogenic outcomes. *Sci Rep.* (2017) 7:45232. doi: 10.1038/srep45232
119. O'Neill LA, Sheedy FJ, McCoy CE. MicroRNAs: the fine-tuners of Toll-like receptor signalling. *Nat Rev Immunol.* (2011) 11:163–75. doi: 10.1038/nri2957
120. Fitzgerald KA, Kagan JC. Toll-like receptors and the control of immunity. *Cell.* (2020) 180:1044–66. doi: 10.1016/j.cell.2020.02.041
121. Wu J, Meng Z, Jiang M, Zhang E, Trippler M, Broering R, et al. Toll-like receptor-induced innate immune responses in non-parenchymal liver cells are cell type-specific. *Immunology.* (2010) 129:363–74. doi: 10.1111/j.1365-2567.2009.03179.x
122. Yokoyama T, Komori A, Nakamura M, Takii Y, Kamihira T, Shimoda S, et al. Human intrahepatic biliary epithelial cells function in innate immunity by producing IL-6 and IL-8 via the TLR4-NF-kappaB and -MAPK signaling pathways. *Liver Int.* (2006) 26:467–76. doi: 10.1111/j.1478-3231.2006.01254.x
123. Pimentel-Nunes P, Roncon-Albuquerque R Jr, Goncalves N, Fernandes-Cerqueira C, Cardoso H, Bastos RP, et al. Attenuation of toll-like receptor 2-mediated innate immune response in patients with alcoholic chronic liver disease. *Liver Int.* (2010) 30:1003–11. doi: 10.1111/j.1478-3231.2010.02251.x

124. Stadlbauer V, Mookerjee RP, Wright GA, Davies NA, Jurgens G, Hallstrom S, et al. Role of Toll-like receptors 2, 4, and 9 in mediating neutrophil dysfunction in alcoholic hepatitis. *Am J Physiol Gastrointest Liver Physiol.* (2009) 296:G15–22. doi: 10.1152/ajpgi.90512.2008
125. Gustot T, Lemmers A, Moreno C, Nagy N, Quertinmont E, Nicaise C, et al. Differential liver sensitization to toll-like receptor pathways in mice with alcoholic fatty liver. *Hepatology.* (2006) 43:989–1000. doi: 10.1002/hep.21138
126. Mahmoudi J, Mahmoodpoor A, Amirnia M, Kazemi T, Chokhachi Baradaran P, Sheikh Najafi S, et al. The induced decrease in TLR2 and TLR4 by cerebrolysin in the alcoholic liver of rats. *J Cell Physiol.* (2019) 218:237–45. doi: 10.1002/jcp.28293
127. Kirpich IA, Feng W, Wang Y, Liu Y, Barker DF, Barve SS, et al. The type of dietary fat modulates intestinal tight junction integrity, gut permeability, and hepatic toll-like receptor expression in a mouse model of alcoholic liver disease. *Alcohol Clin Exp Res.* (2012) 36:835–46. doi: 10.1111/j.1530-0277.2011.01673.x
128. Seo B, Jeon K, Moon S, Lee K, Kim WK, Jeong H, et al. Roseburia spp. abundance associates with alcohol consumption in humans and its administration ameliorates alcoholic fatty liver in mice. *Cell Host Microbe.* (2020) 27:25–40 e6. doi: 10.1016/j.chom.2019.11.001
129. Roh YS, Zhang B, Loomba R, Seki E. TLR2 and TLR9 contribute to alcohol-mediated liver injury through induction of CXCL1 and neutrophil infiltration. *Am J Physiol Gastrointest Liver Physiol.* (2015) 309:G30–41. doi: 10.1152/ajpgi.00031.2015
130. Luo P, Wang F, Wong NK, Lv Y, Li X, Li M, et al. Divergent roles of kupffer cell TLR2/3 signaling in alcoholic liver disease and the protective role of eGCG. *Cell Mol Gastroenterol Hepatol.* (2020) 9:145–60. doi: 10.1016/j.jcmgh.2019.09.002
131. Petrasek J, Mandrekar P, Szabo G. Toll-like receptors in the pathogenesis of alcoholic liver disease. *Gastroenterol Res Pract.* (2010) 2010. doi: 10.1155/2010/710381
132. Bala S, Csak T, Kodys K, Catalano D, Ambade A, Furi I, et al. Alcohol-induced miR-155 and HDAC11 inhibit negative regulators of the TLR4 pathway and lead to increased LPS responsiveness of Kupffer cells in alcoholic liver disease. *J Leukoc Biol.* (2017) 102:487–98. doi: 10.1189/jlb.3A0716-310R
133. Chiu CC, Ching YH, Li YP, Liu JY, Huang YT, Huang YW, et al. Nonalcoholic fatty liver disease is exacerbated in high-fat diet-fed gnotobiotic mice by colonization with the gut microbiota from patients with nonalcoholic steatohepatitis. *Nutrients.* (2017) 9:1220. doi: 10.3390/nu9111220
134. Miura K, Ohnishi H. Role of gut microbiota and Toll-like receptors in nonalcoholic fatty liver disease. *World J Gastroenterol.* (2014) 20:7381–91. doi: 10.3748/wjg.v20.i23.7381
135. Diniz AB, Antunes MM, Lacerda VAS, Nakagaki BN, Freitas Lopes MA, Castro-Oliveira HM, et al. Imaging and immunometabolic phenotyping uncover changes in the hepatic immune response in the early phases of NAFLD. *JHEP Rep.* (2020) 2:100117. doi: 10.1016/j.jhepr.2020.100117
136. Miura K, Yang L, van Rooijen N, Brenner DA, Ohnishi H, Seki E. Toll-like receptor 2 and palmitic acid cooperatively contribute to the development of nonalcoholic steatohepatitis through inflammasome activation in mice. *Hepatology.* (2013) 57:577–89. doi: 10.1002/hep.26081
137. Cengiz M, Ozenirler S, Elbeg S. Role of serum toll-like receptors 2 and 4 in non-alcoholic steatohepatitis and liver fibrosis. *J Gastroenterol Hepatol.* (2015) 30:1190–6. doi: 10.1111/jgh.12924
138. Cheng C, Tan J, Qian W, Zhang L, Hou X. Gut inflammation exacerbates hepatic injury in the high-fat diet induced NAFLD mouse: attention to the gut-vascular barrier dysfunction. *Life Sci.* (2018) 209:157–66. doi: 10.1016/j.lfs.2018.08.017
139. Munukka E, Wiklund P, Partanen T, Valimaki S, Laakkonen EK, Lehti M, et al. Adipocytes as a link between gut microbiota-derived flagellin and hepatocyte fat accumulation. *PLoS ONE.* (2016) 11:e0152786. doi: 10.1371/journal.pone.0152786
140. Singh V, Chassaing B, Zhang L, San Yeoh B, Xiao X, Kumar M, et al. Microbiota-Dependent Hepatic Lipogenesis Mediated by Stearoyl CoA Desaturase 1 (SCD1) promotes metabolic syndrome in TLR5-Deficient mice. *Cell Metab.* (2015) 22:983–96. doi: 10.1016/j.cmet.2015.09.028
141. Etienne-Mesmin L, Vijay-Kumar M, Gewirtz AT, Chassaing B. Hepatocyte Toll-Like receptor 5 promotes bacterial clearance and protects mice against high-fat diet-induced liver disease. *Cell Mol Gastroenterol Hepatol.* (2016) 2:584–604. doi: 10.1016/j.jcmgh.2016.04.007
142. Mridha AR, Haczeyni F, Yeh MM, Haigh WG, Ioannou GN, Barn V, et al. TLR9 is up-regulated in human and murine NASH: pivotal role in inflammatory recruitment and cell survival. *Clin Sci (Lond).* (2017) 131:2145–59. doi: 10.1042/CS20160838
143. Garcia-Martinez I, Santoro N, Chen Y, Hoque R, Ouyang X, Caprio S, et al. Hepatocyte mitochondrial DNA drives nonalcoholic steatohepatitis by activation of TLR9. *J Clin Invest.* (2016) 126:859–64. doi: 10.1172/JCI83885
144. Arias-Loste MT, Iruzubieta P, Puente A, Ramos D, Santa Cruz C, Estebanez A, et al. Increased expression profile and functionality of tlr6 in peripheral blood mononuclear cells and hepatocytes of morbidly obese patients with non-alcoholic fatty liver disease. *Int J Mol Sci.* (2016) 17 :5878. doi: 10.3390/ijms17111878
145. Yiu JHC, Chan KS, Cheung J, Li J, Liu Y, Wang Y, et al. Gut microbiota-associated activation of TLR5 induces apolipoprotein A1 production in the liver. *Circ Res.* (2020) 127:1236–52. doi: 10.1161/CIRCRESAHA.120.317362
146. Yan H, Zhong M, Yang J, Guo J, Yu J, Yang Y, et al. TLR5 activation in hepatocytes alleviates the functional suppression of intrahepatic CD8(+) T cells. *Immunology.* (2020) 161:325–44. doi: 10.1111/imm.13251
147. Manigold T, Bocker U, Hanck C, Gundt J, Traber P, Antoni C, et al. Differential expression of toll-like receptors 2 and 4 in patients with liver cirrhosis. *Eur J Gastroenterol Hepatol.* (2003) 15:275–82. doi: 10.1097/00042737-200303000-00011
148. Hackstein CP, Assmus LM, Welz M, Klein S, Schwandt T, Schultze J, et al. Gut microbial translocation corrupts myeloid cell function to control bacterial infection during liver cirrhosis. *Gut.* (2017) 66:507–18. doi: 10.1136/gutjnl-2015-311224
149. Miura K, Ishioka M, Minami S, Horie Y, Ohshima S, Goto T, et al. Toll-like receptor 4 on macrophage promotes the development of steatohepatitis-related hepatocellular carcinoma in mice. *J Biol Chem.* (2016) 291:11504–17. doi: 10.1074/jbc.M115.709048
150. Liu X, Gong J, Xu B. miR-143 down-regulates TLR2 expression in hepatoma cells and inhibits hepatoma cell proliferation and invasion. *Int J Clin Exp Pathol.* (2015) 8:12738–47.
151. Mularczyk M, Bourebaba Y, Kowalczuk A, Marycz K, Bourebaba L. Probiotics-rich emulsion improves insulin signalling in Palmitate/Oleate-challenged human hepatocarcinoma cells through the modulation of Fetuin-A/TLR4-JNK-NF-kappaB pathway. *Biomed Pharmacother.* (2021) 139:111560. doi: 10.1016/j.biopha.2021.111560
152. Brown GD. Dectin-1: a signalling non-TLR pattern-recognition receptor. *Nat Rev Immunol.* (2006) 6:33–43. doi: 10.1038/nri1745
153. Seifert L, Deutsch M, Alothman S, Alqunaibit D, Werba G, Pansari M, et al. Dectin-1 regulates hepatic fibrosis and hepatocarcinogenesis by suppressing TLR4 signaling pathways. *Cell Rep.* (2015) 13:1909–21. doi: 10.1016/j.celrep.2015.10.058
154. Kulaksiz H, Rudolph G, Kloeters-Plachky P, Sauer P, Geiss H, Stiehl A. Biliary candida infections in primary sclerosing cholangitis. *J Hepatol.* (2006) 45:711–6. doi: 10.1016/j.jhep.2006.07.022
155. Kohatsu L, Hsu DK, Jegalian AG, Liu FT, Baum LG. Galectin-3 induces death of Candida species expressing specific beta-1,2-linked mannans. *J Immunol.* (2006) 177:4718–26. doi: 10.4049/jimmunol.177.7.4718
156. Li Y, Komai-Koma M, Gilchrist DS, Hsu DK, Liu FT, Springall T, et al. Galectin-3 is a negative regulator of lipopolysaccharide-mediated inflammation. *J Immunol.* (2008) 181:2781–9. doi: 10.4049/jimmunol.181.4.2781
157. Jouault T, El Abed-El Behi M, Martinez-Esparza M, Breuilh L, Trinel PA, Chamaillard M, et al. Specific recognition of Candida albicans by macrophages requires galectin-3 to discriminate Saccharomyces cerevisiae and needs association with TLR2 for signaling. *J Immunol.* (2006) 177:4679–87. doi: 10.4049/jimmunol.177.7.4679
158. Al Mamun A, Akter A, Hossain S, Sarker T, Safa SA, Mustafa QG, et al. Role of NLRP3 inflammasome in liver disease. *J Dig Dis.* (2020) 21:430–6. doi: 10.1111/1751-2980.12918
159. Bawa M, Saraswat VA. Gut-liver axis: role of inflammasomes. *J Clin Exp Hepatol.* (2013) 3:141–9. doi: 10.1016/j.jceh.2013.03.225
160. Henao-Mejia J, Elinav E, Jin C, Hao L, Mehal WZ, Strowig T, et al. Inflammasome-mediated dysbiosis regulates progression of

NAFLD and obesity. *Nature.* (2012) 482:179–85. doi: 10.1038/nature 10809
161. Tilg H, Moschen AR, Szabo G. Interleukin-1 and inflammasomes in alcoholic liver disease/acute alcoholic hepatitis and nonalcoholic fatty liver disease/nonalcoholic steatohepatitis. *Hepatology.* (2016) 64:955–65. doi: 10.1002/hep.28456
162. Wu X, Dong L, Lin X, Li J. Relevance of the NLRP3 inflammasome in the pathogenesis of chronic liver disease. *Front Immunol.* (2017) 8:1728. doi: 10.3389/fimmu.2017.01728
163. He K, Zhu X, Liu Y, Miao C, Wang T, Li P, et al. Inhibition of NLRP3 inflammasome by thioredoxin-interacting protein in mouse Kupffer cells as a regulatory mechanism for non-alcoholic fatty liver disease development. *Oncotarget.* (2017) 8:37657–72. doi: 10.18632/oncotarget. 17489
164. Chen D, Le TH, Shahidipour H, Read SA, Ahlenstiel G. The role of gut-derived microbial antigens on liver fibrosis initiation and progression. *Cells.* (2019) 8:13241. doi: 10.3390/cells8111324
165. Ko M, Kamimura K, Owaki T, Nagoya T, Sakai N, Nagayama I, et al. Modulation of serotonin in the gut-liver neural axis ameliorates the fatty and fibrotic changes in non-alcoholic fatty liver. *Dis Model Mech.* (2021) 14:dmm048922. doi: 10.1242/dmm.048922
166. Caraceni P, Vargas V, Sola E, Alessandria C, de Wit K, Trebicka J, et al. The use of rifaximin in patients with cirrhosis. *Hepatology.* (2021). doi: 10.1002/hep.31708
167. Fujinaga Y, Kawaratani H, Kaya D, Tsuji Y, Ozutsumi T, Furukawa M, et al. Effective combination therapy of angiotensin-ii receptor blocker and rifaximin for hepatic fibrosis in rat model of nonalcoholic steatohepatitis. *Int J Mol Sci.* (2020) 21:5589. doi: 10.3390/ijms21155589 [Epub ahead of Print].
168. Bergheim I, Weber S, Vos M, Kramer S, Volynets V, Kaserouni S, et al. Antibiotics protect against fructose-induced hepatic lipid accumulation in mice: role of endotoxin. *J Hepatol.* (2008) 48:983–92. doi: 10.1016/j.jhep.2008.01.035
169. Ponziani FR, Zocco MA, D'Aversa F, Pompili M, Gasbarrini A. Eubiotic properties of rifaximin: disruption of the traditional concepts in gut microbiota modulation. *World J Gastroenterol.* (2017) 23:4491–9. doi: 10.3748/wjg.v23.i25.4491
170. Abdel-Razik A, Mousa N, Shabana W, Refaey M, Elzehery R, Elhelaly R, et al. Rifaximin in nonalcoholic fatty liver disease: hit multiple targets with a single shot. *Eur J Gastroenterol Hepatol.* (2018) 30:1237–46. doi: 10.1097/MEG.0000000000001232
171. Pose E, Napoleone L, Amin A, Campion D, Jimenez C, Piano S, et al. Safety of two different doses of simvastatin plus rifaximin in decompensated cirrhosis (LIVERHOPE-SAFETY): a randomised, double-blind, placebo-controlled, phase 2 trial. *Lancet Gastroenterol Hepatol.* (2020) 5:31–41. doi: 10.1016/S2468-1253(19)30320-6
172. Bajaj JS, Salzman N, Acharya C, Takei H, Kakiyama G, Fagan A, et al. Microbial functional change is linked with clinical outcomes after capsular fecal transplant in cirrhosis. *JCI Insight.* (2019) 4:e133410. doi: 10.1172/jci.insight.133410
173. Bomhof MR, Parnell JA, Ramay HR, Crotty P, Rioux KP, Probert CS, et al. Histological improvement of non-alcoholic steatohepatitis with a prebiotic: a pilot clinical trial. *Eur J Nutr.* (2019) 58:1735–45. doi: 10.1007/s00394-018-1721-2
174. Kobyliak N, Abenavoli L, Mykhalchyshyn G, Kononenko L, Boccuto L, Kyriienko D, et al. A multi-strain probiotic reduces the fatty liver index, cytokines and aminotransferase levels in NAFLD patients: evidence from a randomized clinical trial. *J Gastrointestin Liver Dis.* (2018) 27:41–9. doi: 10.15403/jgld.2014.1121.271.kby
175. Depommier C, Everard A, Druart C, Plovier H, Van Hul M, Vieira-Silva S, et al. Supplementation with Akkermansia muciniphila in overweight and obese human volunteers: a proof-of-concept exploratory study. *Nat Med.* (2019) 25:1096–103. doi: 10.1038/s41591-019-0495-2
176. Lambert JE, Parnell JA, Eksteen B, Raman M, Bomhof MR, Rioux KP, et al. Gut microbiota manipulation with prebiotics in patients with non-alcoholic fatty liver disease: a randomized controlled trial protocol. *BMC Gastroenterol.* (2015) 15:169. doi: 10.1186/s12876-015-0400-5
177. Younossi ZM, Ratziu V, Loomba R, Rinella M, Anstee QM, Goodman Z, et al. Obeticholic acid for the treatment of non-alcoholic steatohepatitis: interim analysis from a multicentre, randomised, placebo-controlled phase 3 trial. *Lancet.* (2019) 394:2184–96. doi: 10.1016/S0140-6736(19)33041-7
178. Safadi R, Konikoff FM, Mahamid M, Zelber-Sagi S, Halpern M, Gilat T, et al. The fatty acid-bile acid conjugate Aramchol reduces liver fat content in patients with nonalcoholic fatty liver disease. *Clin Gastroenterol Hepatol.* (2014) 12:2085–91 e1. doi: 10.1016/j.cgh.2014.04.038
179. Traussnigg S, Schattenberg JM, Demir M, Wiegand J, Geier A, Teuber G, et al. Norursodeoxycholic acid versus placebo in the treatment of non-alcoholic fatty liver disease: a double-blind, randomised, placebo-controlled, phase 2 dose-finding trial. *Lancet Gastroenterol Hepatol.* (2019) 4:781–93. doi: 10.1016/S2468-1253(19)30184-0
180. Mingrone G, van Baar AC, Deviere J, Hopkins D, Moura E, Cercato C, et al. Safety and efficacy of hydrothermal duodenal mucosal resurfacing in patients with type 2 diabetes: the randomised, double-blind, sham-controlled, multicentre REVITA-2 feasibility trial. *Gut.* (2021). doi: 10.1136/gutjnl-2020-323608. [Epub ahead of print].
181. Bajaj JS, Khoruts A. Microbiota changes and intestinal microbiota transplantation in liver diseases and cirrhosis. *J Hepatol.* (2020) 72:1003–27. doi: 10.1016/j.jhep.2020.01.017
182. Ferrere G, Wrzosek L, Cailleux F, Turpin W, Puchois V, Spatz M, et al. Fecal microbiota manipulation prevents dysbiosis and alcohol-induced liver injury in mice. *J Hepatol.* (2017) 66:806–15. doi: 10.1016/j.jhep.2016.11.008
183. de Groot P, Scheithauer T, Bakker GJ, Prodan A, Levin E, Khan MT, et al. Donor metabolic characteristics drive effects of faecal microbiota transplantation on recipient insulin sensitivity, energy expenditure and intestinal transit time. *Gut.* (2020) 69:502–12. doi: 10.1136/gutjnl-2019-318320
184. Allegretti JR, Kassam Z, Carrellas M, Mullish BH, Marchesi JR, Pechlivanis A, et al. Fecal microbiota transplantation in patients with primary sclerosing cholangitis: a pilot clinical trial. *Am J Gastroenterol.* (2019) 114:1071–9. doi: 10.14309/ajg.0000000000000115
185. Bajaj JS, Gavis EA, Fagan A, Wade JB, Thacker LR, Fuchs M, et al. A randomized clinical trial of fecal microbiota transplant for alcohol use disorder. *Hepatology.* (2021) 73:1688–700. doi: 10.1002/hep.31496
186. Ma X, Hua J, Li Z. Probiotics improve high fat diet-induced hepatic steatosis and insulin resistance by increasing hepatic NKT cells. *J Hepatol.* (2008) 49:821–30. doi: 10.1016/j.jhep.2008.05.025
187. Li J, Sung CY, Lee N, Ni Y, Pihlajamaki J, Panagiotou G, et al. Probiotics modulated gut microbiota suppresses hepatocellular carcinoma growth in mice. *Proc Natl Acad Sci USA.* (2016) 113:E1306–15. doi: 10.1073/pnas.1518189113
188. Grander C, Adolph TE, Wieser V, Lowe P, Wrzosek L, Gyongyosi B, et al. Recovery of ethanol-induced Akkermansia muciniphila depletion ameliorates alcoholic liver disease. *Gut.* (2018) 67:891–901. doi: 10.1136/gutjnl-2016-313432
189. Routy B, Le Chatelier E, Derosa L, Duong CPM, Alou MT, Daillere R, et al. Gut microbiome influences efficacy of PD-1-based immunotherapy against epithelial tumors. *Science.* (2018) 359:91–7. doi: 10.1126/science. aan3706
190. Bao T, He F, Zhang X, Zhu L, Wang Z, Lu H, et al. Inulin exerts beneficial effects on non-alcoholic fatty liver disease via modulating gut microbiome and suppressing the lipopolysaccharide-Toll-Like receptor 4-Mpsi-NUCLEAR FACTOR-kappaB-Nod-like receptor protein 3 pathway via gut-liver axis in mice. *Front Pharmacol.* (2020) 11:558525. doi: 10.3389/fphar.2020.558525
191. Hadi A, Ghaedi E, Khalesi S, Pourmasoumi M, Arab A. Effects of synbiotic consumption on lipid profile: a systematic review and meta-analysis of randomized controlled clinical trials. *Eur J Nutr.* (2020) 59:2857–74. doi: 10.1007/s00394-020-02248-7
192. Kowdley KV, Vuppalanchi R, Levy C, Floreani A, Andreone P, LaRusso NF, et al. A randomized, placebo-controlled, phase II study of obeticholic acid for primary sclerosing cholangitis. *J Hepatol.* (2020) 73:94–101. doi: 10.1016/j.jhep.2020.02.033
193. Sun L, Cai J, Gonzalez FJ. The role of farnesoid X receptor in metabolic diseases, and gastrointestinal and liver cancer. *Nat Rev Gastroenterol Hepatol.* (2021) 18:335–47. doi: 10.1038/s41575-020-00404-2
194. Sorribas M, Jakob MO, Yilmaz B, Li H, Stutz D, Noser Y, et al. FXR modulates the gut-vascular barrier by regulating the entry sites for

bacterial translocation in experimental cirrhosis. *J Hepatol.* (2019) 71:1126–40. doi: 10.1016/j.jhep.2019.06.017
195. Fickert P, Hirschfield GM, Denk G, Marschall HU, Altorjay I, Farkkila M, et al. norUrsodeoxycholic acid improves cholestasis in primary sclerosing cholangitis. *J Hepatol.* (2017) 67:549–58. doi: 10.1016/j.jhep.2017.05.009
196. Engelmann C, Sheikh M, Sharma S, Kondo T, Loeffler-Wirth H, Zheng YB, et al. Toll-like receptor 4 is a therapeutic target for prevention and treatment of liver failure. *J Hepatol.* (2020) 73:102–12. doi: 10.1016/j.jhep.2020.01.011
197. Hsieh YC, Lee KC, Wu PS, Huo TI, Huang YH, Hou MC, et al. Eritoran attenuates hepatic inflammation and fibrosis in mice with chronic liver injury. *Cells.* (2021) 10:1562. doi: 10.3390/cells10061562
198. Macnaughtan J, Soeda J, Mouralidarane A, Sandeman S, Howell C, Milkhalovsky S, et al. Effects of oral nanoporous carbon therapy in leptin null mice as a model of non-alcoholic steatohepatitis. *Gut.* (2012) 61:A125–A. doi: 10.1136/gutjnl-2012-302514b.128
199. Suez J, Elinav E. The path towards microbiome-based metabolite treatment. *Nat Microbiol.* (2017) 2:17075. doi: 10.1038/nmicrobiol.2017.75
200. Gao J, Li Y, Wan Y, Hu T, Liu L, Yang S, et al. A novel postbiotic from *Lactobacillus rhamnosus* GG with a beneficial effect on intestinal barrier function. *Front Microbiol.* (2019) 10:477. doi: 10.3389/fmicb.2019.00477
201. Damoogh S, Vosough M, Hadifar S, Rasoli M, Gorjipour A, Falsafi S, et al. Evaluation of E. *coli* Nissle1917 derived metabolites in modulating key mediator genes of the TLR signaling pathway. *BMC Res Notes.* (2021) 14:156. doi: 10.1186/s13104-021-05568-x
202. Isabella VM, Ha BN, Castillo MJ, Lubkowicz DJ, Rowe SE, Millet YA, et al. Development of a synthetic live bacterial therapeutic for the human metabolic disease phenylketonuria. *Nat Biotechnol.* (2018) 36:857–64. doi: 10.1038/nbt.4222
203. Kurtz CB, Millet YA, Puurunen MK, Perreault M, Charbonneau MR, Isabella VM, et al. An engineered E. coli Nissle improves hyperammonemia and survival in mice and shows dose-dependent exposure in healthy humans. *Sci Transl Med.* (2019) 11:au7975. doi: 10.1126/scitranslmed.aau7975
204. Hendrikx T, Duan Y, Wang Y, Oh JH, Alexander LM, Huang W, et al. Bacteria engineered to produce IL-22 in intestine induce expression of REG3G to reduce ethanol-induced liver disease in mice. *Gut.* (2019) 68:1504–15. doi: 10.1136/gutjnl-2018-317232

Conflict of Interest: FT's lab has received research funding by Allergan, Bristol-Myers Squibb, Galapagos, Gilead and Inventiva. He consults for Allergan, Bayer, Boehringer Ingelheim, Galapagos, Galmed, Intercept, Inventiva, NGM bio, Novartis, and Pfizer.

The remaining authors declare that the research was conducted in the absence of any commercial or financial relationships that could be construed as a potential conflict of interest.

Publisher's Note: All claims expressed in this article are solely those of the authors and do not necessarily represent those of their affiliated organizations, or those of the publisher, the editors and the reviewers. Any product that may be evaluated in this article, or claim that may be made by its manufacturer, is not guaranteed or endorsed by the publisher.

Advantages of publishing in Frontiers

OPEN ACCESS
Articles are free to read for greatest visibility and readership

FAST PUBLICATION
Around 90 days from submission to decision

HIGH QUALITY PEER-REVIEW
Rigorous, collaborative, and constructive peer-review

TRANSPARENT PEER-REVIEW
Editors and reviewers acknowledged by name on published articles

Frontiers
Avenue du Tribunal-Fédéral 34
1005 Lausanne | Switzerland

Visit us: www.frontiersin.org
Contact us: frontiersin.org/about/contact

REPRODUCIBILITY OF RESEARCH
Support open data and methods to enhance research reproducibility

DIGITAL PUBLISHING
Articles designed for optimal readership across devices

FOLLOW US
@frontiersin

IMPACT METRICS
Advanced article metrics track visibility across digital media

EXTENSIVE PROMOTION
Marketing and promotion of impactful research

LOOP RESEARCH NETWORK
Our network increases your article's readership